‘Characterising the Role of Basin Margin Structure across a Cleavage Front from the Variscides of South West Ireland’

Number of Volumes: 2

Volume 1 of 2

Chloe Rowena Parker

A thesis submitted for the qualification of Doctorate.

University College Cork,

National University of Ireland,

Cork

Department of Geology, School of BEES.

October 2017

Head of Department: Prof. Sarah Culloty

Supervised By: Dr. Pat Meere (UCC) &

Dr. Carl Stevenson (University of Birmingham)

National University of Ireland, Cork
School of Biological, Earth and Environmental Sciences (Discipline of Geology)
College of Science, Engineering and Food Sciences

‘Characterising the Role of Basin Margin Structure across a Cleavage Front from the Variscides of South West Ireland’

Number of Volumes: 2

Volume 2 of 2

Chloe Rowena Parker

A thesis submitted for the qualification of Doctorate.

University College Cork,

National University of Ireland,

Cork

Department of Geology, School of BEES.

October 2017

Head of Department: Prof. Sarah Culloty

Supervised By: Dr. Pat Meere (UCC) &

Dr. Carl Stevenson (University of Birmingham)

National University of Ireland, Cork
School of Biological, Earth and Environmental Sciences (Discipline of Geology)
College of Science, Engineering and Food Sciences

Table of Contents **Page No.**

Declaration.

This thesis is the candidates own work and has not been submitted for another degree either at University College Cork or elsewhere.

Signed: 

Abstract

Characterising the role of basin margin structure on finite strain patterns across a 'cleavage' front from the Variscides of southern Ireland.

The northern margin of the Munster Basin has been traditionally placed at the Dingle Dungarvan Line (DDL), a line which runs through Dingle Bay in the west and coincides with the Kilarney Mallow Fault Zone (KMFZ) further to the east, on the Iveragh Peninsula, south west Ireland. This region lies at the northern boundary of the Rhenohercynian Zone of the European Variscides. Deformation of a thick (7 km +) Upper Devonian continental clastic sequence and overlying Carboniferous marine carbonate/clastic sequence at the end of the Carboniferous is thought to have consisted of an initial phase of layer parallel shortening, followed by folding, ongoing cleavage development and late stage accommodation thrusting.

Previous models of inversion at the northern margin consist of an initial extensional basin margin fault that was subsequently reactivated as a reverse fault during compression, with resulting higher strain to the south in the Munster Basin and lower strain to the north in the Foreland Zone. Previous suggestions for the location of the northern margin and the mechanisms of inversion with a passive underlying basement, do not account for the nature of deformation observed in the far western vicinity of the basin margin fault. This study proposes an alternative fault - the Coomnacronia Fault (CF), which is a major map scale fault lying to the south of the DDL and laterally to the west of the KMFZ, as the northern margin of the Munster Basin, based on the impact that this fault has had on the northwards directed Variscan strain regime.

The results from the Anisotropy of Magnetic Susceptibility (AMS), strain analysis, structural field work and microstructural studies carried out on Upper Devonian-Old Red Sandstone from the Munster Basin and northern peripheral areas show that the CF marks a significant tectonic boundary. This study proposes three characteristic strain zones including a newly defined zone: The Transition Zone, within the vicinity of the northern margin, which are suggested to be intrinsically related to the geometry of the underlying Caledonian/Acadian basement and the inversion

mechanisms of the CF. To the south of the CF lies the Intrabasinal Zone which is characterised by steeply dipping axial planar cleavage, higher average strain values (DTNNM R_s = 1.296; MRL R_s = 1.269), S_1 controlled AMS ellipsoids (complete tectonic overprint) and microstructures which reflect a zone of higher deformation. To the North of the CF lies the Transition Zone which is characterised by variably dipping passively rotated cleavage, lower average strain values (DTNNM R_s = 1.203; MRL R_s= 1.142), AMS ellipsoids controlled by primary sedimentary fabrics and early LPS fabrics and microstructures indicative of a lower strain regime. The Dingle Peninsula and Kerry head which are already considered to be part of the Foreland to the north display either zero tectonic cleavage or a spaced disjunctive cleavage, bedding controlled AMS ellipsoids and lower average strain values R_s values (DTNNM R_s = 1.069; MRL R_s = 1.048).

Previous studies suggest that the CF was an intrabasinal extensional structure and/or a late stage intrabasinal thrust. This study suggests that the CF was a major basin margin structure. The present day material to the north of the CF consists of foreland deposits that underwent low strain and early LPS and rest upon shallow Caledonian/Acadian basement. The CF was an initial extensional basin margin structure which subsequently acted as a thrust fault during inversion. The CF acted as a structural boundary between the full penetrative cleavage event to the south and a relatively weak cleavage/early LPS to the north. During inversion a shortcut in the footwall developed and rotated the unit to the north of the CF, now defined as ‘The Transition Zone’ resulting in passively rotated weak cleavage/early LPS. The CF is thus considered both a basin margin structure and a northern tectonic boundary to the Variscan front.

Acknowledgements

I would like to thank all of the Geology Department at UCC. I would like to thank my research supervisors, Dr. Pat Meere and Dr. Carl Stevenson. Dr. Pat Meere provided excellent supervision and showed continued enthusiasm and support throughout the entire project. Dr. Carl Stevenson assisted with the AMS analysis and provided very valuable discussions and feedback. Many thanks to Dr. Kieran Mulchrone and to Dr. Dave McCarthy for their assistance with the strain analysis. Dr. Dave McCarthy also gave very helpful discussions on the Munster Basin. I would like to thank Dr. Mark Cooper for discussions and his structural expertise. Thanks to the technicians at UCC for assistance with rock samples and thin section preparation. I also want to thank the administration staff at UCC, for prompt and helpful assistance with various queries.

Also thanks to my family in Ireland and friends in England, Scotland and Ireland for their support and interest along the way.

Thanks to Nick Schofield, who offered both practical and academic advice, as well as support and encouragement in the finishing of the thesis. Jericho Schofield is thanked for being Jericho!

As addendum, I would like to thank Dr. John Reavy and Dr. Robin Shail for their help and encouragement in completing the final version of this thesis.

This project has received funding from IRCSET under the EMBARK initiative.

Chapter 1:
Introduction.

Chapter 1: Introduction

1.1 Generic Basin Inversion Processes

Some of the main foundations of basin inversion mechanisms have been established by authors such as Cooper and Williams (1989), McClay (1989), Williams et al. (1989) and McClay and Buchanan (1992). Tectonic inversion has been defined as ‘conversion of a basin area into a structural high’’ by Glennie and Boegner (1981). Inversion can be both positive where there is uplift or negative where there is subsidence depending on the history of the basin (Glennie and Boegner, 1981). Tectonic inversion features are commonly found in synrift sedimentary basins where the sequence has been extruded from the basin during compression (Cooper et al., 1989). Where there is a notable stratigraphic thickness increase in the hangingwall, this is indicative of synrift sediments (Fig 1.1; Williams et al, 1989). Thickening of sediments close to a basin margin indicates that an extensional fault was active during sedimentation (Hamblin, 1965; Gibbs, 1984). A role-over anticline may also develop in the hanging wall where an extensional fault is active during sedimentation (Fig 1.1 a; Hamblin, 1965; Gibbs, 1984). During inversion there may be negative extension at depth and net contraction higher up in the sequence (Fig 1.1b; Williams et al., 1989).

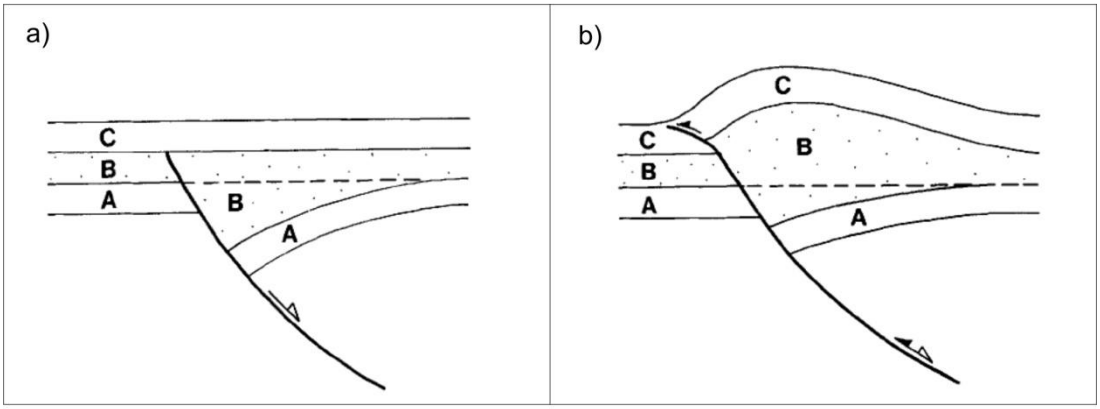

Figure 1.1 a) shows thickening of synrift sediments close to an extensional basin margin fault. b) Inversion may result in negative extension at depth and contraction higher up - from Williams et al. (1989).

The geometries of the reactivated structures in areas of inversion are closely related to the geometry of the initial extensional basin (e.g. McClay and Buchanan, 1992). Thrust faulting in inverted extensional basins is more complicated than thrust faulting in foreland fold and thrust belts due to the pre-existing extensional architecture of the basin (McClay and Buchanan, 1992). McClay and Buchanan (1992) provide a detailed discussion on thrusting in inverted extensional basins based on the interpretation of

sandbox analogue experiments and natural examples (e.g. the Benton Fault system, South Wales, Powell, 1989) and present a sequence of models ranging from the development of an extensional half graben with a role-over anticline through to inversion with a footwall shortcut (Fig 1.2). Based on these conceptual models (McClay and Buchanan, 1992) demonstrate how complex thrust faulting in inverted extensional basin can prove to be.

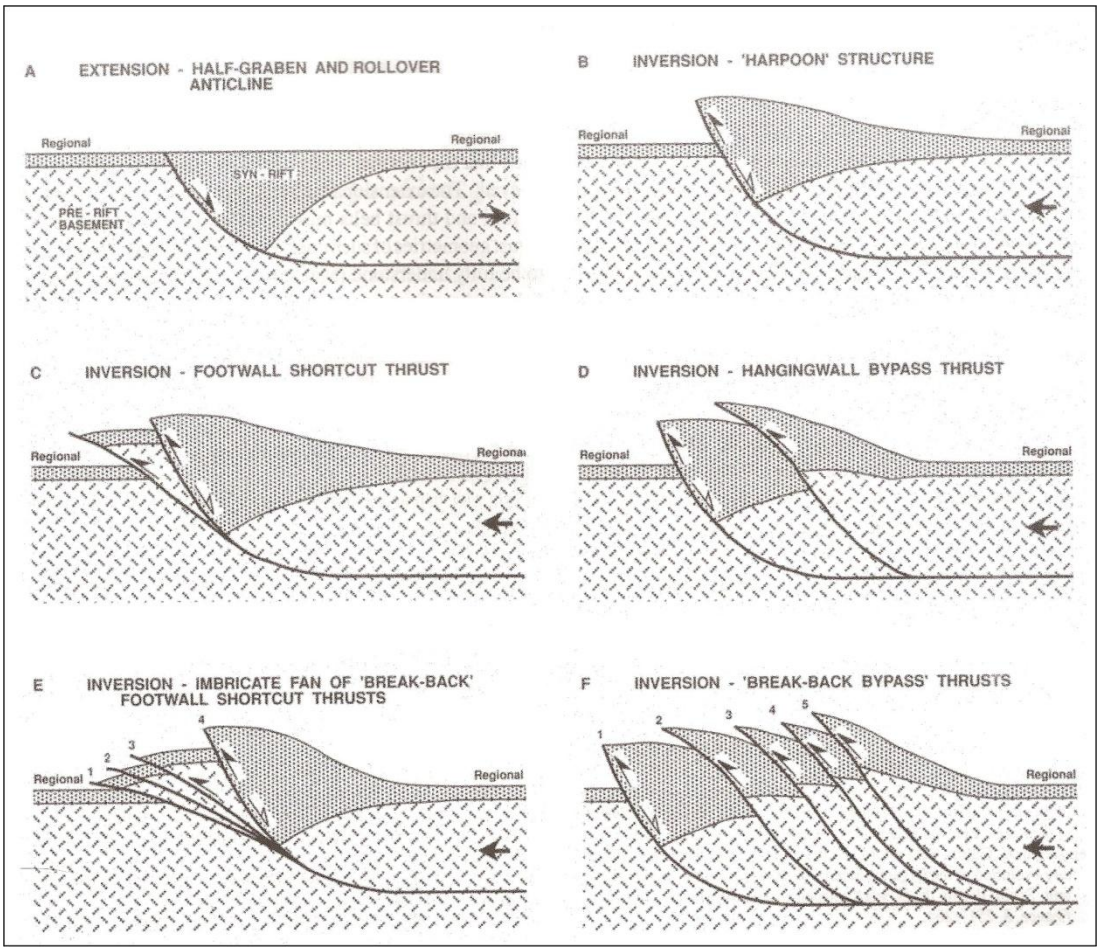

Figure 1.2 A sample of schematic models based on the interpretation of sandbox analogue experiments and natural examples [(e.g. the Benton Fault System, Powell, (1989)] by McClay and Buchanan (1992).

A number of possibilities as to how deformation may be expressed at a basin margin fault during inversion of a half graben are presented by Cooper et al. (1989). One of these is where there is the development of a footwall shortcut, which occurs when there are steeply dipping reactivated extensional faults at the margin (Fig 1.3; Cooper et al., 1989). A footwall shortcut is shallower than the main reactivated basin margin fault and is more efficient in the take up of shortening during compression (e.g. Knipe, 1985; Cooper et al., 1989). Footwall shortcut faults may have a sigmoidal geometry (Fig 1.2 & 1.3; McClay and Buchanan, 1992). Footwall shortcut faults have been documented in

a number of studies as a mechanism for inversion at basement margin faults (e.g. Powell, 1989; Giambiagi, 2009).

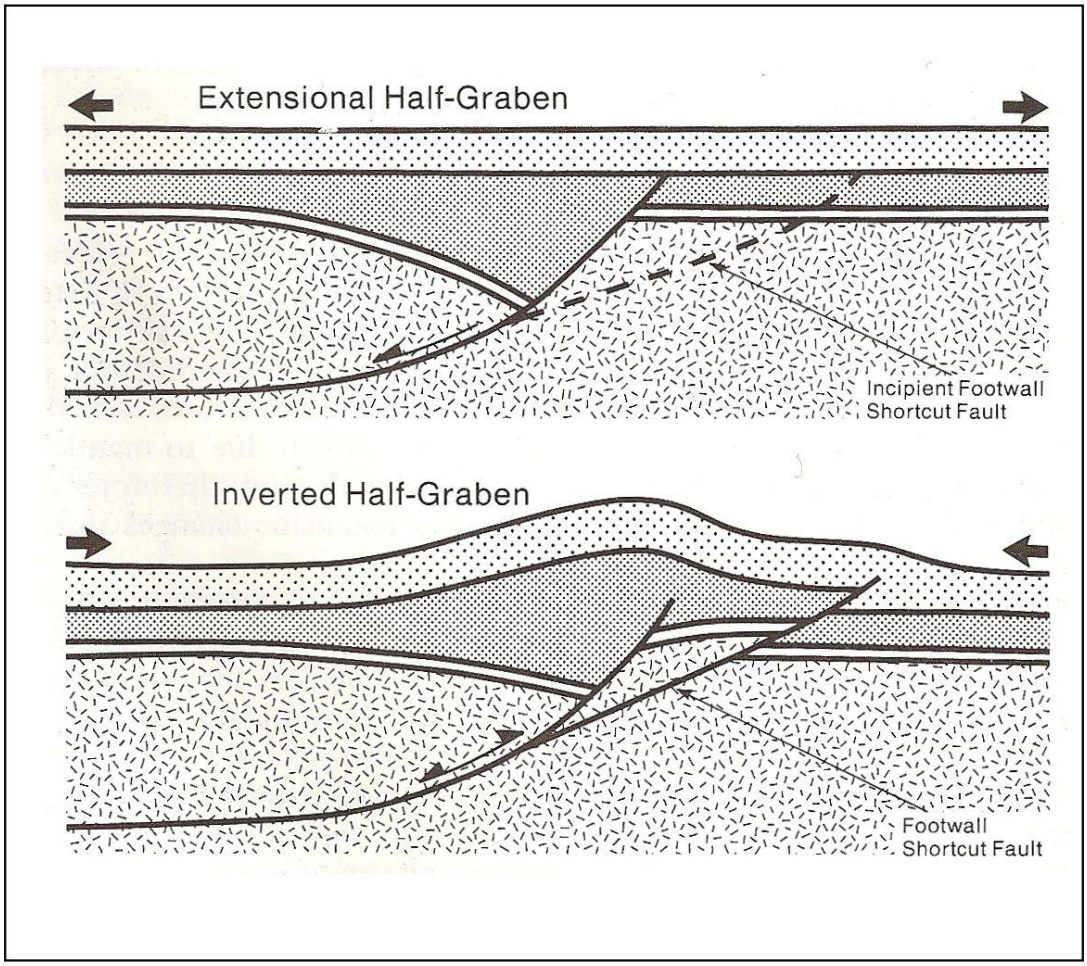

Figure 1.3 shows the development of a footwall shortcut during inversion. From Cooper et al. (1989).

A second mechanism involving basement buttressing (Fig 1.4; Cooper and Williams, 1989) has been previously documented as an important process in a number of studies (e.g. Butler, 1989, 1997; Bailey, 2002). Rigid basement blocks have an important influence on the mechanism of inversion (e.g. Butler, 1989; Hayward and Graham, 1989) and the rheological contrast between basement and cover rocks has been well recognised (e.g. Ramsay, 1982). As a result of basement buttressing, significant deformation and internal folding is found in close proximity to the footwall (e.g. de Graciansky et al., 1989) with a small amount of overspill of the synrift fill (Fig 1.4; Cooper et al., 1989). Consideration of all of the above processes is key to the understanding of the mechanisms involved in both the development and subsequent deformation of the northern margin of the Munster Basin - the focus of this study.

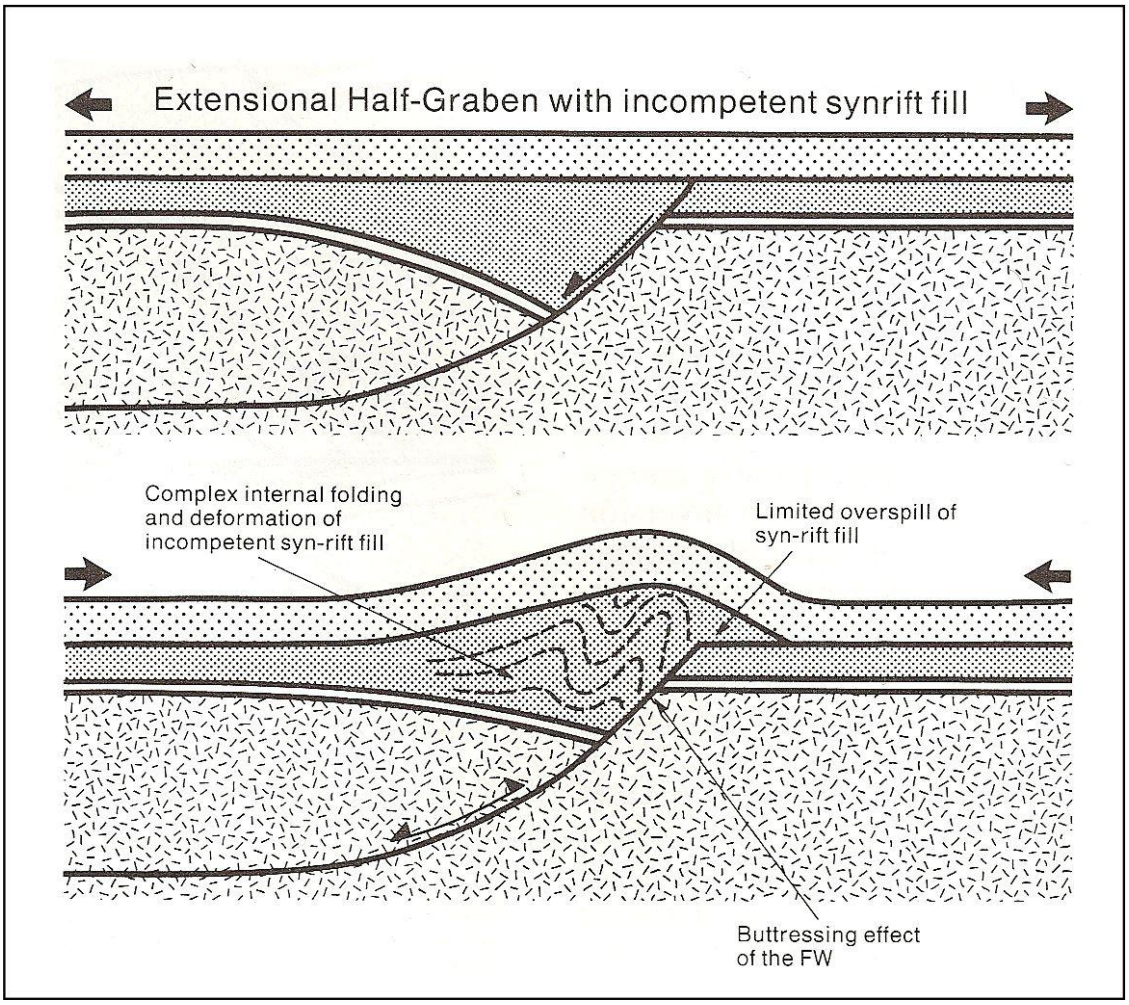

Figure 1.4 Shows the affect of rigid basement buttressing on syn- rift fill from Cooper et al. (1989).

1.2 Rationale

There have been a number of suggestions for the location of the northern margin of the Munster Basin. The northern margin of the Munster Basin has traditionally been placed at the Dingle Dungarvan Line (DDL) or alternatively at the Dingle Bay Galtee Fault Zone (DBGFZ). There has been much ambiguity concerning the precise location of the northern margin of the Munster Basin. A number of recent studies have indicated that the DBGFZ is not likely to be the northern margin. Price and Todd (1988) and Meere (1997) suggest that the Kilarney Mallow Fault Zone (KMFZ), which lies further to the south, is instead the northern margin of the Munster Basin. Recent seismic studies have suggested that the DBGFZ line is in fact a northwards dipping structure that instead bounds the Dingle Basin to the North (e.g. Vermeulen, 1988; Landes, 2000). This study focuses on the Coomnacronia Fault as a potential northern margin to the Munster Basin. The Coomnacronia Fault is a large map scale fault which lies laterally to the west of the Kilarney Mallow Fault Zone. There have been previous suggestions that there is significant southward sedimentary thickening across the Coomnacronia Fault (Williams,

2000) indicating its potential to be a basin margin fault. The hypothesis of this study is that if the Coomnacronia Fault is the basin margin fault then there may be a significant difference in structural deformation styles from the south of the fault to the north of the fault. This study investigates the effect of the Coomnacronia Fault on cleavage and strain regimes in order to assess the role of the Coomnacronia Fault as a potential basin margin fault.

1.3 Study Area

The study area lies in south west Ireland predominantly on the Iveragh Peninsula, but also on the Dingle Peninsula and Kerry Head, Co. Kerry (Fig 1.5). The study is carried out on Middle to Upper ORS that has undergone Variscan deformation at the end of the Carboniferous. The underlying basement has undergone both Caledonian and Acadian deformation. Chapter 2 details the Geological history of the area and the current understandings of the location of the northern margin of the Munster Basin. Chapter 4 outlines the location of the study area.

1.4 Methodology

This regional study incorporates field work, AMS studies, strain analysis and microstructural studies. A preliminary field study of the area was carried out in order to get a general sense of the effect of the Coomnacronia Fault on the cleavage. A number of key sites have been identified that characterise structural styles in relation to cleavage development. AMS has been previously shown in many studies (Chapter 3) to be a very valuable tool in assessing the evolution of sedimentary fabrics to tectonic fabrics, especially in sandstones. It is a rapid and well documented method and has been used in this study as an indicator of the variations in strain. The methodology for AMS is discussed in Chapter 3: Principles of AMS and Chapter 5: AMS Results. A number of the AMS samples were also analysed using variation of magnetic susceptibility with temperature in order to look at the minerals responsible for the magnetic susceptibility. Strain analysis using the Mean Radial Length (MRL) and the Delaunay Triangulation Nearest Neighbour Method (DTTNM) which are both from Mulchrone et al. (2013), was carried out in order to assess the impact of the Coomnacronia Fault on the strain regime. The strain analysis has been carried out on the same hand samples as the AMS in order to compare/integrate the results from the two methods. Microstructural studies were also carried out on samples to the south and north of the Coomnacronia Fault.

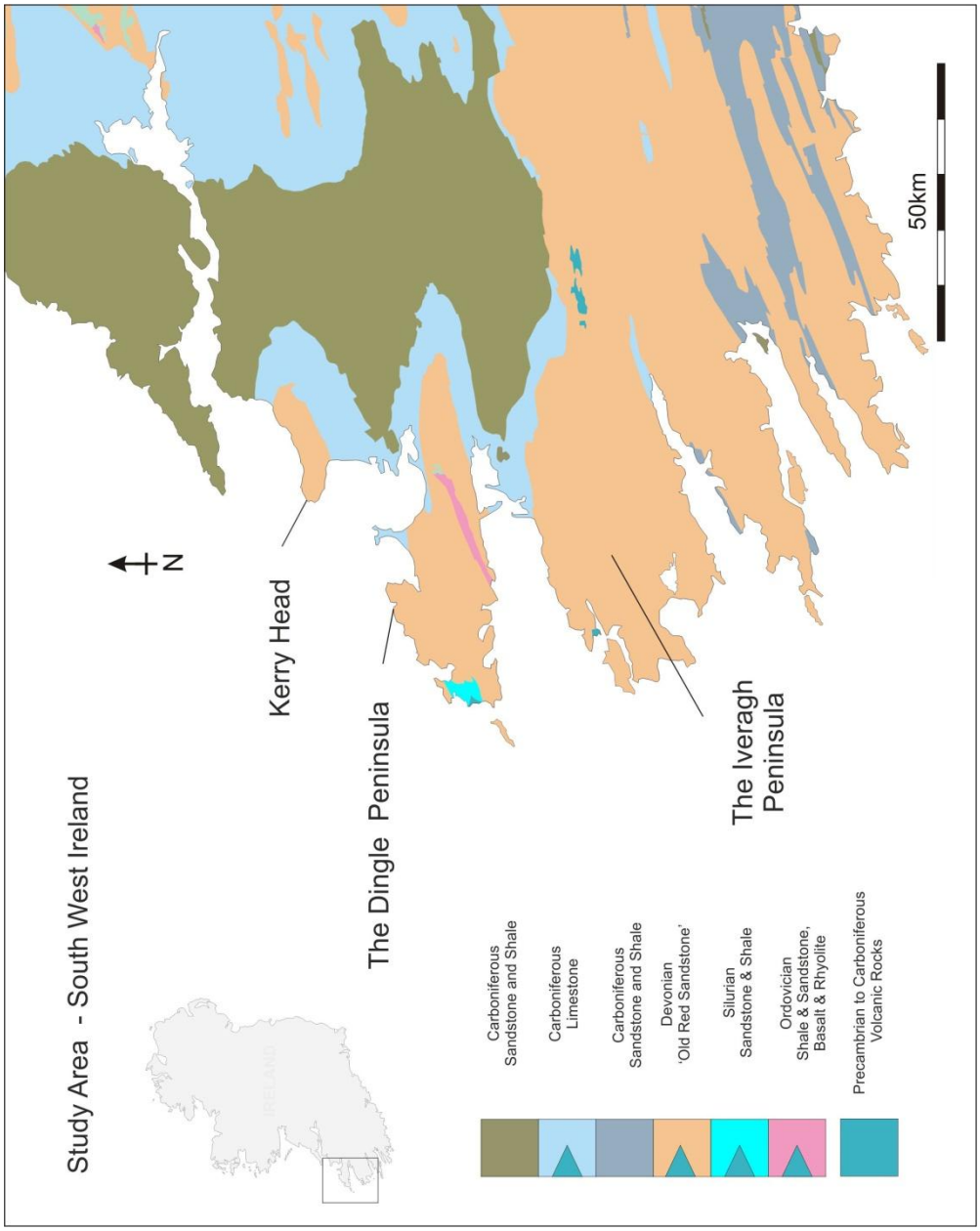

Figure 1.5 shows the location of the study area and the general geological setting of the area (modified from Sleeman et al., 2004)

1.5 Structure of Thesis (Fig 1.6)

Chapter 2: Geological Setting

This chapter gives a brief overview of basin inversion mechanisms and the geological history of the study area. This chapter discusses previous theories on the location of the Munster Basin's northern margin.

Chapter 3: **Principles of AMS**

This chapter discusses the background principles of AMS and how this technique has been effectively applied in terrains similar to the study area.

Chapter 4: Field Work

This chapter investigates the location of the northern margin of the Munster Basin and presents the results from the fieldwork and the interpretation of these findings.

Chapter 5: AMS Results

This chapter presents the results and interpretation of the Anisotropy of Magnetic Susceptibility analysis and thermomagnetic studies carried out in the area.

Chapter 6: Strain Analysis

This chapter presents the results for the strain analysis and compares the results from the strain analysis with microstructural observations in thin section.

Chapter 7: **Discussion**

This chapter brings together the findings for all of the previous chapters and also discusses some relevant further studies.

Chapter 8: Conclusions

Appendix: Contains all the detailed methodologies and field work data.

1.6 Map Inserts

There are four accompanying maps included in this study:

Map Insert 1: Cleavage Results.

Map Insert 2: AMS Results.

Map Insert 3: Strain Analysis Results.

Map Insert 4: Summary of Tectonic Zones.

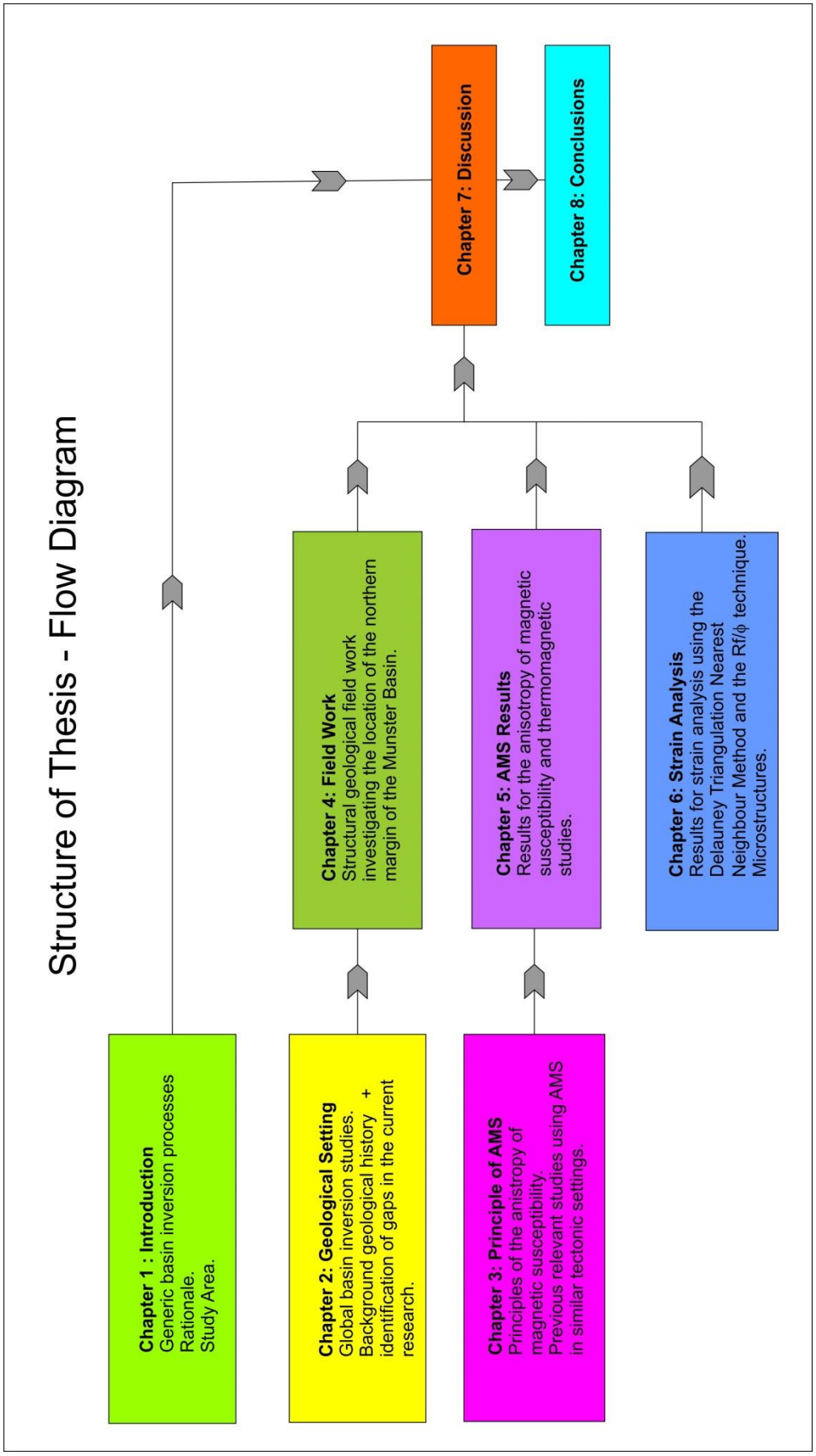

Figure 1.6 Structure of the Thesis

Chapter 2:
Geological Setting.

Chapter 2: Geological Setting

2.1 Part One: Global Inversion Tectonics

Inversion of basins has been recognised as far back as Lamplugh (1920) and Stille (1924). Many of the foundations of basin inversion techniques were established in the late 80's to early 90's e.g. Cooper and Williams (1989), Williams et al. (1989) and McClay and Buchanan (1992), (Section 1.1). Tectonic inversion has been recognized in areas such as the Canadian Cordillera (McClay et al., 1989), the Alps (e.g. Butler, 1989) and the Pyrenees (Todd and Turner, 1989 in Cooper et al., 1989). The term 'inversion' has been suggested by Ziegler (1989) to be used in intra-plate settings where basins developed upon tensional regimes and have subsequently undergone compression/transpression. In terms of deformation intensity, there have been previous debates as to when the term inversion should be used (Ziegler, 1989) and many petroleum geologists in the late 80's argued that inversion not be used in high deformation zones such as the Alps, however Ziegler (1989) discussed the importance of mild inversion that has been subsequently overprinted in high deformation zones. Todd & Turner (1989, in Cooper et al., 1989) suggest that inversion be defined as when a basin transitions from 'net subsidence' and deposition to 'uplift and net erosion'. The timing of inversion can also be diachronous as discussed by Todd and Turner (1989) such as that in the Pyrenean Foreland Basin system. This study is located in an area where Variscan inversion has occurred, an orogeny that is both extensive and highly variable and ranges from Central Europe through the British Isles to North Africa and North America (e.g. Hutton and Sanderson, 1984). Due to the changing nature of the Variscan from granite dominated and high metamorphic zones in Europe to 'Barrovian'metamorphics, with westerly directed thrust sheets in North America, tracing the Variscan across strike has proved to be challenging (e.g. Hutton and Sanderson, 1984). Even within the British Isle's there have been many studies on Variscan inversion tectonics and debates as to the styles of inversion (Section 2.12). South west Ireland and Britain lie in the Rhenohercynian Zone of the Variscan Fold Belt , a zone which has been described as extremely complex due to the nature of the pre-exising Avalonian Terrane, its transpressive regime, and there having been numerous phases of Variscan folding and thrusting (Warr, 2009).

Part Two: Regional Geological Setting

2.2 General Geology and Regional Setting of Southwest Ireland

The geological history of southwest Ireland discussed in this chapter ranges from the Middle Ordovician to Upper Carboniferous and includes the Caledonian, Acadian and Variscan orogenies (Fig 2.1 & 2.2). Old Red Sandstone (ORS) in southwest Ireland is found in Kerry Head, the Dingle Basin, and the Munster Basin (Fig 2.1). The Dingle Basin ranges from the Ordovician to the Upper Devonian (Fig 2.1 & 2.2; Pracht, 1996). The Dingle Basin has been deformed by both the Acadian and the Variscan Orogenies. The Munster Basin and the South Munster Basin (SMB) developed subsequent to the Acadian Orogeny and were both deformed by the Variscan Orogeny which occurred at the end of the Carboniferous. The Munster Basin consists of Middle to Upper Devonian ORS (e.g. MacCarthy, 1990; Pracht, 1996; Bresser and Walter, 1999) and is the main focus of this study. The basement rocks of Ireland consist of two main terrains separated by the Iapetus Suture (Fig 2.3, 2.4); one to the northwest (Laurentian Terrane) which is composed of Grenvillian and Late Proterozoic (Dalradian) rocks (Max and Long, 1985; Woodcock and Strachan, 2012) and one to the south east (Eastern Avalonia), composed of Late Neoproterozoic rocks (e.g. Max and Long, 1985).

2.3 The Caledonian Orogeny

The Caledonian Orogeny occurred as a result of the closure of the Iapetus Ocean, which involved the sinistral oblique docking of Eastern Avalonia from the south east with Laurentia in the northwest and occurred during the Middle Ordovician and Silurian (Fig 2.4; e.g. Soper and Woodcock, 1990; Chew and Stillman, 2009). The Iapetus Ocean had completed closure by the Upper Silurian (e.g. Pickering, 2008). Rocks that were deformed in the Caledonian Orogeny in Ireland have SW-NE orientated structures (e.g. Ryan and Dewey, 1991) and this SW-NE pattern is observed in both the upper crust (e.g. Woodcock and Strachan, 2000) and the lower crust, by seismic studies (Polat et al., 2012). In south east Ireland, there is a large NNE trending granite body, the Leinster Granite, which lies to the east of the Munster Basin (Fig 2.4 b) which is dated at 404 ± 24 Ma based on Rb-Sr isochron age (O' Connor and Bruck, 1978). Rocks that were deformed during the Caledonian Orogeny in southern Ireland crop out in a small number of isolated areas. For example, the Middle to Upper Ordovician Volcanics exist in Co. Waterford, the Rosslare Migmatites in Co. Wexford which are 630 Ma (Max

Personal communication, cited by Naylor et al., 1983) and the Wenlock siltstone formation in the Silvermine Mountains (Naylor et al., 1983). Erosion of the Caledonian Mountain Belt is thought have provided the fill for the Munster Basin (e.g. Friend et al., 2000), however the recent study by Ennis et al. (2015) suggests that the provenance source is instead the later Lower Old Red Sandstone (LORS) that has been recycled from the Dingle Basin.

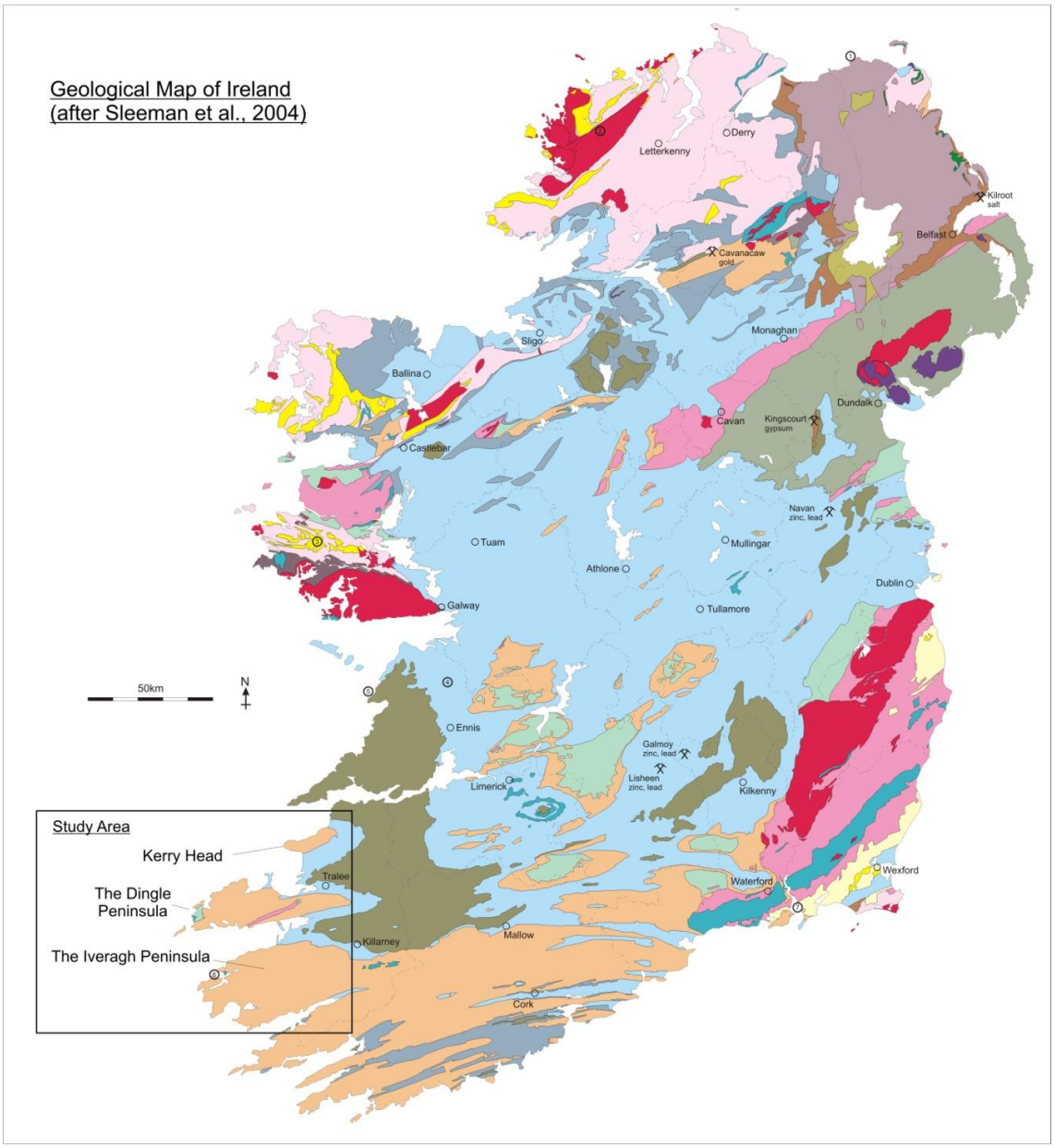

Figure 2.1 Geological Map of Ireland showing the study area in SW Ireland which is dominated by Devonian Old Red Sandstone. Modified from Sleeman et al. (2004), Scale = 1:1,000,000; Legend in Fig 2.2

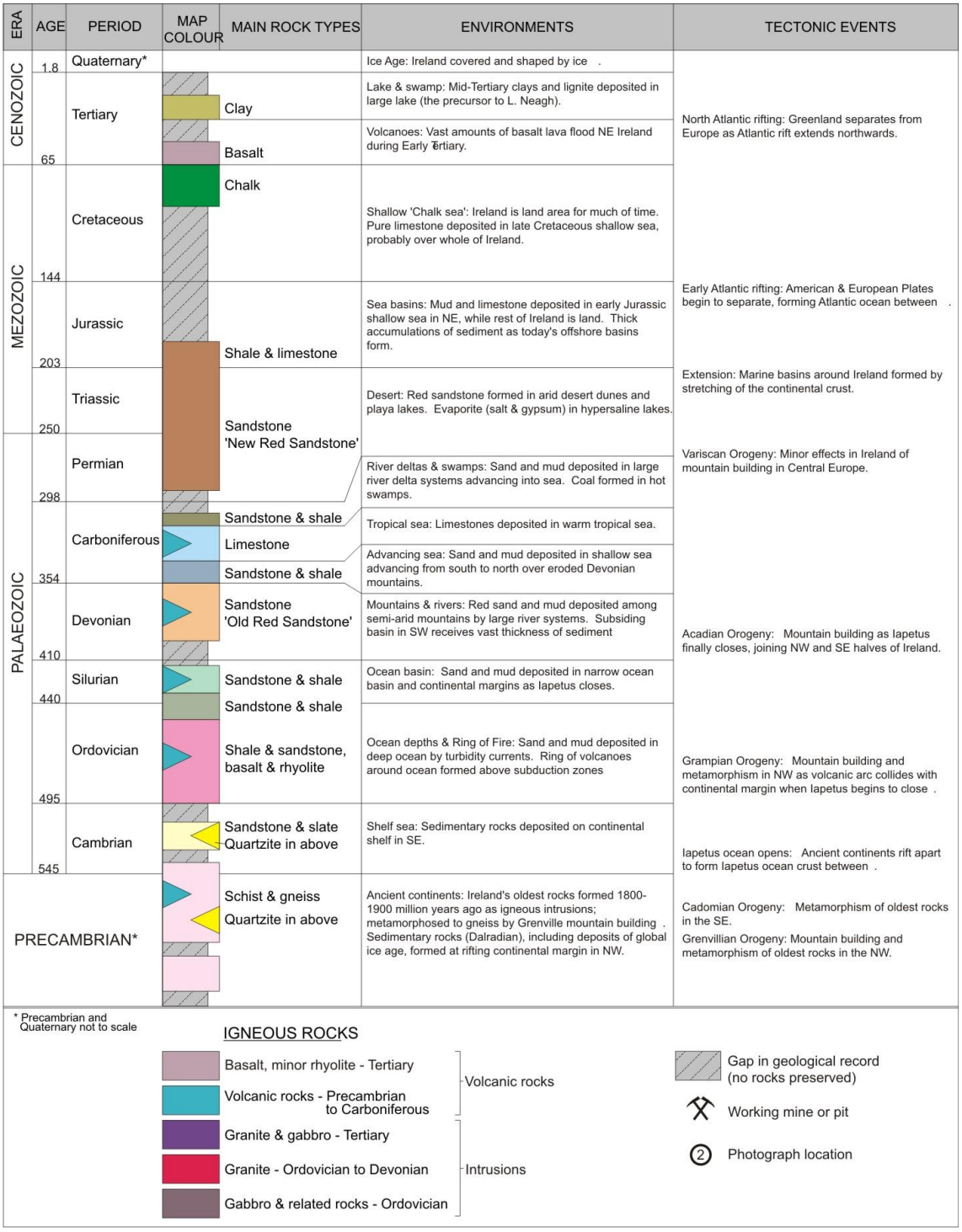

Figure 2.2 Legend for Fig 2.1 and geological timescale for main events in Ireland**.** from Sleeman et al. (2004).

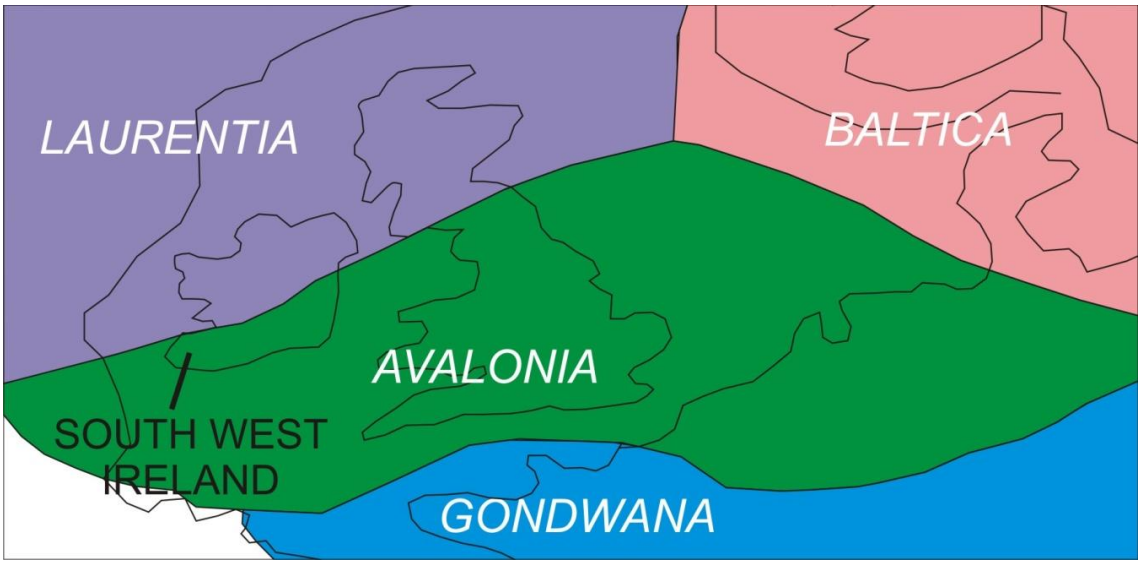

Figure 2.3 The present day geological terranes of Ireland and England. Modified from Stampfli et al. (2013) from Neftex Geodynamic Earth Model. © Neftex Petroleum Consultant.

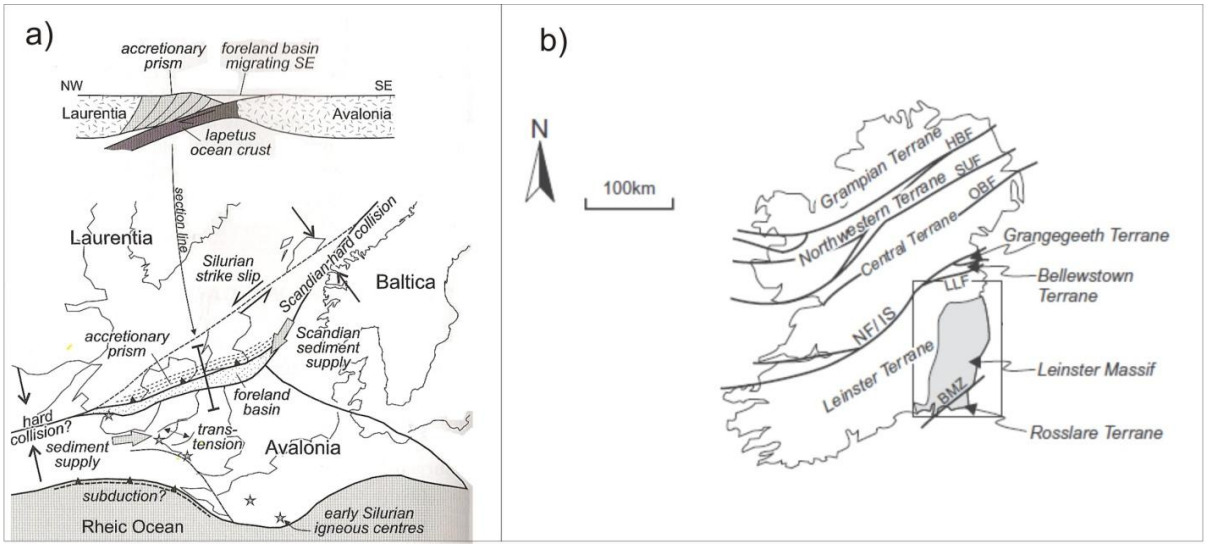

Figure 2.4 a) A cross section and a palaeogeographic map showing the closure of the Iapetus Ocean during the Lower to Middle Silurian (From Woodcock and Strachan, 2012) **b)** the Palaeozoic terrane map of Ireland showing the Iapetus Suture (IS) and Leinster terrane (modified from Clegg and Holdsworth, 2005, after Bluck et al., 1992). HBF = Highland Boundary Fault, SUF = Southern Uplands Fault, OBF = Orlock Bridge Fault, NF/IS = Navan, Fault/Iapetus Suture, LLF = Lowther Lodfe Fault, BMZ = Ballycogly Mylonite Zone.

2.4 Lower to Middle Devonian Sedimentation

After the closure of the Iapetus Ocean, Lower Devonian sediments were deposited in sinistral transtensional basins on Avalonian crust, prior to the onset of Acadian deformation (Woodcock and Strachan, 2012). In Britain and Ireland most of the Lower Devonian ORS was non marine (Woodcock and Strachan, 2012). Fluvial derived ORS in South West England extends as far south as the Looe Basin, which consists of Lower Devonian marine and continental ORS (e.g. Leveridge and Shail, 2011). In South West Ireland, Lower ORS is deposited in the Dingle Basin (Section 2.27; Pracht, 1996).

2.5 The Acadian Orogeny (Pre-Variscan: 385 – 400 Ma)

The Acadian Orogeny was a short lived deformation event that involved low grade regional metamorphism (e.g. Soper and Woodcock, 2003) and was responsible for slate belts in Southern Ireland, England and Wales (Fig 2.5; Soper and Woodcock, 2003; Woodcock and Strachan, 2012). During Acadian deformation, folding, cleavage and shear zones occurred at anchizone and epizone metamorphic grades (Woodcock and Strachan, 2012). The Acadian Orogeny took place in the Lower to Mid-Devonian (385-400 Ma; McKerrow, 1988). Subsequent studies using ^{40}Ar -^{39}Ar to date synkinematic micas from strain shadows of pyritized graptolites from the Welsh Basin dates the cleavage event of the Acadian Orogeny at 394 ± 3.1 to 397 ± 1.8 Ma (Sherlock et al., 2003). Although the Acadian event was previously thought to have involved the final closure of the Iapetus Ocean, Woodcock et al. (2007) suggest that Acadian deformation occurred 20 Ma after the final closure of the Iapetus Ocean and instead may be related to the early closure (Nance et al., 2010) or subduction (Murphy et al., 2004) of the Rheic Ocean which lay further to the south. Alternatively the Acadian deformation event may have involved collision of an oceanic plateau or microcontinent (Nance et al., 2010), by the northward convergence of Armorica with Eastern Avalonia (Fig 2.6; Soper and Woodcock, 2003) or by the collision of Armorica with Laurussia at the end of the early Devonian (Woodcock and Strachan, 2012). The Acadian event in Ireland affected all of Southwest Ireland but is only preserved in the Dingle Peninsula (Fig 2.5), where it is responsible for the main penetrative cleavage event (Meere and Mulchrone, 2006). The Acadian deformation event in Ireland possibly extends south of the Variscan front beneath Southern Ireland (Woodcock and Strachan, 2012). The Avalonian Terrane, which is affected by both the Caledonian and the Acadian orogenic events, forms the basement for the Munster Basin and the later SMB, both of which developed

in an extensional regime (Friend, 2000) and were subsequently deformed during the Variscan Orogeny (e.g. Pracht, 1996).

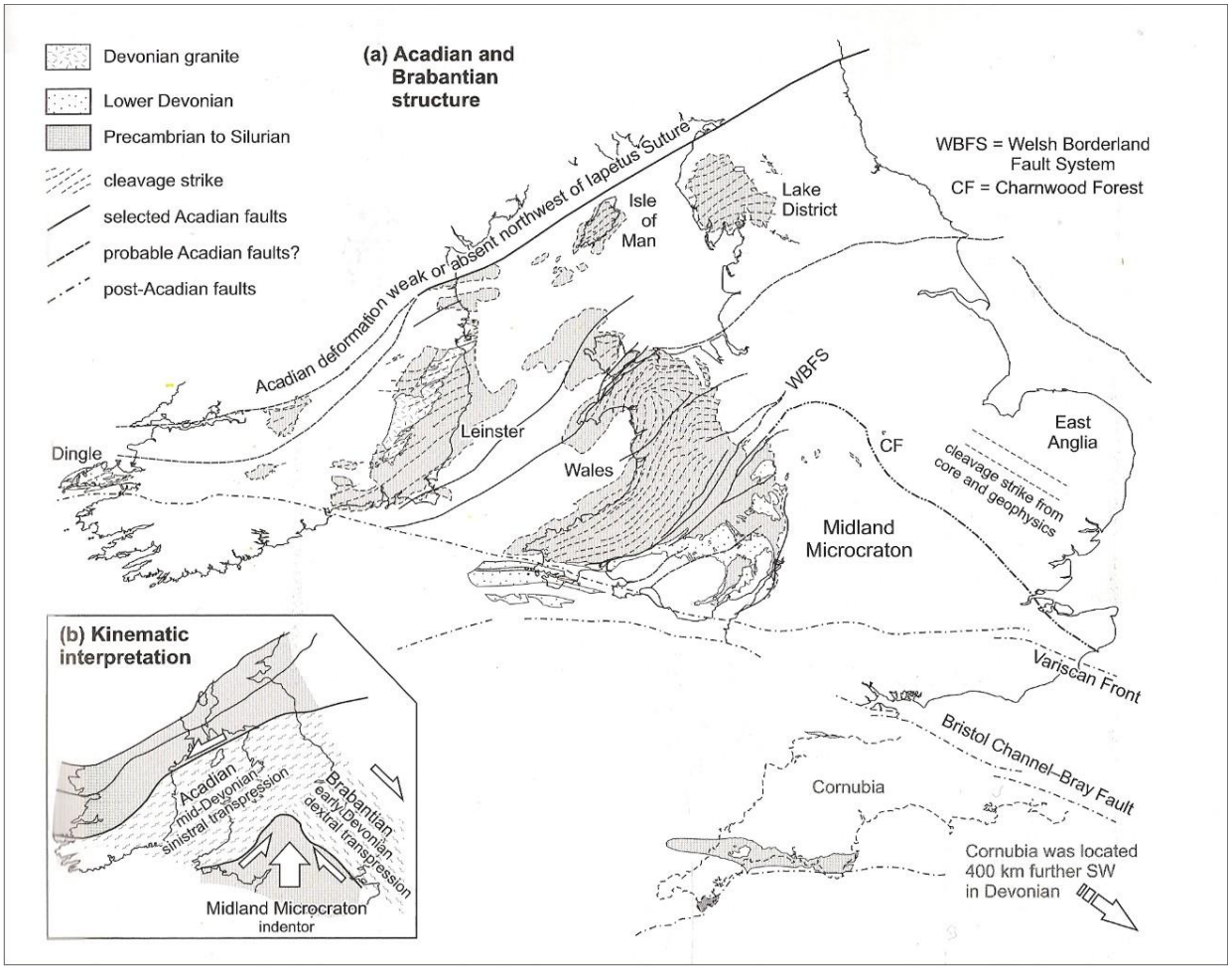

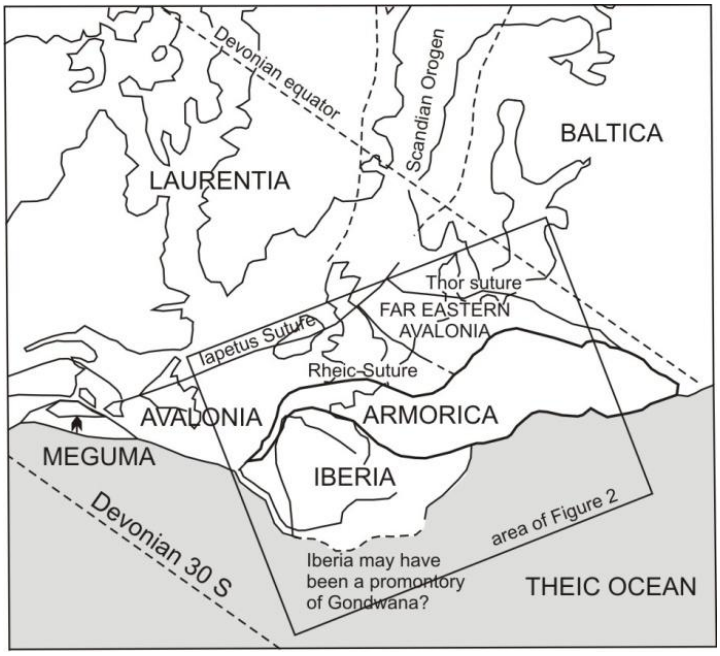

Figure 2.5 Above Acadian structures in the British Isles. The Acadian event affects the Lower ORS of the Dingle Basin but not the Munster Basin. From Woodcock and Strachan (2012). **Figure 2.6 Left** Shows the location of Laurentia, Baltica, Avalonia and Armorica during the Middle Devonian. One explanation for the Acadian event may have been the amalgamation of Armorica and Iberia with Avalonia by the closure of the Rheic Ocean. Redrawn from Woodock et al. (2007) - Modified from the timetrek reconstructions (Smith and Rush, 2006).

2.6 Middle to Upper Devonian Sedimentation

Crustal extension resulting in the development of the Munster Basin initiated in the Frasnian and resulted in the fluvial deposition of Upper Devonian non marine sediments (Woodcock and Strachan, 2012). During the Upper Devonian most of Britain and Ireland were dominated by ORS while to the south, the Rheic Ocean still remained open evidence for which lies in the existence of marine deposition on the Cornubian Terrane (Fig 2.7; Woodcock and Strachan, 2012). Most of Southwest Ireland was covered with ORS in the Middle to Upper Devonian (Pracht, 1996). A marine transgression only occurred very late in the Devonian which was contemporaneous with the development of the SMB (Section 2.29; MacCarthy and Gardiner, 1987).

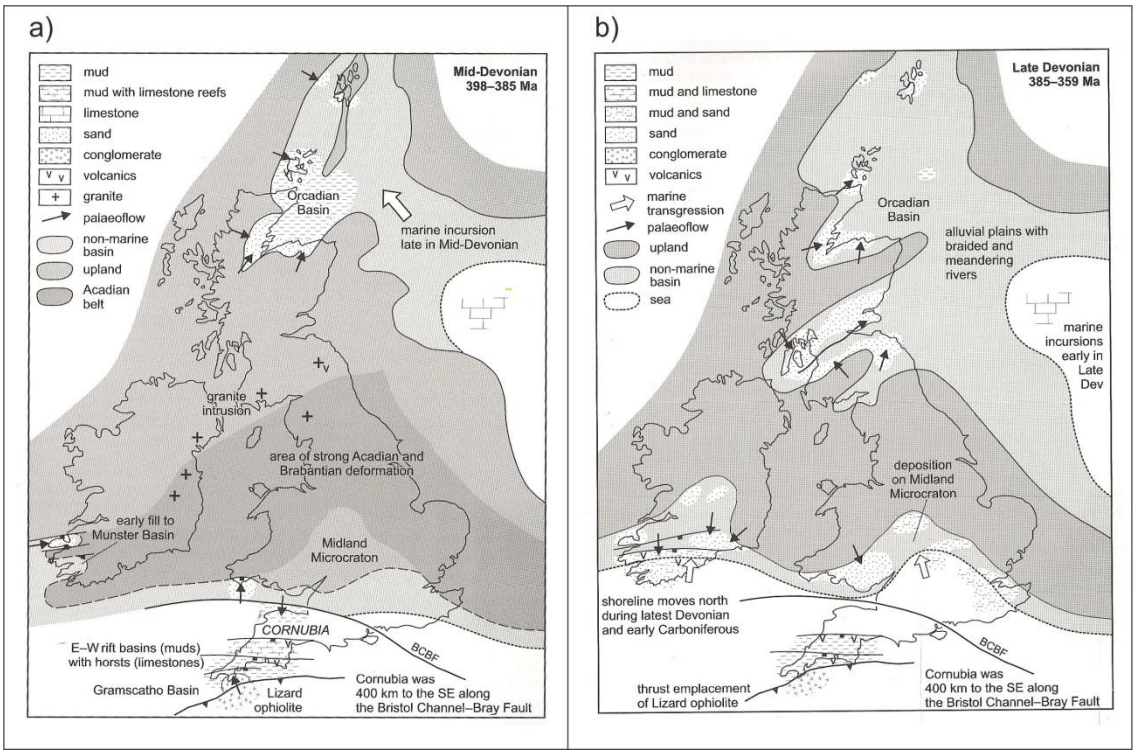

Figure 2.7 Shows a palaeogeographic map for a) the Middle Devonian. The early fill of the Munster Basin consisted of Middle Devonian non marine sediments and b) the Upper Devonian for Britain and Ireland. From Woodcock and Strachan (2012).

2.7 The Variscan Orogeny

The Variscan Orogeny covers an area 8000 km across and 1000 km wide (Franke, 2000; Matte, 2001) and affects North America and much of Europe including the Munster Basin of Southwest Ireland. In Europe, the Variscan Orogeny occurred during the Lower Devonian to Middle Carboniferous due to the collision of Laurussia, the

intervening microplates: Eastern Avalonia and Armorica, and the Gondwanan continent to the south (Fig 2.10; Matte 2001; Woodcock and Strachan, 2012). The Asturian Phase of Variscan Deformation occurred during the Westphalian to Stephanian (Warr, 2012) and was a result of the final amalgamation of Gondwana, Laurussia the intervening Gondwanan microplates to form Pangaea (Fig 2.10; Nance, 2010; Warr, 2012 in Woodcock and Strachan, 2012). The Variscan also involved the closure of two important oceans; The Rheic which existed between Eastern Avalonia and Armorica (Rey et al., 1997) and the Theic which existed between Armorica and Gondwana (Rey, 1997). The Variscan Orogeny lasted over 100 Myr (Warr, 2012 in Woodcock and Strachan, 2012) and in Europe began in the Devonian and was at its most intense at the end of the Carboniferous, and ceased by the Lower Permian (Warr, 2012 in Woodcock and Strachan, 2012). The curvature of the Variscan in Europe is mostly expressed in the Ibero-Armorican arc (Weil et al., 2001; Gutierrez-Alonso et al., 2004; Fig 2.8). The Variscan in Europe has been divided by Kossmat (1927) and Stille (1951) into a number of tectonic zones: including the Saxothuringian Zone, the Rhenohercynian Zone and the Mid German Crystalline Rise (Fig 2.8 & 2.9). The Rhenohercynian Zone occurs through Southern Ireland, Britain, Northern France, Belgium and central Germany (Autran et al., 1980) and is a low grade metamorphic zone ranging from the diagenetic facies (e.g. Warr, 2012) to the lower greenschist facies (Autran et al., 1980). In general, Devonian rocks have undergone a higher degree of metamorphism than the Carboniferous (Warr, 2012). Variscan deformation of the Munster Basin is comparable to that of the Gramscatho Basin (e.g. Shail, 1991), Looe Basin, Trevone Basin, South Devon and North Devon Basins where all of these basins underwent northwards directed deformation resulting in inversion in a dextral transpressive regime where deformation was greatly controlled by the geometry of the basins and pre-existing faults (Warr, 2012). Variscan deformation in Southern Ireland is somewhat comparable to that of Southern England which is considered to be a thin-skinned fold and thrust belt (Shackleton et al., 1982) with thrust movement to the northwest (e.g. Behr et al., 1980; Weber 1981; Leveridge and Hartley, 2006). North of the Rhenohercynian Zone is the Subvariscan Zone in which the intensity of Variscan deformation is greatly reduced and there is a stronger influence exerted by the underlying pre-Variscan structures (Warr, 2012). In the Sub-Variscan zone of Ireland, Variscan deformation consists of gentle folding and faulting controlled by the pre-existing Caledonian and Acadian structural trends (Warr, 2012).

2.8 The Variscan Front

The concept of a Variscan orogenic front dates back as far as Suess (1886) and Gosselet (1888). Dunning (1966, 1980) refers to the Variscan front as a line running through Britain and Ireland. The Variscan front may be considered as the northern margin of the Rhenohercynian Zone (Read and Watson, 1975). Sanderson (1984) considered the Variscan front at the northern margin to consist of extensional and compressional events within a dextral transpressive regime. In the west of Europe dextral strike-slip plate tectonics are thought to be a result of the oblique collision of the European and African Plates (Sanderson, 1984; Badham and Halls, 1975; Badhams, 1982). Figures 2.8 and 2.9 shows two possible locations for the Varsican front as depicted by Woodcock and Strachan (2012) and Bresser and Walter (1999) respectively.

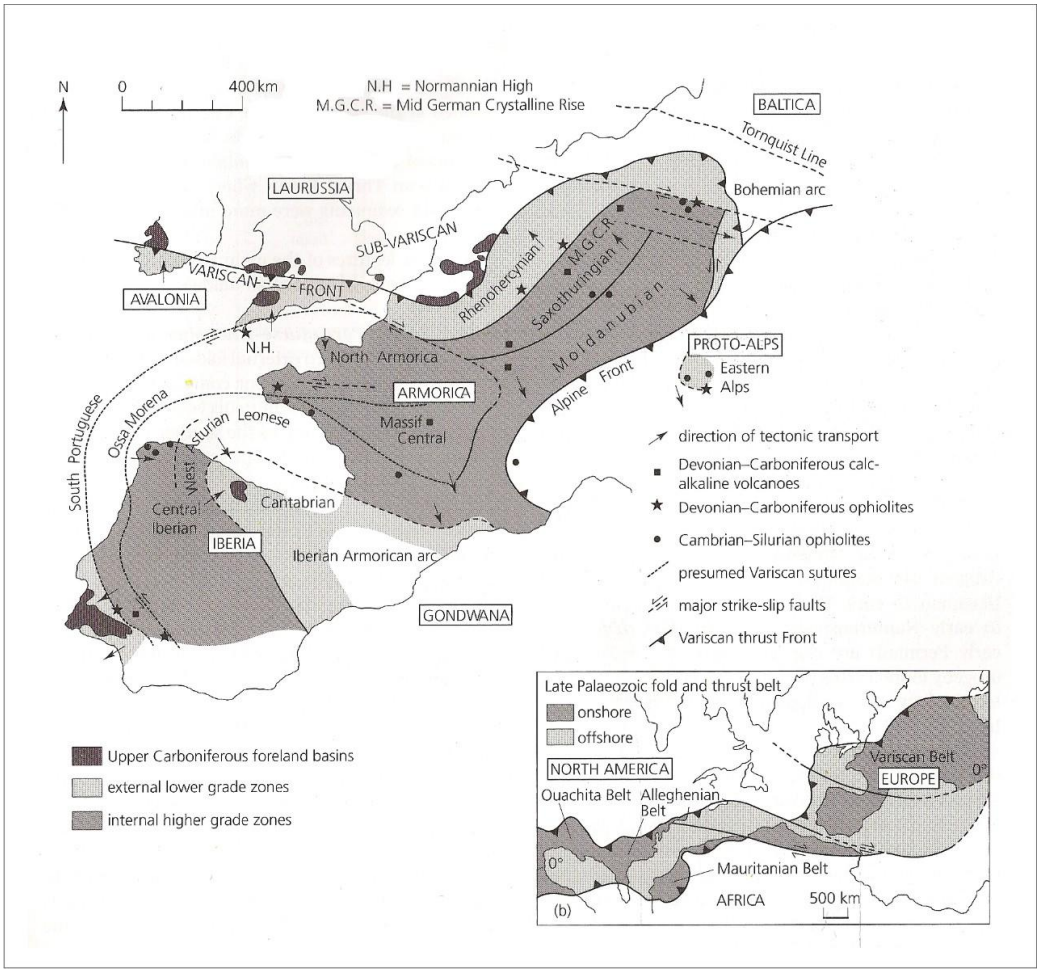

Figure 2.8 a) Variscan Terranes in Europe (with the removal of post Variscan Cover) modified after Franke (1989) from Woodcock and Strachan (2012). B) The Variscan Belt in Europe and its extension to the west to the Alleghenina and Ouachite Belt (after Ziegler, 1989 - with permission from Kluwer Academic Publishers (1999) from Woodcock and Strachan (2012).

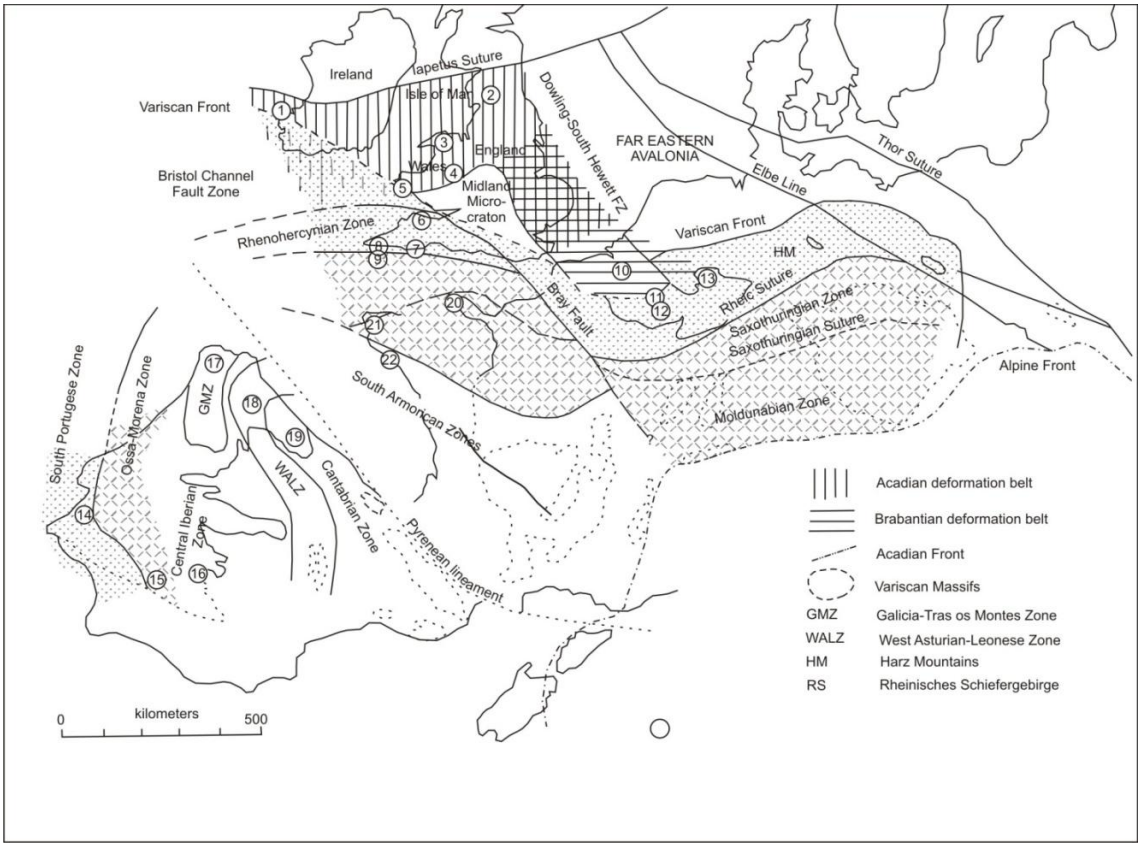

Figure 2.9 Shows the Variscan front in Ireland (Redrawn from Bresser and Walter, 1999; Modified after Rey et al., 1997).

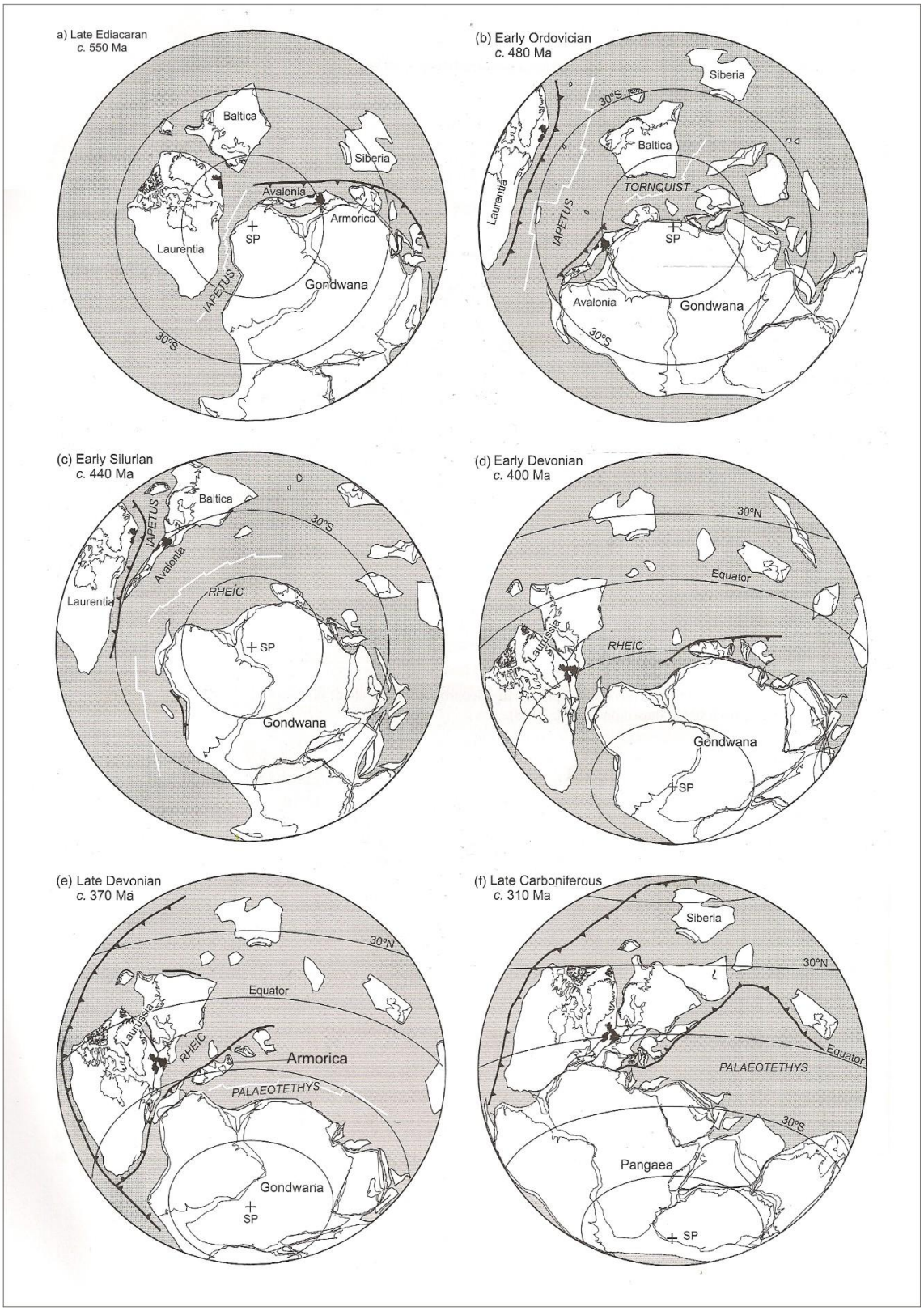

Figure 2.10 Palaeocontinental map from the Late Ediacaran to the Upper Carboniferous modified from Woodcock and Strachan (2012).

Part Three: Geology of South West Ireland - The Munster Basin

2.9 Initiation of The Munster Basin/Pre-Variscan

Extensional basins were widespread in Southern Ireland and Britain during the Upper Silurian-Early Devonian (Williams, 2000) and the Middle to Upper Devonian (Fig 2.11; Friend, 2000). The initiation of the Munster Basin occurred prior to around 385 Ma (Williams et al., 1989) in the late Givetian. Subsidence and development of the Munster Basin upon the pre-existing Avalonian Terrane, is thought to have occurred < 15 Ma subsequent to the Acadian deformation event (Williams et al., 2000). The buoyant terrain of the Leinster Granite inhibited subsidence of the basin to the east (Fig 2.1; Williams, 1989). Post-Caledonian granitic plutons may also lie in the basement beneath the Munster Basin (Howard, 1975; Avison, 1984; MacCarthy and Gardiner, 1987; Meere, 1995). Price (1988) suggests that the subsidence of the Munster Basin was brought about by heterogeneous lithospheric extension (Hellinger and Sclater, 1983; Coward 1986). Extension was brought about by a tensional stress normal to the basin axis (Jackson and McKenzie, 1983). This tension may have reactivated the south Ireland lineament, part of which developed into the Dingle Bay-Galtee Fault Zone (DBGFZ; Fig 2.12; McCarthy, 1990). The Caledonian framework that existed during the rifting stage of lithospheric extension influenced the morphology of the Munster Basin (Price and Todd, 1988). This extension was concentrated along pre-existing Caledonian faults such as the Dingle Bay Lineament (Price and Todd, 1988). The pre-deformational (pre-Variscan) geometry of the Munster Basin is generally considered to be a half-graben (e.g. Naylor and Jones, 1967; Williams et al., 1990; Sanderson 1984; Naylor et al., 1981, 1983; Graham, 1983; Price and Todd, 1988; Price 1989; Williams et al., 1989, 1993; MacCarthy, 1990.), with a NE-SW trend controlled by the Lower Palaeozoic basement (Gardiner and MacCarthy, 1981).

2.10 Sedimentation in the Munster Basin

The Munster Basin is considered to be a post-orogenic molasse type sedimentary basin (e.g. Capewell, 1975) and represents alluvial environments (Gardiner and MacCarthy, 1981; Graham, 1983). The fill of the Munster Basin consists mainly of non-marine Middle and Upper Devonian Old Red Sandstone (ORS) rocks (e.g. Naylor and Jones, 1967; Graham, 1983). The Upper Devonian sequence in the Munster Basin attains a maximum thickness of 6-7 km (Naylor and Jones, 1967; Graham, 1983). There is a

general fining up in the Munster Basin from coarse grained to fine grained to fluvial coastal facies (Graham, 1983, 2009). Sediment transport was from the northerly Laurentian uplands towards the southerly located Rheic Ocean (Fig 2.13; Meere et al., 2013). There is much variation in the thickness of the ORS in southwest Ireland (Fig 2.14, Graham, 1983; 2009). The ORS sequence thickens rapidly from the Dingle Peninsula to the Iveragh and Beara Peninsulas; 565 m of ORS exists in the Slieve Mish Anticline on the Dingle Peninsula (Capewell, 1965), 3850 m is found in the Macgillycuddy Reeks (Walsh, 1968) and 5200 m is found in Sneem (Capewell, 1957). The thickness of the ORS to the east of the basin is 688 m at Slievenamon, (Colthrust 1978); 1200 m at Portlaw (Keegan and Penney, 1978) and 3000 m at the Comeragh Mountains (Penney, 1978). The maximum subsidence of the Munster Basin is considered to have occurred close to the northern margin (Naylor and Jones, 1967; Russell, 1978). Average subsidence rates for the Munster Basin have been calculated at between 0.17-0.25 mm a^{-1} for east Iveragh and 0.18 mm a^{-1} for west Iveragh (Williams et al., 2000).

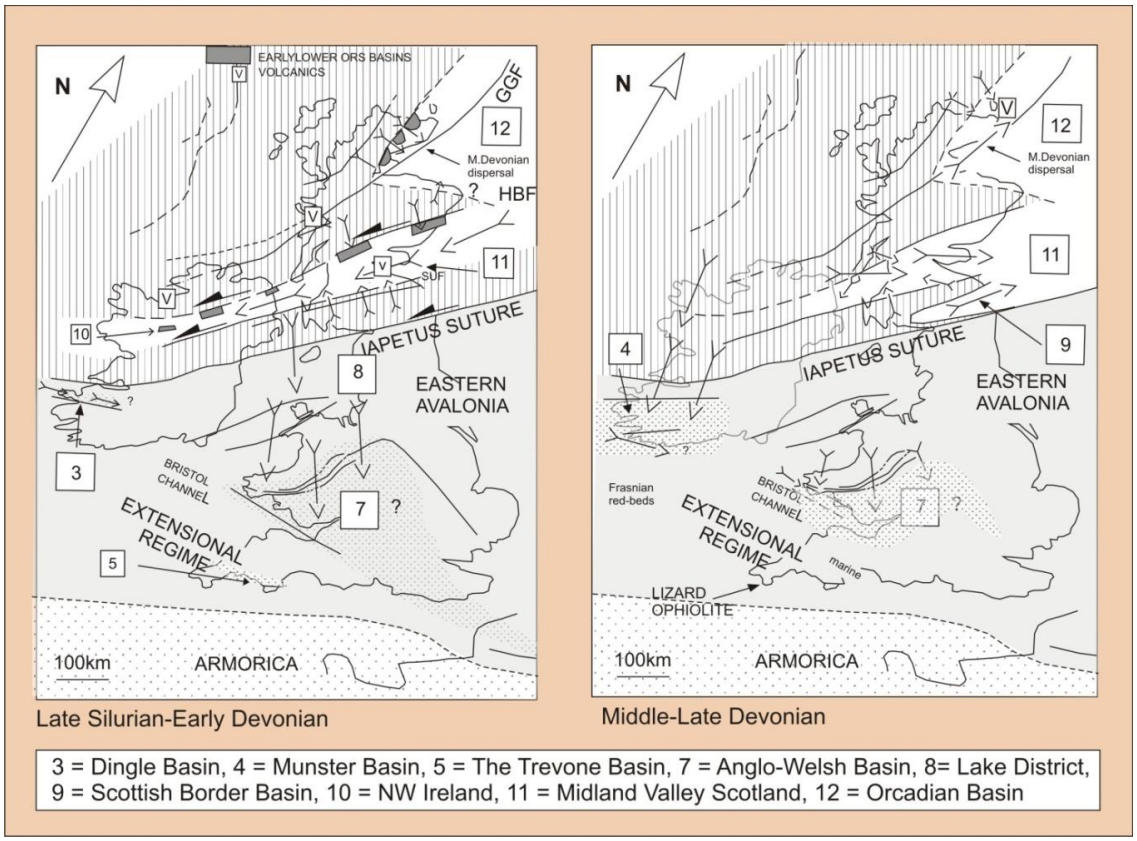

Figure 2.11 Shows the extensional setting of the Munster Basin and Dingle Basin and other contemporaneous basins upon Avalonian terrane in the Late Silurian-Early Devonian and Middle-Late Devonian. Redrawn/Modified from Friend (2000).

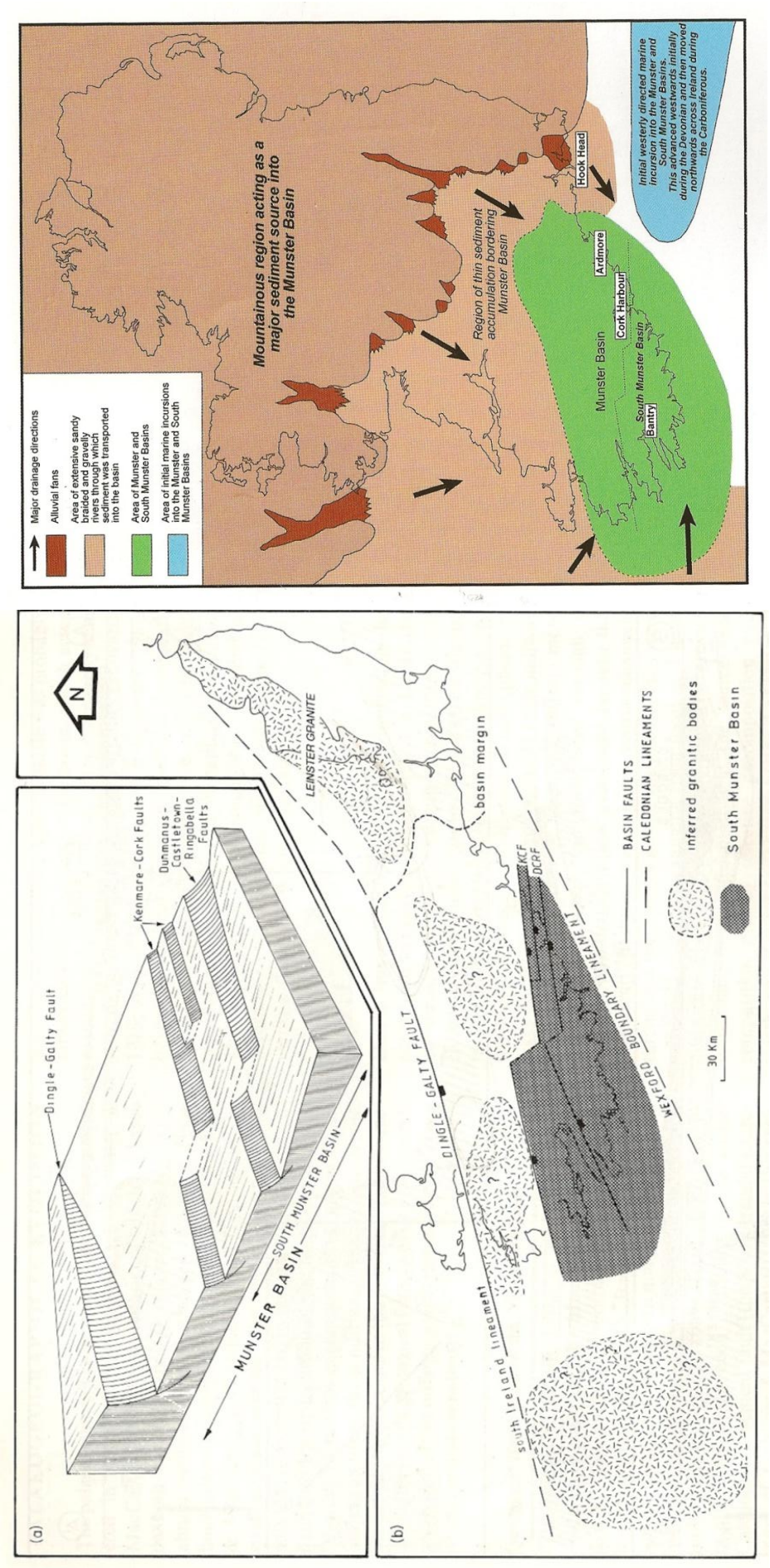

Figure 2.12 Above left a) shows the Munster Basin and south Munster Basin basement fault systems which controlled the sedimentation patterns. b) Shows the South Ireland Lineament and Leinster Granite to the east of the basin. (Macarthy, 1990). **Figure 2.13 Above right** Shows the sediment source to the north for the Munster Basin. From Meere et al. (2013).

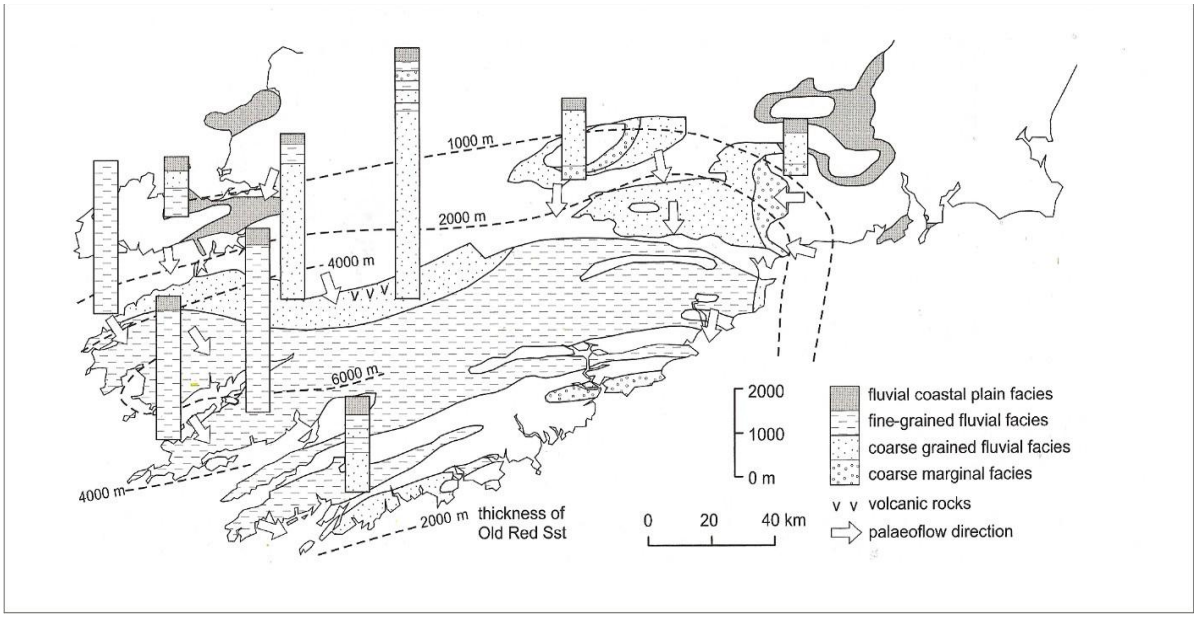

Figure 2.14 shows the thickness and distribution of sedimentary facies of Upper ORS in SW Ireland (from Woodcock and Strachan, 2012- compliled from maps by Graham, 1983 ; 2009).

The oldest known sedimentary rocks exposed in the Munster Basin are late Middle Devonian (late Givetian) in age and are located to the southwest of the Basin (Clayton and Graham, 1974; Russell, 1978; Higgs and Russell, 1981). Much of the dating of the Munster Basin sediments is based on fossil and palynological evidence. Russell (1978) finds a number of locations for vertebrate material on the western coast of the Iveragh Peninsula. Based on the fish fossils found (Acanthodian, Bothriolepis sp. and *Sauripterus* sp.), Russell (1978) gives an age of late Middle to early Upper Devonian for the ORS of the Iveragh Peninsula. Higgs and Russell (1981) studied a spore assemblage from the Chloritic Sandstone Fm. at Molls Gap Quarry and suggested an early Frasnian age. On Clear Island Clayton and Graham (1974) found rocks close to the base of the Munster Basin sequence which contain fossils of late Middle Devonian age. Also, miospores from the Sherkin Fm. on Clear Island have been dated as being late Middle to early Upper Devonian (Clayton and Graham, 1974). Based on the finding of *Rugospora bricei* at Molls Gap, Williams (2000) suggest an age of no more than Middle Frasnian. Miospore assemblages from Molls Gap Quarry give late Givetian-early Frasnian (van Veen and van der Zwan, 1980) and Early Frasnian (Higgs and Russell, 1981). Williams (1997) provides an age of 384.9 ± 0.7 Ma for the ORS using Pb/Pb isotopes on magmatic zircons from the Enagh Tuff (Fig 2.36), but this lacked adequate biostratigraphical correlation. The above led Williams et al. (2000) to carry out

U-Pb geochronology and palynology studies on the Munster Basin in relation to new isotopic dates available (Roden et al., 1990; Tucker and McKerrow, 1995; Tucker et al., 1998 cited by Williams et al., 2000) in order to improve the known age constraints on the Munster Basin. Williams et al. (2000) suggest from U-Pb zircon dates from the Keel, Killeen and Horses Glen Tuff that the earliest ORS is older than 385 Ma.

The sediment for the Munster Basin was sourced from the east, north and west (Fig 2.13; e.g. Gardiner and MacCarthy, 1981; Meere, 2013). Sediment transport in the northern part of the basin came from the north or northwest (Graham, 1983; Russell 1984; Williams et al., 1989). Granitic plutons located to the east and west of the basin influenced the drainage patterns into and within the basin (McCarthy, 1990). Three main entry points exist for the fluvial dispersal systems that filled the basin (Williams et al., 1993). Two of these traversed the DBGFZ while one was within the Galtee Mountains area. The sedimentation of the Munster Basin has been classified into a number of episodes by various authors. Graham (1983), Williams (1989) and MacCarthy (1990) describe the sedimentation in detail.

Graham (1983) proposed a terminal fan model for sedimentation in the Munster Basin and divides it into four major facies:

Facies A: Coarse marginal facies. This facies lies to the north and the eastern margins and consists mostly of conglomerates and pebbly sandstones (Horne, 1971, 1974, 1975; Capewell, 1951, 1965). These formations are alluvial fans (Horne, 1975), braided fluvial deposits (Penney 1980) and some local interbedded aeolian deposits (Horne, 1971, 1975).

Facies B: Coarse grained fluvial facies. This facies consists of sandstones and pebbly sandstone with large scale cross stratification and are interpreted as stack deposits of fluvial channels.

Facies C: Fine grained fluvial facies. Graham (1983) places the Valentia Slate Fm., the St. Finans Sandstone Fm., the Ballinskelligs Sandstone Fm. which lie on the Iveragh Peninsula (Capewell, 1975) in the fine grained fluvial facies. This facies consists mostly of fine sand and silt with sharp bases and ripple cross lamination. The author describes

Facies C as a result of successive flooding which occurred on flat non-channelized alluvial plains.

Facies D: Fluvial Coastal plain facies. This is a fluvial coastal plain facies consisting of sandstone and mudrocks of green grey colour reflecting a higher water table due to climatic changes and the onset of marine transgression (Graham, 1983).

Williams et al. (1989) describes the sedimentary infill of the Munster Basin as consisting of background sedimentation and two major fluvial influxes. The background sedimentation consists of 95% purple coloured fine sandstone and siltstone and was deposited by sheet floods across a low relief environment. The initial fluvial influx consisted of proximal sediments from a high energy environment and a distal part which consists of sandy sheet floods. This initial fluvial influx includes the Chloritic Sandstone Fm., which is the lateral equivilant of the St. Finans Sandstone Fm. (Fig 2.18). Williams (1989) describes this as a distributary system with a fan like form about 90-110 km in radius. The second fluvial influx is interpreted as a ”prograding distributary alluvial cone” (Williams et al., 1989) and is represented by the Gun Point Fm. (Fig. 2.18).

MacCarthy (1990) considers four main episodes of deposition which includes, three main fluvial influxes having occurred over the course of the sedimentation in the Munster Basin (Fig 2.15). MacCarthy (1990) divides the fill of the Munster Basin into 5 facies associations: **A:** Basin margin, alluvial fan and braided complex. **B:** floodplain sheetfloods and ephemeral lakes which includes the Valentia Slate Fm. **C:** Fluvial influx 1, **F1** which comes from the north west and west and contains the St. Finans Sandstone Fm. **D:** Fluvial influx 2, **F2** comes from the north-east, north and north-west and **E**: Fluvial influx 3, **F3** which comes from the west and represents the coastal plain in the South Munster Basin. This includes the Toe Head Fm.

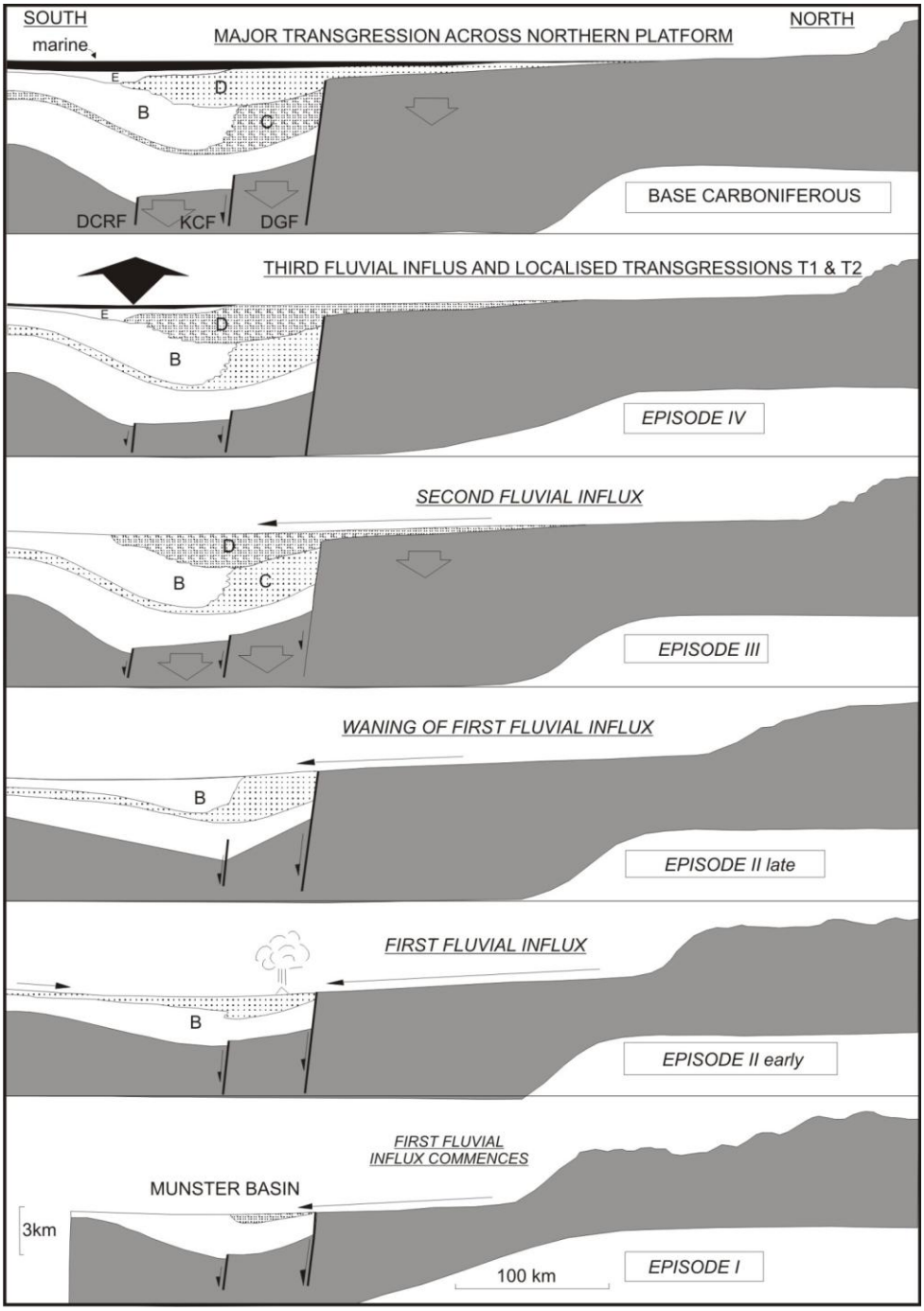

Figure 2.15 Shows four episodes of deposition, which includes three fluvial influxes in the Munster Basin during the Upper Devonian and a major marine transgression in the Early Carboniferous (from MacCarthy, 1990). (DCRF = Dunmanus-Castletown-Ringabella Fault, KCF = Kenmare - Cork Fault, DGF = Dingle Bay-Galty Fault), (Pallinspastic N-S, Pre-Variscan Horizontal Scale) B, C, D, E = refer to Facies associations (MacCarthy, 1990).

2.11 Extent of Basin Margins: Pre – Variscan

2.11.1 The Northern Margin: Pre - Variscan

There have been a number of suggestions for the location of the northern margin of the Munster Basin. The northern margin has been previously placed at the Dingle Bay Lineament (Fig 2.16; Price and Todd, 1988; Todd, 1988), however further attention has been paid to the Dingle Bay Galtee Fault Zone (DBGFZ; Fig 2.17, 2.18; Gill, 1962; Graham, 1983; Sanderson, 1984; Price, 1989; Williams et al., 1989; MacCarthy, 1990) which is also termed the DBGML (e.g. Landes et al., 2000, 2003). The DBGFZ has been described as a southward downthrowing listric fault (Williams et al., 1989; Todd, 1989) or as a growth fault dipping to the south (Todd, 1988), which runs from Dingle Bay across to the north of the Galtee Mountains Williams et al. (1989). The DBGFZ coincides with a thin 1 km isopach following a line from Dingle Bay across to the Galtee Mountains (Fig 2.17; Naylor and Sevastopulo, 1979). Sanderson (1984) describes the northern margin of the Munster Basin to be located where there is major southward thickening of upper ORS which traces in an E-W direction from Dingle across to the Galtees and the Comeragh Mountains. The basin margin swings to a more NE-SW trend in County Waterford (MacCarthy et al., 1990, Fig 2.12). The DBGFZ possibly terminates north of Slievenamon close to the Granite Leinster Massif (Williams et al., 1989). Palinspastic restoration indicates that differential displacement along the DBGFZ has resulted in WSW thickening of ORS fill (Williams et al., 1989). It has been suggested by Williams et al. (1989), that this fault zone had little topographic relief due to the absence of what they term ‘significant’ alluvial fan deposits and that a high rate of sedimentation exceeded subsidence rates. Williams et al. (1989) suggest that there was no significant erosion of the footwall of the DBGFZ in the provision of sediment to the basin. However later studies by Williams (2000) suggest that the trace line of the DBGFZ denotes the southern boundary of the Siluro-Devonian Dingle Basin which lies to the north of the Munster Basin. Williams (2000) suggests that the DBGFZ may have at that time had the opposite sense of downthrow to that employed for the Munster Basin northern margin. The position of the DBGFZ may have been controlled by the previously existing Caledonian South Ireland Lineament (Fig 2.12; Gardiner and MacCarthy, 1981). Although the northern margin has previously been placed at the DBGFZ, Price and Todd (1988) place the Munster Basin’s northern margin at the Kilarney Mallow Fault Zone (KMFZ) which lies further to the south.

Price and Todd (1988) show that the strike of the KMFZ is parallel to the strike of Caledonian inliers in Waterford, Slievnamom, Galtee Mountains and central Ireland, and thus consider it to be a reactivated Caledonian Fault. The KMFZ may be a hanging wall shortcut fault to the DBGFZ (Ford et al., 1991). The KMFZ is considered by Meere (1997) to be the northern margin of the Munster Basin (Fig 2.19). Landes (2000) supports this and suggests that the development of the Munster Basin as a half graben occurred by normal displacement on the KMFZ. Landes et al. (2000, 2003) interpret seismic data from Varnet-96 Line A and B and suggest that the Dingle Bay Mountains Line (DBGML) is instead a north dipping structure and therefore cannot be the northern margin of the Munster Basin. Landes et al. (2000, 2003) actually propose that the DBGML marks the southern margin of the Dingle Basin and are in agreement with the suggestion of Price and Todd (1988) and Meere (1997) that the more southerly KMFZ as the northern margin of the Munster Basin (Fig 2.19, 2.20).

2.11.2 The Southern, Western and Eastern Margins of the Munster Basin

It has been suggested that the Dunmanus-Casteltown Fault (DCF) bounds the half graben of the Munster Basin to the south (Williams et al., 1989; Fig 2.17). The DCF lies 130 km to the south of the DBGFZ and it has been described as an intrabasinal fault based on facies thickness and palaeodispersal (Williams, 1989). Ford et al. (1991) have looked at gravity modelling across the DCF and Masson et al. (1998) have looked at seismic refraction data and they both interpret significant crustal changes associated with the DCF. Williams (1989) suggest that the DCF must have had a northward downthrow during deposition of the Munster Basin. However MacCarthy (1990) suggests that the DCF had a southerly downthrow during sedimentation (Fig 2.15). Naylor et al. (1983) suggest that there is no onshore expression of a southern margin of the Munster Basin. The southern margin of the basin is inferred to lie close to the south coast based on geophysical and sedimentary evidence (Naylor et al., 1983; Price, 1988). Landes (2003) do not find a southward termination of the Munster Basin, based on seismic evidence. Continental Red beds and tuffs of possible Frasnian age have been drilled 155 km offshore to the SSE of Toe Head (South Munster Basin), (Robinson, 1981). However these sediments may not be an offshore continuation of the Munster Basin, but instead may have been produced by rifted crust (Williams, 2000). To the south of the basin lies a Caledonian Fault, the Wexford Boundary Lineament, (Fig 2.12; cf. Gardiner and MacCarthy, 1981, cited by MacCarthy, 1990) which may be related to

the southern margin of the basin, although there is no known Devonian dip-slip movement on the fault (MacCarthy, 1990).

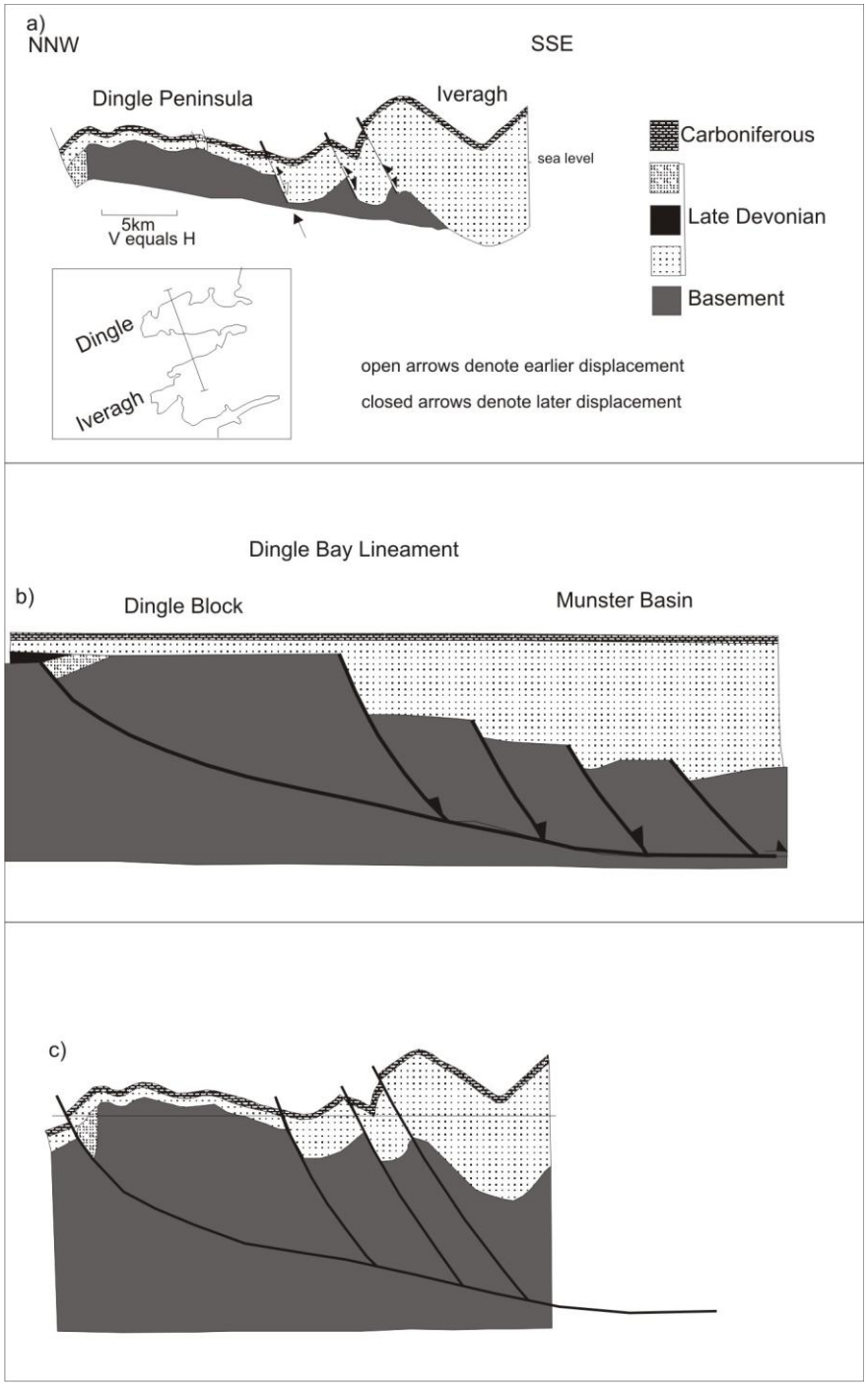

Figure 2.16 Shows the previous suggestion of the northern margin of the Munster Basin at the Dingle Bay Lineament, a) and b) deformation at the early Carboniferous and c) deformation at the end of the Carboniferous. After Price and Todd (1988).

The western margin of the Munster Basin possibly lies offshore (Graham, 1983) based on ESE directed dispersal patterns of the Sherkin Fm. in the Sheeps Head area (Graham and Reilly, 1972; Williams, 2000). It has also been suggested by Ford et al. (1992) that the western margin lies offshore, based on deep seismic data (Makris et al., 1988; Conroy and Brock, 1989; Klemperer et al., 1991).

The eastern margin of the Munster Basin is marked by the Comeragh Mountains, (Capewell, 1956) consisting of a 3000 m thick accumulation of sandstones and conglomerates (Capewell, 1957b; Penney, 1978) and trending in a N-S direction (Penney, 1980).

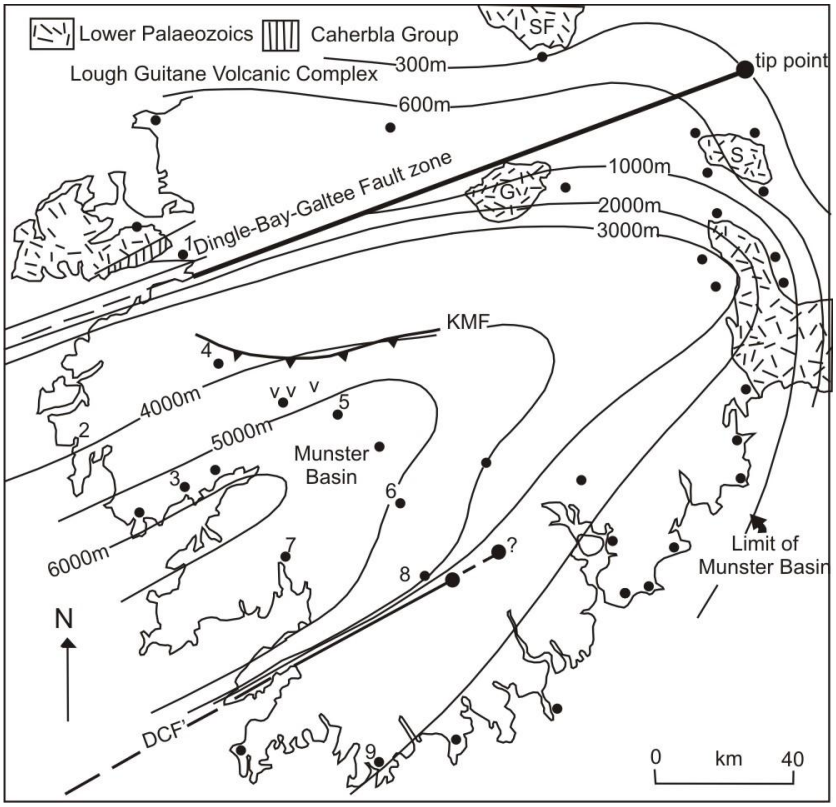

Figure 2.17 Pre-Variscan pallinspastic restoration of the Upper ORS isopachs from the Munster Basin. The position of the Dingle-Bay Galtee Fault Zone and the 1 km isopach of the Munster Basin are shown. Redrawn from Williams (1989). DCF' = Restored position of Dunmanus-Castletown Fault and KMF', the Kilarney Mallow Fault Zone. Corrected for 50% shortening in Zone 1 and eastern transition zone (Cooper et al., 1986) of the Irish Variscides. 1 = Slieve Mish Dingle, 2 = Iveragh Peninsula, 3 = Sneem, 4 = Kilarney, 5 & 6 = Derrynassagarts, 7= Beara-Bantry, 8 = East Shehy Mountains, 9 = Toe Head.

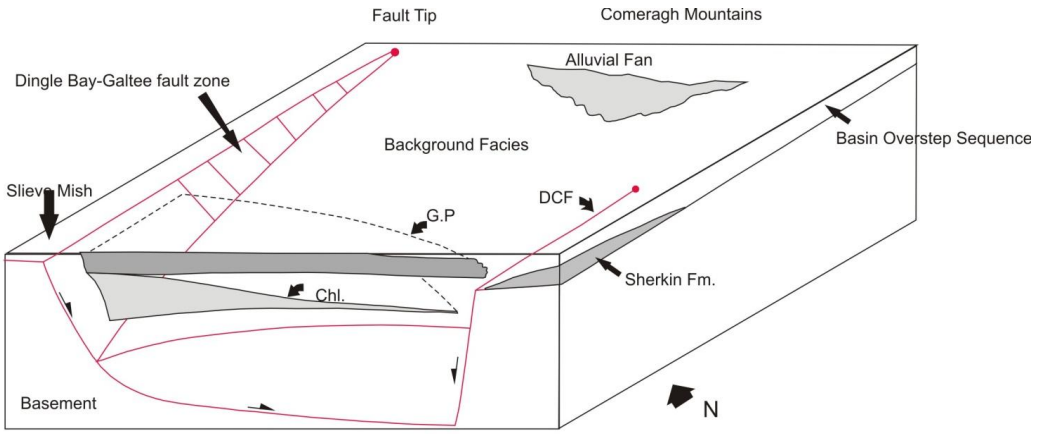

Figure 2.18 Shows the extensional half graben nature of the Munster Basin with the DBGFZ in the north and the Dunmanus-Castletown Fault (DCF) in the south. Sedimentation consists of background sedimentation and two fluvial influxes represented by the Chloritic-Gortanimill Fm. (Chl) and the Gunpoint Fm. (GP). Redrawn from Williams (1989).

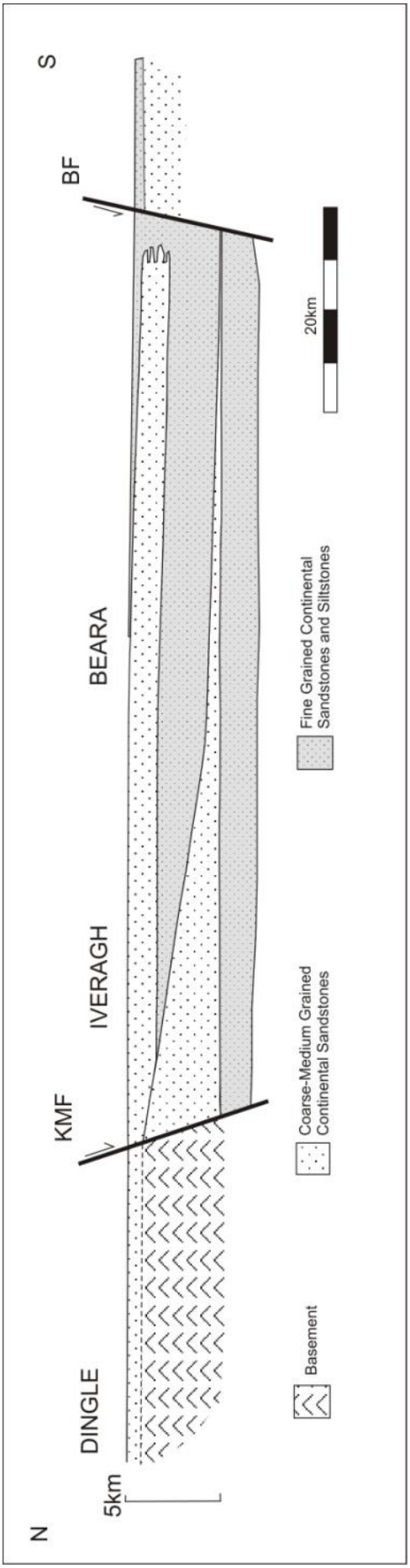

Figure 2.19 Shows the Killarney Mallow Fault as the main northern margin basin fault, prior to Variscan deformation. Redrawn from Meere (1997).

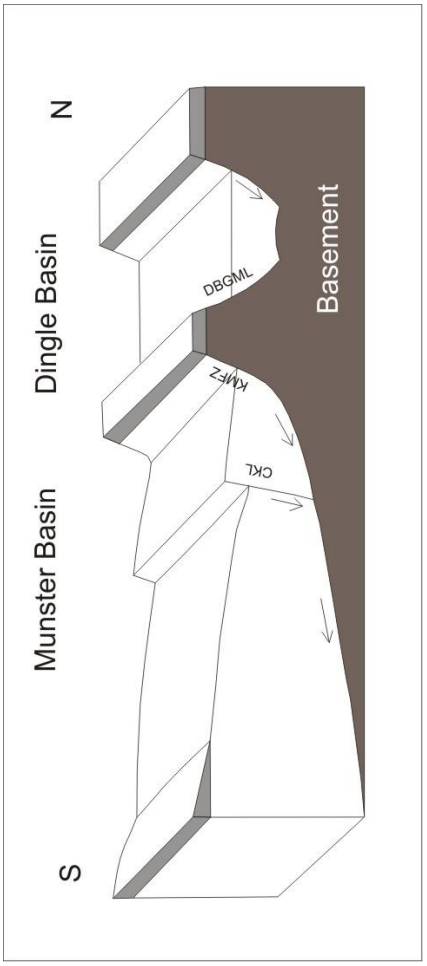

Figure 2.20 Left Sketch of the extensional development of the Munster Basin during Devonian times (Modified after Williams et al. (1989). CKL = Cork-Kenmare line; KMFZ = Killarney Mallow Fault Zone; DBGML = Dingle Bay Galtee Mountains Line. Redrawn from Landes (2003).

Part Four: Variscan Deformation of the Munster Basin

2.12 Inversion of the Munster Basin

Variscan deformation is generally considered to have progressed from the south to the north (e.g. Cooper et al., 1984, 1986). Previous authors have discussed the importance of basin morphology in subsequent basin deformation (e.g. Gardiner, 1978; Naylor et al., 1983; Sanderson, 1984; Cooper et al., 1986). Inversion of the Munster Basin reused the pre-existing structural extensional template (Price and Todd, 1988; Meere, 1995; Landes, 2003). The Munster Basin is considered to be an asymmetrical half-graben based on isopachs and Bouguer anomaly maps (Murphy, 1960). Gravity anomaly maps (Murphy, 1960, 1962) show contours oblique to the Variscan trend possibly influenced by the Caledonian basement (Naylor et al., 1983; Readman et al, 1997). A strong negative gravity anomaly exists to the western end of the Munster Basin on the south side of Dingle Bay and may be accounted for as due to significant depth of the sedimentary basin (Naylor and Jones, 1967) or due to the existence of a large felsic igneous body at depth similar to the Leinster Granite (Howard, 1975). Traditionally deformation is thought to have occurred in three main stages; 1) Initial cleavage formation (2) Folding (3) Thrusting (Cooper et al., 1986). There are two main models for the tectonic deformation of southern Ireland: a thick skinned model where deformation extends to a greater depth in the crust (e.g. Mathews et al., 1983; Sanderson, 1984) and a thin skinned model where deformation involves only the upper crust (e.g. Cooper et al., 1984, 1986; Shackleton, 1984; Allmendinger et al., 1987; Ford, 1987).

2.12.1 Thick-skinned Model of Deformation

Sanderson (1984) put forward a thick-skinned model involving dextral transpression of the Munster Basin with significant crustal thickening. Sanderson (1984) suggested a model that involved an active role of the basement in deformation where dextral transpression occurred via faults that extended deep into the crust. Sanderson (1984) has interpreted gravity data with reference to McKenzie's basin development model and suggests that significant crustal thickening occurred during Variscan deformation. Folded basement observed in the Galtees-Ballyhoura Mountains to the east indicate basement may core the major Variscan folds (Ford et al., 1991) and therefore indicates that deformation is not truly detached from the basement (Williams, 2000). Price and

Todd (1988) suggest that the Munster Basin is more than likely underlain by a low angle detachment, however Sanderson's (1984) thick-skinned model does not include a basal detachment (Bresser and Walter, 1999). Seismic evidence suggest a decollement zone lying approximately 10 km beneath the fold and thrust belt of the Rhenohercynian implying the possibility of a thin skinned model for deformation (Warr, 2012), however a thick-skinned model of deformation is more conducive to the existence of strike slip shear, precollisional rifting and the existence of very steep structures in the Munster Basin (Warr, 2012).

2.12.2 Thin-Skinned Model of Deformation

Cooper et al. (1984, 1986) suggests a thin-skinned model of deformation for the Munster Basin, with a passive basement and an overlying thin-skinned northwards thrusting décollement. Shackleton (1984) supports a thin-skinned mechanism of deformation where the tip of the décollement zone represents the Variscan front. A thin skinned deformational model is supported by Ford (1987). A thin skinned surge zone created as a result of the basin morphology has been proposed by Murphy (1990; Fig 2.28). Bresser and Walter (1999) support a thin skinned model based on field work and their interpretation of seismic data, however they place the basal detachment in Co. Clare instead of at the KMF (Cooper et al., 1984; Ford, 1987). The thin skinned model of Bresser and Walter (1999) includes the involvement of the basement and dextral transpression. Landes et al. (1998) from seismic evidence support a thin skinned model where deformation does not affect the entire crust, as they only find evidence for upper crustal Variscan deformation. The only deep crustal structure of relevance to deformation is the Caledonian Iapetus Suture Zone (Landes, 2003).

2.13 Zonation of the Irish Variscides

Gill (1962) proposed three structural zones of the Irish Variscides which have been further modified by Cooper et al. (1986; Fig. 2.21, 2.22).

Zone 1: This is the zone of intense deformation south of the DDL.

Transition Zone: The Transition Zone contains characteristics between Zone 1 and Zone 2.

Zone 2 a: In this zone, structural trends are highly influenced by Caledonian basement.

Zone 2 b: There is less Caledonian basement control on structural trends and deformation intensity dies out gradually.

Zone 3: This zone lies furthest to the north of Zones 1 and 2 and is considered to be the foreland of the Variscides with rare folding (Dixon, 1972) and N-E trending Caledonian controlled faults.

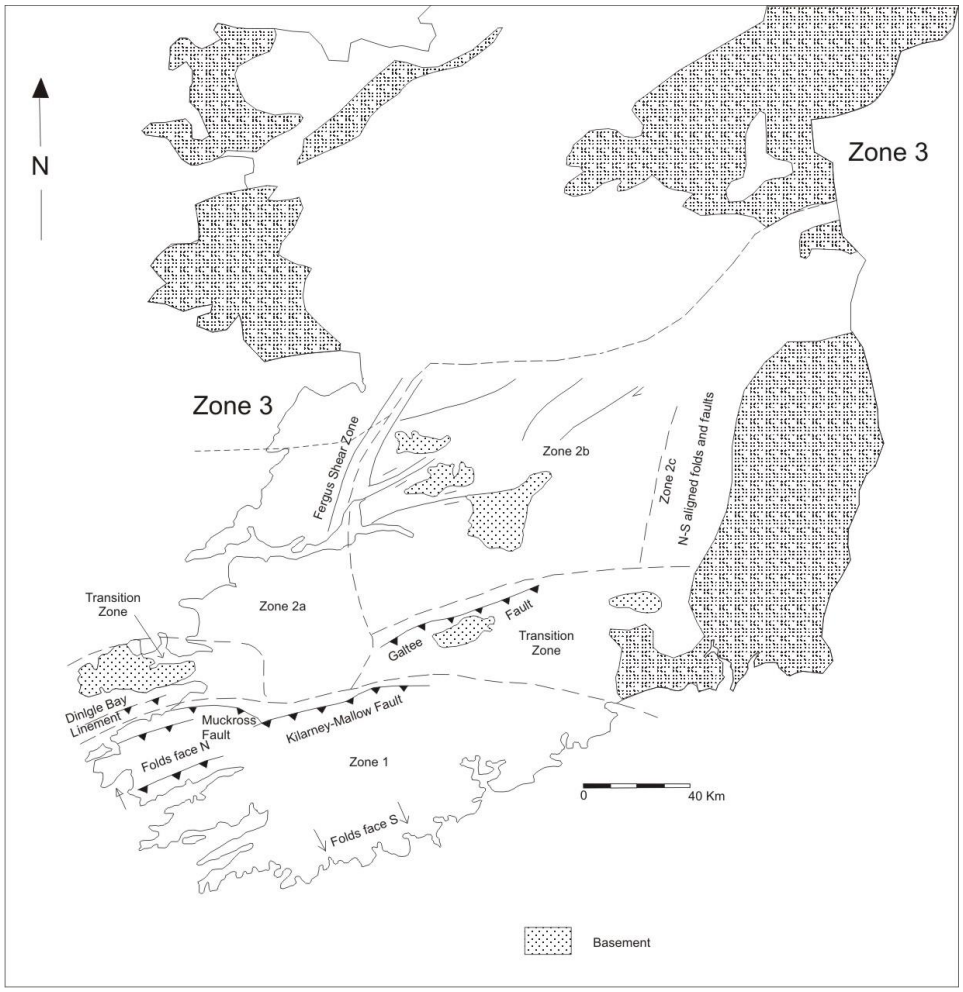

Figure 2.21 Shows the zonation of the Irish Variscides. Redrawn from Price and Todd (1988) and Cooper et al. (1986).

2.14 The Variscan Front in Ireland

There have been many suggestions for the location of the Variscan front in Ireland (e.g. Dunning, 1966; Capewell, 1975; Max and Riddihough, 1975; Ziegler, 1978; Naylor and Sevastopoulo, 1979; Naylor, 1983; Cooper et al., 1984; Sanderson, 1984; Shackleton, 1984; Bresser and Walter, 1999) and some authors consider the idea of a front as having no definitive meaning (e.g. Mathews, 1978; Keely, 1996). Shackleton (1984) considers the Variscan thrust front to be marked by a change in the orientation of deformational

structures from a Variscoid trend to a more Caledonoid trend. Shackleton (1984) also distinguishes between the idea of a present day thrust front, which he defines as where the décollement surface currently crops out or exists as a blind thrust, as oppose to the original thrust front which may have existed structurally higher up and much further to the north and has since been eroded e.g. towards the Highlands of Scotland. Capewell (1975) considers the Variscan front to be marked by a continual reduction in the degree of fold axial plane dip. Naylor and Sevastopulo (1979) and Cooper et al. (1984) suggest that the Variscan front in southern Ireland exhibits a more gradational change in tectonic intensity from south to north rather than ending as a sharp boundary. Sanderson (1984) considers the Munster Basin to be the zone with most intense deformation and the rest of Ireland to be a foreland zone with some minor areas of equally intense deformation. Bresser and Walter (1999) suggest that the Variscan orogenic front in Ireland be defined as where the sole thrust or basal detachment appears at the surface or where there is no longer any displacement along the basal detachment. Bresser and Walter (1999) place the present day Variscan thrust front in Co. Clare based on Variscan folds and thrusts recorded north of the KMFZ (Fig 2.23). Bresser and Walter (1999) describe deformation as gradually decreasing towards the north with virtually no Variscan deformation to have occurred in the Upper Carboniferous limestones of north Co. Clare. Bresser and Walter (1999) suggest that the basal detachment lay 12 km at depth to the south and rose to 3-4 km in the north.

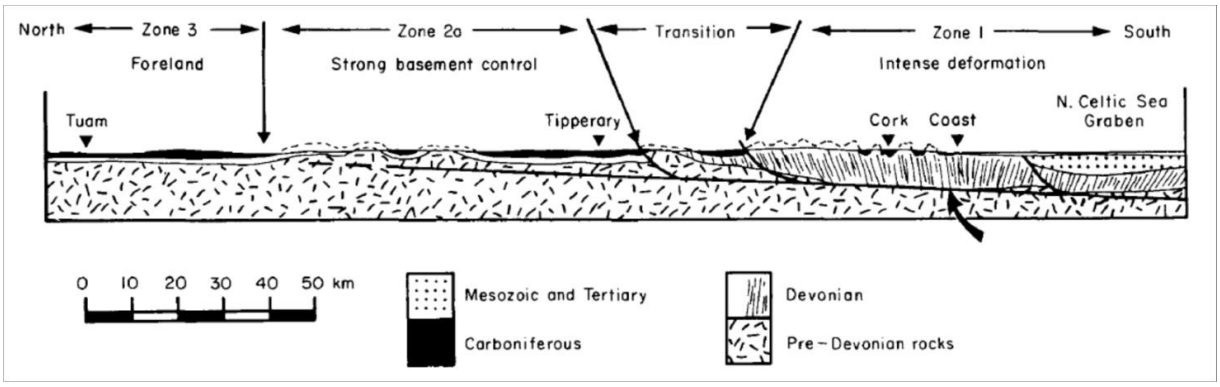

Figure 2.22 a representative cross section through the Irish Variscides. From Cooper et al. (1986).

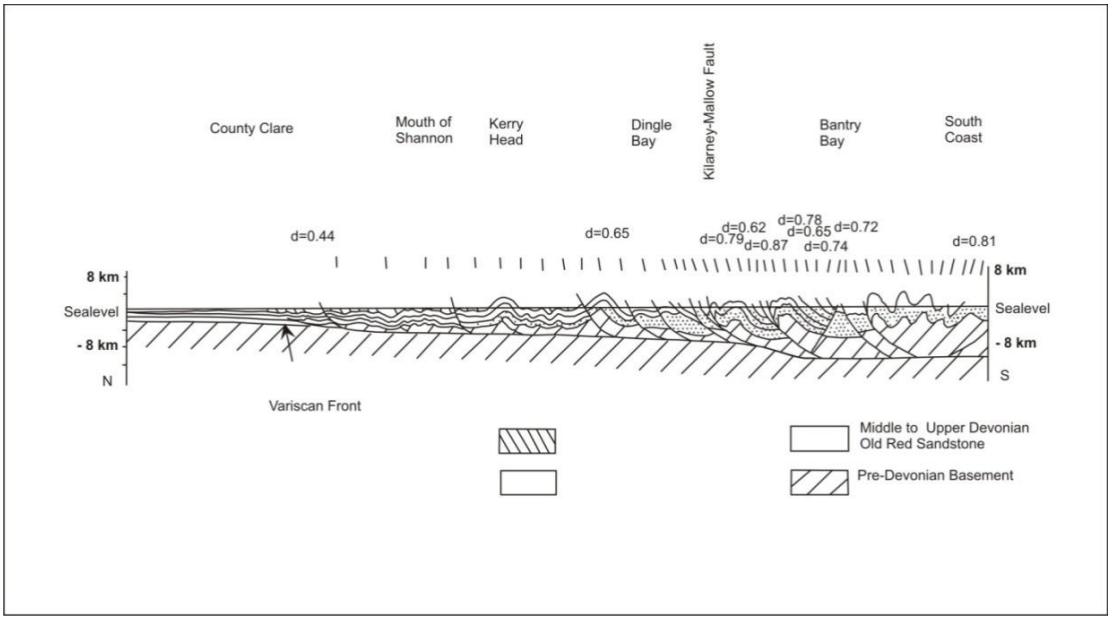

Figure 2.23 Shows the location of the Variscan front and where the regional cleavage dissipates, in Co. Clare. The cleavage is consistently steeply dipping. The space between cleavage dashes represents the relative intensity of cleavage. Redrawn from Bresser and Walter (1999).

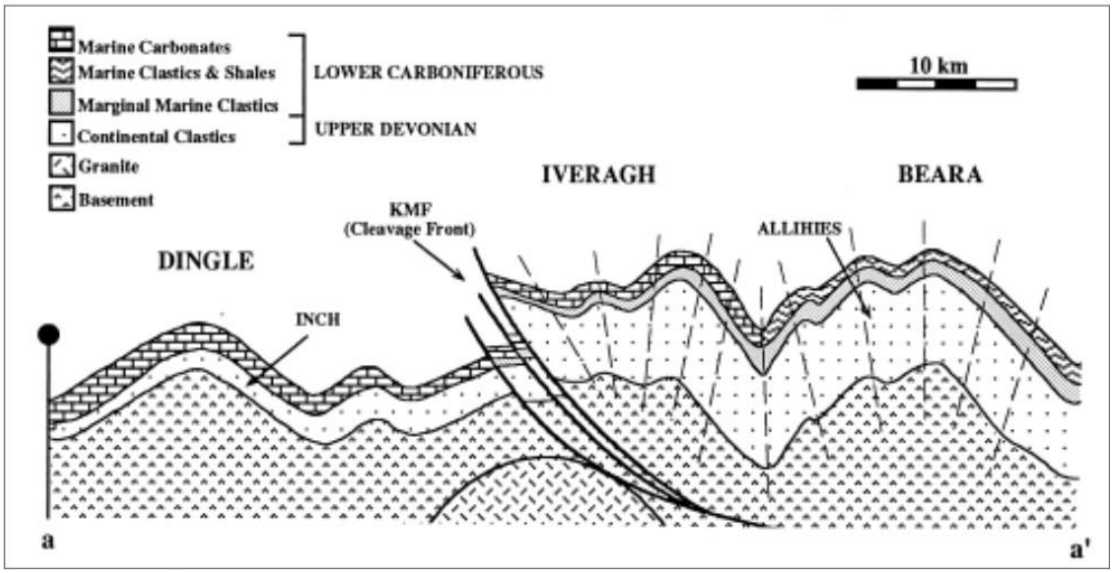

Figure 2.24 Shows a cleavage front at the Kilarney Mallow Fault (KMF) area. From Meere (1997).

2.14.1 The Variscan Front - The Dingle Dungarvan Line (DDL)

Gill (1962) first described the Variscan front as a divide between a fold and thrust belt to the south and a relatively undeformed foreland to the north. Gill (1962) suggested that a line running from Dingle Bay to Dungarvan (the Dingle Dungarvan Line, DDL; Fig 2.25) was representative of a change from deformed to undeformed. Cooper et al. (1986) consider the DDL to be the northern most boundary of the most intense zone of deformation which consists of LPS, buckling and accommodation by thrusting.

Shortening south of the DDL is estimated to be 42 % at the centre of the Irish Variscides area while it is around 33% in the east of the area (Cooper et al., 1984). Between Kilarney and Mallow the DDL exists as a northward propagating thrust (the KMFZ), e.g. Ford (1987) and towards the east the DDL is a stratigraphic boundary (e.g. Ford, 1992). In the eastern part of the Irish Variscides, Murphy (1990) suggests that the Variscan front coincides with the limb of the Dungarvan Syncline. It is suggest that the variation in the expression of the Variscan front from west to east is a function of Caledonian basement controls including the effect of Caledonian granites (Ford, 1991). Max and Lefort (1984) suggest that the DDL Line had an element of dextral strike slip movement and can be traced across to Pembrokeshire.

Price and Todd's (1988) original model for the northern margin of the Munster Basin considers the DDL to be the northern most boundary for the Munster Basin. However, there are some reports of Variscan deformation north of the DDL Line (e.g. Dewey, 1982; Bresser and Walter, 1999). North of the DDL there is very gentle folding and with almost an absence of cleavage even in pelitic layers (Masson et al., 1988).

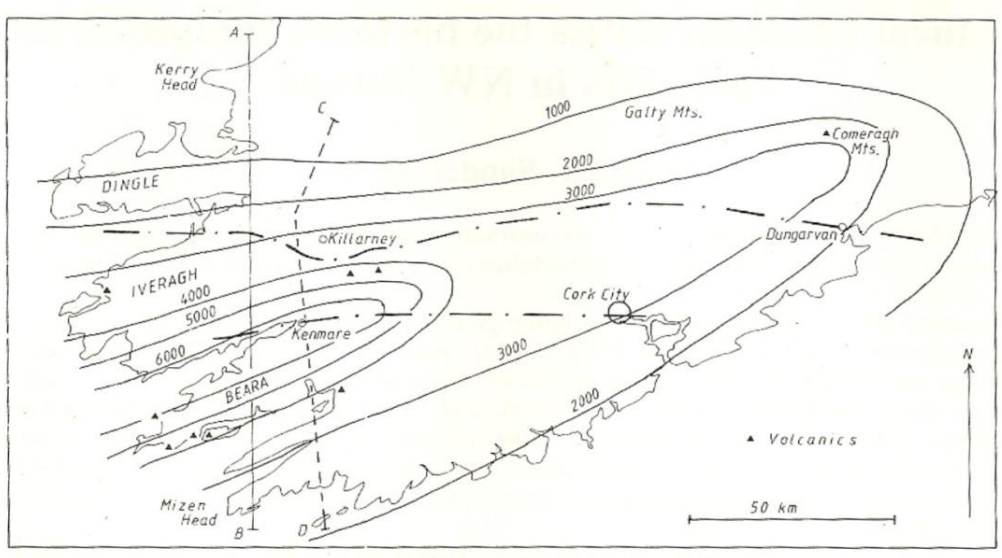

Figure 2.25 Shows the Dingle - Dungarvan line (DDL, dashed line to the north) and the Cork Kenmare Line (dashed line to the south-the northern margin of the South Munster Basin), from Sanderson (1984).

As previously discussed, Williams et al. (1989) suggested another line the Dingle Bay Galtee Fault Zone (DBGFZ), as the northern margin of the Munster Basin. However, Vermeulen (1998) considers the DBGFZ to be a north dipping structure based on seismic interpretation of Varnet-96 Line B (After Landers et al., 2000). Also Landes (2000) consisder the DBGFZ or Dingle Bay Galtee Mountains line, DBGML (which is

a line drawn from Dingle Bay to the Galtee Mountains Thrust Fault, Williams et al., 1989) to be a north dipping structure which bounds a separate basin to the north (Fig. 2.26). Landes (2000) therefore suggest that the DBGML cannot be the northern margin of the syn-rift Devonian Munster Basin. Landes (2000) suggests that Variscan inversion reused the pre-existing extensional faults and that only a small amount of inversion occurred at the DBGML.

2.14.2 The Variscan Front on the Iveragh Peninsula (to the South of the DDL)

Walsh (1968) suggests that the front is located where there is a significant change in structural elevation and Capewell (1975) considers this to occur near Coomnacronia and the Cahersiveen Valley on the Iveragh Peninsula (Fig 2.32). Capewell (1975) suggests that at the Variscan front there may be a decrease in dip value of the axial planes of folds and suggests that the front be located in a zone of maximum overfolding which he suggests lies in the 'zone of tilted folds' located along the northern coast of the Iveragh Peninsula. Capewell (1975) suggests that this zone may structurally be part of the foreland to the north of the Hercynian front (Fig 2.32).

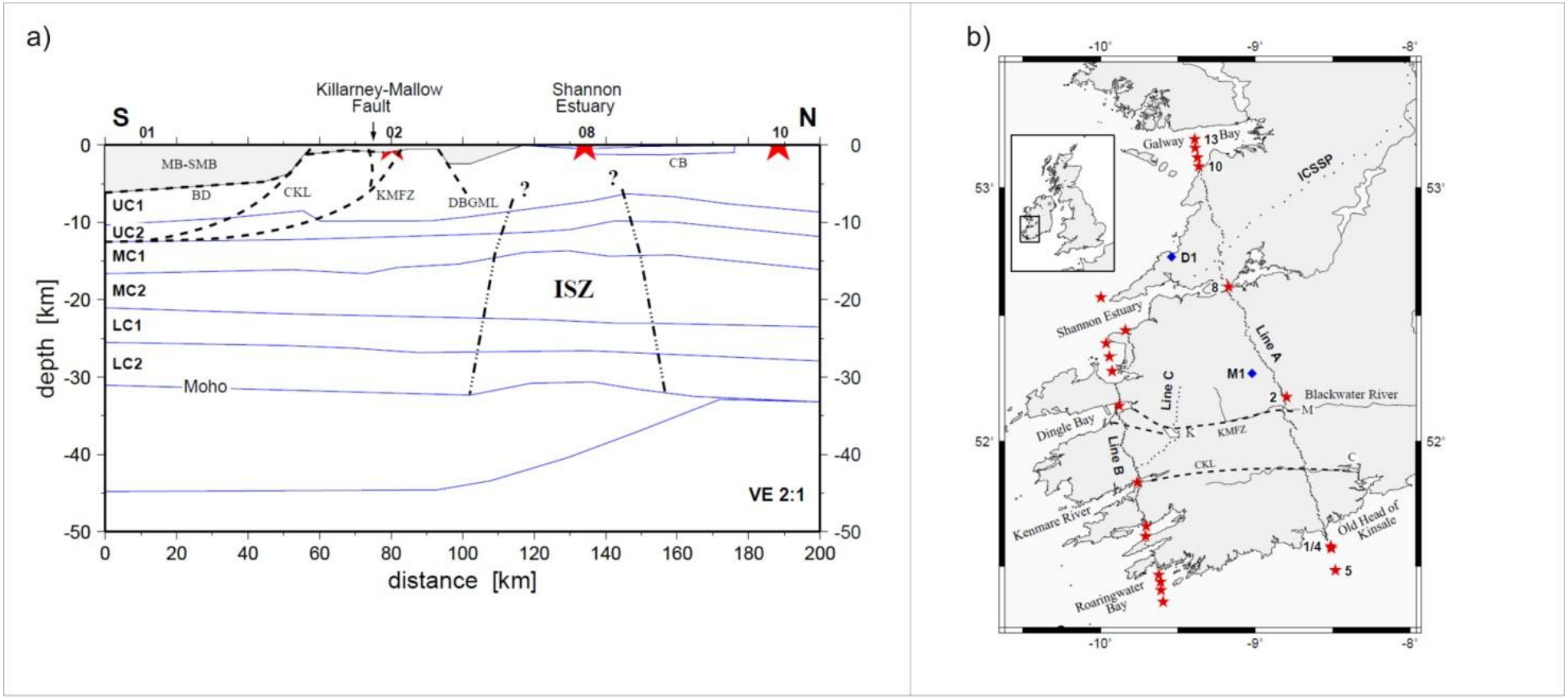

Figure 2.26 Shows Landes (2000) interpretation of Varnet-96 Line A. grey area equals sediments. MB-SMB = Munster Basin-South Munster Basin; BD = Basal detachments; CKL = Cork-Kenmare Line;KMFZ= Kilarnery Mallow Fault Zone; DBGML = Dingle Bay Galtee Mountains Line; CB=Clare Basin, ISZ = Iapetus Suture Zone, After Landes (2000) B) shows location of Line A.

2.15 Variscan Deformation in the Foreland

Variscan deformation in the foreland (in Central Ireland) consists of ENE-WSW major trending dextral faults zones (Sanderson, 1984) which are strongly controlled by the basement, for example the Navan-Silvermines Fault which is congruent to the trace of the Iapetus suture (Phillips et al., 1976). In this zone, Variscan deformation has been suggested to have occurred in the Lower Carboniferous (e.g. Brown, 1979). Variscan deformation in the foreland (of the British Isles) has also been noted further to the north in the Midland Valley of Scotland (e.g. Sanderson, 1984).

Rothery (1989) has studied cleavage in Carboniferous shaly limestones and limestone turbidites from the localities of Belgard and Boston Hill Quarries in the Midlands of Ireland. Rothery (1989) finds cleavage to be either a pressure solution cleavage and or a tectonic stylolitc cleavage and is sporadic, weak and axial planar to folding. The only deviations from axial planar cleavage include extensional asymmetric cleavage in thin shale between massive limestones and some rotation of cleavage in close proximity to en echelon vein arrays and some cleavage shear zones both in proximity to the en echelon vein arrays and flexural slip during folding. The relationship of the general orientation of cleavage with the vein arrays, Rothery (1989) argues for cleavage having been formed during ‘orthogonal wrench tectonic regimes’ (Harland and Baly, 1958). This area lies in subzone 2A of Cooper et al. (1986; Fig 2.21). In the Foreland, the regional cleavage dissipates at around 75 km north of the Dingle-Dungarvan Line (Max, 1980). The cleavage front has also been placed in County Clare (Fig 2.27) and further to the east in Cashel (Le Gall, 1991).

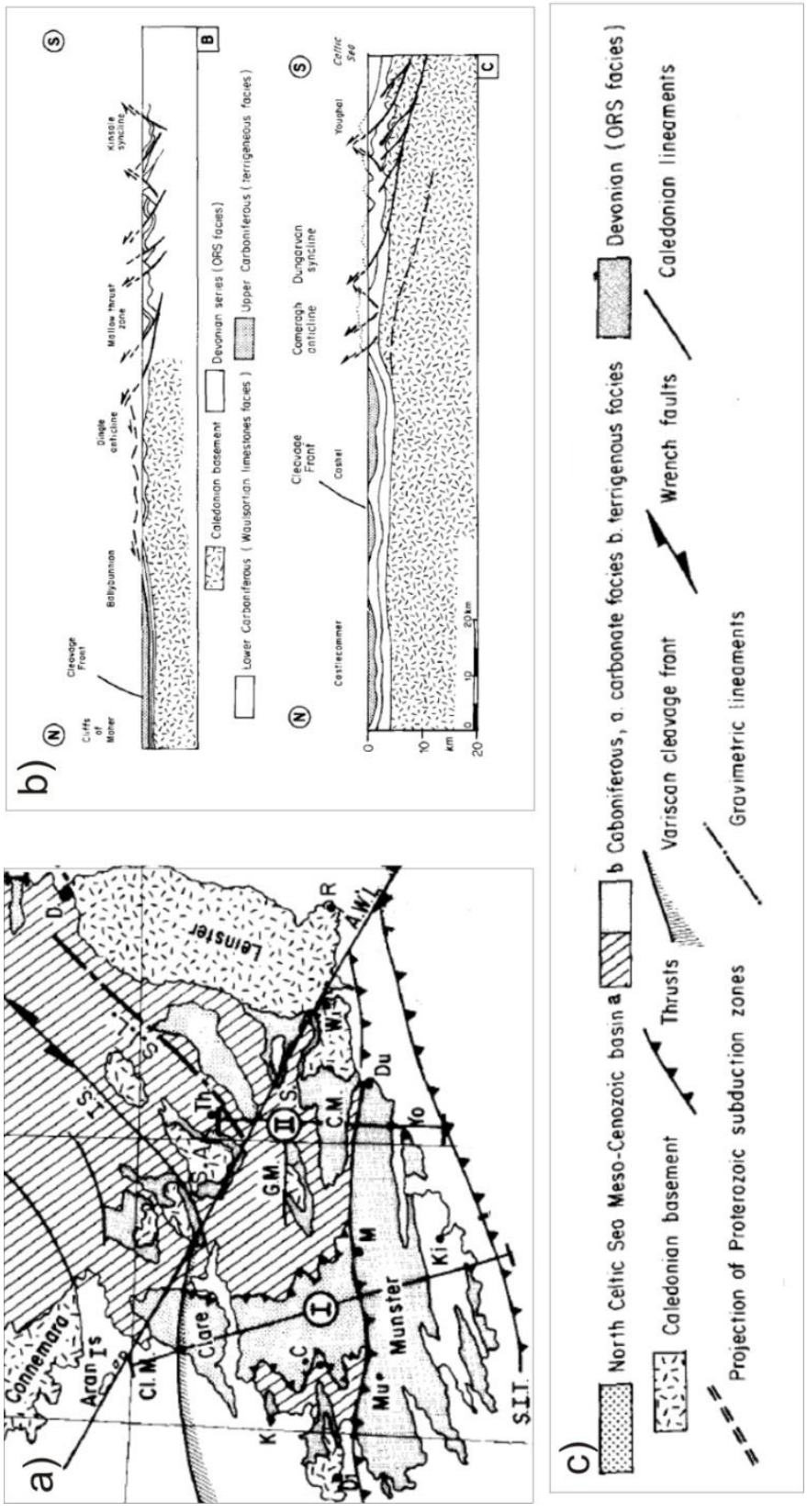

Figure 2.27- Shows the cleavage front in Co. Clare (west of Ireland) and Cashel, Co. Tipperary (Midlands). From Le Gall (1991).

2.16 The Arcuate Nature of the Orogen in the Irish Variscides

South of the DDL, the Variscan fold structures have ENE-WSW to E-W trends (e.g. Cooper et al., 1984). To the east the general NE-SW Variscan trend becomes a more N-S trend due to the influence of the Leinster Massif (Gardiner and Sheridan, 1981). Overall, crustal shortening has been estimated at 50% in a NNW-SSE direction (Ford, 1987). The arcuate nature of the orogen (Fig 2.28) may be due to differential shortening along strike, with 33% in the east and 42% in the west, as interpreted from balanced cross sections (Cooper et al., 1984). Towards the west the fold trends close to 055° (Murphy, 1985), to the centre it is 070° (Cooper et al., 1986) and to the east it is 110° (Cooper et al., 1986). Bedding/cleavage intersection lineations trend WNW-ESE in the east and ENE-WSW in the centre of the basin (Cooper et al., 1984). Murphy (1990) suggested that a surge zone occurs towards the centre of the basin. Murphy (1985) suggests that temporary sticking points both in the east and in the west may contributed to the arcuate nature especially in the east where there is N-S dextral wrench faults.

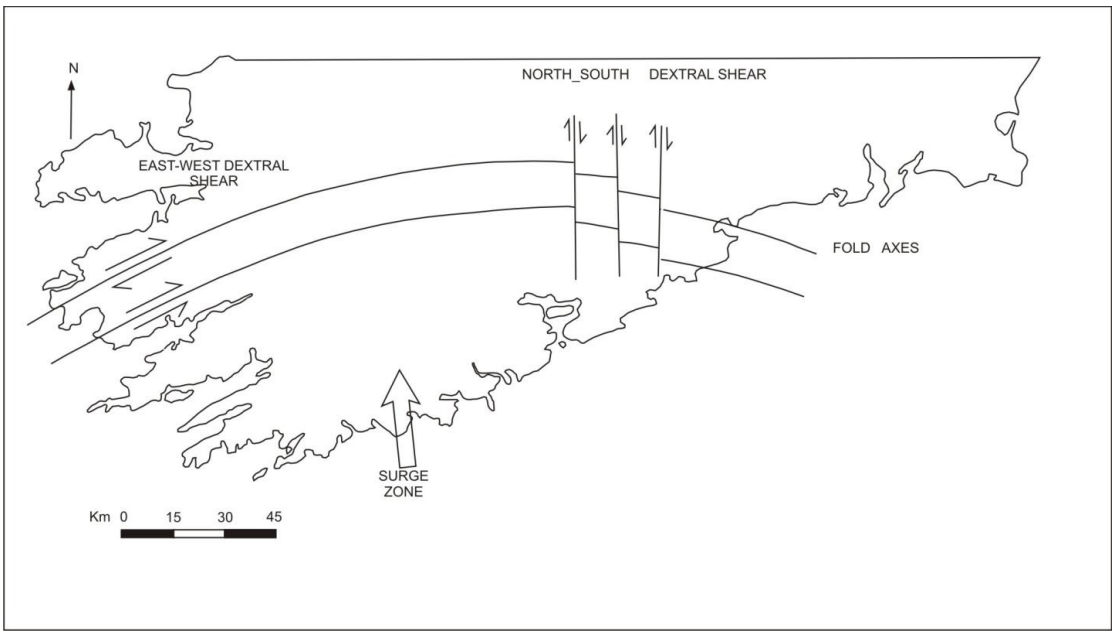

Figure 2.28. The arcuate nature of the Irish Variscides. Redrawn from Murphy (1985).

2.17 Metamorphic Grade

The Munster Basin is considered to have experienced lower greenschist facies regional metamorphism (e.g. Avison, 1982, 1984 a). The metamorphic grade due to Variscan deformation of rocks in the Munster Basin is low, only reaching the anchizone to epizone conditions (Blackmore, 1995; Meere, 1995a; Woodcock and Strachan, 2012;

Fig 2.29). Metamorphic temperatures of > 250 ° C have been determined by conodont colour and vitrinite reflectance indices (Clayton, 1989). Temperatures attained during metamorphism of 280-315ºC have been determined by chlorite geothermometry (Meere, 1995 b) and of 275° to 325 ° C by illite crystallinity studies (Meere, 1995). Meere (1995) suggests that peak metamorphic temperatures were attained during extension prior to Variscan deformation. Temperatures of 340-350° C have been suggested by Blackmore (1995) based on vitrinite reflectance and white mica crystallinity studies across the basin.

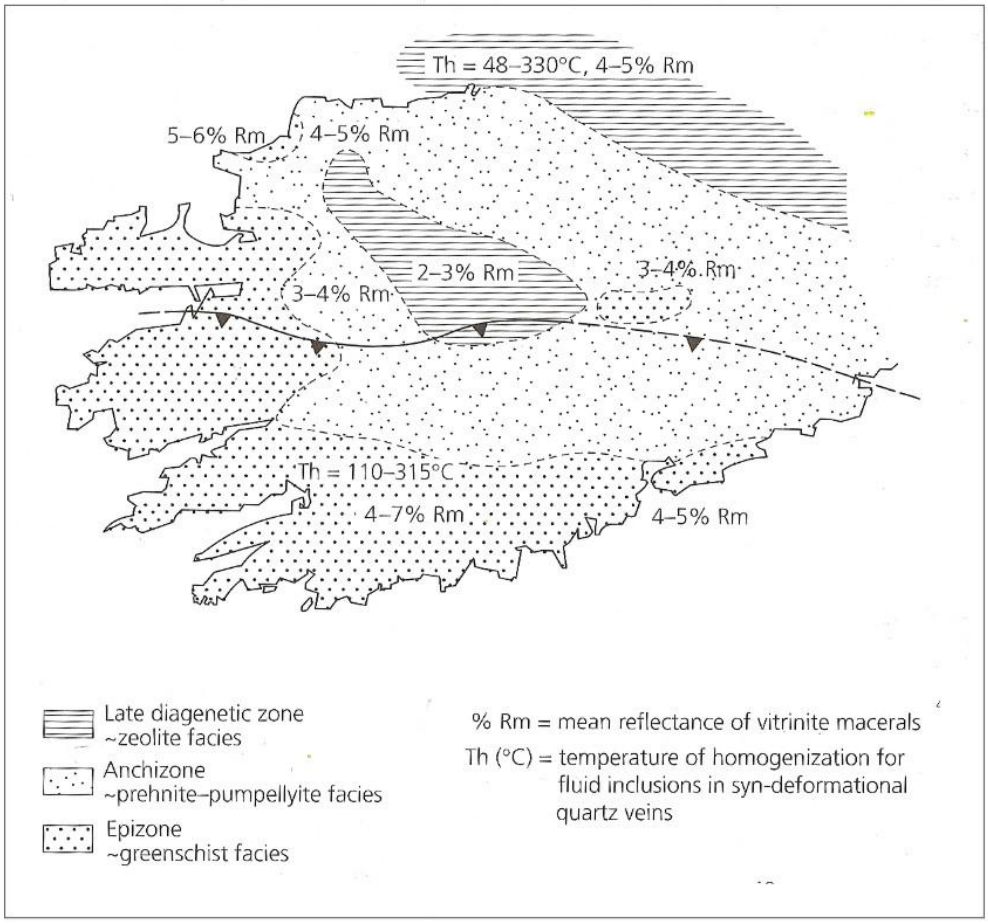

Figure 2.29 shows metamorphic zones of south west Ireland. Modified from Woodcock and Strachan (2012).

2.18 Timing of Variscan Deformation

Sanderson (1984) suggests that the onset of Variscan deformation varies both temporally and spatially across the region of the British Isles and France. K-Ar dating on syntectonic veins in the south of the Munster Basin dates Variscan deformation at around 290 Ma (Halliday and Mitchell, 1983). Igneous intrusions in the south on the

Beara Peinsula are suitable for constraining the timing of Variscan deformation (Quinn et al., 2005; Wartho et al., 2006). $^{40}Ar/^{39}Ar$ dating has been used by Quinn et al. (2005) on an undeformed dyke from the South Munster Basin, who suggest that Variscan deformation had ceased by 296.88 ± 0.60 Ma. Also Wartho et al. (2006) dates a penetratively deformed pipe on Blackball Head at 314.4 ± 1.0 Ma, and 302.0 ± 1.5 to 298.1 +- 0.6 Ma for later stage brittle deformation of dyke material.

2.19 Cleavage in the Munster Basin

There is generally one single pervasive cleavage which dips steeply both to the south and to the north (e.g. Bresser and Walter, 1999) and is predominantly parallel to the fold axial planes (e.g. Capewell, 1957, 1975; Naylor et al., 1981; Sanderson, 1984; Cooper et al., 1986; Pracht, 1996). There is both a spaced disjunctive cleavage in coarse lithologies (e.g. Sanderson, 1984; Cooper et al., 1986, Naylor et al, 1983) and a continuous cleavage in slates (Bresser and Walter, 1999). Quartz rich microlithons are observed between the phyllosilicate cleavage domains (e.g. Naylor et al., 1983). In thin section, sutured boundaries exist between the detrital chlorite and quartz and there are fibrous quartz/chlorite/mica pressure fringes (Sanderson, 1984). The deformation process that operated during cleavage formation in both the mudstones and the coarser sedimentary rocks was a pressure solution controlled diffusion creep (Sanderson, 1984). There is also some authigenic growth of white micas along the cleavage plane (Bresser and Walter, 1999). The timing of cleavage development in the Irish Variscides has been debated. Cleavage development has been considered to be an early LPS event (Coe and Selwood, 1963; Cooper et al., 1986) and considerable LPS is thought to have occurred prior to buckling and reverse faulting (Cooper et al., 1986; Ford, 1987). Cooper et al. (1986) suggest from their field evidence that both layer parallel shortening and cleavage formation occurred prior to or at the early stages of folding and that an early LPS is responsible for the cleavage formation based on the high angle of cleavage to bedding, sheared cleavage and the deformation of burrows which have axes that plunge down the cleavage dip. It is also suggested by Trayner and Cooper (1984), that sheared cleavage may indicate cleavage being formed during the early stages of folding. Cooper et al. (1986) describes a deformation sequence consisting of initial layer parallel shortening, followed by folding and then thrusting (Fig 2.30). Bresser and Walter (1999) observe shearing parallel to cleavage planes which they attribute to a component of dextral strike slip movement. Price (1986) suggests synfolding cleavage as did Meere (1992) who suggests that synfolding cleavage developed by continuous shortening and is a

result of the whole kinematic history. The overall cleavage pattern in the Munster Basin is suggested to reflect the entire Variscan deformation history rather that a set of discrete events (Meere, 1992).

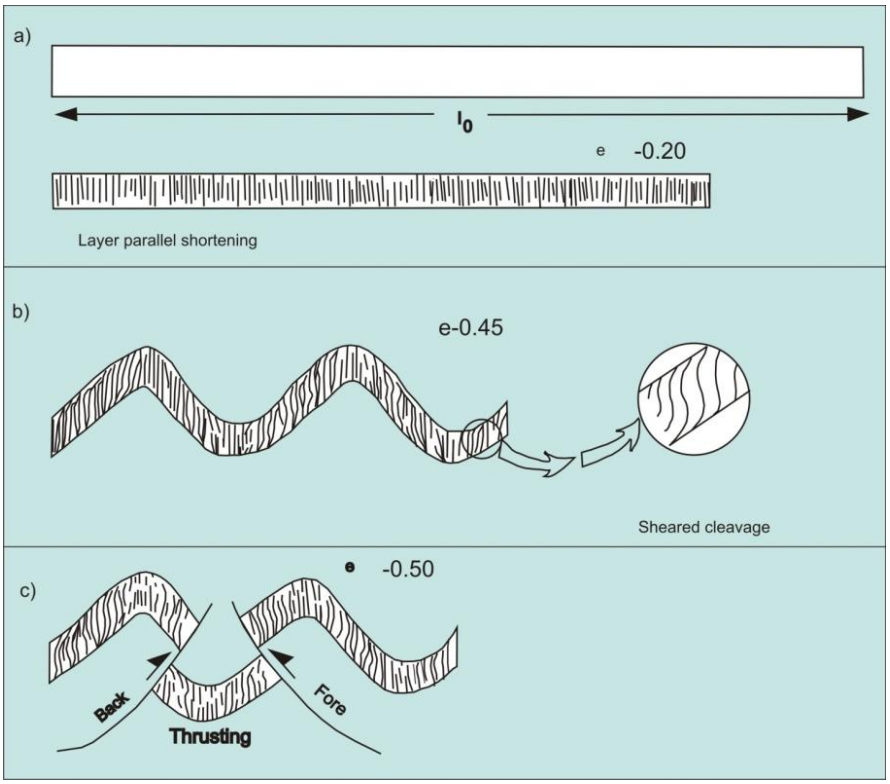

Figure 2.30 Shows the deformation sequence in the Irish Variscides. a) LPS, b) Buckling, c) Accommodation thrusting. Redrawn from Cooper et al. (1986).

There are some deviations to the typical axial planar steeply dipping cleavage. Cleavage refraction and fanning has been observed (e.g. Bresser and Walter, 1999) but only a small amount exists (Sanderson, 1984). There is an anticlockwise deviation from regional folding of the strike of the cleavage on the Beara Peninsula (Sanderson, 1984). Crenulation cleavage is generally only a feature found close to faults or syntectonic veins and is not significant regionally (Sanderson, 1984). Capewell (1975) notices a cleavage dip decreasing from 80° to 20 ° in siltstones of the Valentia Slate Fm. in northern Iveragh (towards Dingle Bay, near the zone of vertical folds, Fig 2.32) and cleavage with a dip of 25° to 30° to the south east in the Valentia Slate quarries. Similarly some less steeply dipping cleavage is noted by Wingfield (1966), where he finds cleavage dipping to the south at 40-60 ° to the south of the Lough Leane area. Bresser and Walter (1999) discuss a local secondary cleavage found exclusively to the south as a result of cleavage rotation during late Variscan deformation and consider this cleavage rotation to be related to minor accommodation faults (Cooper et al., 1986; Bresser and Hilgers, 1996) which are a result of a late deformation stage subsequent to

folding, faulting and cleavage formation. Towards the south (in the SMB), Coe and Selwood (1963) and Gill (1962) find evidence for a second cleavage on the Beara peninsula and Mizen Peninsula (Naylor et al., 1981). Gill (1962) suggests the possible existence of polyphase deformation. Coe (1966) and Coe and Selwood (1963) suggest a two-phase development of cleavage on the Beara Peninsula based on diorite intrusions that cross cut folds and display cleavage. Sanderson (1984) however believes these to be syntectonic intrusions during one continuous deformation regime as there is no other direct evidence of two phases of cleavage in the field. On the Iveragh Peninsula, Capewell's (1975) tectonic interpretation allows for only one episode of compression and accounts for the existence of only one cleavage. Meere (1992; 1997) places a cleavage front at the KMFZ (Fig. 2.24) and Bresser and Walter (1999) observe that cleavage becomes more spaced and less intense north of the KMFZ. Bresser and Walter (1999) find cleavage domains in Co. Clare and diagrammatically show the change in dip and intensity of cleavage along a cross section from the south coast to County Clare (Fig. 2.23). Kink bands which postdate cleavage and folding (Sanderson, 1984) have been suggested to have formed by deformation of cleavage and to a lesser extent by kinking of sedimentary laminae (Murphy, 1988). Conjugate pairs exist but dextral kink bands are most common with a N-S orientation (Sanderson, 1984) which may represent a late sinistral shear in the Irish Variscides (Dewey, 1966).

2.20 Folding in the Munster Basin

The Munster Basin has a number of major folds which are generally upright or steeply inclined and trend ENE-WSW in the main part of the basin to a more E-W trend towards the east (Cork city), (Sanderson, 1984). In the western part of the Munster Basin the trend of Hercynian (Variscan) folds is controlled by the Caledonian basement (Capewell, 1975). Folding geometry has been described as periclinal by Bresser and Walter (1999). Major folds may have basement in their cores based on the bouguer anomaly map (Ford et al., 1991). There are also small scale folds and parasitic folds superimposed on the larger folds (Capewell, 1975; Bresser and Walter, 1999). Some of the minor small scale folding has been described as assymetrical and rounded (Sanderson, 1984). Minor occurrences of step folds have also been noted (Coe and Selwood, 1963). Fold vergence on the south coast (in the South Munster Basin) is to the south (Cooper et al., 1984) and northwards facing towards the thrust front (Cooper et al., 1984). Structurally the Iveragh Peninsula is composed of two main anticlines, and

one intervening syncline; the Kilcrohane Anticline to the south, the Portmagee Anticline to the north and the Inny Syncline in between with also numerous superimposed folds (Capewell, 1975; Fig 2.36). On the Portmagee Anticline, in the northern part of the Iveragh Peninsula, Capewell (1975) describes in detail the folding style that occurs across the strike of the Coomnacronia Fault in the areas close to the three lakes of Coomasahrn, Coomaglaslaw and Coomnacronia (Fig 2.31). At Coomasahrn, Capewell (1975) notes twelve folds with subvertical to 80° axial planes dipping to the south east and with flanks dipping mostly 30° but some also up to 70° in less than 2 km across strike. Further north, across strike, Capewell (1975) describes 11 folds at the corries of Coomaglaslaw and Coomnacronia and describes how the folding style changes, where there is overturning with the northern limbs of folds going from vertical to 20° overturning dip. The southerly limbs dip at about 30° and the axial planes are 60° to the south east (Capewell, 1975). A cross section showing the relationship of the Coomnacronia Fault to the Portmagee anticline is shown in Fig 2.35. Close to this area, north of the Coomnacronia Fault in Kells Quarry fold axial planes dip 45° to the south or south east (Capewell, 1975). In Kells Bay (Fig 2.31) the fold axial plane are subvertical with limb dips of usually no more than 30°. As previously discussed, in relation to the Variscan front, there is a zone of tilted folds that runs along the northern coast of the Iveragh Peninsula and may be structurally part of the foreland to the north (Capewell, 1975; Fig 2.32). Overturning of folds has also been observed further to the east near to Kilarney (Sanderson, 1984). There are quartz slickenside fibres on bedding surfaces of folds indicating that flexural slip has occurred (Bresser and Walter, 1999). Slickenside fibres are not always perpendicular to the fold axial planes, and their relative orientation may be a result of periclinal fold formation during olique convergence (Bresser and Walter, 1999).

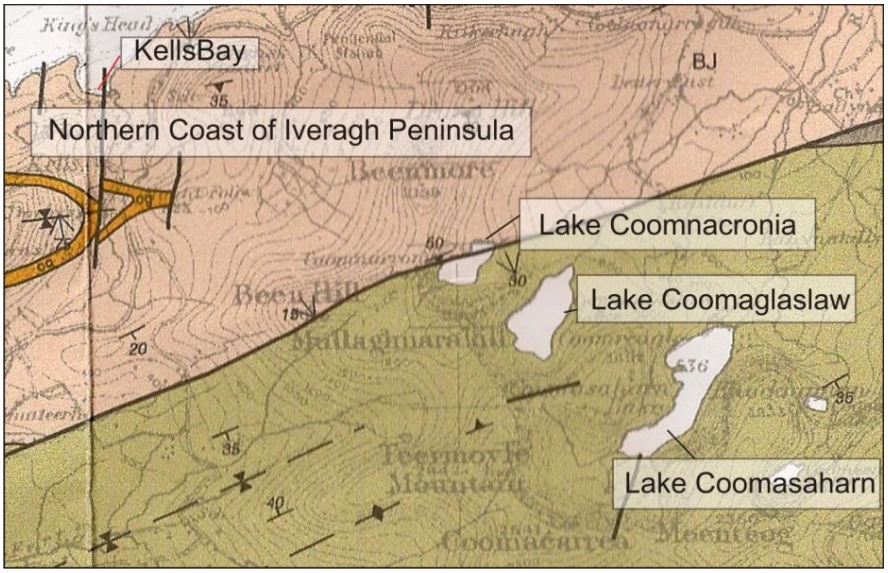

Figure 2.31 Left Shows the area of Lake Coomnacronia and Kells Bay on the northern coast of the Iveragh Peninsula. Modified from the Geological Survey of Ireland Sheet 20 (Pracht, 1996).

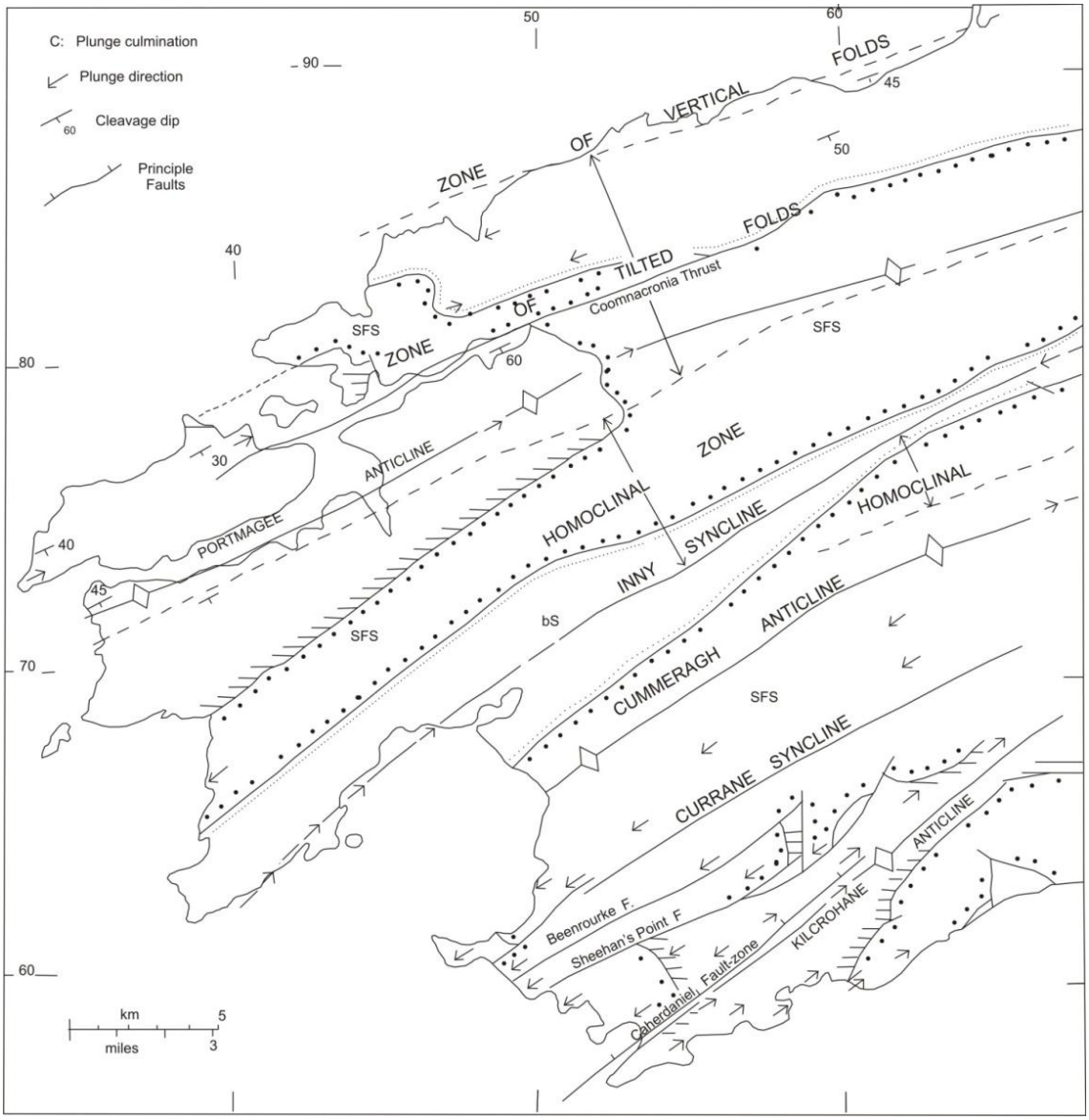

Figure 2.32 Shows the anticlines and synclines on the Iveragh Peninsula and the zone of tilted folds and the zone of vertical folds to the north of the Peninsula. There are also some records of gently dipping cleavage shown on the diagram (redrawn from Capewell, 1975).

2.21 Faulting in the Munster Basin

Sanderson (1984) describes two main types of faults in the Munster Basin: Strike faults which formed early in the deformation history and cross faults which formed later in the deformation history. Strike faults are numerous and lie parallel to the orogenic strike (Naylor et al., 1981; Reilly and Graham, 1972; Naylor, 1969) and some strike faults have reverse displacement (Naylor, 1978; Naylor and Sevastopulo, 1979; Naylor et al., 1981). Three types of strike faults have been described by Sanderson (1984):

1) Early basin development faults which were normal pre-tectonic faults, cited at the northern margin of the Munster Basin and probably had an effect on the location of the Variscan front (Sanderson, 1984).

2) Low angle listric thrust faults which are found locally with reverse movement to the north and the south (Sanderson, 1984; Cooper, 1984).

3) E-W dextral strike slip faults which occur on the Iveragh Peninsula (Capewell; 1957) and on the Beara Peninsula to the south (Reilly and Graham, 1972; Sanderson, 1984).

Cross faults which generally trend under 045° and cross cut folds are thought to have formed late in the deformational history (Sanderson, 1984). However, these faults have also been known to compartmentalize folding (Philcox, 1964). Cooper et al. (1984) use McClay's (1981) definition of a thrust fault being a 'map scale contractional fault' and considers that many of the previously termed strike faults (Naylor et al., 1981; Reilly and Graham, 1972) are in fact thrust faults. Based on balanced cross sections from locations towards the middle and eastern part of the Munster Basin, Cooper et al. (1984) shows that thrust faults are as significant in orogenic shortening as folding. There are also a number of minor northward propagating thrusts within the Munster Basin typical of a thrust front (e.g. Cooper et al., 1984). In the area between Kilarney and Mallow, major thrusts typical of a thrust front are present but there is no existence of thrusts east of Mallow, which is a result of the stratigraphic level of the sole thrust (Cooper et al., 1984). In general, Cooper et al. (1984) suggest that there is limited exposure of major thrusts. Towards the west, reverse faults are considered to be high angle extensional structures that have been subsequently reactivated (Price and Todd, 1988; Meere, 1992). Cooper et al. (1984) suggest that minor faults may have acted as boundary structures at

the northern margin of the Munster Basin, based on facies changes, but do not consider them to have been that significant in terms of boundary faulting. Map scale faults of significance around the northern margin are the KMFZ, the Coomnacronia Fault and the Black Lake Fault (Fig 2.33). Bresser and Walter (1999) consider that the basin margin faults of the Munster Basin located at Dingle Bay were reactivated by Variscan deformation. Bresser and Walter (1999) describe some of the major faults as having an orientation of 10-15° clockwise to the orientation of the major folds axes, which they suggest is a result of a combination of strike slip movement on the faults and transpression during fold development. Towards the northern margin, at the Gap of Dunloe, the Black Lake Fault is considered to be a significant crustal scale reverse fault with a dip of approximately 55-60 ° S and a throw of about 1.5-2 km (Meere, 1995). The Black Lake Fault lies to the east of the Coomnacronia Fault (Fig 2.33). In the southern part of the Iveragh Peninsula the faults are sub-parallel to the regional strike (Capewell, 1975). The Caherdaniel Fault Zone (CFZ) consists of NE- SW culmination of fractures, close to the axial trace of the Kilcrohane Anticline and dies out north-eastwards (Capewell, 1975). Given that there is no evidence of thrusting in any of the CFZ, these faults are considered to be post -variscan rotational dip-slip faults formed as a result of tensional rebound subsequent to the main Variscan compressive phase (Capewell, 1975).

2.22 The Killarney Mallow Fault Zone (KMFZ)

The KMFZ is considered to be a Variscan thrust structure (Cooper et al., 1984, 1986; Williams et al., 1989, 1990). It has been suggested by Price and Todd (1988), that the Muckross Fault (Fig 2.33) may have been a transfer zone which linked the KMFZ and the Dingle Bay Lineament. Cooper (1986) and Cooper et al. (1984) describe the KMFZ as a major thrust zone with a 5-7 km of reverse displacement. To the west of the KMFZ (at Kilarney) around 2.5 km of reverse displacement has been estimated (Avison, 1984). The strike of the KMFZ is parallel to the strike of Caledonian inliers in Waterford, Slievenamon, the Galtee Mountains and Central Ireland, and has been suggested to be a reactivated Caledonian Fault (Price and Todd, 1988). Williams et al. (1990) however, dispute Price and Todd's (1988) model for pre-existing Caledonian control on the extensional aspect of the KMFZ, suggesting that the KMFZ in fact has a more Variscan orientation than Caledonian. Williams et al. (1990) disagree with Price and Todd's (1988) description of the KMFZ being a reactivated normal fault. Williams et al. (1990)

argue that the KMFZ can only be a thrust fault based on its sinuosity, moderate inclination, SSE dip and NNW verging imbricates both on the hanging wall and the footwall. Williams et al. (1990) also suggest that the lack of alluvial fan deposits along it does not reflect proximity to a marginal structure and also argue that the simplistic SSE palaeoflow directions do not conform to an expected radial pattern associated with a fan deposit. Williams et al. (1990) also find no evidence for soft sediment deformation in the hanging wall of the KMFZ as proposed by Leeder (1987) to indicate proximity to a basin margin fault. Willliams et al. (1990) also suggest the KMFZ may be a hanging wall shortcut (Powell, 1987) to the basin margin fault. As previously discussed, the KMFZ has been considered by some authors to be a reactivated basin margin fault (Sanderson, 1984; Price and Todd, 1988; Price, 1989; Meere, 1995 a; Vermeulen et al., 1998-1999, 2000) and marks boundary between lower strain to the north (12-30% shortening), (Ford et al., 1991; Meere, 1995) and higher strain to the south (40-50% shortening), (Meere, 1995; Cooper, 1986). Bresser and Walter (1999) do not consider the KMF to be the location of the Variscan front as described by Gill (1962) as they describe the area to the north of the KMF as being intensely deformed and they suggest that a basal detachment must have existed beneath this area in order for this to have occurred. However, Bresser and Walter (1999) describe the KMFZ instead as a ‘splay of the basal detachment’ and suggest that the KMFZ is a basinal marginal fault that was reactivated during Variscan compression. Vermeulen (1998) agree that the KMFZ is the northern margin of the Munster Basin based on interpretation of VARNET 96 Seismic Line B (Masson et al., 1998, Fig 2.34). Vermeulen, (1998) suggest that Caledonian granites may exist in the basement at the northern margin of the Munster Basin as interpreted from seismic evidence and the change in swing of strike of the KMFZ from an ENE to a more WNW trend may be caused by a deep igneous body (Meere, 1995). Landes (2000) consider that significant Variscan deformation exists in the hangingwall of the KMFZ but do not find a deep trace of the KMFZ from their seismic interpretation.

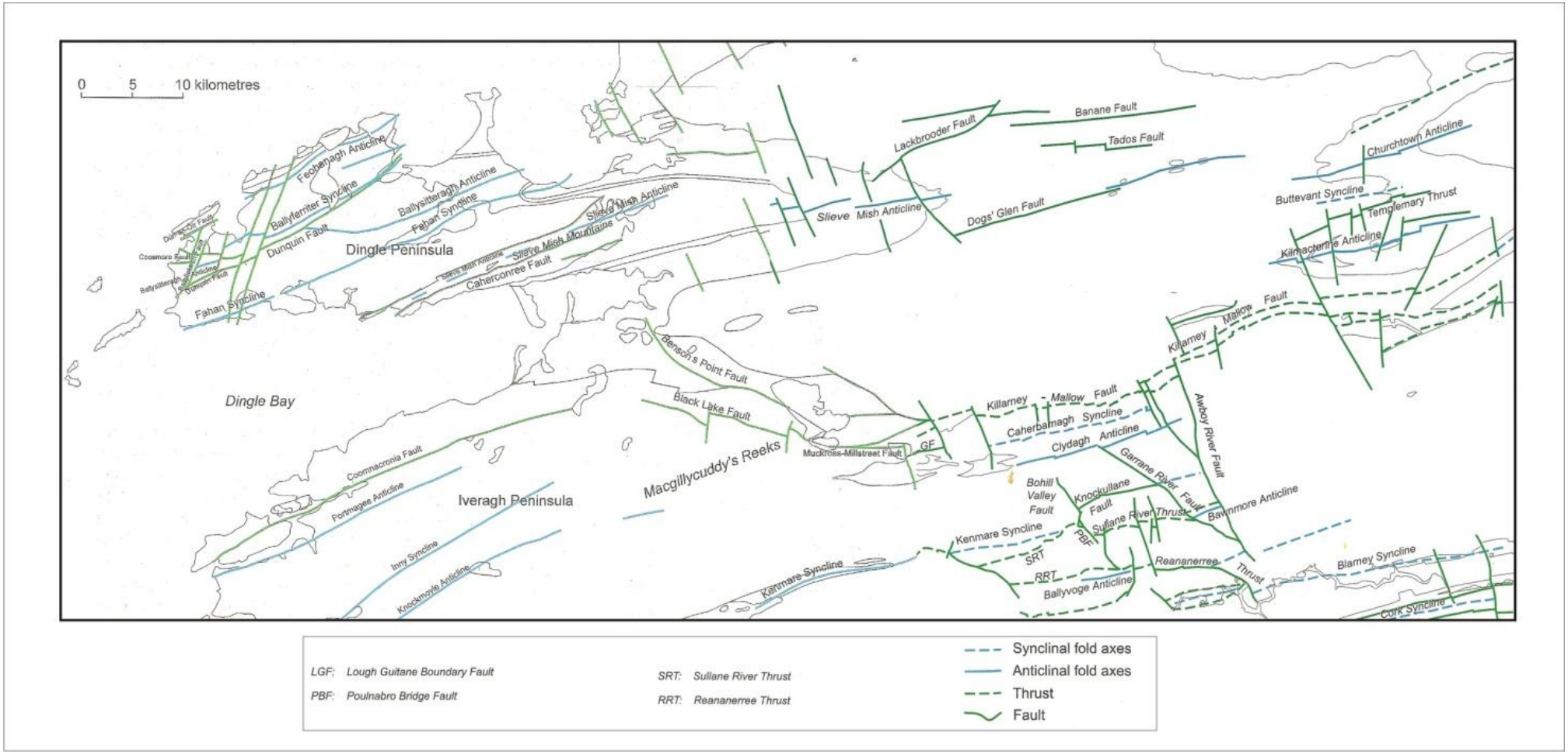

Figure 2.33 Shows the Coomnacronia Fault, the Black Lake Fault, the Muckcross-Milstreet Fault and the Kilarney Mallow Fault and other structures on the Iveragh Peninsula and Dingle Peninsula-compiled from Pracht (1996, 1997)

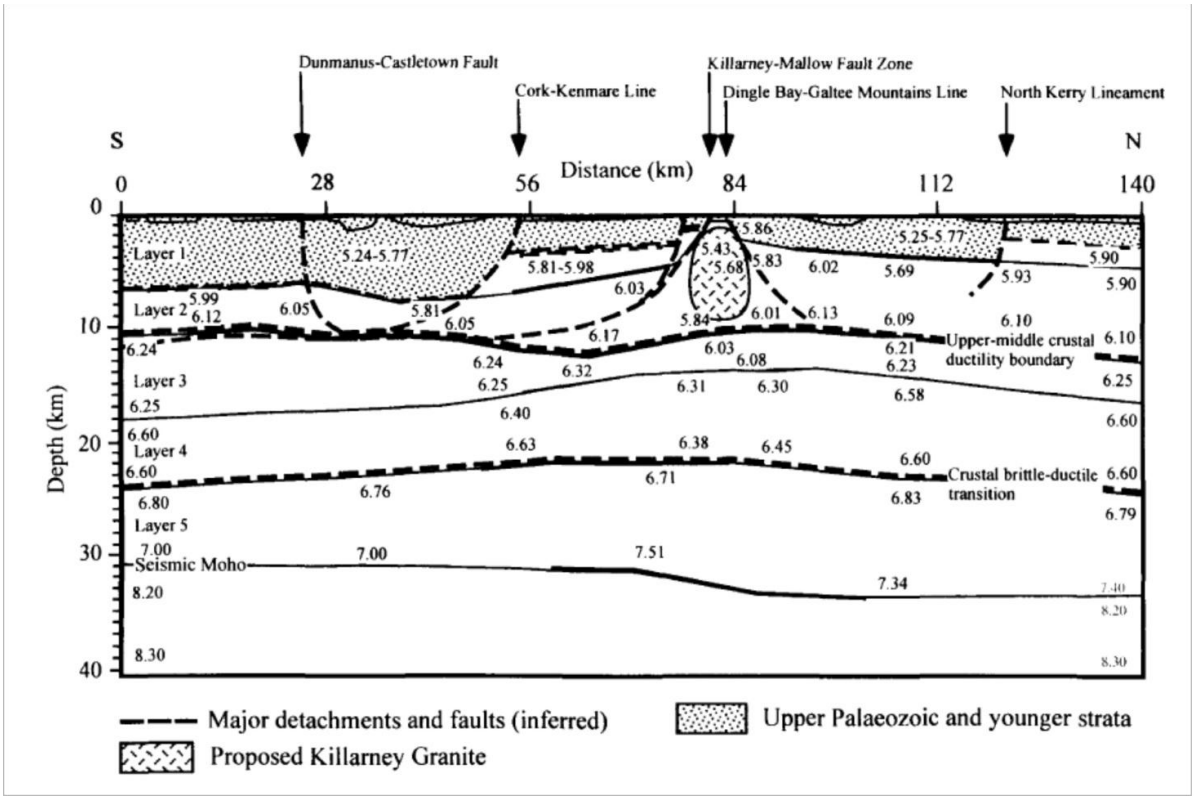

Figure 2.34 A (2D) seismic interpretation (Vermeulen, 1998) of Varnet-96 Line B (after Masson et al., 1998). The location of the south dipping KMFZ and the north dipping Dingle Bay Galtee Mountains line are shown.

2.23 The Coomnacronia Fault (CF)

The Coomnacronia Fault (CF) lies towards the northern part of the Munster Basin and laterally to the west of the KMFZ (Fig 2.33). The CF is inferred to continue down the Ferta Valley, paralleling the Valentia River and as far as Glanleam on Valentia Island (Capewell, 1975). The CF has been described as as a steep angle thrust that crops out on the northern limb of the Portmagee Anticline and forms the boundary between the St. Finans Sandstone Fm. and the Ballinskelligs Sandstone Fm. (Fig 2.35; Capewell 1975). As discussed in section (2.20), the dip of the fold axial planes is observed to decrease from south to north in the vicinity of the CF (at Lake Coomnacronia by Capewell, 1975). Marked Bouger and filtered gravity signatures have been observed at the CF (Morris, 1980; Ford et al., 1991; Readman, 1997; cited by Williams et al., 2000). Towards the east on the footwall of the CF the basement is shallow (Masson et al., 1998). Seismically this has been interpreted as a buried granite body (Masson et al., 1998; Vermeulen et al., 1998, 1999). The Keel Tuff and the Enagh Tuff beds which

have been previously correlated (Russel, 1984; Stossel, 1993; Graham et al., 1995; Williams et al., 1997) are found at different stratigraphic levels across the CF and can be used in correlating the lithostratigraphy across the CF (Williams et al., 2000). The Keel and the Enagh Tuffs have the same $^{207}Pb/^{206}Pb$ mean ages and very similar REE patterns and are thus interpreted to have originated from the same magmatic system representing one explosive event (Williams et al., 1997, 2000). The Keel-Enagh Tuff has been dated by Williams et al. (2000) at 384.9 +_0.4 Ma. To the south of the CF, the Keel tuff is found close to Keel Bay on the south western side of the Iveragh Peninsula. This 5.1 m thick tuff bed lies in the Valentia Slate Fm., 766 m below the base of the St. Finans Sandstone Fm. (Williams et al., 2000). The Enagh Tuff is 11.6 m thick (Russell, 1984) and is located in northeast Iveragh in the footwall of the CF (Russell, 1984, Williams et al., 1987) in the Ballinskelligs Fm. at the base of the St. Finans Sandstone Fm. (Williams et al., 2000). The Keel-Enagh Tuff is located at the base of the St. Finans Sandstone Fm. to the north in the footwall of the CF, but occurs midway up the Valentia Slate Fm. to the south of the fault (Fig 2.36; Williams et al., 2000). This is achieved by major south thickening of the St. Finans Sandstone Fm. south of the CF (Fig 2.36, Williams et al., 2000). Based on this major southward stratigraphic sedimentary thickening, the CF is interpreted as a major intrabasinal extensional structure (Williams et al., 2000; Fig 2.36). However, Williams et al. (2000) do account for the outcrop pattern of the Valentia Slate Fm. to the north and the south of the fault as being due to some element of reverse displacement (approx 2.2 km).

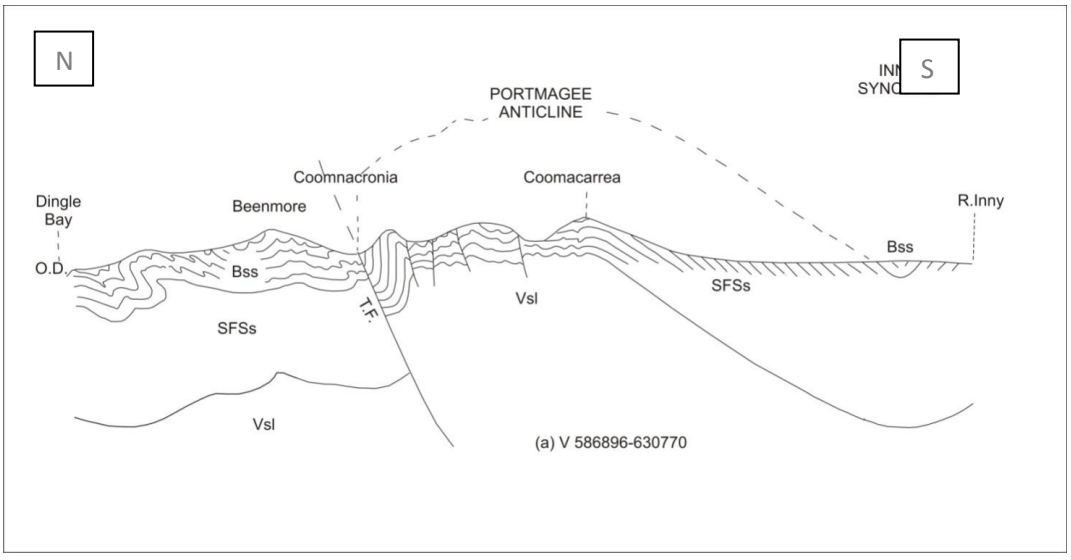

Figure 2.35 The Portmagee Anticline and the CF Redrawn and modified from Capewell., (1975). Bss = Ballinskelligs Sandstone Fm., SFSs = St. Finans Sandstone Fm. Vsl = Valentia Slate Fm.

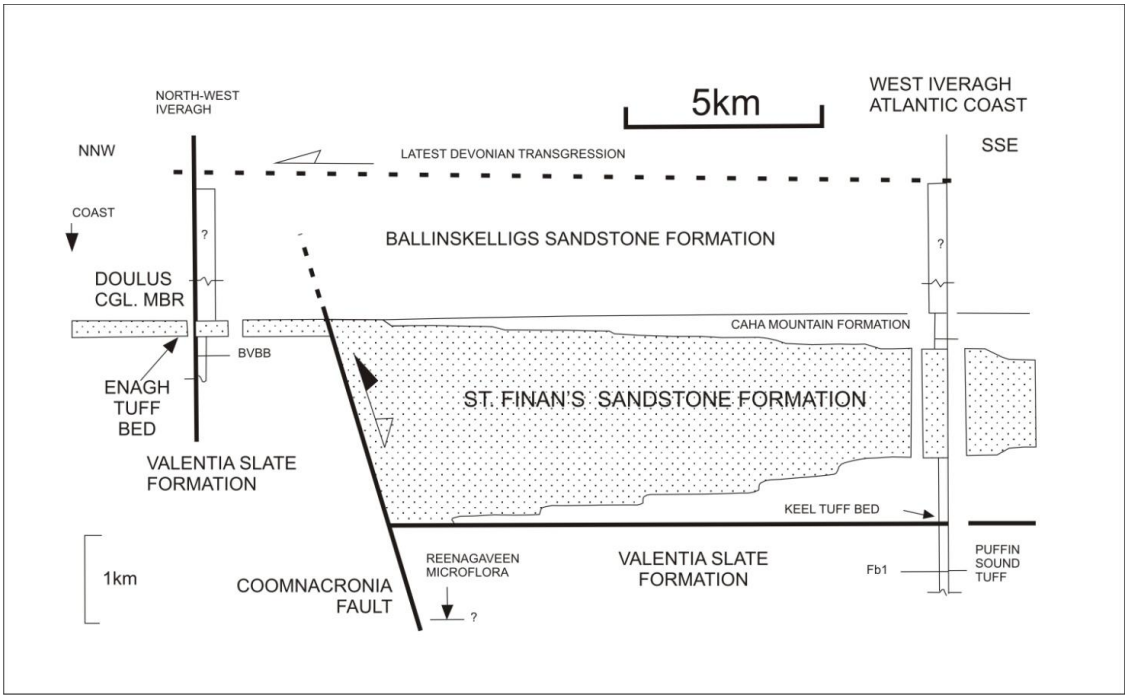

Figure 2.36 The CF and the stratigraphic relationships on the Iveragh Peninsula based on correlative dating of the Keel-Enagh Tuff. Williams et al. (2000) suggest that the CF is a major intrabasinal structure. Redrawn from Williams et al. (2000).

2.24 Boudinage

There is boudinage in West Cork (Coe, 1959) that has been interpreted to result from strike parallel extension (Sanderson, 1984). Shearing of boudinage is noted at Bantry Bay and may be a result of dextral shear (Bresser and Hilgers, 1996).

2.25 Veining

Sanderson (1984) described six main types of veins in the Irish Variscides:

1) Bedding parallel slickensides which are not common in Devonian rocks but are more frequently found in Carboniferous rocks are often folded by the main cleavage and form as a result of flexural slip folding (Sanderson, 1984)

2) Early extensional veins which are more common on the Beara Peninsula and are often strongly folded by cleavage and therefore predate cleavage. These veins are generally N-S trending and steeply dipping. They are a result of strike parallel extension that occurred prior to cleavage formation (Sanderson, 1984)

3) Late steep extension veins which formed along joints which cross cut cleavage, but some of these veins also minorly deflect some local cleavage. Late steep extension veins

are a result of a late tectonic extension that occurred throughout cleavage development. Both early extensional veins and late steep extensional veins indicate strike parallel extension prior to and during the formation of cleavage (Sanderson, 1984).

4) Flat extension veins which occur in steeply dipping sandstone beds as a result of subvertical extension (Sanderson, 1984).

5) Inclined extension veins which are a result of a combination of subvertical extension and E-W dextral shear. These veins are an intermediate type of vein between the flat extensional veins and the steep extensional veins (Sanderson, 1984).

6) E-W veins which occur along faults and joints and may have formed at the same time as folding and cleavage (Sanderson, 1984).

Part Five: Stratigraphy

2.26 Stratigraphy of The Iveragh Peninsula

The ORS group of Iveragh was first mapped by Jukes (1861) and consists of four main formations; the Valentia Slate Fm. (3200 m thick; Capewell, 1975), the St. Finans Sandstone Fm. (2160-2440 m thick; Capewell, 1975), the Ballinskelligs Sandstone Fm. (over 1180 m thick) and the Lough Acoose Sandstone Fm. (1000 m, e.g. Capewell (1975; Pracht, 1996; Fig 2.37). The base of the ORS is not exposed on the Iveragh Peninsula (Capewell, 1975; Williams et al., 1989). All three formations found on the Iveragh Peninsula are a result of a fluvial environment of deposition, evidence being the occurrence of channel scours, unidirectional palaeocurrents, ripples and dessication cracks (e.g. Russell, 1978)**.**

The lowest formation on the Iveragh Peninsula is the Valentia Slate Fm. which consists of fine and medium grained purplish/grey and green/grey siltstones with axial planar cleavage and purple and purple/grey quartzitic sandstones (Capewell, 1975). The Valentia Slate Fm. coarsens upwards with the occurrence of an increasing proportion of cross-laminated fine grained sandstones and coarse siltstones (Russell, 1984). It has been suggested by Capewell (1975) that conglomerates found within the Valentia Slate Fm. on the north coast of Valentia Island at Coosagauna and Reasaclagh may be a thin continuation of the Inch Conglomerate which is interpreted as a piedmont deposit.

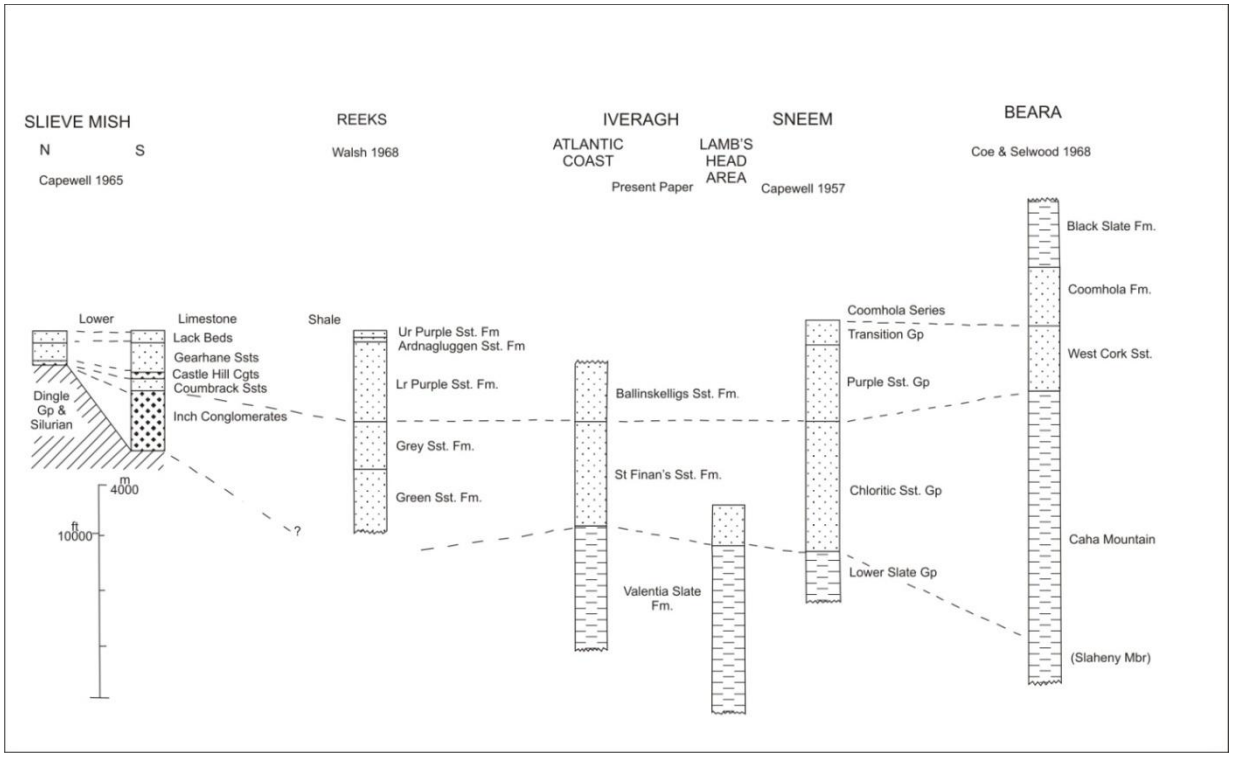

Figure 2.37 Stratigraphy of Slieve Mish, Iveragh and Beara and the lateral equivalents of the Valentia Slate Fm., the St. Finans Sandstone Fm. and the Ballinskelligs Sandstone Fm. Redrawn from Capewell, (1975).

The St. Finan's Sandstone Fm. lies conformably upon the Valentia Slate Fm. and consists of grey medium-grained sandstones and purple-grey/green siltstones (Capewell, 1975). The St. Finan's Sandstone Fm. is interpreted by Walsh (1968) and Graham (1983) as a fluvial deposit with occasional lacustrine deposits. The St. Finan's Sandstone Fm. found in the western part of the Iveragh Peninsula represents an initial fluvial influx (Capewell, 1975). In the Iveragh Peninsula this first fluvial influx is represented by the St. Finan's Sandstone Fm. (Capewell, 1975), and to the east by the Chloritic and Gortanimill Fms. (Capewell, 1965; Horne, 1974). A Fransian age has been suggested for the St. Finans Sst, based on palynological data from Moll's Gap (Higgs and Russsell, 1981). The base of the St. Finans Sandstone Fm. turns into coarse sandstone and is located just south of Keel Strand (Capewell, 1975). The St. Finans Sandstone Fm. is the lateral lithostratigraphical equivilant of, and grades eastwards into, the Green Chloritic Sandstone Fm. (or Glenflesk Chloritic Sandstone Fm.), (Walsh, 1968; Capewell, 1975; Williams, 1989). The Glenflesk Chloritic Sandstone Fm. is Upper Devonian in age (Williams et al., 1989). The mineral chlorite is responsible for the green colour of this unit. The Glenflesk Chloritic Sandstone Fm. represents 1 of 2

large radius fluvial dispersal systems (Williams, 1989), the other being the Gun Point Fm.

The Lough Acoose Sandstone Fm. overlies the St. Finan's Sandstone Fm. and underlies the Ballinskelligs Sandstone Fm. (Pracht, 1996). This formation consists of grey and purple-grey medium grained sandstones (Pracht, 1996) and reaches a thickness of 1000 m in the Reeks area (Pracht, 1996). To the west this formation thins and is replaced by the St. Finans Sandstone Fm. (Pracht, 1996).

In the west of the Iveragh Peninsula, The St. Finan's Sandstone Fm. passes conformably up into the Ballinskelligs Sandstone Fm. which consists of medium-grained purple sandstones with fracture cleavage with some minor cleaved siltstones (Capewell, 1975). This formation outcrops on the Inny Syncline and on the northern flank of the Portmagee Anticline (Fig 2.36; Capewell, 1975).

The Ballinskelligs Sandstone Fm. also contains the Dolous Head Conglomerate (e.g Pracht, 1996). The Dolous Head Conglomerate member is 30 m thick, clast supported and poorly sorted (Pracht, 1996) and is probably a lateral continuation of the conglomerates found at Reenadrolaun Point, Valentia Island (Capewell, 1975). These conglomerates were deposited as pebbly sheetflood deposits and viscous debris flows (Russell, 1984). Conglomerate members such as the Doulus Conglomerate Membermay have been formed by local movement on the Dingle Bay Galtee Fault zone (Williams et al., 1989).

Part Six: Geology of areas surrounding the Munster Basin- The Dingle Peninsula, South Munster Basin and Kerry Head.

2.27 The Dingle Peninsula

During the Ordovician and the Silurian the area that is now the Dingle Peninsula lay on the Eastern Avalonian microplate on the southern margin of the Iapetus Ocean (Pracht, 1996; Fig 2.10). The Dingle Basin was initiated by transpressional sinistral strike slip movements during Caledonian convergence (Sloan, 1991; Todd, 1989 b; Todd et al., 1988) which involved the closure of the Iapetus Ocean by the docking of eastern Avalonia with Laurentia (e.g. Soper and Woodcock, 1990; Chew and Stillman, 2009). The fill of the Dingle Basin accrued during and just after transpressional docking of

Avalonia with Laurentia (Soper et al., 1987; McKerrow, 1988). The stratigraphy of the Dingle Basin is shown in Figs 2.38 & 2.39. The earliest fill of the Dingle Basin is the Dunquin Group which is of Upper Wenlock to Middle Ludlow age (Boyd and Sloan, 2000; cited by Friend et al., 2000) and consists of siliclastic marine and non marine sediments along with subducted related basaltic and rhyolitic volcanic rocks (Boyd and Sloan, 2000). The Dunquin Group have been deformed during the Caledonian Orogeny (e.g. Pracht, 1996) and passes conformably to ORS in the centre of the basin (Friend et al., 2000) but unconformably at the edges (Holland, 1987; Todd, 1991).

The ORS of the Dingle Peninsula can be divided into Lower-Middle ORS and Upper ORS and consists of the following lithostratigraphic units:

- The Dingle Group (Lower ORS) is the oldest group of the ORS and overlies the Silurian Dunquin Group (e.g. Meere and Mulchrone, 2006). The Dingle Group represents continental sedimentation in a pull apart basin that was approximately 60 km long following a Caledonian trend (Todd et al., 1988).

- The Smerwick Group (Middle ORS) lies at the NW of the Dingle Peninsula unconformably upon the Dingle Group (e.g. Meere and Mulchrone, 2006). The Smerwick Group is Middle to Late Devonian (Todd et al., 1988; Todd, 1989) and represents fluvial and aeolian environments. The Acadian Unconformity on the Dingle Peninsula lies between the Dingle Smerwick Groups and the Pointgare Group (Richmond and Williams, 2000).

- The Caherbla Group (Middle ORS) is eroded from high grade metamorphic basement to the south of the Dingle Bay Lineament (Todd, 2000) and predates the initiation of the Munster Basin (Williams et al., 1997, 2000). The Caherbla Group is a fluvio-aeolian sediment and is post-Acadian (Friend, 2000).

- The Pointgare Group (Upper ORS) is a fluvio-aeolian sediment , is post-Acadian (Friend, 2000) and lies unconformable upon the Dingle and Smerwick Groups (Richmond and Williams, 2000). Both the Smerwick Group and the Pointgare Group are thought to have been deposited in a half graben located on the northern margin of the Munster Basin (Pracht, 1996; Todd et al., 1988).

Subsequent to the deposition of the Smerwick Group and the Pointgare Group, was the deposition of the Slieve Mish Group and contemporaneously the Iveragh Group of the Munster Basin (Pracht, 1996).

- The Slieve Mish Group (Upper ORS) is considered to be coeval with the latest fill of the Munster Basin (MacCarthy, 1990; Williams, 1993). This group is considered to be an ORS deposit marginal to that of the Munster Basin (Pracht, 1996). Higgs and Russell (1981) correlate the Slieve Mish Group on the Dingle Peninsula with the Kerry Head ORS and Munster Basin ORS (Meere and Mulchrone, 2006). The Slieve Mish Group is about 850 m thick (Capewell, 1965; Horne, 1974) and lies unconformably upon the Silurian Dingle Group (Holland, 1987) and the Mid-Devonian Caherbla Group (Horne, 1974). The Slieve Mish Group was deposited in the late Devonian (Higgs and Russell, 1981). The Slieve Mish Group consists of the Lough Slat Conglomerate unit which is composed of cross bedded sandstones with quartz, jasper and quartzite clasts (Capewell, 1951), the Cappagh Sandstone Fm. which is a fluvial-lacustrine sandstone and the Lack Sandstone Fm. which is a marginal marine fluvial sandstone (Meere and Mulchrone, 2006).

The Dingle Basin lies just to the south of the Iapetus Suture (Woodcock and Strachan, 2012) and is bound to the north by the North Kerry Lineament and to the south by the Dingle Bay Lineament (Fig 2.39; Todd, 2000). The Dingle Peninsula has undergone Caledonian, Acadian and Variscan deformation (e.g. Todd, 2015). There are some small-scale Caledonian Folds in the last formation of the Dunquin Group (the Derrymore Glen Fm.), (Pracht, 1996; Parkin, 1976 a). It has been concluded that Acadian transpression during the Lower to Middle Devonian is responsible for the main penetrative cleavage event on the Dingle Peninsula, below the Acadian unconformity (Meere and Mulchrone, 2006). This Acadian cleavage is found to transect local fold axes in an anticlockwise orientation which is a result of dextral transpression of the Dingle Basin, fitting with the Acadian Orogeny kinematics (Meere and Mulchrone, 2006).

Above the Acadian unconformity, there is a weak disjunctive steeply dipping cleavage which is Variscan (Meere and Mulchrone, 2006). Variscan fold axial traces on the Dingle Peninsula lie ENE-WSW and are approximately parallel to the previous Acadian

trend (e.g. Meere and Mulchrone, 2006). Pressure solution cleavage in all of the ORS of Dingle had traditionally been considered to have formed during Variscan deformation at the end of the Carboniferous (Parkin, 1976; Todd, 2000). The Variscan cleavage gently overprints the earlier Acadian cleavage below the unconformity and is the only cleavage present in the upper ORS of the Dingle Peninsula (Meere and Mulchrone, 2006). Variscan cleavage is found in the Upper Devonian Slieve Mish Group rocks and is a minimal fracture cleavage (Parkin, 1976). Cleavage is absent in the eastern end of the Dingle Peninsula (Capewell, 1965; Hudson et al., 1966; Meere, 1995). Cleavage in the Slieve Mish Group is disjunctive and occurs more so in the western outliers of the Slieve Mish Group on the Dingle Peninsula (Meere and Mulchrone, 2006). Variscan cleavage on Bulls Head Peninsula occurs in the Upper ORS (Slieve Mish Group) and is disjunctive and is steeply dipping (Meere and Mulchrone, 2006; Fig: 2.40).

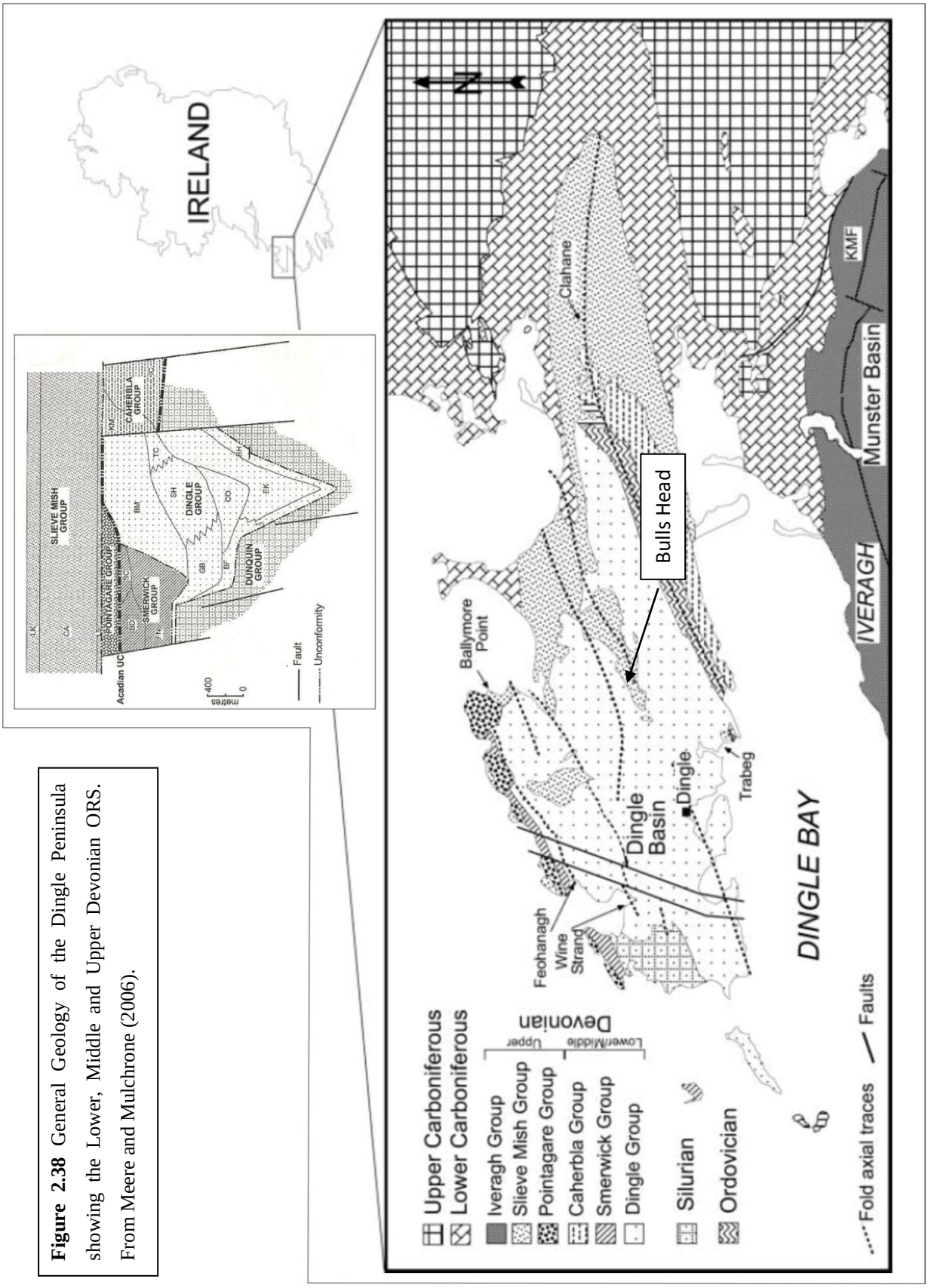

Figure 2.38 General Geology of the Dingle Peninsula showing the Lower, Middle and Upper Devonian ORS. From Meere and Mulchrone (2006).

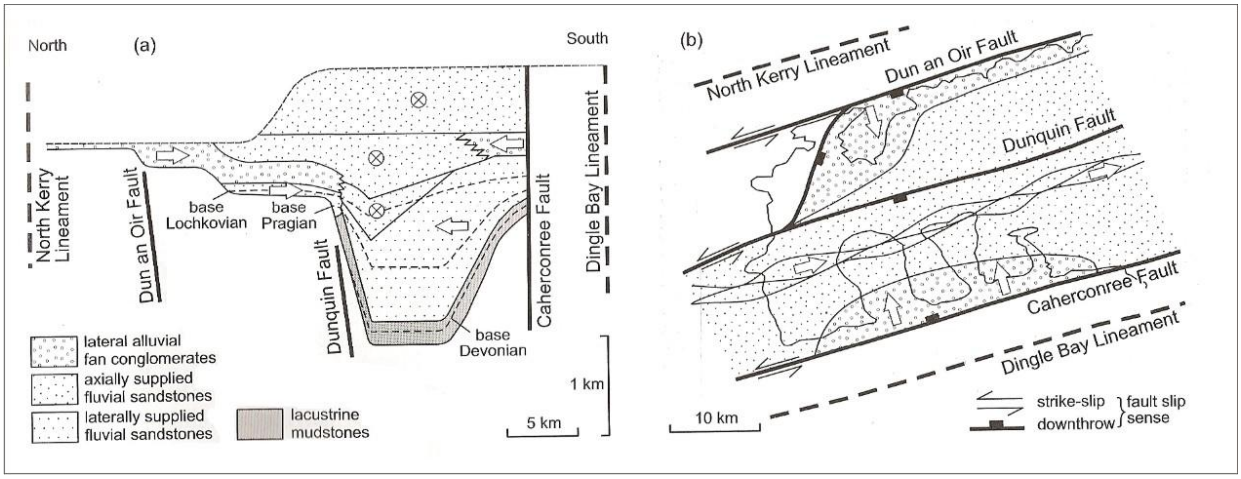

Figure 2.39 a) Facies of the Dingle Basin b) the Palaeogeography during the early Emsian for the Dingle Basin (after Todd 2000, from Woodcock and Strachan, 2012).

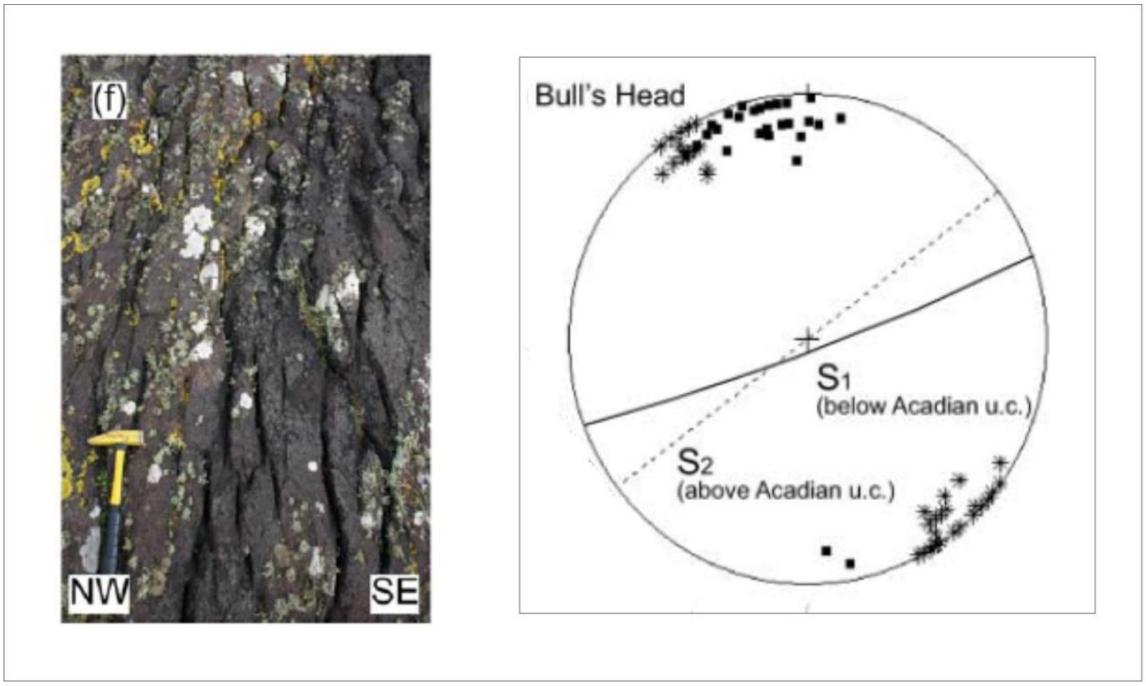

Figure 2.40 a) Spaced disjunctive steeply dipping Variscan cleavage found in Upper ORS (Slieve Mish Group) at Bulls Head (Fig 2.38), Dingle Peninsula B) plot of cleavage below and above Acadian unconformity at Bulls Head (From Meere and Mulchrone, 2006).

2.28 Kerry Head

The ORS of Kerry Head consists of Upper Devonian ORS sandstones and mudstone beds from northward sourced laterally migrating river channels and floodplains (Diemer, 1987). There are three main ORS formations: the Glandahalin Fm. (> 321m thick, mainly Famennian in age), the Inshaboy Fm. (174m thick, Famennian-Tournaisian in age), and the Kilmore Fm. (208 m thick), (Fig 2.41; Diemer, 1987).

There is one Lower Carboniferous formation, the Clashmelcon Fm. (> 88 m thick) which is a lower limestone shale. Kerry Head is an east west trending anticline (e.g. Diemer, 1987). There is also some minor folding along with small inclined thrusts (Diemer, 1987). An unusual pattern of north verging folds on the northern limb and south verging folds on the southern limb exists on Kerry Head (Diemer, 1987). Kerry Head is a major upright noncylindrical fold (Diemer, 1987) plunging 20 ° to the west with a general dip of 25 ° of bedding on the limbs. There is an upright ENE-WSW trending cleavage which is developed in the argillacious sandstones in Kerry Head (Diemer, 1987). At Ballyheige, the Kilmore Sandstones consist of yellow, brown and olive sandstones and green siltstones with some minor red siltstones (Diemer, 1987).

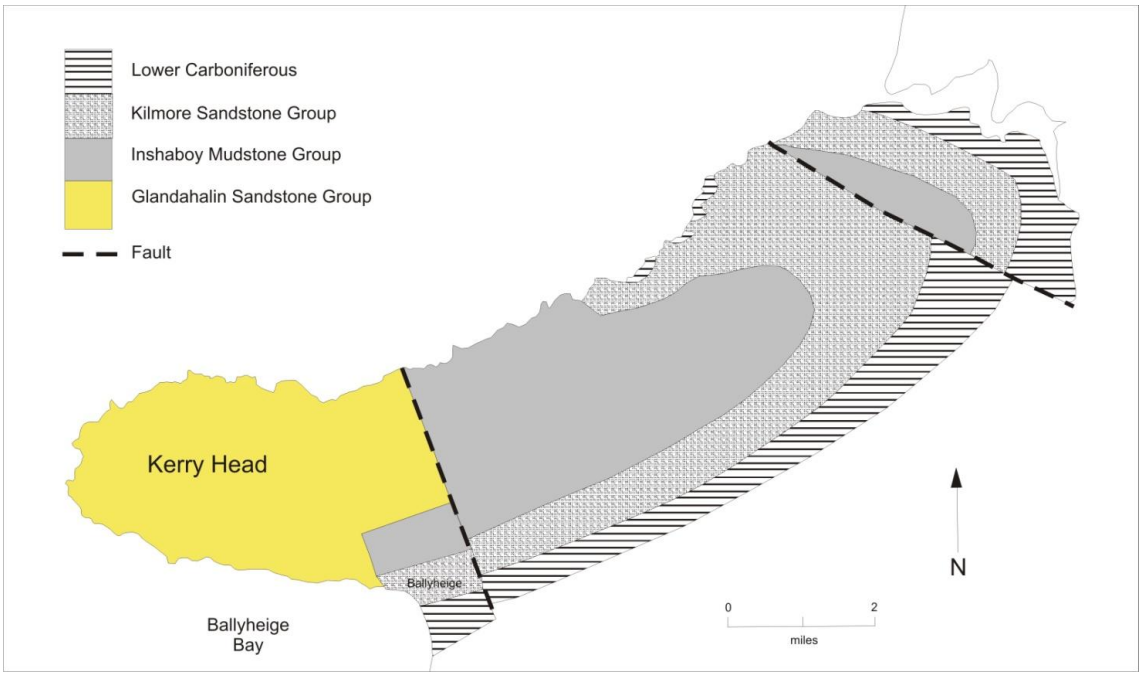

Figure 2.41 Geological map of Kerry Head. From Diemer (1987).

2.29 The South Munster Basin (SMB)

During most of the Carboniferous, Britain and Ireland were submerged under a shallow sea - the Euramerican Seaway (e.g. Woodcock and Strachan, 2012). The Carboniferous in Ireland is represented by the SMB and by a carbonate shelf area in the centre and the north (e.g. the Shannon Trough, the Dublin and Ulster Basins; Woodcock and Strachan, 2012). Parts of the SMB can be correlated with some of the Irish Midlands Carbonates which are Waulsortian in age (Williams et al., 1989). In south west Ireland, the ORS of the Munster Basin passes conformably upwards from Upper Devonian to Lower

Carboniferous marine clastic sequence observed at Sneem (Capewell, 1957; Higgs and Russel, 1981), Kenmare (Husain, 1957) and Kilarney (Walsh, 1968; Higgs et al., 1988). The beginning of the Carboniferous and the initiation of the SMB witnessed the cessation of alluvial conditions in the Munster Basin (Williams et al., 1989), except some minor terrigenous influx from the north and north-east (MacCarthy, 1990). This onset of marine conditions was brought about by a marine transgression from the south (MacCarthy and Gardiner, 1987). The top of the Toe Head Fm. which consists of grey-green sandstones and overlying marine grey heterolithic beds (Graham, 1975), represents the onset of marine conditions (Cotter and Graham, 1991). The SMB (George et al., 1976) is considered to be Devonian to Namurian in age (Clayton et al., 1980; Naylor et al., 1983) or late Devonian-Strunian in age (MacCarthy, 1987). The northern boundary of the SMB is represented by the Cork-Kenmare Line (Jukes, 1864; Naylor, 1969, Fig 2.42) which may be controlled by basement faulting (Naylor & Sevastopulo, 1979). The SMB has been described as a dextral transtensional half graben by Williams et al. (1989). The SMB consists of shallow marine, marine shelf and deep basinal sediments (MacCarthy and Gardiner, 1987) consisting of Strunian marine sandstones and mudrocks (Clayton et al., 1979). The SMB has undergone Variscan defomation at the end of the Carboniferous (e.g Pracht and Sleeman, 2002) and lies in Cooper's (1986) Zone 1 of the Irish Rhenohercynian. In the SMB there are large scale Variscan folds, thrust faulting with axial planar cleavage (e.g. Cooper et al., 1984; Pracht and Sleeman, 2002). In the SMB, a markedly different relationship of cleavage to bedding than is typical of the Munster Basin and elsewhere in the SMB is observed at the Galley Head peninsula (Ford, 1990). In this area there is secondary phyllosillicate growth along the cleavage planes, consisting of chlorite and muscovite representing upper anchizone to lower greenschist metamorphism (Ford, 1985). Ford (1990) argues a more complex deformational history for findings at the Galley Head area and suggests that there has been a component of early layer parallel shortening resulting in a weak cleavage. Ford (1990) suggests that folding occurred prior to cleavage development on an overturned limb of a periclinal fold pair at Galley Head which has resulted in bedding parallel cleavage (Fig. 2.43; Ford and Bamford, 1990) which has not been observed in other folds to the north or within the Irish Variscides and recognises an early cleavage, a main cleavage and a late cleavage as three distinct developments. Ford (1990) has linked southward facing and overturned folds to proximity to the southern margin of the SMB and suggests that this is caused by hinterland escape of the basin

fill. Ford (1990) accounts for structural facing direction in the southwest due to the geometry of the basin rather than transport direction, which was to the north.

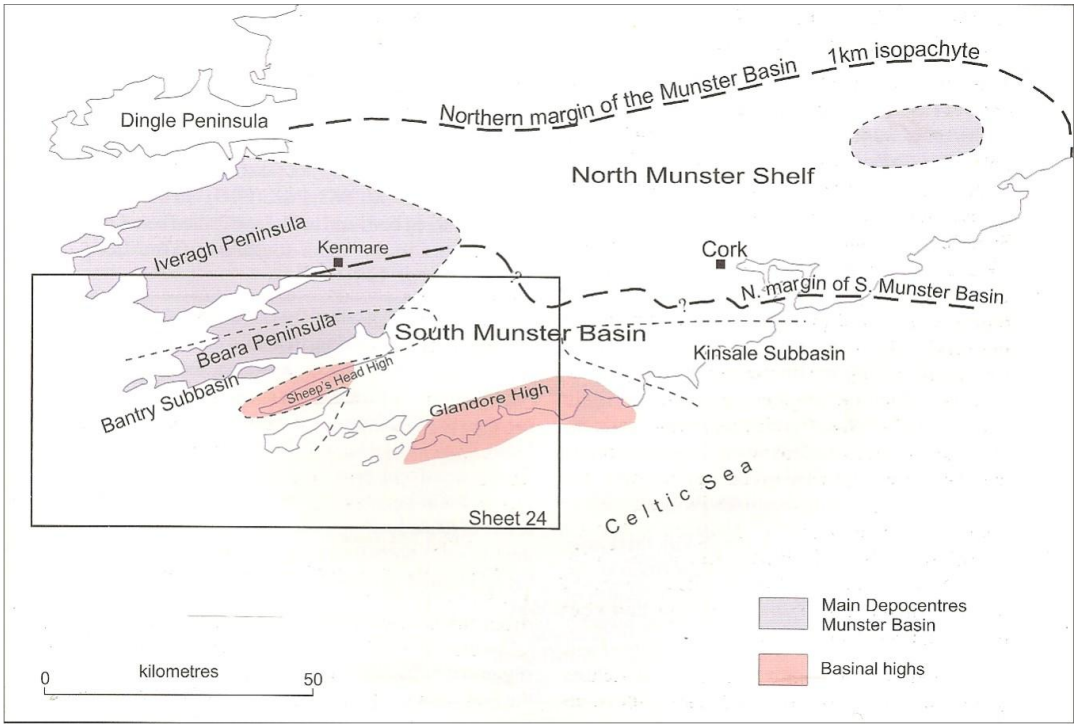

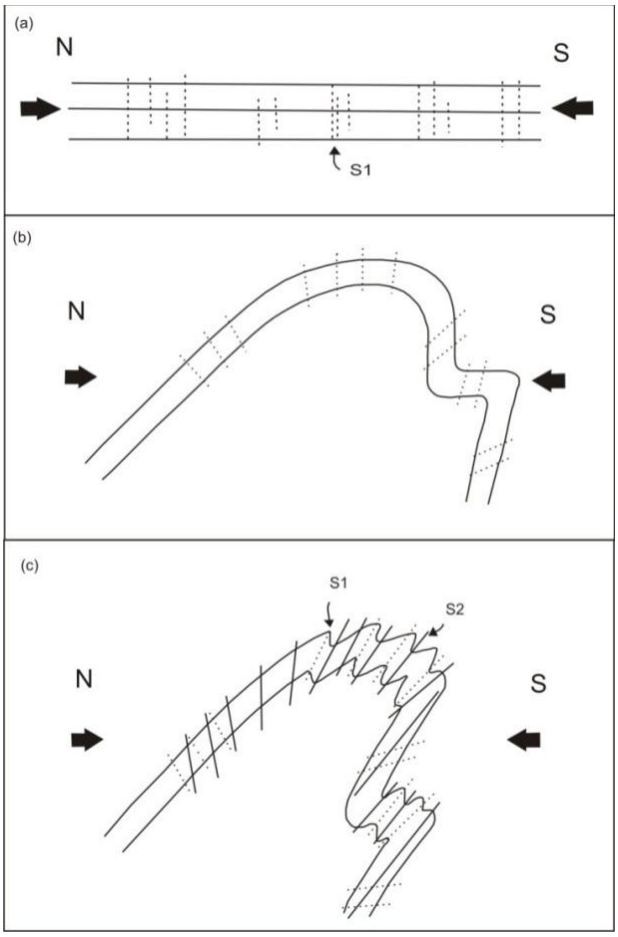

Figure 2.42 Above shows the location of the South Munster Basin (SMB). (From Pracht and Sleeman, 2002)

Figure 2.43 Left Shows the deformation history and cleavage formation of the Kilkeran Anticline. a) initial amounts of minor LPS (S1) b) Buckling. C) Main cleavage formation (S2) either parallel to or at a low angle to bedding on southern limb. Redrawn from Bamford and Ford (1990).

Chapter 3:
Principles of AMS

Chapter 3: Principles of AMS.

Part one: Introduction, Principles of AMS and Methodology

3.1 Introduction

The anisotropy of magnetic susceptibility (AMS) has been used to determine petrofabrics in a range of rock types (e.g. Hrouda, 1982; Borradaile, 1998; Jezek and Hrouda, 2002; Borradaile and Jackson, 2010). AMS, or magnetic fabric studies, can be used to enhance rock fabric analysis for the purpose of analysing preferred grain orientation and crystallographic preferred orientations, which can lead to interpretations of palaeocurrent directions, magmatic flow paths or strain analysis (e.g. Fuller, 1963; Jackson, 1991; Rochette et al., 1992). AMS has been previously used to study tectonic deformation (e.g. Hrouda, 1976, Rathore and Heinz, 1980; Kligfield et al., 1981, 1982, 1983; Rathore and Henry, 1982; Bakhtari, 1998; Mattei et al., 1999; Pares et al., 1999). The magnetic susceptibility of a rock is influenced by the magnetic anisotropies of the individual grains and the alignment of these grains within a rock sample (Tarling and Hrouda., 1993). Thus the AMS signal is controlled by the orientation and distribution of crystals in a rock sample (e.g. Uyeda, 1963; Hrouda, 1982; Stephenson et al., 1986; Borradaile and Henry, 1997). The AMS of individual minerals was recognised as far back as 1899 (Borradaile and Jackson, 2009) and was first measured in 1907 by Voight and Kinoshita. AMS was first used as a petrofabric indicator by Ising (1942) and Graham (1954). Every mineral present in a rock has a magnetic susceptibility (Hrouda, 1982; Rochette, 1987; Borradaile et al., 1987).

3.2 Principles of Magnetic Susceptibility

Magnetisation is caused by the motion of electrically charged particles (e.g. Tarling and Hrouda, 1993). Electrons have magnetisation due to their axial spin and due to their orbital motion around a nucleus (e.g. Tarling and Hrouda, 1993). Magnetic susceptibility is the ease to which a material becomes magnetised in an applied external magnetic field measured in a low field compared to the Earth's Field (Borradaile, 1997). The Kappabridge is an instrument used for AMS analysis, which measures the magnetic susceptibility of samples in weak magnetic fields in the range of 2 A/m to 700 A/m (A = Amperes, m = meters; [www.agico.com]). The magnetic susceptibility (k) of a rock is its intrinsic magnetizability (e.g. Butler, 1992) which is the relationship between the intensity of an applied external field (H) and magnetization (M).

When magnetisation is applied in a low field (< 1 mT; mT = microTesla) the induced magnetisation, M, is not parallel to the applied field H and can be represented by three orthogonal components (Tarling and Hrouda, 1993):

$$M_x = k_{xx}H_x + k_{xy}H_y + k_{xz}H_z$$
$$M_y = k_{yx}H_x + k_{yy}H_y + k_{yz}H_z$$
$$M_z = k_{zx}H_x + k_{zy}H_y + k_{zz}H_z \quad (3.1)$$

Which is equivalent to:

$$M_i = K_{ij}H_j . \quad (i= 1, 2, 3) \quad (3.2)$$

Or:

$$M = KH = K\left(\frac{B}{\mu_0}\right) \quad (3.3)$$

Where:

$$K_{ij} = \begin{bmatrix} k_{xx} & k_{xy} & k_{xz} \\ k_{xy} & k_{yy} & k_{yz} \\ k_{xz} & k_{yz} & k_{zz} \end{bmatrix} \quad (3.4)$$

K_{ij} is the second-order AMS tensor. Where: K is the magnetic susceptibility, M is the magnetic dipole of the induced field per unit volume (in A/m), H is the magnetic field strength (A/m), B is the magnetic field measured in Tesla, μ_0 is the permeability of free space ($4\pi \times 10^{-7}$ henry/m; Tarling and Hrouda, 1993). The magnetic susceptibility (K) is dimensionless in the SI system and has no units (Tarling and Hrouda, 1993).

Based on the above matrices (Equation 3.4), a minimum of six measurement axes are required to resolve six unknown tensor components of the AMS (Fig 3.1; Hext, 1963; Girdler, 1961; Jelinek, 1977; Borradaile and Shipausky, 1995; Owens, 2000 a). The directions must be chosen so as to prevent inversion of matrices and this is achieved using the Girdler (1961) positions (Fig. 3.1).

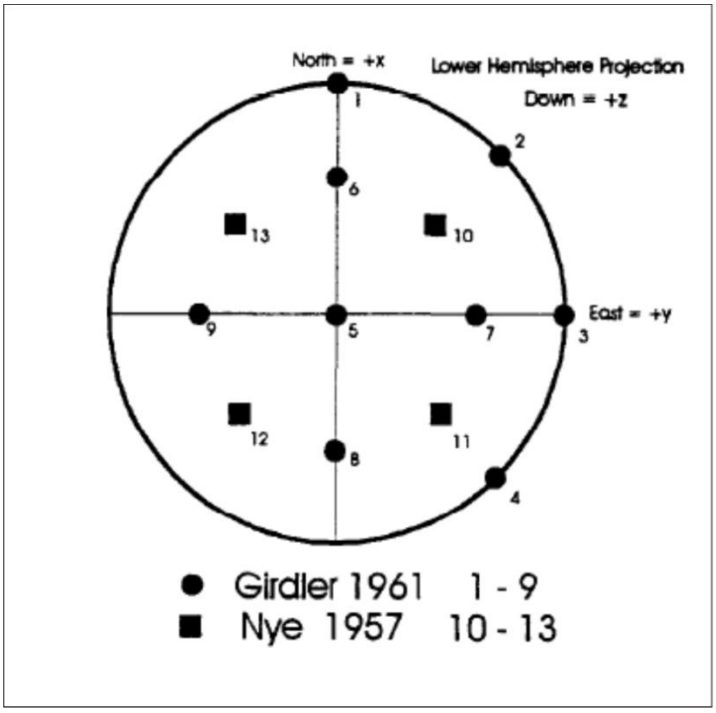

Figure 3.1. A combination of directions 1-9 (Girdler, 1961) are usually used to calculate AMS, and also body diagonal measurements 10-13 (Nye, 1957) may also be used in the case where there is low magnetic susceptibility (Borradaile and Stupavsky, 1995). From Borradaile (1997).

3.3 The AMS Fabric Ellipsoid

AMS can be represented as an ellipsoid with maximum (K_{max} or K1), intermediate (K_{int} or K2) and minimum (K_{min} or K3) principal susceptibilities along its semi-axes (Nye, 1957). The greatest intensity of induced magnetisation runs parallel to the maximum susceptibility axes, K_{max} and the least intensity of magnetisation runs along the minimum susceptibility axes, K_{min} where:

$$K_{max} > K_{int} > K_{min} \qquad \text{(Hrouda, 1982).}$$

K_{max}, K_{int} and K_{min} are usually plotted on equal area stereographs for the purpose of interpretation (e.g. Tarling and Hrouda, 1993). For the purpose of the description of AMS fabrics, three types of ellipsoids are used: prolate, oblate and neutral (Fig. 3.2). A prolate ellipsoid is an ellipsoid that has K_2 and K_3 of approximately equal length and one longer axis, K_1. An oblate ellipsoid has two longer axes of approximately equal length (K_1 and K_2) and one shorter axis (K_3). A neutral ellipsoid also referred to as spheroidal or isotropic and has all three axes (K_1, K_2 and K_3) of approximately equal length (Fig 3.2, b). The AMS ellipsoid is similar to the fabric finite strain ellipsoid, first introduced by Flinn (1965) to describe oblate and prolate fabrics in structural geology.

A Flinn type plot is used to plot the AMS ellipsoid shapes and show their distribution in the oblate and prolate fields (Fig. 3.3).

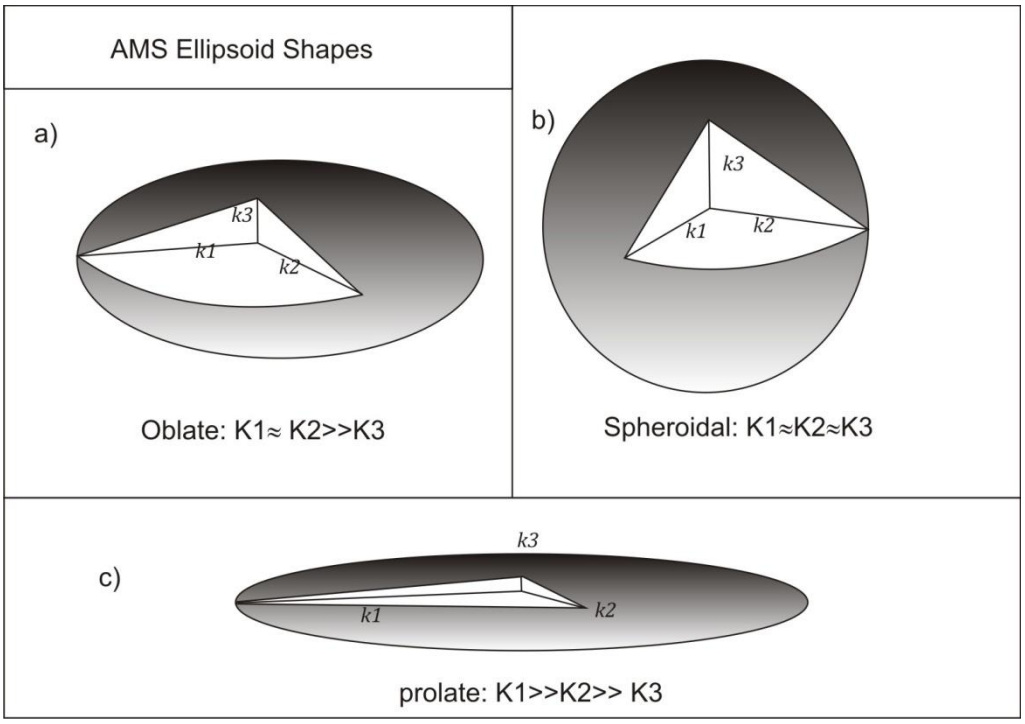

Figure 3.2 Shows three main types of AMS fabric ellipsoid: a) oblate b) spheroidal or neutral and c) prolate. Redrawn from Winkler et al. (1997).

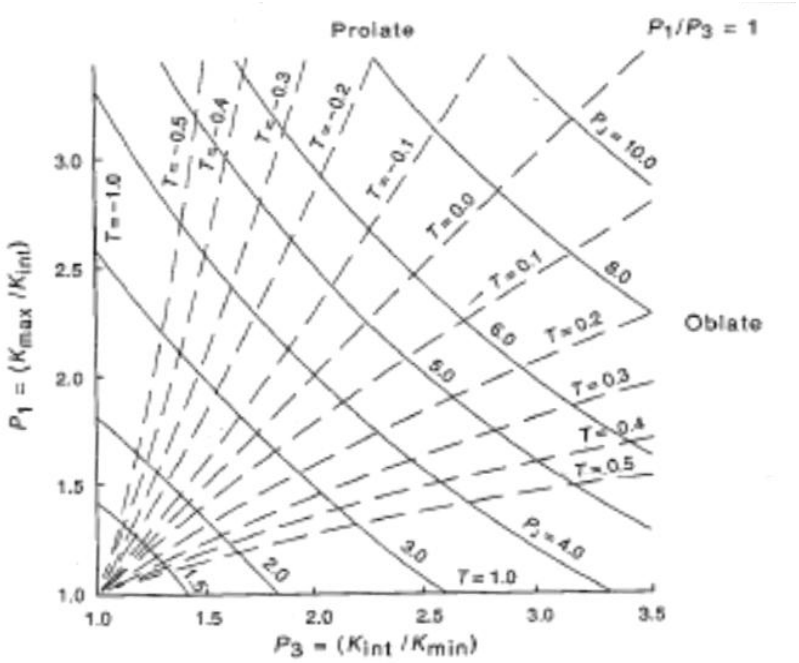

Figure 3.3 A Flinn type plot showing the magnetic lineation (K_{max}/K_{int}) against the magnetic foliation (K_{int}/K_{min}). This plot shows the oblate and the prolate fields of the AMS ellipsoid. (From Tarling and Hrouda, 1993; modified after Flinn, 1962; 1965 a,b).

There are a number of equations derived from the values of K_{max}, K_{int}, and K_{min}, (Tarling and Hrouda, 1993). The most commonly used parameters are; the mean susceptibility, K, the magnetic lineation, L; the magnetic foliation, F; the μ value, the anisotropy degree Pj and the shape parameter, Tj. These parameters are discussed next and used in the AMS analysis (Chapter 5: AMS Results).

The Mean Susceptibility, K_{mean}:

$$K_{mean} = \frac{K_1+K_2+K_3}{3}$$ (e.g. Nagata, 1961; Janak, 1965)

The Magnetic Lineation, L:

$$L = \left(\frac{Kmax}{Kint}\right)$$ (e.g. Borradaile, 1997)

The Magnetic Foliation, F:

$$F = \left(\frac{Kint}{Kmin}\right)$$ (e.g. Borradaile, 1997)

The μ Value.

The μ value determines the degree of oblateness or prolateness of the AMS ellipsoids:

On a Flinn plot (Fig 3.3), the μ value is related to the L (the magnetic lineation) and the F (the magnetic foliation) parameters as follows:

μ = the arctan or $\tan^{-1}$ of L/F (answer needs to be converted from radians to degrees):
or:

$$\mu = (\tan^{-1} L/_F)*(180/\pi)$$

The μ value is the angle between X axis and the line joining the origin (0, 0) to the point (F, L) on the graph (Fig 3.3).

Where $0° < \mu < 45°$ the AMS ellipsoid is oblate (Fig 3.3).

Where 45° < μ < 90°, the AMS ellipsoid is prolate (Fig 3.3).

The Anisotropy Degree/Eccentricity of the ellipsoid, Pj

The magnitude or eccentricity of the ellipsoid is also known as the anisotropy degree and can be described using the Parameter Pj (Jelenik, 1981) where;

$$P_j = \exp\sqrt{\{2[(\eta_1 - \eta_m)^2 + (\eta_2 - \eta_m)^2 + (\eta_3 - \eta_m)^2]\}} \qquad \text{(Jelinek, 1981)}$$

$$\eta_1 = \ln K_1; \eta_2 = \ln K_2; \eta_3 = \ln K_3$$

$$\eta_m = \sqrt[3]{(\eta_1 \cdot \eta_2 \cdot \eta_3)} \qquad \text{(Geometric mean)}$$

The geometric mean needs only to be used when there are differences in the range of values of an order of magnitude (Tarling and Hrouda, 1993).

$$\eta_m = (\eta_1 + \eta_2 + \eta_3) / 3 \qquad \text{(Arithmetic mean)}$$

The arithmetic mean is used by Tarling and Hrouda (1993) as it is adequate for data sets which are of a similar order of magnitude.

The shape parameter, Tj

To describe the shape of the ellipsoid, the shape parameter, T_j is used:

$$T = \left[\frac{2\ln(K_2/K_3)}{\ln(K_1/K_3)}\right] - 1 \qquad \text{(Jelenik, 1981).}$$

When T = +1 the ellipsoid is oblate. When T = -1, the ellipsoid is prolate. When T = 0, the ellipsoid is neutral, (i.e. $K_1 = K_2 = K_3$).

3.4 The Effects of Mineralogy on Bulk Magnetic Susceptibility

AMS is influenced more or less by all of the minerals present (e.g. Borradaile and Henry, 1997). In order to interpret the magnetic fabrics in rocks it may also be important to also consider the effects of grain size and grain relationships (Tarling and

Hrouda, 1993) and mineralogy (e.g. Chadima et al., 2006). Minerals affecting the bulk magnetic susceptibility can be classified into diamagnetic, paramagnetic and ferromagnetic minerals. The mean susceptibility (K_m) may come from a combination of the diamagnetic, paramagnetic and ferromagnetic minerals in relation to the bulk volume (e.g. Siegesmund, 1996).

3.4.1 Diamagnetic Minerals

In diamagnetic materials the electron shell is complete and magnetization is caused by electrons orbiting around the nucleus (Tarling and Hrouda, 1993). Susceptibility is weak and only present in the presence of an applied magnetic field (Tarling and Hrouda, 1993). When a magnetic field is applied to diamagnetic minerals the magnetization produced is in the opposition direction to that of the applied field (Fig 3.4; Tarling and Hrouda, 1993). Diamagnetic minerals therefore have negative susceptibilities in the region of -10^{-5} SI (e.g. Tarling and Hrouda, 1993; Borradaile and Jackson, 2010). Diamagnetic minerals include mainly quartz, calcite and feldspars (Tarling and Hrouda, 1993). Diamagnetic minerals have no remanent magnetisation once the magnetic field is removed (Tarling and Hrouda, 1993; Fig. 3.4). Diamagnetic minerals are considered to be only important magnetic carriers when there is almost a complete absence of ferromagnetic minerals, i.e. less than 0.001% and when less than 10% of the rock is paramagnetic (Tarling and Hrouda, 1993).

Diamagnetic minerals do not change into ferromagnetic minerals during metamorphism, but the initial fabric created by the diamagnetic minerals e.g. quartz can be replaced by paramagnetic or ferromagnetic minerals (Tarling and Hrouda, 1993). The mechanical behaviour of the rock during metamorphism may be controlled by diamagnetic minerals (Friedman and Higgs, 1981).

3.4.2 Paramagnetic Minerals

Paramagnetism is due to the electron spin of unpaired electrons (Tarling and Hrouda, 1993). In paramagnetic minerals the electron shells are incomplete and magnetisation occurs in the same direction as the applied field (Tarling and Hrouda, 1993; Fig 3.4). Susceptibility is weak and only present in an applied magnetic field (Carmichael, 1982). Paramagnetic minerals have positive, low susceptibilities in the region of 10^{-2} to 10^{-4} (S1) (Tarling and Hrouda, 1993; Fig 3.4). Paramagnetic minerals do not retain a remanent magnetisation after the magnetizing field is removed (Tarling and Hrouda,

1993; Fig 3.3). Paramagnetic minerals include biotite, chlorite and muscovite (Tarling and Hrouda, 1993). In rocks containing about 10 % paramagnetic minerals, where the susceptibility is greater than 5 x 10^{-3} (SI), the anisotropy is carried by the ferromagnetic fraction (Hrouda and Kahan, 1991). Only in the absence of ferromagnetic minerals will paramagnetic dominate over diamagnetic minerals, unless they are <1% of the rock (Tarling and Hrouda, 1993). The AMS of rocks displaying a bulk low susceptibility may be controlled by the paramagnetic phyllosillicates (e.g. Borradaile et al., 1986; Rochette, 1987; Hrouda and Jelinek, 1990).

3.4.3 Ferromagnetic Minerals

The magnetic susceptibility of ferromagnetic minerals is positive and large. (Carmichael, 1982). Ferromagnetism occurs in minerals containing Fe where the atomic magnetic moments are strongly aligned with one another (Tarling and Hrouda, 1993). Ferromagnetism is a property of the first transition series of elements. The electron spins have been spontaneously coupled which aligns the spin magnetisations (Tarling and Hrouda, 1993). Ferromagnetic minerals have stronger positive susceptibilities than paramagnetic minerals (Fig 3.4; Tarling and Hrouda, 1993). In ferromagnetic minerals, there is a remnant magnetisation in the absence of an applied external field above temperatures of absolute zero and up to the Curie temperature, Tc of the mineral. Above the Curie temperature, the ferromagnetic material becomes paramagnetic. Ferromagnetic minerals are capable of retaining a permanent magnetisation once the magnetic field is removed (Tarling and Hrouda, 1993). This includes ferrimagnetic and antiferromagnetic minerals which have components of antiparallel magnetisation once the applied magnetic field is removed (e.g. Tarling and Hrouda, 1993; Fig 3.4). The most important ferromagnetic minerals are magnetite and haematite and where both magnetite and haematite exist, magnetite will be the dominant mineral affecting susceptibility as long as it is $\geq$ 0.5% of the iron oxide fraction (Tarling and Hrouda, 1993). Only in the absence or minute concentrations of magnetite do other iron oxide minerals such as goethite, maghaemite and pyrrhotite have importance (Tarling and Hrouda, 1993 based on Hrouda and Kahan, 1991). Magnetite has a high magnetic susceptibility and its grain shape controls AMS as opposed to its crystallographic structure (Borradaile and Henry, 1997). Due to their high susceptibility, ferromagnetic minerals will be the predominant control of the magnetic properties of the sample in cases where they occupy greater than 0.1% volume of the total rock (Tarling and Hrouda, 1993, based on Hrouda and Kahan, 1991). Ferromagnetic grains may also

interact magnetically and may affect the overall magnetism of the rock (Tarling and Hrouda, 1993).

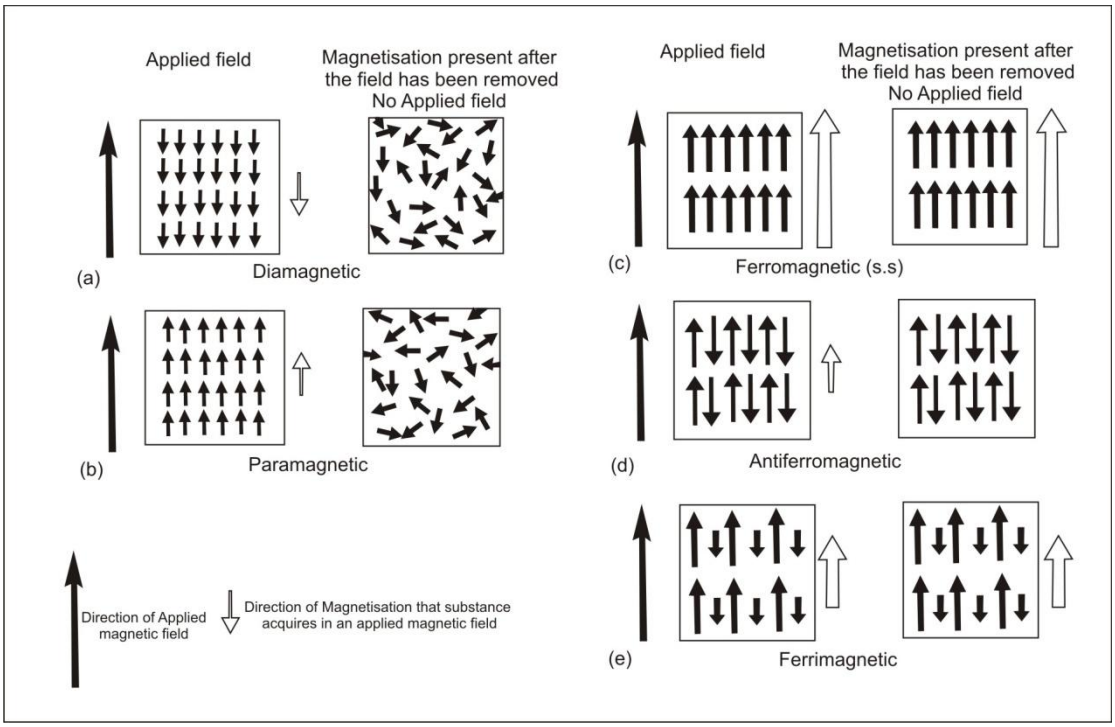

Figure 3.4 Shows different types of magnetisation. **a)** Diamagnetic minerals are weakly magnetised in the opposite direction to the applied field but do not retain magnetisation after the field is removed. **b)** Parramagnetic minerals are weakly magnetised in the same direction as the applied field, but do not retain magnetisation after the field is removed. **c)** Ferromagnetic minerals retain their magnetisation after the magnetic field is removed and in the same direction as the applied magnetic fields. **d)** and **e)** Have components of antiparallel magnetisation after the applied field is removed. Above modified from Tarling and Hrouda (1993).

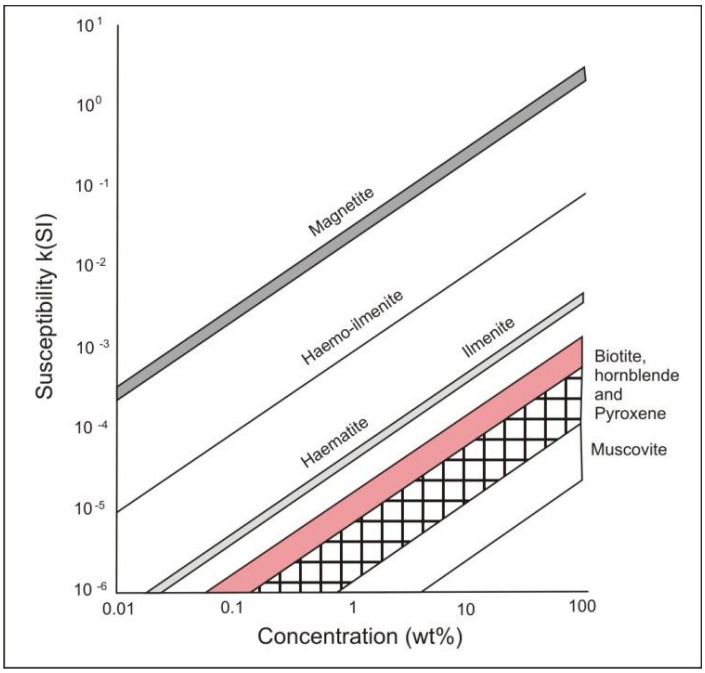

Figure 3.5 Left The susceptibility of a rock depends on the concentration and intrinsic susceptibility of individual minerals, examples are shown of some paramagnetic and ferromagnetic minerals. Modified from Tarling and Hrouda (1993) after Hrouda and Khan (1991).

Tarling and Hrouda (1993) describe three (Fig 3.5) main guidelines for the interpretation of the mineral contributions to AMS based on susceptibility. They are:

1. If 10% of the rock is made up of paramagnetic minerals but its susceptibility is higher than 5×10^{-3}, then the susceptibility of the rocks is carried by the ferrimagnetic portion.

2. If the rock contains approximately 10% paramagnetic minerals and its susceptibility is less than 5×10^{-4} (SI), the magnetic susceptibility is controlled by the paramagnetic minerals.

3. If the rock contains around 10% paramagnetic minerals and its susceptibility is on the range of 5×10^{-4} (SI) and 5×10^{-3} (SI), the susceptibility will be influenced by both paramagnetic and ferromagnetic minerals.

The above however is only a general guideline and the contributions from various types of minerals may not just be due to their relative concentrations but may be affected by other factors such as certain minerals having a stronger preferred lattice orientation (Tarling and Hrouda, 1993).

3.5 Inverse AMS Fabrics

Inverse AMS fabrics may be caused by the presence of single domain magnetite (Potter and Stephenson, 1988). Single domain magnetite is already fully magnetised along its easy axes (long axes) and therefore has zero low field susceptibility along that axes (Tarling and Hrouda, 1993). The grain may be magnetised perpendicular to the easy axes allowing susceptibility to occur perpendicular to the minerals long dimension (e.g. Borradaile and Jackson, 2009). This produces a maximum magnetic susceptibility orthogonal to the direction of magnetization (Tarling and Hrouda, 1993). This can also occur in other high susceptibility minerals such as maghemite (Borradaile and Puumala, 1989) and greigite (Aubourg and Robion, 2002). Single domain magnetite may therefore reduce the AMS signal (Borradaile and Henry, 1997). However SD magnetite is usually only a minor constituent of the AMS signal (Borradaile and Henry, 1997) and may not be important enough to interfere significantly (Rochette et al., 1992). AARM (anisotropy of anhysteretic remanence) can be used to detect SD magnetite which will show up as being orthogonal to the AMS fabric (Borradaile and Henry, 1997). Temperature experiments can also be used to identify the presence of single domain magnetite (Chapter 5).

Interaction of ferromagnetic grains may also cause inverse AMS fabrics (Borradaile, 2010). When the induced magnetisation of individual ferromagnetic particles interact with one another, this affects the overall bulk magnetisation of the population (e.g. Stephenson, 1994; Muxworthy and Williams, 2004; Gaillot et al., 2006) and is termed 'Distribution Anisotropy'. This interaction depends on factors such as the spatial distribution of grains and their grain size and may lead to inverse fabrics (Borradaile, 2010).

Inverse magnetic fabrics may also be produced by sub-equal contributions from diamagnetic and paramagnetic minerals (Borradaile, 2010). Inverse AMS fabrics are also produced by other minerals for example, ferroan calcites (which have positive susceptibilities) as the maximum susceptibility lies along the c -axis (Rochette, 1988).

3.6 The Interpretation of Magnetic Subfabrics/Separation of Subfabrics

Henry (1983) first proposed the idea of separating the AMS contributions of diamagnetic, paramagnetic and ferromagnetic minerals. Separation of subfabrics may be important in the interpretation of AMS as there may be different response and/or growth mechanisms of minerals during tectonic deformation (e.g. Borradaile and Henry, 1997; Robion et al., 1999; Aubourg and Robion, 2002; Martin-Hernandez and Ferré, 2007). Separation into paramagnetic and ferromagnetic subfabrics may be of particular importance (Borradaile and Jackson, 2004). However, Borradaille and Henry (1997) describe two main ways to avoid the need for extra technological approaches to AMS: The first involves taking AMS in areas of strong strain gradients of uniform lithology and the second involves measuring AMS in areas with a different lithology but similar strain.

3.6.1 The Anisotropy of Anhysteretic Remanant Magnetisation, AARM

The anisotropy of anhysteretic remenant magnetisation (AARM) can be used to isolate the contribution of remanence carrying phases such as ferromagnetic minerals (e.g. Stephenson et al., 1986; Jackson, 1991; Tarling and Hrouda, 1993). Remanent grains may occur as low abundance accessory minerals such as oxides or sulphides of iron or manganese and may retain information on a certain part of the strain history (Borradaile, 2001). Although the remanent grains may be volumetrically small, their susceptibility may dominate the AMS signal, in particular the minerals magnetite, titanomagnetite and pyrrhotite (Borradaile, 2001). AARM can also be used to investigate the presence of single domain magnetite as previously discussed (Borradaile and Henry, 1997).

3.6.2 AMS in High and Low Magnetic Fields

High field magnetic anisotropy involves subjecting the sample to a high magnetic field (e.g. Banerjee and Stacey, 1967). Under a high magnetic field the ferromagnetic grains become saturated and this allows for the evaluation of the paramagnetic minerals, by using a high field slope calculation (Kelso et al., 2002). In this study the analysis has been carried out on standard 1 inch cylinders using a vibrating sample magnetometer. Kelso et al., (2002) have compared the high field results with the low field magnetic results and find that high field represents paramagnetic minerals even in the case where ferromagnetic dominates in the low field.

Hrouda (2006) have used low field variation of magnetic susceptibility in order to identify magnetic minerals in various types of rocks. Minerals investigated included titanomagnetites, pyrrohotites, and paramagnetic minerals such as biotite and muscovite. Hrouda (2006) suggests that that this method could be used in routine identification of magnetic minerals although they suggest that the method of low field variation is less effective than the variation of magnetic susceptibility with temperature (as discussed in Chapter 7).

3.6.3 Heating Experiments and AMS

The method involves heating and subsequent cooling prior to AMS measurement (Tarling and Hrouda, 1993). Heating a sample to ≥ 200 ° C or more often 300-350 ° C often results in the growth of new minerals (the paramagnetic minerals are converted to ferromagnetic minerals) and an overall increase in magnetic susceptibility (Tarling and Hrouda, 1993). The newly grown ferromagnetic fabric often replaces that of the original paramagnetic mineral fabric and therefore heating tends to enhance the original fabric (Tarling and Hrouda, 1993). Heating experiments have been carried out to enhance weak fabrics in siltstones (e.g. Abouzakhm and Tarling, 1975) and sandstones (e.g. Perarnau and Tarling, 1985).

Heating experiments have also been used to intensify the contribution by iron oxides (Pernau and Tarling, 1985). However, this can have variable results, where either the newly grown oxides remain parallel to the silicate substrate or they grow in spurious directions and do not thus represent the pre-existing fabric (Borradaile and Henry, 1997). Henry et al. (2003) looks at the AMS of heated rocks, in reference to ferrimagnetic minerals and investigates how to distinguish between an enhanced magnetic fabric and a fabric that is thermally induced and not related to the original

rock fabric. Also, experiments in AMS have been carried out, based on the fact that ferromagnetism may be destroyed by heating in which case the material behaves parramagnetically (Tarling and Hrouda, 1993).

3.6.4 Low Temperature Susceptibility

Low temperature AMS using liquid nitrogen can reveal the contribution by paramagnetic phases (Richter and van der Pluijm, 1994; Pares and van der Pliujm, 2014). The magnetic susceptibility of paramagnetic minerals is increased at low temperatures due to the Curie-Weiss law (Richter and van der Pluijm, 1994; Pares et al., 2000; Pares and van der Pluijm, 2002, 2014).

$Kp = C/(T-\phi)$,

Where:

Kp = paramagnetic susceptibility

C = a constant

T = temperature (degrees Kelvin)

ϕ is the paramagnetic Curie temperature

Submerging the samples into liquid nitrogen at temperatures of 77K for 30 minutes increases the magnetic susceptibility of the K_{max} axes with respect to the K_{min} axes by 3-5 times (Pares and Van der Pluijm, 2002). If the AMS is controlled predominantly by paramagnetic minerals, there will be a steady increase in magnetic susceptibility (Richter and van der Pluijm, 1994).

3.7 AMS and Palaeomagnetism

Natural remanent magnetization (NRM) is the naturally occurring permanent magnetization of a rock (e.g. Borradaile, 1997). Ferromagnetic minerals are capable of carrying a remanant magnetisation subsequent to the removal of an induced magnetic field (Tarling and Hrouda, 1993) and this is the principle behind palaeomagnetic studies (Tarling, 1983). Natural remanent magnetisation (NRM) is not destroyed by AMS, therefore palaeomagnetic studies may be carried out using the AMS cores (Borradaile and Lucas, 2003). AARM however does destroy NRM so AARM cores cannot be used for palaeomagnetic studies (Borradaile and Lucas, 2003).

3.8 Using AMS in Conjunction with other Rock Fabric Analytical Methods

AMS is often used with other rock fabric analytical methods. In some studies the interpretation of AMS is quite straight forward where as in other cases it is more complicated (e.g. Urcia et al., 2009). AMS may be compared with preferred crystal orientation (PCO) which is a recognised feature of tectonic strain (Ramsay, 1967; Ramsay and Huber, 1983).

Neutron texture goniometry can be used to compare PCO of minerals with AMS of specimens (Brokmeier, 1994; Ullemeyer et al., 2000). Similarities between paramagnetic phyllosilicate orientation and AMS axes has been founds using X-ray texture and neutron texture goniometry (Richter et al., 1993 a,b; Chadima et al., 2004; Cifelli et al., 2009). Luneburg et al. (1999) used AMS with X-Ray texture goniometry and electron microscopy to determine mineral orientations and fabric-forming mechanisms respectively. Hansen et al. (2004) show that neutron diffraction for pole figure measurements in sedimentary rocks has been used successfully in conjunction with AMS, as the pole figures for minerals (chlorite and hematite) align closely with the principal AMS axes. Neutron pole figure measurements are a very effective way of measuring grain preferred orientation due to the neutrons high penetration depth (Hansen et al., 2004).

AMS has also been used successfully with the technique of the Electron Back Scatter Diffraction Technique (EBSD) to look at mineral preferred orientation fabrics e.g. in mylonites (Bascou et al., 2002) and igneous intrusions (Feinberg et al., 2006).

Part Two. Interpreting AMS in Deformed Sedimentary Rocks

3.9 Types of AMS ellipsoids

The interpretation of AMS ellipsoids in strained sedimentary rocks is based on the orientations and distribution of the principal axes, K_1, K_2 and K_3. Many previous studies have shown how the AMS ellipsoids evolve from being controlled by primary sedimentary fabrics through intermediate stages to tectonic fabrics (e.g. Averbuch et al., 1992; Bakhtari et al., 1998; Parés et al., 1999; Grelaud et al., 2000; Frizon de Lamotte et al., 2002; Saint-Bezar et al., 2002; Aubourg et al., 2004).

Tarling and Hrouda (1993), describe three types of fabric ellipsoid, these are: oblate, prolate and triaxial (Fig 3.6). Similarly these are described by Robion (2007), (Fig 3.7). These are:

- A planar uniaxial fabric (oblate fabric), where K_3 is clustered and there is a dispersion of K_1 and K_2 orthogonal to K_3.
- A linear uniaxial fabric (prolate fabric) where the K_1 axes is clustered and K_2 and K_3 is dispersed and
- A triaxial fabric which has three distinct clusters. The magnetic lineation corresponds to the K_1 axis.

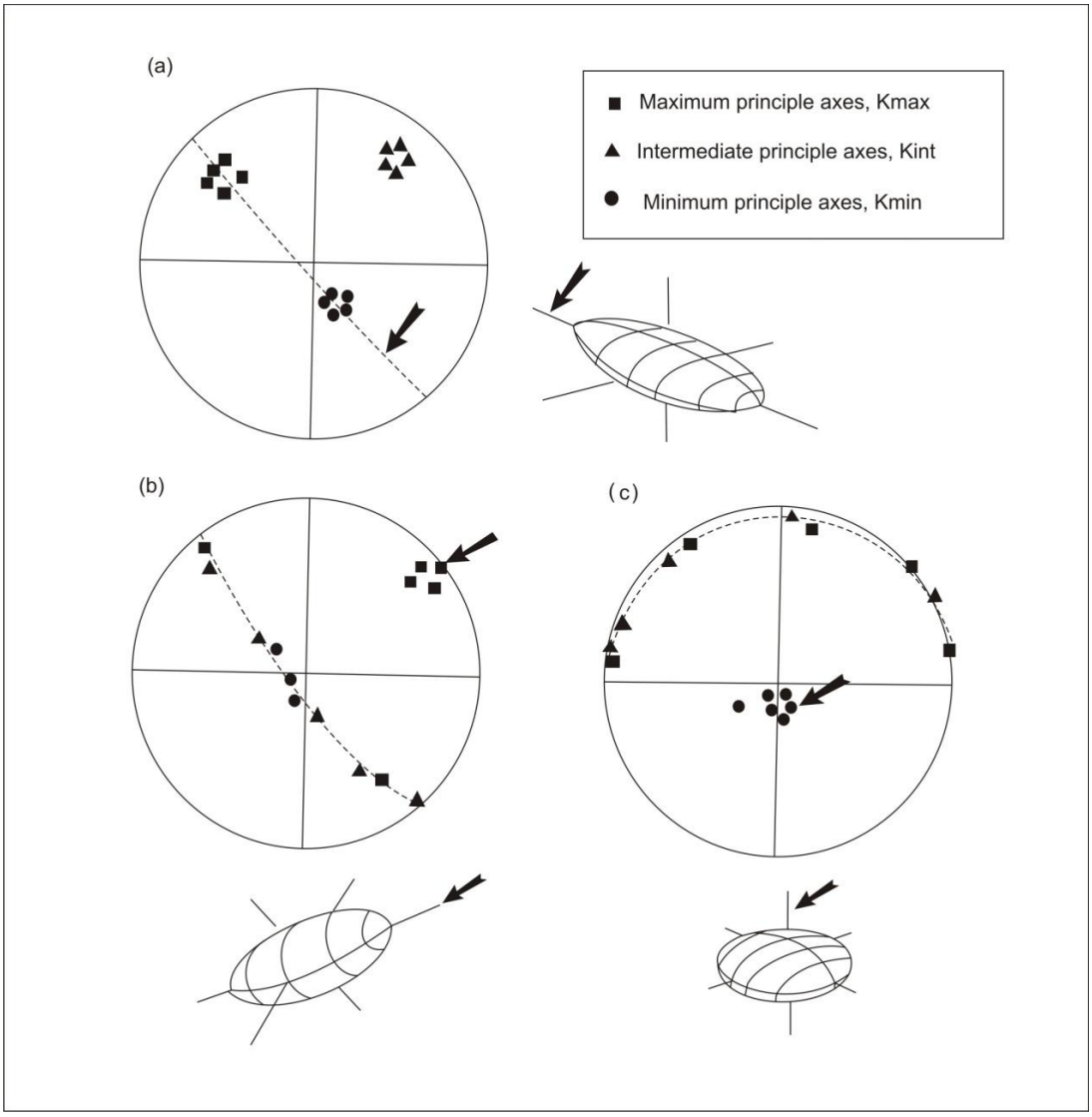

Figure 3.6 How different shaped AMS ellipsoids plot stereographicaly. A) Triaxial ellipsoids have three distinct clusters. b) Prolate ellipsoids have K_{max} closely grouped and K_{int} and K_{min} are distributed within a girdle at 90 degrees to the K_{max} direction. C) Oblate ellipsoids have a well grouped K_{min} axes and the K_{max} and K_{int} axes lie on a girdle at 90 degrees to the K_{min} axes. Redrawn from Tarling and Hrouda (1993).

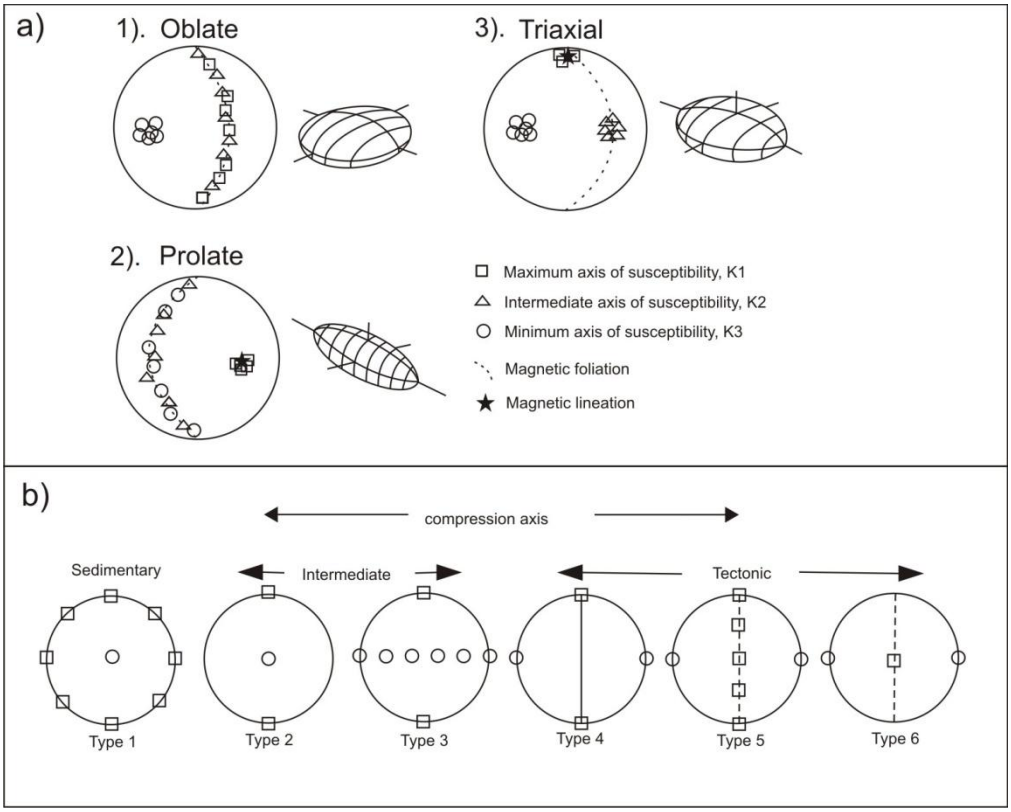

Figure 3.7.a) reiterates from Fig 3.6 and also shows where the magnetic foliation and the magnetic lineation plot on the AMS stereonet. Three type of AMS fabric ellipsoid: 1) planar uniaxial fabric (Oblate Fabric), 2) a linear uniaxial (prolate fabric) 3) a triaxial fabric. **b)** shows the sequence of evolution of magnetic fabrics as deformation increases in fold and thrusts belts. Sequence is illustrated for the case of horizontal bedding. Types 1 to 6 are described in terms of increasing tectonic strain. In Type I K_3 is parallel to the pole to bedding. It is a sedimentary fabric and is uniaxial (Oblate). Type II and type III are intermediate fabrics. Type II still retains the sedimentary indicator of K_3 parallel to the pole to bedding. In Type III as the sedimentary features become compromised K_3 is scattered within the bedding plane. Type IV is classified as the beginning of the tectonic stage where K_3 is within the bedding plane and no longer perpendicular to it. Type V and VI is characterised by K_1 scattered around K_3. (Redrawn from Robion et al., 2007).

3.10 AMS in Foreland Fold and Thrust Belts

The evolution of magnetic fabrics throughout a foreland fold and thrust belt has been well documented in previous studies (e.g. Kissel et al., 1986; Jackson et al., 1989; Lee et al., 1990; Averbuch et al., 1992; Frizon de Lamotte et al., 1997; Pares et al., 1999; Hirt et al., 2004; Weil and Yonkee, 2012). Sedimentary fabrics undergoing deformation gradually lose their sedimentary features to tectonic features (Ramsay and Huber, 1983), and most magnetic fabrics in foreland fold and thrust belts evolve from a primary, through an intermediate to a tectonic phase (Averbuch et al., 1992; Bakhtari et al., 1998; Pares et al., 1999; Grelaud et al., 2000; Frizon de Lamotte et al., 2002; Saint Bezar et al., 2002; Aubourg et al, 2004, Hirt et al., 2004). There are numerous previous studies on the behaviour of AMS ellipsoids in low to moderately strained sedimentary

rocks in: clays (e.g. by Kissel et al., 1986), pelitic rocks (e.g. Debacker et al., 2004), slates (e.g. Luneburg et al., 1999; Hirt et al., 2004) and sandstones (e.g. Bakhtari et al., 1998). AMS can be used in the study of ductile deformation in sedimentary rocks (e.g. Chadima et al., 2006) and on weak internal deformation found in sedimentary rocks of fold and thrust belts (e.g. Hrouda., 1991; Pares et al., 1999). Some of the first studies using AMS on the early stages of deformation of sedimentary rocks was carried out by Kligfield et al. (1981), Kissel et al. (1986) and Lowrie and Hirt (1987).

3.11 AMS and Primary Sedimentary Fabrics

AMS is an effective tool that may be used in seemingly undeformed terrains (Kissel et al., 1986; Lee et al., 1990). In undeformed sedimentary rocks the AMS is controlled by depositional process (e.g. Pares, 1999). The AMS ellipsoids are typically oblate (or uniaxial) in undeformed sedimentary rocks (e.g. Robion et al., 2007; Fig 3.6 c). Sedimentary compaction is characterised by a clustering of the minimum susceptibility axes, K_3 about the pole to bedding and an increase in magnetic anisotropy (e.g. Imaz et al., 2000). In relatively undeformed sedimentary rock, the magnetic foliation often lies in the same plane as the bedding and the magnetic lineation may be parallel to the palaeocurrent direction (e.g. Hamilton and Rees, 1970; Pares, 1999; Chadima et al., 2006). In some cases, the magnetic lineation may be parallel to the flow direction and a foliation may be found between the bedding plane and foreset laminea (Borradaile et al., 1999). The AMS fabric may be affected by some degree by sedimentary re-working and slumping (Lagroix and Banerjee, 2002, 2004). Pedalogical processes may also affect the anisotropy of bedding which in turn affects the AMS fabric (in sandstones and siltstones; Robion, 2007). AMS has also been used to look at diagenetic events for example in folded aeolian Permian sandstones (e.g. Callot et al., 2010).

Summary of AMS in Primary Sedimentary Fabrics/Bedding

- AMS in sedimentary rocks reflects depositional processes (e.g. Pares, 1999), diagenesis (Callot et al., 2010) and compaction (Imaz et al., 2000).
- Oblate AMS ellipsoids are found in bedding planes (e.g Robion et al., 2007) and the magnetic foliation is parallel to bedding (e.g. Chadima, 2006).
- The K_3 axes are clustered and lie parallel to the pole to bedding (e.g. Imaz et al., 2000).
- The K_1 and K_2 axes are often dispersed within the bedding plane (e.g. Robion et al., 2007).

- K_1 or the magnetic lineation may be parallel to the palaeocurrent direction (Chadima, 2006).
- Factors such as sedimentary reworking, slumping (Lagroix and Banerjee, 2002, 2004), pedalogical processes (Robion, 2007) and the presence of a stylolitic cleavage plane should be considered (Borradaile and Tarling, 1981).
- In low strain deformation of sedimentary beds where there is folding the magnetic lineation, K_1 may parallel to the fold axial plane (Kissel et al., 1986).

3.12 Weak Deformation of Primary Sedimentary fabrics

Where deformation intensity is low the magnetic lineation has been observed to parallel the fold axes such as those reported in weakly deformed Cenozoic clays in Greece (Kissel et al., 1986). Where the bedding is completely overprinted by tectonic fabric it may not be possible to decipher whether the original bedding fabric was not truly oblate or altered by current lineations (Borradaile and Henry, 1997). Scale is also an important factor when applying the technique of AMS on bedding and cleavage fabrics (Borradaile, 1989). For example, the AMS ellipsoid may be affected on a local scale by a stylolitic cleavage depending on whereabouts it is taken from the sample (Fig 3.8).

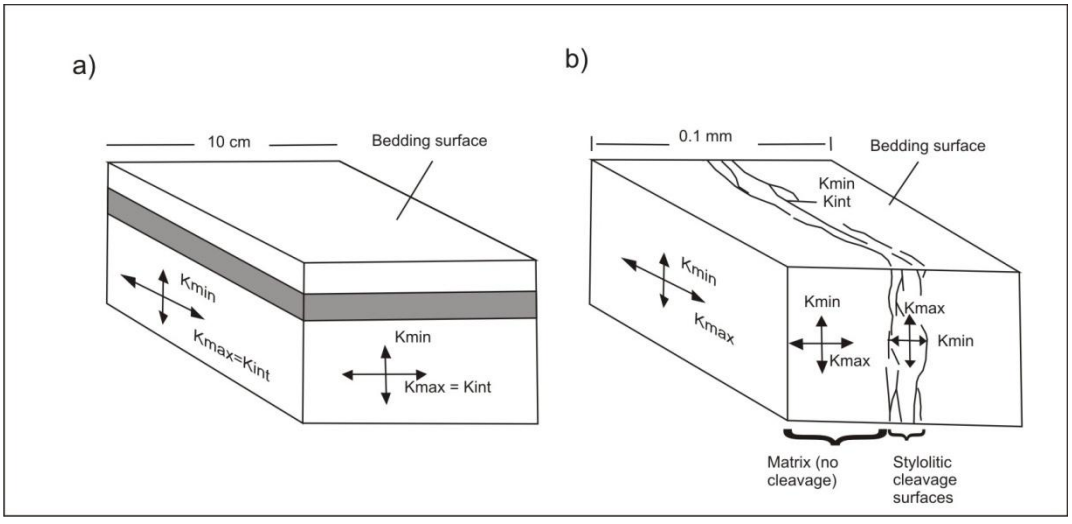

Figure 3.8 Scale is important when looking at bedding and cleavage fabrics. a) shows only bedding but b) shows bedding and cleavage. Redrawn from Hrouda 1993(after Borradaile, 1989).

3.13 The Magnetic Lineation in Low Deformation Zones

The magnetic lineation is often parallel to the intersection of two planar fabrics (Borradaile and Tarling, 1981; Richter et al., 1993). The magnetic lineation may also correspond with the bulk extension direction (e.g. Kligfield et al., 1981; Ferré and Améglio, 2000; Hirt et al., 2000). In shales and slates, K_{max} has been shown to represent

either a stretching lineation (e.g. Hirt et al., 2004) or a bedding/cleavage intersection lineation (e.g. Borradaile and Tarling, 1981; Rochette and Vialon, 1984; Parés and Dinarès, 1993). Similarly numerical and experimental models by Housen et al. (1993), show that K_{max} may represent the intersection of two planar mineral fabrics. Different scenarios for the magnetic lineation are shown in Fig 3.9.

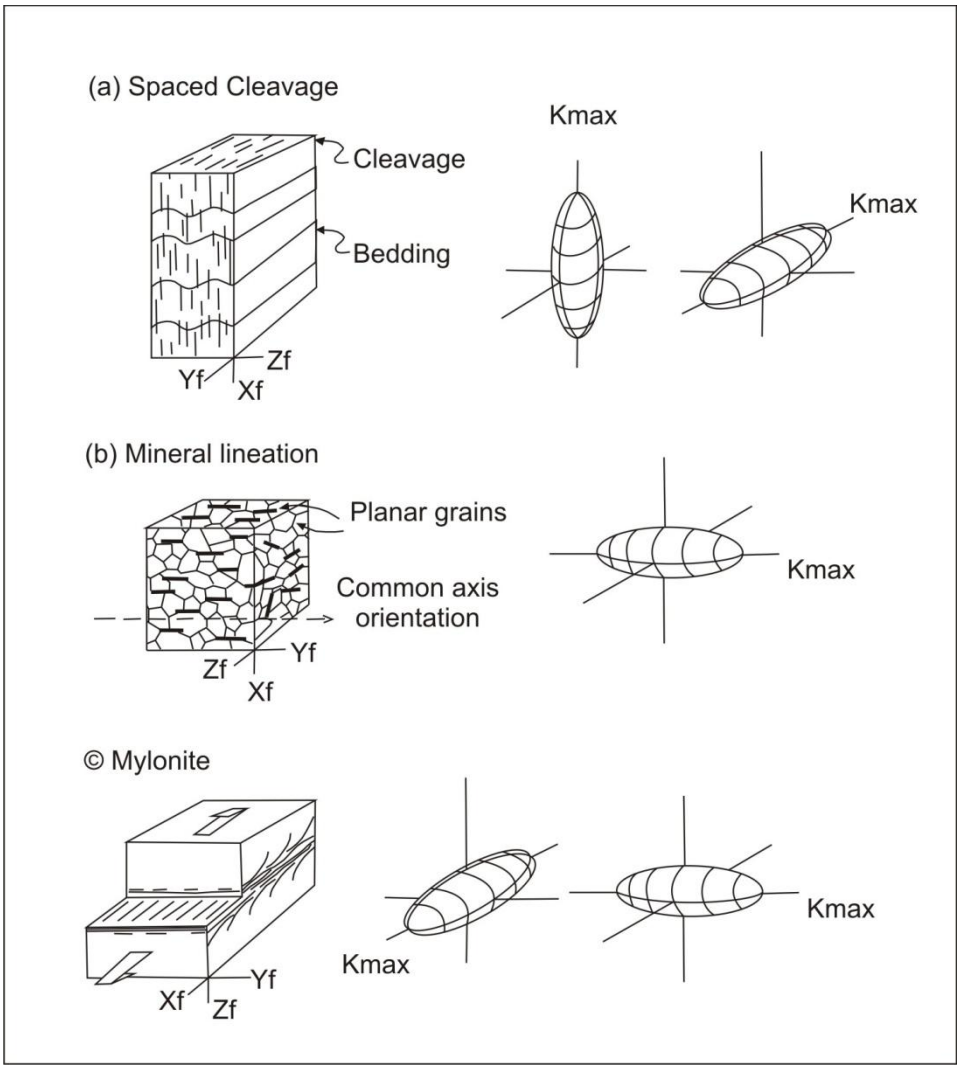

Figure 3.9 Shows three scenarios for the magnetic lineation represented by $K_{max.}$ In a) the magnetic lineation may lie in the cleavage plane or may be parallel to the bedding/cleavage intersection lineation. In b) the magnetic lineation is parallel to the mineral elongations. In c) the magnetic lineation is parallel to the shearing direction in the mylonite. Redrawn from Pares and Van der Pluijm (2002).

3.14 AMS and Layer Parallel Shortening

AMS has been used to recognise layer parallel shortening (LPS), (Graham, 1966; Kligfield et al., 1977; Kligfield et al., 1981; Borradaile and Tarling, 1981; Kissel et al., 1986, Lowrie and Hirt, 1987; Lee et al., 1990; Roure et al., 2005; Weil and Yonkee, 2012). AMS has been shown to be sensitive to pre-folding LPS strain in sandstones and siltstones (Averbuch et al., 1992; Bakhtari et al., 1998). Where LPS has occurred, the

magnetic fabric typically evolves from a relatively undeformed sedimentary state with the magnetic foliation parallel to the bedding and evolves through an intermediate stage where the magnetic lineation (K_{max}) is normal to the shortening direction and the magnetic foliation is parallel to bedding (Bakhtari et al., 1998; Sagnotti et al., 1998; Pares et al., 1999; Fig 3.6 b). This is also re-iterated by (Mattei et al., 1999) who highlighted that during the early stages of deformation K_{max} may align itself perpendicular to the shortening direction. Similarly, AMS can record an early LPS that precedes folding and is often preserved throughout folding, often the LPS does not totally overprint the sedimentary fabric but expresses itself as 90° to the bedding magnetic foliation (Averbuch et al., 1992; Frizon de Lamotte et al., 2002). In weakly to moderately deformed mudstones, grouping of K_{max} and a girdle containing K_{min} and K_{int} may be indicative of the first signs of LPS, observed by e.g. (Parés and Dinarès, 1993; Sagnotti and Speranza, 1993). As deformation increases the fabric may evolve from zero LPS to low LPS to high LPS (Fig 3.10, Saint-Bezar et al., 2002).

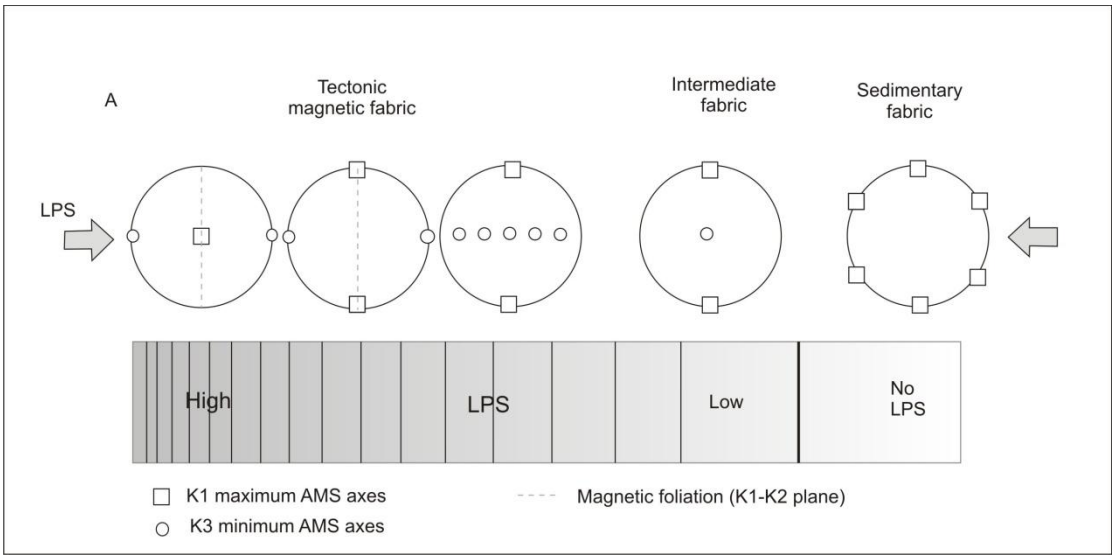

Figure 3.10. Shows the evolution of the magnetic fabric in terms of layer parallel shortening (LPS). Deformation increases from right to left. In the sedimentary fabric the magnetic foliation is parallel to bedding. The intermediate fabric has the magnetic foliation parallel to bedding while the magnetic lineation is normal to the shortening direction, this fabric has been reported in fold and thrust belts (Bakhtari et al., 1998; Sagnotti et al., 1998; Pares et al., 1999). Redrawn from Saint-Bezar et al. (2002) based on Graham (1966); Averbuch et al. (1992) and Bakhtari et al. (1998).

Summary of LPS AMS fabrics.

- K_1 lies parallel within the LPS plane or normal to the shortening direction (e.g. Mattei 1999).

- The first signs of LPS are indicated by the K_1 axes being normal to the shortening direction while the magnetic foliation remains parallel to the bedding plane (Bakhtari et al., 1998; Sagnotti et al., 1998; Pares et al., 1999).
- The first signs of LPS are indicated by the grouping of K_1 and a girdle of K_2 and K_3 (Parés and Dinarès, 1993; Sagnotti and Speranza, 1993).
- Where higher amounts of LPS have occurred (Fig 3.10) K_1 is perpendicular to shortening and K_3 is parallel to the pole to cleavage (Saint-Bezar et al., 2002).

3.15 AMS and Cleavage

In weakly deformed sedimentary rocks where a bedding and cleavage fabric exist, K_1 is often parallel to the bedding/cleavage intersection lineation (e.g Chadima et al., 2006) but K_3 can occupy a location either perpendicular to bedding (Saint Bezar et al., 2002; Pares and Van der Pluijm, 2002) or perpendicular to cleavage or intermediate between the pole to bedding and the pole to cleavage (e.g. Robion et al., 1995; Luneburg et al., 1999; Frizon de lamotte et al., 2002). With the onset of cleavage there may be an incomplete tectonic overprint of cleavage on bedding (Borradaile, 1997; Fig 3.12 b). In deformed sedimentary rocks the K_{min} axes is often normal to the cleavage or the flattening plane (Pares, 1999). Pares (2004) suggest from AMS studies on mudrocks that cleavage begins forming at the early stages of deformation and gradually develops rather than it being a discrete event at a certain amount of strain. In foliated rocks K_3 is often perpendicular to the foliation while K_1 is often parallel to either the cleavage/bedding intersection lineation or a tectonic extensional direction (e.g. Rathore, 1979; Hrouda, 1982; Aubourg et al., 1991; Nakamura and Borradaile, 2001; Pares and Van der Pluijm, 2002). Where there is the influence of both bedding parallel and cleavage parallel fabrics on the AMS fabric, a girdled distribution may be observed (eg. Housen et al., 1993; Parés and Van der Pluijm, 2003). There may be an important influence of the initial rock anisotropy on the cleavage and its expression in AMS (Pares and Van der Pluijm, 2002; Pares, 2004). Where the deformation is very strong, the slaty cleavage exhibits parallelism with the magnetic foliation (Chadima et al., 2006). Hirt et al. (2004) reinforce the idea that as deformation reaches it most intense in a sedimentary foreland fold and thrust setting, that the AMS fabrics become more prolate in nature. However, the AMS ellipsoid can evolve to being strongly oblate when there has been deformation resulting in a cleavage e.g. a slaty cleavage in black shales (Chadima et al., 2006). Increasing deformation may cause K_{max} to evolve from parallelism with the structural foliation to obliquity with the structural foliation (Rathore, 1985;Aranguren et al., 1996; Borradaile et al., 1998).

Summary of AMS and Cleavage

- The onset of cleavage may be marked by K_1 being parallel to the bedding/cleavage intersection lineation (e.g. Chadima et al., 2006) and K_3 lying somewhere between the pole to bedding and the pole to cleavage (e.g. Robion et al., 1995; Luneburg et al., 1999; Frizon de lamotte et al., 2002; Fig 3.12 b).
  Or:
- With the onset of cleavage, the magnetic lineation (K_1) is parallel to the bedding cleavage intersection lineation and the magnetic foliation (K_2 and K_3) is parallel to bedding (e.g. Pares, 1999).
- With further deformation, in foliated rocks, K_3 is parallel to the pole to cleavage and K_1 is parallel to bedding cleavage intersection lineation.
- With further deformation, the magnetic foliation is parallel to the cleavage plane and the AMS ellipsoid is oblate in the cleavage plane (e.g. Pares, 1999).
- With further deformation K_{max} may evolve from being parallel to structural foliation to being oblique to it (Rathore, 1985; Aranguren et al., 1996; Borradaile et al., 1998).

3.16 AMS and Metamorphic Rocks

Interpretation of AMS should accompany a good understanding of the metamorphic conditions (e.g. Borrradaile and Jackson, 2010). AMS may reflect a complex array of subfabrics mostly likely to have developed during metamorphism (Oliva Urcia et al., 2010). An example of this may be the growth of new minerals such as chlorite along cleavage planes (e.g. Housen et al., 1993; Hirt et al., 2004). Even in low-grade zones, with increasing deformation, the AMS fabric may be affected by the metamorphic growth of new minerals (Rochette and Lamarche, 1986; Borradaile, 1987). Growth of new minerals may affect the lineation (L) and foliation (F) parameters associated with strain (Borradaile, 1987; Rochette, 1988). The magnetic lineation (L_m) in metamorphic terrains, often tracks mineral elongations (e.g. Aranguren et al., 1996; Fig. 3.9). The nature of a lineation may also be affected by dynamic recrystalisation (Piazolo and Passchier, 2002).

AMS has also been used in the study of shear zones and mylonites (Goldstein, 1980; Goldstein and Brown, 1988; Ruf et al., 1988; Housen et al., 1995). In transpressional regimes and in shear zones, magnetic lineations may be variable and may be parallel or perpendicular to the shear direction (Tikoff and Greene, 1997, cited by Parés and van

der Pluijm, 2002). The study of AMS in moderate to high grade metamorphism is not relevant to this study.

3.17 AMS and Strain analysis

3.17.1 General Relationship between AMS and Strain Analysis

AMS has been previously correlated with finite strain (Fuller, 1964; Graham 1966). A long term objective has been to quantitatively correlate AMS with finite strain (e.g. Kneen, 1976; Wood et al., 1976; Rathore et al., 1983; Kligfield et al., 1981; Borradaile 1991; Hirt et al., 1993; Lüneburg et al., 1999; Parés and van der Pluijm, 2003). In some cases, the axial orientations of the magnetic susceptibility ellipsoid and the finite strain ellipsoid have been noted to coincide (Henry and Daly, 1993; Borradaile and Henry, 1997). Borradaile (1991) has reviewed a number of case studies correlating AMS with strain (Fig 3.11, Tarling and Hrouda, 1993). The graphs in Fig 3.11 show the Pj(k) - the degree of magnetic anisotropy, plotted against Pj (ε) - the magnitude of strain based on different types of strain markers: synthetic sandstone samples (Borradaile and Allford, 1987), Welsh Slates (Wood et al., 1976; Kneen, 1976), oolites (Kligfield et al., 1982), reduction spots (Kligfield et al., 1981), concretions (Hirt et al., 1988) and xenoliths (Cogné and Perroud, 1988), mica subfabrics (Rathore et al., 1983; Rathore and Hugon, 1987) and lapilli (Borradaile and Motherhill, 1984; reviewed by Borradaile, 1991; cited by Tarling and Hrouda, 1993). In these studies reviewed by Borradaile (1991) there appears to be a correlation between the magnetic anisotropy, Pj and the magnitude of strain Pj (ε). Borradaile (1991) notes from these studies that Pj parameter correlates well with strain, however Borradiale (1991) suggests that AMS is only effective as a qualitative petrofabric tool and cannot be used to assess the intensity of strain.

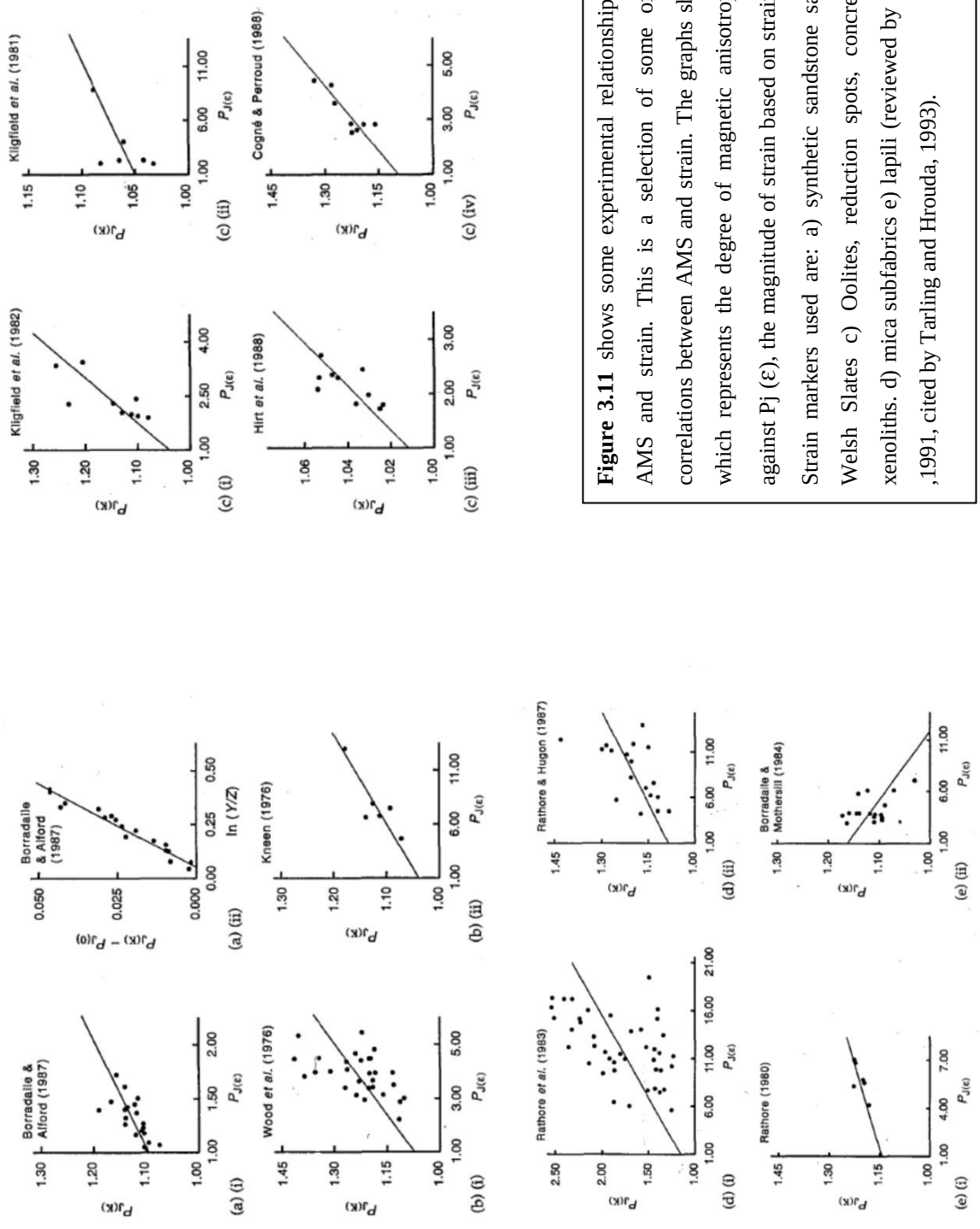

Figure 3.11 shows some experimental relationships between AMS and strain. This is a selection of some of the best correlations between AMS and strain. The graphs show Pj (k) which represents the degree of magnetic anisotropy plotted against Pj (ε), the magnitude of strain based on strain markers. Strain markers used are: a) synthetic sandstone samples. b) Welsh Slates c) Oolites, reduction spots, concretions and xenoliths. d) mica subfabrics e) lapili (reviewed by Borradaile ,1991, cited by Tarling and Hrouda, 1993).

3.17.2 Modelling of AMS and Strain

The relationship between magnetic anisotropy and strain has been modelled theoretically by Owens (1974), Hrouda (1987), Rochette (1988), Fitter (1989), Henry and Hrouda (1989) and Hrouda and Lanza (1989). These models are based on uniaxial magnetic grains that do not interact magnetically, do not acquire magnetism during deformation, have no pre-existing fabric and are set in a matrix with no susceptibility (Tarling and Hrouda, 1993). There have also been previous experimental models of AMS with strain experimentally (e.g. Owens and Rutter, 1978; Borradaile and Alford, 1987, 1988; Borradaile and Puumala, 1989). A study by Hrouda and Jezek (1999), theoretically models the relationship between magnetic anisotropy and strain using triaxial magnetite grains. They conclude that despite the complex behaviours of individual triaxial grains, there is an averaging out process involved that allows a correlation of strain and magnetic anisotropy. They show that this model of AMS and strain on triaxial grains is similar to previous models of systems containing prolate/oblate spheroidal bodies (e.g. Owens and Rutter, 1978; Borradaile and Alford, 1987, 1988; Rathore, 1988; Borradaile and Puumala, 1989; Borradaile, 1991; Tarling and Hrouda, 1993 cited by Hrouda and Jezek, 1999). Hrouda and Jezek (1999) suggest from this that AMS is a good method for the estimation of cumulative strain.

3.17.3 Correlating AMS with strain: Limitations

There are a number of issues in attempting to correlate AMS with strain analysis. The magnetic fabric may not deform in the same path as tectonic strain and the interpretation of AMS may require an assumption that there is no anisotropy prior to tectonic deformation (Hrouda and Janak, 1976; Borradaile and Tarling, 1981; Kligfield et al., 1981, 1983; Tarling and Hrouda, 1993). Relating AMS to strain sometimes requires assumptions about the magnetic behaviour of minerals in the sample (Jezek and Hrouda, 2002). The AMS ellipsoid is controlled by the alignment of minerals brought about by discrete metamorphic and solid state flow events (Borradaile, 2010) and its evolution cannot parallel the same path as a continuum strain ellipsoid (Borradaile, 2010; Fig 3.14). The continuum strain ellipsoids sums the total accumulation of events where as the AMS ellipsoids may reflect only discrete mineral subfabrics (Borradaile, 2010; Fig 3.14).

3.17.4 Using AMS as an Indicator of Strain

The relationship of the shape parameter Tj to the anisotropy degree Pj may be used to show the evolution of the AMS fabric ellipsoids with increasing deformation (Hrouda, 1982; Borradaile, 1997; Fig. 3.12 a). A polar plot, where T_j is plotted against P_j, can be used to show a distribution of the ellipsoid shapes and in looking at the deformation paths of the AMS ellipsoid (Borradaile and Jackson, 2004; Fig. 3.13). The Tj verses Pj plot shows the evolution of the magnetic fabrics with increasing deformation (Jelenick 1981; Borradaile, 2010). In order to relate the parameters (P_j, T_j) to strain it is important to do this on a similar scale to the AMS scale (Borradaile and Henry, 1997). The T_j parameter has been shown to be a useful indicator of increasing deformation in low strained mudrocks (e.g. Pares et al., 2001; Parés and van der Pluijm, 2003).

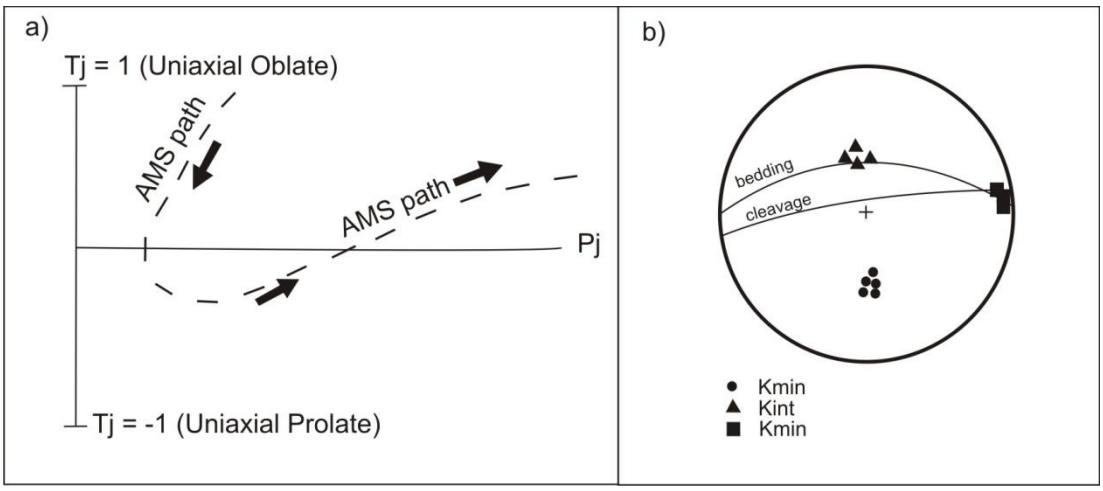

Figure 3.12. a) shows the evolution of the AMS path with increasing deformation based on the parameters Pj and Tj. The expected AMS path in terms of the shape ellipsoid is shown where Tj is plotted against Pj (Jelenick, 1981) (b) shows the AMS plot when the bedding is incompletely overprinted by cleavage. The bedding cleavage intersection lineation is parallel to K_{max}. (Borradaile and Tarling, 1984). Redrawn from Borradaile, (1997).

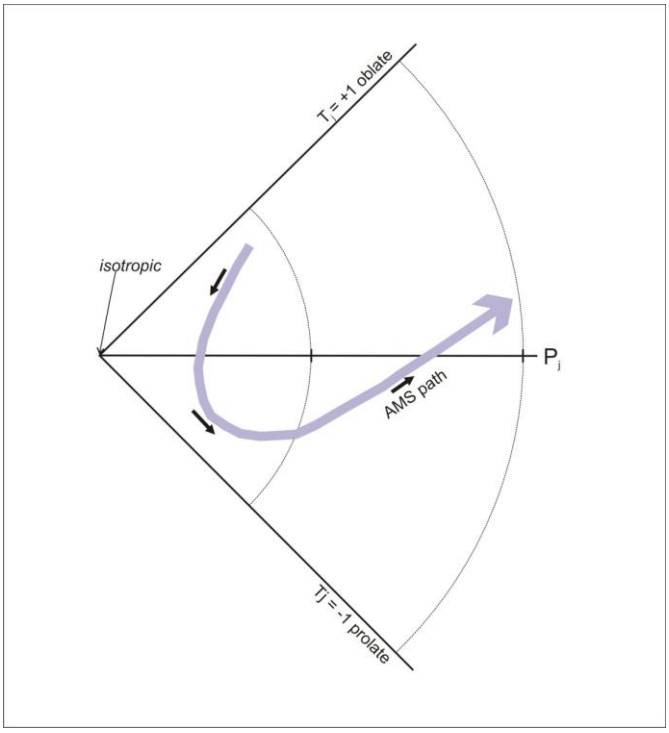

Figure 3.13 Left Shows a polar plot with Tj plotted against Pj. The polar plot is useful for displaying low Pj values. Redrawn from Borradaile and Jackson (2004).

Figure 3.14 below It is not possible to correlate the AMS ellipsoid path with an ideal strain ellipsoid as shown by this idealised diagram. Redrawn from Borradaile and Jackson (2010).

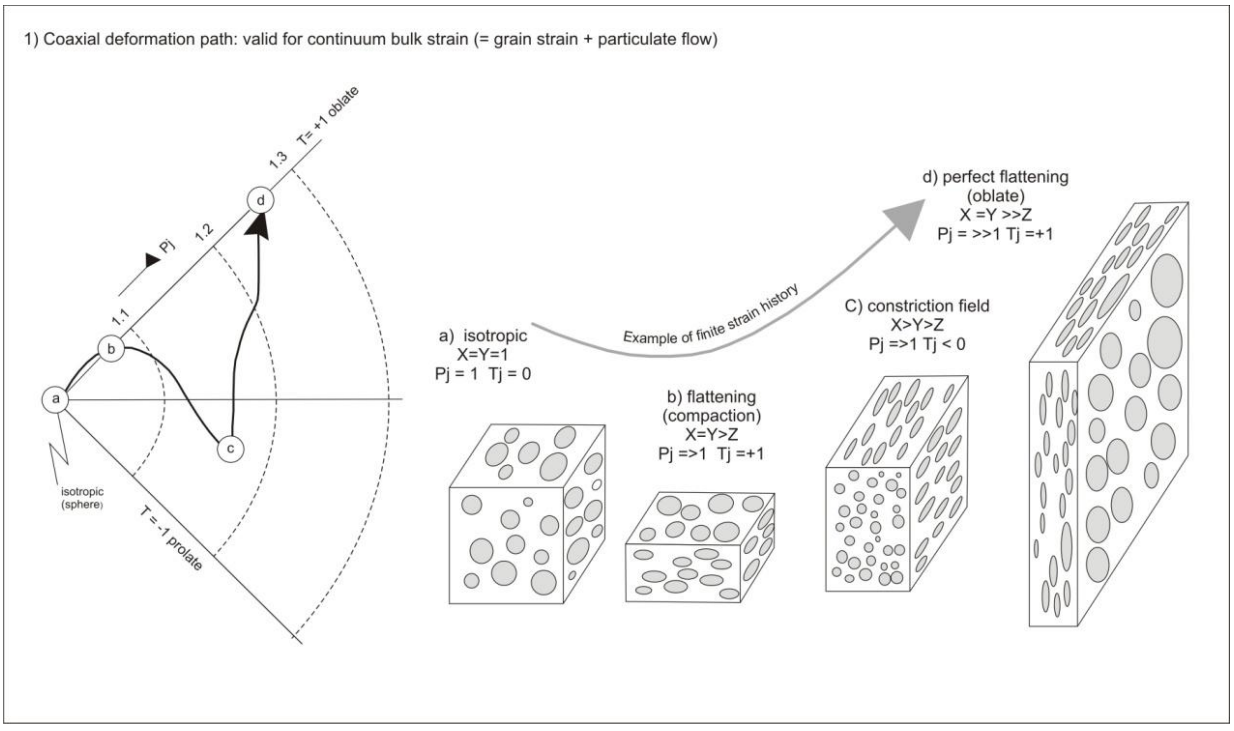

3.17.5 The Interchanging of the Principal AMS Axes

Borradaile (1997) characterises the evolution of the AMS ellipsoid from primary sedimentary fabric to tectonic fabric in relation to the principal strain axes in a series of simplified diagrams (Fig. 3.15). Progressive strain may cause K_{min} to evolve to K_{int} and then to K_{max} (Borradaile and Henry, 1997; Fig 3.15). The interchanging of the principal AMS axes (also known as axis swapping) has also been observed in laboratory

experiments (Borradaile and Alford, 1987, 1988; Borradaile and Puumala, 1989) and predicted through mathematical modelling (Daly, 1972; Hrouda and Hruskova, 1990). The overall AMS fabric may be a result of the blending of various subfabrics and the swapping of AMS ellipsoids may reflect this (Borradaile, 2010; Fig. 3.16).

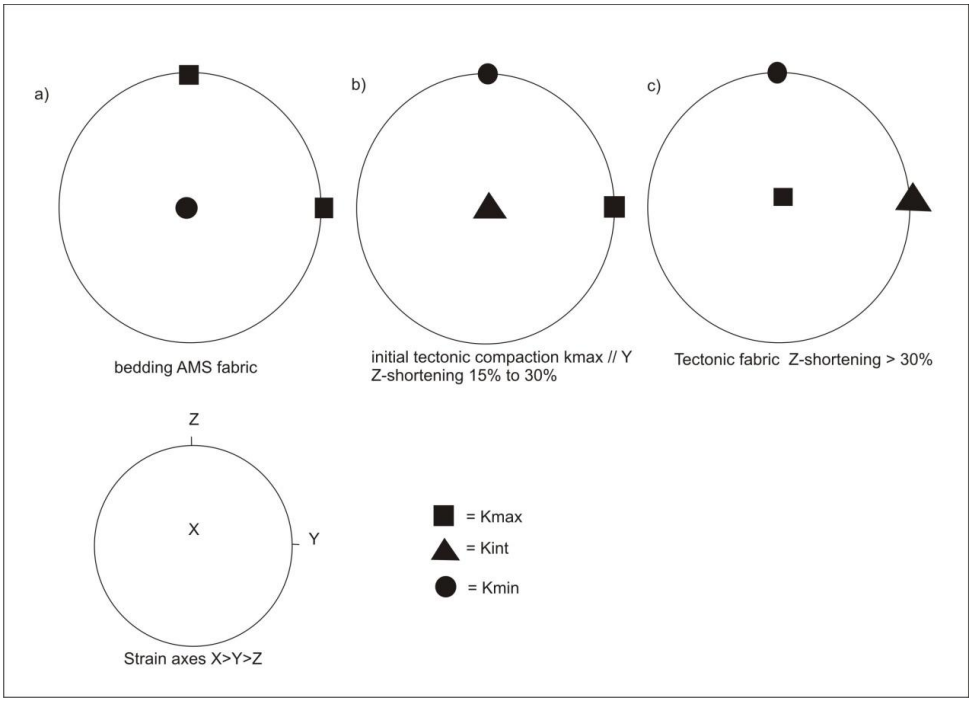

Figure 3.15. Shows the idealised evolution from a) a primary bedding AMS fabric to b) an intermediate AMS fabric to c) a tectonic AMS fabric in relation to the principal strain axes. The K_{min} axis evolves from being parallel to the pole to bedding to being in the same plane as the pole to the shortening direction. The AMS axes correspond to the strain axes only with sufficient strain. Redrawn from Borradaile (1997).

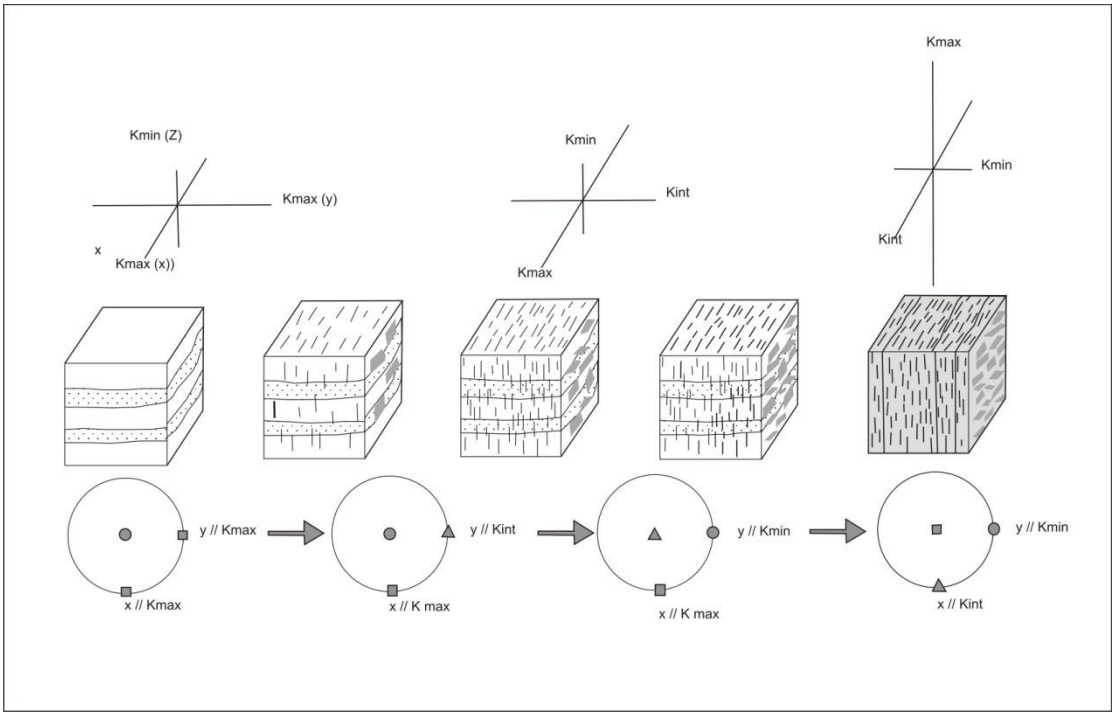

Figure 3.16 Shows the progressive deformation of a sedimentary rock where there is blending or switching of subfabrics and the end member AMS may be a blended result of the primary bedding (left) and cleavage (right) fabrics. During deformation the degree of fabric blending may vary (centre). The swapping of AMS axes will reflect this blending or switching of subfabrics. Redrawn from Borradaile and Jackson (2010).

3.17.6 Previous Studies: Comparing AMS and Strain Analysis

Burmeister et al. (2009) have carried out AMS and strain analysis using the Fry technique on very low strain sandstones from two localities of the Appalachian fold and thrust belt, which ranges from lower Devonian to Carboniferous (Pennsylvanian). They find that the long axes (K_1 axes) of the AMS axes cluster parallel to the structural grain (faults, cleavage and fold hinges) but the Fry ellipse long ellipsoids do not, implying that AMS is more sensitive to strain in low strain sandstones than the Fry technique.

Oliva-Urcia et al. (2010) have combined the techniques of AMS with strain analysis and X-ray texture goniometry on phyllites from Greece. Oliva-Urcia et al. (2010) use low temperature AMS to look at the paramagnetic subfabric, the projected dimension strain method (Ring and Brandon, 1999; Rahl, 2005) for strain analysis and XTG and SEM to look at the paramagnetic mineral assemblages and their orientation. Oliva- Urcia et al. (2010) find a qualitative relationship between AMS and strain in phyllites from Greece where directional strain data correlates well with AMS ellipsoids (they find K_{min}

parallel to Sz and K_{max} parallel to Sx). The quantitative relationship is less definable and the discrepancies have been accounted for by the effect of microstructural deformation processes including the dissolution and precipition of quartz and recrystallisation of phyllosilicates (Oliva-Urcia et al., 2010). However Oliva-Urcia et al. (2010) do note a weak correlation of the Sx and Sz axes with K_{max} of the AMS ellipsoid.

Pares et al. (2003) have carried out AMS studies on pencil structures found in Ordovician Mudstones of the Knobb's Fm. in the Valley and Ridge province of the US Appalachians. They find that the shape parameter Tj shows more sensitivity to strain than the magnetic intensity parameter Pj.

Jezek and Hrouda (2007) have developed a Matlab programme enabling the estimation of irrotational strain from AMS data, based on a theoretical relationship of strain and AMS. The programme only requires the input of anisotropy degree, P, shape parameter, T, and K_{max}, K_{int} and K_{min} values. Although the programme has been tested and shown to work for a strained laboratory specimen, they have found many limitations which make it unsuitable for use on field samples.

Part 3: Previous Studies using AMS in Sedimentary Rocks

3.18 General Previous Studies using AMS

Hirt et al. (2004) have used high and low field AMS in combination with X-ray Texture Goniometry (XTG) to look at the behaviour of paramagnetic minerals during deformation in shales and slates from the central Appalachian foreland fold and thrust belt, Pennsylvania. Hirt et al. (2004) find that the paramagnetic minerals (chlorite and mica) evolved from being parallel to the bedding fabric to being reorientated into the cleavage plane and the AMS fabric also evolved from being oblate in the bedding plane through to prolate in the pencil structure and prolate in the subsequent cleavage plane.

Anderson and Morris (2004) show that AMS can reveal information about the later stages of deformation and post-orogenic history. Anderson and Morris (2004), have used AMS to investigate the Bude Formation in Cornwall, which is Variscan crust in south west England. Anderson and Morris (2004) have found that there are prolate AMS ellipsoids which have their long axes (K_{max}) perpendicular to the fold hinges. They interpret this as being a result of late stage Variscan or post-Variscan subhorizontal stretching. They suggest that in this case the previous tectonic AMS fabrics that would have been expected in this type of setting have been completely

overprinted by this late stage extension. They attribute the extension to possible simple shear caused by the change from chevron to recumbent folding as modelled by Sanderson (1979) or post-orogenic extensional features such as late normal faulting (Freshney et al., 1972, cited by Anderson et al., 2004). Anderson and Morris (2004) have therefore demonstrated the importance of considering the subsequent post orogenic events to the main orogenic event when interpreting AMS.

Parés and Van der Pluijm (2002) show that predeformational fabrics influence the subsequent effects of strain. Parés and Van der Pluijm (2002) have carried out AMS on mudstones, slates and schists from the Pyrenees and Appalachians and noted the importance of lithology as well as strain in the outcome of the magnetic lineation direction. Parés and Van der Pluijm (2002) find that rocks with a weak pre-deformational fabric are more predisposed to the development of a magnetic lineation parallel to the tectonic extension direction.

Robion et al. (2007) have compared AMS from the Minervois Basin (NE Pyrenees France) and the Potwar Basin (SW Himalaya, Pakistan). Despite the fact that both basins have undergone deformation, the Minervois Basin has lost its primary sedimentary fabric while the Potwar Basin retains some of its sedimentary features (Robion et al., 2007). They suggest that the loss of sedimentary fabric in the Minervois basin is due to two mains reasons: Firstly there is the effect of coupling between basement and cover and secondly there is a low initial anisotropy caused by pedological process. Robion et al. (2007) suggest that pedalogical processes acted on sediments removing the primary bedding fabric leading to a more isotropic sediment which is more susceptible to recording subsequent deformation. This leads to an apparent high internal deformation in the Minervois Basin (NE-Pyrennees, France).

Pares et al. (1999) have used AMS to characterise the stages of cleavage development in mudrocks from the Southern Pyrenean Foreland Basin. They have deciphered from low temperature and anhysteretic remenant magnetisation that the AMS signal is dominated by paramagnetic minerals. Pares et al. (1999) suggest that the sediments were only partially lithified with the onset of deformation.

Mallik et al. (2009) have carried out AMS on 35 Jurassic sandstone samples from the both the forelimbs and back limbs of anticlines associated with two major reverse faults in the Kachchh region, western India. Mallik et al. (2009) have applied AMS as a

technique for fabric analysis of the anticlines in order to decipher the deformational history of the area. By characterising AMS fabrics into stages ranging from a primary sedimentary to tectonic overprint, and recognising three stages of magnetic fabric development and Mallik et al. (2009) were able to deduce that transpressional deformation is causing variations in stress and limb rotation of the anticline.

Oliva-Urcia et al. (2009) demonstrate the need to separate the magnetic fabric into subfabrics due to variation of the bulk AMS, orientations in an area of homogenously deformed Cretaceous limonites. Oliva-Urcia et al. (2009) have studied the contribution to AMS by the paramagnetic and ferromagnetic minerals using low temperature AMS and the Anisotropy of Anhysteretic Remenant Magnetisation (AARM) respectively. Oliva-Urcia et al. (2009) were then able to investigate the role of paramagnetic minerals and ferromagnetic minerals in tectonic deformation. Oliva-Urcia et al. (2009) observe long euhedral white mica crystals lying parallel to the cleavage plane and suggest that these are brought about by authigenic growth during deformation.

Schmidt et al. (2007) have looked at the separation of diamagnetic and paramagnetic minerals using high field torque measurements at both room temperature and low temperatures. Schmidt et al. (2007) use a theory that paramagnetic minerals have perfect oblate or prolate AMS ellipsoids and that a ratio of the paramagnetic fraction at room temperature to low temperature can be deciphered. Factoring this in with the fact that diamagnetic susceptibility is temperature independent but the paramagnetic susceptibility increases with decreasing temperature, then the diamagnetic contribution can be isolated.

Robion and Frizon de Lamotte (1995) have carried out AMS studies on the France-Belgium Ardennes Variscan Front. Robion and Frizon de Lamotte (1995) show that different mineralogical assemblages can contribute to and/or control different types of magnetic fabric. Robion and Frizon de Lamotte (1995) make three main associations between mineralogy and structural interpretation. These are: 1) phyllosilicates and hematite with the intersection lineation. 2) pyrrhotite and magnetite and possible maghemite with the transport direction and 3) post tectonic minerals; including multiple magnetic carriers with diffuse and planar fabrics and an undefined magnetic lineation.

Mattei et al. (1999) suggest that AMS may be used to differentiate extensional and compressional regimes in weakly deformed sedimentary basins. Mattei et al. (1999)

have used AMS to look at weakly deformed sedimentary rocks of the Amantae Basin, Calabria, Italy which have undergone a predominantly synsedimentary extensional regime. Mattei et al. (1999) find that while the magnetic foliation is parallel to the bedding planes, the magnetic lineations were subparallel to the dip of bedding. Mattei et al., (1999) suggest that this magnetic lineation is parallel to the stretching directions based on the analysis of faults and basement architecture. The study suggests that in extensional basins the magnetic lineation is parallel to the dip of the bedding while in compressional basins the magnetic lineation is parallel to the strike of the bedding.

3.18.1 Previous AMS Studies in the Munster Basin

McCarthy (PhD, 2014) has carried out AMS analysis towards the eastern margin of the Munster Basin (The Dingle Dungarvan Line, Chapter 2). Thermomagnetic studies on these samples suggest that predominantly paramagnetic minerals with some minor ferromagnetic (haematite) are responsible for the AMS fabric (McCarthy, 2014). In this study McCarthy (2014) finds that the AMS ellipsoids range from bedding controlled to cleavage controlled and that there is a general decrease in tectonic control of the AMS fabics from south to north across the eastern part of the Munster Basin's northern margin (the Dingle-Dungarvan Line). McCarthy (2014) also shows that tectonic controlled AMS ellipsoids lie to the south of the DDL (within the basin), intermediate types exist around the margin and bedding controlled AMS ellipsoids are found north of the DDL. This is the only previous study using AMS in the region of the Munster Basin.

Chapter 4:
Field Work

Chapter 4. Field Work

4.1 Introduction to the Field Area

Structural field work has been carried out on the Iveragh Peninsula Co. Kerry, south west Ireland in order to examine the effect of the Coomnacronia Fault on cleavage. A brief examination of cleavage on the Dingle Peninsula and Kerry Head is also discussed. These areas have been well established in the literature to lie in the Foreland to the north (Fig 4.1; Chapter 2). The Munster Basin is composed of Upper Devonian Old Red Sandstone (ORS) that has been deformed by the Variscan Orogeny. The Dingle Peninsula consists of Silurian and Lower to Upper ORS, whilst Kerry Head to the north consists of Upper ORS. The ORS has been deformed at the end of the Carboniferous by the Variscan Orogeny. The background geology of the area has been discussed in detail in Chapter 2. This regional study is mainly focused on the mid-section and the western part of the Iveragh Peninsula as this area provides the best opportunity to study the change in structural deformation across the strike of the Coomnacronia Fault. The field data has been collected from sites both inland and along the coast. There is excellent exposure along the coastal areas and moderate/good exposure inland where sites are selected for road cuts, quarries, corrie lakes and the areas of higher topography. The lowland inland areas on the south western part of the peninsula do not have good outcrop exposure however. The topography ranges from sea level to the highest at 1040 m at Carrauntoohil in the MacGillycuddy's Reeks, but the majority of sites are taken close to sea level or within the first 100 m to 300 m as at these levels the accessibility to outcrop is the best allowing for numerous sites to be visited. The area generally becomes more mountainous further inland towards the east (the MacGillycuddy’s Reeks and the Gap of Dunloe area, Map Insert 3).

4.2 Aims and Objectives

As detailed in Chapter 1, the purpose of this study was to characterise the change in structural styles across the Coomnacronia Fault and in doing so investigate if the Coomnacronia Fault is the northern margin of the Munster Basin. This chapter investigates the macroscopic structural styles, from south to north of the field area, and if the Coomnacronia Fault marks a significant boundary between cleavage styles. The northern margin of the Munster Basin has been traditionally considered to be located at the Dingle Bay Galtee Fault Zone - DBGFZ (part of which is the Kilarney Mallow Fault

Zone - KMFZ, See Map Insert 1), or at the Dingle Dungarvan Line (DDL, part of which is also the KMFZ). However, as discussed in Chapter 2, there is significant southward sedimentary thickening across the Coomnacronia Fault (Williams, 2000), a fault which lies to the south of the DDL and the DBGFZ indicating that this may have been a basin margin fault. In an attempt to assess the validity of the interpretation of the Coomnacronia Fault as a basin margin fault, the strain regime across the fault and the impact that this fault has on the Variscan cleavage front has been investigated.

4.3 Summary of Previous Work Done

Previous work carried out on cleavage on the Iveragh Peninsula, the northern margin and the CF is discussed in detail in Chapter 2. The following summarizes the current key understandings:

4.3.1 Cleavage.

Cleavage in the Munster Basin has generally been described as:

- Axial planar to folding (Capewell, 1957; Naylor et al., 1981; Sanderson, 1984; Cooper et al., 1986) with minor amounts of fanning (Chapter 2).
- Steeply dipping to the south (e.g. Sanderson, 1984) and north (e.g. Bresser and Walter, 1999).
- Occurs less frequently as a spaced disjunctive cleavage in sandstones and more commonly as a slaty cleavage in siltstones.
- The only occurrences of gently dipping cleavage that have been previously recorded are by Capewell (1975) at Valentia Island Slate Quarries (25-30° dip) and by Wingfield (1966), just to the south of Lough Leane area Kilarney (40-60 ° dip). No structural interpretations have been made for these findings.
- There are small amounts of cleavage refraction and fanning (e.g. Bresser and Walter, 1999).
- Cleavage was initiated as an LPS fabric during the early stages of folding and continued to develop throughout Variscan Deformation (e.g. Cooper et al., 1986).
- The Geological Survey of Ireland map shows cleavage generally dipping steeply to the south with some northerly dipping cleavages (Map Insert 1: GSI data Pracht, 1996).

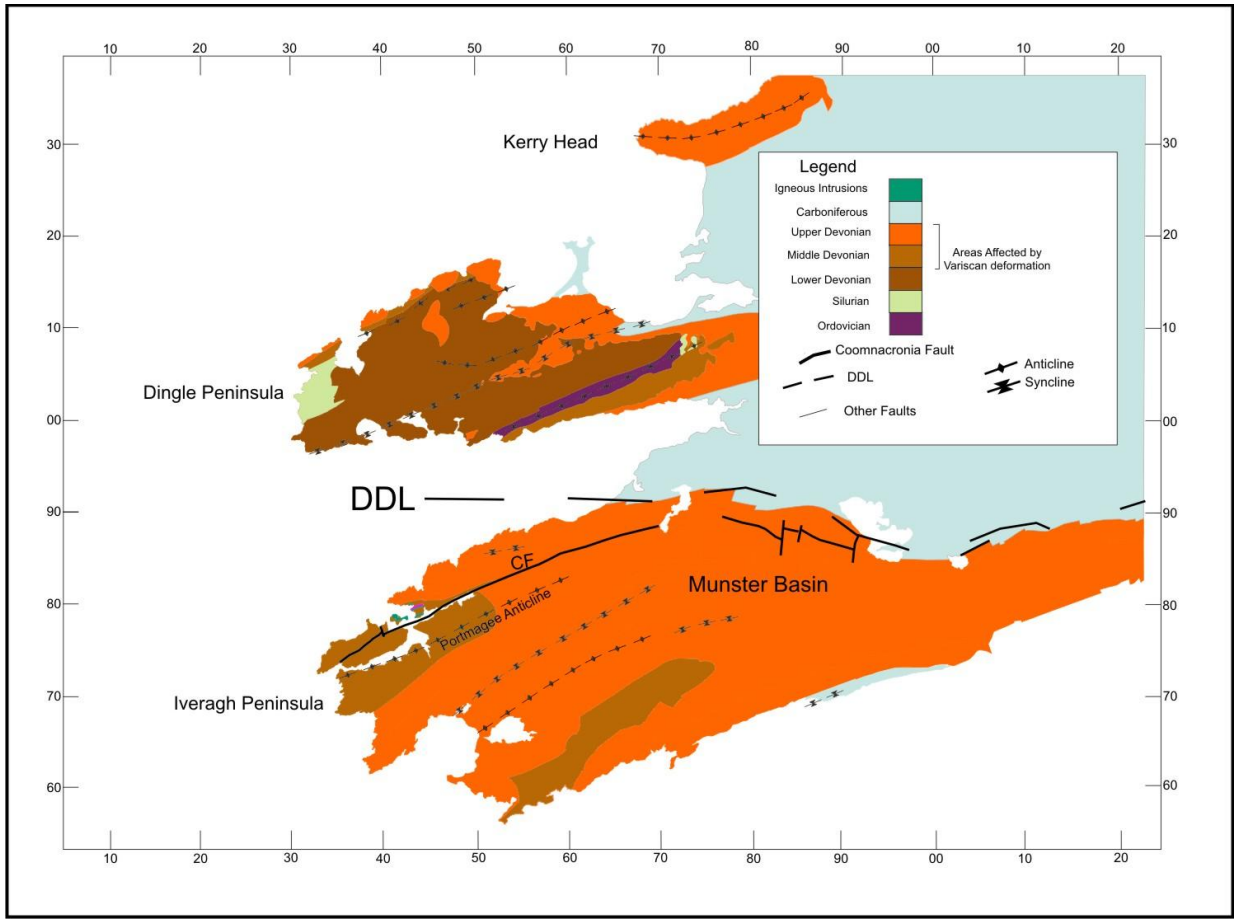

Figure 4.1 The distribution of Lower, Middle and Upper ORS on the Iveragh Peninsula, Dingle Peninsula and Kerry Head. The Dingle Dungarvan Line (dashed line) was one of the lines previously considered to be the northern margin of the Munster Basin. In this study the Coomnacronia Fault (CF) is investigated as a potential northern margin of the Munster Basin.

4.3.2 The DBGFZ & DDL

- The DDL is discussed in Chapter 2 and is one of the previous suggestions for the northern margin.
- The DBGFZ has been previously considered to be a southerly dipping Munster Basin margin fault and the westward lateral equivalent of the KMFZ (e.g. Gill, 1962; Cooper, 1986).
- In more recent studies the DBGFZ has been suggested not to be the Munster Basin margin fault but to be a northerly dipping structure bounding the Dingle Basin as interpreted from seismic evidence (e.g. Vermeulen, 1998; Landes, 2000).

4.3.3 The CF

The Coomnacronia Fault has been suggested to be:

- An intrabasinal fault with major southward stratigraphic thickening by Williams (2000).
- A thrust fault by Capewell (1975).

4.4 Methodology

The field work has been carried out in two main stages:

1. A regional cleavage study has been carried out across the study area. This involved the collection of bedding and cleavage data from a total of 65 sites in order to map out the cleavage pattern across the area. The 65 sites are located mostly to the western and northern areas of the Iveragh Peninsula as these areas provide the best exposure but there are also sites towards the mid section and the east as far inland as Glenflesk Quarry (Map Insert 1: Cleavage Results). Cleavage readings have been taken from both coarse-grained and fine-grained lithologies from all four formations: The Ballinskelligs Sandstone Fm., The Valentia Slate Fm., The Lough Acoose Sandstone Fm. and The St. Finan's Sandstone Fm. across the study area. Of the 65 sites 35 sites are single point readings (1 bedding and/or 1 cleavage depending on outcrop quality). Single point readings were taken in areas where outcrop was poor and also collected from the AMS sample sites (25 sites. Chapter 5). Multiple cleavage readings (30

sites) were taken from selected sites where there was good outcrop spread across the study area. Multiple cleavage data was collected in order to show the consistency of the cleavage orientations for each site. All site data can be found in Appendix A. Based on these results, a regional cleavage map of the Iveragh Peninsula has been compiled. The cleavage results have been compiled onto a map along with the pre-existing Geological Survey or Ireland (GSI) data.

2. Of the 65 sites, field work was carried out on 13 key sites that showed excellent examples of the behaviour of cleavage on a macroscale. At these sites the relationship between cleavage and folding was investigated and used as an indication of how much Variscan deformation has occurred (See sections-4.5.4.3 & 4.5.5.3). This involved measuring the angle between bedding and cleavage across a fold profile. The key sites along with field data are listed in Appendix A: Coosfada, Canglass Point, Coonama Harbour, Culoo Rocks and Near to Rossbeigh to the north of the Coomnacronia Fault and Ballinskelligs Pier, Ballygasheen Pass, Road to Caherdaniel, Derrynane Beach and Killabounia to the south of the Coomnacronia Fault. Also the angles between bedding and cleavage have been compiled from all the other field locations where there was at least one paired bedding and cleavage reading (Appendix A). A total of (65) angles between bedding and cleavage have been measured in order to demonstrate the behaviour of cleavage in relation to bedding. Field work has been carried out on the Coomnacronia Fault where it outcrops at Lake Coomnacronia. Exposure of the Coomnacronia Fault is generally limited in the study area however this location provides excellent exposure of the Coomnacronia Fault. Cleavage data has been collected in the vicinity of this fault in order to assess the local impact that this fault has on cleavage orientation.

4.5 Field Work Results

4.5.1 Structural Zonation Scheme for the ORS of the Iveragh Peninsula, Dingle Peninsula and Kerry Head.

Three main zones have been identified based on the integration of the field work results and previous published data (Chapter 2) across the Iveragh Peninsula, the Dingle Peninsula and Kerry Head.

- Zone 1: The Intrabasinal Zone.
- Zone 2: The Transition Zone.
- Zone 3: The Foreland Zone.

Zone 1 and Zone 2: Structural field work has been concentrated on the Iveragh Peninsula which contains Zone 1 and Zone 2 as this is the area where the potential basin margin fault, the Coomnacronia Fault, lies. The Foreland Zone lying to the north of the Munster Basin Margin has been already established in the literature as being part of the foreland to the north (Chapter 2: Geological Setting).

4.5.2 Regional Cleavage Map of the Iveragh Peninsula

A detailed cleavage map of the Iveragh Peninsula has been compiled in order to investigate the effect that the Coomnacronia Fault has on the cleavage orientations on the Iveragh Peninsula. This has been done in order to assess if the Coomnacronia Fault is a potential basin margin fault. It is proposed that if the Coomnacronia Fault is a basin margin fault then it would affect the orientations of the Variscan cleavage to the south of the Fault. The regional cleavage map of the Iveragh Peninsula shows that the Coomnacronia Fault does have a clear impact on the cleavage orientations.

In Zone 1: the Intrabasinal Zone, the cleavage is generally steeply dipping and axial planar to folding. The cleavage predominantly dips steeply to the south, but there is also some cleavage which is steeply dipping to the north (section 4.5.4).

In Zone 2 the cleavage orientations become much more variable and the dip ranges from steeply dipping to the south to gently dipping to the south (section 4.5.5).

Zone 3 will be discussed in section 4.5.6-Zone 3: The Foreland Zone. This zone has not been included on the regional cleavage map, as the map was focused on the effect of the

Coomnacronia Fault on cleavage and therefore required the map to be a detailed map of the Iveragh Peninsula where the Coomnacronia Fault exists.

4.5.3 The Coomnacronia Fault

The Coomnacronia Fault is a major map scale fault that runs along the northern part of the Iveragh Peninsula and marks a boundary between the Saint Finan's Sandstone Fm. to the south and the Ballinskelligs Sandstone Fm. to the north (Cleavage Results Map). The Coomnacronia Fault may be considered to be the westward continuation of the Black Lake Fault at the Gap of Dunloe and the KMFZ (Chapter 2). The KMFZ is considered to be a basin margin fault (Price and Todd, 1988; Meere, 2007). The CF can be clearly seen at Lake Coomnacronia, close to Glenbeigh (Fig 4.2 i & ii). The findings of this study show that the Coomnacronia Fault marks the boundary between two different structural zones: the Intrabasinal Zone to the south and the Transition Zone to the north. Cleavage orientations have been observed in close proximity to the Coomnacronia Fault (Fig 4.2). Due to access and steep topography the numbers of cleavage and bedding readings in these locations are limited. However the local data from this site indicates that this fault marks a boundary between two very different structural areas and is in agreement with these findings as shown on the regional cleavage map.

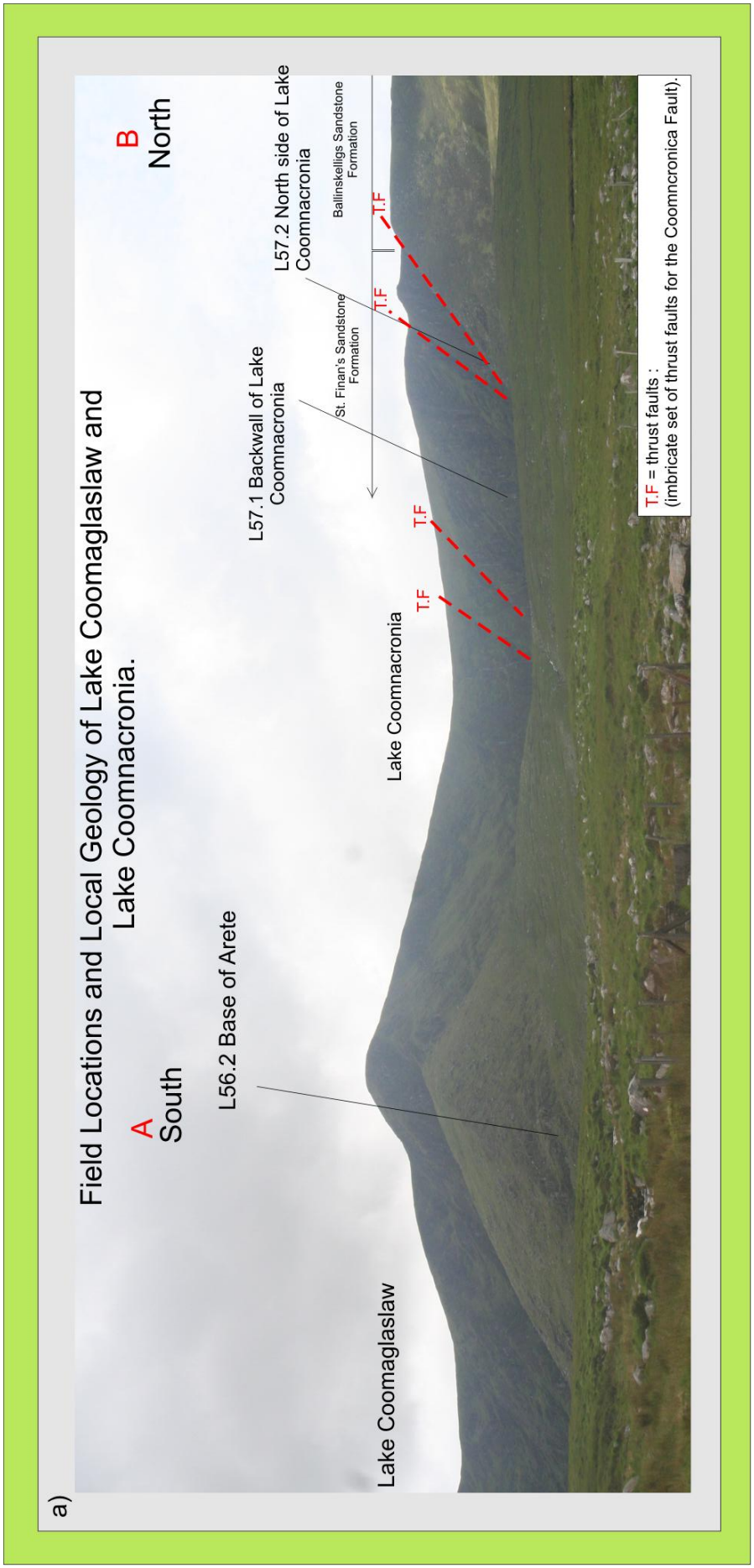
a)
Field Locations and Local Geology of Lake Coomaglaslaw and Lake Coomnacronia.
A South
B North
L56.2 Base of Arete
L57.1 Backwall of Lake Coomnacronia
L57.2 North side of Lake Coomnacronia
Ballinskelligs Sandstone Formation
St. Finan's Sandstone Formation
T.F
Lake Coomnacronia
Lake Coomaglaslaw
T.F = thrust faults :
(imbricate set of thrust faults for the Coomncronica Fault).

Fig 4.2 i)

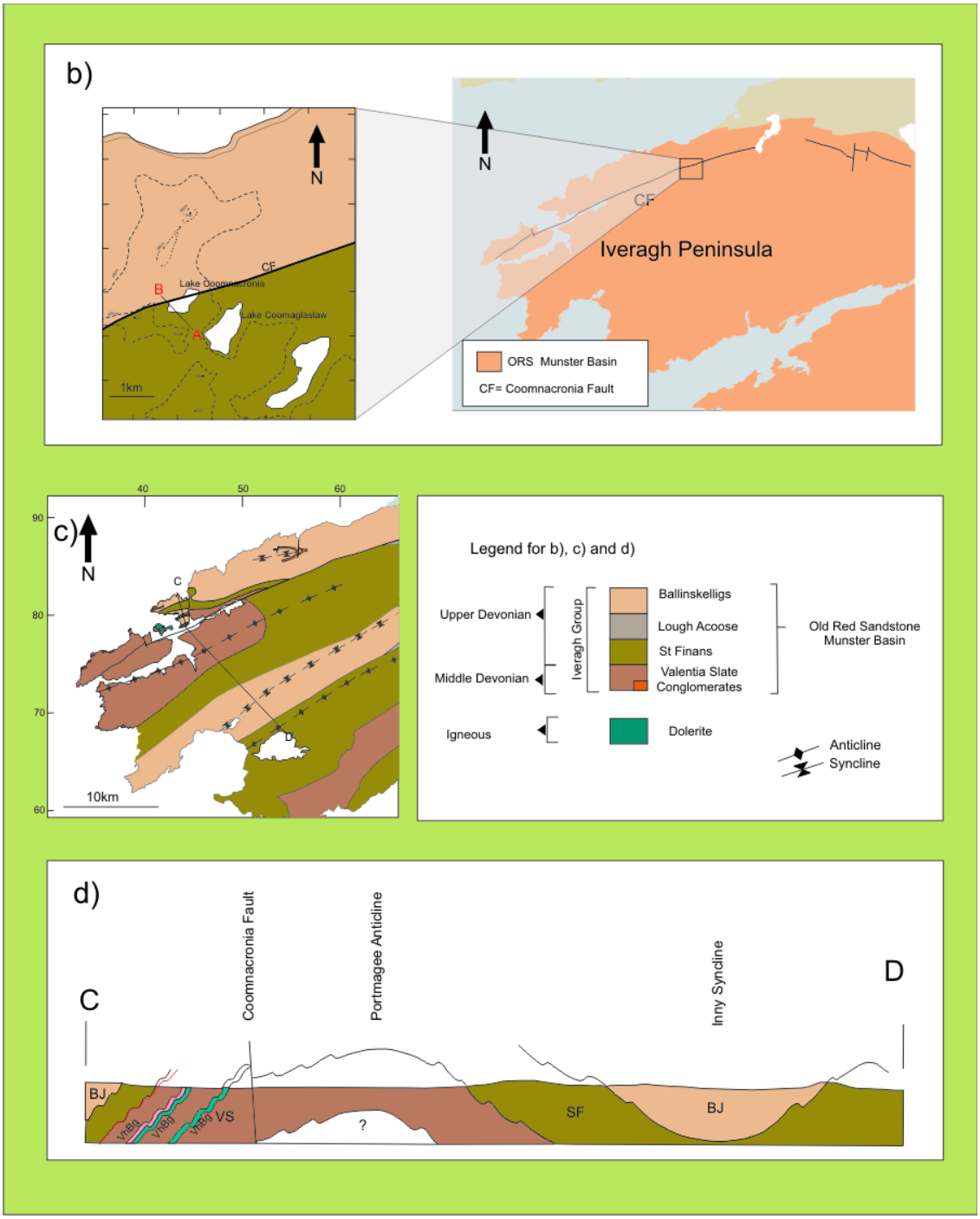

Figure 4.2i) overleaf **a)** Lake Coomaglaslaw and Lake Coomnacronia showing the field locations L56-L57. Line A-B is shown in b). **4.2ii) b)** The local geology of the Coomnacronia Fault (CF). The Ballinskelligs Sandstone Fm. (BJ) lies to the north and the St Finan's Sandstone Fm. (SF) lies to the south of the CF (modified from Pracht, 1996) **c) & d)** Line C-D is a cross section showing the Coomnacronia Fault as a thrust fault on the northern Limb of the Portmagee Anticline. Redrawn from GSI; Pracht ,1996).

Lake Coomaglaslaw (L56.2)

L56.2 is located in the St Finan's Sandstone Fm. at the base of the arete between Lake Coomaglaslaw and Lake Coomnacronia (Fig 4.2i). There is some gentle to moderate folding with steeply dipping axial planar cleavage with a dip of 50-70° S. Cleavage is generally steeply dipping to the south (Fig 4.3).

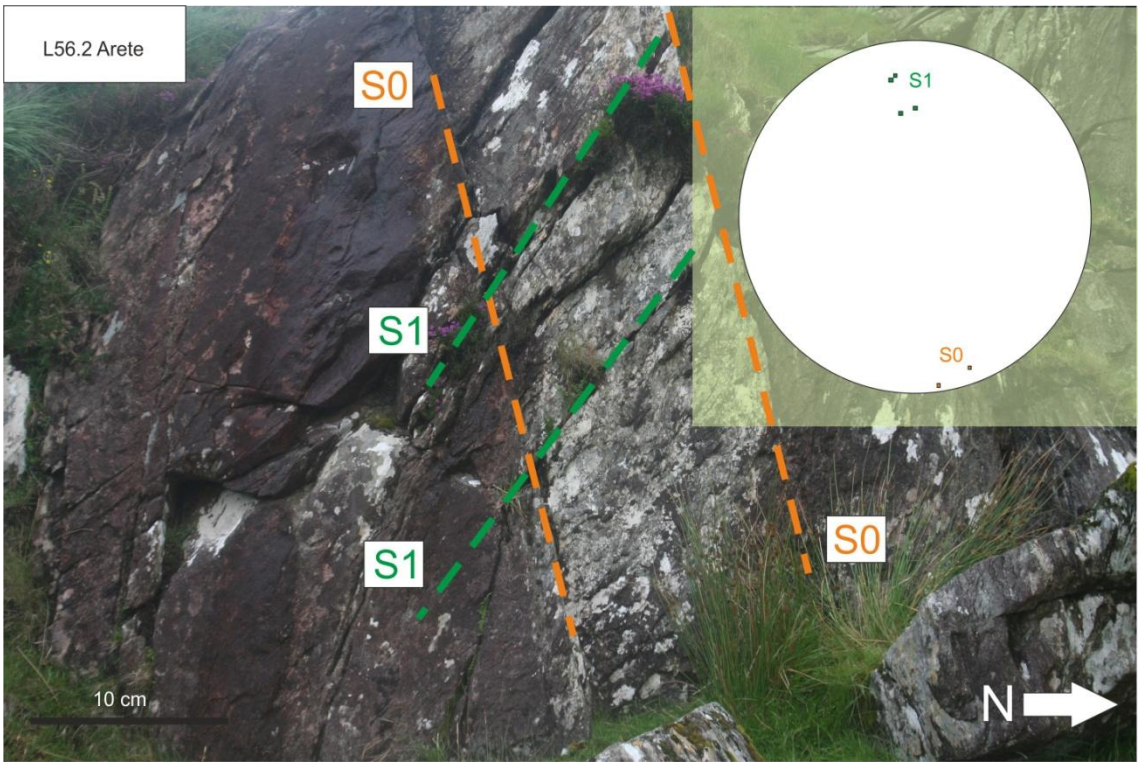

Figure 4.3 Base of the arete between Lake Coomaglaslaw and Lake Coomnacronia (L56.2) shows steeply dipping cleavage.

Lake Coomnacronia (L57.1 & L57.2)

The Coomnacronia Fault (CF) is located at Lake Coomnacronia (Fig 4.2) and appears to consist of a number of imbricate thrusts which have chevron folds spanning across the fault zone in the hangingwall (Fig 4.4). In the hanging wall towards the south of the lake Coomnacronia, the cleavage is moderately to steeply dipping (Fig 4.5). At the left hand side of the backwall of Lake Coomacronia (Fig 4.4), access is poor but cleavage is observed to dip at 80 ° S. There are numerous tight chevron folds (Fig 4.5, 4.6) as observed from the north side of the lake. Moving further north along the backwall of Lake Coomnacronia towards the main thrust faults it is possible to view the cleavage up close (Fig 4.6 & 4.7). The cleavage becomes more gently dipping and begins to show a passive rotation with bedding (Fig 4.7).

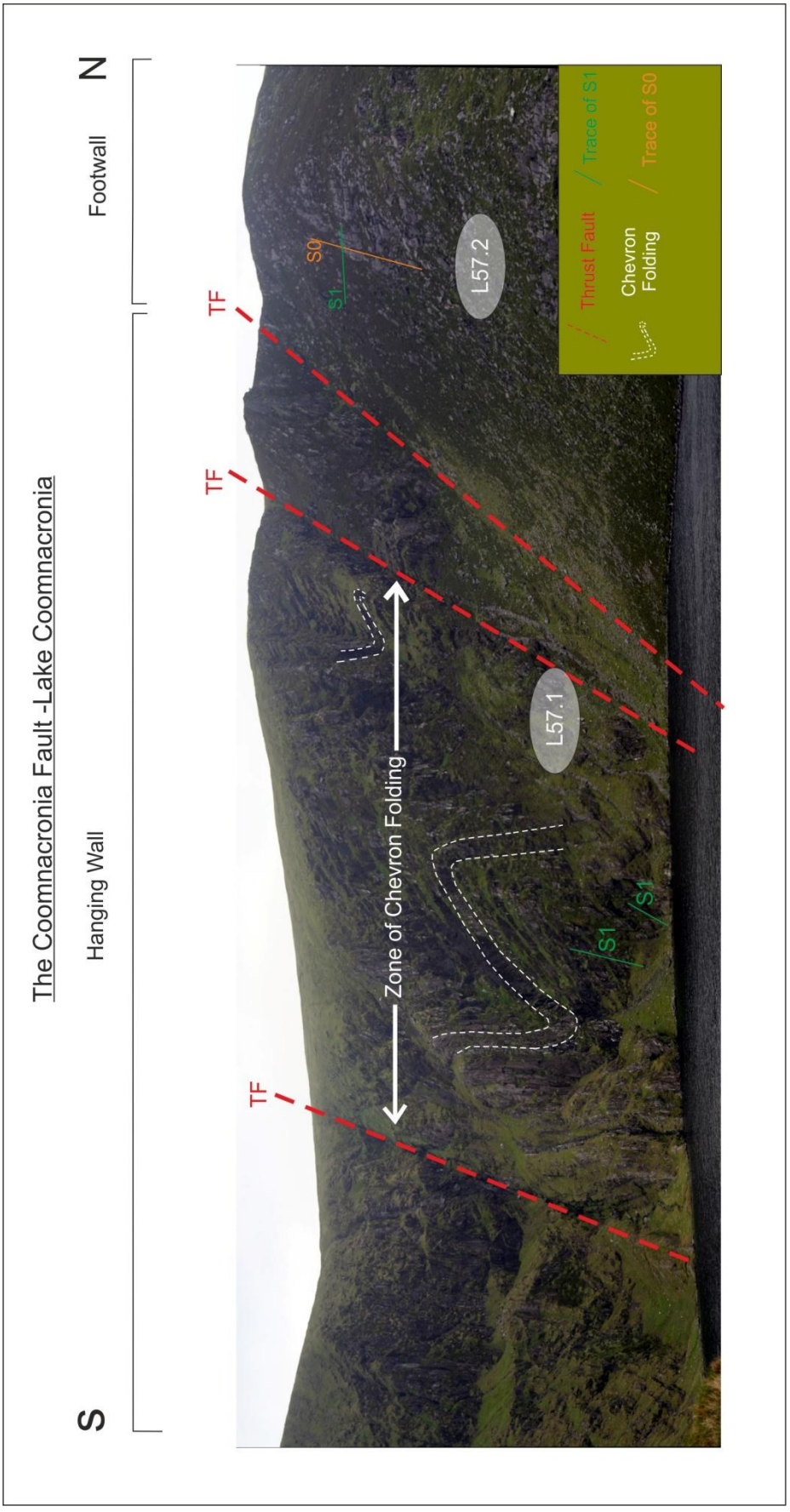

Figure 4.4 The Coomnacronia Fault viewed from Lake Coomnacronia shows imbricate thrust sheets and chevron folding. This type of chevron folding is not found to the south of this location in the Munster Basin.

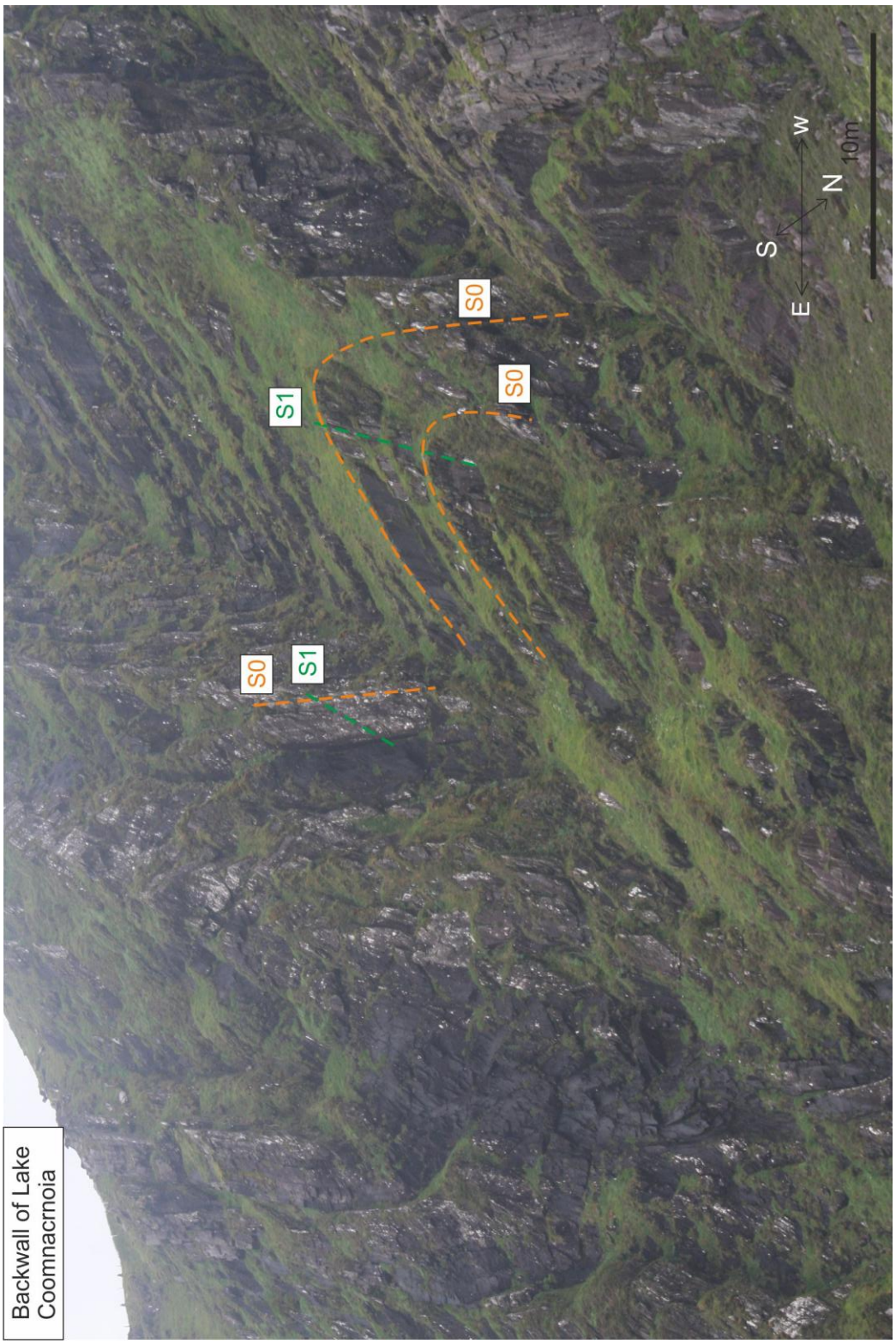

Figure 4.5 Steep chevron folding at central/ left hand side of the backwall of Lake Coomnacronia showing steeply dipping cleavage.

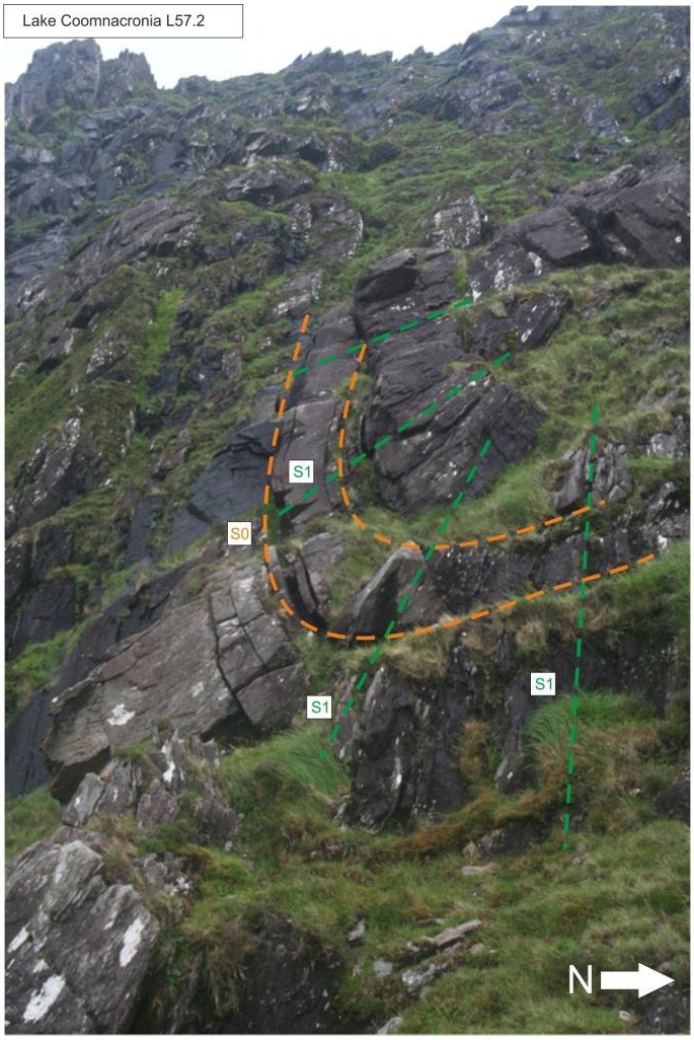

Figure 4.6 Above L57.1 on the north side of Lake Coomnacronia, the fabric (S1) begins to rotate to around 40° dipping to the south.

Figure 4.7 Left L57.2 a fold at the right hand side/back section of Lake Coomnacronia, possibly to the north of the imbricate thrusts or within the last set of thrusts, on the north hand face of the escarpment. In this fold the fabric (S1) appears to rotate with the bedding.

L57.2b North Side of Lake Coomnacronia

At the north side of Lake Coomnacronia, the lithology is the Ballinskelligs Fm. (L57.2). The bedding is steeply dipping and the cleavage is gently inclined at 25-30° S (Fig 4.8). This location (L57.2) lies to the north of the visible imbricate thrusts and may be within or close to the footwall at this point.

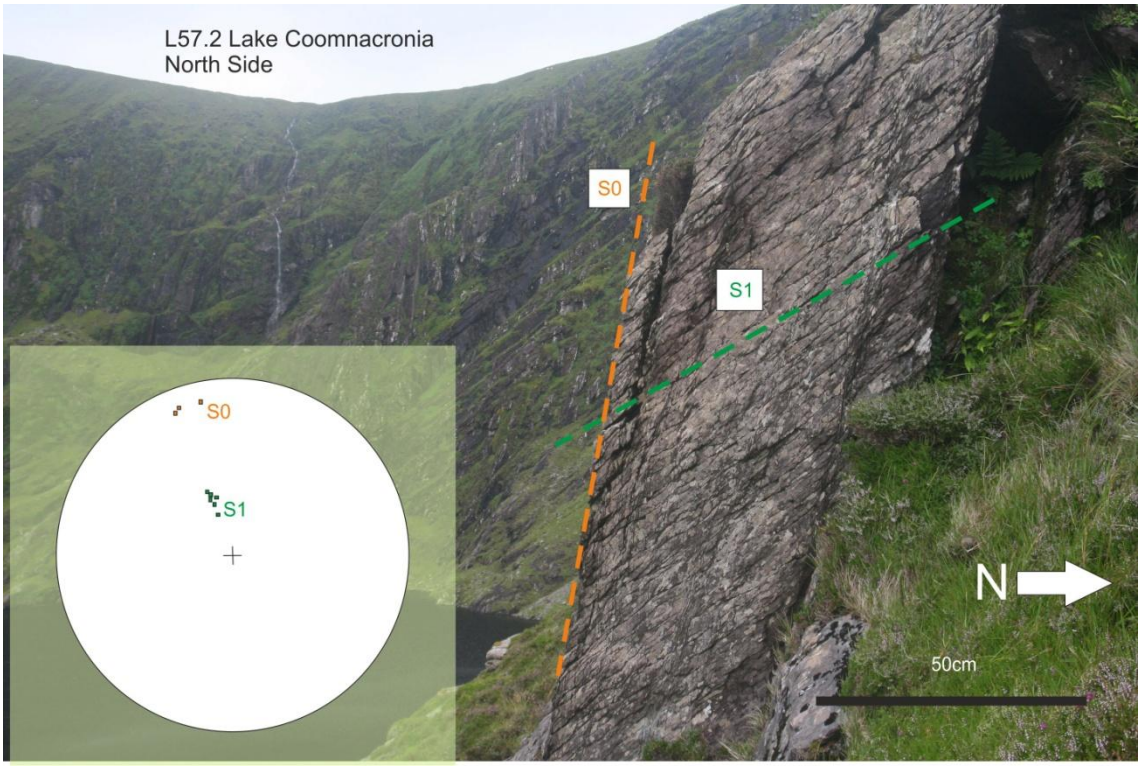

Figure 4.8: in the foreground (north side of the Lake Coomnacronia) steeply dipping beds from the limb of a chevron fold with a shallow dipping fabric (S1) set against the backdrop (backwall of Lake Coomnacronia) of chevron folding. The bedding /S1 relationship indicates overturned bedding.

4.5.3.1 Summary of Field Work on the Coomnacronia Fault

Overall this area clearly demonstrates that the set of imbricate thrusts which make up the Coomnacronia Fault has a direct impact on the orientation of the cleavage. In a relatively short transect (approximately 1.5 km) from south to north, the cleavage dip changes significantly from dipping at 80 ° S to 25° S. Across the section the folding changes from gentle to moderate folds in the south to tight chevron folds at Lake Coomnacronia. No other major faults with associated chevron folding and passive rotation of cleavage have been previously recorded or observed in this study in the Munster Basin.

4.5.4 Zone 1: The Intrabasinal Zone

The Intrabasinal Zone encompasses all of the Iveragh Peninsula south of the Coomnacronia Fault. It has been called the Intrabasinal Zone as it is the main infill material of the Munster Basin. The folding in the Munster Basin on the Iveragh Peninsula generally consists of two large scale anticlines: the Portmagee Anticline to the north and the Kilkrohane Anticline to the south with the Inny Syncline in between (Chapter 2, Fig 2.40). The Coomnacronia Fault is exposed on the northern limb of the Portmagee Anticline. The folds are generally large scale with some minor amounts of small scale parisitic folds. Bedding is generally uniformly dipping and forms part of the north and south limbs of the large scale anticlines and synclines. Common features to be found include joints, veins, ripple marks, bedding-cleavage intersection lineations and slickensides. Bedding thickness have been found to range from 10-80 cm in the sandstones. The faulting consists of syndeformational to late stage small scale thrust faults and late stage cross faults (discussed in detail in Chapter 2). The only major map scale fault on the Iveragh Peninsula is the Coomnacronia Fault.

4.5.4.1 Zone 1: The Intrabasinal Zone - General Cleavage Orientations

In the Intrabasinal Zone, the cleavage is generally axial planar and steeply dipping to the south and to the north. Cleavage dip generally ranges from about 60- 88° S and 80-90° S and N (Map Insert 2: Cleavage Results). The steeply dipping south and north cleavage is a result of cleavage fanning across the large scale anticlines and synclines. On a local scale the cleavage fanning occurs on small scale folds (for example: L53 Derrynane). In most sites the cleavage is found to be dipping to the south and the northerly dipping cleavage is noted at Keel Bay (A3M), SE of Keel (A4), Rossmore (A8) and Kilgarvan (A14). The cleavage data plotted on the stereonets is generally closely grouped showing the consistency of the cleavage and demonstrating that these cleavage data are representative of the regional cleavage (Cleavage Map Insert 1).

There has been no gently dipping cleavage observed in any parts of the study area in the Intrabasinal Zone. Cleavage is well developed in both the finer grained slaty horizons and also can be observed in much of the coarser lithologies. Cleavage in the sandstones may be spaced and disjunctive but is generally a very faint fabric, sometimes not visible and sometimes more obvious towards the bedding surface where it begins to refract. There are clearly developed bedding/cleavage intersection lineations in much of the sandstones.Some refraction of cleavage is observed between the sandstone and the

siltstones, especially in smaller scale gentle folds where there is flexural slip (for example Ballinskelligs Pier, Fig 4.14). A number of key locations show particularly well the intrabasinal cleavage on the Iveragh Peninsula (Section 4.5.4.2).

The strike of the cleavage maintains a close relationship to the strike of the Coomnacronia Fault in the west of the study area. In the east of the study area, at the faults at Torc Waterfall, the cleavage strike swings slightly to maintain a concordant relationship with the strike of the faults. The dip of the cleavage is around 60° in close proximity to the Coomnacronia Fault, which itself has a dip of 60° (See Chapter 2, Coomnacronia Fault Section).

4.5.4.2 Key Locations showing Axial Planar Cleavage in the Intrabasinal Zone

L53 Derrynane Beach

The lithology in this area consists of the St. Finan's Sandstone Fm. The area consists of number of small scale gentle folds which plunge gently (10-40 °) to the west and have steeply dipping axial planar cleavage (Figs 4.9 - 4.12).

Derrynane Beach Fold 1

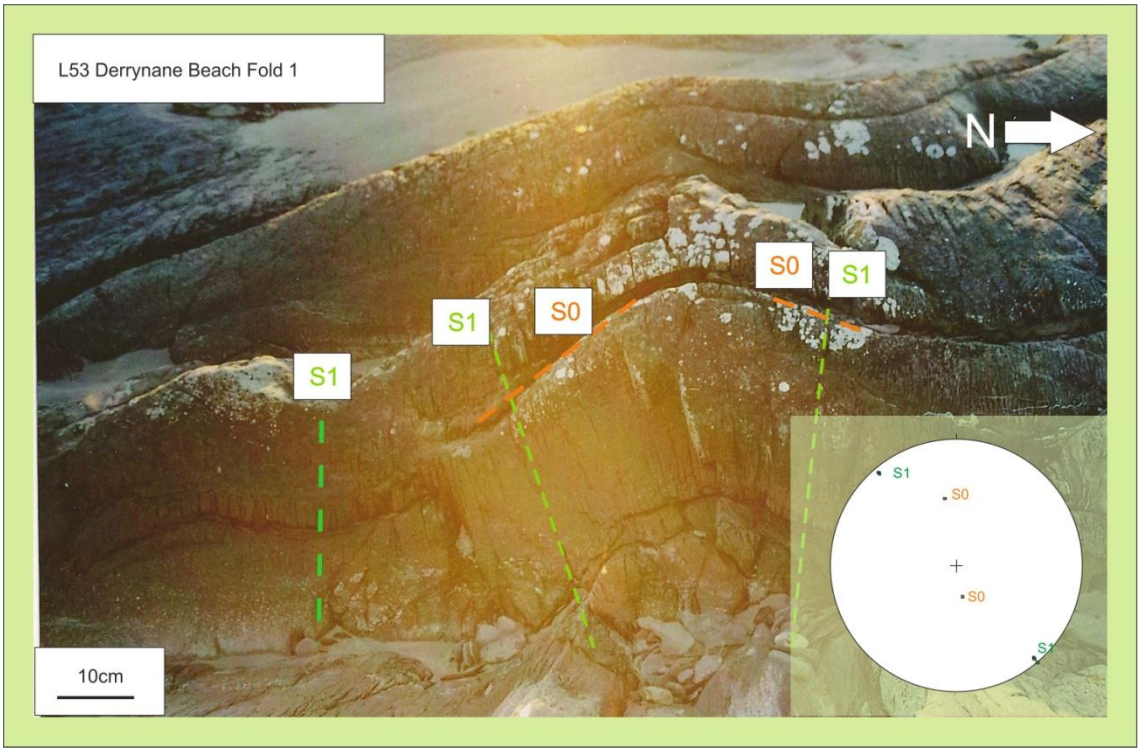

Figure 4.9 shows axial planar cleavage from the Munster Basin. Location: Derrynane Beach. Fold plunge = 38-235; S1 ranges from 050 85 N-050 85 S.

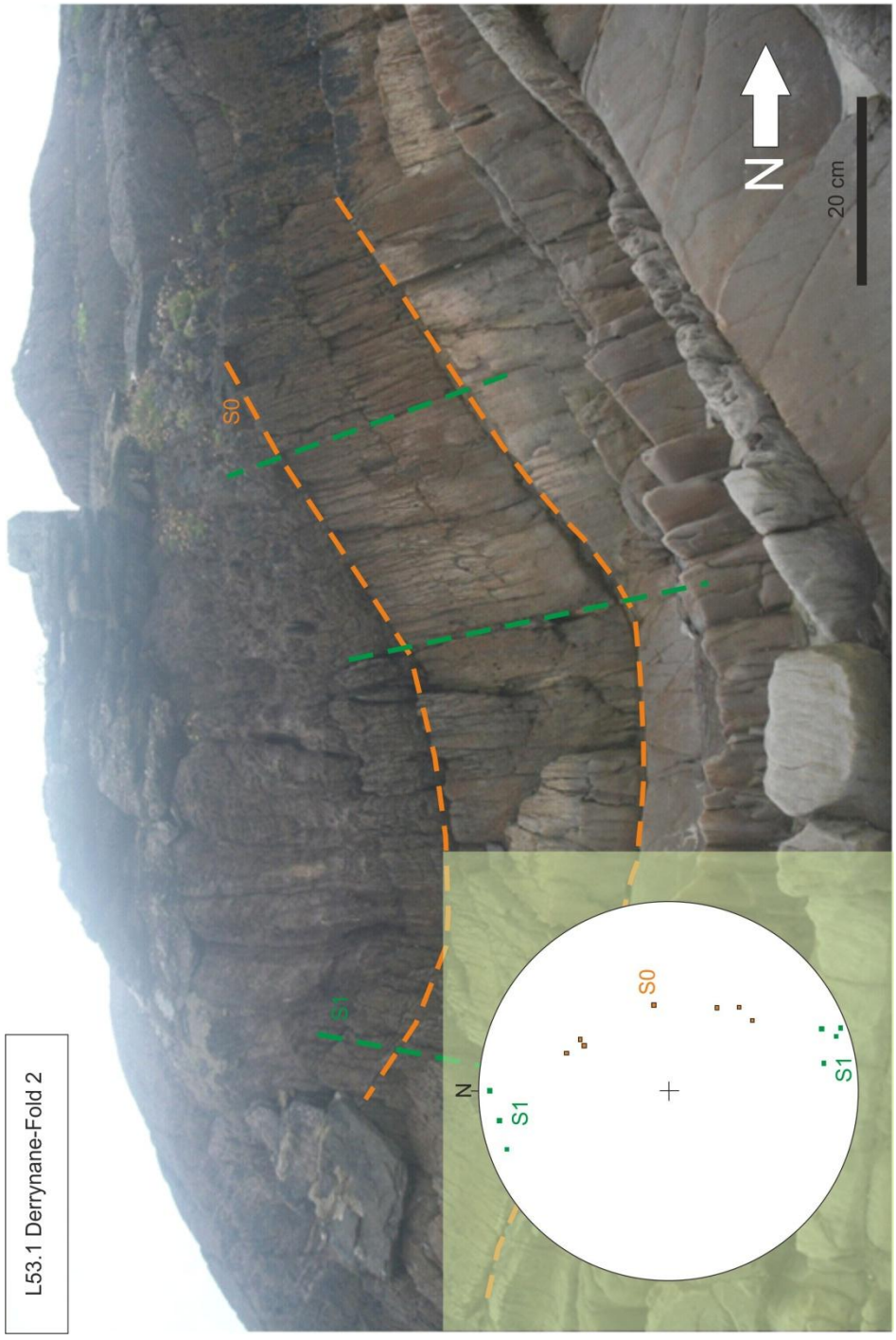

Figure 4.10 L53 Fold 2 north side of Derrynane Beach- showing axial planar cleavage.

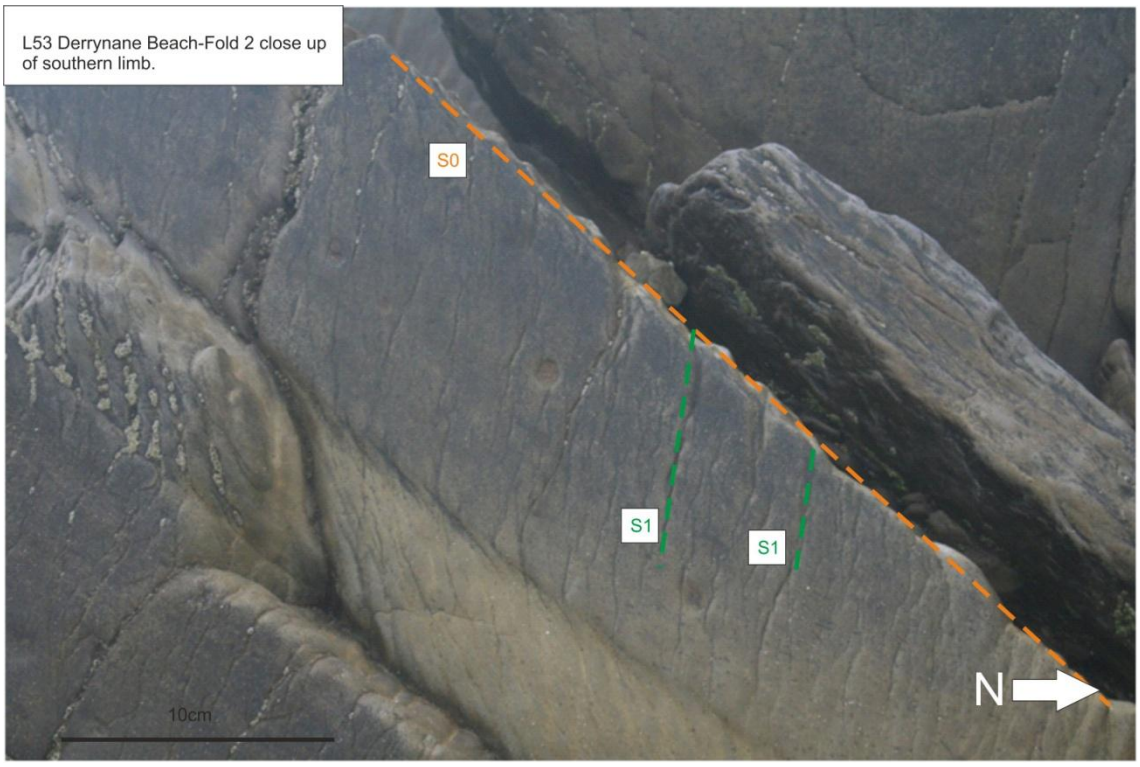

Figure 4.11 L53.1 Derrynane Beach - Fold 2: close up of southern limb showing bedding and cleavage.

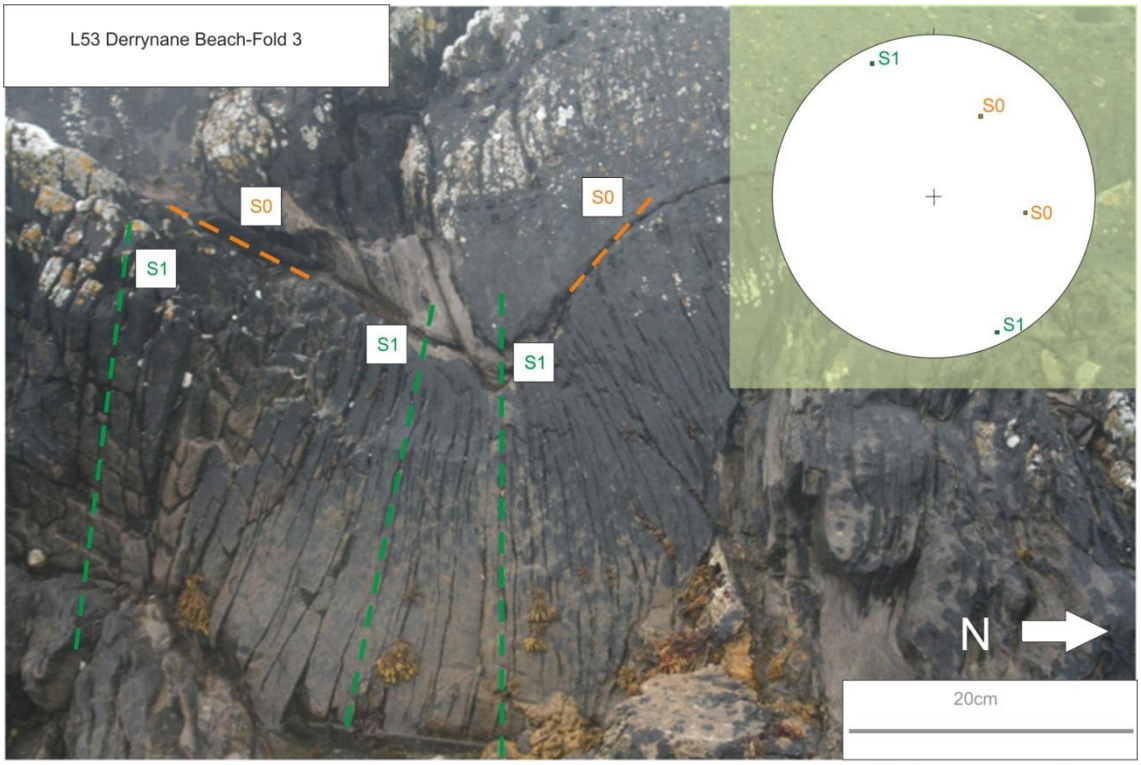

Figure 4.12 L53.1 mid section of Derrynane Beach – Fold 3: axial planar cleavage.

A6.1 near Caherdaniel

This area consists of steeply dipping south-westerly beds with a steeply dipping southerly cleavage (Fig 4.13). The beds form part of the southern limb of the Currane syncline (Capewell, 1975; Chapter 2) which plunges to the south west. An AMS sample (A6) has been taken within 100 m of this site (Chapter 5. AMS Results).

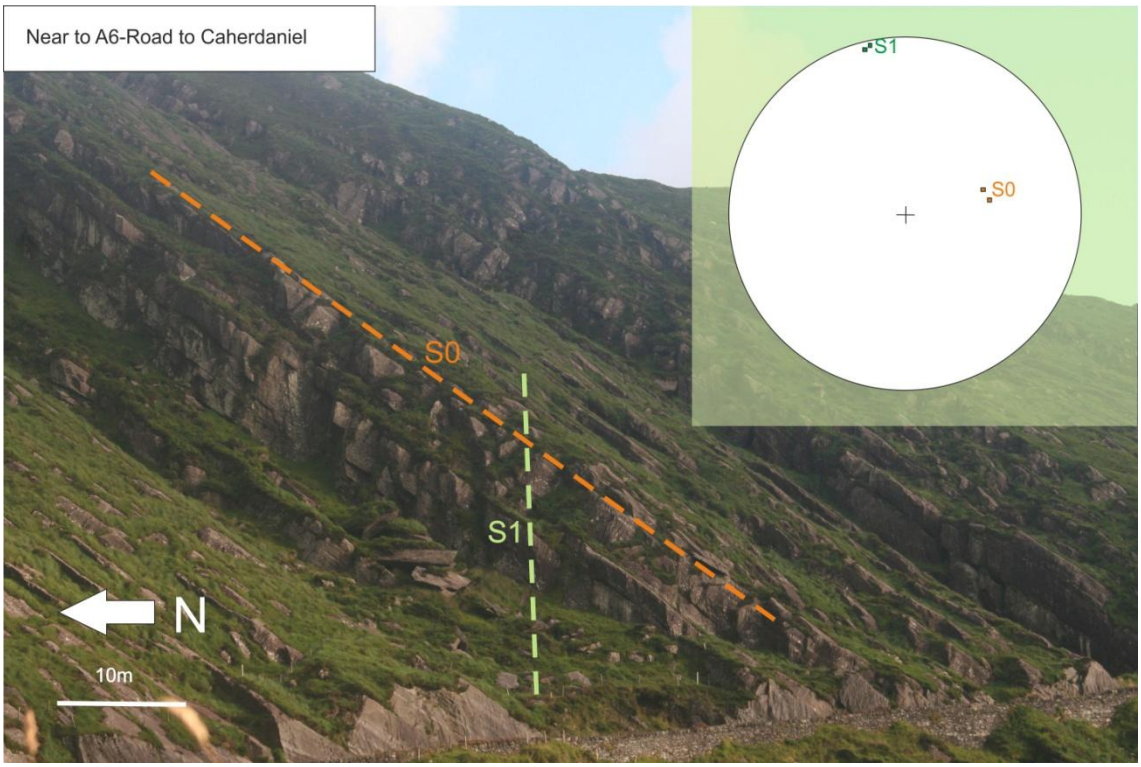

Figure 4.13. Steeply dipping bedding near to location A6: Road to Caherdaniel. The beds are orientated at 162 38 S and the axial planar cleavage is orientated at 078 88 S

L54 Ballinskelligs Pier

In this location the lithology is the Ballinskellig's Sandstone Fm. The beds are approximately 10- 40 cm thick and are uniformly dipping to the north. The cleavage is generally steeply dipping to the south and there is some evidence of cleavage refraction in the layers (Fig 4.14).

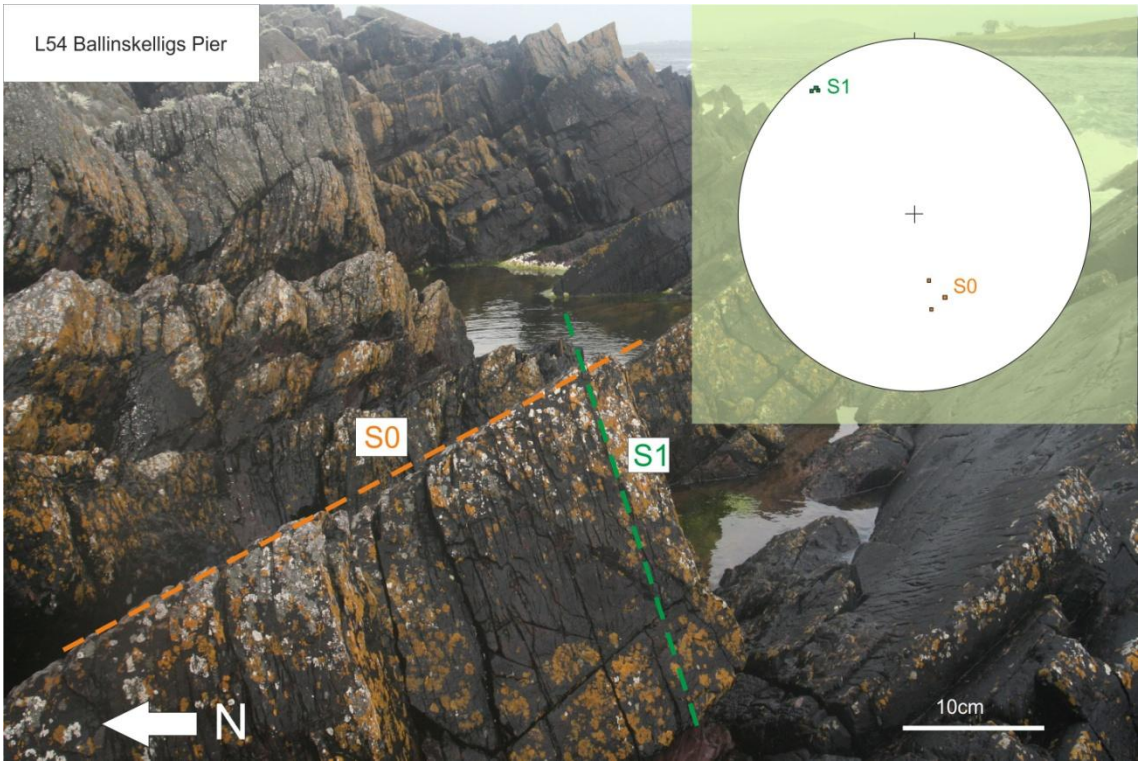

Figure 4.14 L54 Ballinskelligs Pier with moderately dipping beds and steeply dipping cleavage.

L52 Ballygasheen Pass

This area consists of steeply N-dipping beds with a steeply dipping to the south cleavage. Beds are orientated at 056 56 N and the cleavage is orientated at 060 62 S (Fig 4.15).

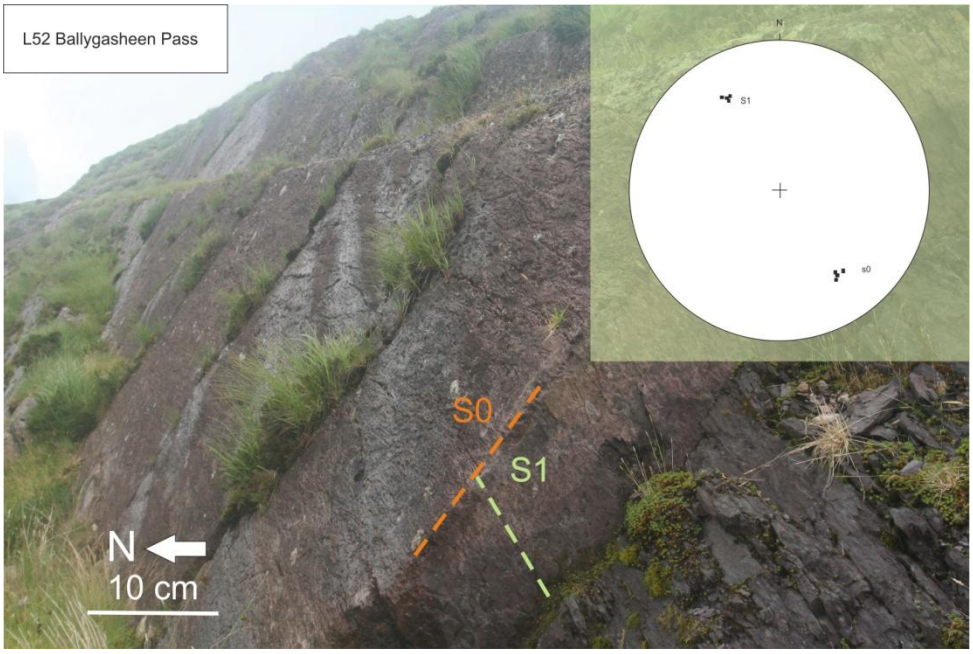

Figure 4.15 L52: Ballygasheen Pass. Bedding is steeply dipping to the north while cleavage is steeply dipping to the south.

A2.1 Killabounia

This site is located to the south of the Coomnacronia Fault in the Valentia Slate Fm. An AMS sample has been taken < 10 m from this site (Chapter 5). This site also shows the typical steeply dipping axial planar cleavage of the Munster Basin (Fig 4.16). The area is located on the southern limb of the Portmagee Anticline. The beds are uniformly dipping and have an average thickness of 30 cm. The lithology is medium to coarse grained sandstones. Cleavage is axial planar to folding and maintains an average orientation of 052 83 S.

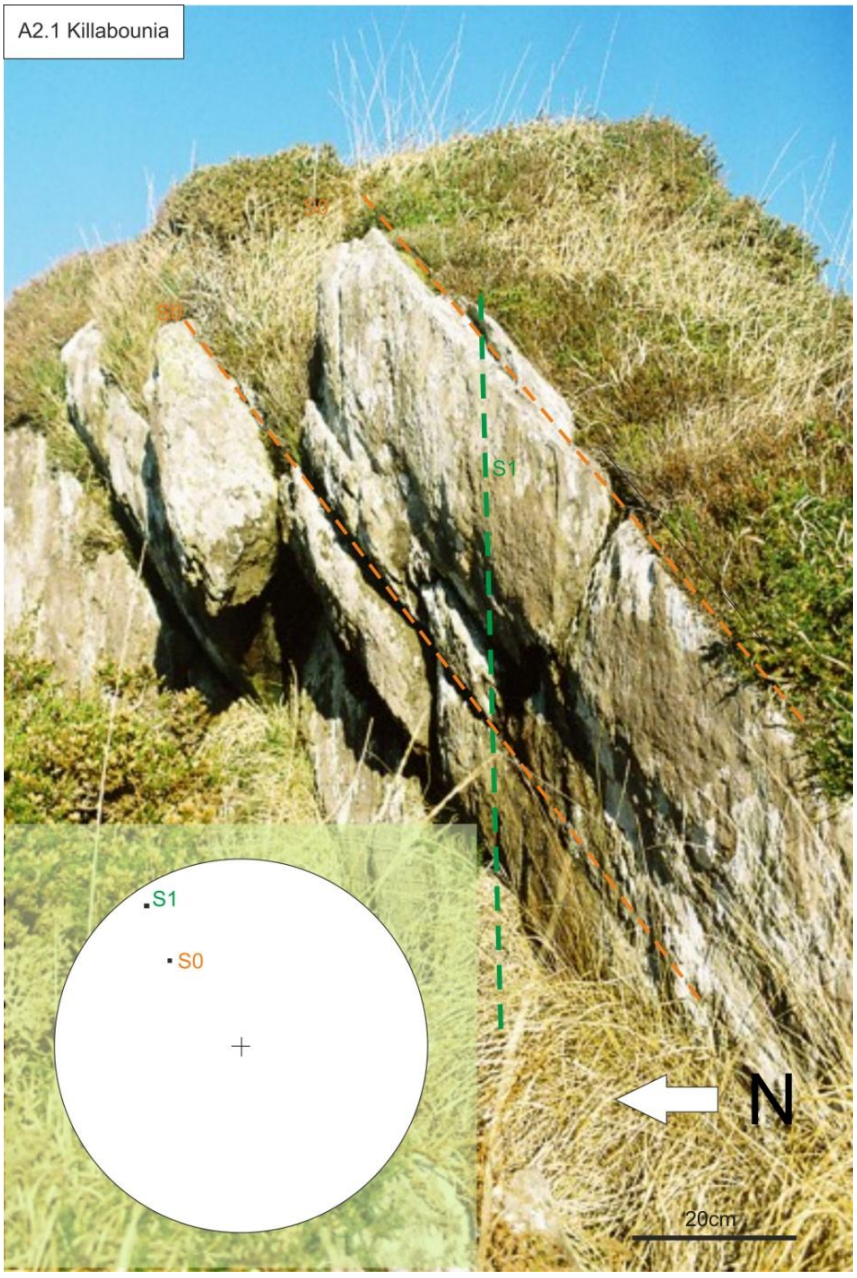

Figure 4.16 Intrabasinal axial planar cleavage. Location A2 Killabounia. This is a fine to medium sandstone and the cleavage fabric is visible.

4.5.4.3 Zone 1. Relationship of Cleavage to Folding

A useful way to show that cleavage is axial planar to folding is to measure the angle between bedding and cleavage on an equal area stereonet for various locations across the Intrabasinal Zone. For the folds in the Intrabasinal Zone, the angles between bedding and cleavage have been measured from the various key sites and during the collection of the AMS samples (Chapter 5). The AMS sites consist of just one S1 and S0 readings which have been measured from the same bed. Where the folds are small scale folds, it was possible to measure multiple pairs of angles. A total of 29 angles between bedding and cleavage for the Instrabasinal zone have been measured (See Table 4.2). The results of these measurements have been plotted (Fig 4.17-21, Fig 4.40) and show that for the Intrabasinal Zone there is a variation in the angle between bedding and cleavage from 12° to 86° as would be expected from axial planar cleavage.

Table 4.2 The angle between bedding (S0) and cleavage (S1) for the Intrabasinal Zone.

The Intrabasinal Zone: South of the Coomnacronia Fault:		S0	S1	Angle between S0 and S1
L53 Derrynane Beach Fold 1	a	088 52 S	050 85 N	56°
	b	080 45 S	050 86 N	56°
Derrynane Beach fold 2:	a	110 48 S	068 76 N	70°
	b	170 38 W	070 86 N	82°
	c	118 42 S	072 82 N	70°
	d	120 45 S	080 72 N	72°
	e	050 48 N	070 80 S	55°
	f	040 48 N	080 80 S	64°
	g	030 42 N	090 84 S	74°
Derrynane Mid section small Fold 3	a	010 48 S	065 80 S	58°
	b	120 48 S	065 82 N	71°
At fold axial plane	c	145 38 S	050 90 S	86°
AMS sites:				
A1Portmagee Quarry		060 45 S	062 72 S	28°
A2 Kilabounia		050 40 S	056 80 E	40°
A3M Keel Bay		046 60 S	052 78 N	42°
A4 SE of Keel Bay		050 70 S	060 75 N	36°
A6 Caherdaniel		120 32 S	065 88 S	72°
A6.1 Near A6		162 38 S	078 88 S	84°
A8 Rossmore		250 18 N	070 85 N	66°
A9 Molls Gap		070 52 S	058 80 S	30°
A12 Gap of Dunloe south		040 30 S	076 72 S	50°
A14 Kilgarvan		072 30 S	065 85 N	65°
M5 Lough Acoose		100 40 S	075 55 S	24°
AM1 Lough Caragh North		078 42 S	070 85 S	42°
L52 Ballygasheen Pass		056 56 N	060 68 N	12°
L54 Ballinskelligs Pier		080 46 N	065 82 N	38°
L56.2 Arete	a	082 86 N	082 50 S	44°
	b	070 80 N	080 68 S	34°
L62 Near Ballykneally		070 64 S	068 78 N	37°

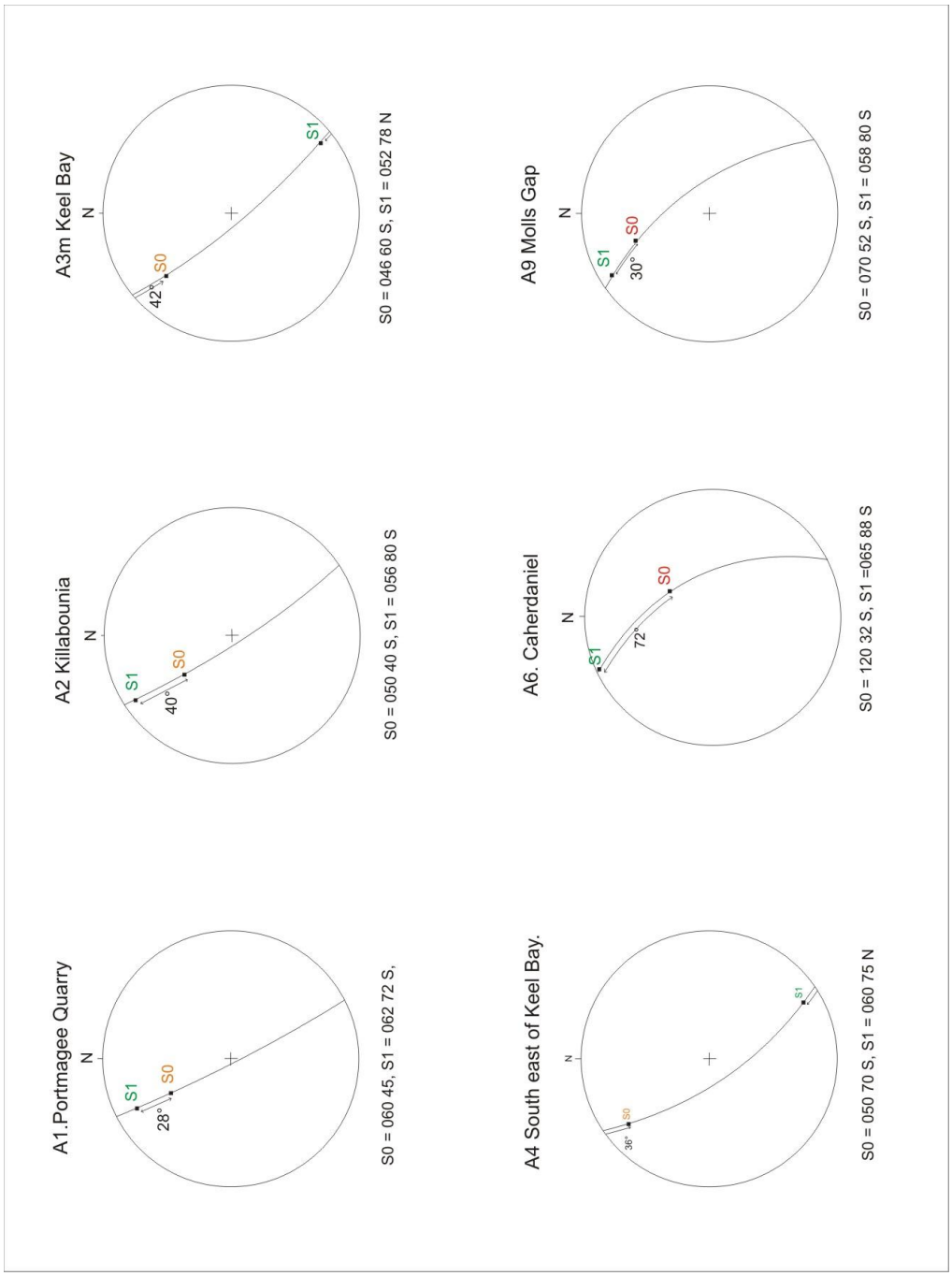

Figure 4.17 Stereonets showing the angle measured between bedding and cleavage for the Intrabasinal Zone.

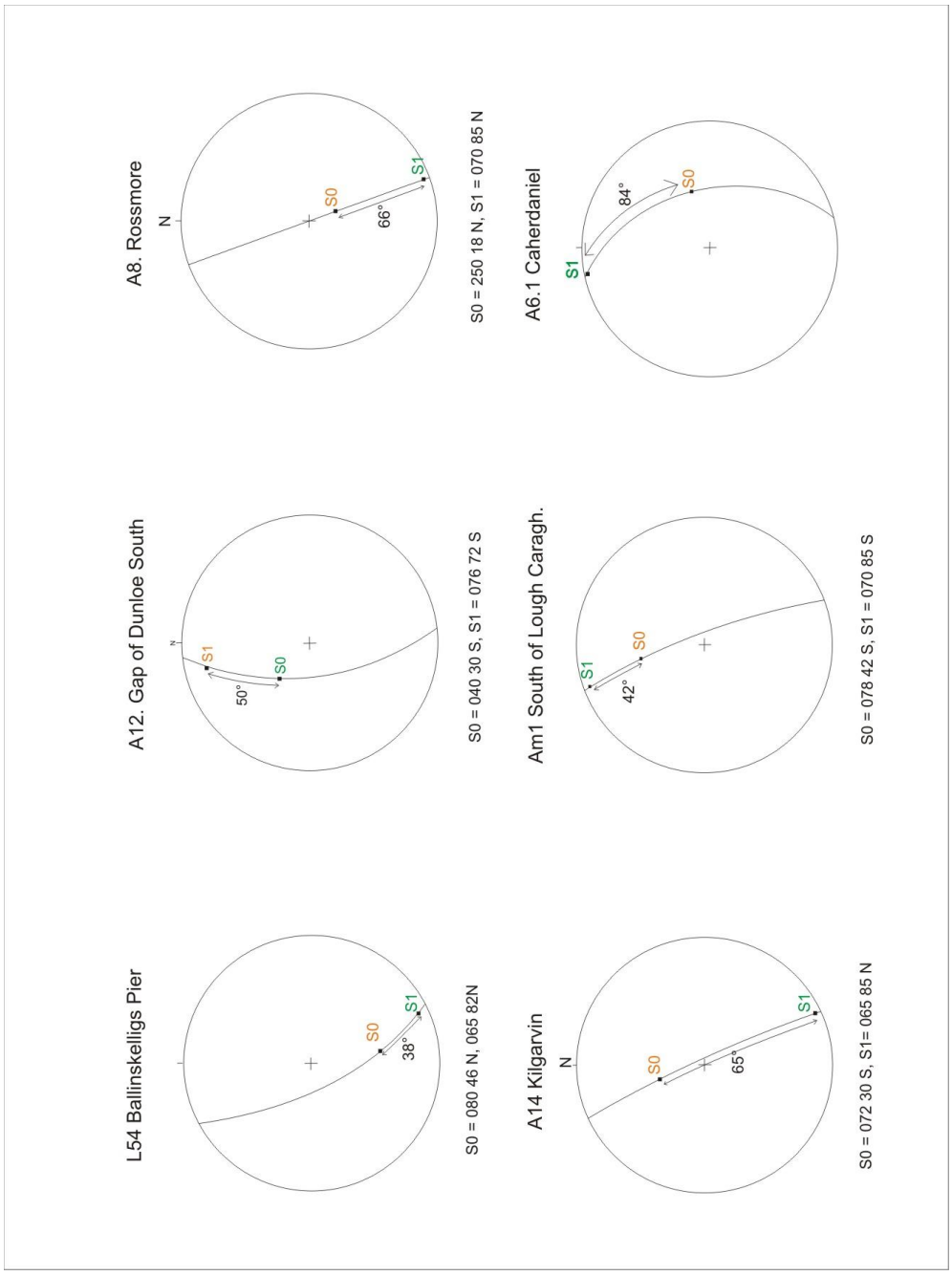

Figure 4.18 Stereonets showing the angle measured between bedding and cleavage for the Intrabasinal Zone

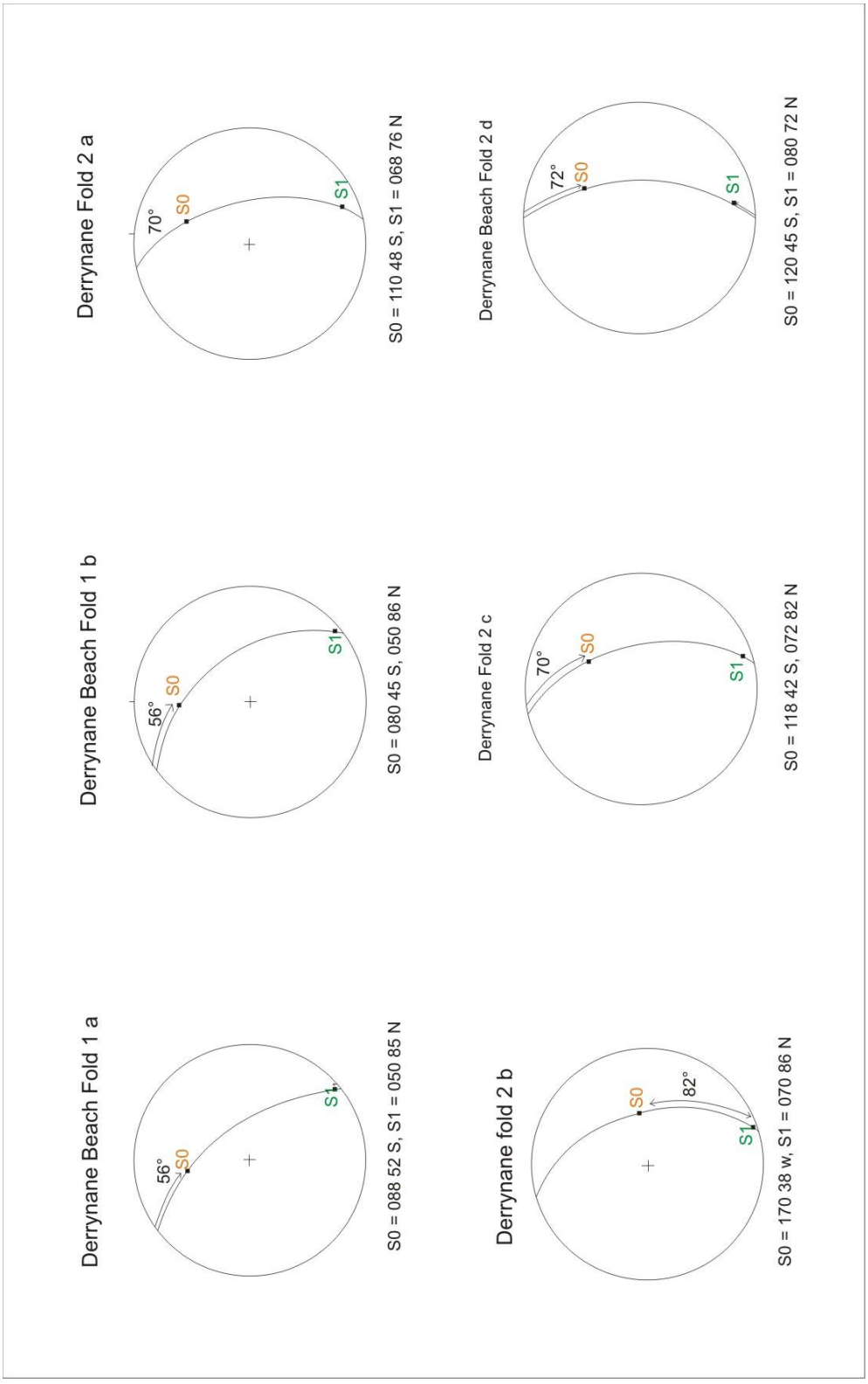

Figure 4.19 Stereonets showing the angle measured between bedding and cleavage for the Intrabasinal Zone.

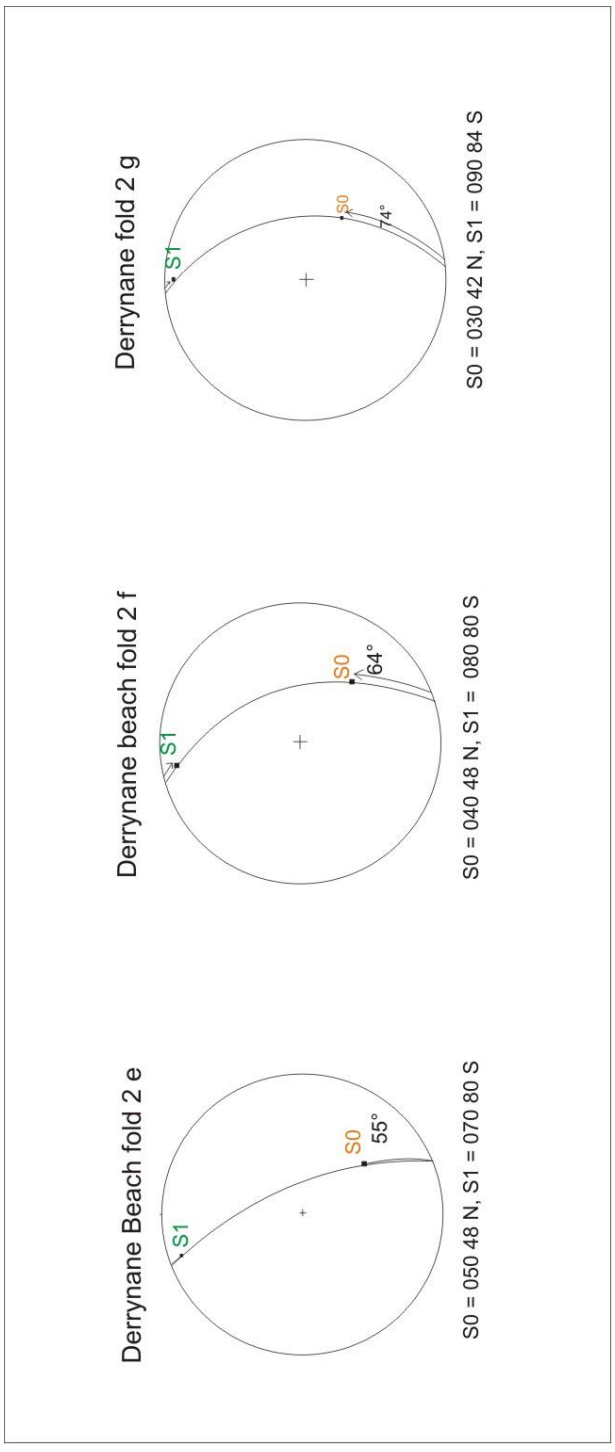

Figure 4.20 Stereonets showing the angle measured between bedding and cleavage for the Intrabasinal Zone.

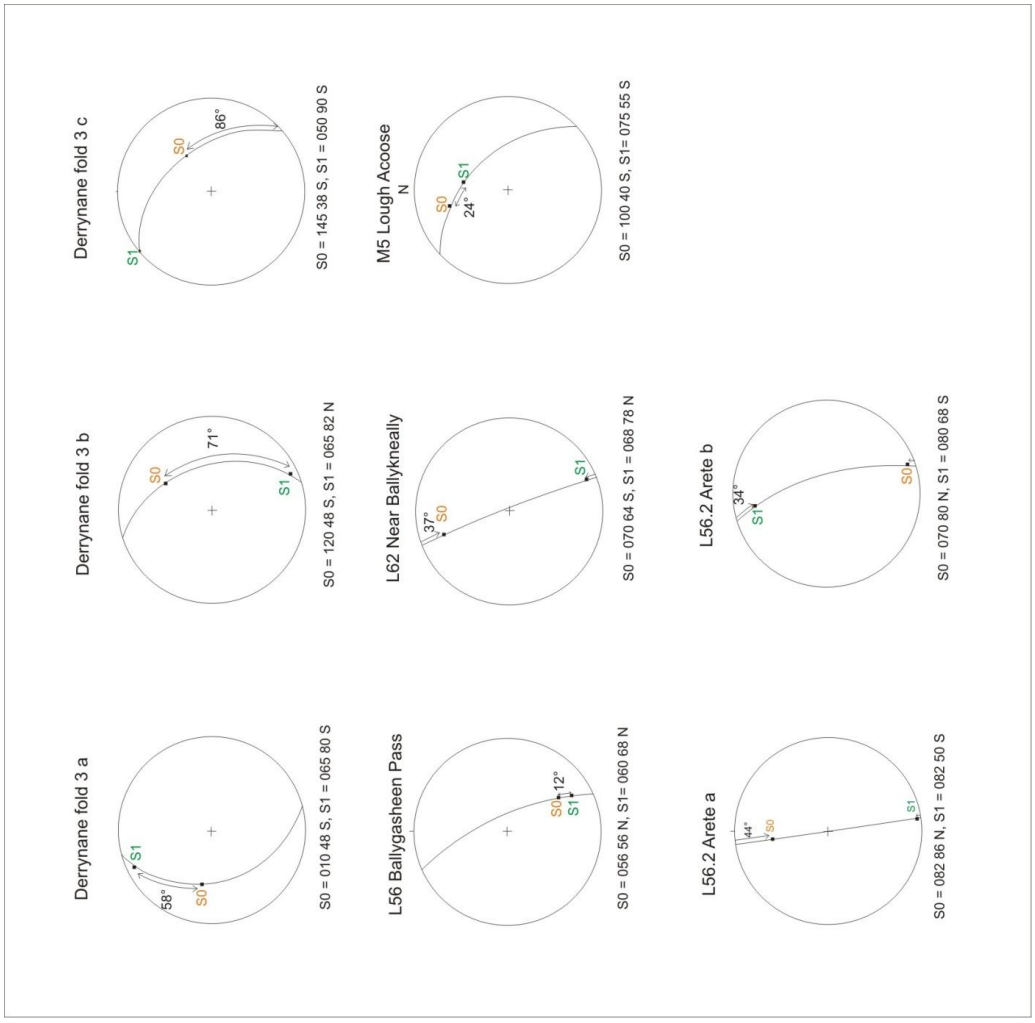

Figure 4.21 Stereonets showing the angle measured between bedding and cleavage for the Intrabasinal Zone.

4.5.4.4 Summary of Cleavage in Zone 1: The Intrabasinal Zone

To the South of the Coomnacronia Fault the cleavage is:

1) Axial planar to folds.
2) Steeply dipping mostly to the south but also some steeply dipping to the north (A3M Keel Bay, A6 Caherdaniel, A14 Kilgarvan).
3) Closely spaced and mostly visible in the finer grained lithologies.
4) Some closely spaced cleavage faintly observed in sandstones.
5) The angle between bedding and cleavage ranges from low to high and changes significantly across a fold profile.
6) No evidence of passively rotated cleavage.
7) Large scale anticlines and synclines with minor amounts of parasitic folding.

4.5.5 Zone 2. The Transition Zone

The Transition Zone is located to the north of the Coomnacronia Fault along the northern coast of the Iveragh Peninsula. This zone has been named The Transition Zone as it exhibits structural features which are intermediate between the higher deformation Intrabasinal Zone and the lower deformation Foreland Zone.

Structurally, the northern part of the Iveragh Peninsula is made up of the northern limb of the Portmagee Anticline with numerous superimposed small scale parasitic folds which tend to verge to the north. The smaller scale folds in the Transition Zone consist of some open to gentle folds (e.g. L31 Valentia Island, L44 Culoo Rocks,) and also some northward verging folds (e.g. Fig 4.29, L48 Canglass Point) with overturned bedding on the northern limbs. In the Transition Zone, there are many overturned folds with a small wavelength and high amplitude (e.g. Canglass Point). Many of the beds appeared to be overturned as there are inverted ripple marks on the northern surfaces (Fig 4.29). Other structural features in the Transition Zone include early extensional veins, tension gashes and late stage north-south jointing. There are no major map scale faults north of the Coomnacronia Fault within the Transition Zone. Faulting in the Transition Zone consists of late stage north-south cross faults, some minor reverse faults, normal faults and oblique slip faults with very little displacement (discussed in Chapter 2 and observed at L44 Culoo Rocks, L31 Valentia Island).

4.5.5.1 Cleavage in the Transition Zone

To the north of the Coomnacronia Fault, the cleavage is much different to that of the Intrabasinal Zone to the south. As previously discussed the cleavage in the Intrabasinal Zone is steeply dipping and axial planar to folding, however in the Transition Zone the cleavage dip becomes highly variable ranging from 20-90° across fold profiles (Cleavage Results Map). Previously only a couple of gently dipping cleavage readings have been recorded in this area on the GSI map. The mean strike of the cleavage ranges from (053 at Beenakryraka Head) in the west to (076 at A10 Gap of Dunloe North) in the east. The cleavage maintains a high angle to bedding and is passively rotated during folding with the bedding i.e. as the bedding has been folded the cleavage has been reorientated from steeply dipping to gently dipping There are no previous studies documenting this passive rotation of cleavage in the Irish Variscides. Also, this study shows that passive rotation of cleavage with bedding is unique to the Transition Zone. Passive rotation of cleavage has been observed from east to west across the Transition Zone from L44 Culoo rocks in the west to L55 Rossbeigh in the East. In the Transition Zone, gently dipping cleavage is consistently found on the northern limb of the folds. There are six key locations discussed here that show particularly well in the field the structural characteristics of the Transition Zone: L55 Rossbeigh, L44 Culoo Rocks, L31 Reednadrolaun Point, L48 Canglass Point, L47 Coosfada, L1 Coonama Harbour and Near to Rossbeigh. Note L44, L31 and L47 are also AMS sites (Chapter 5. AMS Results). The cleavage in the Transition Zone is considered to be an early LPS fabric.

4.5.5.2 Key Localities – The Transition Zone

L55 Near to Rossbeigh

The lithology in this area is made up of coarse grained red sandstones, which are fluviatile in origin and are part of the Ballinskelligs Sandstone Fm. This area consists of gentle, moderate and overturned folds (Fig 4.22 - 4.25). Cleavage is well displayed in some of the folds and absent in other folds. In the folds affected by cleavage the cleavage appears to passively rotated with bedding.

L55 Near to Rossbeigh –Bedding Set 1

Cross bedding is clearly displayed in the sandstones in this sequence of beds. The beds show no visible cleavage fabric (Fig 4.22).

Figure 4.22 Part of an eroded fold at location: L55: Rossbeigh. The bedding dips gently and there is no evidence of a tectonic fabric.

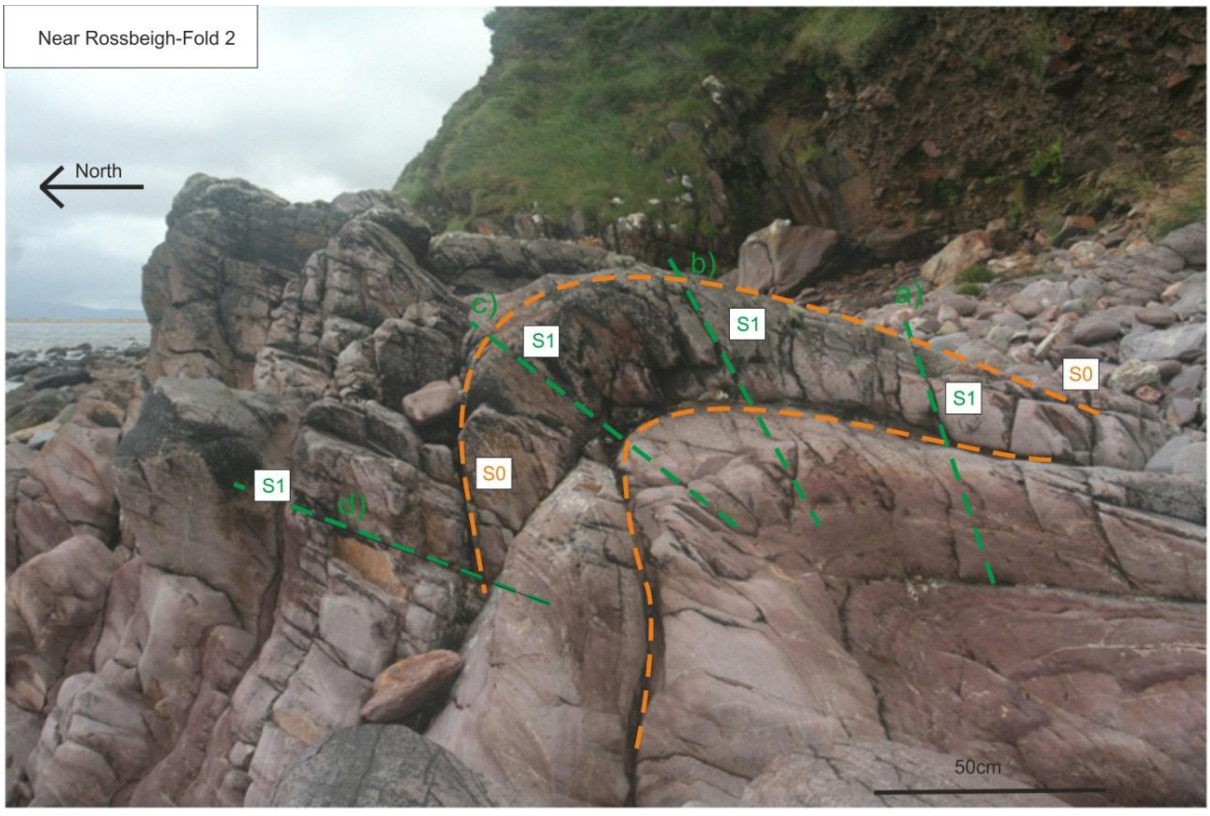

Figure 4.23 Fold 1 – L55: Near to Rossbeigh .On the southern limb the cleavage is steeply dipping while on the northern limb the S1 fabric is gently dipping (see Table 4.3).

Near to Rossbeigh Fold 2

Fold 2 also clearly displays passively rotated cleavage. The paired bedding and cleavage orientations are plotted on the stereonet (Fig 4.24).

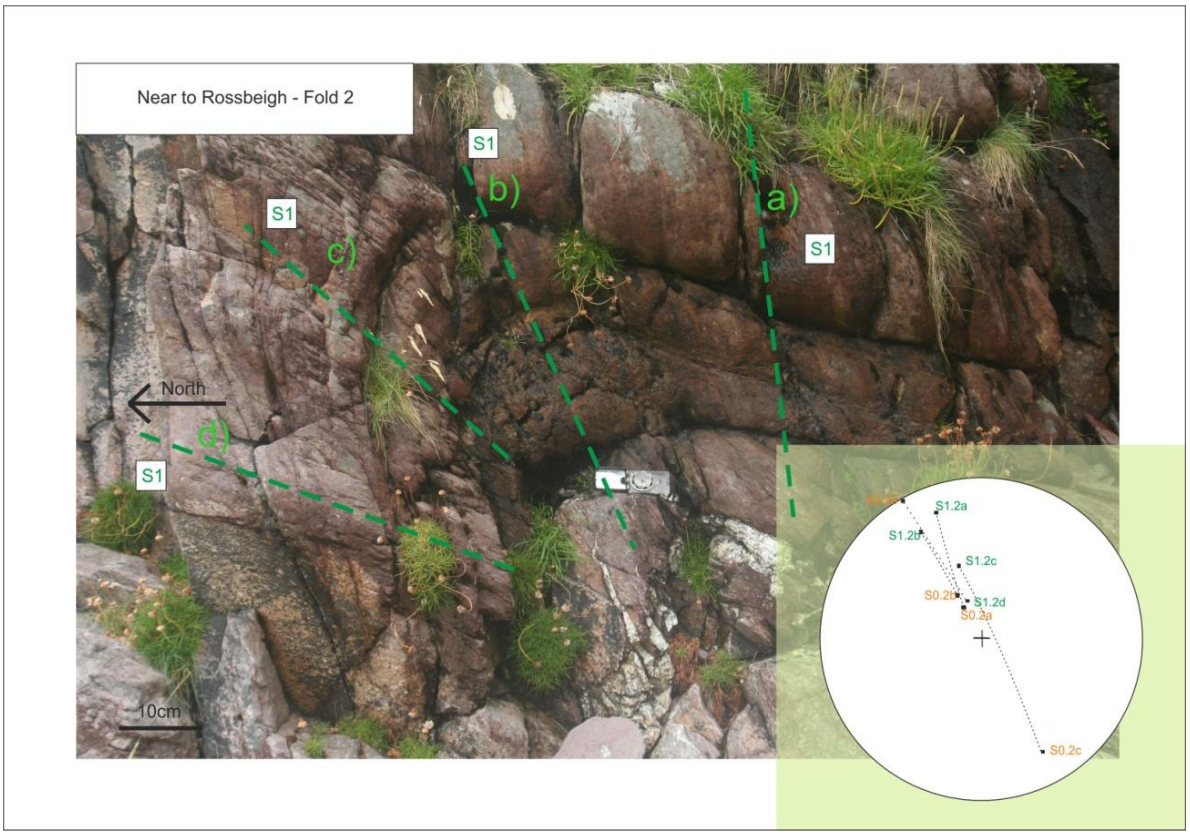

Figure 4.24 northward-verging fold with gently dipping S1 fabric on the northern limb-Near to Rossbeigh

Near Rossbeigh - Fold 3: This folded sandstone shows a very minor amount of passively rotated disjunctive cleavage (Fig 4.25).

Figure 4.25 Fold 3, L55 Near to Rossbeigh – shows only minor amounts of a disjunctive S1 fabric. The fold verges to the north.

L44 Culoo Rocks, Valentia Island

This site is located within the Valentia Slate Fm. An AMS sample has also been taken from this site (Chapter 5: AMS Results). The bedrock consists of cleaved medium grained sandstones and fine grained mudstones/siltstones. Culoo Rocks consists of one main gentle to open anticline of approximately 40 m in wavelength verging to the north. Bed thickness ranges from 20-40 cm. Cleavage ranges from finely laminated pervasive cleavage in the siltstones to a more widely spaced fabric in the coarser sandstones. A small amount of cleavage refraction is observed between the coarse and fine beds, but this only penetrates into the first 3-4 cm of the edge of the beds in some locations. Within the main anticline, cleavage is observed to range from steeply dipping in the gently dipping beds to very gently dipping in the steeper dipping northern limb of the anticline. The angle between cleavage and bedding is approximately constant throughout the fold profile indicating passive rotation of cleavage has occurred and is plotted on a stereonet (Fig 4.26). There is a minor reverse fault on the anticline with very little net movement (5-10 cm).

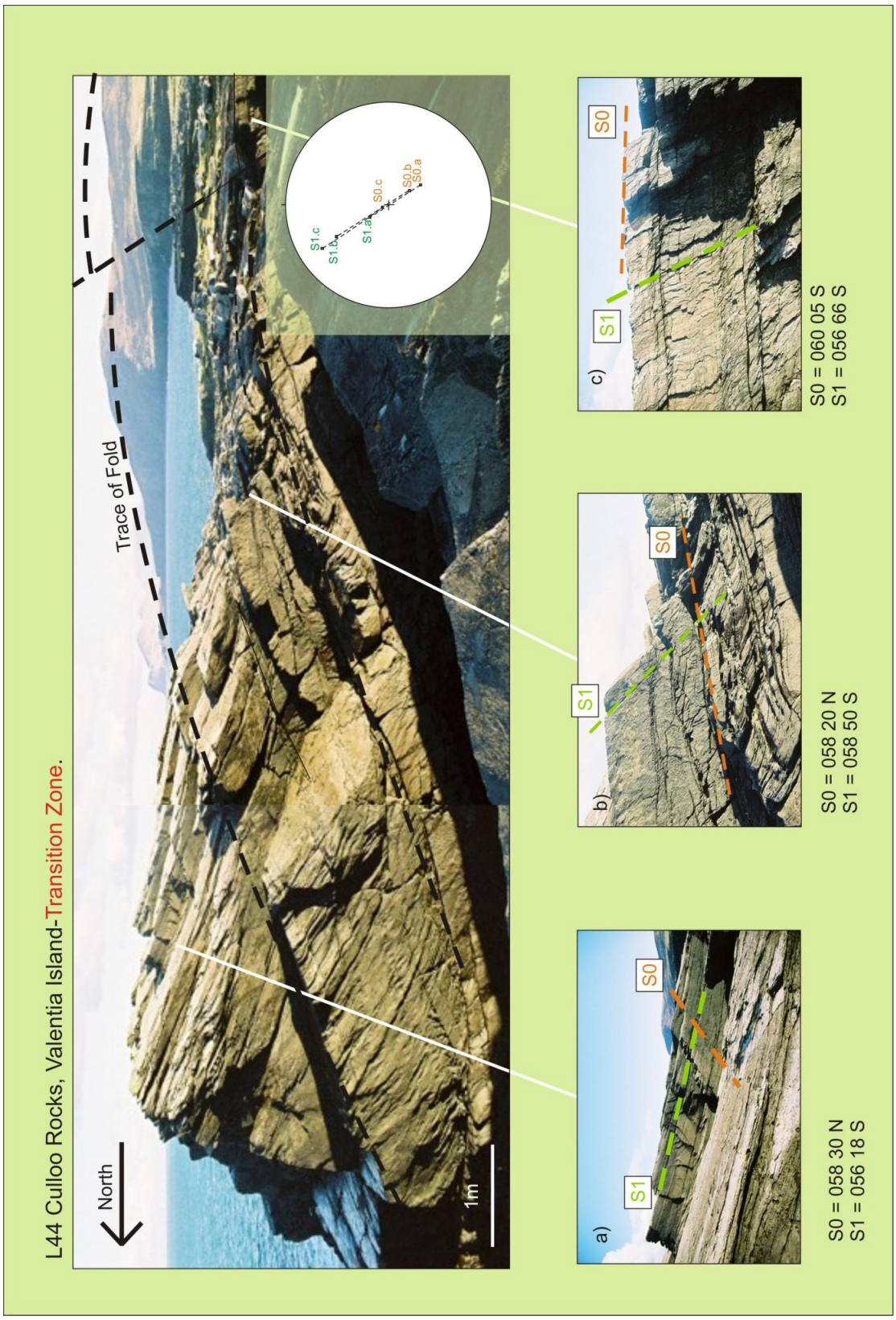

Figure 4.26 Culoo Rocks (L44) shows the S1 fabric maintaining a high angle with bedding across the fold profile.

L47 Coosfada

These are medium to coarse grained red fluvial sandstones of the Ballinskelligs Sandstone Fm. The beds are 10-30 cm in thickness and only consist of coarse grained sandstones. The area is characterised by a number of large upright isoclinal/tight to recumbent folds verging to the north. Fold amplitude ranges from 10-20 m. There is a visible spaced weak cleavage/LPS fabric with a spacing of 2-5 cm. No cleavage refraction is observed in this locality. The cleavage to bedding angle is maintained at a high value throughout the fold profiles (Fig 4.27, 4.28). This relationship of cleavage to bedding can be explained as a passive rotation of cleavage with respect to bedding. This may indicate an early LPS/cleavage event prior to or at the early stages of folding.

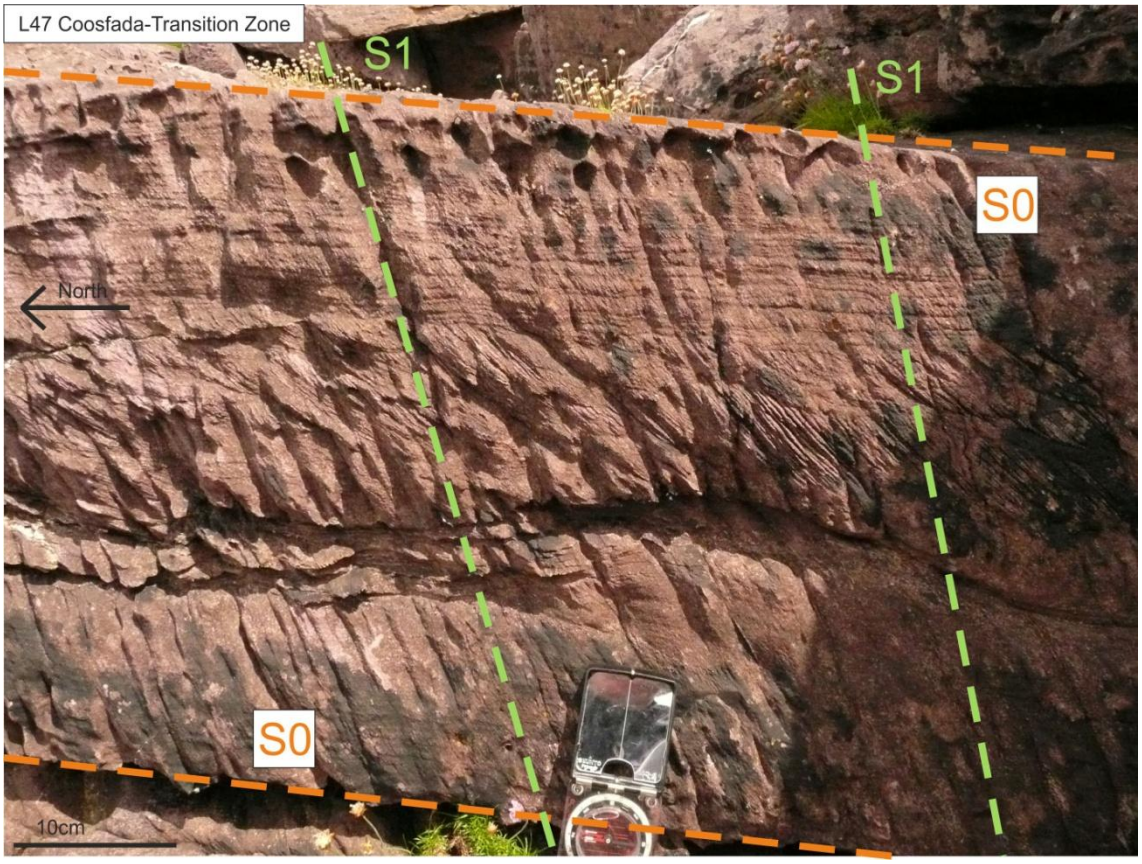

Figure 4.27 L47 Coosfada: The Transition Zone - Shows a faint S1 fabric at a high angle to bedding.

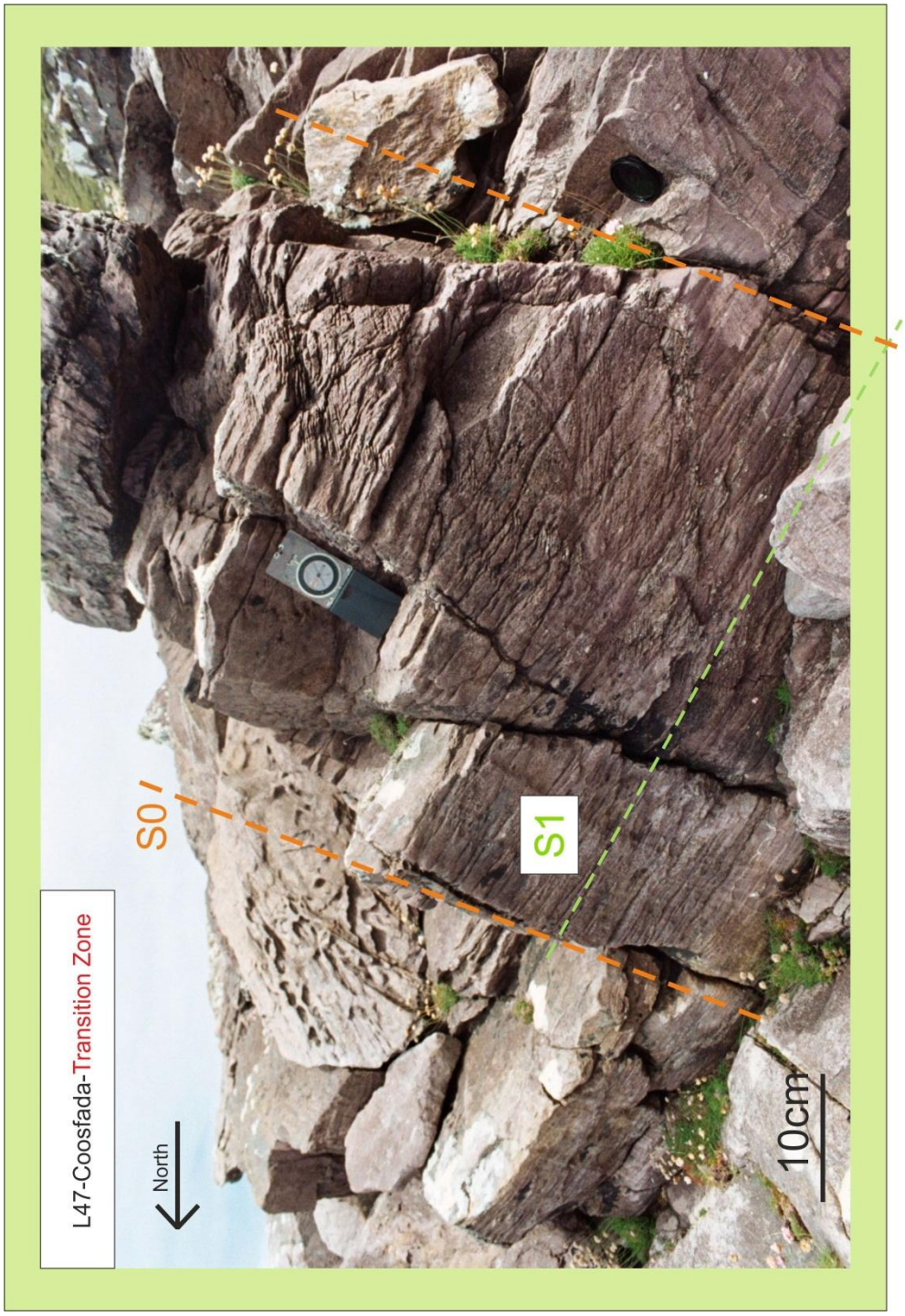

Figure 4.28. L47 Coosfada: The Transition Zone shows bedding steeply dipping to the north and a faint S1 fabric at a high angle to bedding.

L47 b Canglass Point. GR: 4522 8445

This area just north of Coosfada consists of the Ballinskelligs Sandstone Fm. There is a series of northward verging overturned folds. There is visible cross laminations within the sandstone beds and ripple marks indicating the way up of beds. The beds on the northern limbs of the folds are often overturned as indicated by inverted ripple marks. The beds range from 10-40 cm thickness. These folds are similar folds (Fig 4.29). The cleavage maintains a high angle to bedding indicating that cleavage has been passively rotated (Fig 4.30).

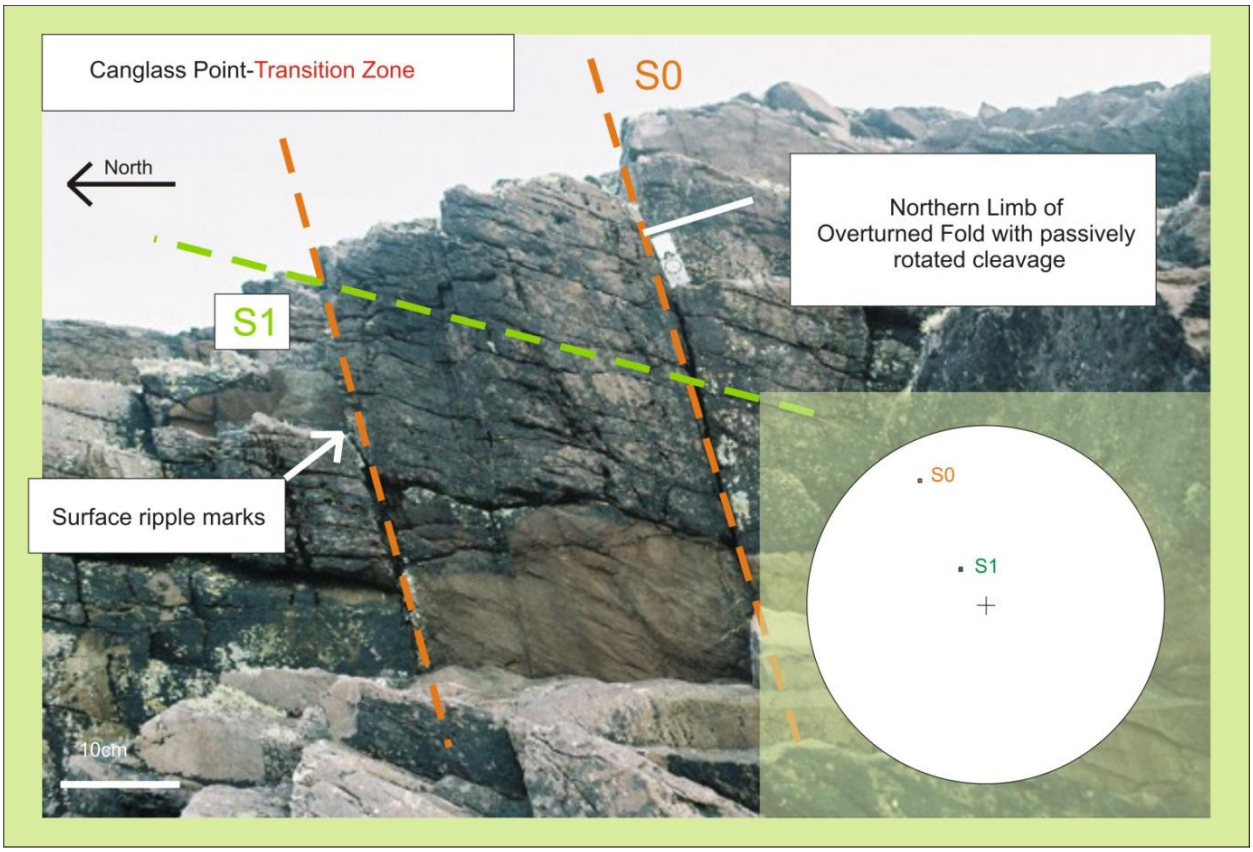

Figure 4.29 shows overturned steeply dipping bedding (with ripple marks on surface) with a gently dipping S1fabric.

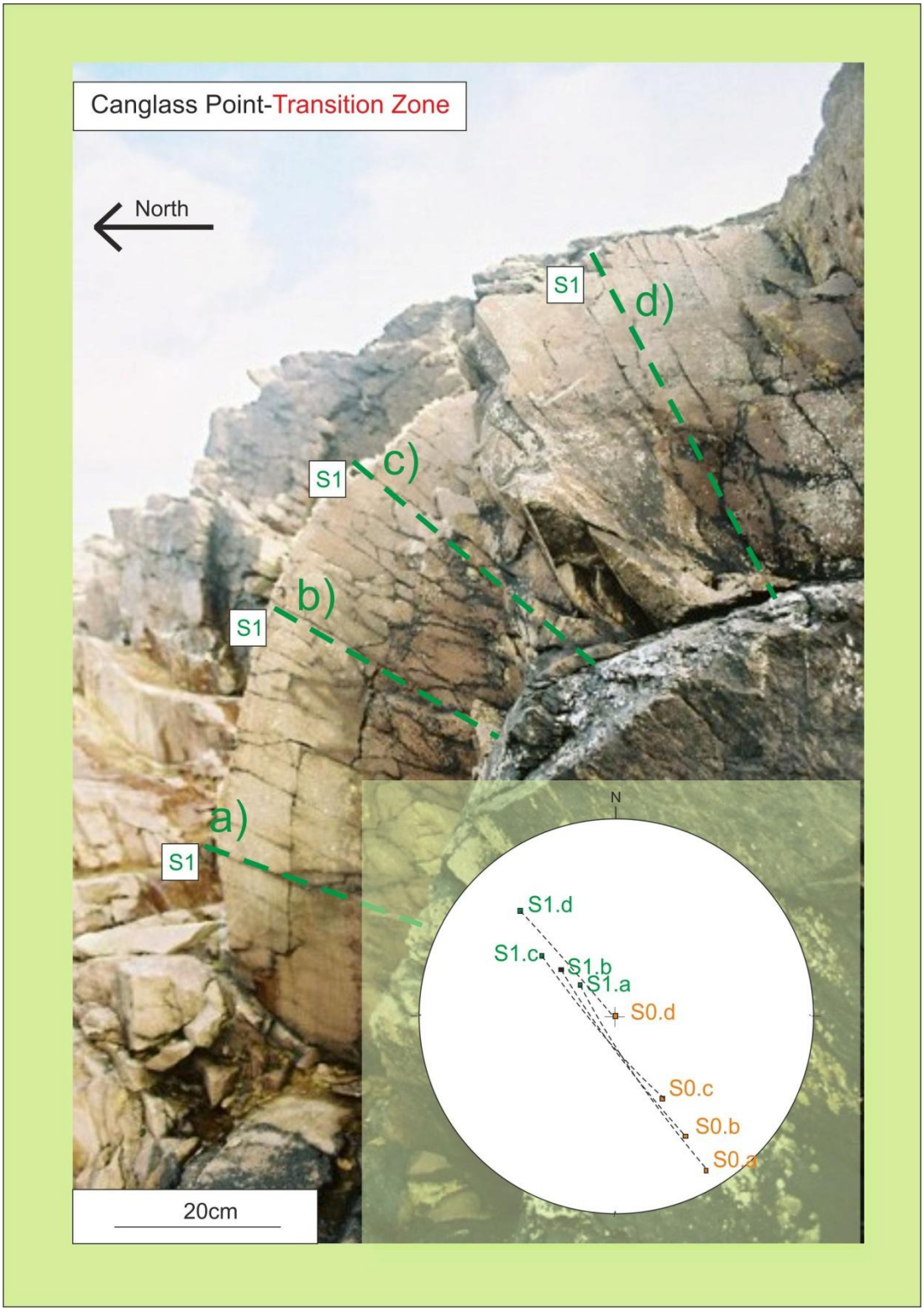

Figure 4.30 Canglass Point –The Transition Zone- The S1 fabric maintains a high angle to bedding

L31-Reenadolaun Point-Valentia Island

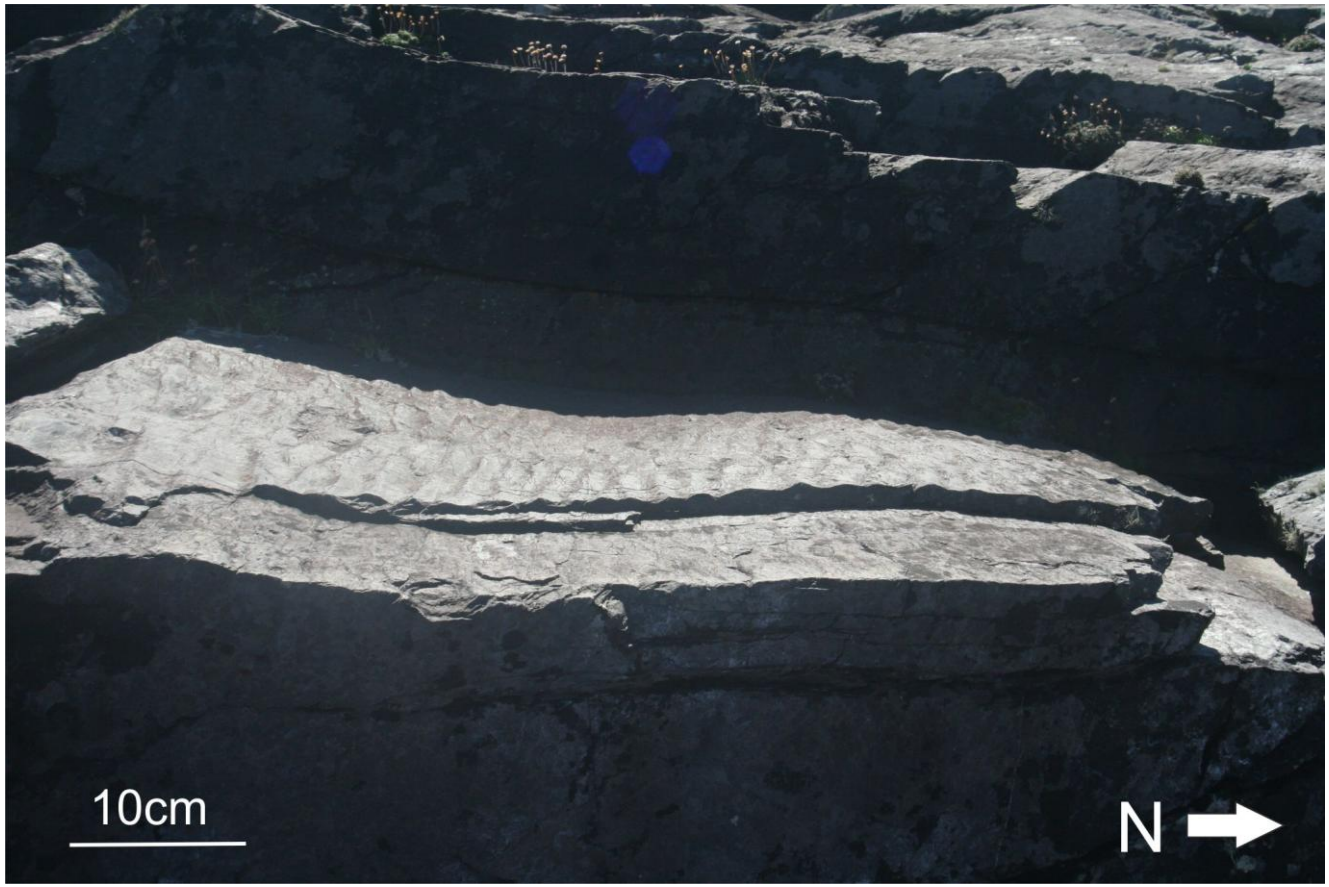

Figure 4.31. L31 Reenadrolaun Point-The Transition zone: area consists of gentle folds with ripple marks on the surface of the beds.

L31- Reedadrolaun Point, Valentia Island

This location lies in the Valentia Slate Fm. At Reenadrolaun Point there are both sandstone beds and siltstone beds. In the sandstones there are implicit ripple marks on the surface and a faint disjunctive cleavage fabric (Fig 4.31). In the siltstones there is a well developed cleavage that is gently dipping (Fig 4.32).

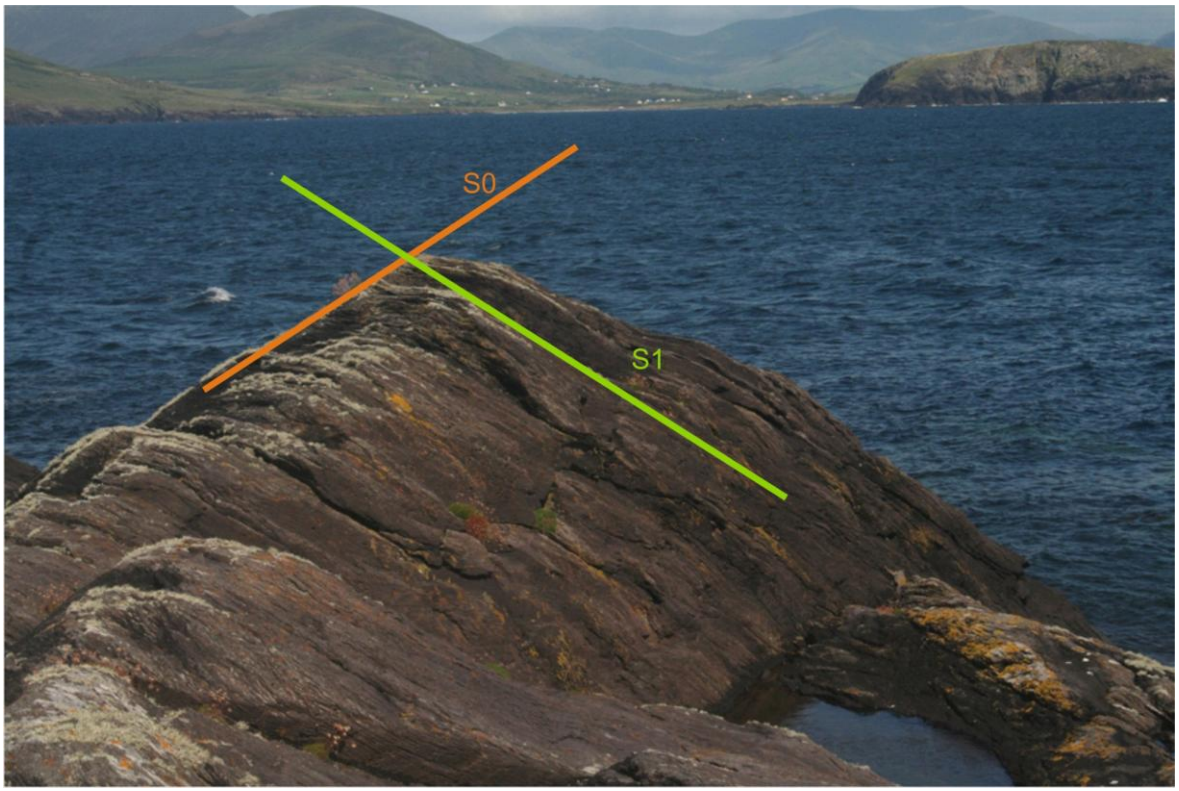

Figure 4.32 L31.b Reenadrolaun Point approximately 100 meters from L31.a (Fig 4.31) - showing a well developed gently dipping S1 fabric in the siltstones of the Valentia Slate Fm.

L1- Coonama Harbour

This area is located in the Ballinskelligs Sandstone Fm. The lithology is a medium to coarse grained sandstone. The area is characterised by gentle folds (Fig. 4.33). This fold verges to the N and plunges gently to the SW (12-220). The cleavage is steep on the southern limb and becomes shallower on the northern limb. The cleavage appears to maintain a high angle to bedding and to be passively rotated with the bedding. The paired readings of bedding and cleavage are plotted on Fig 4.33.

Figure 4.33: Fold at Coonama Harbour .There is a high angle between bedding and the S1 fabric.

4.5.5.3 Relationship of Cleavage to Folding –The Transition Zone

The results of the measured angle between bedding and cleavage have been presented in the Table 4.3. A total of 36 measurements for the Transition Zone were made from key sites and from single point cleavage and bedding data. The stereonet plots for each measurement are shown in Fig 4.34 - 4.39.The results for both the Transition Zone and the Intrabasinal Zone angles are plotted in Fig 4.40. The results show that for the Transition Zone the angle between bedding and cleavage ranges from 40 ° to 90 ° and never below 40°.These consistently high angles between bedding and cleavage in the Transition Zone are a result of passively rotated cleavage.

Table 4.3 shows coupled cleavage and bedding data from the transition zone, north of the Coomnacronia Fault. The calculated angle between bedding and cleavage is presented in Fig 4.5, scatter plot. (The acute angle is used in all cases).* = key site

Location		Bedding (S0)	Cleavage (S1)	Angle between bedding and cleavage
North of the Coomnacronia Fault.				
Near Rossbeigh*				
Fold 1:	a	060 20 S	078 80 S	60°
	b	060 05 S	078 65 S	60°
	c	080 40 N	060 48 S	86°
	d	070 70 N	070 25 S	86°
	e	080 88 N	080 18 S	72°
	f	070 72 S	070 25 S	48°
Fold 2 :	a	060 18 S	070 72 S	54°
	b	060 25 S	060 65 S	40°
	c	062 70 N	072 38 S	72°
	d	060 88 S	068 20 S	68°
Canglass Point*				
Fold 1:	a)	060 80 N	040 20 S	80 °
	b)	060 60 N	040 30 S	88 °
	c)	060 40 N	040 40 S	78 °
	d)	horizontal	048 62 S	62 °
Other beds beside Fold 1	e)	055 10 S	056 68 S	58°
	f)	062 68 S	055 20 S	48°
	g)	040 15 S	056 68 S	54°
Culoo Rocks*				
From 1 fold profile	h)	060 05 S	056 66 S	62°
	i)	horizontal	045 62 S	62°
	j)	058 20 N	058 50 S	70 °
	k)	058 30 N	056 18 S	48 °
	l)	056 28 N	050 20 S	48°
	m)	052 14 N	052 48 S	62°
	n)	050 15 N	052 52 S	68°
	o)	048 10 N	052 52 S	62°
	p)	036 04 S	050 60 S	56°
Coosfada*				
L47		240 58 N	060 30 S	88°
Coonama* Harbour fold		**Fold plunges 12 - 220**		
	a	234 60 N	060 30 S	88°
	b	232 54 N	060 38 S	88°
	c	132 08 S	050 60 S	58°
	d	235 20 S	050 70 S	50°
Single Pair readings from AMS samples and other sites.				
AM11 Lough Caragh north		262 52 N	068 40 S	90 °
A21 Cooscrome		250 80N	060 25 S	76°
A21.1 Cooscrome		255 68 N	060 20 S	77°
V25 ReenadrolaunPoint		060 40 N	070 40 S	80°
Lake Coomnacronia-north side 1		070 78 S	074 28 S	50°

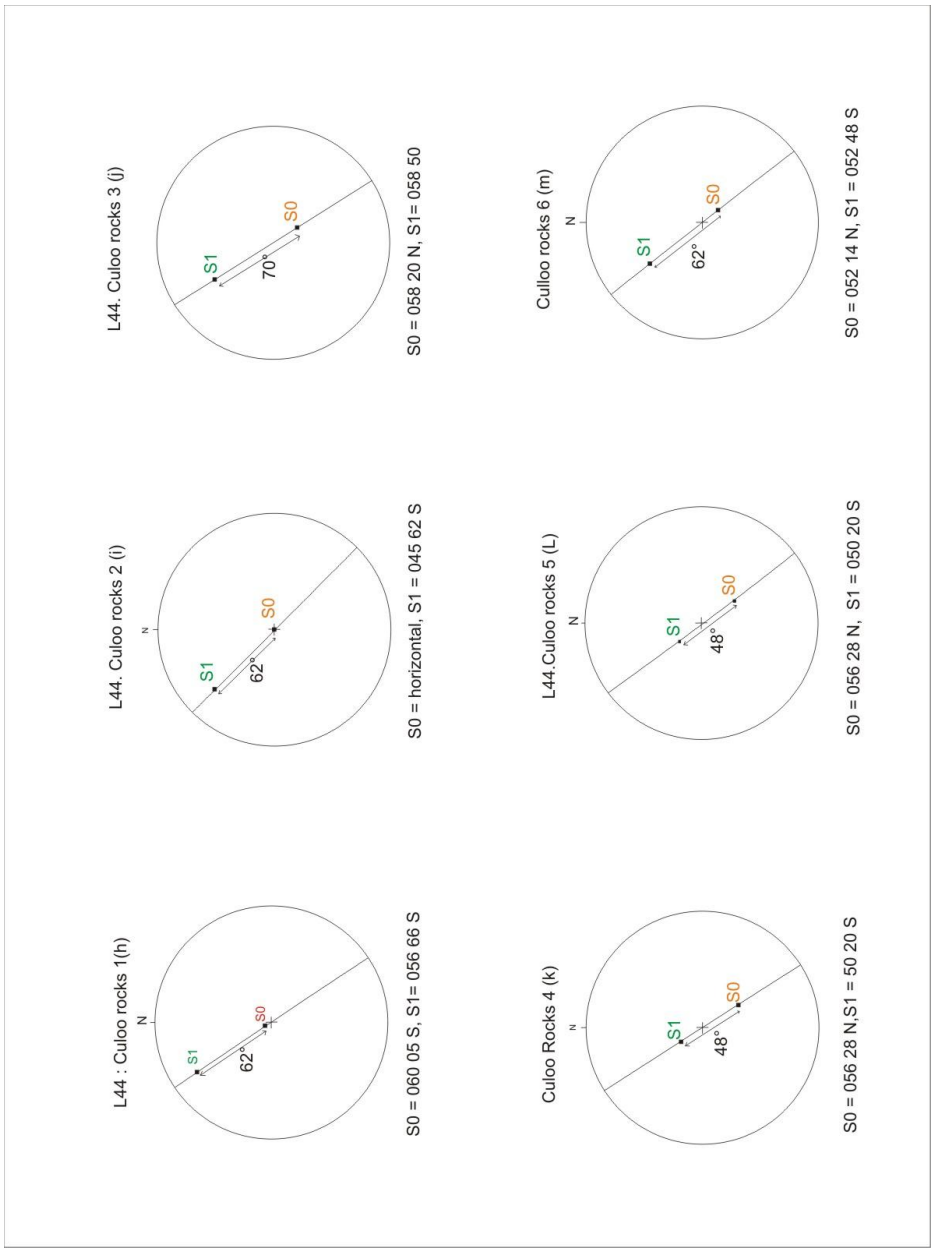

Figure 4.34 Stereonet plots showing the angle between bedding and cleavage for each location in the Transition Zone.

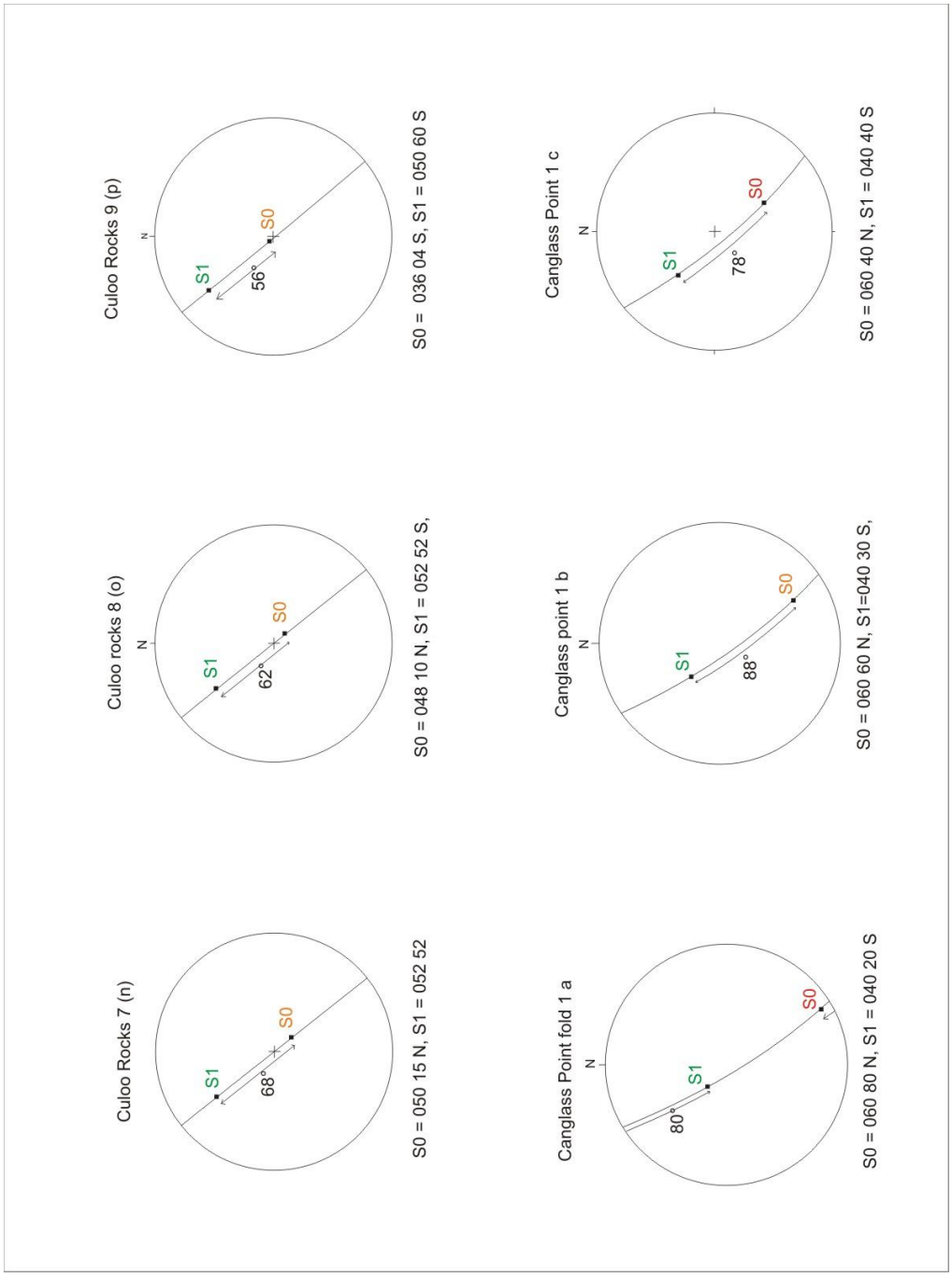

Figure 4.35 Stereonet plots showing the angle between bedding and cleavage for each location in the Transition Zone.

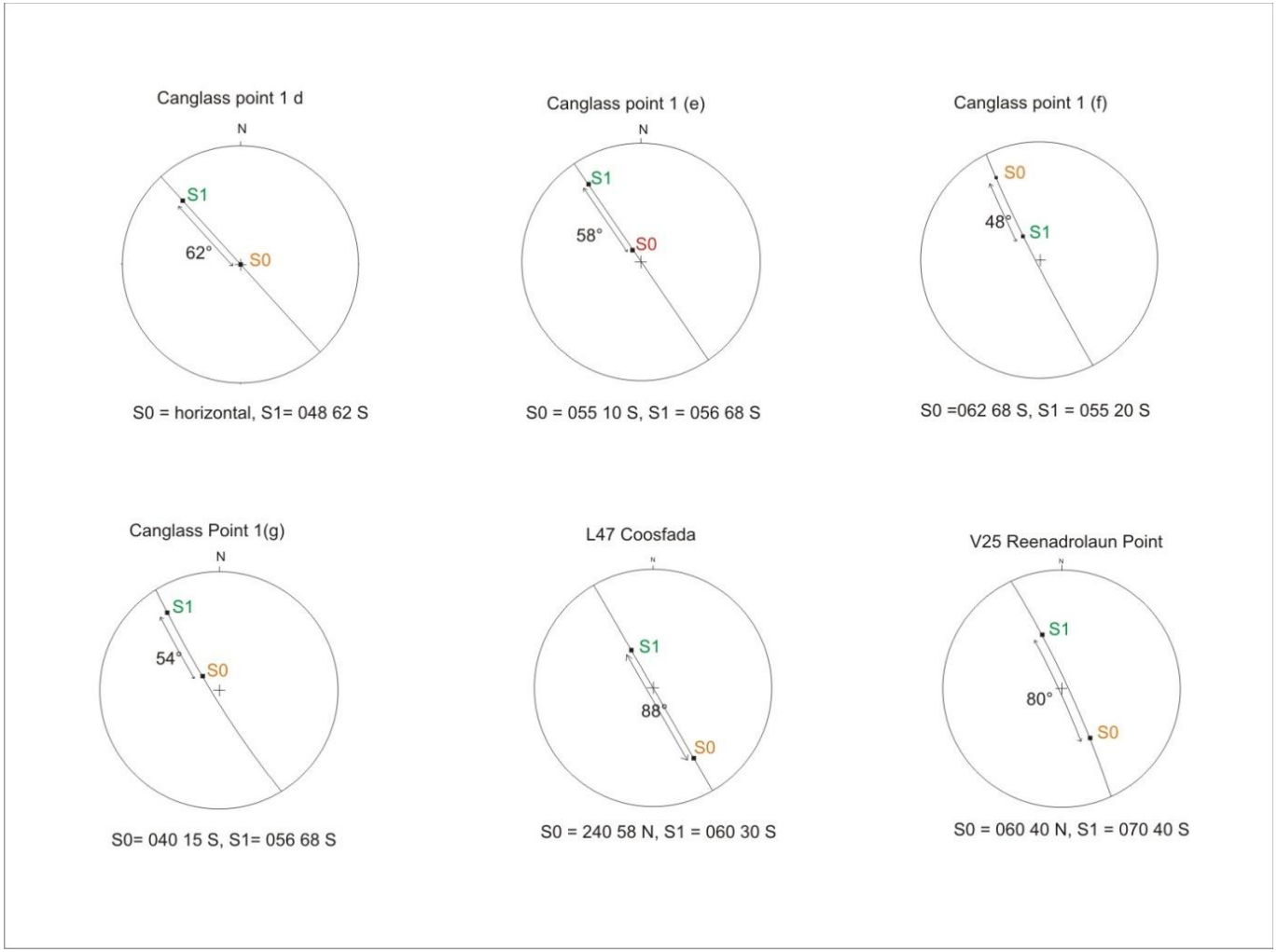

Figure 4.36 Stereonet plots showing the angle between bedding and cleavage for each location in the Transition Zone

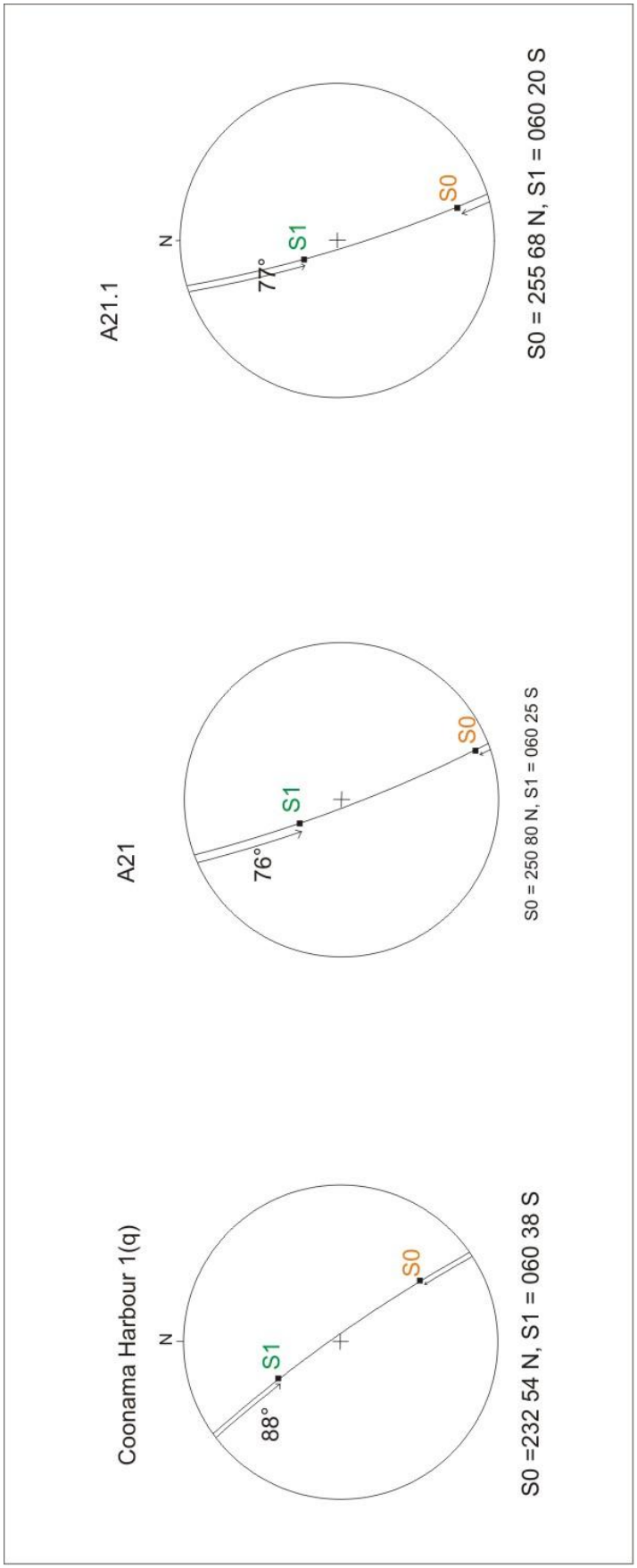

Figure 4.37 Stereonet plots showing the angle between bedding and cleavage for each location in the Transition Zone.

Figure 4.38 Stereonet plots showing the angle between bedding and cleavage for each location in the Transition Zone

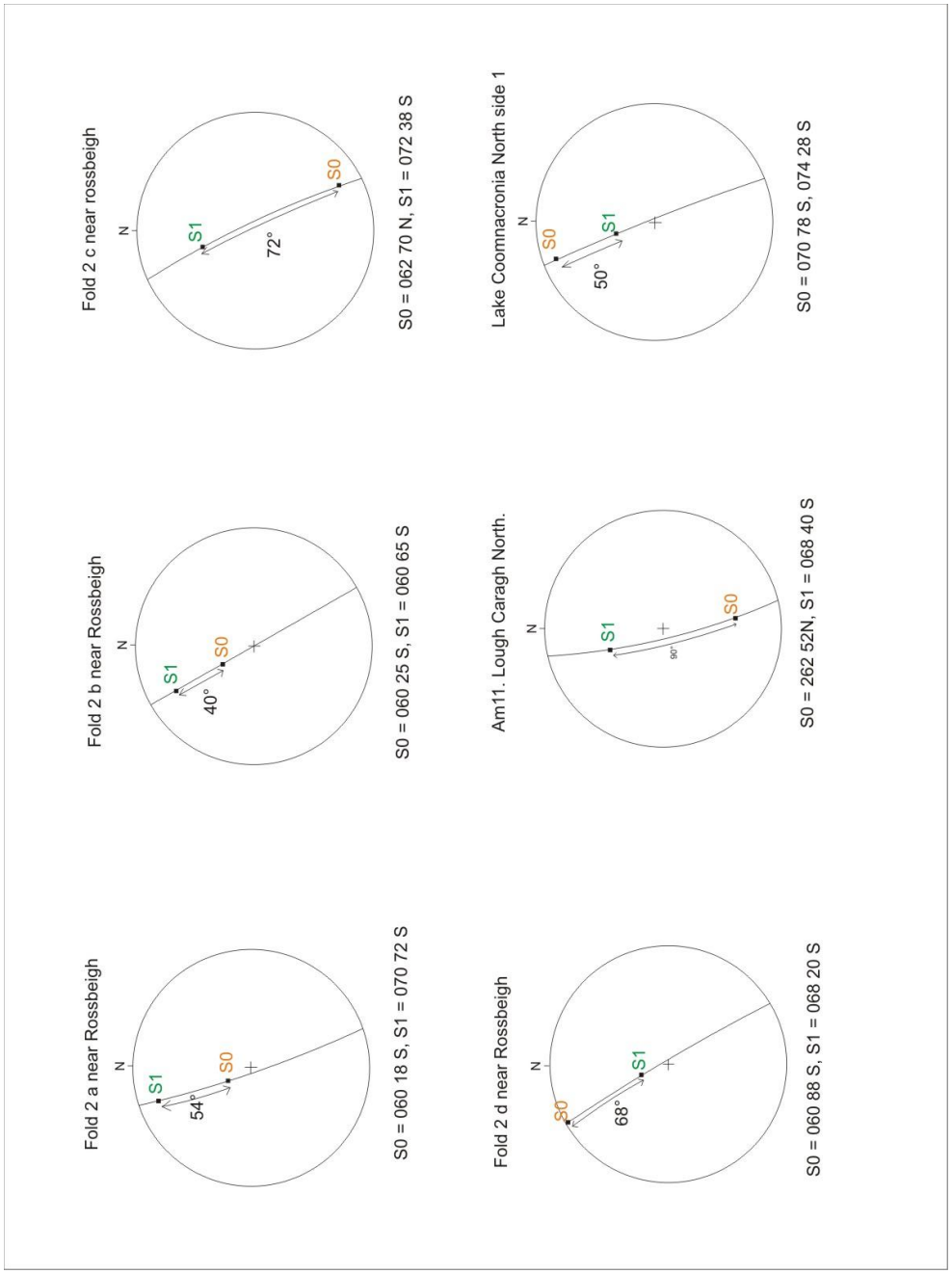

Figure 4.39 Stereonet plots showing the angle between bedding and cleavage for each location in the Transition Zone.

4.5.5.4 Overburden and Lithological Controls on Passively Rotated Cleavage

Passively rotated cleavage is observed to the north of the Coomnacronia Fault in both the Ballinskelligs Sandstone Fm. and the Valentia Slate Fm. Given that passively rotated cleavage occurs in both of these lithologies, it can therefore be assumed that it is not controlled by variations in lithology or overburden.

4.5.5.5 Summary of Cleavage in the Transition Zone

To the north of the Coomnacronia Fault cleavage is:

1) Less frequently found with some locations showing no cleavage. Slaty cleavage is found in the Valentia Slate Fm. and a spaced disjunctive fabric in sandstones i.e. the Ballinskelligs Sandstone Fm., which may be an early LPS fabric.
2) More variable in orientation. The slaty cleavage and the LPS fabric are passively rotated i.e. the cleavage plane maintains a high to the bedding plane. The angles between bedding and cleavage are generally high (> 40 °, see Fig 4.40).
3) Folding consists of small scale gentle to open folds and small scale overturned folds all of which verge to the north and are superimposed on the northern limb of the Portmagee Anticline.

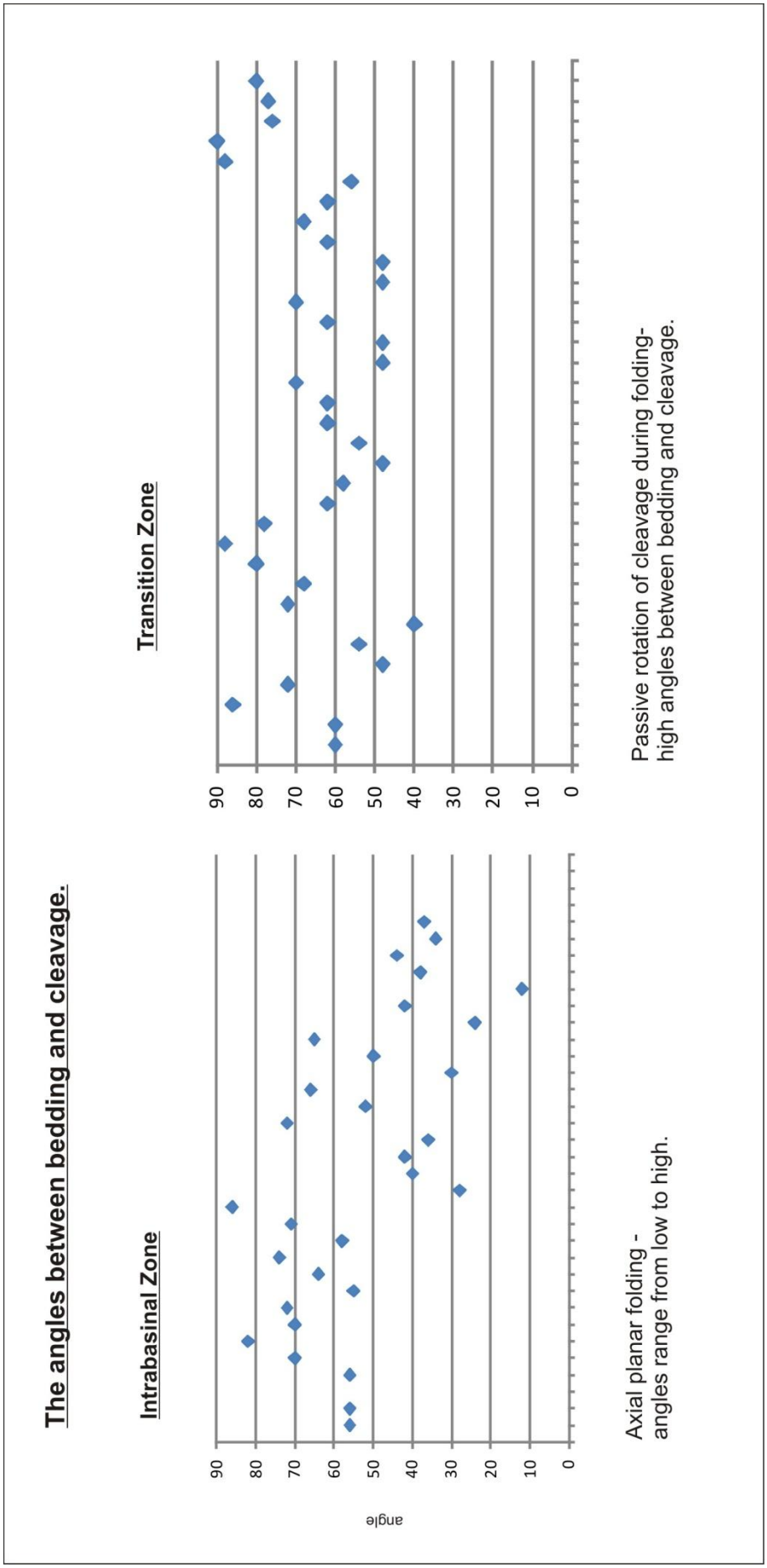

Figure 4.40 The angle between bedding and cleavage. South of the Coomnacronia Fault (Intrabasinal Zone) exhibits a broader range of angles, typical of axial planar cleavage. North of the Coomnacronia Fault (Transition Zone) shows non axial planar cleavage where the angle between cleavage and bedding maintains a high angle.

4.5.6 Zone 3 - The Foreland Zone

The Dingle Peninsula and Kerry Head

The Dingle Peninsula and Kerry Head which lie to the north of the Iveragh Peninsula have already been established as part of the Foreland (Chapter 2) and therefore this study takes a brief look at cleavage in this zone. As discussed in Chapter 2, cleavage in the Upper ORS of the Foreland has been well documented as being a disjunctive steeply dipping cleavage e.g. Upper ORS at Bulls Head (Fig 2.40: Chapter 2; Meere and Mulcrhone, 2006), a fracture cleavage (e.g. Parkin, 1976) or absent (e.g. Capewell, 1965; Hudson, 1966). The Upper ORS equivalent of the Munster Basin (Chapter 2) on the Dingle Peninsula can be seen at Brandon's Pier (M7, See Map Insert 3: AMS Results). Kerry Head (M6) which also lies to the north of the Dingle Peninsula can be correlated with the Upper ORS of the Munster Basin. AMS analysis has also been carried out for each of these sites (Chapter 5: AMS Results).

M7 Brandon Pier (See AMS Results Map for location)

At M7: Brandon Pier, which lies on the north coast of the Dingle Peninsula, the lithology is the Capagh Sandstone Fm. which is part of the Slieve Mish Group. At Brandon Pier the cleavage is absent and the area consists of gently dipping coarse red sandstones.

M6 Ballyheige (See AMS Results Map for location)

At M6: Ballyheige on Kerry Head, there is similarly no cleavage observed. At Ballyheige, the lithology is the Kilmore Sandstone Group which is Upper Old Red Sandstone. The bedding ranges from 10-30 cm, is gently dipping and shows cross bedding. Previous studies have found an upright ENE-WSW cleavage on Kerry Head (Chapter 2: Geological setting).

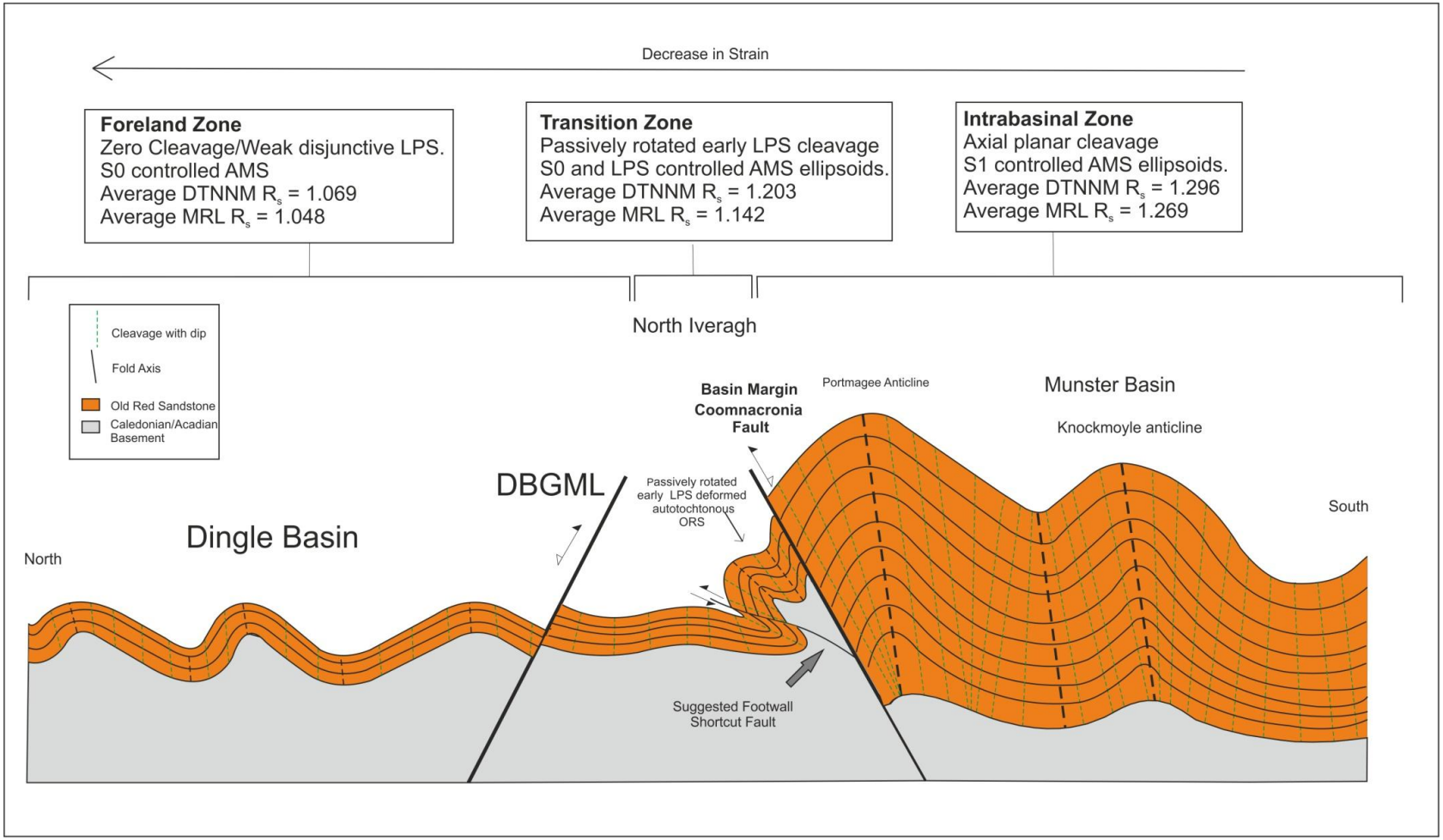

Figure 4.41 shows a cross sectional model illustrating the behaviour of cleavage from south to north across the three tectonic zones (Pre-Erosion) based on S1 and S0 data from the Cleavage Map

Table 4.6 Summarizes the structures found in the three tectonic zones.

Zone	Fold Style	Cleavage Style
Intrabasinal Zone	• Large scale anticlines and synclines with minor amounts of small scale parasitic folds which are overturned folds and gentle open folds. • Chevron folding found in the hangingwall close to the Coomancronia Fault.	• Steeply dipping to the south and to the north axial planar cleavage in all lithologies. Mostly found in slatey horizons but also abundant in coarser lithologies. • Dips at 60° to the south in close proximity to the Coomancronia Fault which also is estimated to dip at 60° S. • Small amounts of cleavage refraction.
Transition Zone	• Small scale overturned folds and gentle folds superimposed on the northern limb of a large scale anticline (The Portmagee Anticline). • Northwards verging isoclinals folds on north coast of Iveragh.	• Passively rotated cleavage in all lithologies. • Variable intensity of cleavage-weak to absent in some areas, spaced and disjunctive and more pervasive in the siltsones. • Cleavage is an early LPS fabric.
Foreland Zone	• Gentle open folds.	• Very weak disjunctive steeply dipping or absent cleavage.

4.6 Discussion of Field Work Results

The Coomnacronia Fault marks an obvious boundary between two different tectonic zones. To the south of the Coomnacronia Fault, cleavage is steeply dipping, axial planar and cleavage poles are tightly clustered. Folds to the south of the Coomnacronia Fault are mostly large scale anticlines and synclines with smaller scale parasitic folds.

To the north of the Coomnacronia Fault the cleavage is considered to be an early LPS fabric and is passively rotated with bedding. There is the presence of a number of small scale overturned folds which verge to the north. This area (north coast of the Iveragh Peninsula) has previously been documented by Capewell (1975), as the zone of tilted folds and he suggests that this area may be part of the foreland to the north (Chapter 2).

During sedimentation in the Munster Basin, it is proposed in this study that the Coomnacronia Fault was a south dipping extensional structure which acted as the northern bounding structure in the western part of the Munster Basin. Most of the ORS infill was confined to the south of this fault, however there was a thin succession of Upper ORS deposited to the north on the footwall (now the northern coast of the Iveragh Peninsula). The onset of Variscan deformation at the end of the Carboniferous affected the ORS in the Munster Basin and the ORS to the north of the Coomnacronia Fault

The Intrabasinal material of the Munster Basin took up most of the deformation as shown by the intensity of cleavage due to it being bound to the north by the Coomnacronia Fault. In the early stages of deformation both the Intrabasinal succession and that to the north of the Coomnacronia Fault, underwent layer parallel shortening and gentle folding. Variscan deformation reactivated the once extensional Coomnacronia Fault and brought about reverse movement on this fault. During inversion of the CF, the rest of the Intrabasinal material remained within the basin and underwent continued Variscan deformation in the form of ongoing cleavage development and further folding. The steeply dipping axial planar cleavage was directly impacted by the geometry of the Coomnacronia Fault. The Intrabasinal material underwent the full extent of Variscan deformation and forms The Intrabasinal Zone.

The material to the north of the Coomnacronia Fault was sheltered from the full effects of Varsican deformation due to it lying on a horst block to the north of the basin margin.

The material to the north of the Coomnacronia Fault therefore preserves the early stages of Variscan deformation in the form of LPS. A footwall short cut may have developed in response to the inversion on the CF allowing possible rotation of this unit (*Cooper, M.A., 2016 pers comms*). This rotated unit may have included some of the Caledonian basement. This LPS fabric/cleavage fabric was passively rotated as a result of further folding and/or rotation of the unit via the footwall shortcut.

The material to the north on the Dingle Peninsula and Kerry Head only underwent gentle folding with some minor amounts of steeply dipping disjunctive cleavage. It is affected to a lesser degree by Variscan deformation than the material to the south on the Iveragh Peninsula.

Figure 4.41 shows a cross sectional model illustrating the behaviour of cleavage from south to north (orthogonal to strike) across the three tectonic zones based on the bedding and cleavage data.

4.7 Summary of Field Work Results

- The Coomnacronia Fault is a major basin margin fault, which was initially an extensional fault and subsequently acted as reverse fault during Variscan inversion.
- The Coomnacronia Fault marks a significant boundary between two proposed different tectonic zones: the Intrabasinal Zone and the Transition Zone.
- Cleavage is axial planar to the south of the Coomnacronia Fault and passively rotated to the north of the Fault.
- The zone proposed to the north of the CF is termed the Transition Zone as it exhibits features transitional between the Intrabasinal Zone and the Foreland Zone to the north.
- LPS occurred and was preserved in the Transition Zone. LPS in the Intrabasinal Zone was overprinted by continual cleavage development during further Variscan deformation.

Chapter 5:
AMS Results.

Chapter 5. AMS Results

5.1 Introduction & Objectives of Using AMS

As discussed in Chapter 4, the study area, which forms part of the Variscan foreland fold and thrust belt in south west Ireland has been divided into three proposed distinct tectonic zones. Zone 1: the Intrabasinal Zone, Zone 2: the Transition Zone and Zone 3: the Foreland Zone. Zone 1 and 2 are separated by the Coomnacronia Fault which is proposed to be the northern margin of the Munster Basin. The aim of this chapter is to characterise how the AMS ellipsoids vary across these zones. As previously discussed in Chapter 3: Principles of AMS, AMS is a useful tool in assessing the relative variation in the degree of deformation across a foreland fold and thrust belt. In this study AMS is used in order to:

1) Characterise the strain across the Coomnacronia Fault (the northern margin of the Munster Basin) and investigate if this fault marks a strain boundary.
2) Compliment the already defined structural zones across the northern margin of the Munster Basin based on field observations.

5.2 AMS Methodology

5.2.1 Sample Collection and Core Preparation

The anisotropy of magnetic susceptibility has been carried out on a total of 25 arenaceous sandstone block samples which were collected from selected locations on the Iveragh Peninsula, Dingle Peninsula, Kerry Head and also one form Broad Strand (South Munster Basin) and another external to the study area from Dunmore East, Co. Waterford (as a control sample; AMS Results Map). Samples of similar grain size and mineralogy (quartz arenites) were selected in order to maximize their comparability. Samples have been taken from mostly medium/coarse grained arenite sandstones and a few are fine/medium grained quartz arenite sandstones (Table: 5.1. The samples consist mostly of quartz (80 - 90%), Micas and matrix (< 15%) made of micas, quartz and minor amounts of accessory minerals (i.e. oxides). Block samples were orientated in the field with a magnetic compass/clinometer using the left hand rule with bedding as the main reference (Appendix A). Block samples were taken where bedding thicknesses were consistent and of uniform lithology. Depending on the quality of the outcrop data, at each site field data ,S_0, S_1 and L_1 readings, were collected either from the same bed set as the sample was taken or within close proximity to the sample point (within 10-20 m). A list of all field data collected at each sample site along with the AMS sample readings are shown in Appendix A. Numerous structural readings were

taken from sites which had high quality outcrop and sites with limited exposure consist of just one of each structural reading. The block samples were then taken to the University of Birmingham for core preparation and AMS analysis.

5.2.2 AMS Analysis Methodology using the Kappabridge

AMS analysis was carried out using the AGICO KLY-3S Kappabridge at the University of Birmingham. The Kappabridge works in a magnetic field of 300 A/m and at a frequency of 875Hz (Magee PhD, 2011). The Kappabridge can detect susceptibility variations as small as 10^{-8}. The specimen is placed in the holder in three separate positions. Prior to each measurement the Kappabridge is zeroed. For each of the positions the specimen is slowly rotated while the Kappabridge takes measurements. The Kappabridge takes 64 measurements per rotation. Also a single bulk susceptibility reading is taken along one axis (www.agico.com). The AMS raw data obtained from the Kappabridge is analysed using software which consists of a number of programmes called Anisosoft programmes under the heading Susar - See Appendix B.

Table 5.1 List of AMS locations. See AMS Results Map. BSF = Ballinskelligs Sandstone Fm, VSF = Valentia Slate Fm, LASF = Lough Acoose Sandstone Fm, SFSF = St. Finan's Sanstone Fm, LS = Lough Slat Conglomerate, CA = Capagh Sandstone Fm , WS = White Strand Fm., KS = Kilmore Sandstone Fm, TF = Templetown Fm.

AMS Samples									
Location No.	**Location**	**Grid Reference**	**Fm.**	**Lithology**	**Location**	**Sample Bedding (S0)**	**No of Cores analysed**	**Strain analysis**	**Thermomagnetic studies**
A1	Portmagee Quarry	44439 57185	SFSF	SST	South	060 45 S	13	✓	
A2	Killabounia.	44155 56981	SFSF	SST	South	050 40 S	10	✓	✓
A3M	Keel Bay.	43905 56853	SFSF	SST	South	046 60 S	9	✓	
A4	SE of Keel Bay.	44006 56658	SFSF	SST	South	050 70 S	9	✓	
A6	Road to Caherdaniel.	45215 55997	SFSF	SST	South	120 32 S	11	✓	
A8	Turn off Rossmore.	47562 56618	BSF	SST	South	250 18 N	19	✓	✓
A9	Molls Gap.	48637 57730	SFSF	SST	South	070 52 S	16	✓	
A10	Gap of Dunloe South.	48768 58788	BSF	SST	North	100 30 S	13	✓	
A12	Gap of Dunloe North.	48765 58806	SFSF	SST	South	040 30 S	9	✓	
A13	Dunmore East.	66894 60087	TF	SST	External to Munster Basin	140 08 S	9	✓	
A14	Kilgarvin.	50763 58097	SFSF	SST	South	072 30 S	10	✓	✓
A15	Bulls Head Dingle Peninsula.	44950 59752	LS	SST	North	062 35 S	8	✓	
L44	Culoo Rocks	43545 57635	VSF	SST	North	056 28 N	13	✓	✓
L47	Coosfada	44457 58350	BSF	SST	North	240 58 N	8	✓	
L31	Valentia Island	43836 57850	VSF	SST	North	050 20 S	15	✓	✓
M2	Rheencaheragh.	43565 57288	VSF	SST	South	090 42 N	21	✓	

AMS Samples Continued								
Location No.	**Location**	**Grid Reference**	**Fm.**	**Lithology**	**Location**	**Sample Bedding (S0)**	**No. Of Cores analysed**	**Strain Analysis**	**Thermomagnetic studies**
M3	Kells Bay.	45568 58796	BSF	SST	North	085 52 S	16	✓	
M4	Broad Strand.	55147 54114	WS	SST	South	075 80 S	25	✓	
M5	Lough Acoose.	47609 58494	LASF	SST	South	100 40 S	13	✓	
M6	Ballyheige.	47472 62801	KS	SST	North	060 20 S	26	✓	✓
M7	Brandon Pier.	45255 61516	CA	SST	North	038 38 S	7	✓	
M8	Glenflesk Quarry.	50666 58614	SFS	SST		232 80 N	28	✓	

5.3 The Variation of Magnetic Susceptibility with Temperature

5.3.1 Introduction

In order to determine the minerals responsible for the magnetic susceptibility of the AMS samples, temperature dependant susceptibility experiments have been carried out. These experiments help to reveal whether these minerals are diamagnetic, paramagnetic or ferromagnetic. A curve where the magnetic susceptibility (K) is plotted against temperature (T) may also be referred to as a thermomagnetic curve.

5.3.2 Theory

Hrouda (1994) discusses in detail the technique for the measurement of the variation of magnetic susceptibility with temperature using the KLY-2 Kappabridge. Thermomagnetic curves can reveal what types of magnetic mineral are present and can also give information about grain size distribution (Hrouda, 2003; Petrovský and Kapička, 2006). The three types of minerals: diamagnetic, paramagnetic and ferromagnetic exhibit different types of thermomagnetic curves. Diamagnetic minerals such as quartz and calcite have negative susceptibilities and are temperature independent (e.g. Schmidt, 2007) and therefore will be represented by a horizontal line on a K/T plot. In weakly magnetic rocks the susceptibility is significantly influenced by paramagnetic minerals (e.g. Owens and Bamford, 1976; Rochette, 1987). The magnetic susceptibility of paramagnetic minerals is inversely proportional to the temperature according to the Curie Weis Law (Chapter 3) and the thermomagnetic curves produced are in the shape of a hyperbolic curve (Hrouda, 2010). For example, on heating, biotite shows typical paramagnetic behaviour with a gently decreasing susceptibility versus temperature slope (Fig 7.1; Hrouda, 1997). Thermomagnetic curves are also used to find the Curie temperatures, which are used to identify the presence of certain magnetic minerals (Petrovský and Kapička, 2006). There is a significant decrease in the magnetic susceptibility at the Curie temperature for ferromagnetic minerals (Dunlop and Ozdemir, 1997). The Curie temperature is the temperature at which ferromagnetic, ferrimagnetic or antiferromagnetic mineral lose their magnetism and becomes paramagnetic in behaviour i.e. its induced magnetisation is directly proportional to the strength of the applied field (Petrovský and Kapička, 2006). A Curie temperature of 580 ° C indicates the presence of pure magnetite (Fig 7.1; O' Reilly, 1984; Hrouda, 1997) and on a thermomagnetic curve this appears as a sudden drop in the magnetic susceptibility at 580°C (e.g. Silva et al., 2001). Haematite shows a sharp inflection of the curve at 670-680 °C (Fig 7.1; Hrouda, 1997). The Hopkinson effect is where there is

an increase in magnetic susceptibility near the Curie point (O' Reilly, 1984). This has been observed in fine grained magnetite (Dunlop, 1974).

Thermomagnetic curves can be made up of contributions from both paramagnetic and ferromagnetic minerals and can be resolved into separate fractions (Fig 7.2; Hrouda, 2010). Examples of thermomagnetic curves for bulk rocks are shown by Hrouda (2010, Fig 5.1); Granodiorite, which is made up of predominantly ferromagnetic minerals shows a flat curve with a sudden drop between 560-600 ° C, greywacke which is mostly made up of paramagnetic minerals shows a steady inverse relationship between magnetic susceptibility and temperature and two granites are shown: one with mostly paramagnetic minerals and one with equal amounts of paramagnetic and ferromagnetic minerals, both showing inverse relationships between magnetic susceptibility and temperature (Fig 5.1).

One drawback of the thermomagnetic method is that heating may cause transformations of the minerals (Petrovský and Kapička, 2006). If the susceptibility is lower during cooling than it was during heating, then the original magnetic minerals have undergone changes during the experimental process (Silva et al., 2001). Heating a rock sample results in the growth of iron oxides (Dunlop, 1974; Thompson and Oldfield, 1986). At temperatures of around 320° C there may be a transformation of maghemite to heamatite (Dunlop and Ozdemir, 1997) or pyrrhotite to magnetite (Bina and Daly, 1994). Higher magnetic susceptibility on the cooling curve indicates the formation of magnetite during the experiment. Lower magnetic susceptibility is less common and may be a result of magnetite dissolving into a less magnetic material (Fig 7.3; Chadima (online Pdf; after Hrouda, 2003). However, consideration of the possible mineral changes during the experimental process may help in the interpretation of the sample.

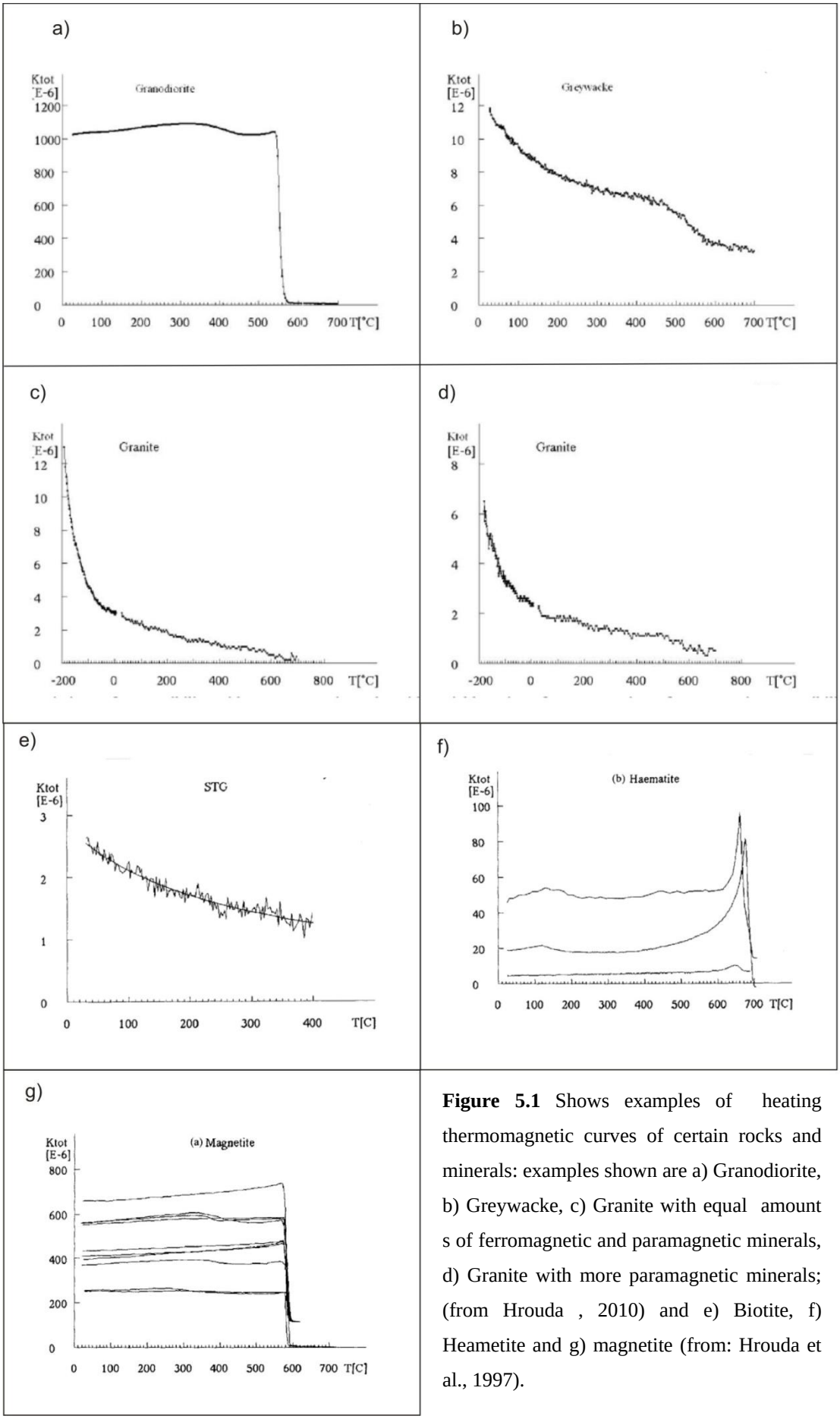

Figure 5.1 Shows examples of heating thermomagnetic curves of certain rocks and minerals: examples shown are a) Granodiorite, b) Greywacke, c) Granite with equal amount s of ferromagnetic and paramagnetic minerals, d) Granite with more paramagnetic minerals; (from Hrouda , 2010) and e) Biotite, f) Heametite and g) magnetite (from: Hrouda et al., 1997).

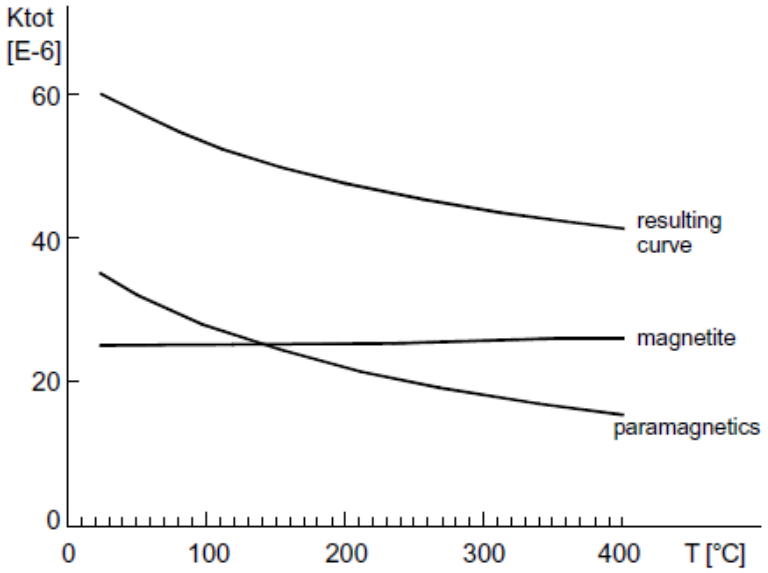

Figure 5.2 shows how the overall thermomagnetic curve can be a product of both the paramagnetic fraction and the ferromagnetic fraction. From Hrouda (2010).

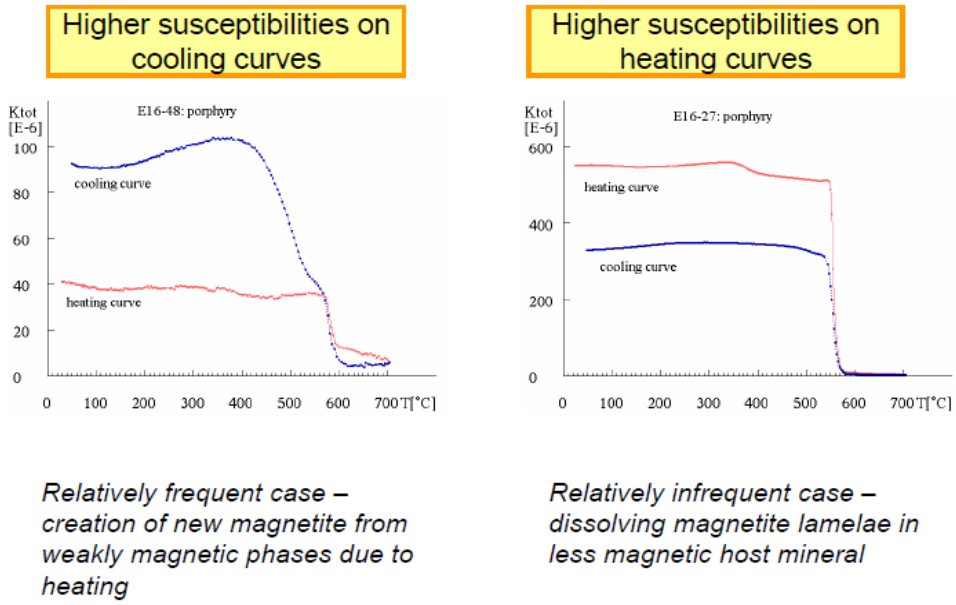

Figure 5.3 Higher magnetic susceptibility on the cooling curve indicates the formation of magnetite during the experiment. Lower magnetic susceptibility is less common and may be a result of magnetite dissolving into a less magnetic material. From Chadima (online Pdf) after Hrouda (2003).

5.3.3 Methodology

The variation of magnetic susceptibility with temperature experiments have been carried out at the University of Birmingham. A total of 8 of the AMS samples selected from each of the structural zones (Chapter 4) were analysed (AMS Results Map). The magnetic susceptibility of powdered samples is measured from room temperature to between 600-700° C and then on cooling back to about 100°. Oxidation of the minerals

may occur due to heating in air. Alternatively heating experiments may be carried out in argon in order to prevent oxidation. However argon was unavailable to use and the experiments were carried out in air. A detailed description of the methodology is found in Appendix E. All specimens were corrected for the susceptibility of the holder which is approximately (-140). As the holder is diamagnetic its susceptibility is temperature independent, therefore this correction has been used for whole range of data points.

5.3.4 Results of the Variation of Magnetic Susceptibility with Temperature

Intrabasinal Sample Results

Sample No. A2-G21 Kilabounia –The Intrabasinal Zone

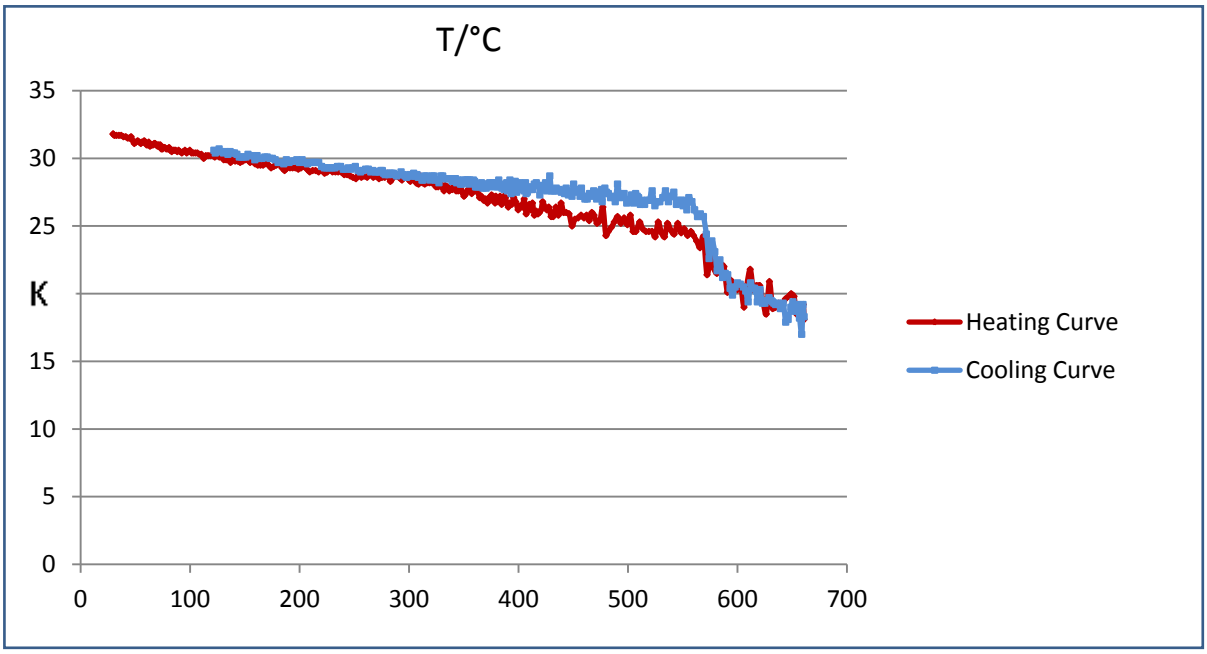

Figure 5.4 Thermomagnetic curve for sample no. A2-G21: Kilabounia- a med/coarse grained quartz arenite from the St Finans Sandstone Fm.

A2: On heating there is a steady decrease in the magnetic susceptibility of this sample (Fig 5.4), indicating the presence of paramagnetic minerals. On heating there is a minor drop at 580°C indicating that there is also some magnetite present. On cooling, the magnetic susceptibility increases and then returns to a similar susceptibility value as the heating curve. The fact that the cooling curve returns back along a similar path as the heating curve indicates that not much alteration occurred during the experimental process.

Sample No. A8-M11: Turn off Rossmore-the Intrabasinal Zone

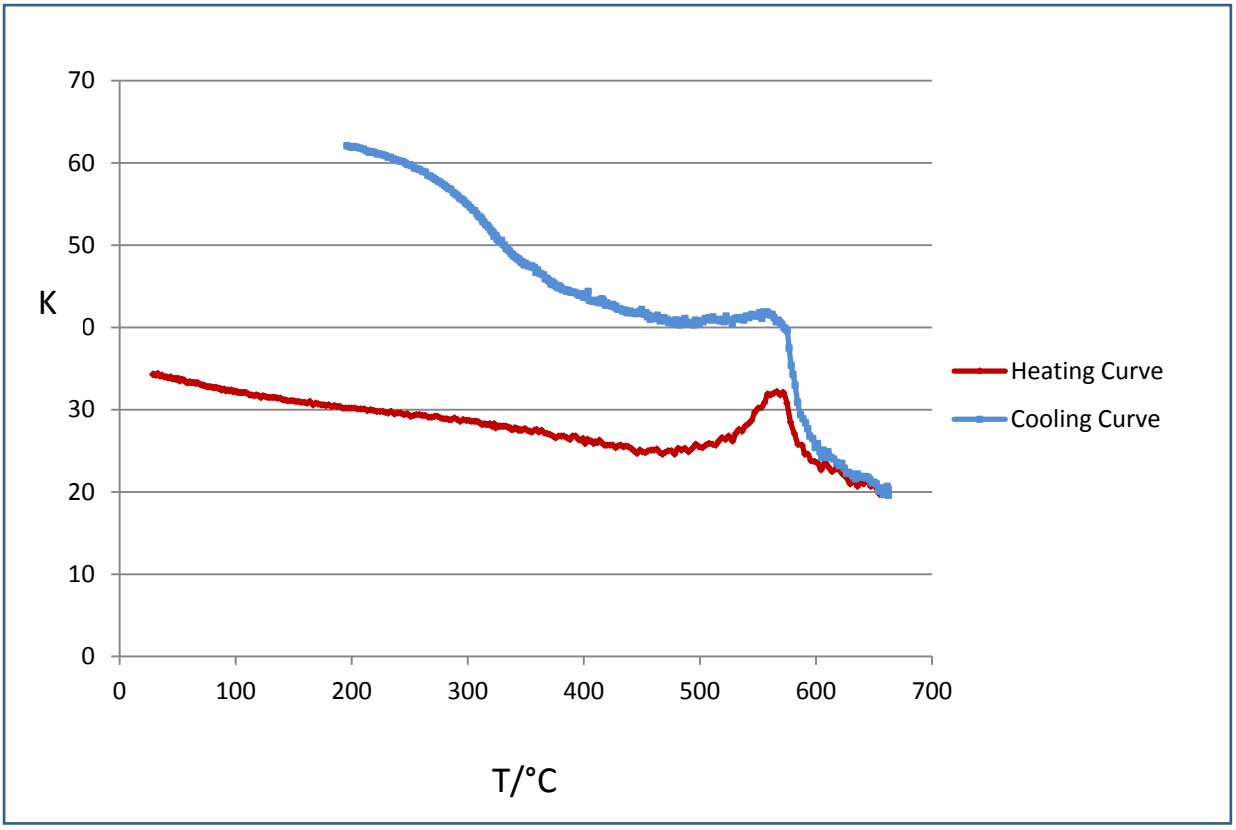

Figure 5.5 Thermomagnetic curve for sample no. A8-M11: Turn off Rossmore a med/coarse grained quartz arenite.

A8: On heating there is a gently decreasing curve indicating paramagnetic minerals (Fig 5.5). The sample also shows a characteristic Hopkinson's Peak (1889), where there is an increase in the magnetic susceptibility close to the Curie temperature. This indicates the presence of single domain magnetite. The cooling curve follows a higher magnetic susceptibility path and indicates that mineral transformations have occurred during the experimental process. This is probably due to paramagnetic minerals being oxidised to ferromagnetic minerals.

Sample No. A14-H1 Kilgarvan -The Intrabasinal Zone

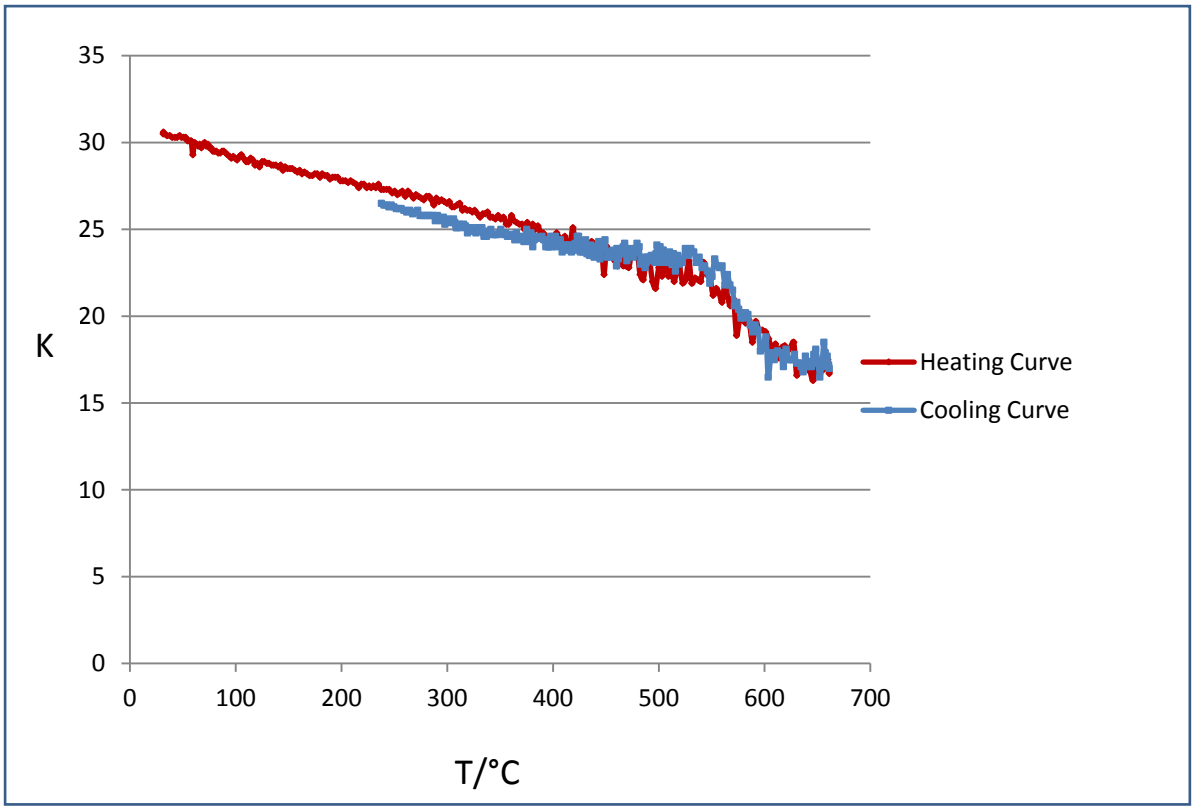

Figure 5.6 Thermomagnetic curve for sample no. A14-H1: Kilgarvan a med grained quartz arenite.

A14: This sample shows similar behaviour to sample A2-G21, with an inverse relationship between susceptibility and temperature on both heating and cooling as a result of paramagnetic minerals and a minor inflection on the cooling curve at 580°C caused by some lesser amounts of magnetite possibly formed during the experiment (Fig 5.6). The magnetic susceptibility is slightly lower on cooling indicating some minor mineral transformations during the experimental process.

Sample No. AM1-H21: South of Lough Caragh-The Intrabasinal Zone

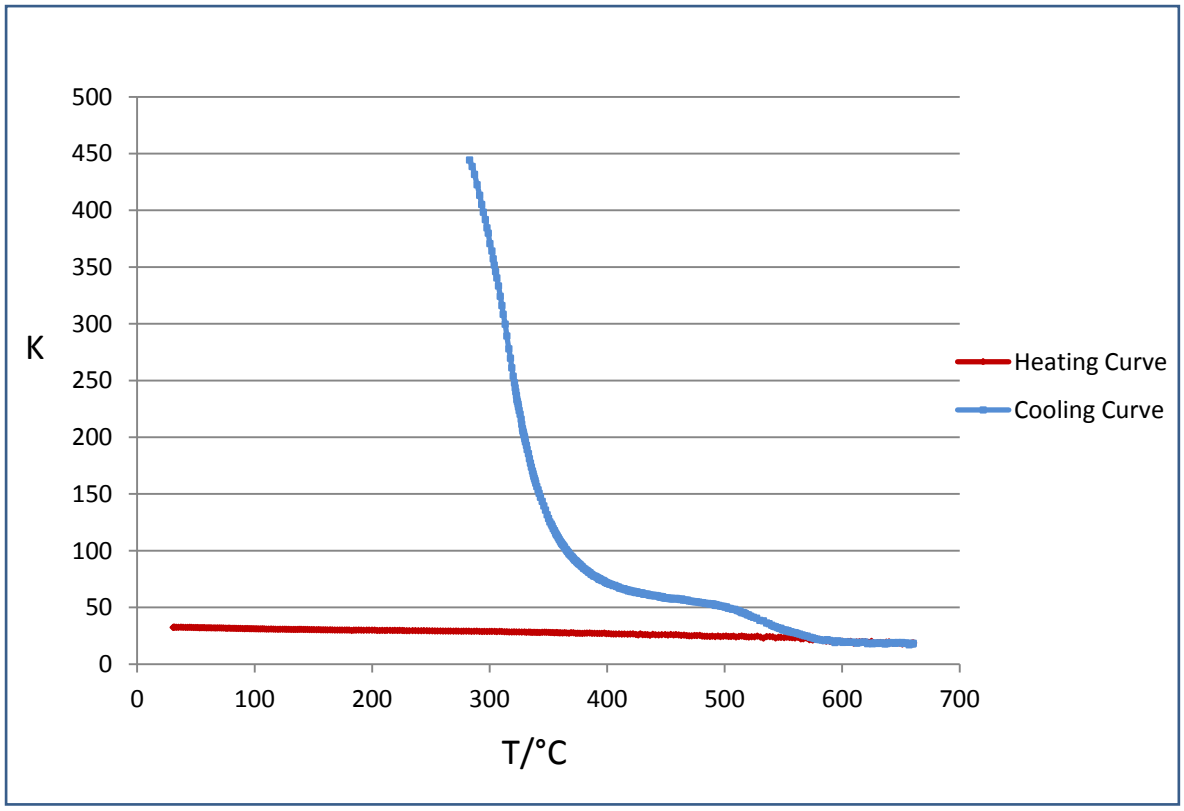

Figure 5.7 Thermomagnetic curve for sample no. AM1-H21: South of Lough Caragh a medium grained quartz arenite.

AM1: The heating curve shows a steady but very gradual decrease in magnetic susceptibility with temperature indicating the presence of paramagnetic minerals (Fig 5.7). The cooling curve shows a significantly higher susceptibility than the heating curve which may be a result of a high degree of oxidation and the formation of maghaemite during the experimental process. This oxidation may be a result of higher amounts of Fe in the micas in this sample. The high amount of Fe in the micas could be a result of authigenic growth along the cleavage plane.

Sample No. AM11-K21: Lough Caragh North-The Intrabasinal Zone

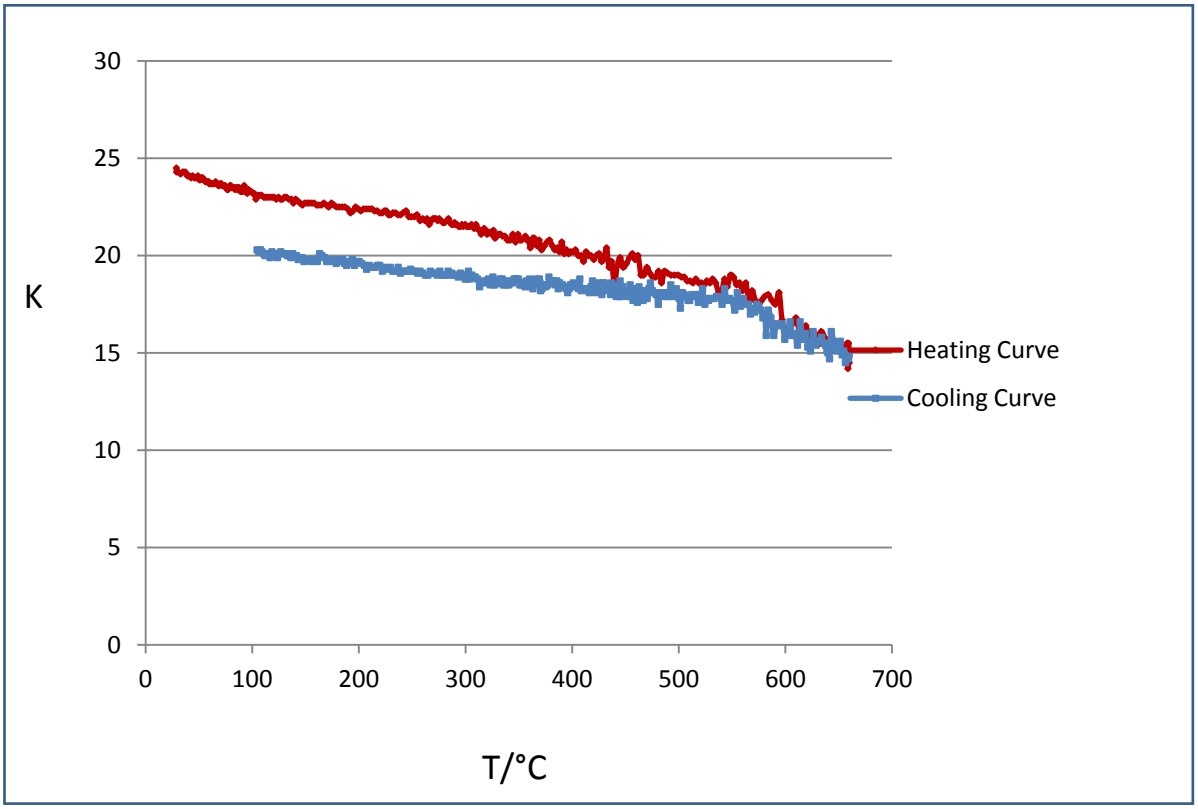

Figure 5.8 Thermomagnetic curve for sample no. AM11-K21: Lough Caragh North a med/coarse grained quartz arenite.

AM11: The gently decreasing curve indicates the presence of paramagnetic minerals (Fig 5.8). The cooling curve has a lower susceptibility than the heating curve indicating some mineral transformations during the heating process. The lower susceptibility on the cooling curve indicates that magnetite has dissolved into the less magnetic material.

Transition Zone and Foreland Zone Sample Results

Sample No. L31-G11: Reenadrolaun Point -The Transition Zone

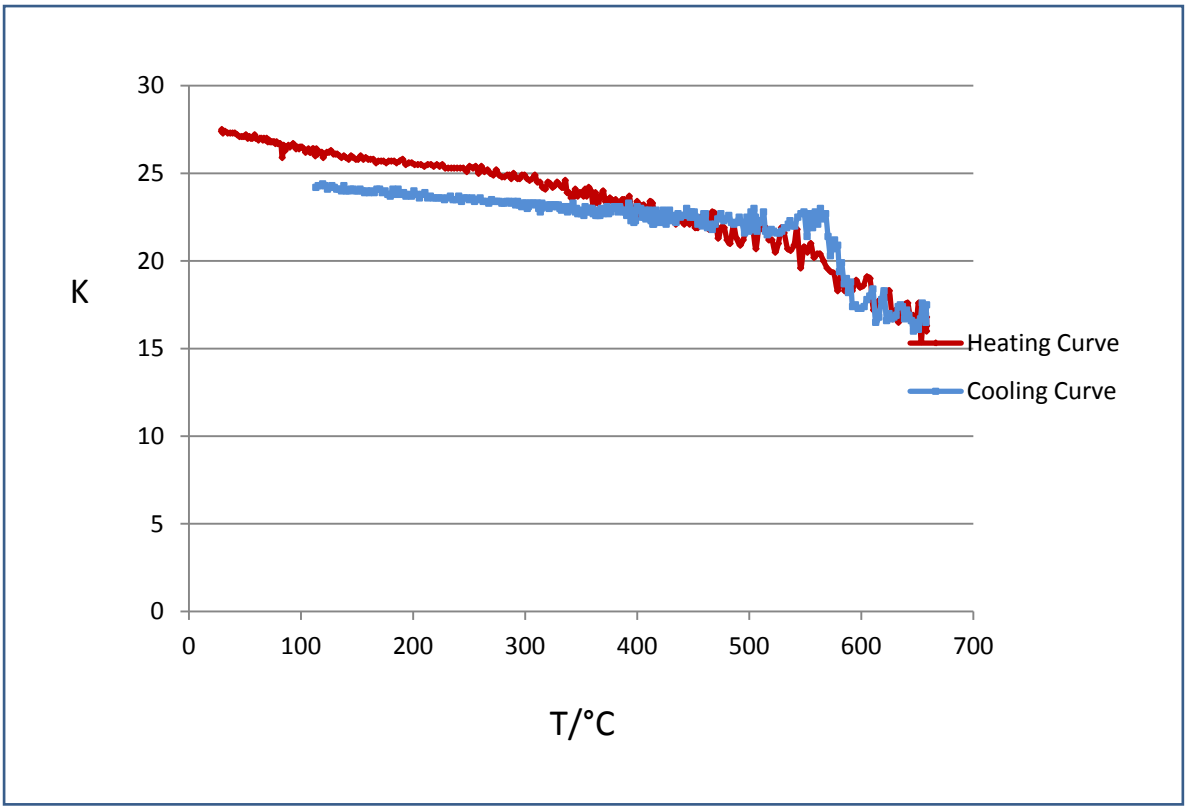

Figure 5.9 Thermomagnetic curve for sample no. L31-G11: Reenadrolaun Point a medium grained quartz arenite.

L31: The heating curve shows a gradual decreasing curve indicating the presence of paramagnetic minerals (Fig 5.9). On the cooling curve there is an inflection at 580 ° C indicating the formation of magnetite during the experimental process. The lower susceptibility on the cooling curve indicates that magnetite has dissolved into the less magnetic material.

Sample No. L47-E1: Coosfada-The Transition Zone

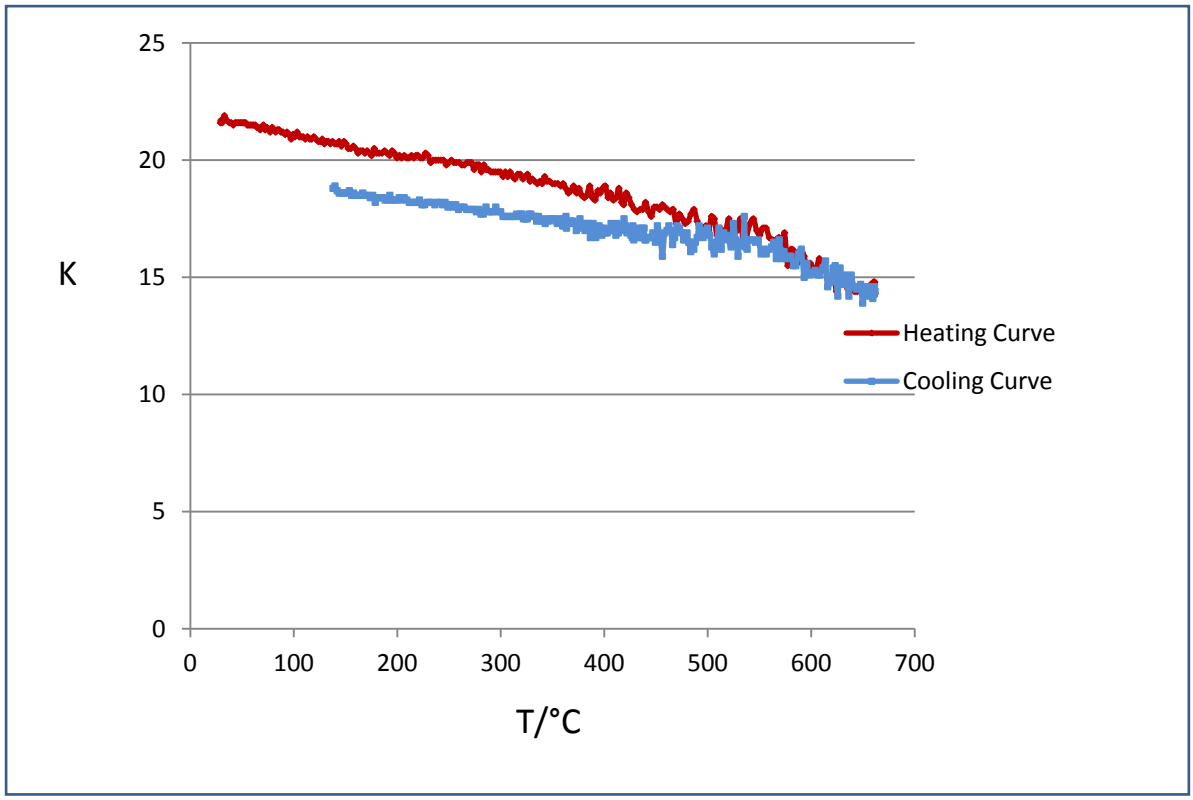

Figure 5.10 Thermomagnetic curve for sample no. L47-E1: Coosfada a medium/coarse grained quartz arenite.

L47: This sample is very similar to AM11-K21.The gently decreasing curve indicates the presence of paramagnetic minerals (Fig 5.10). The lower susceptibility on cooling curve indicates that magnetite has dissolved into the less magnetic material.

Sample No. M6-L11: Ballyheige -The Foreland Zone

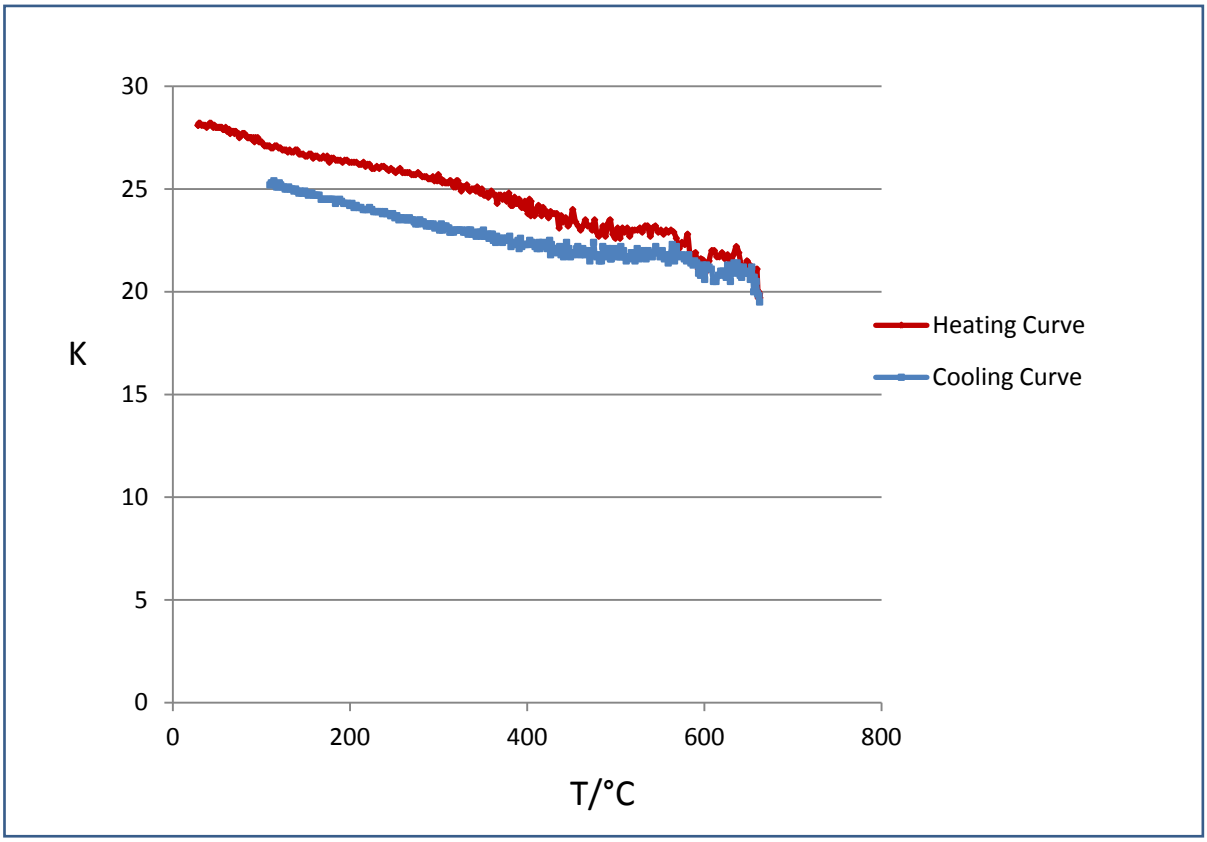

Figure 5.11 Thermomagnetic curve for sample no. M6-L11: Ballyheige a medium grained quartz arenite.

M6: This sample is very similar to AM11-K21 and L47-E1.The gently decreasing curve indicates the presence of paramagnetic minerals. The lower susceptibility on the cooling curve indicates that magnetite has dissolved into the less magnetic material.

Table 5.2 Summarizes the results for the thermomagnetic analysis.

Sample No.	**Location:**	**Characteristics of K/T Curve:**	**Magnetic Mineralogy:**	**Zone:**	**AMS fabric controlled by:**
A2-G21	Kilabounia	Steady inverse relationship between K and T + drop at 580°C.	Paramagnetic Minerals + minor Magnetite	Intrabasinal	Cleavage
A8-M11	Turn off Rossmore	Steady inverse relationship between K and T + Hopkinson's Peak.	Paramagnetic Minerals + Single Domain Magnetite	Intrabasinal	Cleavage
A14H1	Kilgarvan	Steady inverse relationship between K and T.	Paramagnetic Minerals	Intrabasinal Zone	Cleavage
AM1-H21	South of Lough Caragh	Steady inverse relationship between K and T, High amount of oxidation cooling.	Paramagnetic Minerals	Intrabasinal Zone	Cleavage
AM11-K21	Lough Caragh	Steady inverse relationship between K and T.	Paramagnetic Minerals	Transition Zone	LPS
L31-G11	Reenadrolaun Point	Steady inverse relationship between K and T, Formation of magnetite on cooling.	Paramagnetic Minerals	Transition Zone	Bedding
L47-E1	Coosfada	Steady inverse relationship between K and T.	Paramagnetic Minerals	Transition Zone	LPS
M6-L11	Ballyheige	Steady inverse relationship between K and T.	Paramagnetic Minerals	Foreland Zone	Bedding

5.3.5 Discussion of Thermomagnetic Studies Results

Table 5.2 summarizes the results for the thermomagnetic analysis of each of the samples and shows what structural zones (Chapter 4) they lie in.

In the Intrabasinal Zone: Samples A14-H1, AM1-H21 exhibit paramagnetic minerals (muscovite and biotite) as the main magnetic carrier. Sample A2-G21 exhibits paramagnetic minerals and some minor amounts of magnetite. Sample A8-M11 exhibits paramagnetic minerals and single domain magnetite. In these samples, the paramagnetic minerals lie in the cleavage plane.

In the Transition Zone: Samples L31-G11, L47-E1 and AM11-K21 exhibit paramagnetic minerals as the main magnetic carriers. In L31: the paramagnetic minerals lie in the bedding plane. For samples AM11-K21 and L47-E1 the paramagnetic minerals lie in the LPS plane.

In the Foreland Zone the sample M6-L11 exhibits paramagnetic minerals as the main magnetic carrier. In M6-L11 the paramagnetic minerals lie in the bedding plane.

These thermomagnetic experiments show that the magnetic mineralogy for most of the selected samples consists of paramagnetic minerals. Paramagnetic minerals dominate the magnetic susceptibility in all three structural zones. This indicates that paramagnetic minerals (i.e. micas) have been rotated from the bedding plane into the LPS plane/cleavage plane during deformation, as these are the magnetic minerals responsible for the AMS ellipsoids in these samples. The cleavage planes may have a strong component of detrital micas except for sample AM1-H21-south of Lough Caragh which may have authegenic mica's. These results also correspond to the low mean susceptibilities of samples (Section 5.8).

5.4 Interpretation of the AMS Data

The AMS ellipsoids have been interpreted as to whether they are controlled by bedding (i.e. the primary sedimentary fabric), by cleavage (i.e. a tectonic fabric), or a mixture of both bedding and cleavage. Spatially across the tectonic zones, the AMS ellipsoids have been used to assess the evolution of a primary sedimentary fabric through to a complete tectonic overprint fabric. The following AMS parameters are used in the interpretation of the AMS data:

- The orientations of the K_{min} axes, K_{int} axes and K_{max} axes in relation to the collected field data are used to understand which structural features the AMS is

sensitive to. Each AMS stereonet plots the orientation of the principal axes K_{max}, K_{int} and K_{min} for each sample and the numbering on the stereonets is for each core taken within the block sample. Numbering is useful in the case of any anomalies; the individual core and its location within the block sample can be re-checked. The relationship of the K_{min} axes to the pole to bedding or the pole to cleavage is one of the key characteristics when interpreting the AMS ellipsoids with respect to the structural field data, as the orientation of the K_{min} axes defines the orientation of the AMS ellipsoid. The angular relationship between the average K_{min} axes and the pole to S_0 and S_1 is used to show the variations in the degree of control of the S_0 or S_1 on the AMS axes for all of the AMS sites and this is described in the Section 5.5.

- The μ value indicates the shape of the AMS ellipsoid. Where $0 < \mu < 45°$, the ellipsoid is oblate and where $45° < \mu < 90°$, the ellipsoid is prolate. The degree of oblateness or prolatess reflects both the strength of the primary sedimentary fabric and the amount of subsequent deformation that has occurred.

The anisotropy degree, Pj and the shape parameter, Tj are plotted together on a Jelenick plot (Jelenick, 1981; Borradaile, 1997) in order to show the evolution of the AMS ellipsoids with increasing deformation.

To describe the shape of the ellipsoid, the shape parameter, T_j is used:

$$T = \left[\frac{2\ln(K_2/K_3)}{\ln(K_1/K_3)}\right] \quad -1 \qquad \text{(Jelenik,1981).}$$

When T = +1 the ellipsoid is oblate. When T = -1, the ellipsoid is prolate. When T = 0, the ellipsoid is neutral, (i.e. $K_1 = K_2 = K_3$).

The magnitude or eccentricity of the ellipsoid is also known as Pj, the anisotropy degree (Jelenik, 1981).

$$P_j = \exp\sqrt{\left\{2\left[(\eta_1 - \eta_m)^2 + (\eta_2 - \eta_m)^2 + (\eta_3 - \eta_m)^2\right]\right\}} \qquad \text{(Jelinek, 1981)}$$

$$\eta_1 = \ln K_1;\ \eta_2 = \ln K_2;\ \eta_3 = \ln K_3$$

$$\eta_m = \sqrt[3]{(\eta_1 \cdot \eta_2 \cdot \eta_3)} \text{ (Geometric mean)}$$

- Also a Flinn plot (Flinn 1962) is used to show the distribution of AMS ellipsoid shapes.

All of the above criteria have been used to classify the AMS ellipsoids into zones of zero to low, moderate and high deformation. An overall summary of the behaviour of the AMS fabrics and using them to define tectonic zones has been provided at the end of the chapter.

5.5 AMS Results

As discussed in Chapter 4: Field work, three tectonic zones have been proposed across the study area. The AMS ellipsoids display behaviour reflecting the structural styles in these three tectonic zones. To recap from Chapter 4, Zone 1: The Intrabasinal zone is located south of the Coomnacronia Fault and is characterised by large scale folding and by a penetrative uniformly steeply dipping axial planar cleavage. Zone 2: The Transition zone is located north of the Coomnarcronia Fault and is characterised by overturned folding with a passively rotated LPS/Cleavage fabric. Zone 3: The Foreland Zone is characterised by gentle folding and zero to minor amounts of a spaced disjunctive cleavage.

The AMS results for each site within the zones are described individually. For each site, field data is recorded in the form of bedding, cleavage and bedding/cleavage intersection lineations. All of the AMS ellipsoids have also been compiled onto a map which shows the characteristic behaviour of the AMS ellipsoids within the zones. (AMS Results Map).

5.5.1 AMS Stereonets Results: Zone 1. The Intrabasinal Zone

Sample A1: Portmagee Quarry - Zone 1: Intrabasinal Zone

The sample is taken from the St. Finan's Sandstone Fm. on the southern limb of the Portmagee Anticline to the south of the Coomnacronia Fault. The area consists of uniformly dipping sandstones with an average orientation of 067 50 S and with an average bed thickness of 10-20 cm. A faint cleavage fabric is observed in some parts of the sandstone beds, with more apparent bedding cleavage intersection lineations. The main cleavage can be observed in slaty horizons interbedded within the sandstones.

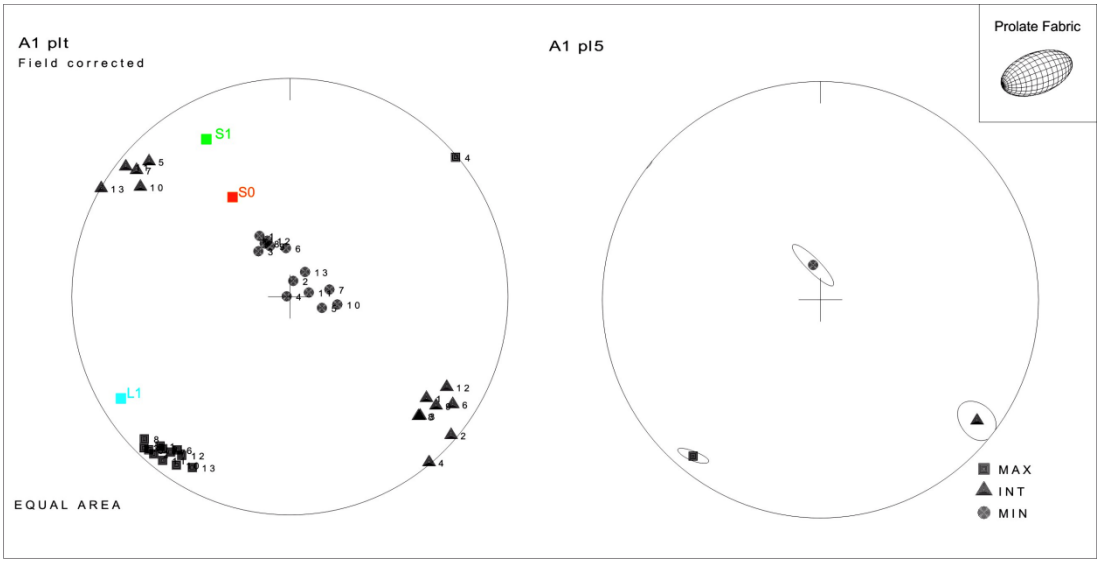

Figure 5.12 AMS ellipsoid and confidence ellipsoid for A1, Portmagee Quarry.

The K_{int} axes lie close to parallelism with the pole to cleavage (S_1). The K_{min} axes lies sub parallel to the pole to S_0, however S_0 could also be interpreted not to be represented by the AMS axes (Fig 5.12). L_1 lies close to parallelism with the K_{max} axes. This indicates that the primary sedimentary fabric has been overprinted by a tectonic fabric. There is roughly a ten degree rotation to the left (anticlockwise) of the AMS fabric with respect to the intersection lineation (L_1) and the pole to cleavage. This may be an indication of further tectonic strain (Chapter 3: Rathore, 1985; Aranguren et al., 1996; Borradaile et al., 1998). This is a prolate fabric with a μ value of 66. The combination of the K_{int} being parallel to S_1, the rotation of the fabric and the degree of prolateness can be interpreted as this ellipsoid representing a high deformation zone.

Sample A2: Kilabounia - Zone 1: Intrabasinal Zone

The sample is taken from the St. Finan's Sandstone Fm. on the southern limb of the Portmagee Anticline. In this location there are uniformly dipping medium grained sandstones with moderate thickness (average 20-30 cm beds), which display ripple marks on surface. There are also visible bedding/cleavage intersection lineations. There is a very weak cleavage fabric in the sandstone bed, but the main cleavage readings are taken from some finer grained slates that are interbedded within the sandstone and in close proximity to the sample bed (< 10 m). The K_{max} axes are parallel to the bedding/cleavage intersection lineation. The K_{min} axes are parallel to the pole to cleavage. The pole to bedding, $S_{0,}$ does not appear to be represented by any of the AMS axes. This is indicative of a complete tectonic overprint fabric. This is a prolate fabric with a μ value of 62.7. Based on the prolateness and the control of the AMS ellipsoid by the cleavage fabric only, this AMS ellipsoid may be classified as coming from a high deformation zone (Fig 5.13).

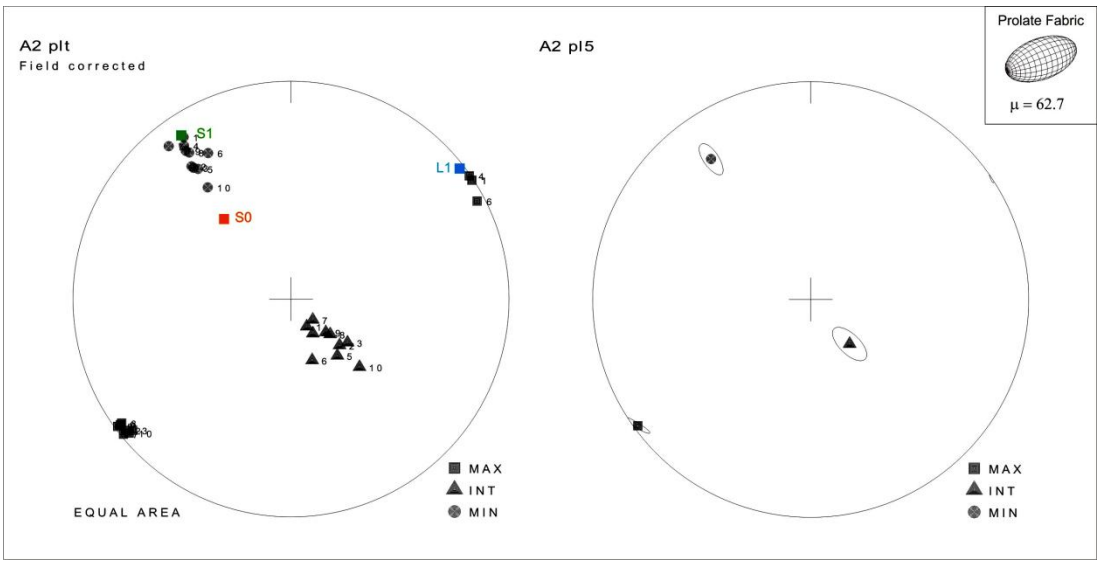

Figure 5.13 AMS stereonet and confidence ellipsoid for A2, Killabounia.

Sample A3M: Keel Bay - Zone 1: Intrabasinal Zone

Keel Bay marks a lithological boundary between the St. Finan's Sandstone Fm. to the south east and the Valentia Slate Fm. to the north west. Cleavage ranges from steeply dipping to the north to steeply dipping to the south. The bed thickness range from 10 cm to 40 cm on average and are uniformly dipping to the south. Bedding cleavage intersection lineations are visible on the bedding surfaces. The K_{max} axes are parallel to the bedding/cleavage intersection lineation L_1. The K_{min} axes lie close to parallelism with the pole to cleavage. The pole to bedding S_0 is not interpreted to be represented by the AMS ellipsoid (Fig 5.14). This AMS ellipsoid may be interpreted as a complete tectonic overprint. This is an oblate fabric with a μ value of 36. This is interpreted as a high deformation zone. The AMS ellipsoid may have evolved from being oblate to prolate to oblate again with increasing deformation.

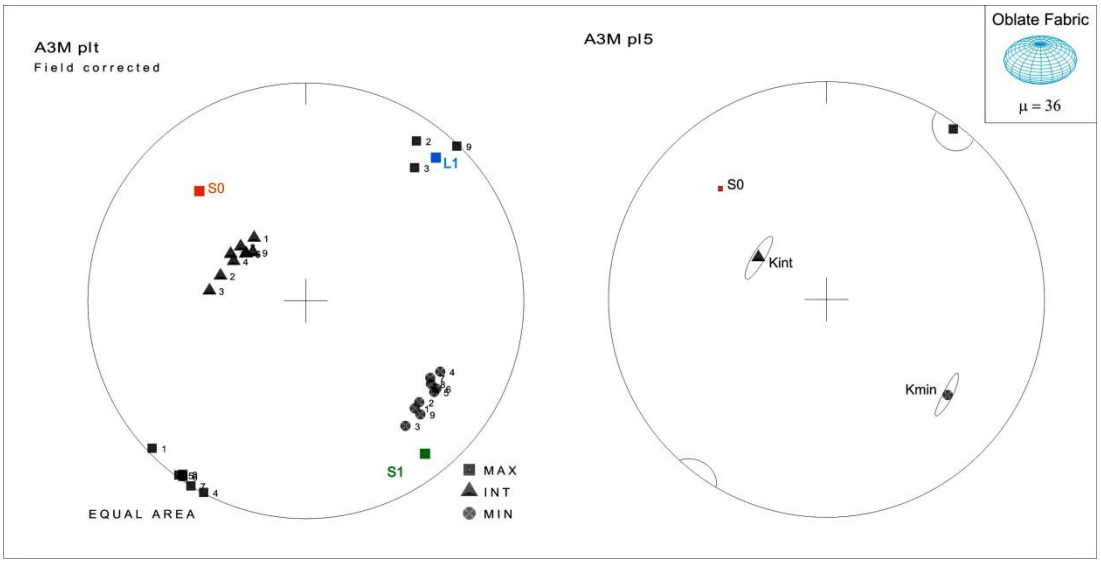

Figure 5.14 AMS stereonet and confidence ellipsoid for A3M, Keel Bay.

Sample A4: East of Keel Bay - Zone 1: Intrabasinal Zone

This sample is taken to the south east of Keel Bay in the St. Finan's Sandstone Fm. on the southern limb of the Portmagee Anticline. It is taken from uniformly dipping beds of 20-50 cm thickness. The K_{min} axes are parallel to the pole to bedding but are also close to the pole to cleavage. The K_{max} axes are close to parallelism with the bedding/cleavage intersection (Fig 5.15). Due to the close proximity of the orientation of the bedding and the cleavage this may be interpreted as bedding or a cleavage controlled fabric. This is an oblate fabric with a μ value of 33.1.

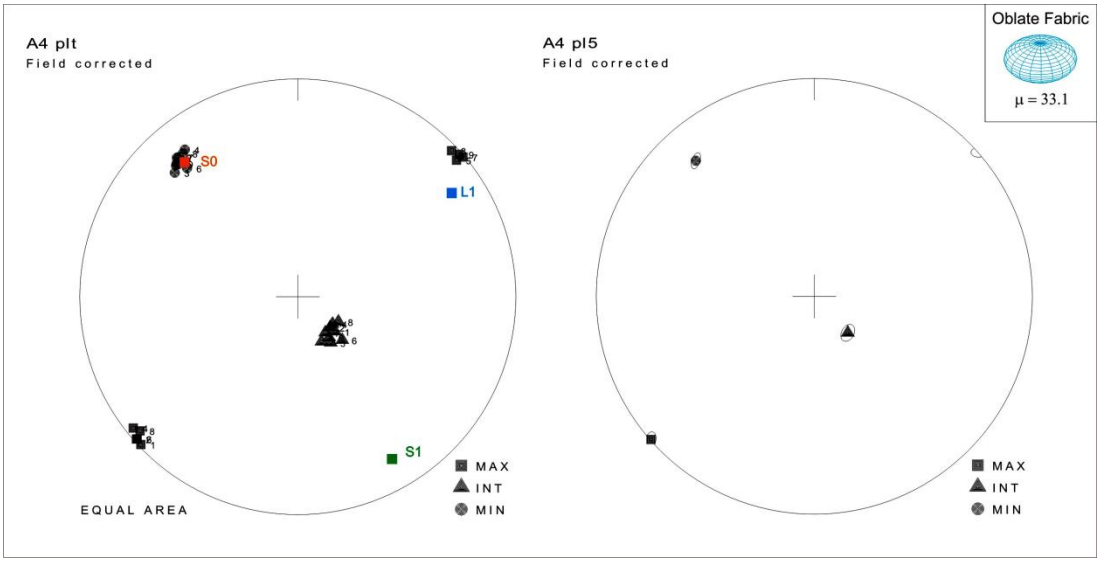

Figure 5.15 AMS stereonet and confidence ellipsoid for A4, south east of Keel Bay.

M2: Rheencaheragh - Zone 1: Intrabasinal Zone

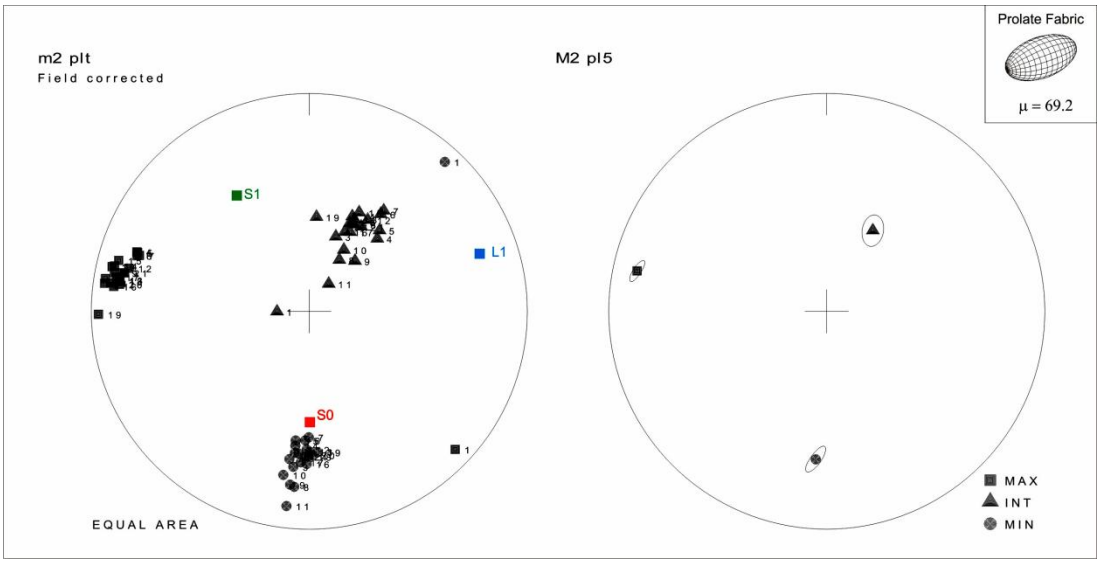

Figure 5.16 AMS stereonet and confidence ellipsoid for M2, Rheencaheragh.

The K_{min} axes for M2 are parallel to the pole to bedding. The K_{int} and K_{max} axes lie intermediate to the L_1 and pole to S_1 (Fig 5.16). This shows that the AMS ellipsoid is mainly bedding controlled. This sample is the only bedding controlled sample found in the Intrabasinal zone. However this location lies very close to the boundary between the Intrabasinal Zone and the Transition Zone (AMS Results Map).This is a prolate fabric with a μ value of 69.2. The prolate fabric indicates that the AMS ellipsoids has been deformed from the original oblate shape lying in the bedding plane, so a moderate amount of deformation has occurred.

Sample A6: Caherdaniel - Zone 1: Intrabasinal Zone

These are uniformly dipping green/grey sandstones from the St. Finan's Sandstone Fm. There is little or no cleavage fabric visible in the bedded sandstone, but there is a good regional slaty cleavage in slates 10-20 m away from the site. The K_{max} axes lie parallel to the bedding/cleavage intersection lineation. The K_{min} axes and the K_{int} axes occupy an intermediate position between the pole to S_1 and the pole to S_0. This represents an incomplete tectonic overprint fabric where the AMS fabric has begun a rotation form a primary sedimentary fabric towards a complete tectonic overprint fabric. This may represent a moderate deformation intensity zone. This is a prolate fabric with a μ value of 64.5 (Fig 5.17).

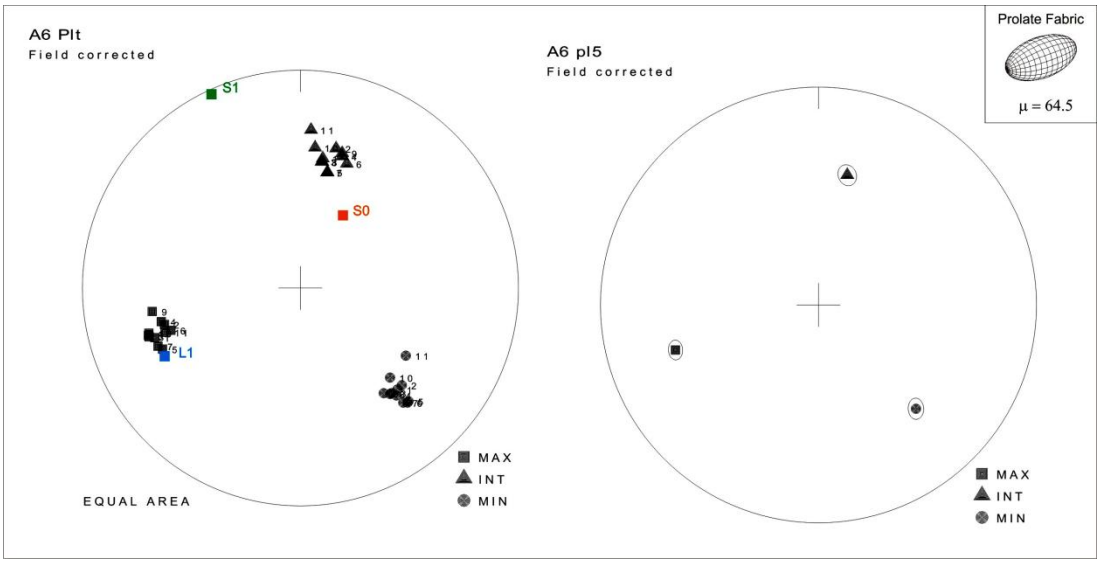

Figure 5.17 AMS stereonet and confidence ellipsoid for A6, Caherdaniel.

Sample A8: Turn Off Rossmore - Zone 1: Intrabasinal Zone

The sample is taken from the Valentia Slate Fm. The K_{min} axes are parallel to the pole to cleavage indicating a tectonic cleavage controlled AMS fabric. The K_{max} axes are parallel to the bedding/cleavage intersection lineation. The K_{int} axes are parallel to the pole to bedding (Fig 5.18). This is a prolate fabric with µ value of 58.2. This is interpreted as a high deformational zone.

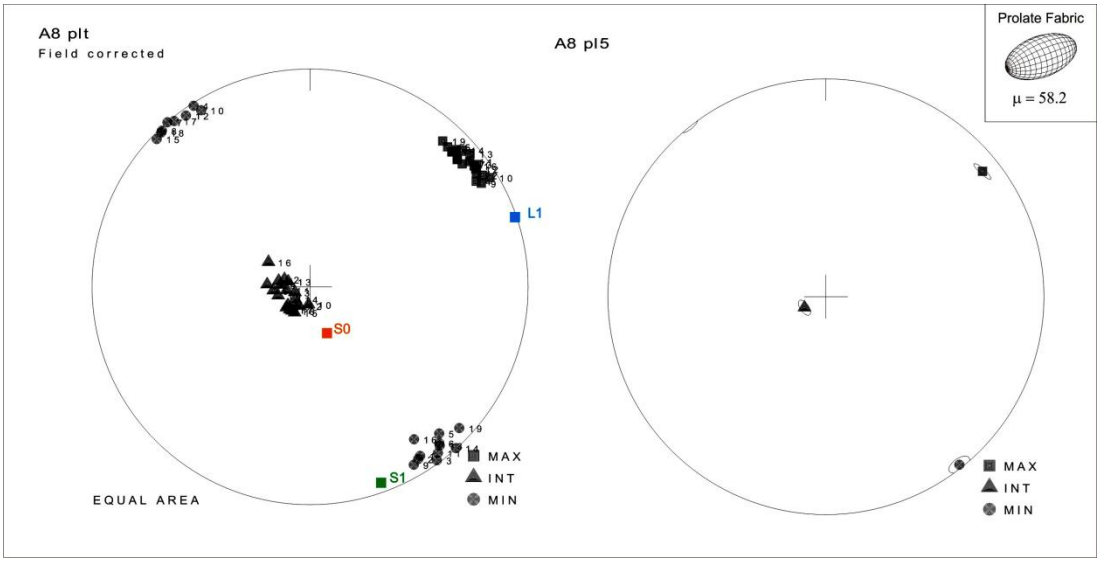

Figure 5.18 AMS stereonet and confidence ellipsoid for A8-Turn off Rossmore.

Sample A9: Molls Gap - Zone 1: Intrabasinal Zone.

The sample is taken from the St. Finan's Sandstone Fm. The area has moderate to steeply dipping uniform beds of approximately 20-40 cm thickness. In close proximity there are slaty horizons within the sandstones, from which cleavage readings have been taken. The AMS fabric appears to be rotated approximately 10° to the right from the main structural elements, S_0, S_1, and L_1 (Fig 5.19). This obliquity with the main structural elements may be interpreted as further deformation (e.g. Rathore, 1985). This is an oblate fabric with a µ value of 22.8. The AMS ellipsoids have evolved from a primary sedimentary oblate fabric to a prolate cleavage fabric to an oblate cleavage fabric. As deformation increases fabrics may evolve from oblate to prolate to oblate. This intensity of deformation would fit well with obliquity resulting from increase deformation (Rathore, 1985), therefore this AMS ellipsoid indicates a high deformation zone.

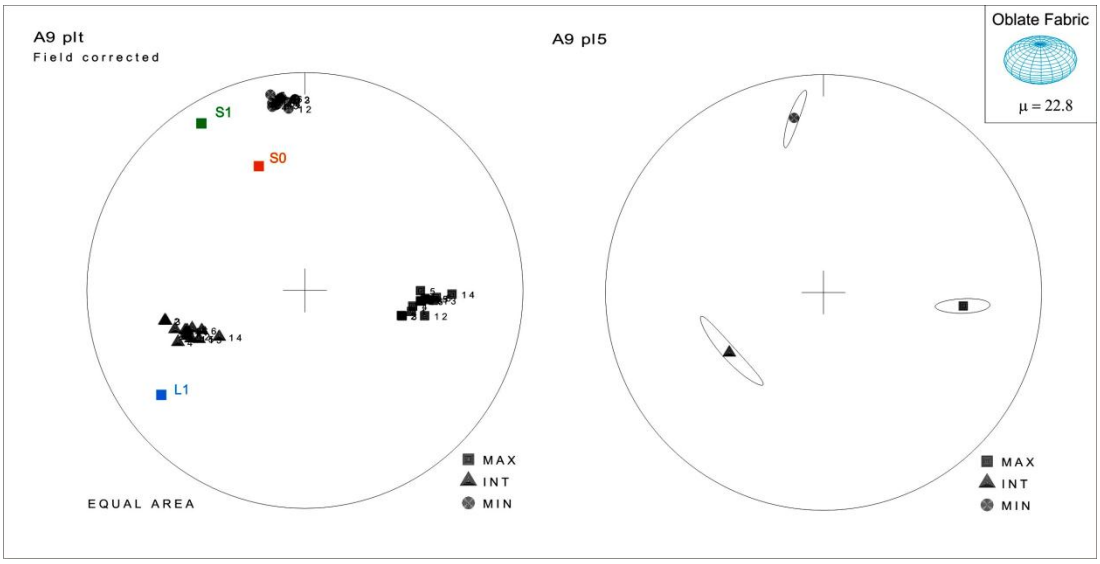

Figure 5.19 AMS stereonet and confidence ellipsoid for A9 Molls Gap.

Sample A12: Gap of Dunloe South - Zone 1: Intrabasinal Zone

The sample is taken from the St. Finan's Sandstone Fm. There is little or no cleavage visible in the beds but cleavage is recorded in fine grained slaty beds approximately 10-20 m away. This site is located just to the south of the Black Lake Fault, which could be considered to be an eastwards lateral continuation of the Coomnacronia Fault, at the Gap of Dunloe (Chapter 2). K_{max} is parallel to L_1. The pole to S_0 is not obviously represented by the axes of the AMS ellipsoid. The K_{min} axes are parallel to the pole to cleavage, indicating S_1 and L_1 are the primary control on AMS fabric (Fig 5.20). However, the K_{min} axes and the K_{int} axes are spread in a girdle in the plane containing the pole to bedding and the pole to cleavage. This girdled AMS fabric may indicate early signs of LPS (Chapter 3: Principles of AMS, e.g. Parés and Dinarès, 1993; Sagnotti and Speranza, 1993). This is a prolate fabric with a μ value of 59. The prolate fabric may be a result of deformation intensified in the hanging wall of the fault. This is interpreted to be an LPS controlled ellipsoid of moderate deformation.

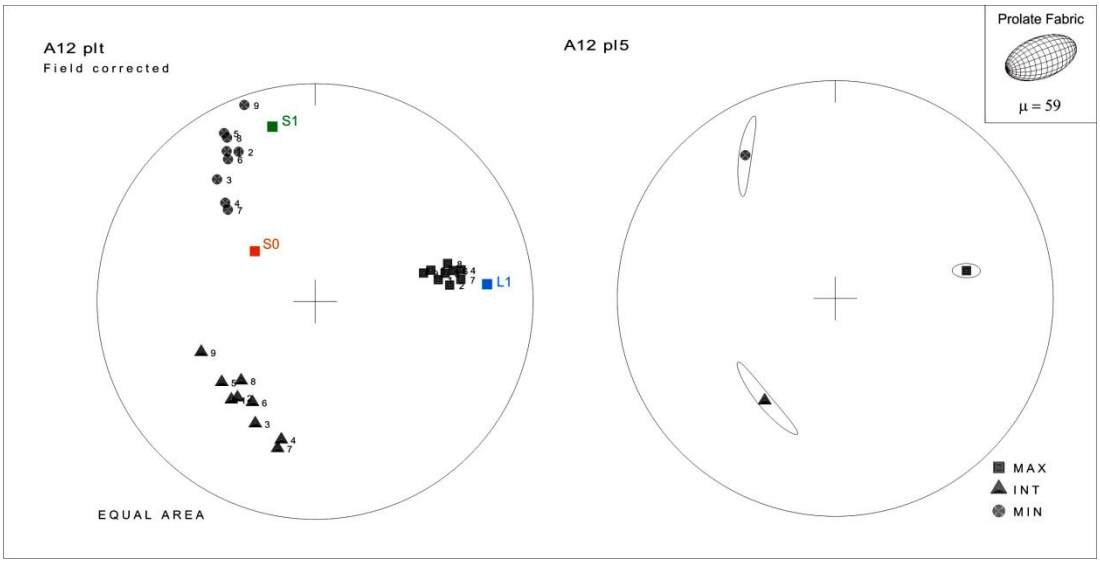

Figure 5.20 AMS stereonet and confidence ellipsoid for A12: Gap of Dunloe South

Sample A14: Kilgarvin - Zone 1: Intrabasinal Zone

This area consists of moderately dipping 20-30 cm thick beds of sandstone of the St. Finan's Sandstone Fm. This area lies in the west of the study area (AMS Results Map). The K_{int} axes are parallel to the bedding/cleavage intersection lineation (Fig 5.21). The K_{min} axes are parallel to the pole to S_1. S_0 is not represented in the AMS ellipsoid. This represents a complete tectonic overprint fabric. This is an oblate fabric with a μ value of 9.1. The oblate fabric indicates high deformation. Deformation intensity may be higher to the west of the Intrabasinal zone due increased strain caused by the curvature of the northern bounding faults.

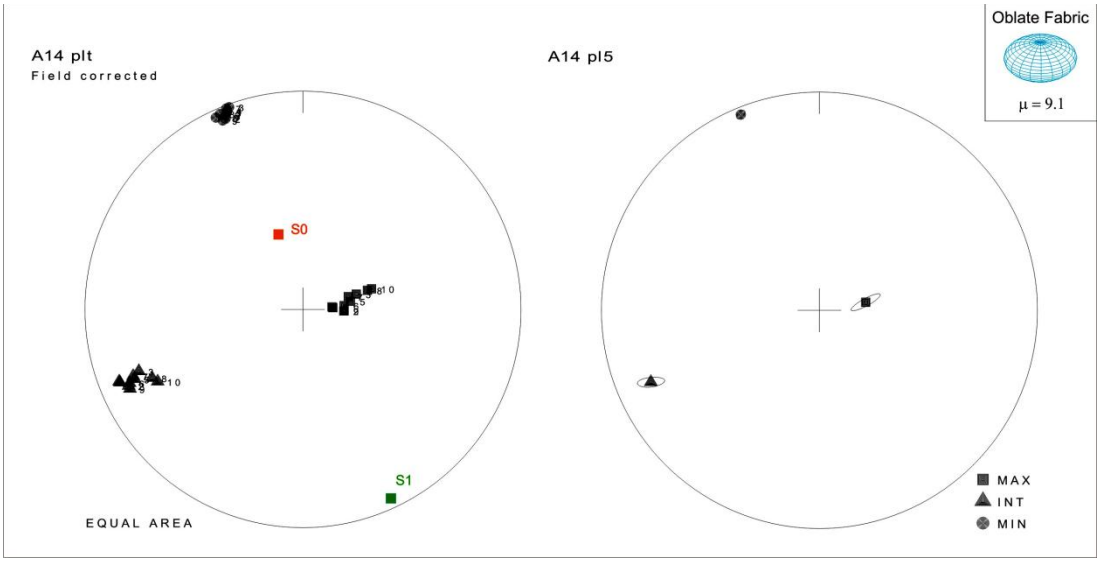

Figure 5.21 AMS stereonet and confidence ellipsoid for A14 Kilgarvin

Sample M8: Glenflesk Quarry - Zone 1: Intrabasinal Zone

The sample is taken from Glenflesk Quarry within the Glenflesk Chloritic Sandstone. This area lies in the east of the study area. Cleavage is not obvious in the sandstones but is found in slaty horizons within 20 m proximity. The K_{min} axes are parallel to the pole to cleavage and the K_{int} axes are parallel to the bedding/cleavage intersection lineation (Fig 5.22). S_0 is not represented in the AMS ellipsoid. This is a complete tectonic overprint fabric and represents a high deformation zone. This is an oblate fabric with a μ value of 21.6. The oblateness in the cleavage plane also indicates high deformation.

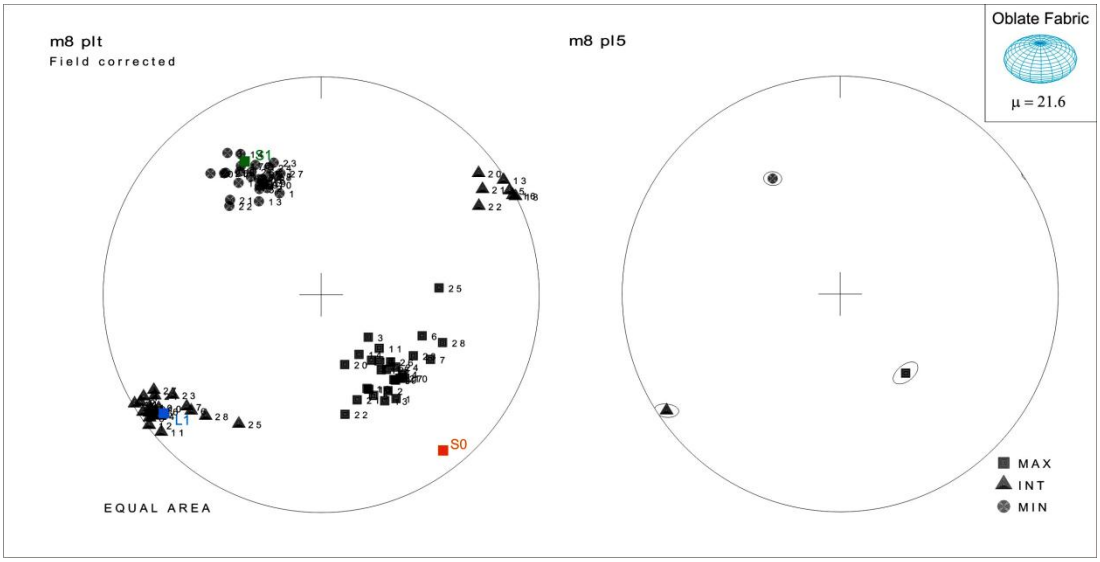

Figure 5.22 AMS stereonet and confidence ellipsoid for M8, Glenflesk Quarry.

Sample M5: Lough Acoose - Zone 1: Intrabasinal Zone

The sample is taken from the Lough Acoose Sandstone Fm. from uniformly dipping beds of 10-40 cm thickness. The area lies in the mid section of the study area beside Lough Acoose (AMS Results Map). The K_{min} axes are parallel to the pole to cleavage (Fig 5.23). The K_{int} axes are close to parallelism with L_1, the bedding/cleavage intersection lineation. The pole to bedding is not represented by the AMS ellipsoid. The AMS ellipsoid is only controlled by L_1 and S_1 and therefore represents a complete tectonic overprint. This is an oblate fabric with a μ value of 42.9. This AMS ellipsoid is interpreted to represent high deformation. The AMS ellipsoid has evolved from oblate to prolate to oblate during deformation.

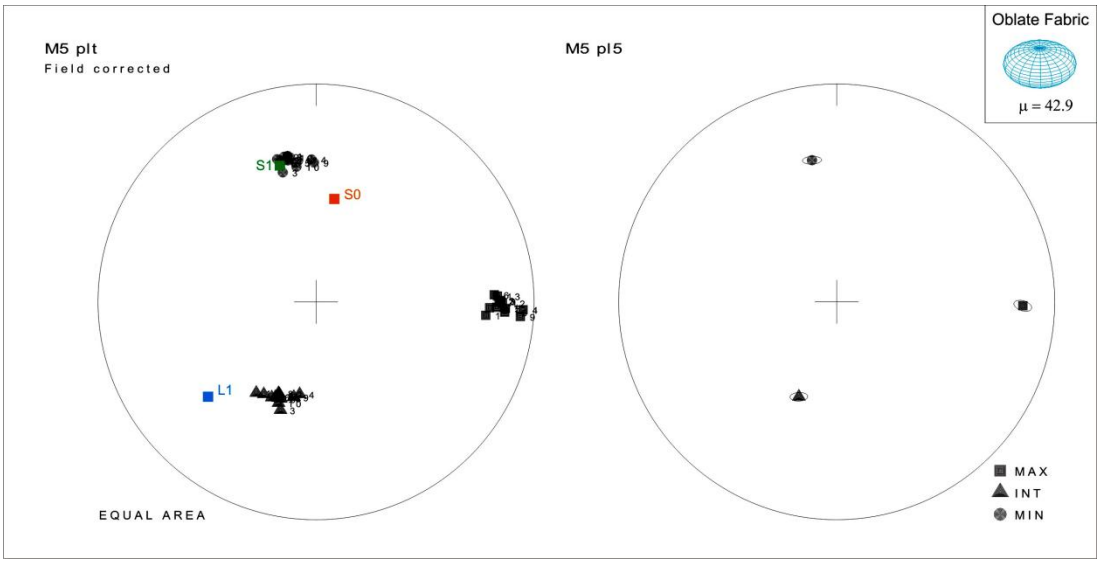

Figure 5.23 AMS stereonet and confidence ellipsoid for M5-Lough Acoose.

AM1: South of Lough Caragh - Zone1: Intrabasinal Zone

The sample comes from moderately dipping beds of the Ballinskelligs Sandstone Fm. in the mid-section of the Intrabasinal Zone (Fig 5.24, AMS Results Map). The area consists of moderately dipping beds 20-30 cm thickness. Cleavage is uniformly dipping and displayed in the slaty horizons some 10-20 m away from the sample point. The K_{min} axes are parallel to the pole to cleavage. The K_{max} axes are parallel to the bedding/cleavage intersection lineation (Fig 5.24). S_0 is not represented in the AMS ellipsoid. This is a cleavage controlled fabric and represents a complete tectonic overprint. The individual axes are tightly clustered. This is a prolate fabric with a μ value of 54.9. The prolateness indicates high deformation.

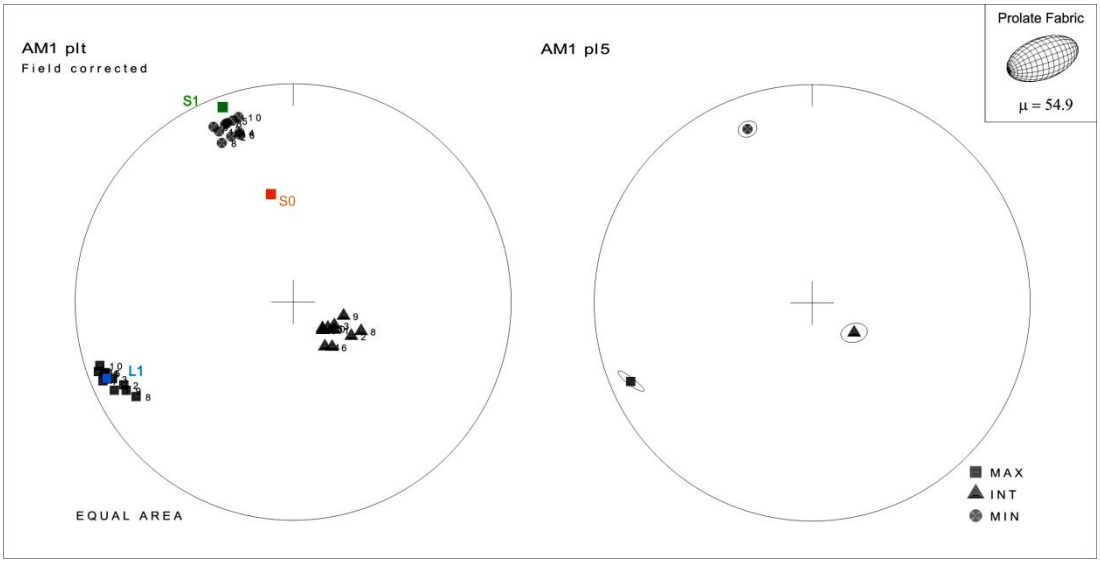

Figure 5.24 AMS stereonet and confidence ellipsoid for AM1 south of Lough Caragh.

Sample M4: Broad Strand - Zone 1: Intrabasinal Zone

The sample is taken from the White Strand Fm. This site is located further to the south in the South Munster Basin (AMS Results Map), but has been included as it clearly demonstrated a tectonic fabric as a result of Variscan deformation. The area consists of steeply dipping beds of approximately 20 cm thickness (Fig 5.25). The beds shows surface ripples marks and sedimentary laminations. The cleavage reading is taken from some slaty horizons with well-developed cleavage and bedding cleavage intersection lineations close to the site. The K_{min} axes are parallel to the pole to cleavage (Fig 5.26). The K_{max} axes are parallel to the bedding/cleavage intersection lineation. S_0 is not represented by the AMS axes. Despite the sample showing strong primary sedimentary features in the field, this AMS ellipsoids represents a complete tectonic overprint. This is a prolate fabric with a μ value of 49.4. The AMS ellipsoid is interpreted to represent moderate to high deformation.

Figure 5.25 sample location for M4, Broad Strand, South Munster Basin. This sample lies external to the study area but still shows typical Variscan overprinting in the AMS ellipsoid.

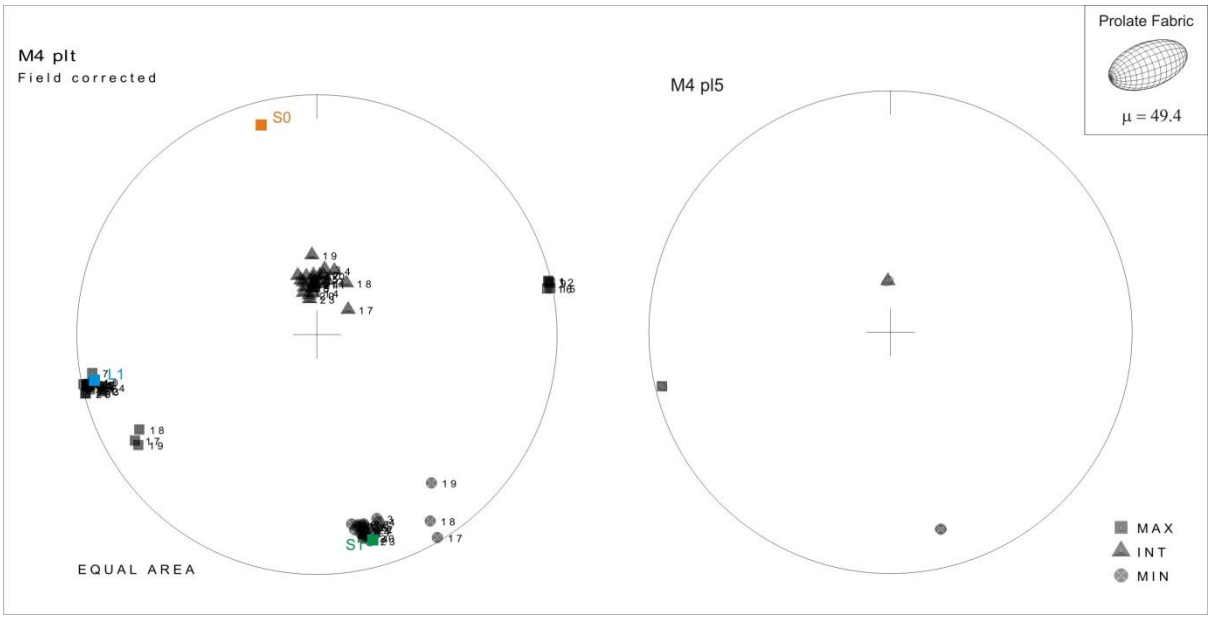

Figure 5.26 Stereonet and confidence ellipsoid for M4 Broad Strand-Located in the South Munster Basin.

5.5.1.1 Summary of Intrabasinal Zone Results

This zone is characterised by predominantly tectonic fabric controlled AMS ellipsoids. In most of the AMS ellipsoids, the K_{min} axes lie parallel or sub parallel to the pole to cleavage and bedding is not represented. These tectonic controlled AMS ellipsoids indicate a high deformation zone. In the Intrabasinal Zone the cleavage is a tectonic penetrative cleavage that exists in both the siltstones and the sandstones. In the hanging wall of the Coomnacronia Fault the AMS ellipsoid are prolate indicating moderate to high deformation (AMS Results Map).

5.5.2 AMS Results: Zone 2: The Transition Zone - North of the Coomnacronia Fault, Iveragh Peninsula

Sample A10: Gap of Dunloe North - Zone 2: Transition Zone

The sample is taken from the Ballinskelligs Sandstone Fm. just to the north of the Black Lake Fault at the Gap of Dunloe. The AMS sample has been taken from beds dipping 30° to the south with a thickness of 10-20 cm in an area with minor thrusts and slickenfibres present on the bedding surface (Fig 5.28). There is no visible cleavage in the sandstones but cleavage is taken from slaty horizons within the sandstones approximately 10-20 m away. The pole to S_1 and the pole to S_0 lie in between the K_{max} and K_{min} axes (Fig 5.27). This may be interpreted as the AMS fabric having been incompletely rotated from the bedding plane into the cleavage plane and represents an incomplete tectonic overprint and it may be considered to represent low to moderate

deformation. The K_{int} axes are parallel with the bedding/cleavage intersection lineation. This is an oblate fabric with a μ value of 14.4.

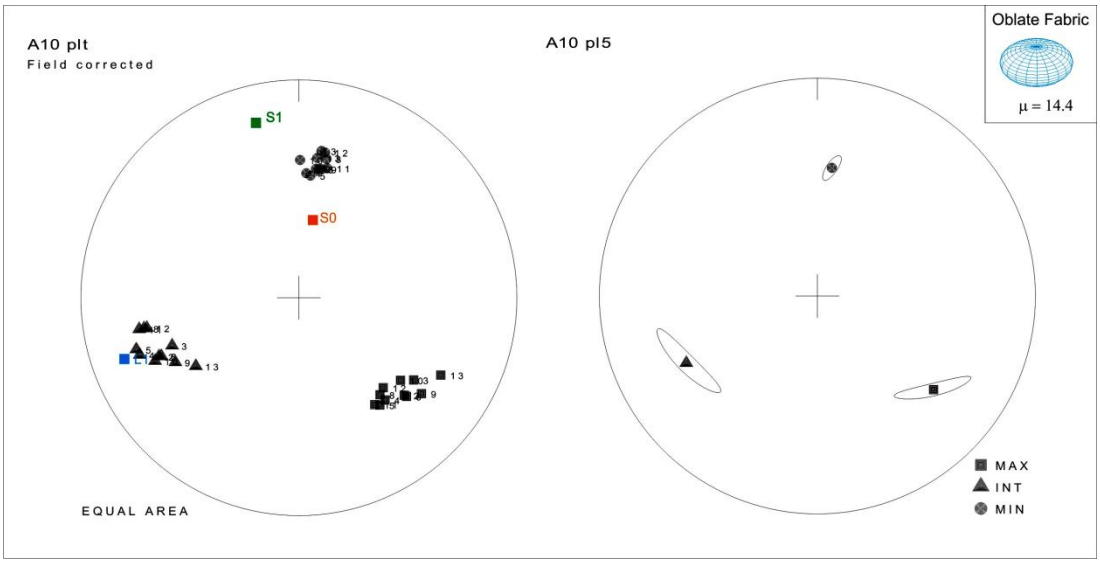

Figure 5.27 AMS stereonet and confidence ellipsoid for A10 Gap of Dunloe North.

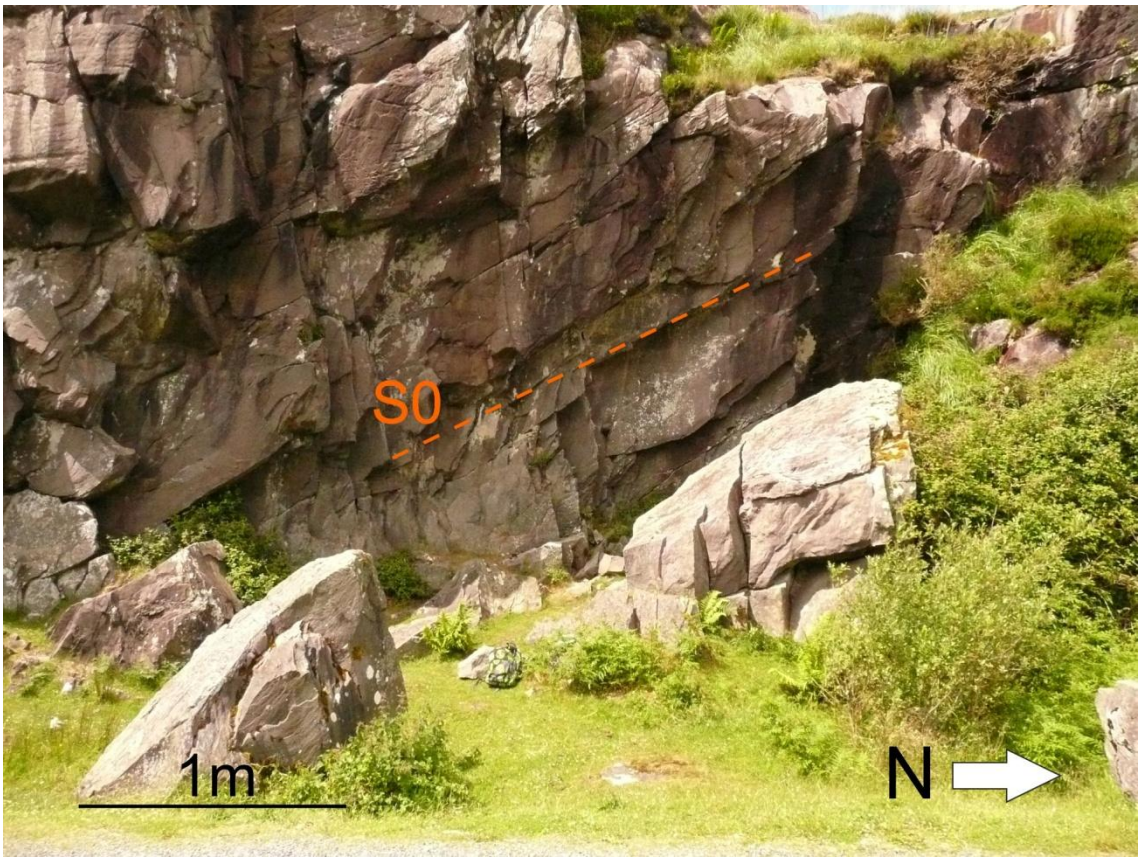

Figure 5.28 Location A10 Gap of Dunloe North. This represents an incomplete tectonic overprint.

Sample AM11: Lough Caragh North - Zone 2: Transition Zone

The sample is taken from moderately dipping beds of 20-30 cm thickness. There is a well developed cleavage and bedding cleavage intersection lineations on the beds, 10m away from the sample point (Fig 5.30). The sample is taken from the Ballinskelligs Sandstone Fm. just beside the north western shore of Lough Caragh (AMS Results Map). The site is located just to the south of the boundary between the Ballinskelligs Sandstone Fm. and the Dinantian limestones (undiffrentiated) to the north. The K_{min} axes are parallel to the pole to cleavage (Fig 5.29). The K_{max} axes are parallel to the pole to bedding. Where K_{max} is normal to the regional shortening direction and parallel to the pole to bedding, this indicates an early LPS fabric (Chapter 3: Principles of AMS, Bakhtari et al., 1998; Sagnotti et al., 1998; Pares et al., 1999; Mattei, et al., 1999). The K_{int} axes are parallel to the bedding/cleavage intersection lineation. This is an oblate fabric with a μ value of 15.6. This is interpreted as a low to moderate deformation LPS controlled AMS ellipsoid.

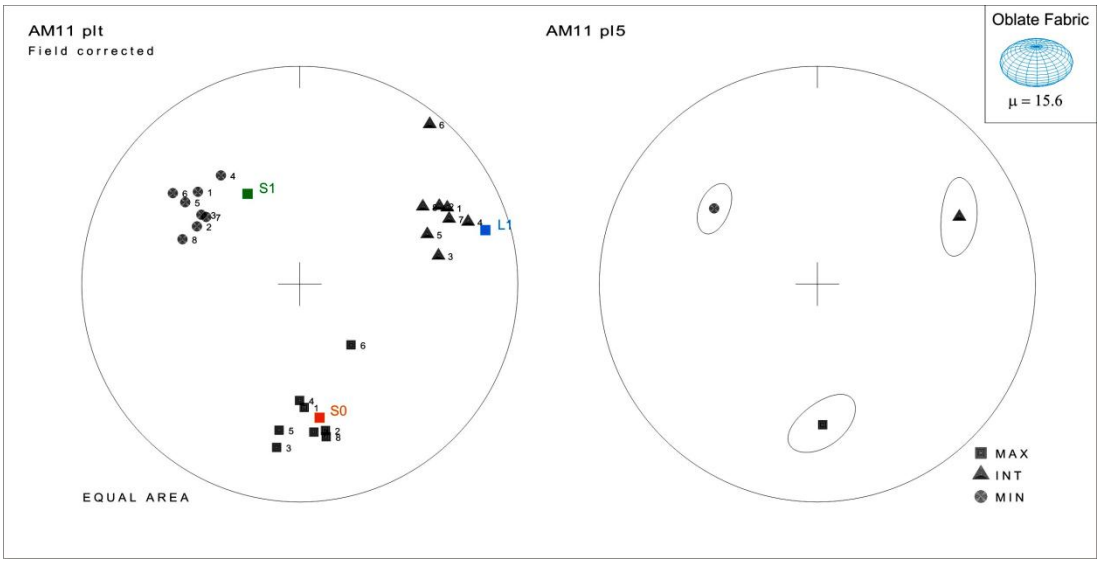

Figure 5.29 AMS stereonet and confidence ellipsoid for AM11 Lough Caragh North.

Figure 5.30 Picture taken close to sample point AM11. Bedding/cleavage intersection lineations are clearly developed. The tectonic fabric is well developed in the sandstones. Location AM11, Lough Caragh.

Sample L47: Coosfada - Zone 2: Transition Zone

The sample is taken from the Ballinskelligs Sandstone Fm. at Coosfada Point, northern Iveragh Peninsula (AMS Results Map). The lithology is a red medium/coarse grained sandstone with uniform bedding with an average thickness of 30 cm. The beds are a series of tight isoclinal overturned folds. The cleavage fabric is quite spaced and disjunctive and is considered to be an early LPS fabric. This strong layer parallel shortening fabric maintains a high angle to bedding across the fold's profiles indicating that passive rotation of the LPS fabric has occurred (Fig 5.31, as discussed in Chapter 4: Field Work). The K_{max} axes are parallel to the pole to bedding, or the K_{max} axes may be described as being normal to the shortening direction. This is indicative of LPS (Fig 5.32) as in sample AM11: Lough Caragh North. The K_{int} axes are parallel to the intersection lineation, L_1. The K_{min} axes are parallel to the pole to cleavage which is an early LPS fabric. This ellipsoid has all three structural elements (S_0, S_1 and L_1) represented by (K_{max}, K_{min} and K_{int}, respectively). This may be interpreted as the AMS ellipsoid being locked into position in a similar way to the LPS fabric being locked into position with the bedding during passive rotation of cleavage (Chapter 4: Field work). The AMS ellipsoid lies in an oblate plane controlled by bedding/LPS and L_1. This oblate fabric has a μ value of 9.4. This is interpreted to represent low deformation.

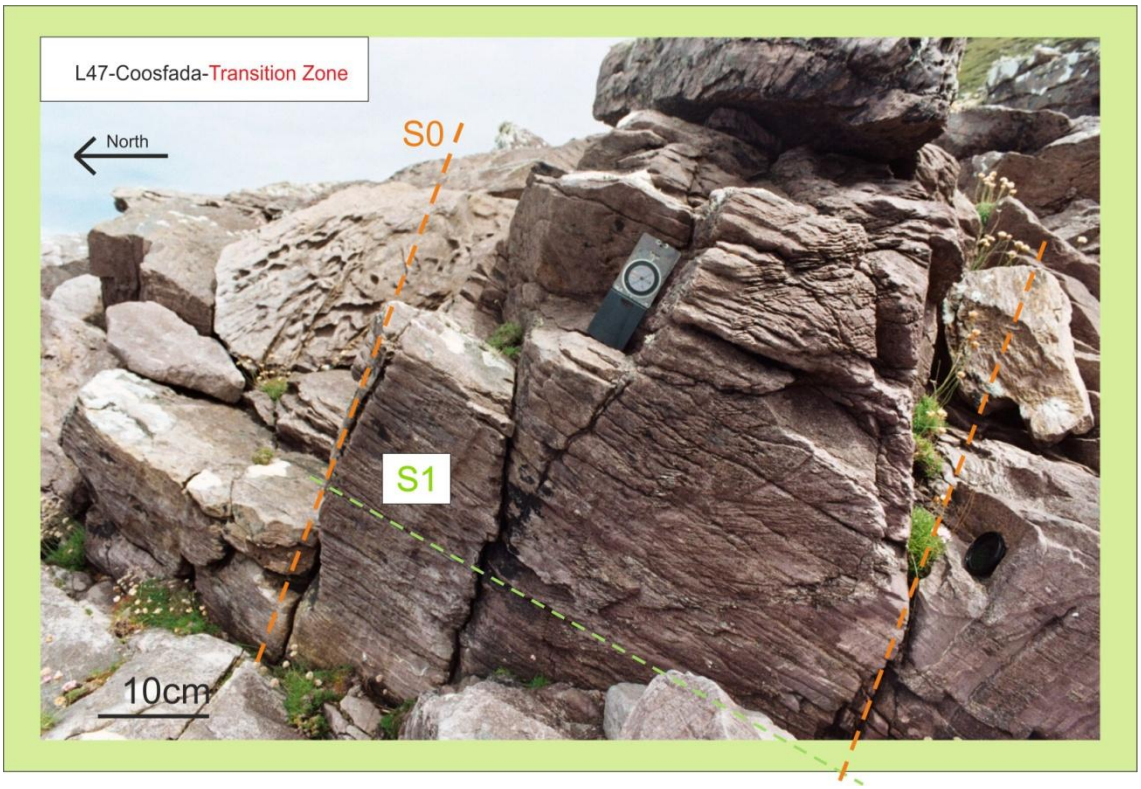

Figure 5.31 Location L47: Coosfada shows steeply dipping beds and a faint tectonic fabric.

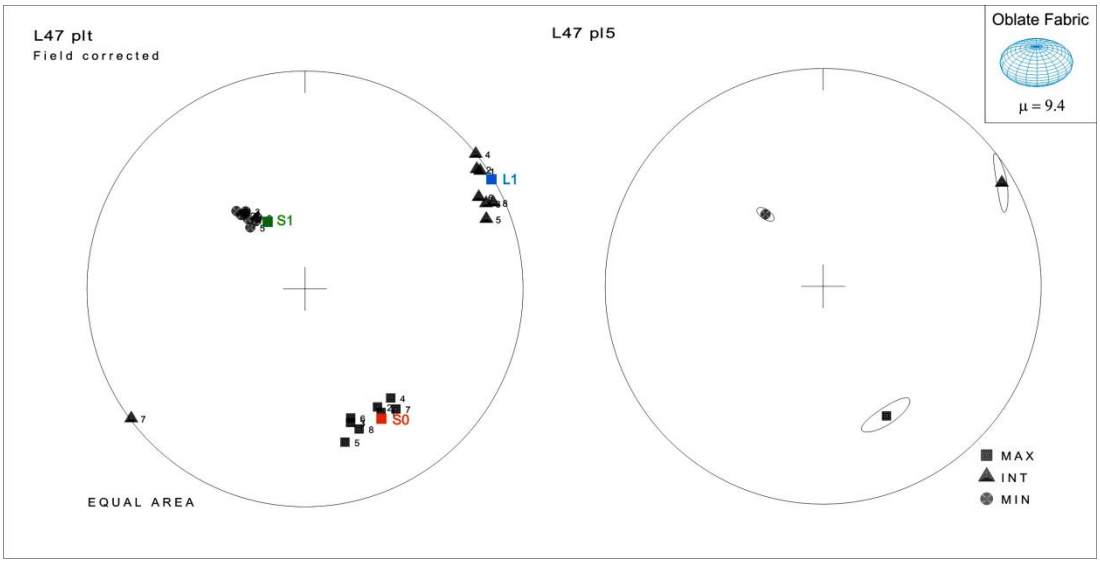

Figure 5.32 AMS stereonet and confidence ellipsoid for L47 Coosfada

Sample L35: Dooneen - Zone 2: Transition Zone

The sample is taken from the Ballinskelligs Sandstone Fm. in Dooneen on the northern part of the Iveragh Peninsula. This area lies on the northern limb of the Portmagee Anticline. The area is characterised by gently dipping beds of approximately 20-30 cm thickness. There is a very faint tectonic fabric in the sandstones and minor occurrences of a cleavage in the interbedded slates in close proximity to the site. The K_{min} axes are parallel to the pole to bedding (Fig 5.33). This indicates a strong element of bedding controlled AMS fabric. The K_{max} axes are parallel to the pole to cleavage. The K_{int} axes are parallel to the bedding/cleavage intersection lineation. This AMS ellipsoid represents a weak deformational fabric. This is an oblate fabric lying in the bedding plane with a μ value of 30.7 and represents low deformation.

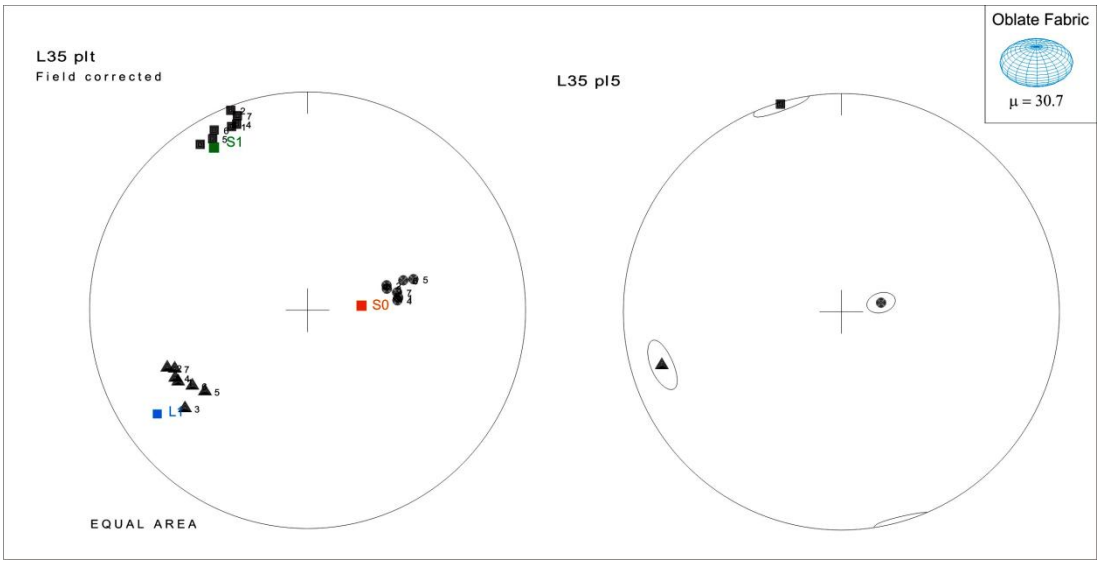

Figure 5.33 AMS stereonet and confidence ellipsoid for L35 Dooneen.

Sample L31: Reenadrolaun Point, Valentia Island - Zone 2: Transition Zone

The sample is taken from 10-40 cm thick beds form gentle rolling open folds approximately 3-4 m in wavelength. It is taken from the Valentia Slate Fm. from Reenadrolaun Point, on Valentia Island. The beds range from approximately 10 - 40 cm with and are predominately medium grained sandstone. There is no obvious cleavage in this sample but there is a LPS/cleavage fabric close by in the area of Reenadrolaun Point. The K_{int} axes are parallel to the pole to bedding (Fig 5.34). The pole to bedding is the only structural feature controlling the orientation of the AMS ellipsoid. S_1 and L_1 are not represented. This is a primary bedding fabric. This is a prolate fabric with a μ value of 52. The S_1 reading is taken from the area approximately 30 m away. The prolate fabric may suggest that there is some degree of deformation, but it is primarily bedding controlled. The K_{int} axes being parallel to the pole to bedding may indicate a low amount of strain where axis swapping has begun. The K_{max} axes may be representative of NE to SW directed palaeocurrents which has been documented (Chapter 2 & Chapter 6; Graham, 1983; Russell, 1984; Williams et al., 1989). The prolate fabric could be a result of palaeocurrents.

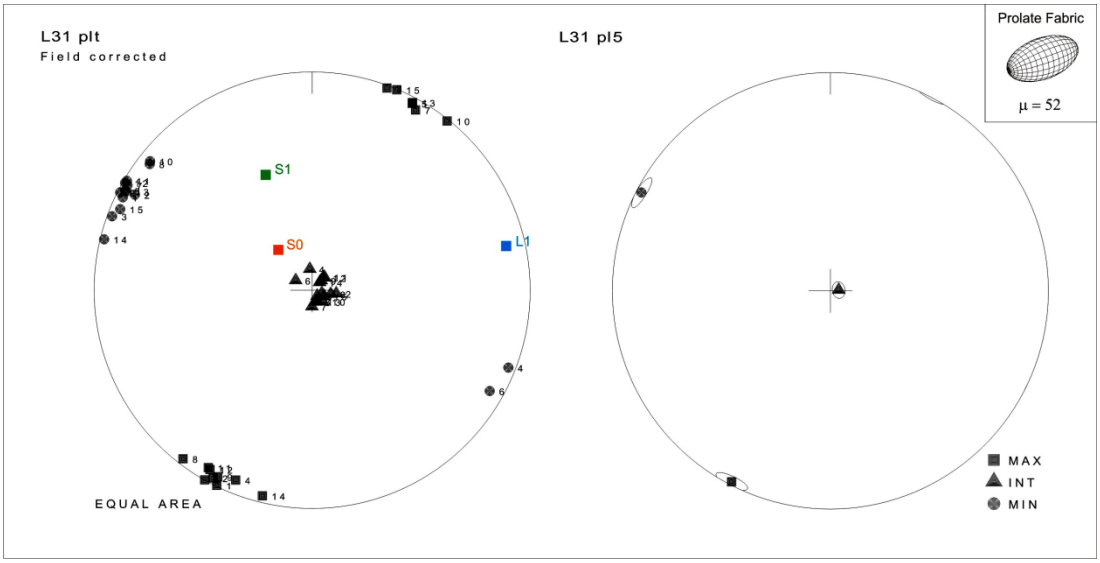

Figure 5.34 AMS stereonet and confidence ellipsoid for L31, Reenadrolaun Point, Valentia Island.

Sample M44: Culoo Rocks -Zone 2: Transition Zone

The sample is taken from the Valentia Slate Fm. from a medium grained sandstone with moderately to well-developed cleavage and cleavage bedding intersection lineations. It consists of beds of both medium grained sandstone and finer siltstone. The site is an

open syncline with a 40 m wavelength (Fig 5.36). There is a strong cleavage fabric in the finer-grained sandstones/siltstones and a weak fabric in the medium grained sandstone. In this area passive rotation of LPS/cleavage occurs. There appears to be some degree of axis swapping between the K_{int} and the K_{min} axes (Fig 5.35). Axes swapping, as a result of progressive deformation has been previously shown numerically and experimentally and occurs during progressive deformation (Chapter 3: Principles of AMS). Also the resulting girdle containing the K_{min} and K_{int} axes may be the early signs of LPS (Chapter 3: e.g. Pares, 1999). The L_1 axes lies close to parallelism with the K_{max} axes. The K_{max} axes also lies close to a NE-SW directed palaeocurrent lineation as previously observed at L31. The AMS ellipsoid is a prolate fabric lying in a plane represented by all three structural elements, S_0, S_1 and L_1. This is a prolate fabric with a μ value of 80.4. This sample is interpreted as low to moderate deformation. The AMS ellipsoid is affected by both primary sedimentary features and an early LPS fabric.

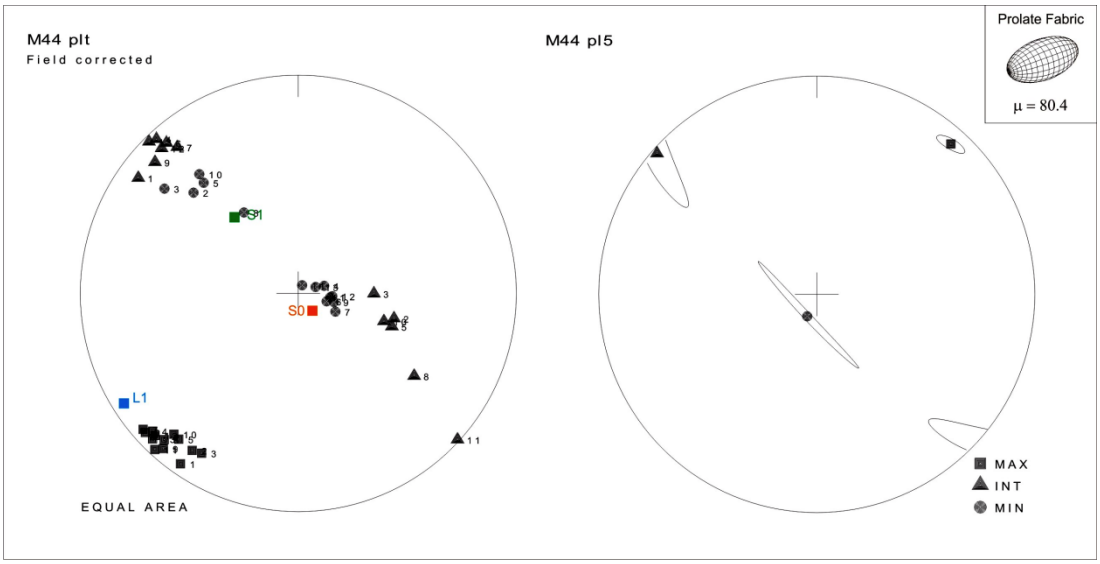

Figure 5.35 AMS stereonet and confidence ellipsoid for M44: Culoo Rocks.

Figure 5.36 L44: Culloo Rocks with passively rotated tectonic fabric.

Sample M3: Kells Bay - The Transition Zone

These are uniformly dipping well bedding coarse red sandstones of 20-40 cm in thickness and with no apparent cleavage. There is visible cross stratification in the sandstones. There is no cleavage fabric to be found in this area (at least within + 400 m either side of the bay). The K_{min} axes are parallel to the pole to bedding (Fig 5.37). The K_{max} axes and K_{int} axes form a girdle perpendicular to the pole to bedding (in the bedding plane). This girdle may be due to cross stratification in the sandstones. This is a primary bedding controlled fabric. This is an oblate fabric with a μ value of 16.9. It is considered to be a zero to low deformational zone. There are no signs of LPS or cleavage in the area or from the AMS stereonet.

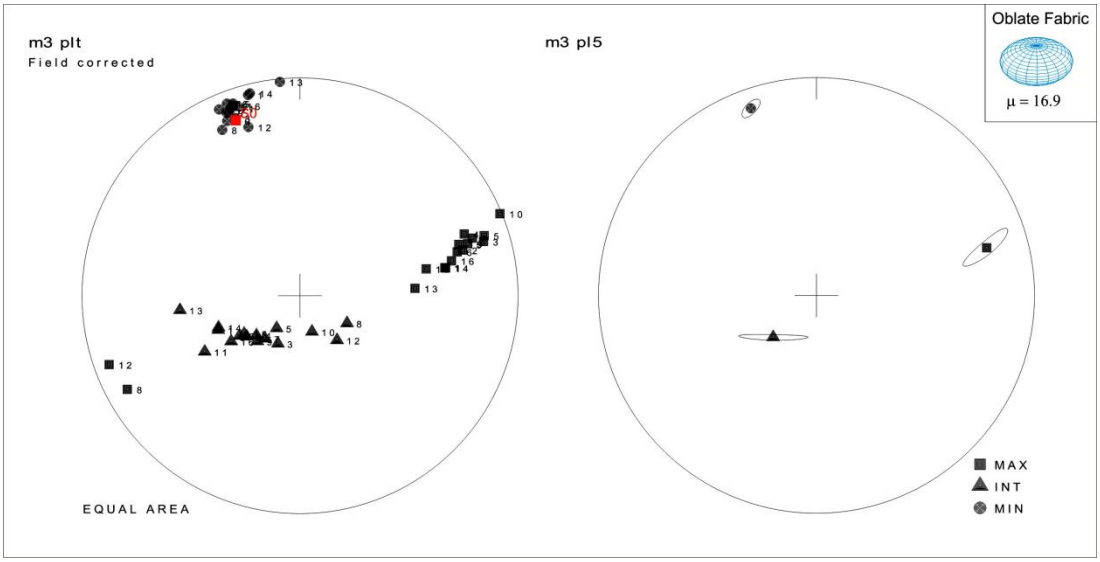

Figure 5.37 Stereonet and confidence ellipsoid for M3, Kells Bay, Northern Iveragh Peninsula.

5.5.2.1 Summary of The Transition Zone - AMS Ellipsoid Results

The Transition Zone lies to the north of the Coomnacronia Fault on the Iveragh Peninsula. There is a significant change in the behaviour of the AMS ellipsoids from the south (Intrabasinal Zone) to the north (Transition Zone) of this fault. In the Transition Zone the AMS ellipsoids consist of a mixture of bedding controlled and/or LPS controlled. There is also a mixture of oblate and prolate ellipsoids, in either the bedding plane or the LPS plane or both. They represent low deformation. The bedding fabric and the LPS fabric in the transition zone has been preserved in the early stages and protected from subsequent ongoing Variscan deformation which affects the Intrabasinal Zone (Chapter 4: Field Work). The reason why S1 exists north of the Coomnacronia Fault but is not represented in some of the AMS ellipsoids may be because it is a disjunctive non penetrative LPS fabric. It occurs only in certain areas and exists as a passively rotated LPS fabric (Chapter 4: Field Work).

5.5.3 AMS stereonets: Zone 3: The Foreland Zone - The Dingle Peninsula and Kerry Head

A15: Dingle Peninsula - Zone 3: Foreland Zone

This sample is taken from a coarse-grained sandstone bed from the Lough Slat Conglomerate Fm, in the Slieve Mish Group (Upper Devonian). It is taken from gently dipping beds of 10-20 cm thickness. The K_{min} axes are parallel to the pole to bedding and the K_{max} axes are tightly clustered in an area close to an expected S_0/S_1 lineation (Fig 5.38). The AMS ellipsoid is controlled by a primary sedimentary fabric. This is an oblate fabric with a μ value of 37.2. This is interpreted as a low deformational zone.

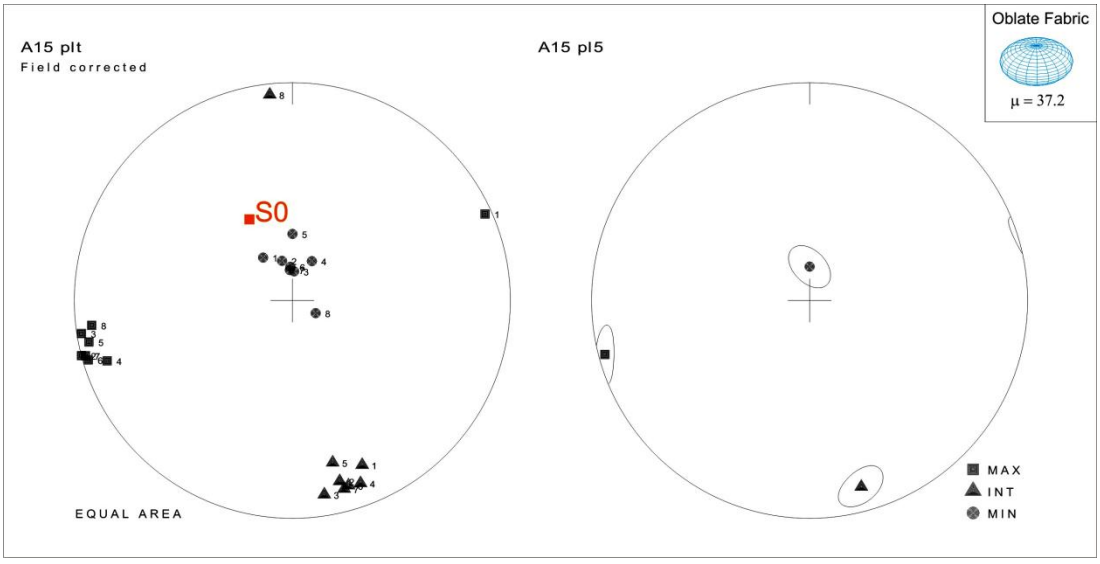

Figure 5.38 AMS stereonet and confidence ellipsoid for A15-Bulls Head, Dingle Peninsula.

M6: Ballyheige - Zone 3: Foreland Zone

This sample is taken from Ballyheige, Kerry Head which lies to the north of the Dingle Peninsula. These are well bedded fine-to medium grained red sandstones from the Kilmore Sandstone Fm. They are uniformly dipping beds with a thickness of 10-20 cm. There is some gentle folding in the area. There is no visible LPS, cleavage or bedding cleavage intersection lineations in the area. This site is interpreted as a low deformational zone. The K_{min} axes are parallel to the pole to bedding and the K_{max} axes are tightly clustered in an area close to an expected S_0/S_1 lineation (Fig 5.39). This is an oblate fabric with a μ value of 13.5.

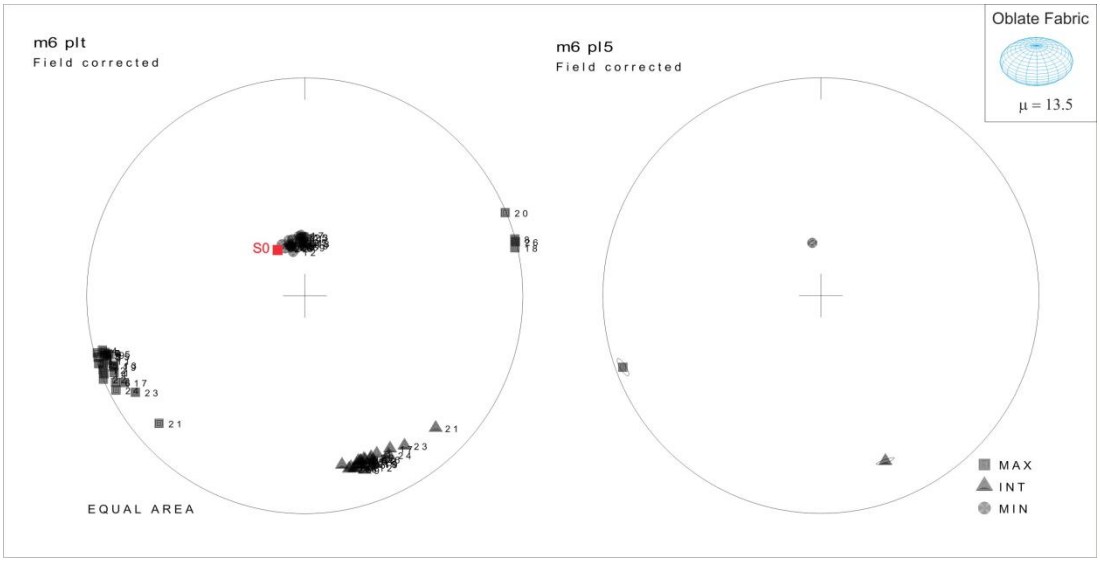

Figure 5.39 AMS stereonet and confidence ellipsoid for M6: Ballyheige, Kerry Head.

M7: Brandon Pier - Zone 3: Foreland Zone

The sample is taken from red coarse-grained sandstones from the Capagh Sandstone Fm. The beds are approximately 20-30 cm thick and moderately-dipping. There is no apparent cleavage in the area. The K_{min} axes are parallel to the pole to bedding (Fig 5.40). This is a primary sedimentary controlled fabric that is oblate with a μ value of 19.6. The oblate fabric lies in the bedding plane. There is girdling of the K_{int} and K_{max} axes within the bedding plane which may be due to depositional features such as compaction, cross bedding or palaeocurrents or could be the first signs of a tectonic overprint. This is interpreted as an area of low deformation.

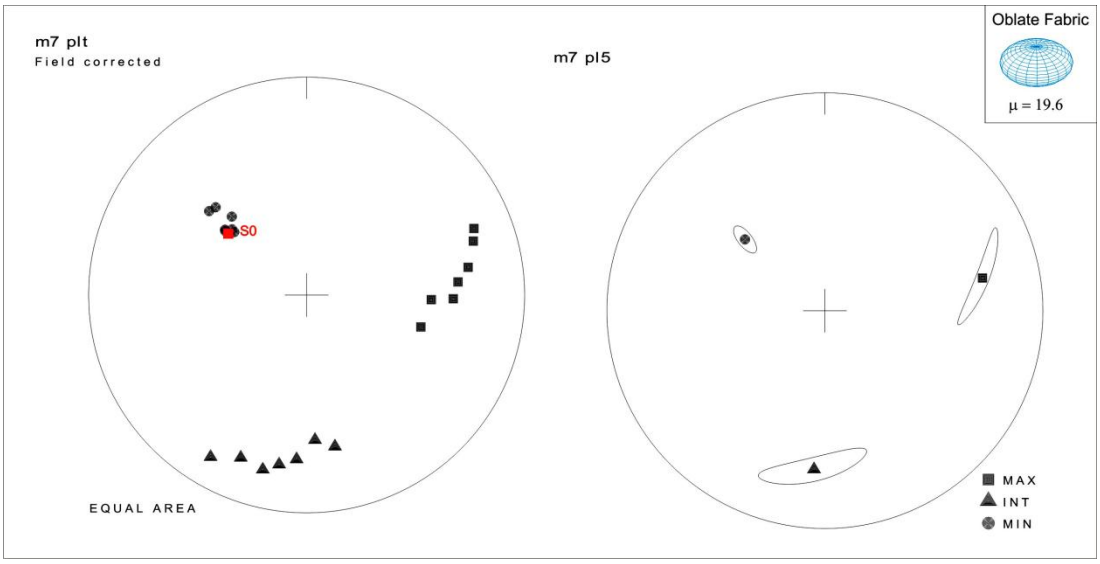

Figure 5.40 AMS stereonet and confidence ellipsoid for M7, Brandon Pier, The Dingle Peninsula.

A13: Dunmore East - Co. Waterford. Old Red Sandstone external to The Munster Basin

The sample is taken from coarse red sandstones from the Templetown Fm. It is taken from 10-30 cm beds of gently dipping laminated red sandstone. There is no cleavage in this area. The sample has been taken external to the Munster Basin, as a control sample, in order to show the characteristics of AMS in a typical primary sedimentary fabric in Devonian ORS that has not undergone tectonic (Variscan) deformation. The K_{min} axes are parallel to the pole to S_0 (Fig 5.41). It is a primary sedimentary fabric controlled ellipsoid and is not affected by deformation. This is an oblate fabric lying in the bedding plane with a μ value of 9.8. This sample comes from ORS outside of the Munster Basin which has not been affected by Variscan deformation and is used as an example of undeformed ORS.

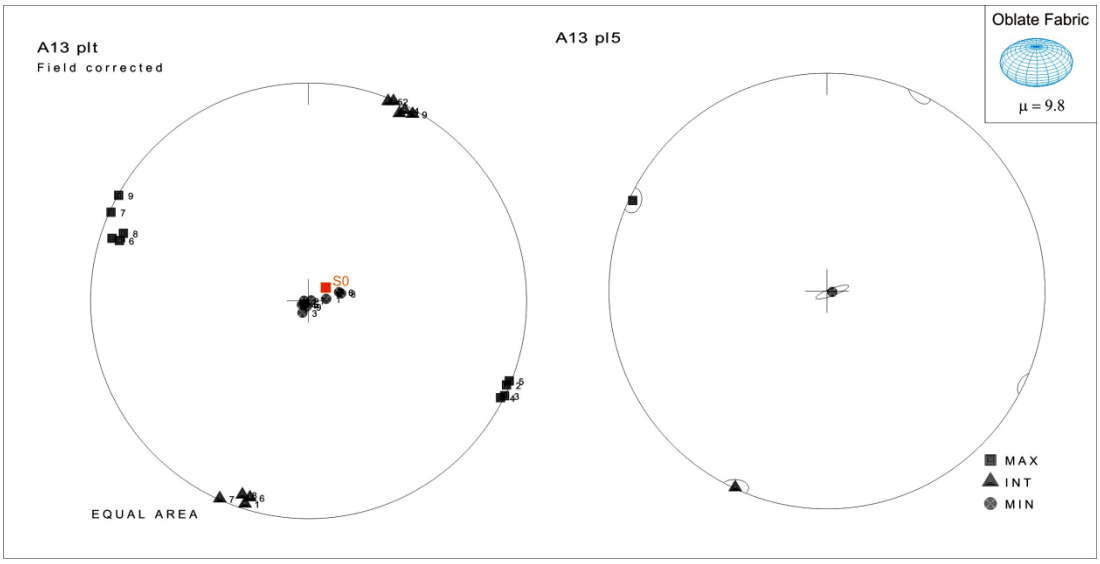

Figure 5.41 A13 AMS stereonet and confidence ellipsoid from Dunmore East, Co. Waterford. Taken from ORS external to the Munster Basin with no deformation.

5.5.3.1 Summary of Foreland Zone AMS Ellipsoids Results

The AMS ellipsoids in the foreland zone are bedding-controlled and there is no expression of any cleavage fabric in the ellipsoids. The ellipsoids are oblate ellipsoids lying the in the bedding plane and represent low deformation.

5.6 Measured Angles between the K_{min} AMS axis (Pl5 average) and the pole to Bedding (S_0) or Cleavage (S_1)

This section quantitatively summarizes the relationship between the average K_{min} AMS axis and the poles to bedding and/or the pole to cleavage. Pl5 files (five fold-normalized measurements; Owens, 2000) show the orientation of the average K_{min} and the 95% confidence ellipsoids of all the AMS axes. Using these AMS ellipsoids, the angle between the average K_{min} axis and the pole to S_1 and/or the pole to S_0 is measured (Fig 5.42 - 5.46). The angle between the K_{min} axis and the pole to cleavage (S_1) and/or the pole to bedding (S_0) is used as the K_{min} AMS axis predominantly lies close to either the pole to cleavage or the pole to bedding and is a defining axis when analysing the type of AMS ellipsoid. However in some locations the nearest axis is the K_{int} or K_{max}. Where the closest axis to the pole is instead the K_{int} or K_{max} this is measured and shown. The results are shown in Table 5.3. The measured angles are then plotted on a graph (Fig 5.47).The results of the measured angles fit well with the division of the field area into three structural zones in described in Chapter 4.

Table 5.3. Measure angles between K_{min} and the pole to S_0 or S_1. All samples are used except for A1 and A12 which have alot of spread in the K_{min} axes.

Zone 1: Intrabasinal Zone	**Angle between K_{min} and the pole to S_0.**	**Angle between K_{min} and the pole to S_1.**	**Type of AMS ellipsoid.**
A6 Caherdaniel	70°	42°	Incomplete tectonic overprint
A2 Killabounia	26°	11°	Tectonic
A3M Keel Bay	60°	24°. K_{int} and S_1 = 30°	Tectonic
A4 South of Keel Bay	1°	35°	Sedimentary
A8 Rossmore	72°	20°	Tectonic
M5	24°	4°	Tectonic
A14 Kilgarvin	55°	8°	Tectonic
AM1 South of Lough Caragh	34°	10°	Tectonic
M8 Glenflesk Quarry	49°	8°	Tectonic
M4 Broad Strand	28°	4°	In the south Munster Basin.
M2 Rheencaheragh	16°	78°	Sedimentary.
Outside the study area: A13 Dunmore East	6°	S_1 Not present.	Example of pure bedding AMS fabric. ORS external to Munster Basin
Others not used.			
A1 Portmagee Quarry	K_{min} Girdled with K_{int}	N/A	Not used. Gridled fabric.
A9 Molls Gap	20°	22°	Rotated-transpression
A12 Gap of Dunloe	Spread in K_{min} and K_{int} axes		Not used. Girdled fabric

Zone 2: The Transition Zone	**Angle between average K_{min} and the pole to S0**	**Angle between average K_{min} and the pole to S_1**	**Interpretation of AMS ellipsoid**
M44 Culoo Rocks	8°	42°	Bedding/LPS
L31 Reenadrolaun Pt, Valentia Island.	**K_{int}** and S0 = 20°	S_1 and **K_{int}** = 50 °	Bedding
AM11 Lough Caragh north	**K_{max}** and S0 = 8°	24°	LPS fabric

Zone 2 Contnd	**Angle between average K_{min} and pole to S0**	**Angle between average K_{min} and the pole to S1**	**Interpretation of AMS ellipsoid**
M3 Kells Bay	30°	S_1 not present	Bedding
A10 Gap dunloe, north.	20°	28°	Bedding
L47 Coosfada	**K_{max}** and S0 = 4°	K_{min} and S_1 = 6°	LPS Fabric
L35 Dooneen	4°	**K_{max}** and S_1 = 8°	Bedding/Early LPS

Zone 3: The Foreland Zone	Angle between Kmin and the pole to S_0	Angle between Kmin and the pole to S_1	Type of AMS ellipsoid
A15 Dingle	24°	S_1 not present	Bedding
M7 Brandon Pier	3°	S_1 not present	Bedding
M6 Ballyheige	6°	S_1 not present	Bedding

In Zone 1: The Intrabasinal Zone, the angle between the K_{min} axis and the pole to S_1 is significantly lower than the angle between the K_{min} axis and the pole to S_0 (Fig 5.47).

In Zone 2: The Transition Zone there is a mixture of K_{min} being closest to the pole to S_1 and K_{min} being closest to the pole to S_0 (Fig 5.47). In some locations of the Transition Zone the pole to S_0 or S_1 is instead represented by the K_{int} or K_{max}. This interchanging of AMS axes occurs in the Transition Zone as in this zone the AMS ellipsoids represent the evolution from bedding controlled to LPS controlled. Where the closest axis to the pole to S_0 is K_{max} this indicates an early LPS fabric (Chapter 3: Principles of AMS). It is clear from the graphs that the Coomnacronia Fault- the boundary between Zone 1 and Zone 2 - marks a major change in the angular relationship between the AMS axes and the poles to S_0/S_1.

In Zone 3: The Foreland Zone (the Dingle Peninsula), K_{min} is closest to the pole to S_0 and cleavage (S_1), if present, does not influence the AMS ellipsoid or found in these locations. In the Foreland Zone K_{min} has a low angle to the pole to S_0 (Fig 5.47).

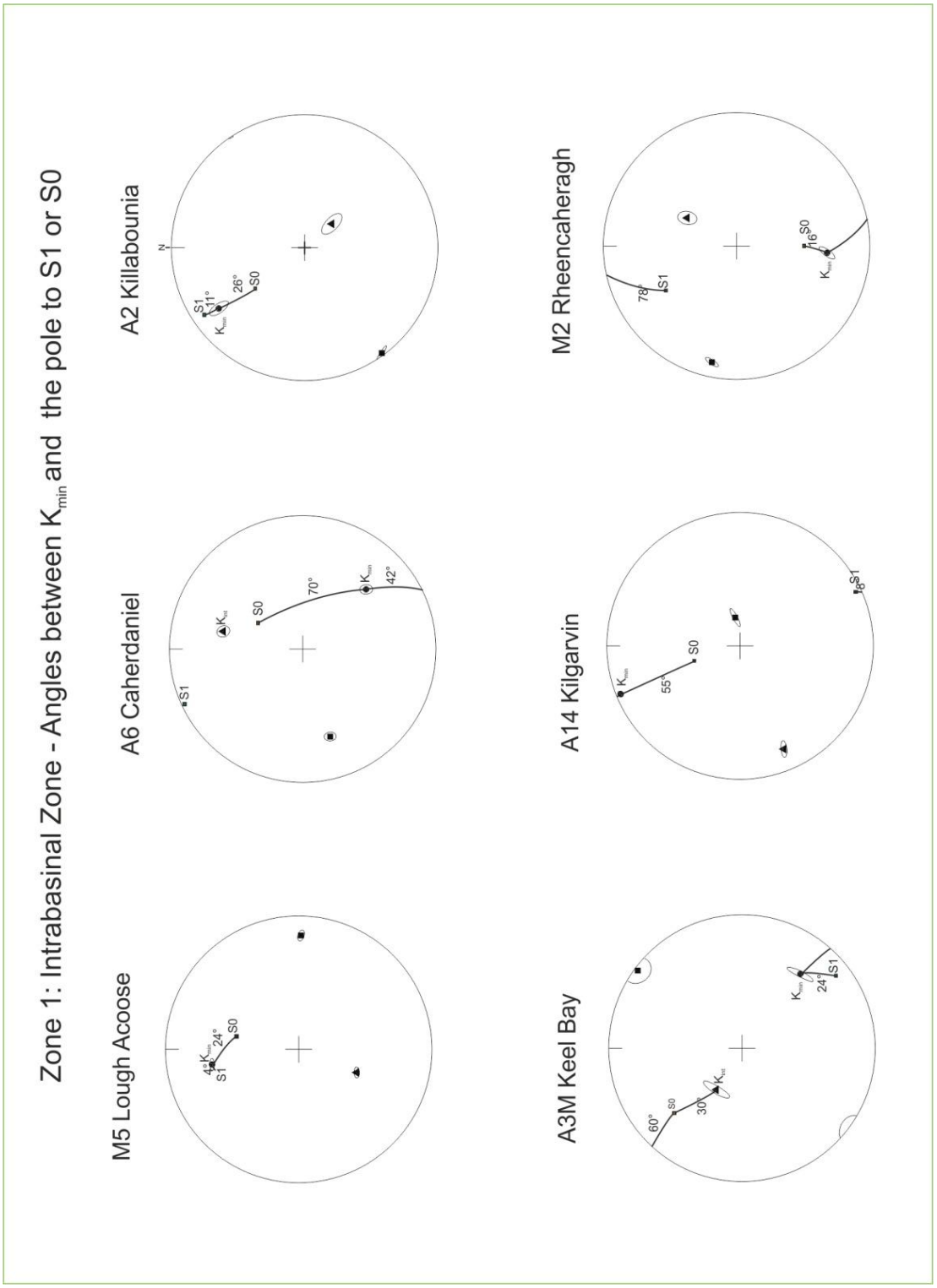

Figure 5.42 AMS stereonets (the P15 plots), showing the measured angles between K_{min} and the pole to S_0 and/or S_1 for the Intrabasinal Zone.

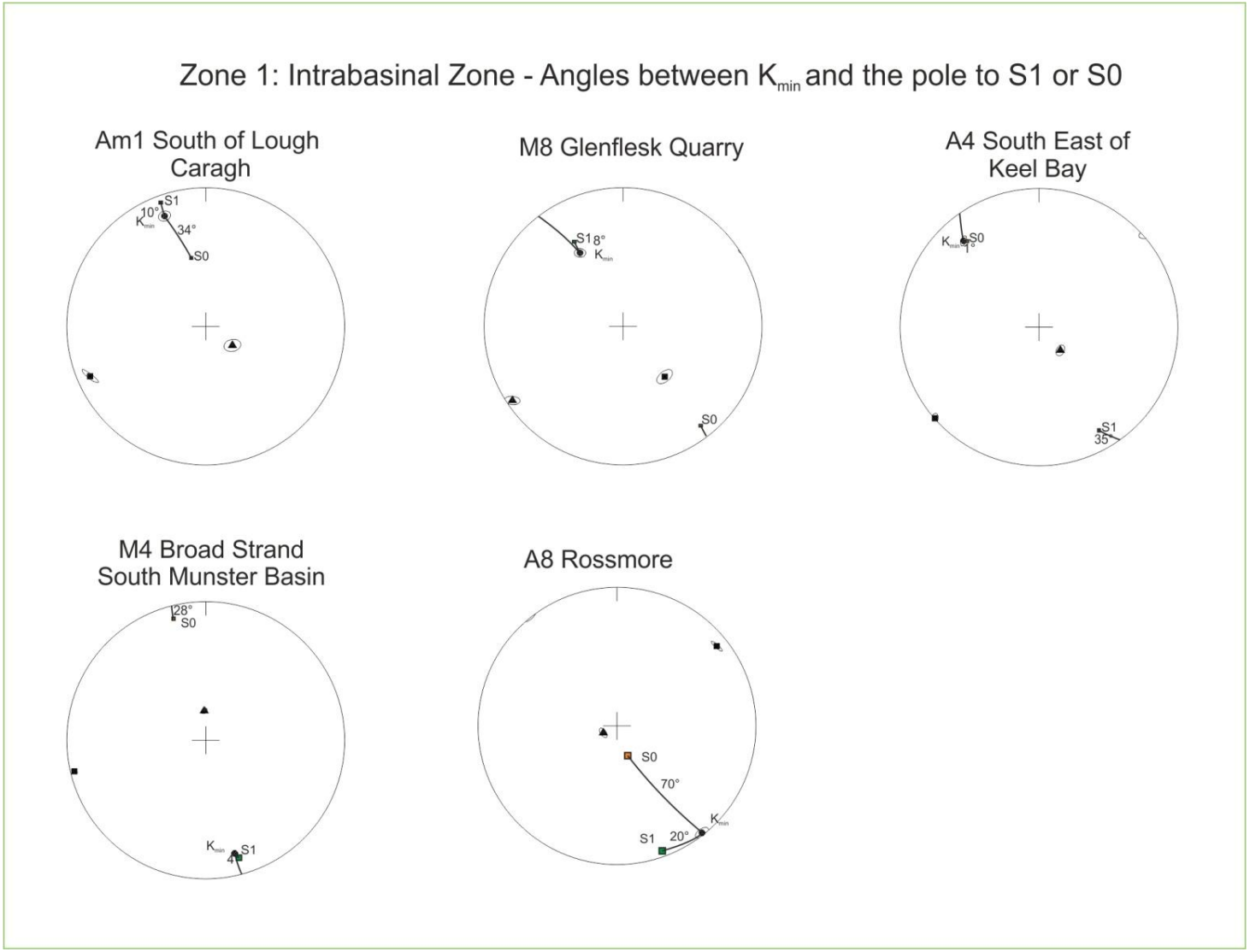

Figure 5.43 AMS stereonets (the Pl5 plots), showing the measured angles between K_{min} and the pole to S_0 and/or S_1 for the Intrabasinal Zone.

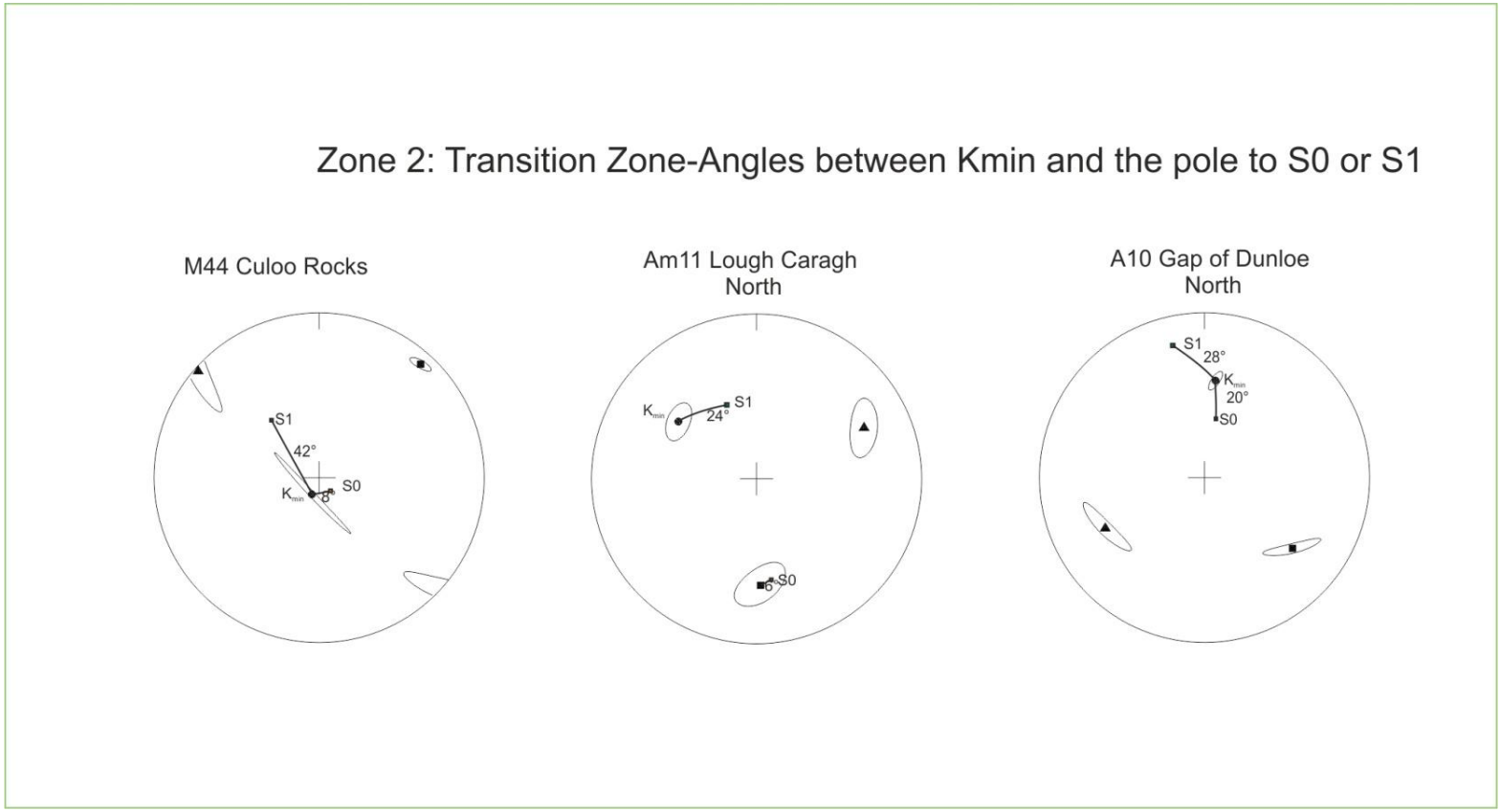

Figure 5.44 AMS stereonets (the Pl5 plots), showing the measured angles between K_{min} and the pole to S_0 and/or S_1 for the Transition Zone.

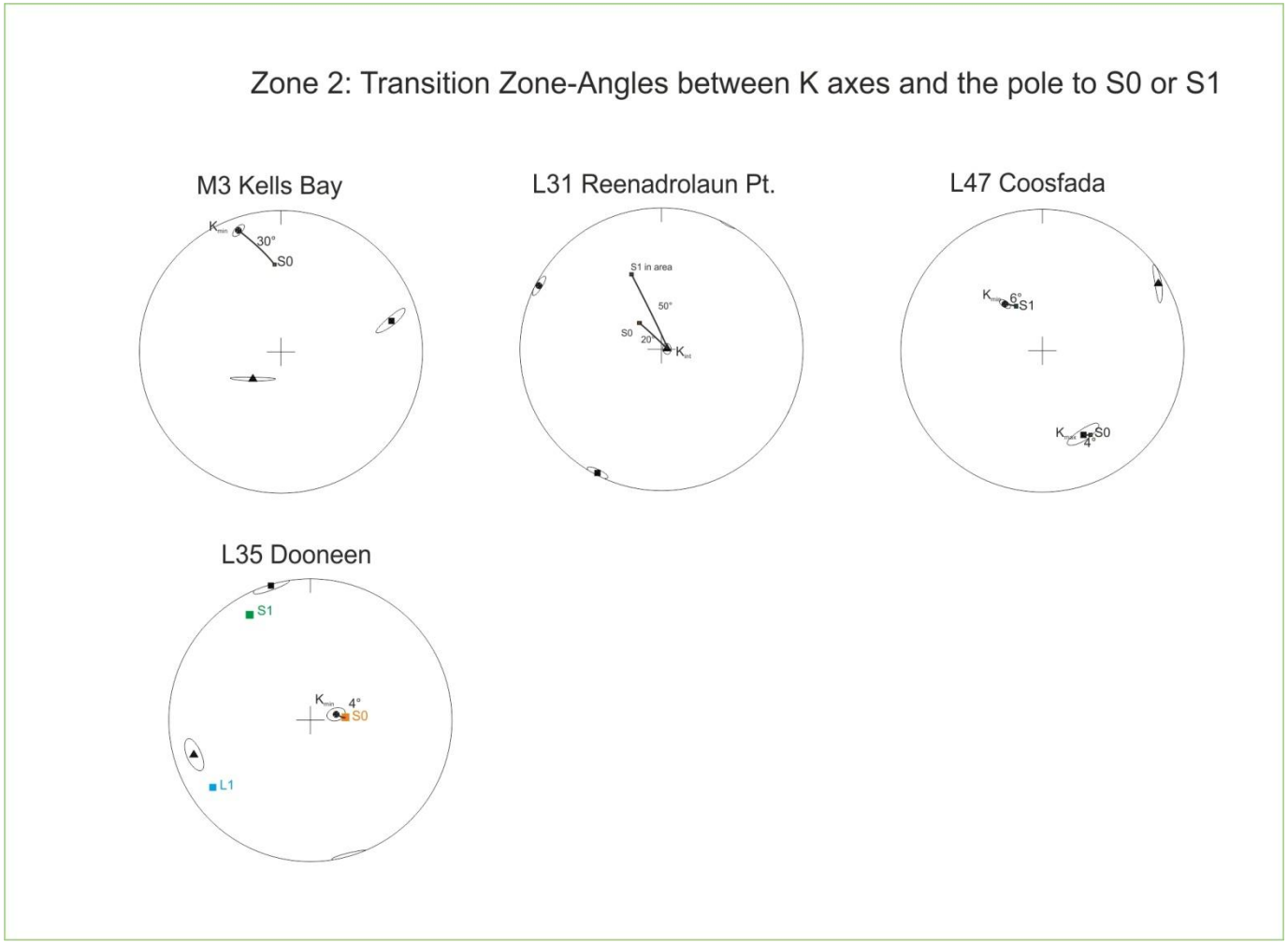

Figure 5.45 AMS stereonets (the Pl5 plots), showing the measured angles between K_{min} and the pole to S_0 and/or S_1 for the Transition Zone.

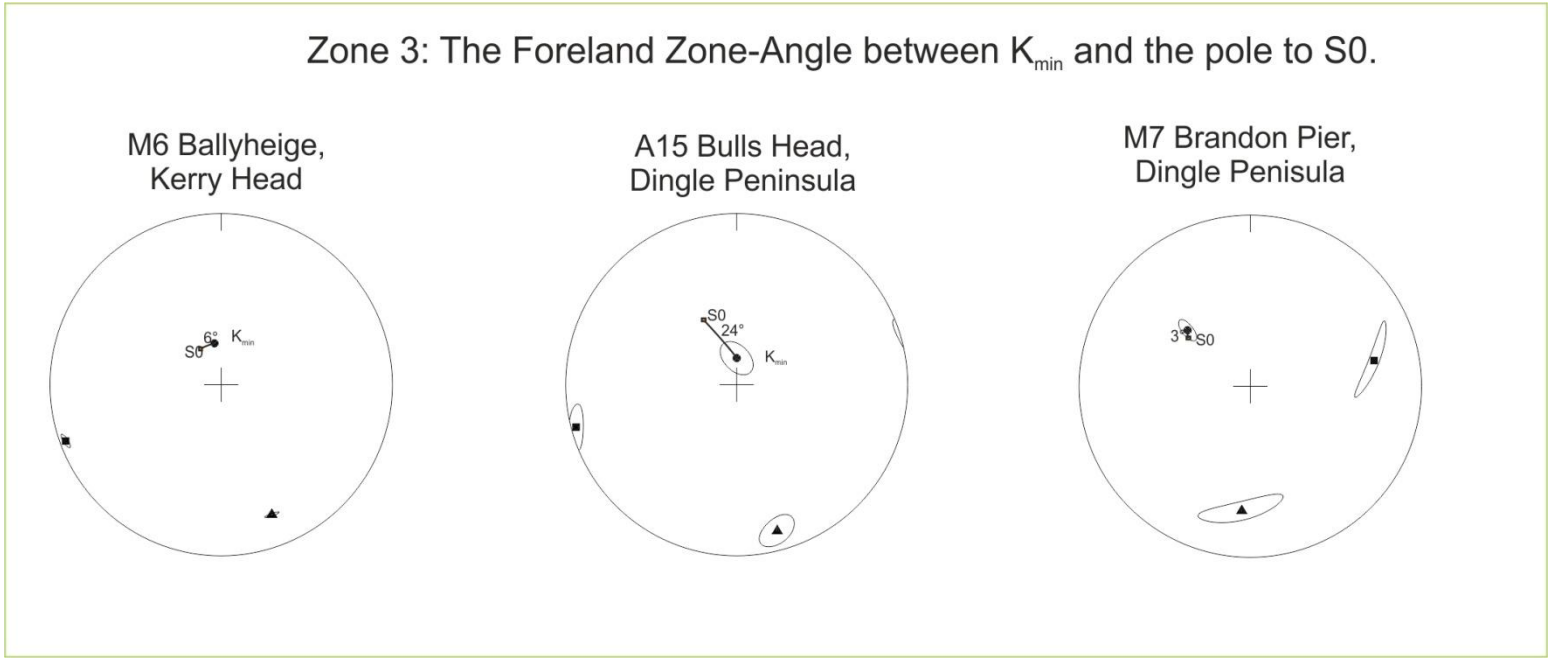

Figure 5.46 AMS stereonets (the Pl5 plots), showing the measured angles between K_{min} and the pole to S_0 and/or S_1 for the Foreland Zone.

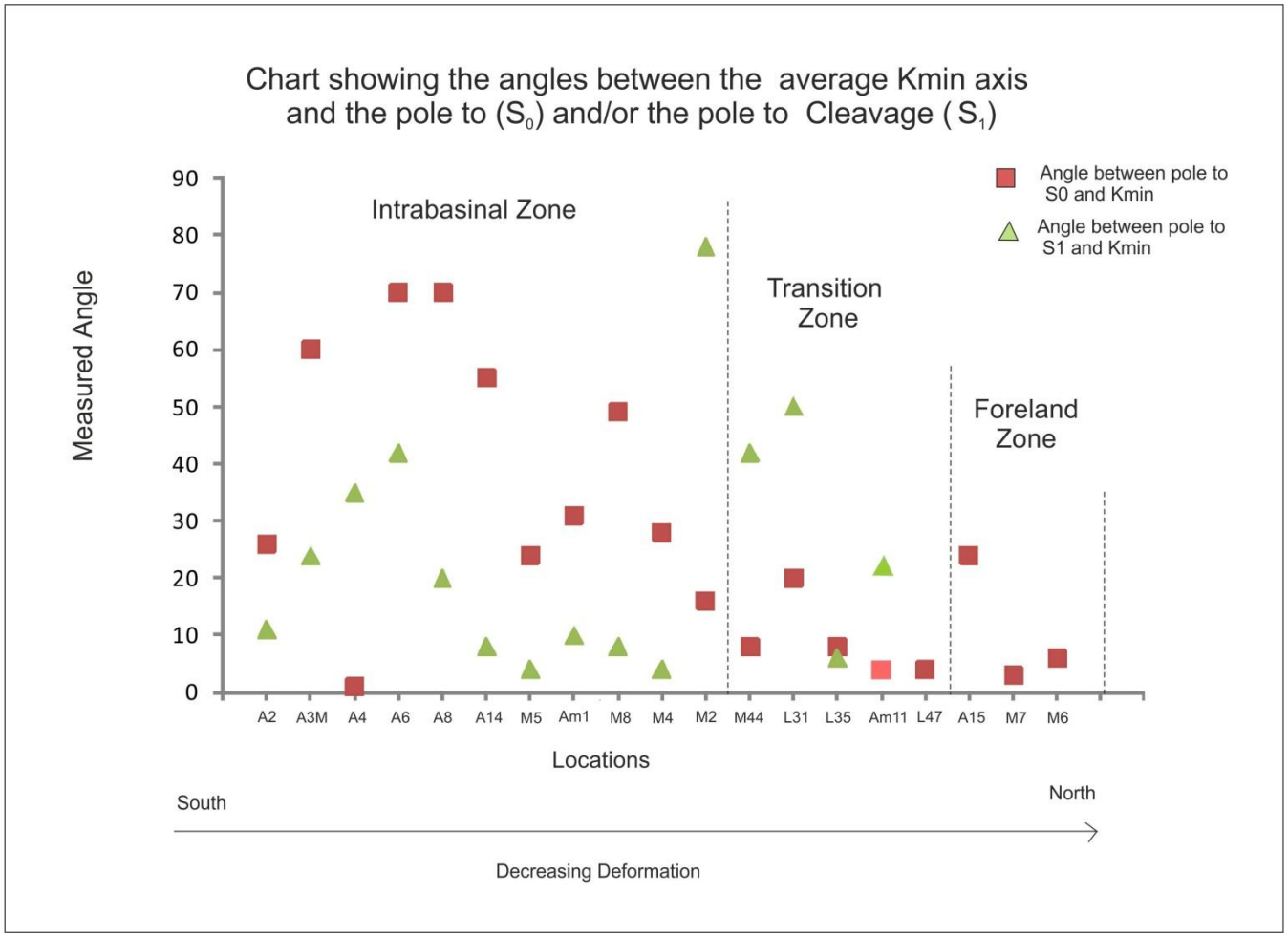

Figure 5.47 Graphs showing the measured angle between K_{min} and the pole to S_0 or S_1. The K_{min} axes is closer to the pole to S_1 than S_0 in the Intrabasinal Zone. This changes to K_{min} being closer to the pole to S_0 in the Transition Zone and Foreland Zone (note L35 green triangle = angle between K_{max} axes and Pole toS1, AM11 red square = angle between the K_{max} axes and S_0 axes)

5.7AMS interpretation summary Table based on the Interpretation of the AMS Ellipsoids

Sample	Location.	AMS features.	Tectonic Interpretation.	North/South of CF	Zone.
A1	Portmagee Quarry	K_{int} // pole to S_1, K_{max} // L_1, S_0 not represented, 10 ° anticlockwise rotation of AMS fabric. Prolate fabric.	Complete Tectonic Overprint.	South –Iveragh Peninsula.	1: Intrabasinal Zone
A2	Killabounia	K_{min} // pole to S_1, K_{max} // L_1, S_0 not represented. Prolate fabric.	Complete Tectonic Overprint.	South –Iveragh Peninsula.	1: Intrabasinal Zone
A3m	Keel Bay	K_{max} // L_1, K_{min}// pole to S_1, S_0 not represented. Oblate fabric.	Complete Tectonic Overprint.	South –Iveragh Peninsula.	1: Intrabasinal Zone
A4	South of Keel Bay	K_{min} // pole to S_0 + S1, K_{max}// L_1, intermediate between S_1 and S_0, Oblate.	Complete Tectonic Overprint.	South –Iveragh Peninsula.	1: Intrabasinal Zone
A6	Caherdaniel	K_{max} // L_1, K_{min} and K_{int} lie intermediately between the pole to S_1 and the pole to S_0.	Incomplete Tectonic Overprint.	South –Iveragh Peninsula.	1: Intrabasinal Zone
A8	Rossmore	K_{max} // L_1, K_{int} // pole to S_0, K_{min} // pole to S_1, prolate,	Complete Tectonic Overprint.	South –Iveragh Peninsula.	1: Intrabasinal Zone
A9	Molls Gap	10 ° clockwise rotation of AMS fabric,	Complete Tectonic Overprint	South –Iveragh Peninsula.	1: Intrabasinal Zone
A12	Gap of Dunloe	K_{max} // L_1, K_{min} // pole to S_1, S_0 not represented, K_{min} and K_{int} form a girdle indicating LPS.	Early LPS	South –Iveragh Peninsula.	1: Intrabasinal Zone
M5	Lough Acoose	K_{min} //pole to S_1, K_{int} // L_1, S_0 not represented, Oblate	Complete Tectonic Overprint.	South –Iveragh Peninsula.	1: Intrabasinal Zone
AM1	South of Lough Caragh	K_{max} // L_1, K_{min} // pole to S_1, S_0 not represented, Prolate,	Complete Tectonic Overprint.	South –Iveragh Peninsula.	1: Intrabasinal Zone

Sample	Location	AMS Features	Tectonic Interpretation	North/South of CF	Zone
A14	Kilgarvan	Kint// L_1, K_{min} // pole to S_1, S_0 not represented, Oblate.	CompleteTectonic Overprint.	South –Iveragh Peninsula.	1: Intrabasinal Zone
M8	Glenflesk Quarry	K_{min} // pole to S_1, K_{int} // L_1, S_0 not represented, Oblate	Complete Tectonic Overprint	South –Iveragh Peninsula.	1: Intrabasinal Zone
A10	Gap Dunloe north	K_{int} // L_1, Oblate	Incomplete tectonic overprint.	North of Black Lake Fault (lateral equivalent of CF)	2: Transition Zone
L31	Reenadrolaun Pt	K_{int} // pole to S_0	Bedding	North-Northern Iveragh Peninsula	2: Transition Zone
L35	Dooneen	K_{min}// pole to S_0, K_{max}// pole to S_1, Oblate	Bedding	North-Northern Iveragh Peninsula	2: Transition Zone
L47	Coosfada	K_{max} // pole to S_0 or normal to shortening direction, K_{int}// K_1, K_{min} // pole to S_1,	Early LPS	North-Northern Iveragh Peninsula	2: Transition Zone
M44	Culoo Rocks	K_{int} and lie in a girdle between pole to S_1 and pole to S_0, K_{max} //L_1, Prolate	Early LPS	North-Northern Iveragh Peninsula	2: Transition Zone
M2	Rheencaheragh	K_{min} // pole to S_0, K_{int} and K_{max} lie intermediately between L_1 and pole to S_1,	Bedding or Incomplete Tectonic Overprint.	North-Northern Iveragh Peninsula	2: Transition Zone
M3	Kells Bay	K_{min} // pole to S_0, oblate	Bedding	North-Northern Iveragh Peninsula	2: Transition Zone
AM11	Lough Caragh	K_{min} // pole to S_1, Kmax // pole to S_0 or K_{max} normal to shortening direction, K_{int} // L_1, Oblate	Early LPS	North-Northern Iveragh Peninsula	2: Transition Zone
M6	Ballyheige	K_{min} // pole to S_0, oblate	Bedding.	North-Dingle Peninsula	3: Foreland Zone
M7	Brandon Pier	K_{min} // pole to S_0, oblate	Bedding.	North-Dingle Peninsula	3: Foreland Zone
A15	Dingle Peninsula.	K_{min} // pole to S_0, oblate	Bedding.	North-Dingle Peninsula	3: Foreland Zone
Other	Locations				
M4	Broad Strand	K_{min} // pole to S_1, Kmax //L_1, S_0 not represented, prolate	Complete Tectonic Overprint	South Munster Basin	Intrabasinal: South Munster Basin.
A13	Dunmore East	K_{min} // pole to S_0, oblate	Bedding	Co. Waterford	Extrabasinal (ORS to the East of Munster Basin)

5.8 The μ value, Anisotropy degree, Pj and shape factor Tj , and Mean Susceptibility.

The μ value is calculated and given in the AMS files (RS5 files see appendix (Normalised data; Owens, 2000). Where $0 < \mu < 45°$ the AMS ellipsoid is oblate. Where $45 < \mu < 90$, the AMS ellipsoid is prolate. The μ value is related to the L (the magnetic lineation) and the F (the magnetic foliation) parameters as follows:

μ = the arctan or $\tan^{-1}$ of L/F (answer needs to be converted from radians to degrees):

or:

$$\mu = (\tan^{-1} L/F)*(180/\pi)$$

The L and F parameters have been plotted on a Flinn Plot (Flinn, 1962; Fig 5.48), which also shows the μ values. The μ value is the angle between X axis and the line joining the origin (0, 0) to the point (F, L) on the graph. The Flinn plot is used to show the distribution of AMS ellipsoid shapes. The oblate field lies below the 45° line and the prolate field lies above the 45 ° line (Fig 5.48). As can be seen from Fig 5.48, most of the Transition Zone and Foreland Zone ellipsoids have low μ values and lie in the oblate field. This reflects primary bedding controlled and LPS controlled AMS ellipsoids with low deformation. Most of the intrabasinal ellipsoids which are cleavage controlled have higher μ values and lie closer to the prolate field, which indicates higher deformation. A few of the intrabasinal ellipsoids lie in the oblate field as they have undergone further deformation from the prolate phase into the oblate phase (lying in the cleavage plane).

The projected μ values are plotted along a line perpendicular to the regional strike (AMS Results Map) in order to show the variation in the μ value from south to north across the three tectonic zones (Fig 5.49). There is a drop off in the μ values across the Coomnacronia Fault.

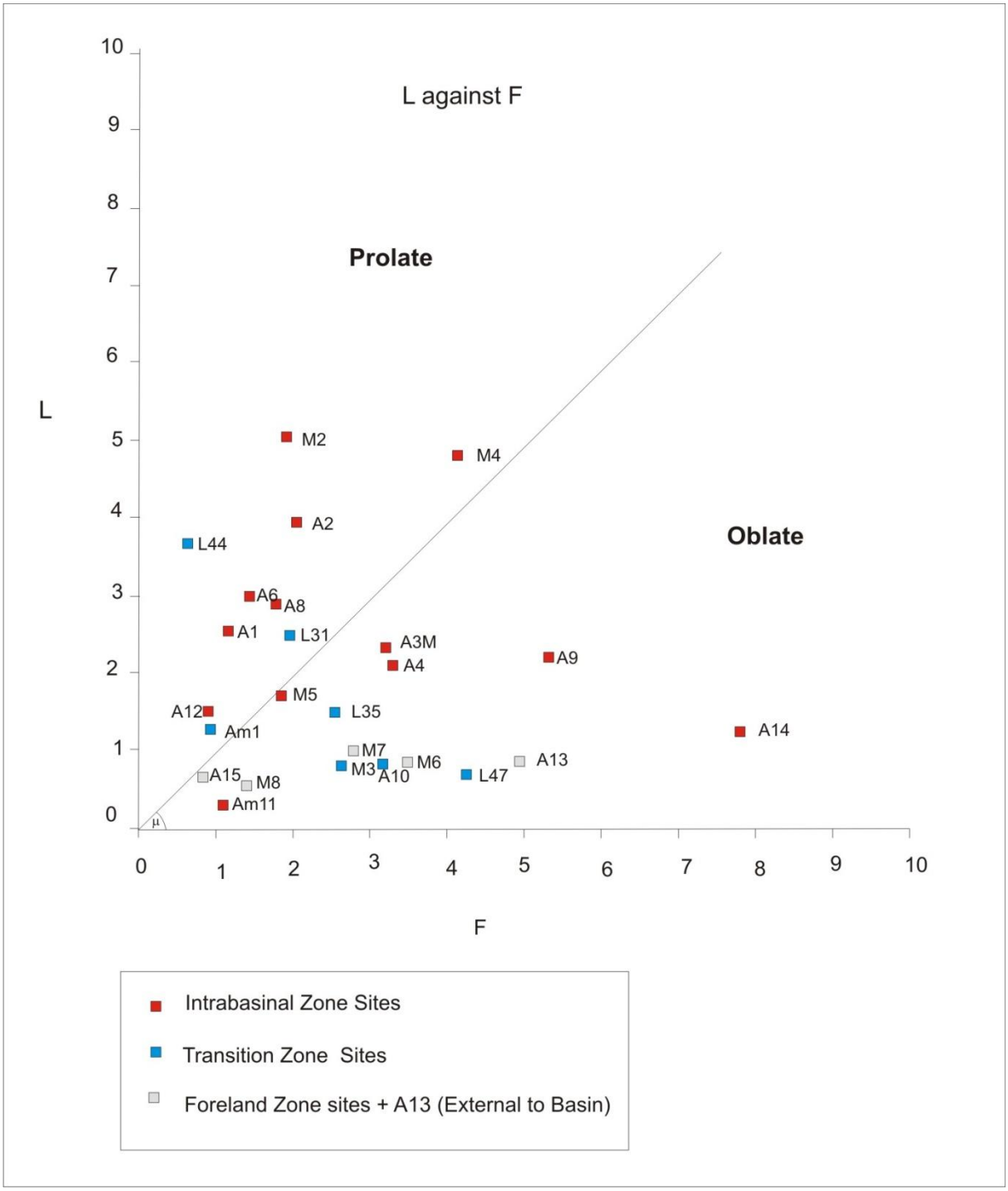

Figure 5.48 A Flinn Plot showing the magnetic lineation (L) against the magnetic foliation (F) for the AMS sites. The μ value is the angle between X axis and the line joining the origin to the point (F, L).The Flinn plot shows the distribution of AMS ellipsoid shapes for each of the Zones: The Intrabasinal Zone, The Transition Zone and the Foreland Zone.

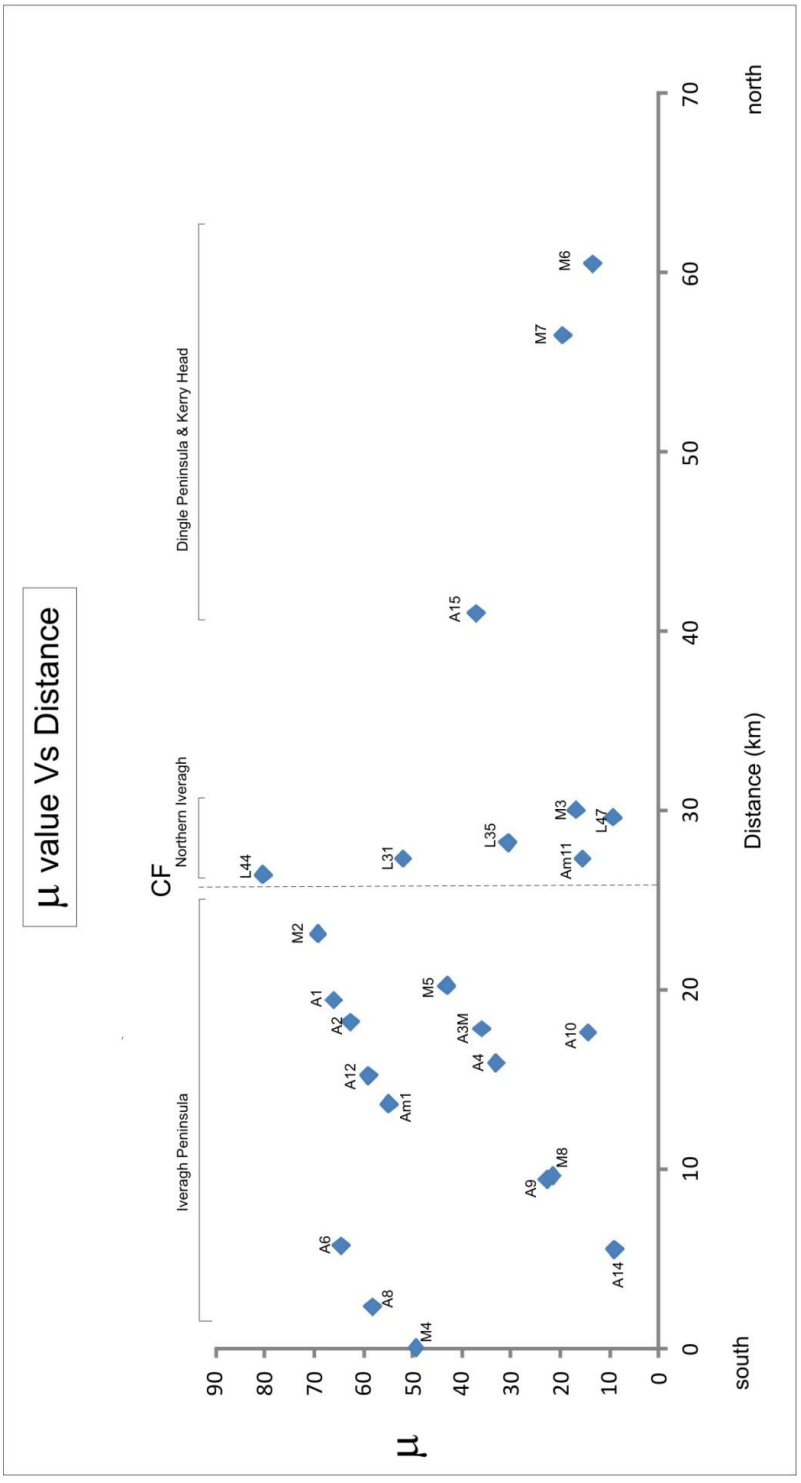

Figure 5.49 μ value against distance from south to north (CF = Coomnacronia Fault; See AMS Results Map; note M4 lies outside of study area in the south Munster Basin).

The Anisotropy Degree, Pj

The magnitude or eccentricity of the ellipsoid is also known as the anisotropy degree and can be described using the parameter P_j (Jelenik, 1981) where;

$P_j = exp\sqrt{\{2[(\eta_1 - \eta_m)^2 + (\eta_2 - \eta_m)^2 + (\eta_3 - \eta_m)^2]\}}$ (Jelinek, 1981)

$\eta_1 = \ln K_1; \eta_2 = \ln K_2; \eta_3 = \ln K_3$

$\eta_m = \eta_m = (\eta_1 + \eta_2 + \eta_3)/3$ (arithmetic mean).

or

$\eta_m = \sqrt[3]{(\eta_1 \cdot \eta_2 \cdot \eta_3)}$ =The geometric mean and needs only to be used when there are differences in the range of AMS values of an order of magnitude (Tarling and Hrouda, 1993).

The arithmetic mean is used by Tarling and Hrouda (1993) as it is adequate for data sets which are of a similar order of magnitude.

The Shape Parameter, Tj

To describe the shape of the ellipsoid, T_j is used (Jelenik, 1981).

$$Tj = \left[\frac{2\ln(K_2/K_3)}{\ln(K_1/K_3)}\right] \quad - 1$$

When $0 < T_j \leq +1$ the ellipsoid is oblate. When $0 > T_j \geq -1$, the ellipsoid is prolate. When $T_j = 0$, the ellipsoid is neutral.

The Tj verses Pj plot (Jelenick, 1981; Borradaile, 2010) of all of the samples shows the evolution of the magnetic fabrics with increasing deformation. As deformation increases an AMS path can be tracked from the samples from the Foreland Zone to the Transition Zone to the Intrabasinal Zone. The fabric evolves from oblate (primary sedimentary bedding controlled) through to prolate (tectonic cleavage) and through to oblate again (tectonic cleavage). The path that these AMS samples follow in this study fits with the model of Borradaile (2010; Fig 5.50).

Table 5.5 shows the calculated Pj and Tj values based on the equation from K1, K2 and K3 RS5 files. Pj is the anisotropy degree and Tj is the shape parameter.

Location	K_1	K_2	K_3	Anisotropy degree, Pj	Shape Parameter, Tj
A1 Portmagee Quarry	1.021	0.995	0.984	1.038599	-0.39766
A2 Killabounia	1.033	0.994	0.973	1.062527	-0.28631
A3M Keel Bay	1.026	1.003	0.971	1.056946	0.177
A4 SE of Keel Bay	1.025	1.004	0.971	1.056136	0.235032
A6 Caherdaniel	1.025	0.995	0.981	1.045801	-0.35407
A8 Rossmore	1.025	0.996	0.979	1.047486	-0.25013
A9 Molls Gap	1.033	1.01	0.957	1.081704	0.410701
A10 Gap of Dunloe north	1.016	1.008	0.976	1.043475	0.606375
A12 Gap of Dunloe South	1.013	0.998	0.989	1.02451	-0.24437
A13 Dunmore East	1.022	1.014	0.964	1.06547	0.730988
A14 Kilgarvan	1.034	1.022	0.944	1.104179	0.743624
A15 Dingle Peninsula	1.007	1.001	0.992	1.015226	0.203598
AM1 South of Lough Caragh	1.012	0.999	0.989	1.023317	-0.12478
AM11 Lough Caragh North	1.005	1.003	0.992	1.014125	0.693997
L31 Reenadrolaun Pt, Valentia Island	1.023	0.998	0.979	1.045064	-0.12556
L35 Dooneen	1.018	1.003	0.978	1.041365	0.259363
L47 Coosfada	1.019	1.012	0.969	1.056069	0.725985
M5 Lough Acoose	1.017	1	0.982	1.03565	0.037316
M44 Culoo Rocks	1.027	0.99	0.984	1.047367	-0.71574
M2 Rheencaheragh	1.04	0.99	0.97	1.074274	-0.41421
M3 Kells Bay	1.014	1.006	0.98	1.036343	0.535511
M4 Broad Strand	1.046	0.998	0.956	1.094174	-0.04424
M6 Ballyheige	1.017	1.009	0.974	1.047082	0.63439
M7 Brandon Pier	1.016	1.006	0.978	1.040355	0.481031
M8 Glenflesk Quarry	1.008	1.003	0.989	1.019935	0.477363

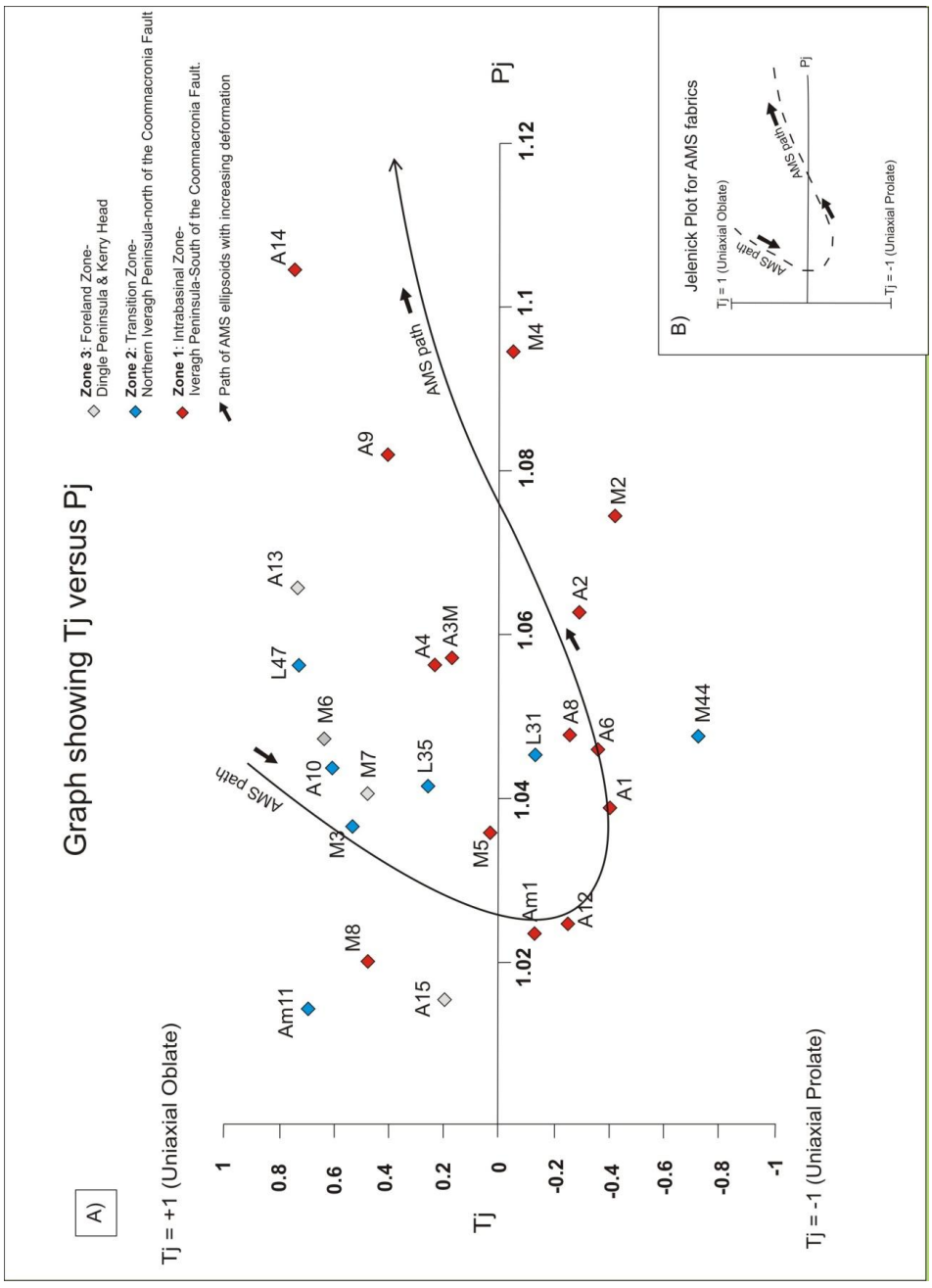

Figure 5.50 A) This graphs plots the Tj values against the Pj values (Table 5.5 for each site).The AMS ellipsoids from each of the three zones fit well with the mode l for the evolution of the AMS ellipsoids with increasing deformation in shown in B) (Jelenick, 1981; Borradaile, 1997). The AMS path passes from the Foreland Zone to the Transition Zone and to the Intrabasinal Zone with increasing deformation.

The AMS results can be considered in terms of the mean susceptibility of each sample. The mean susceptibility of each sample is relatively low (Table 5.5). For most of the samples, the mean susceptibility is generally low ranging from 43.05 x 10^{-6} to 238.02 x 10 $^{-6}$ SI and may indicate that the AMS ellipsoids are controlled by paramagnetic minerals (Chapter 3). A low mean susceptibility of the samples may be a result of lower amounts of ferromagnetic minerals and higher amounts of paramagnetic minerals (Section 5.3).

5.9 Summary of AMS Ellipsoid Types

There are five different types of AMS ellipsoid each of which relate to a structural zone (Table 5.7).

In order of increasing tectonic deformation:

i) Bedding controlled AMS ellipsoid - Primary sedimentary controlled.
ii) Bedding controlled/ Early LPS controlled.
iii) Intermediate between bedding and cleavage - Incomplete tectonic overprint
iv) Cleavage controlled AMS ellipsoid - Complete tectonic overprint.
v) Cleavage controlled with minor rotation of AMS fabric -Tectonic Overprint with transpression.

5.10 Summary of AMS Results Chapter

- Three tectonic zones are proposed in this study defined by the AMS ellipsoids. The Intrabasinal Zone: Zone 1, The Transition Zone: Zone 2 and The Foreland Zone-Zone 3. Zone 1 and Zone 2 are separated by the Coomnacronia Fault - the proposed basin margin fault.
- AMS ellipsoids indicate a strong strain gradient from south to north across the Basin margin fault- The Coomnacronia Fault- where deformation decreases from Zone1 to Zone 2.
- AMS is very sensitive to the tectonic fabric in the Intrabasinal Zone and to the LPS fabric and bedding fabrics in the Transition Zone.
- The results from the AMS ellipsoids from each zone fit accordingly with the model of Jelenik (1981) of the behaviour of AMS ellipsoids with increasing deformation.

Table 5.6 shows the values for the magnetic lineation (L), the magnetic foliation (F), the μ values, and the Mean Susceptibility which is taken from the RS6 file.

AMS Site number	**Location**	**L**	**F**	**μ**	**mean susceptibility (RS6)** x 10^{-6} SI
A1	Portmagee Quarry	2.57	1.15	66	77.34 ± 7.92
A2	Kilabuonia	3.95	2.04	62.7	152.02 ± 5.54
A3M	Keel Bay	2.32	3.2	36	235.36 ± 12.95
A4	East of Keel Bay	2.13	3.28	33.1	162.93 ± 3.9
A6	Caherdaniel	2.97	1.42	64.5	155.05 ± 2.15
A8	Turn Off Rossmore	2.87	1.78	58.2	238.02 ± 6.96
A9	Molls Gap	2.23	5.31	22.8	202.97 ± 4.15
A10	Gap of Dunloe North	0.81	3.14	14.4	65.73 ± 2.59
A12	Gap of Dunloe South	1.5	0.9	59	116.63 ± 7.8
A13	Dunmore East	0.85	4.94	9.8	210.83 ± 9.64
A14	Kilgarvin	1.24	7.78	9.1	135.78 ± 4.55
A15	Dingle	0.65	0.86	37.2	67.62 ± 7.7
AM1	South of Lough Caragh	1.31	0.92	54.9	175.71 ± 21.57
AM11	Lough Caragh	0.3	1.06	15.6	51.98 ± 51.98
L31	Reenadrolaun Pt	2.49	1.94	52	83.85 ± 2.28
L35	Dooneen	1.5	2.54	30.7	155.67 ± 2.46
L47	Coosfada	0.7	4.23	9.4	43.05 ± 1.01
M5	Lough Acoose	1.7	1.83	42.9	67.82 ± 2.15
M44	Culoo Rocks	3.69	0.62	80.4	135.53 ± 4.02
M2	Rheencaheragh	5.06	1.92	69.2	341.68 ± 7.53
M3	Kells Bay	0.79	2.62	16.9	73.35 ± 2.77
M4	Broad Strand	4.81	4.13	49.4	214.15 ± 9.24
M6	Ballyheige	0.83	3.46	13.5	109.93 ± 5.76
M7	Brandon Pier	0.98	2.74	19.6	116.82 ± 47.91
M8	Glenflesk Quarry	0.55	1.39	21.6	107.72 ± 4.00

Table 5.7 shows the types of ellipsoids and the zones they are found in.

Type	**AMS sites**	**AMS Ellipsoid controlled by:**	**AMS ellipsoid Type**	**Zone of AMS sites:**	**Relationship to CF**
i)	M3, M6, M7, A15, A10, L35, L31.	S0 controlled.	Zero Tectonic Overprint	Foreland Zone and Transition Zone,	North
ii)	L47, AM11, M44, A12.	LPS controlled.	Early LPS	Transition Zone + Intrabasinal	North and South
iii)	A6, A10.	Intermediate between S0 and S1.	Incomplete Tectonic Overprint	Intrabasinal	South
iv)	A2, A3M, M8,A8, M5, AM1, A14, A4, M2.	S1 controlled.	Complete Tectonic Overprint	Intrabasinal	South
v)	A1, A9.	S1 controlled.	Complete Tectonic Overprint with rotation.	Intrabasinal	South

Chapter 6:
Strain Analysis

6.1 Introduction

Finite strain analysis has been carried out on 33 sandstone samples of Upper Devonian Old Red Sandstone from the Iveragh Peninsula, the Dingle Peninsula and Kerry Head in order to investigate the change in strain regime across the Coomnacronia Fault (Strain Analysis Results Map). There have been various strain analysis studies carried out previously in the study area but none have specifically examined the effect of the Coomnacronia Fault. Strain analysis has been carried out using the Delaunay Triangulation Nearest Neighbour Method (DTNNM) and the Mean Radial Length (MRL) Method (Mulchrone, 2002, 2005; Mulchrone et al., 2013).

6.2 The Delaunay Triangulation Nearest Neighbour Method (DTNNM)

The DTTNM method was developed by Mulchrone (2002) based on a number of previously existing strain analysis methods. Initially Ramsay (1967) first put forward the idea that measuring the centre to centre distance of objects could be used as a method for strain analysis. This nearest neighbour method (NNM) of Ramsay (1967) was not widely used due to a number of limitations (Erslev, 1988). These include labour intensity, subjectivity as to what the nearest neighbour is and problems with interpretations (Erslev, 1988). Subsequent to and based upon Ramsay's original NNM, was the development of the Fry Method (Fry, 1979) which was modified to the Normalized Fry method (Erslev, 1988) and the Enhance Normalized Fry method (Erslev and Ge, 1990). McNaught further developed these techniques by using best fit ellipses for non-elliptical shaped objects. Mulchrone (2002) improved upon these previous techniques and developed the DTNNM method. A Delaunay Triangulation is composed of lines joining the centres of objects to their nearest neighbours (Fig 6.1; Perparate and Shamos, 1985; O' Rourke, 1993). In the simulation study by Mulchrone (2002), the objects are represented as ellipses and Mulchrone (2002) discusses how the DTNNM can be used on objects of variable shape. DTNNM analyses are carried out in 2D sections (Mulchrone, 2005).

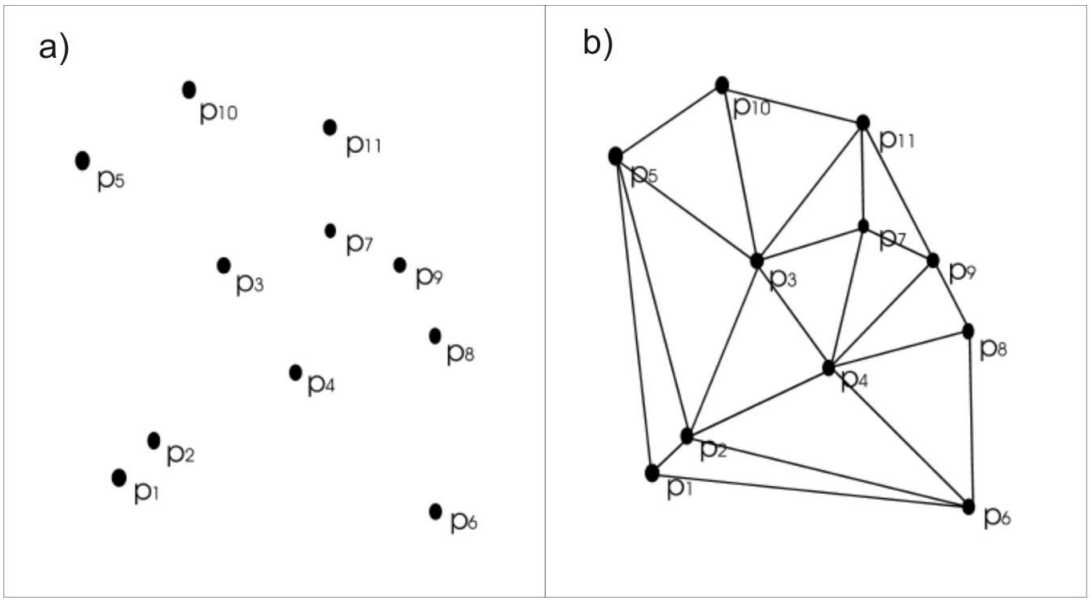

Figure 6.1 shows how a Delaunay triangulation in b) is composed from points in a), (Modified from Mulchrone, 2002).

An advantage of the DTNNM is that it is computationally more efficient than the previously existing Fry, NNM and Normalised Fry methods all of which are graphical methods (Mulchrone, 2002). The efficiency of the DTNNM is important when dealing with large data sets and data sets that are analysed using automated image analysis techniques (Mulchrone, 2002; Aillieres and Champenois, 1994; Aillieres et al., 2005). The DTNNM method makes the assumption that the objects are anticlustered prior to the uptake of strain (Mulchrone, 2005). With increasing strain the precision of DTNNM may decrease (Mulchrone, 2002). Mulchrone (2002) finds that in order to reduce error in analysis the DTNNM is best used in investigating low to moderate strains ($R_s < 6$). Mulchrone (2002) has demonstrated the effectiveness of the DTNNM method using a simulation study and on real data from an ironstone oolite image from Ramsay and Huber (1983). It was found that strain results acquired using the DTNNM are comparable to results obtained from previous methods and the DTNNM can produce strain data with a 95% confidence ellipse. Another advantage of DTNNM is that the method can be used on markers that passively deform within the matrix (Mulchrone, 2005). Centre to centre methods such as the DTNNM are not suitable for use on a recrystallized quartzite as the centres of the grains are not comparable to the centre of the original grains (Passchier and Trouw, 2005).

6.3 The Mean Radial Length (MRL) Methods

MRL is a measure of the grain shapes and their distributions and has its origins in the R_f/ϕ Method (Ramsay, 1967). The R_f/ϕ method was first introduced by Ramsay (1967) for strain analysis which involves measuring the axial ratios R_i and orientations ϕ (Fig 6.2a) of a number of deformed objects and compiling this data in order to obtain a principal strain tensor in two dimensions (e.g. Choudhury and Mulchrone, 2006).

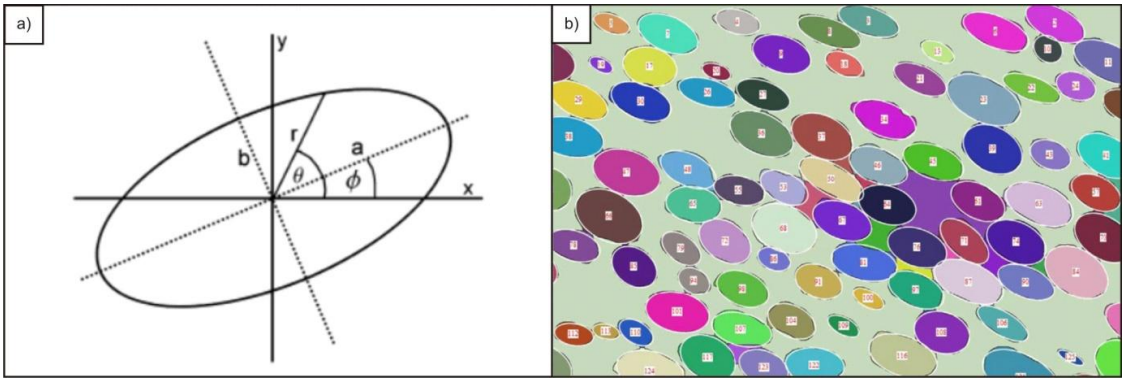

Figure 6.2 a) a = long axis of the ellipse, b = short axis of the ellipse, ϕ = the angle with the positive x-axis, θ and r = polar coordinates for a point on the ellipse-from Mulchrone et al. (2003). **b)** Strain analysis software written on Mathematica, identifies clast boundaries and calculates the best fit ellipses in order to allow both DTNNM and MRL analyses - from Mulchrone et al. (2013).

There has been much research in relation to the R_f/ϕ method (e.g. Dunnet, 1968; Elliot, 1970; Dunnet and Siddans, 1971; Mathews et al., 1974; Shimamoto and Ikeda, 1976; Robin, 1977; Le Theoff, 1979; Lilse, 1977; Borradaile, 1976; De Paor, 1980; Yu and Zheng, 1984; Mulchrone and Meere, 2001). Mulchrone et al. (2003) developed the MRL method for strain analysis which is based on the principle that prior to strain the MRL of ellipses equates to a circle, and subsequent to strain the MRL evaluates to a strain ellipse. They have demonstrated the use of the MRL technique using both a simulation study and on Irish Variscan sandstone samples from Meere's (1995) study. The results from the MRL analysis of Mulchrone et al. (2003) on Meere's (1995) samples correlate well with that of the analysis by Meere and Mulchrone (2001) on the same samples. The R_f/ϕ method and hence the MRL method can be used on objects that were not originally spherical (Ramsay and Huber, 1983; Robin and Torrance, 1987; Mulchrone et al., 2003; Meere and Mulchrone, 2003). There are two main assumptions that need to be considered when interpreting the results for the MRL analysis: these are that the objects are uniformly randomly distributed prior to deformation and that the distribution of axial ratios is not dependant on their orientation (Mulchrone et al., 2003).

The R_f/ϕ method, (from which MRL has been developed), makes the assumption that objects deform passively with respect to the matrix (e.g. Choudhury and Mulchrone, 2006). In reality there are competency contrasts between clasts and the matrix which lead to non passive behaviour, especially when analysing sedimentary clasts in sub-greenschist terrains (Meere, 2008). This effect of competency contrast was first noted by Gay (1968) and is most notable in conglomerates (Ramsay, 1967; Gay, 1968 a,b).

The Bootstrap method is an error estimation method created by Efron (1979) for use on complex statistical data and is recommended for use with the MRL method by Mulchrone et al. (2003). Simulation studies have been carried out by Mulchrone et al. (2003) in order to test the effectiveness of the Bootstrap method on strain data using the MRL method. Mulchrone et al. (2005) have also demonstrated the suitability of the Bootstrap method on real sandstone samples from Meere's (1995) study.

6.4 Previous Strain analysis Studies in the Munster Basin and Dingle Peninsula

Meere and Mulchrone (2006) have carried out strain analysis on samples from the Dingle Peninsula. They investigated strain in the Upper Devonian Slieve Mish Group which is considered to be the equivalent to the Upper Devonian ORS of the Munster Basin and Kerry Head (Higgs and Russell, 1981). The Upper Devonian Slieve Mish Group lies above the Acadian unconformity (Richmond and Williams, 2000) and has been affected by Variscan deformation (Meere and Mulchrone, 2006). Meere and Mulchrone (2006) conclude that the main cleavage found on the Dingle Peninsula is a weak Variscan cleavage. Meere and Mulchrone (2006) have carried out R_f/ϕ analysis on clasts from sandstones and conglomerates from Slieve Mish, Bulls Head, Ballymore Point and Clahane on the Dingle Peninsula. They have used the MRL method of Mulchrone et al. (2003). They find strain values between $R_s = 1.1$ to $R_s = 1.3$ for these lithologies and conclude from this that there is little to no penetrative tectonic strain. Overall Meere and Mulchrone (2006) conclude that penetrative strain is weak for the Upper Devonian lithologies of the Dingle Peninsula. This low strain correlates with the distribution of cleavage on the Dingle Peninsula with a weak disjunctive cleavage in the west (Meere and Mulchrone, 2006) and zero tectonic fabric in the east (Capewell, 1965; Hudson et al., 1966) and Meere (1995). Strain analysis has been carried out by Meere (1995) on 23 sandstone samples to the north and to the south of the Kilarney Mallow Fault (KMF), a fault which lies laterally to the east of the Coomnacronia Fault (Fig 6.3), using the R_f/ϕ method. R_s values range from 1-3. North of the KMF the orientations of

the principal strain axes are randomly distributed and this may be a result of either primary sedimentary fabric control or rotation of strain ellipsoids by further folding (Meere, 1995). These values have been plotted on a Flinn diagram by Meere (1995), who concludes that the strain state of these samples to the north of the KMF relates to an early deformation stage (Ramsay and Huber, 1983). To the south of the KMF the principal strain axes are more uniform in direction and parallel the cleavage direction (Meere, 1995). Based on Flinn plots for samples to the south of the KMF, Meere (1995) suggests that these fabrics are a result of the superimposition of tectonic fabrics upon burial fabrics (Ramsay and Huber, 1983).

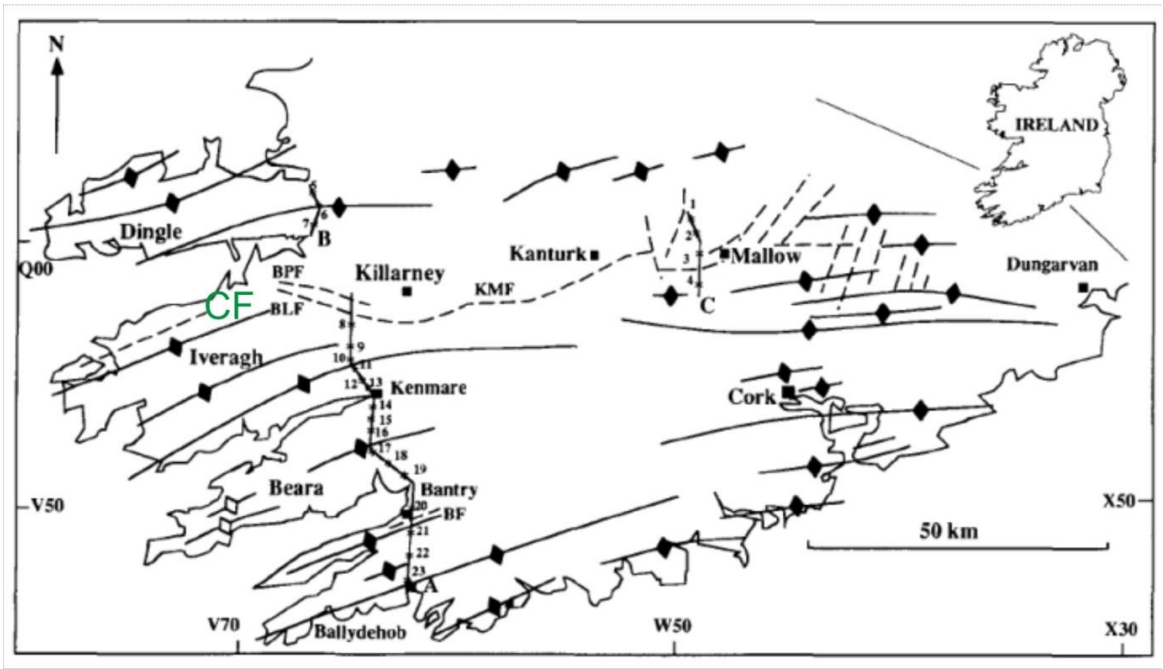

Figure 6.3 Location map for Meere's (1995) strain analysis samples to the south and the north of the Kilarney Mallow Fault (KMF). CF (dashed line) = The Coomnacronia Fault lies to the west of the KMF. Modified from Meere (1995).

Bresser and Walter (1999) carried out strain analysis using the Fry method (Fry, 1979) on 15 fine grained cleaved samples taken across the Variscan front in the West of Ireland (Fig 6.4). In the cleavage plane they find R_s values ranging from 1.1-1.43. In the ac plane of the fold axis they find strain values ranging from 1.3-2.2 (Fig 6.4).

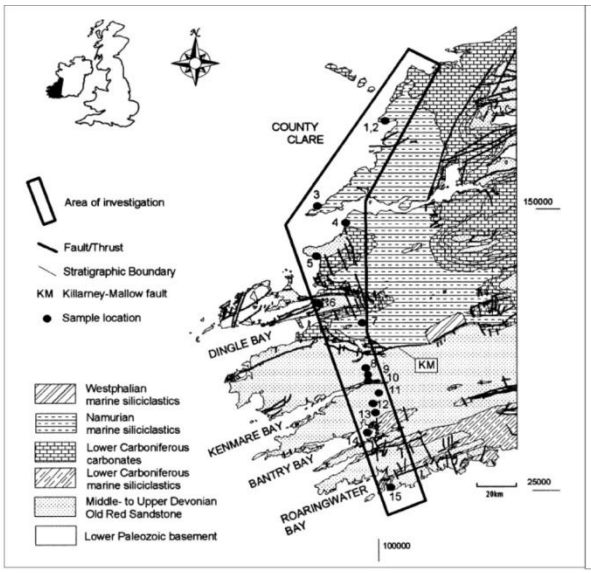

Sample	Irish grid	R_{ac}	R_{xy}
1	104485, 187701	1.4	1.3
2	104482, 187698	1.3	–
3	073519, 150643	1.7	–
4	086176, 141641	1.6	–
5	074746, 128024	1.3	–
6	070712, 106167	1.85	1.2
7	093059, 100668	1.3	–
8	095886, 080205	1.8	1.3
9	096518, 077733	2.0	1.3
10	098690, 073340	2.2	1.3
11	098797, 067449	2.0	1.3
12	097996, 061790	1.8	1.2
13	098376, 059337	1.8	1.1
14	096112, 050442	2.1	1.3
15	104661, 026505	1.7	1.43

Figure 6.4 Bresser and Walter's (1999) Strain analysis results on fine grained samples from the Variscan Front. R_{ac} is taken in the ac plane of the fold axes and R_{xy} lies in the cleavage plane- from Bresser and Walter (1999).

McCarthy (2014) has carried out both strain analysis using DTNNM and the MRL method and AMS studies on the far eastern side of the Munster Basin, Co. Waterford. In the study by McCarthy (2014), R_s values in the bedding plane across the eastern margin of the Munster Basin (which in that area is considered to be the DDL) range from 1.03-1.9 for DTNNM and 1.02 – 1.6 for MRL. McCarthy (2014) shows that most of the higher strain values occur south of the DDL.

6.5 Strain Analysis Methodology

Mulchrone et al. (2013) have developed new software that can be used for both the MRL and the DTNNM method. In the software by Mulchrone et al. (2013), DTNNM is applied to measure the relative orientations of the objects and MRL is applied in order to analyse the shape of the objects. The software code is designed for use in Mathematica and produces a graphical output of the strain analysis data (Mulchrone et al., 2013). This software calculates the best fit ellipses for objects of arbitrary shapes (Fig 6.2 b) and subsequently calculates the strain analysis results for DTNNM and MRL (Mulchrone et al., 2013). The authors have tested and demonstrated the software's suitability for use on three samples: arenite, oolite and quartzite.

In this study, strain analysis has been carried out using the DTNNM and the MRL method using the software developed by Mulchrone et al. (2013) on Mathematica. A total of 33 samples + 1 external to the Basin (A13 Dunmore East, Co. Waterford), have

been analysed across the study area and 20 of these samples are from the same hand sample as the AMS samples (Strain Analysis Results Map), in order to allow a comparison of the strain data with the AMS data. Thin sections have been cut parallel to the bedding plane as this orientation is mostly likely to minimise the effects of sedimentary fabrics on the finite strain estimates. In order to keep the samples consistent and comparable, the samples chosen are all med/coarse sandstones taken from bedding surfaces. The samples are quartz arenite sandstones and the locations for the samples are shown in the Strain Analysis Results Map. The samples consist mostly of quartz, with a matrix made of micas, quartz and minor amounts of accessory minerals (i.e. oxides). A brief outline of some of the microstrucutral characteristics observed in thin section is also included (section 6.10.3) in order to compare any microstructural fabric seen in thin section with the strain analysis results.

Mulchrone et al. (2013) describe the methodology for using the software package for DTNNM and MRL analysis. The traces can be carried out on the quartzofeldspathic grains of sandstone samples only (Mulchrone et al., 2013) allowing comparison between samples of similar rheology. Elongate minerals such as biotite can be left out of the analysis (Mulchrone et al., 2013). The optimum number of clasts to be traced from each thin section is 150 (Meere and Mulchrone 2003). Tracing of grain boundaries is carried out on photomicrographs taken in cross polarised light (Mulchrone et al., 2013). The grain boundaries need to be trace with a pen of 0.5 mm thickness and the trace must be a closed loop (Mulchrone et al., 2013). The software also calculates the error associated with the strain analysis methods using the Bootstrap method and suggests that when the confidence ellipses do not overlap that the different techniques (DTNNM and MRL) are sensitive to different behaviours. In this study a minimum of 150 clasts have been traced for each sample. Examples of the steps and graphical outputs for 3 of the samples are shown in Figures 6.5-6.10**.** Graphs for the rest of the samples can be found in Appendix D.

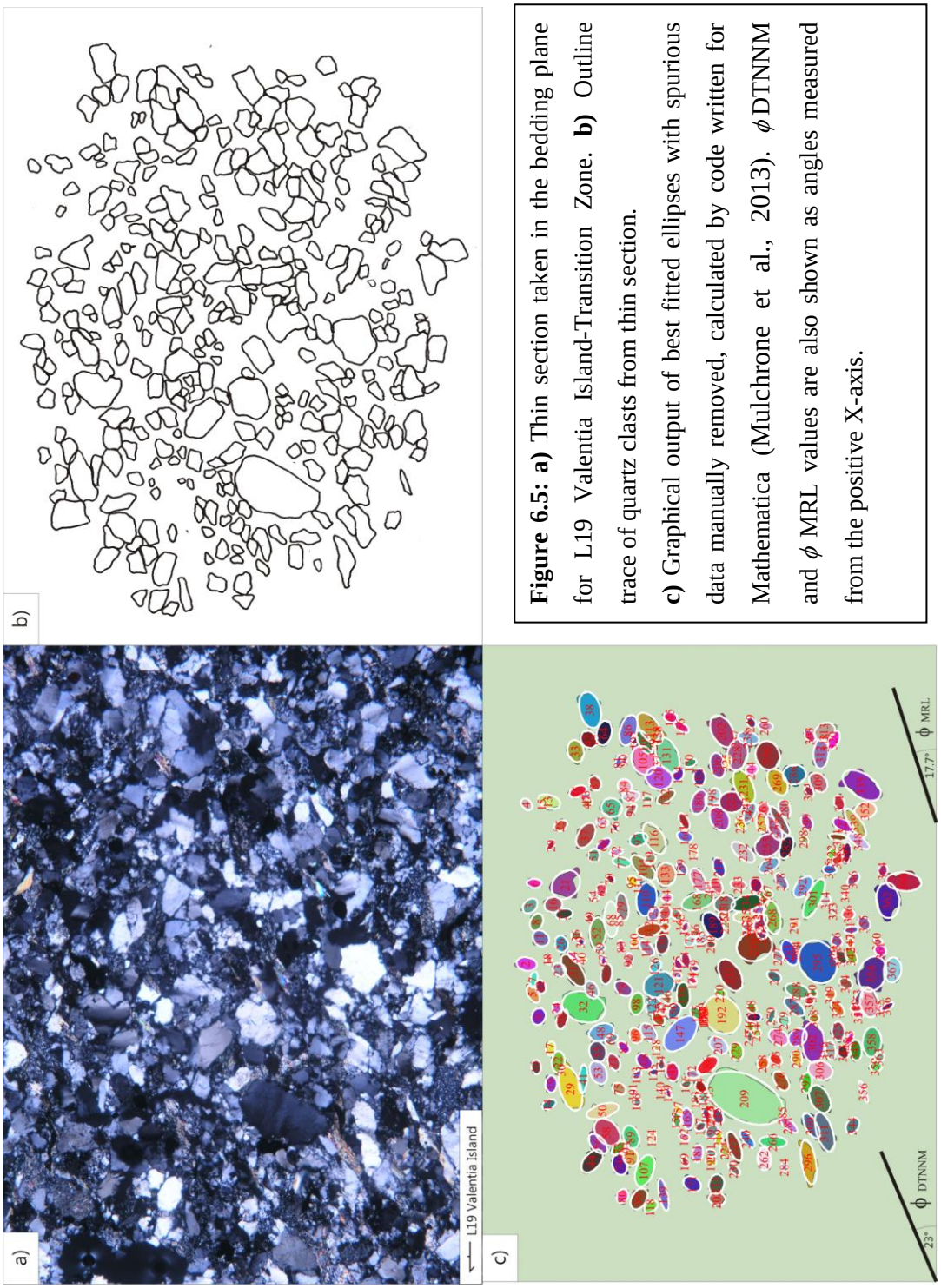

Figure 6.5: a) Thin section taken in the bedding plane for L19 Valentia Island-Transition Zone. **b)** Outline trace of quartz clasts from thin section. **c)** Graphical output of best fitted ellipses with spurious data manually removed, calculated by code written for Mathematica (Mulchrone et al., 2013). ϕDTNNM and ϕ MRL values are also shown as angles measured from the positive X-axis.

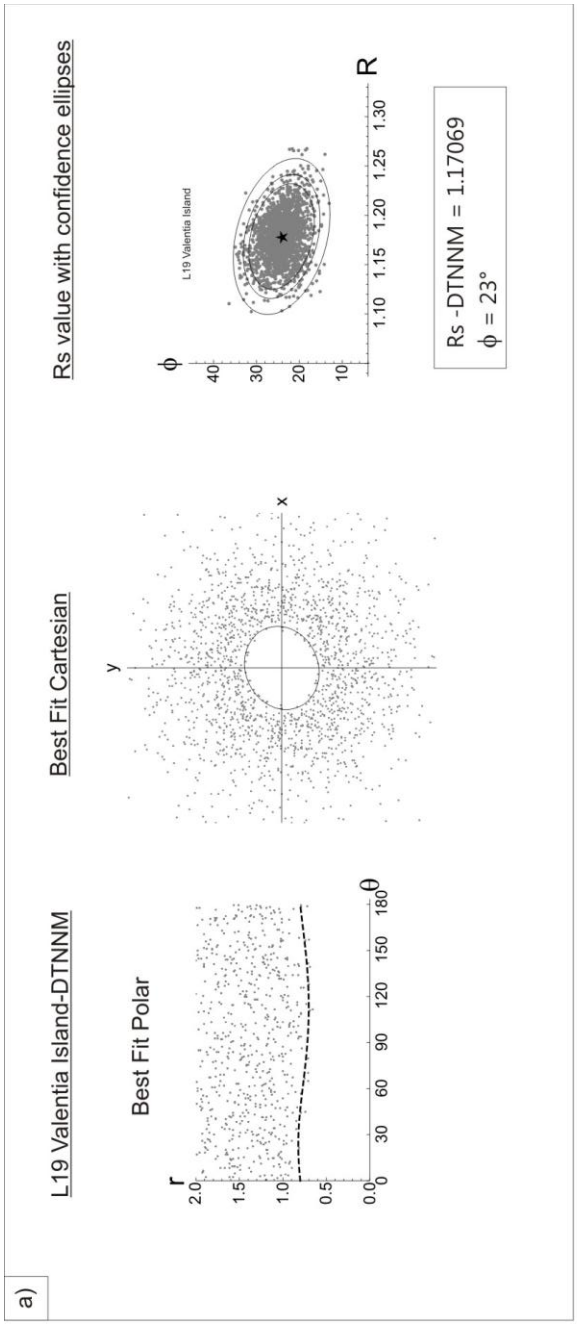

Figure 6.6 L19 Valentia Island.

a) Shows the best fit polar plot, best fit cartesian plot and the bootstrap analysis with 90, 95 and 99% confidence ellipses for the DTNNM. Star symbol is the calculated R_s value.

b) Shows the bootstrap results for the MRL. Star symbol is the calculated R_s value for MRL.

Figure 6.7: a) Thin section taken in the bedding plane for M5 Lough Acoose in the Intrabasinal Zone. **b)** Outline trace of quartz clasts. **c)** Graphical output of best fitted ellipses with spurious data manually removed, calculated by code written for Mathematica (Mulchrone et al., 2013). ϕ DTNNM and ϕ MRL values are also shown as angles measured from the positive X-axis.

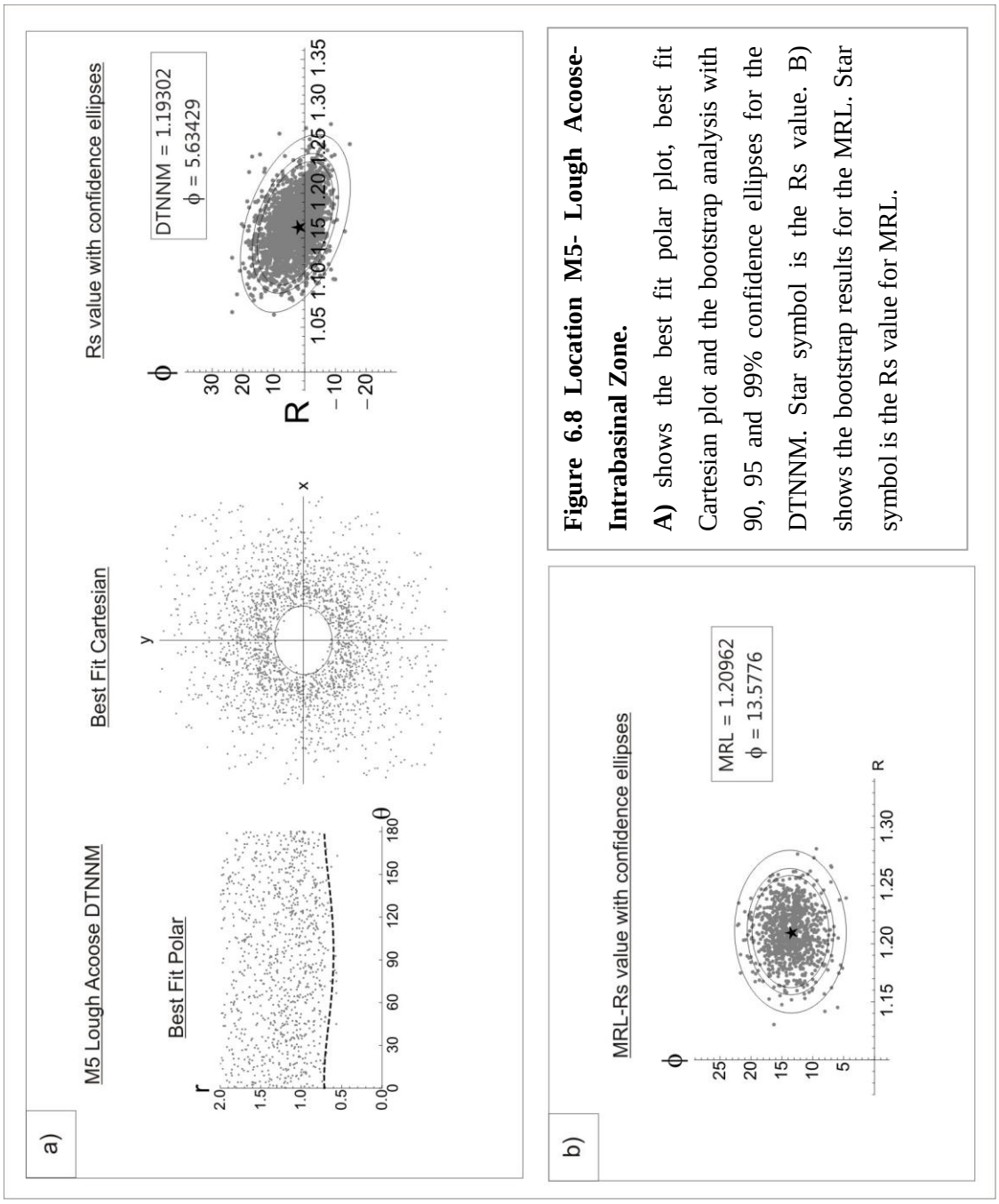

Figure 6.8 Location M5- Lough Acoose- Intrabasinal Zone.

A) shows the best fit polar plot, best fit Cartesian plot and the bootstrap analysis with 90, 95 and 99% confidence ellipses for the DTNNM. Star symbol is the Rs value. B) shows the bootstrap results for the MRL. Star symbol is the Rs value for MRL.

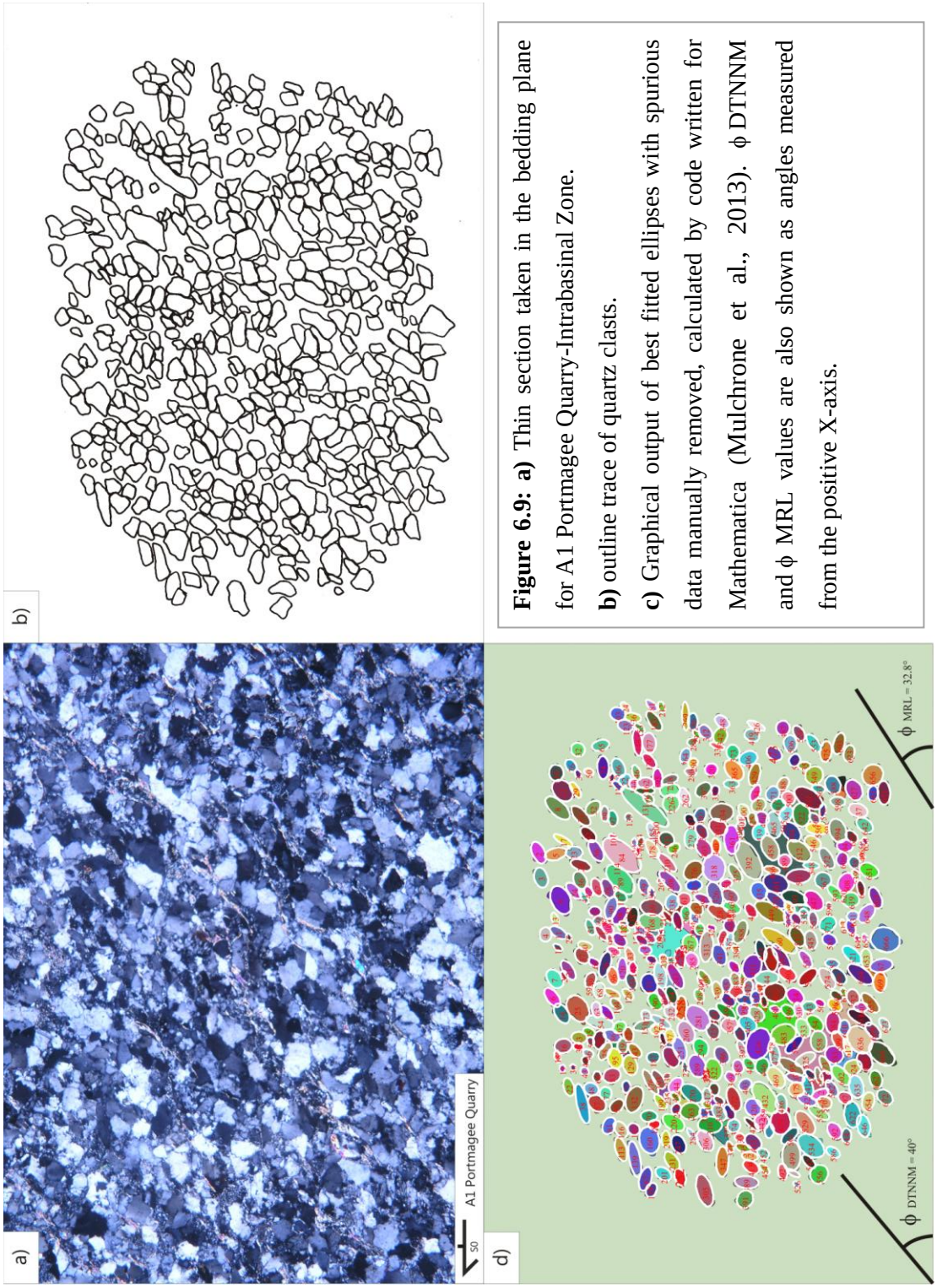

Figure 6.9: a) Thin section taken in the bedding plane for A1 Portmagee Quarry-Intrabasinal Zone.
b) outline trace of quartz clasts.
c) Graphical output of best fitted ellipses with spurious data manually removed, calculated by code written for Mathematica (Mulchrone et al., 2013). ϕ DTNNM and ϕ MRL values are also shown as angles measured from the positive X-axis.

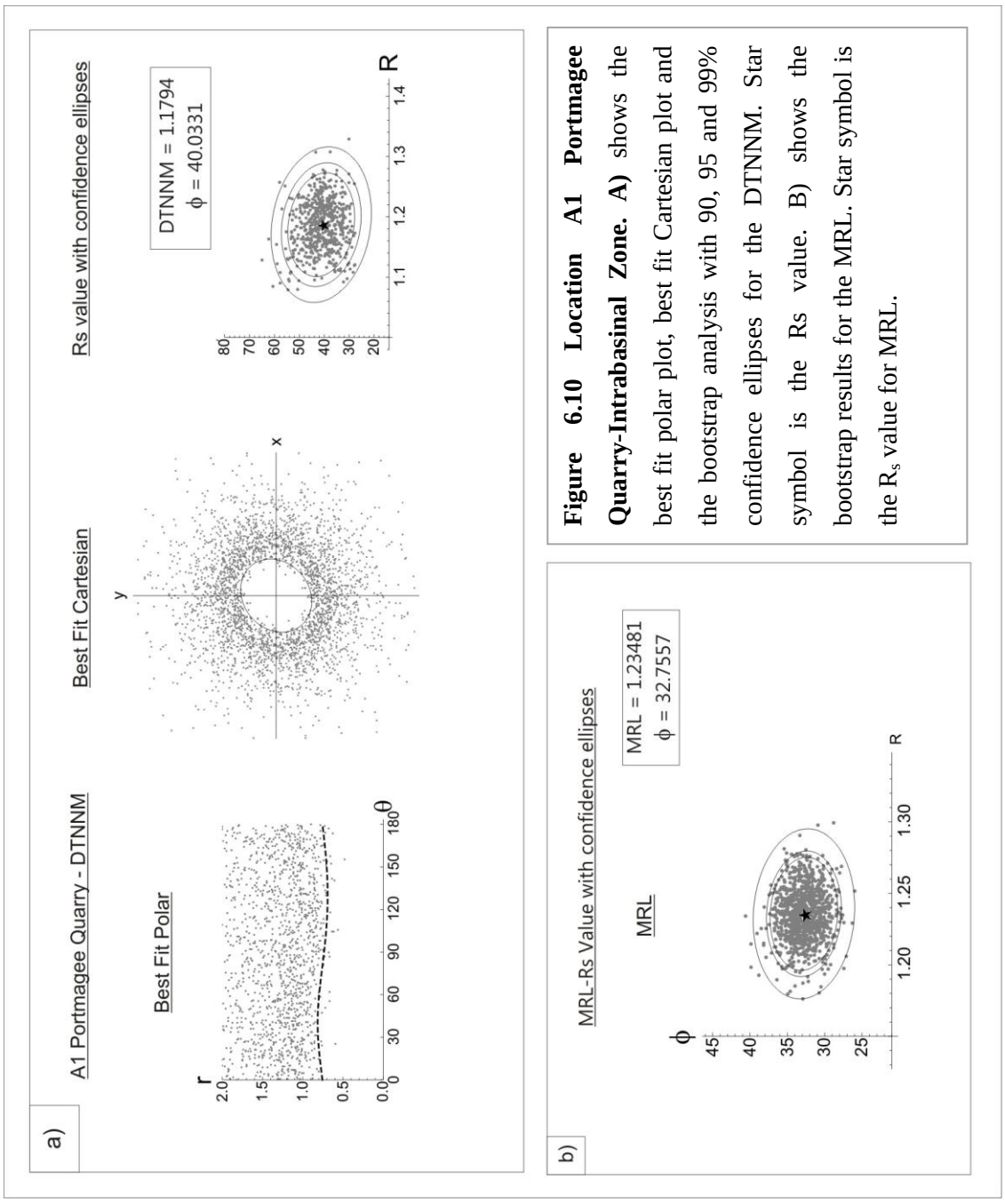

Figure 6.10 Location A1 Portmagee Quarry-Intrabasinal Zone. A) shows the best fit polar plot, best fit Cartesian plot and the bootstrap analysis with 90, 95 and 99% confidence ellipses for the DTNNM. Star symbol is the Rs value. B) shows the bootstrap results for the MRL. Star symbol is the R_s value for MRL.

6.6 Strain Analysis Results

There is a general decrease is strain from south to north for both the DTNNM and MRL methods (Fig 6.11, 6.12, 6.13, 6.14). The strain analysis results reflect the three proposed tectonic zones across the study area (Chapter 4: Field Work). The Intrabasinal Zone (south of the Coomnacronia Fault) ,which has slightly higher strain values, the Transition Zone (north of the Coomnacronia Fault) which has intermediate to low strain values and the Foreland Zone (north of the Coomnacronia Fault on the Dingle Peninsula, which has low strain values. The Coomnacronia Fault marks a boundary between higher strain results and lower strain results for both the DTNNM and the MRL. This gradual decrease in strain intensity is more obvious in the MRL. In the DTNNM there is a decrease in strain value however there are some anomalies within the DTNNM results.

6.6.1 Results – DTNNM

The average DTNNM R_s value for the Intrabasinal Zone is 1.296 (based on 15 samples). The average DTNNM R_s value for the Transition Zone is 1.203 (based on 16 samples) and the average DTNNM R_s value for the Foreland Zone is 1.069 (based on 2 samples).

In the Intrabasinal Zone the R_s values for the DTNNM range between 1.14 - 1.57 (Fig 6.11, 6.12, Table 6.1). Overall the results for the DTNNM in the Intrabasinal Zone are relatively moderate to high indicating this zone to be a moderate to high strain zone. In the Transition Zone the strain results for the DTNNM range from 1.08 – 1.44 (Fig 6.11, 6.12, Table 6.1). They are mostly generally lower with occasional higher results. In the Foreland Zone there are 2 samples and the DTNNM values for these are low at 1.04 (M7- Brandon Pier) and 1.09 (Ballyheige), (Fig 6.11 and 6.12, Table 6.1).

The best fit ellipses for samples L19 (Fig 6.6 a), M5 (Fig 6.8 a) and A1 (Fig 6.10 a) and the rest are shown in the Appendix D. For all of the plots, there are a low amount of central inliers which indicates good quality data (Mulchrone et al., 2013). The best fit ellipses are obtained by choosing a suitable zeta value while using the software from Mulchrone et al. (2013) in Mathematica. The zeta value is normally set at values between 100-4000 until the best fit ellipse is achieved and any changes in the zeta value can alter the strain analysis results (Mulchrone et al., 2013).

Table 6.1 DTNNM Rs Values with lower and upper 95% confidence limit

Locations	Distance along line (km) - Map Insert 3	R_s Value - DTNNM	Lower Value (95% confidence limit)	Upper Value (95% confidence limit)
M4 Broad Strand	0	1.57413	1.325	1.835
A7 Lambs Head	2.1	1.20096	1.132	1.292
A8 Rossmore	2.3	1.14232	1.078	1.284
A14 Kilgarvin	5.5	1.50258	1.364	1.508
A6 Caherdaniel	5.7	1.20397	1.138	1.275
A9 Molls Gap	9.4	1.30942	1.14	1.51
AM1 South of Lough Caragh	13.6	1.32629	1.258	1.398
A4 South east of Keel Bay	15.9	1.21603	1.114	1.325
A3M Keel Bay	17.8	1.53916	1.46	1.632
A2 Killabounia	18.2	1.3484	1.165	1.55
A1 Portmagee Quarry	19.4	1.1794	1.084	1.291
M5 Lough Acoose	20.2	1.19302	1.088	1.245
L23 Rheencaheragh Bay	23.1	1.24869	1.034	1.575
L26 Reenard Pt	25.5	1.30125	1.174	1.382
M8 Glenflesk	9.6	1.15664	1	1.208
A10 Gap of Dunloe North	17.6	1.09039	1.049	1.182
L44 Culloo Rocks	26.4	1.28436	1.208	1.402
L19 Valentia Island	27.2	1.17069	1.116	1.242
AM11 Lough Caragh North	27.3	1.20934	1.146	1.294
L31 Reenadrolaun Point	27.3	1.29031	1.22	1.44
L35 Dooneen	28.2	1.34795	1.19	1.518
L11 Enagh Point	28.4	1.13601	1	1.226
L6 Cooscrome Harbour	28.5	1.11671	1.063	1.181
L7 Cooscrome Harbour	28.6	1.10647	1.063	1.195
L10 Dolous Head	28.7	1.11863	1	1.28
L41 Knocknatobar	28.8	1.1293	1.056	1.222
L22 Kells Post Office	29.2	1.1708	1.092	1.292
L39 Knocknatobar	29.4	1.29153	1.236	1.35
L47 Coosfada	29.6	1.44428	1.344	1.539
M3 Kells Bay	30	1.13481	1.048	1.243
L21 Kells Bay	30.1	1.2043	1.092	1.301
M7 Brandon Pier	56.5	1.04481	1	1.121
M6 Ballyheige	60.5	1.09317	1.038	1.148

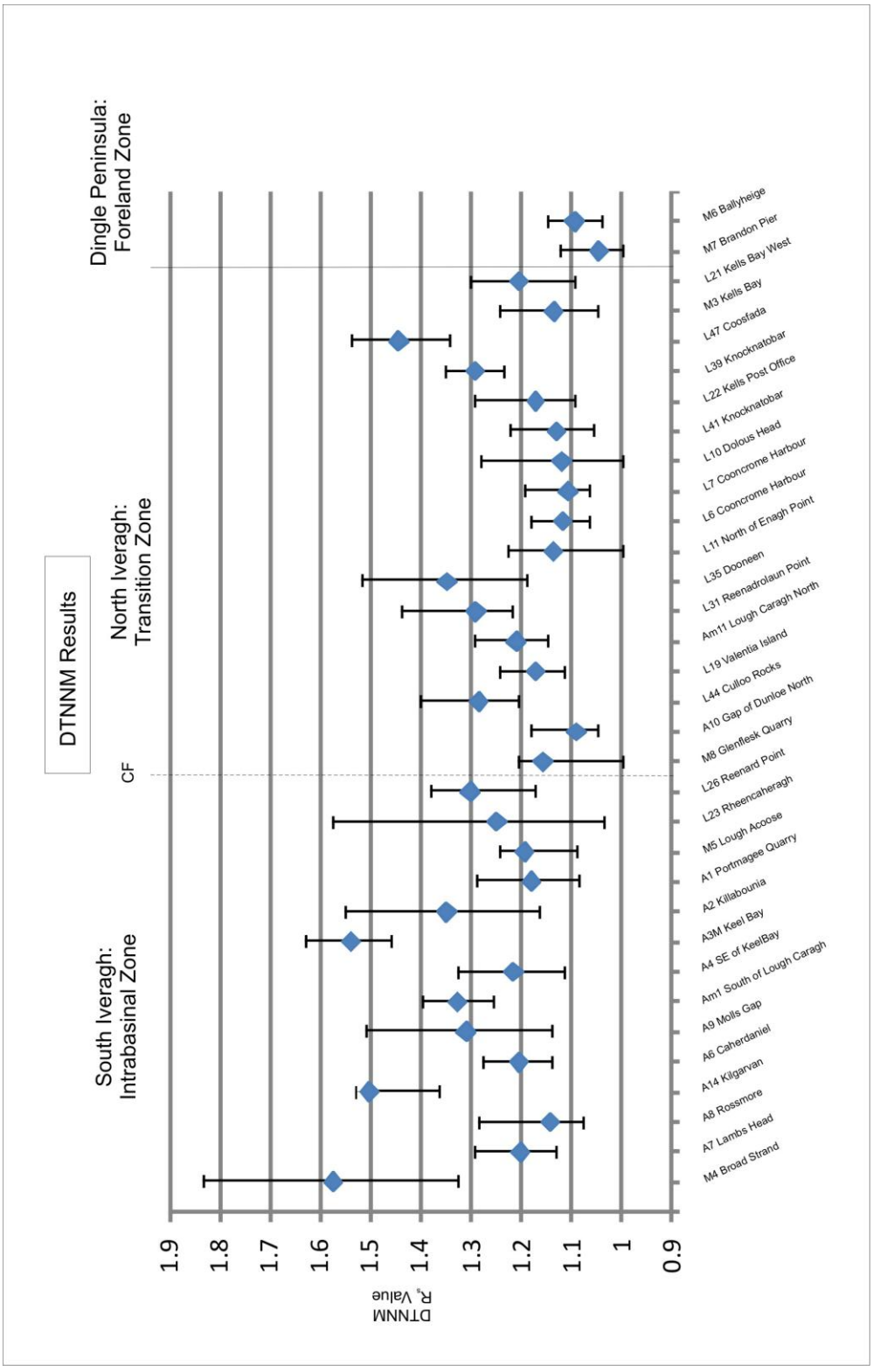

Figure 6.11 The results for the DTNNM analysis. R_s values are plotted on the Y-axis and locations in order from south to north are plotted on the X –axis. R_s values are generally higher south of the Coomnacronia Fault (CF) than to the north of it, with a few exceptions at e.g. L47.

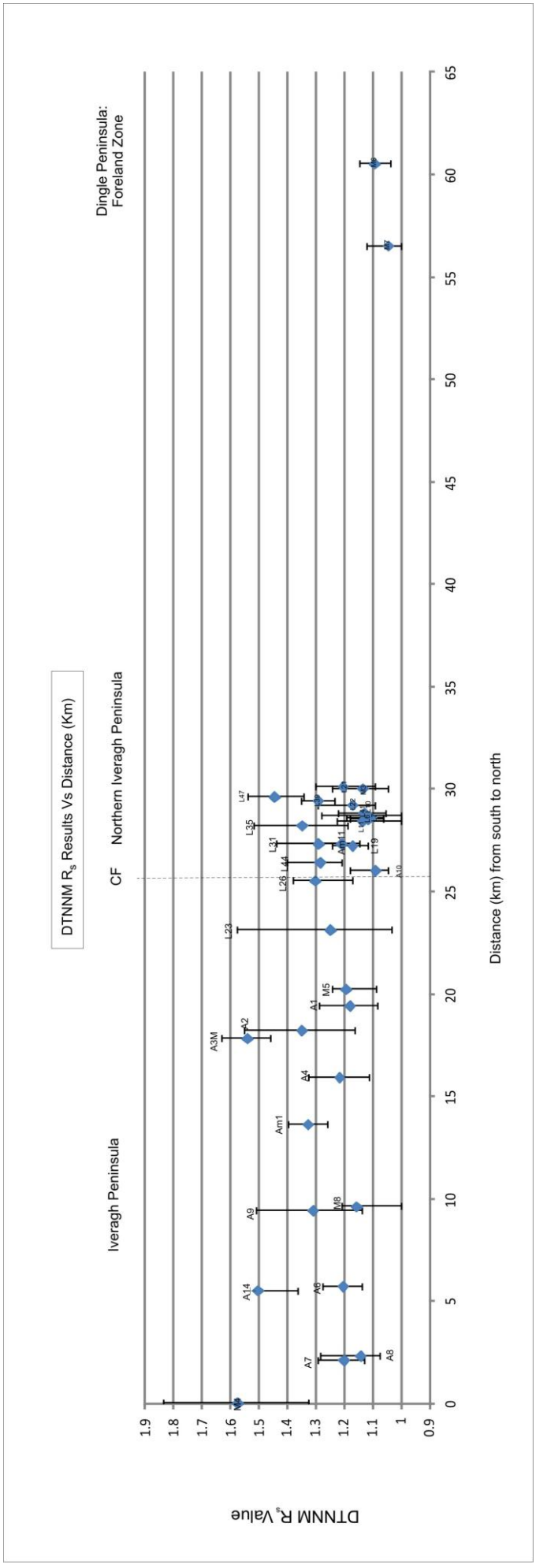

Figure 6.12 DTNNM R_s values with upper and lower error bars for 95% confidence, plotted against distance in km for the Iveragh Peninsula and Dingle Peninsula.(Note M4 is placed at 0Km as it lies outside of the Iveragh Peninsula, to the south-See Strain Analysis Map Insert).

6.6.2 Results – MRL

The MRL results show a steady decrease in R_s values from south to north (Fig 6.13, 6.14). The average MRL R_s value in the Intrabasinal Zone is 1.269 (based on 15 samples). In the Intrabasinal zone, R_s ranges from 1.13-1.43 (Fig 6.13). The average MRL R_s value in the Transition Zone is 1.142 (based on 16 samples). In the Transition Zone the R_s value range from 1.01-1.26 and in the Foreland Zone there are 2 samples and the R_s values are 1.03 (Brandon Pier) and 1.07 (Ballyheige, Fig 6.13). The average R_s value in the Foreland Zone is 1.048 (based on 2 samples). The best fit ellipses for examples L19 (Fig 6.6 a), M5 (Fig 6.8a) and A1 (Fig 6.10a) and the rest are shown in Appendix D. There is a low amount of central inliers indicating good quality data. The MRL bootstrap zeta value is set at 1000 for all the samples (Mulchrone et al., 2013).

Table 6.2 MRL R_s values with lower and upper 95% confidence limits.

Location	Distance along line (km) - Map Insert 3	MRL	Lower MRL	Upper MRL
M4 Broad Strand	0	1.27605	1.185	1.375
A7 Lambs Head	2.1	1.30891	1.255	1.368
A8 Rossmore	2.3	1.15988	1.044	1.284
A14 Kilgarvin	5.5	1.4265	1.358	1.496
A6 Caherdaniel	5.7	1.38196	1.324	1.412
A9 Molls Gap	9.4	1.19938	1.121	1.28
AM1 South of Lough Caragh	13.6	1.26302	1.217	1.31
A4 South East of Keel	15.9	1.16514	1.04	1.31
A3M Keel Bay	17.8	1.35498	1.272	1.44
A2 Killabounia	18.2	1.23626	1.081	1.4
A1 Portmagee Quarry	19.4	1.2349	1.193	1.28
M5 Lough Acoose	20.2	1.20962	1.156	1.265
L23 Rheencaheragh Bay	23.1	1.30956	1.242	1.382
L26 Reenard Point	25.5	1.24331	1.181	1.306
M8 Glenflesk Quarry	9.6	1.24014	1.187	1.298
A10 Gap of Dunloe north	17.6	1.06922	1.022	1.124
L44 Culloo rocks	26.4	1.16775	1.116	1.219
L19 Valentia Island	27.2	1.14383	1.089	1.204
AM11 Lough Caragh North	27.3	1.08096	1.031	1.136
L31 Reenadrolaun Point	27.3	1.19617	1.122	1.269
L35 Dooneen	28.2	1.15595	1.093	1.218
L11 North of Enagh Point	28.4	1.16224	1.099	1.234
L6 Cooscrome Harbour	28.5	1.18987	1.138	1.25
L7 Cooscrome Harbour	28.6	1.14187	1.104	1.184
L10 Dolous Hd	28.7	1.18854	1.132	1.248
L41 Knocknatobar	28.8	1.08372	1.039	1.134
L22 Kells Post office	29.2	1.11133	1.07	1.156
L39 Knocknatobar	29.4	1.23496	1.185	1.288
L47 Coosfada	29.6	1.23221	1.17	1.296
M3 Kells Bay	30	1.08335	1.038	1.132
L21 Kells Bay	30.1	1.03498	1	1.084
M7 Brandon Pier	56.5	1.02682	1	1.07
M6 Ballyheige	60.5	1.0693	1.041	1.101

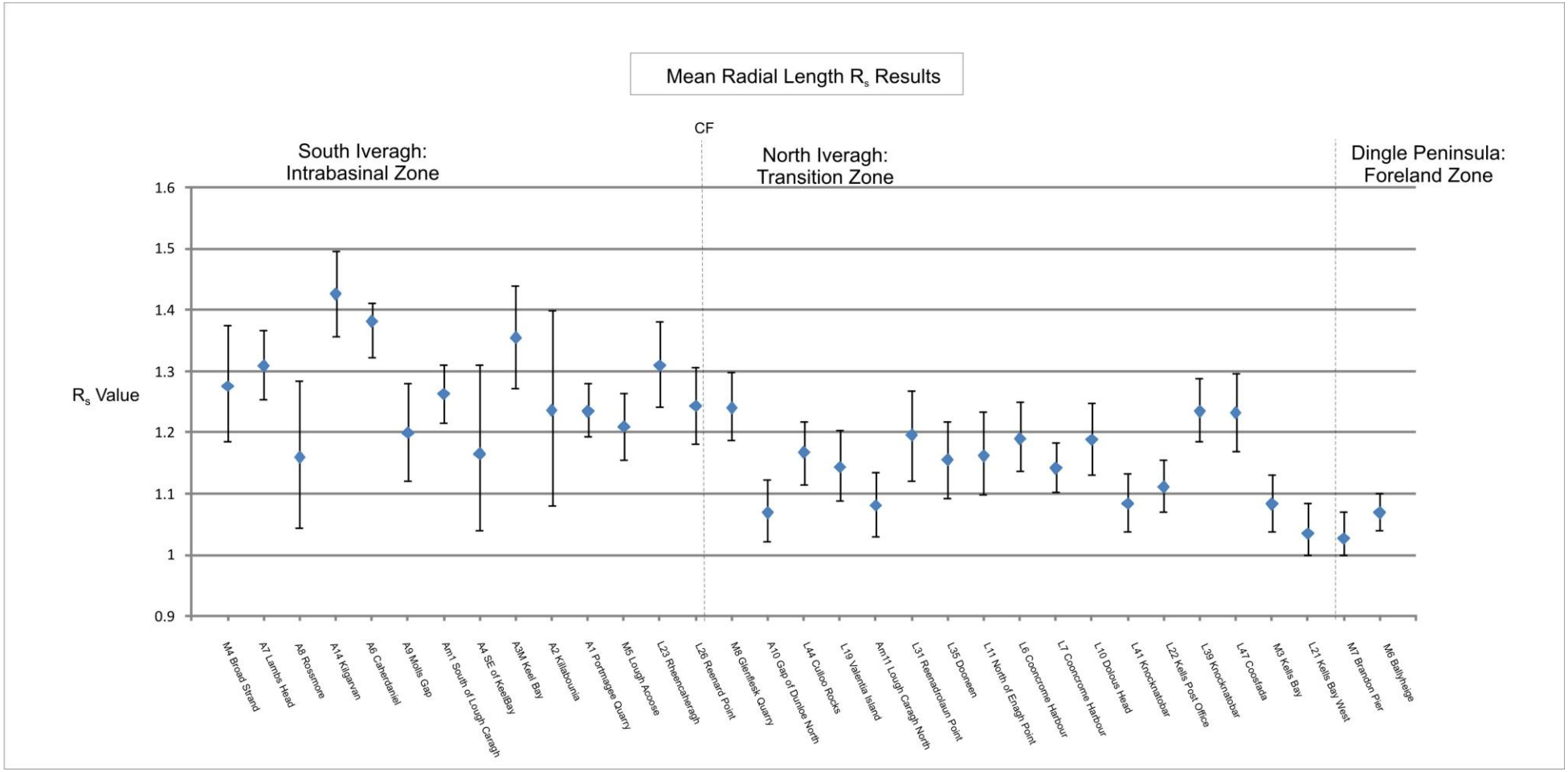

Figure 6.13 -MRL R_s values with upper and lower 95% confidence limits. There is a general decrease in the R_s values from south to north. Locations are plotted on the X-Axis while R_s values are plotted on the Y-Axis. R_s values are higher south of the Coomnacronia Fault (CF) than to the north of it.

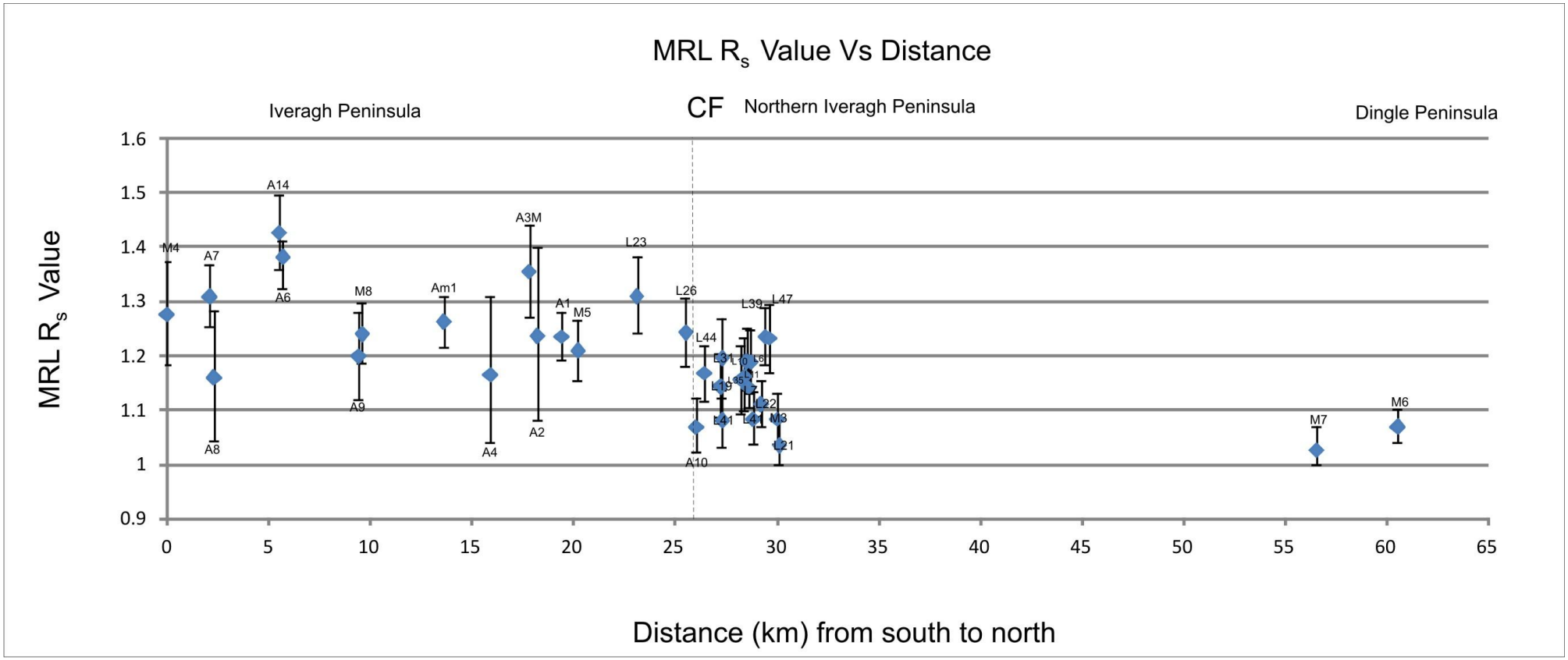

Figure 6.14: MRL R_s values with upper and lower error bars for 95% confidence, plotted against distance in km for the Iveragh Peninsula and Dingle Peninsula. (Note M4 is placed at 0km as it lies outside of the Iveragh Peninsula, to the south).

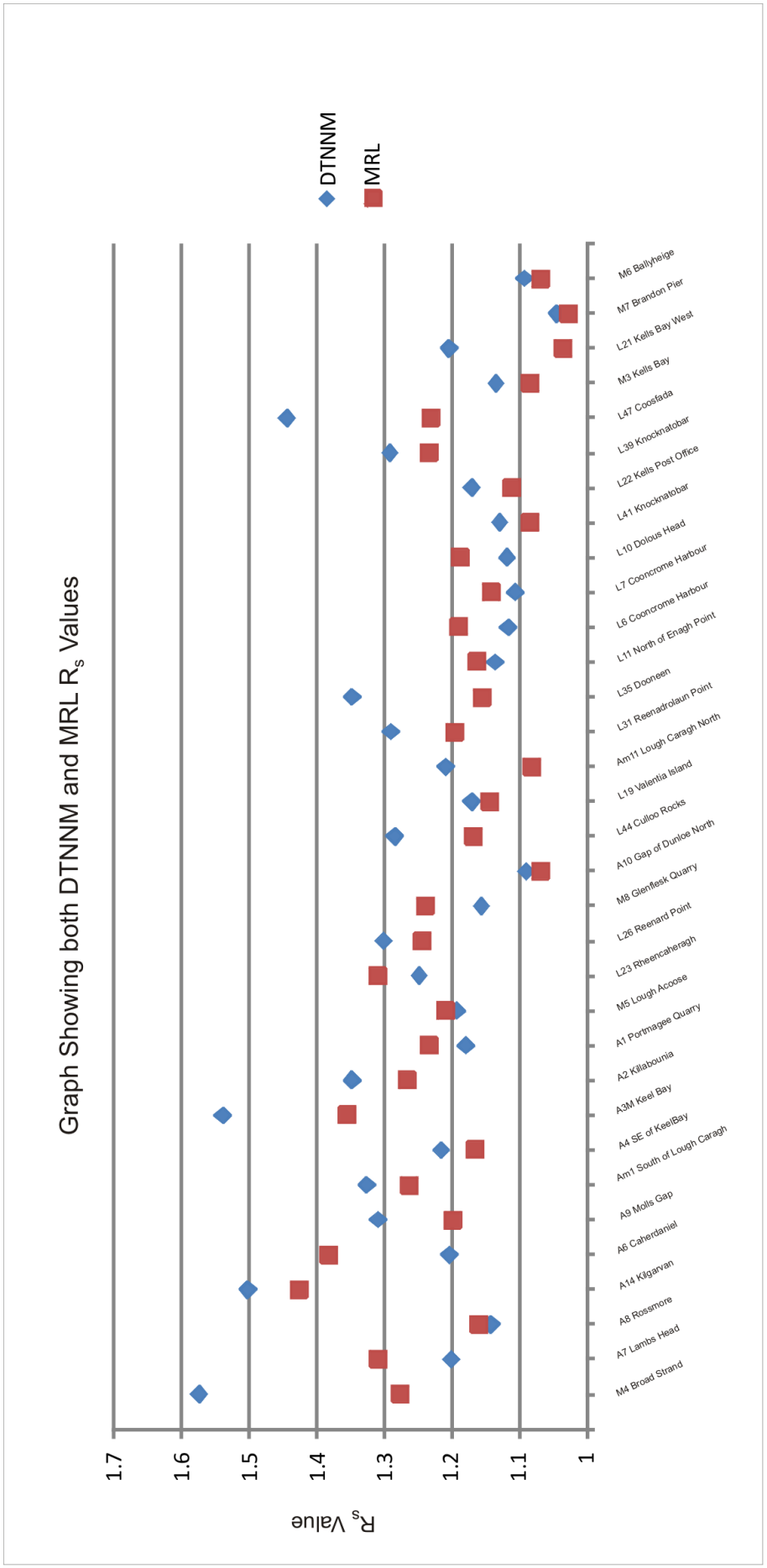

Figure 6.15- shows both the DTNNM and MRL R_s results plotted together on the same graph.

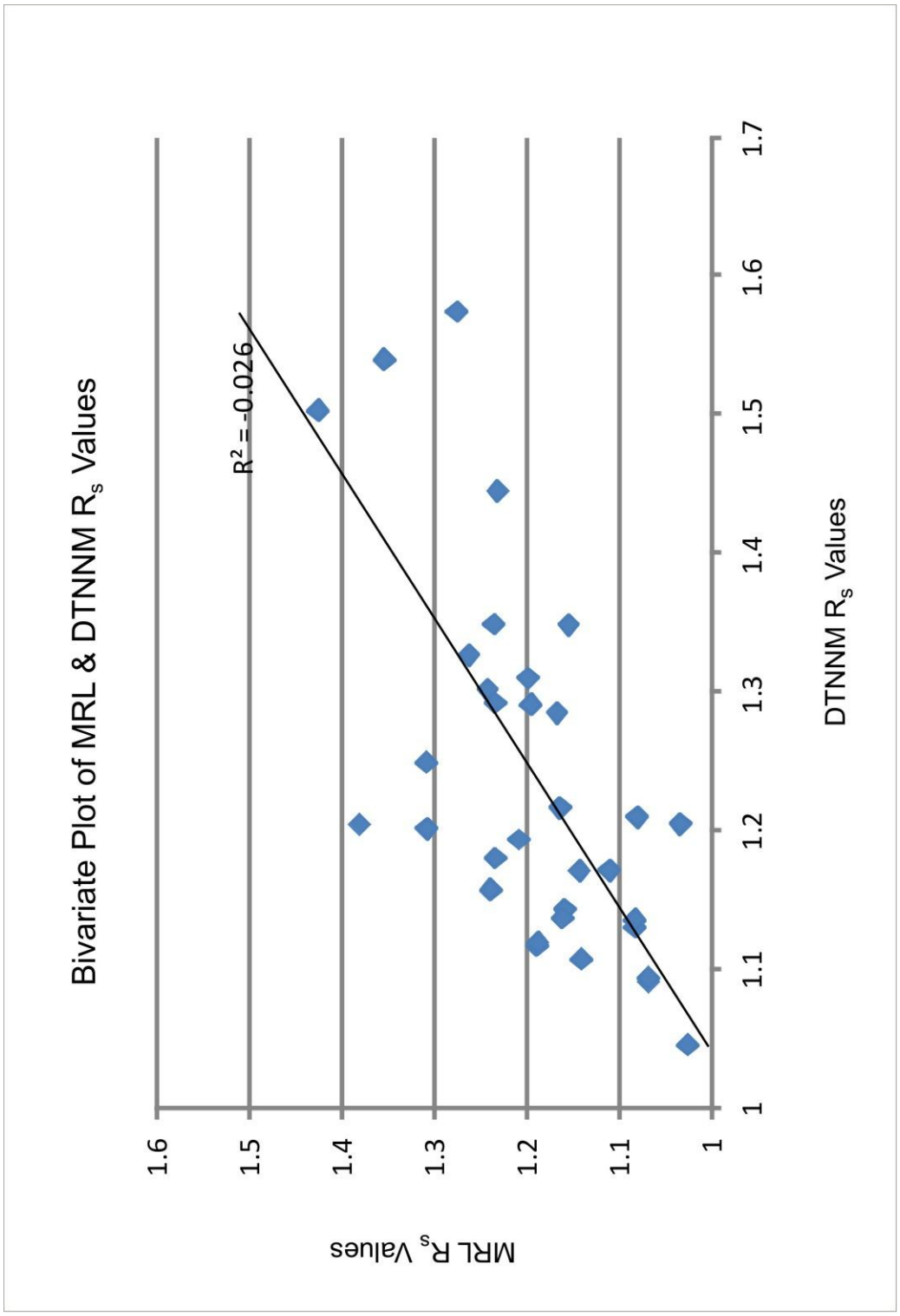

Figure 6.16 Bivariate plot showing R^2 - the correlation coefficient between DTNNM and MRL results in order to show any linear relationship between the two.

6.7 Discussion of DTNNM and MRL R_s Results

There are a number of lower strain values in the Intrabasinal Zone, and these may be a result of the fact that the DTNNM method and MRL results cannot account for smaller grain sizes caused by dynamic recrystallization and brittle deformation – processes that occur in low grade metamorphism (Passchier and Trouw, 2005). In the Intrabasinal Zone some of the grains may have had the centre of their ellipticity changed due to these deformation processes. The long axis of the grain orientation of these grains may still be similar in orientation to the long axis had the grain not be distorted by these processes.

In the Transition Zone there are some occasional higher values for DTNNM strain values. In these samples the ellipticity of the grains as a result of deformation is well preserved, as there is no significant evidence in these samples of dynamic recrystallization, pressure solution processes or grain boundary migration (section 6.10.3). Therefore these grains have had their deformation history well preserved as opposed to some of the grains in the Intrabasinal Zone that have been distorted (section 6.10.3). As previously discussed the DTNNM for these sample may be recording a combination of a preferred orientation due to palaeocurrent directions from the NE-SW and subsequent deformation during early LPS. These grains therefore may show a higher result for the strain analysis. At Coosfada (L47) and Culloo Rocks (L44) the DTNNM values are relatively high. There is a strong LPS fabric at Coosfada and Culloo Rocks. In both of these locations the ϕ value for DTNNM and MRL plot closely to the bedding cleavage intersection lineation indicating that the strain ellipse is tracking the tectonic fabric. The MRL for these locations is lower than the DTNNM. The MRL may be more sensitive to the palaeocurrent in these samples and the DTNNM is sensitive to both the palaeocurrent and the deformation of the matrix by early LPS.

The results from the strain analysis for both the DTNNM and the MRL compare well with the previous field data and AMS data. The DTNNM results are more variable than the MRL results and this suggests that these methods are accounting for different parts of the strain history. The DTNNM may be more closely related to the strain history of the entire sample i.e. quartz clasts and matrix while the MRL method is related to the ellipticity of the quartz grains only. The DTNNM method is carried out on the quartz grains but may be more sensitive to the deformation of the overall fabric including the

micas. Overall however, the DTNNM and MRL results compare well with each other as can be seen from where both DTNNM and MRL are plotted on the same graph (Fig 6.15) and the bivariate plot of MRL against DTNNM (Fig 6.16).

6.8 DTNNM and MRL ϕ Values

The strain analysis has been carried out in the bedding plane, and therefore the calculated DTNNM and MRL ϕ values can be plotted as a lineation pitching on the bedding plane. Plotting the ϕ value as a lineation shows the orientation of the fabric that produces the long axes of the strain ellipse for the DTNNM and MRL methods. For the MRL and DTNNM the ϕ value in Mathematica is the angle that the long axis of the strain ellipse makes with the positive x-axis measured counter-clockwise from the x-axis (Mulchrone, 2002; 2003; Fig 6.2a). ϕ represents the long axis of the overall calculated strain ellipse for both methods (Mulchrone, 2002; Mulchrone et al., 2003). The ϕ value has been plotted as a lineation pitching on the S_0 plane for all of the strain analysis locations and reveals if the strain fabric is related to the regional cleavage, to primary sedimentary processes or is not defined (Fig 6.17 – 6.33). Bedding (S0) and cleavage (S1) are plotted as great circles and the beta axis is obtained in order to approximate the bedding/cleavage intersection lineation (L1). This is done in order to maximize the comparability of 2D lineation (L1) in thin section with the strain analysis data. The ϕ values have also been plotted with the principal AMS axes in order to compare the R_s long axis orientations with AMS axes orientations.

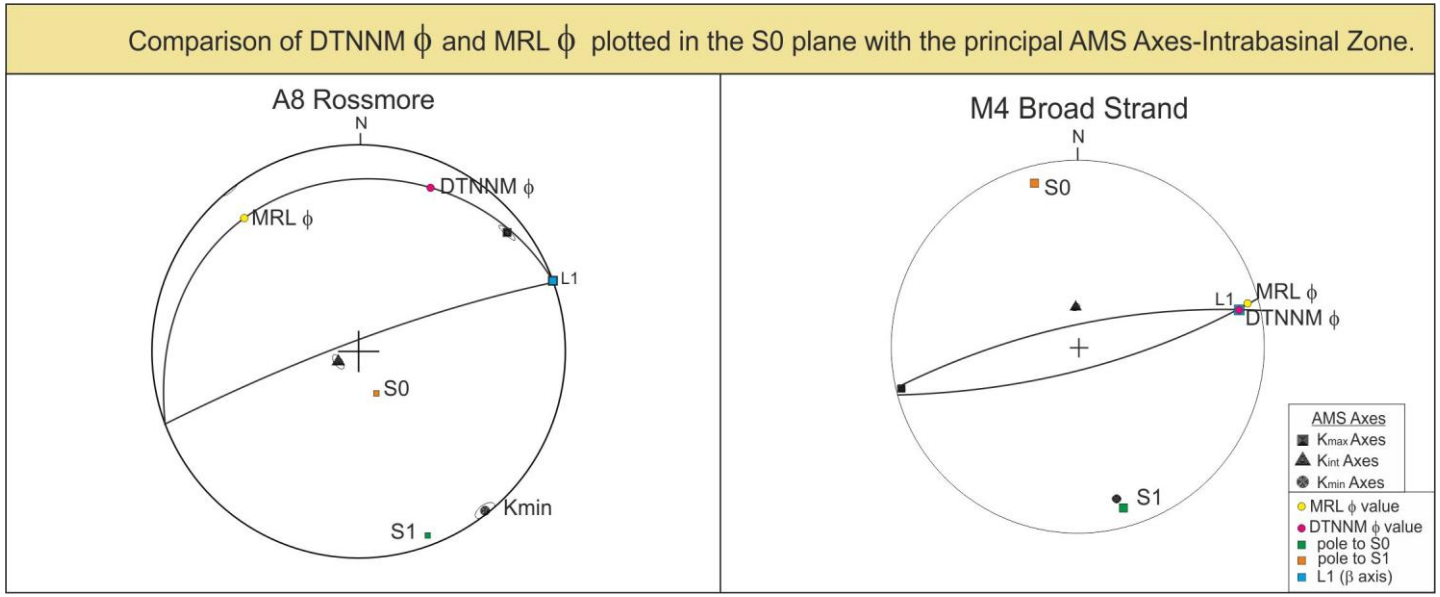

Figure 6.17 Stereonet plots for locations A8 & M4 (Intrabasinal Zone) showing the planes S_0 and S_1 and the AMS principal axes . The ϕ values for DTNNM and MRL are plotted as lineations on the S_0 plane.

Location A8 (Fig 6.17): DTNNM ϕ does not lie particularly close to K_{max} or L_1. MRL ϕ lies closest to the K_{min} axes. This sample has been shown to contain single domain magnetite (Chapter 5: Thermomagnetics) which may have resulted in an inverse fabric. An inverse fabric means that the K_{max} and K_{min} may have swapped places. Therefore MRL may actually lie parallel to K_{max} .DTNNM R_s =1.142 MRL R_s = 1.16. The strain values for both DTNNM and MRL are low. **Location M4 (Fig 6.17)** DTNNM and MRL ϕ lie close to both the L_1 and K_{max} axes. For this location the strain values are relatively high where DTNNM R_s = 1.57 and MRL R_s = 1.276 .This high strain value is associated with ϕ, L_1 and K_{max} coinciding due to the existence of a strong tectonic fabric.

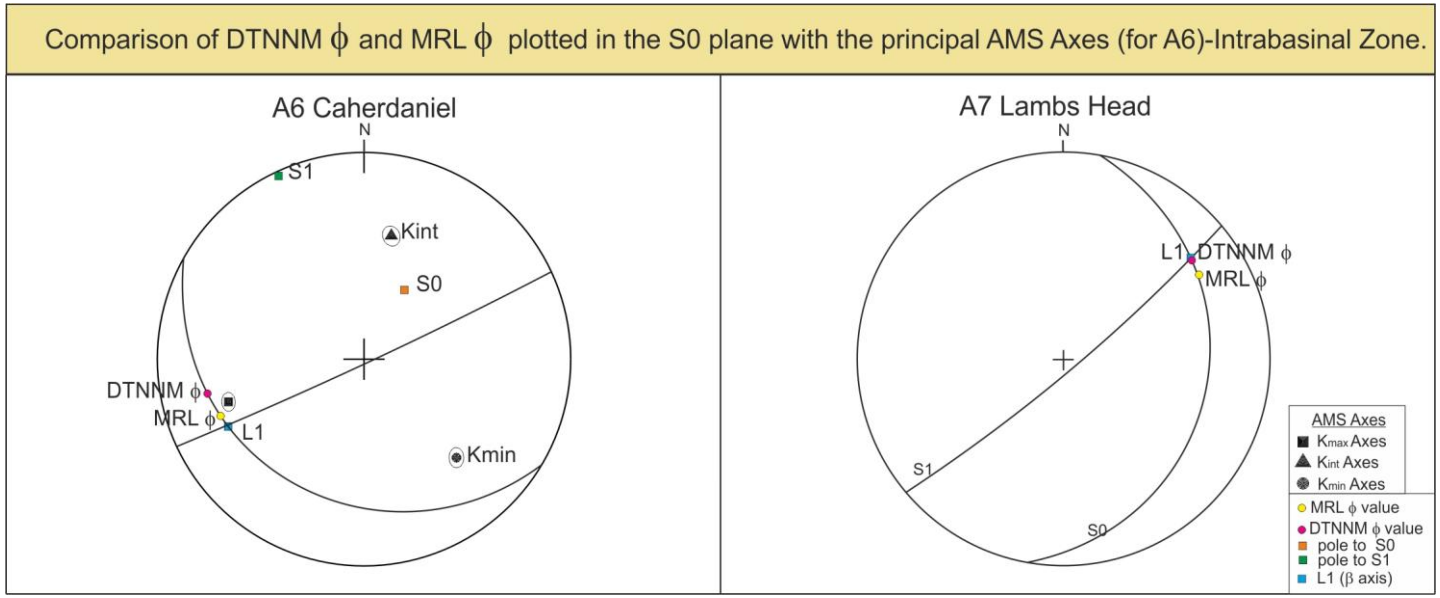

Figure 6.18 Stereonet plots for locations A6 & A7 (Intrabasinal Zone) showing the planes S_0 and S_1 and the AMS principal axes (for A6). The ϕ values for DTNNM and MRL are plotted as lineations on the S_0 plane.

Location A6 (Fig 6.18): DTNNM and MRL ϕ lie close to both the K_{max} axes and L_1. Strain values are relatively moderate to high with DTNNM R_s =1.204 and MRL R_s = 1.382. **Location A7 (Fig 6.18):** DTNNM and MRL ϕ lie close to L_1. DTNNM R_s =1.201 MRL R_s = 1.30

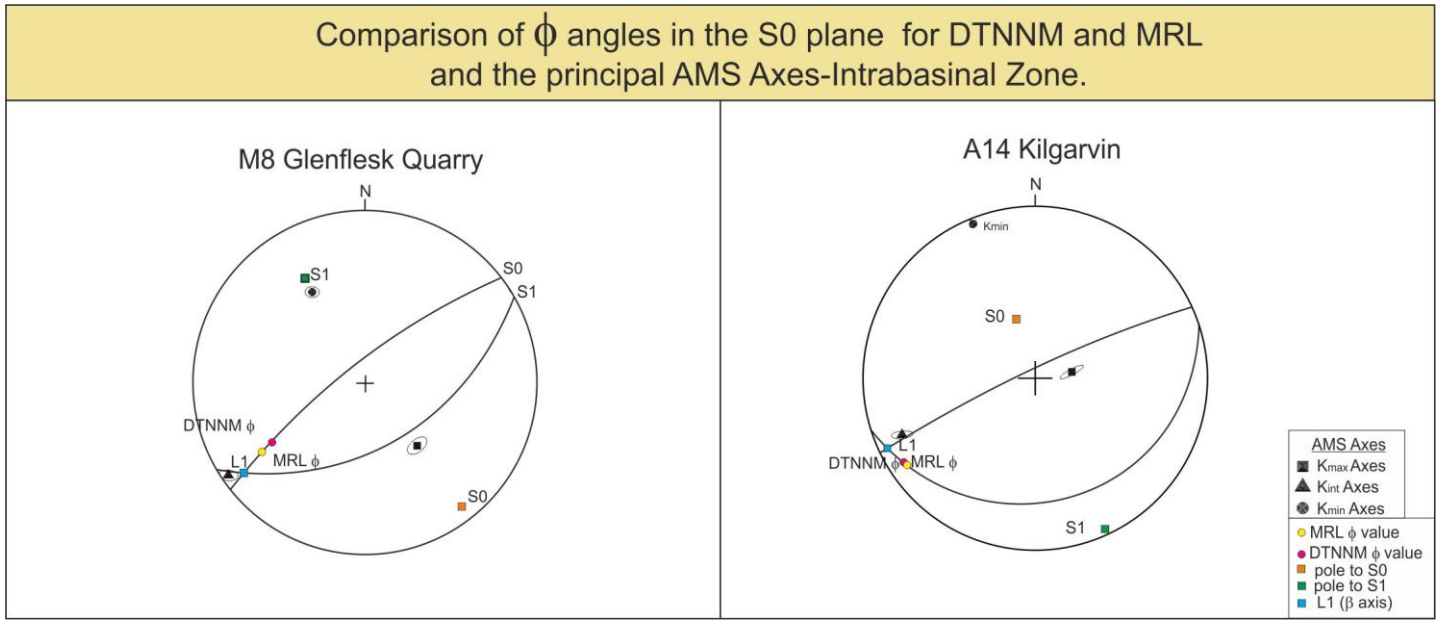

Figure 6.19 Stereonet plots for locations M8 & A14 (Intrabasinal Zone) showing the planes S_0 and S_1 (where applicable) and the principal AMS axes. The ϕ values for DTNNM and MRL are plotted as lineations on the S_0 plane.

Location M8 (Fig 6.19): DTNNM and MRL ϕ both lie close to L_1 and the K_{int} axes. The strain value for DTNNM R_s =1.157 and MRL R_s = 1.24 which is relatively moderate to high. **Location A14 (Fig 6.19):** DTNNM and MRL ϕ both lie close to K_{int} and L_1. The strain values for this location are high with DTNNM R_s = 1.503 and MRL R_s = 1.42

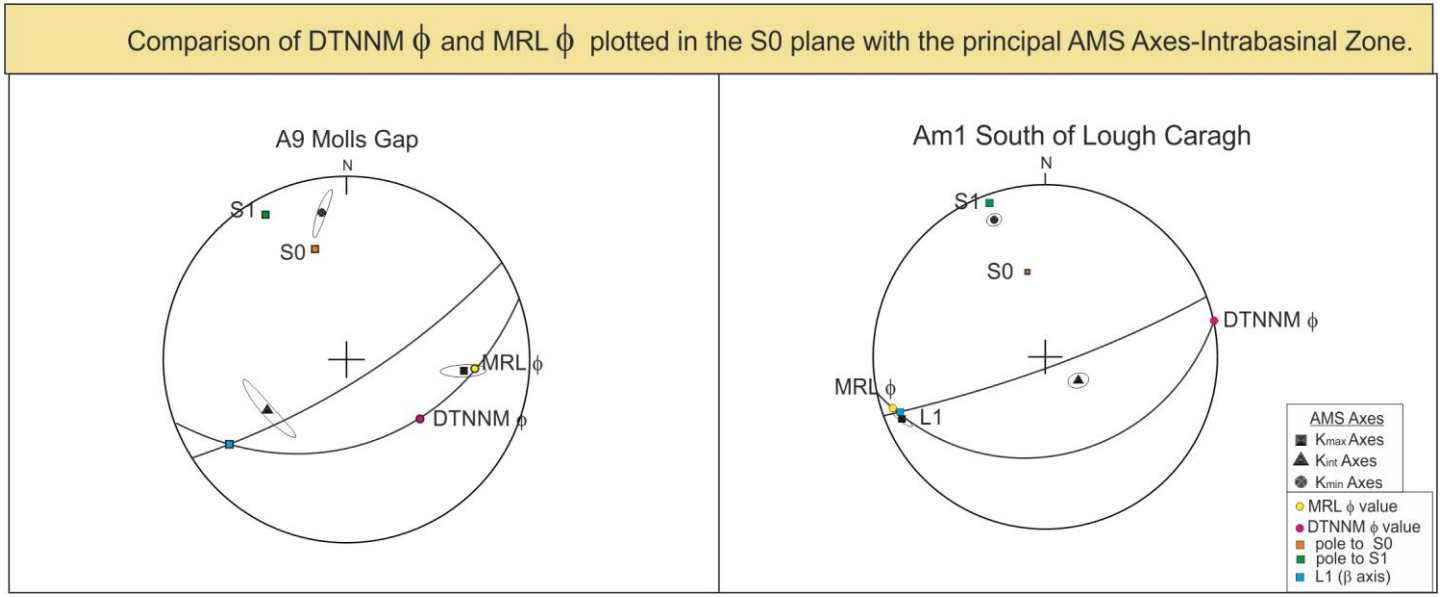

Figure 6.20 Stereonet plots for locations A9 & AM1 (Intrabasinal zone) showing the planes S_0 and S_1 and the principal AMS axes. The ϕ values for DTNNM and MRL are plotted as lineations on the S_0 plane.

Location A9 (Fig 6.20): DTNNM ϕ does not lie particularly close to any of the axes or to L1. MRL ϕ lies very close to K_{max} .DTNNM R_s =1.309 and MRL R_s = 1.199. **Location AM1 (Fig 6.20):** DTNNM and MRL ϕ lie close to K_{max} and L_1.The strain values are relatively high with DTNNM R_s = 1.326 and MRL R_s = 1.263

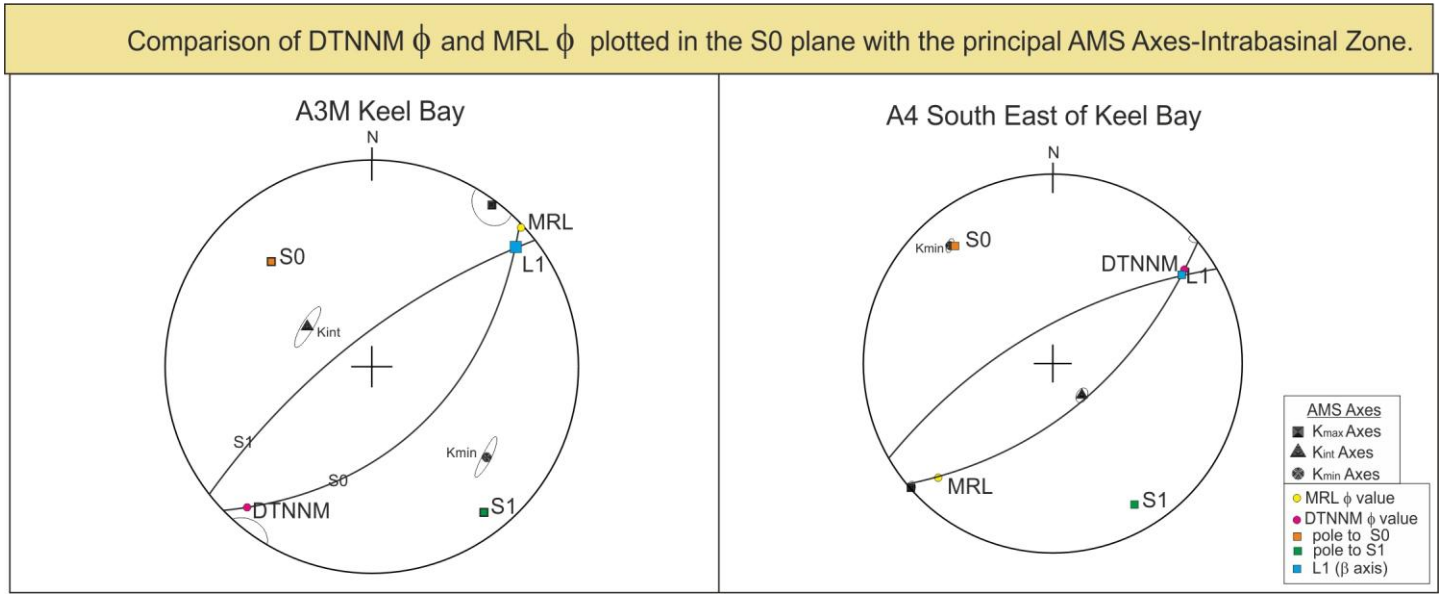

Figure 6.21 Stereonet plots for locations A3M & A4 (Intrabasinal zone) showing the planes S_0 and S_1 and the AMS principal axes. The ϕ values for DTNNM and MRL are plotted as lineations on the S_0 plane.

Location A3M (Fig 6.21): DTNNM and MRL ϕ lie very close to L_1 and also close to the K_{max} axes. Both DTNNM and MRL ϕ lie slightly closer to L_1 than to $K_{max.}$ The strain values are relatively high with DTNNM R_s = 1.539 and MRL R_s = 1.355. **Location A4 (Fig 6.21):** DTNNM and MRL ϕ lie close to K_{max} and L_1. DTNNM R_s =1.216 and MRL R_s = 1.16

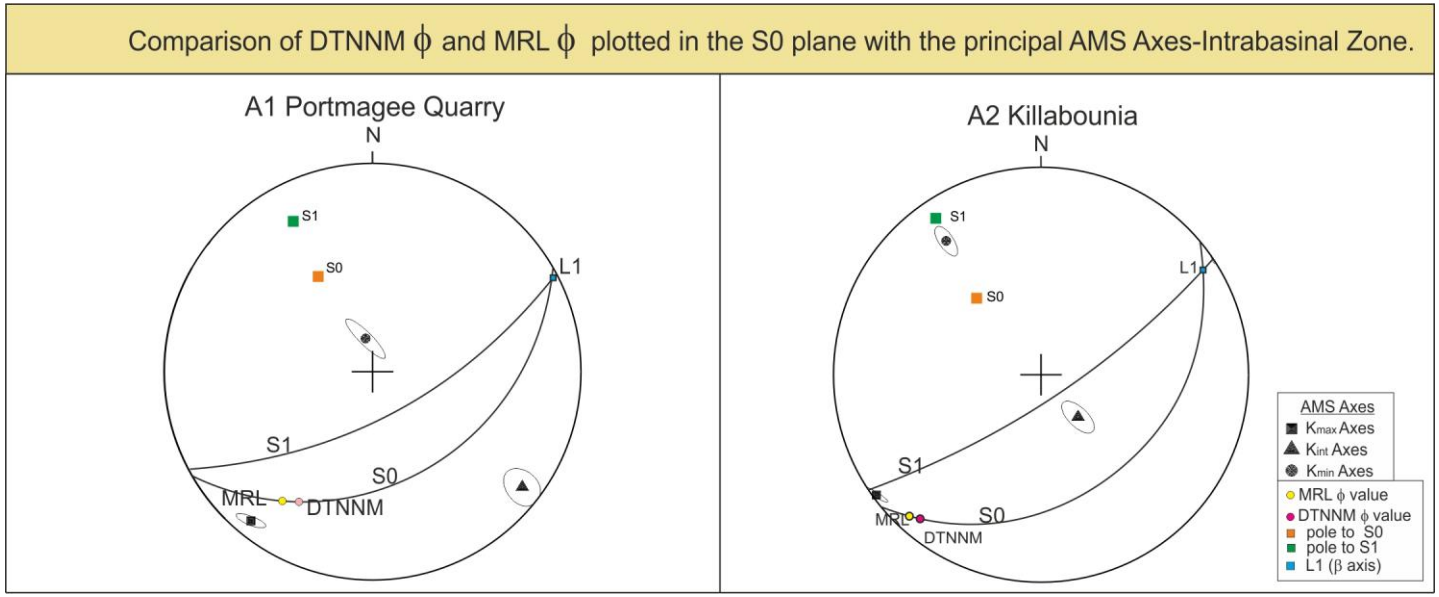

Figure 6.22 Stereonet plots for locations A1 & A2 (Intrabasinal zone) showing the planes S_0 and S_1 and the AMS principal axes. The ϕ values for DTNNM and MRL are plotted as lineations on the S_0 plane.

Location A1 Portmagee Quarry (Fig 6.22): DTNNM and MRL ϕ lie close to the K_{max} axes and moderately close to L_1.In this case DTNNM and MRL ϕ are interpreted to represent L1. As discussed in Chapter 5, the AMS ellipsoid is interpreted to represent a 10° anticlockwise rotation of K_{max} from L1 due to further tectonic strain. This may be the case for DTNNM and MRL also. The strain values for DTNNM is moderate where R_s =1.179 and higher for MRL where R_s = 1.235.**Location A2 Killabounia (Fig 6.22):** Both the DTNNM and MRL ϕ values lie close to the K_{max} axes and L_1. The strain values are relatively high with DTNNM R_s =1.348 and MRL R_s =1.26

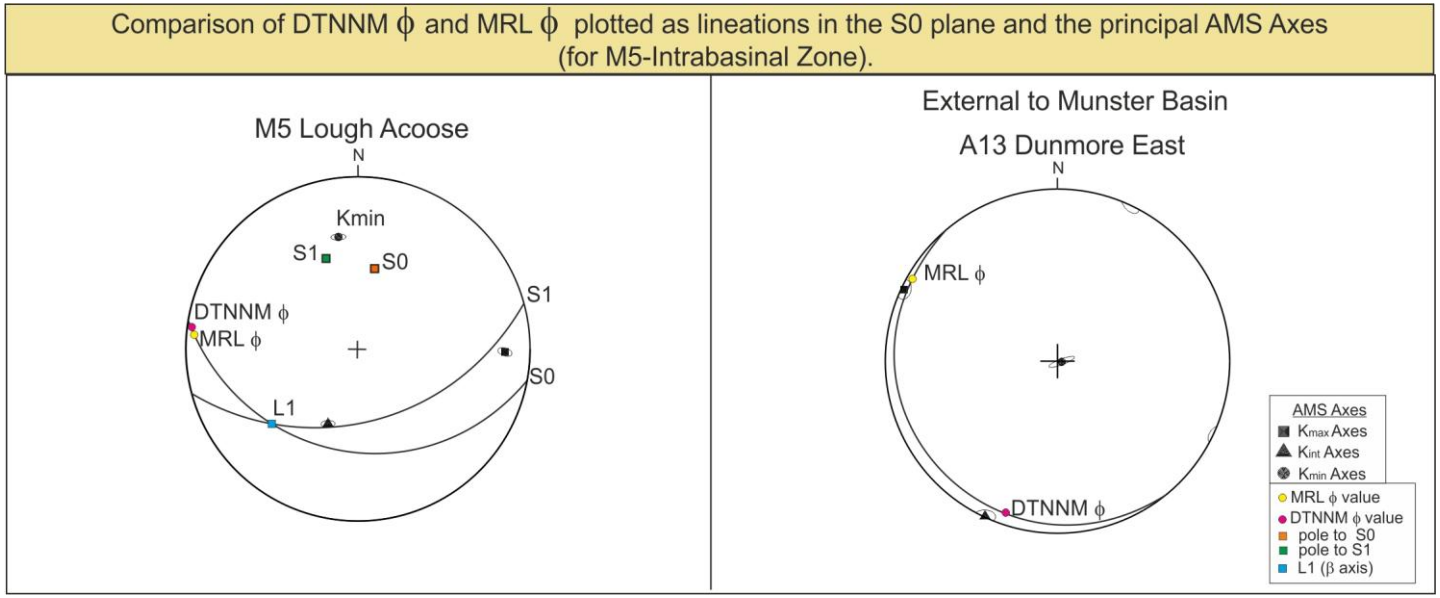

Figure 6.23 Stereonet plots for locations M5 & A13 showing the planes S_0 and S_1 and the principal AMS axes. The ϕ values for DTNNM and MRL are plotted as lineations on the S_0 plane.

Location M5 (Fig 6.23): DTNNM and MRL ϕ lie close to K_{max} but not close to L_1. DTNNM R_s =1.193 and MRL R_s = 1.21.**Location A13 (Fig 6.23):** DTNNM ϕ lies very close to the K_{int} axes and MRL ϕ lies very close to the K_{max} axes. DTNNM R_s = 1.292 and MRL R_s = 1.09. Even at a low strain value MRL lies close to K_{max}. This sample is taken from the Brownstown Head member of the Templetown Fm. in Dunmore East. This basin was a separate basin from the Munster Basin ,which lay to the east of the Munster Basin. Palaeocurrents for the Brownstown Member are mostly orientated in a NNE direction (Ori and Penney, 1982).The DTNNM ϕ and the K_{int} axes may represent a NNE palaeocurrent oreintation while the MRL ϕ may be inicative of cross bedding which has also been documented in the area (Ori and Penney, 1982).

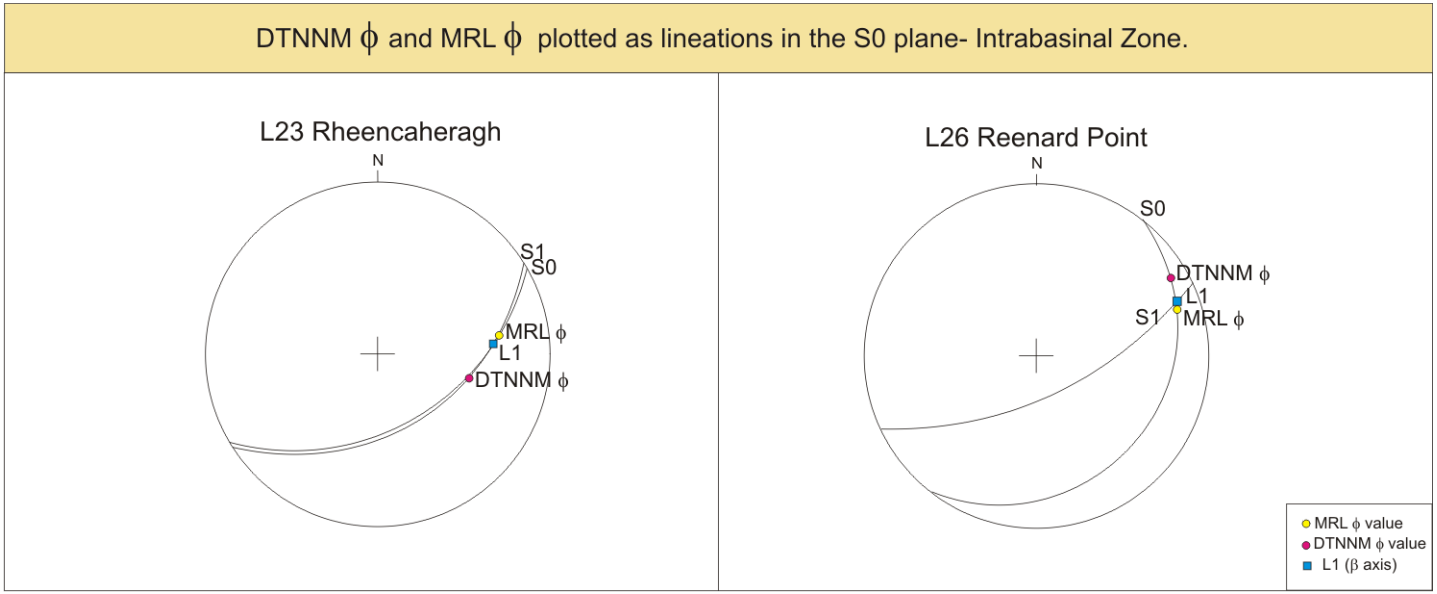

Figure 6.24 Stereonet plots for locations L23 & L26 (Intrabasinal Zone) showing the planes S_0 and S_1.The ϕ values for DTNNM and MRL are plotted as lineations on the S_0 plane.

Location L23 (Fig 6.24): DTNNM and MRL ϕ lie close to L_1. DTNNM R_s =1.249 and MRL R_s = 1.310. **Location L26 (Fig 6.24):** DTNNM and MRL ϕ lie close to L_1. DTNNM R_s =1.301 and MRL R_s = 1.243

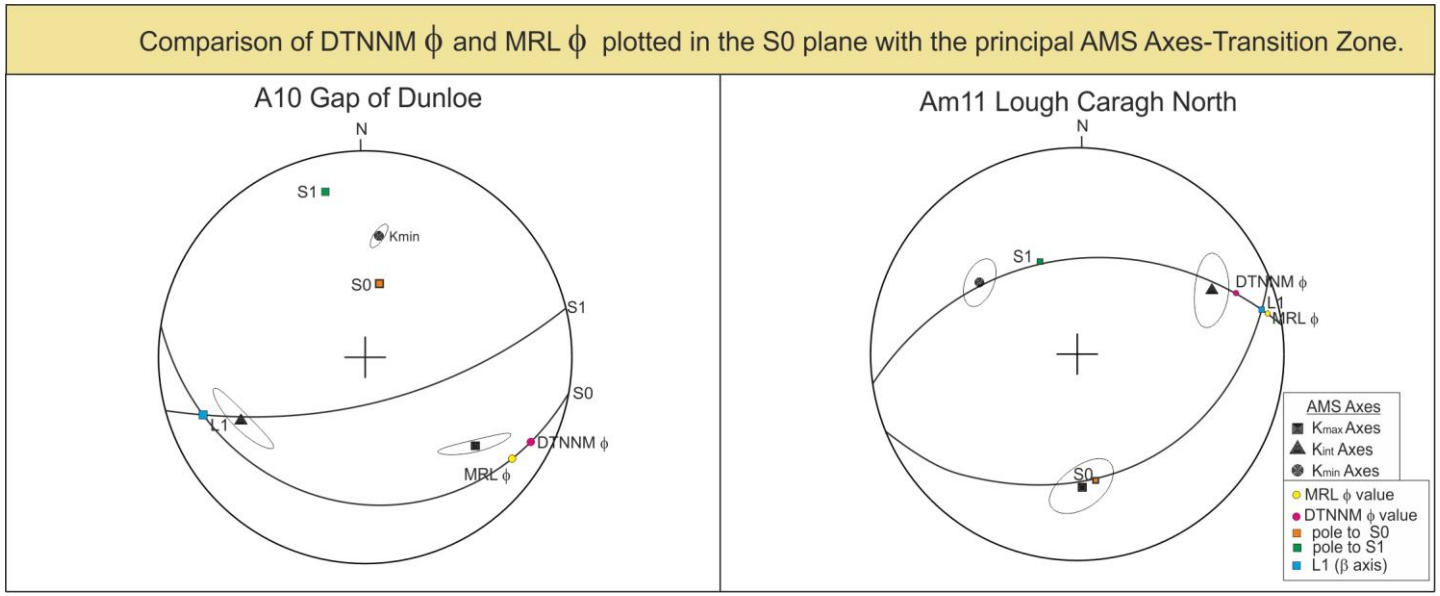

Figure 6.25 Stereonet plots for locations A10 & AM11 (Transition Zone) showing the planes S_0 and S_1 and the AMS principal axes . The ϕ values for DTNNM and MRL are plotted as lineations on the S_0 plane.

Location A10 (Fig 6.25): DTNNM and MRL ϕ both lie close to the K_{max} axes. The strain values are low with DTNNM R_s = 1.09 and MRL R_s = 1.069. A10 lies just to the north of the Black Lake Fault, Gap of Dunloe, in the Transition Zone. This sample demonstrates that even at low strains DTNNM andMRL show a close correlation with the K_{max} axes. **Location AM11 (Fig 6.25):** DTNNM and MRL ϕ lies close to both L_1 and $K_{int.}$ DTNNM R_s = 1.209 MRL R_s = 1.081.

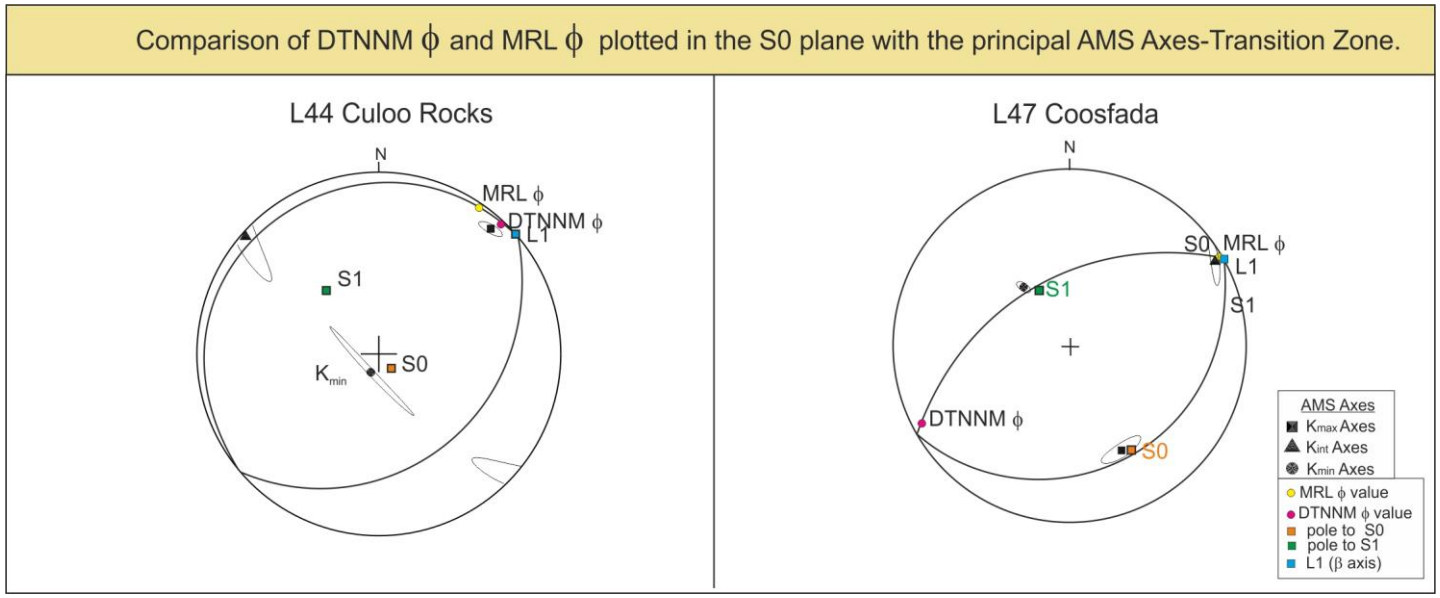

Figure 6.26 Stereonet plots for locations L44 & L47 (Transition Zone) showing the planes S_0 and S_1 and the AMS principal axes. The ϕ values for DTNNM and MRL are plotted as lineations on the S_0 plane.

Location L44 (Fig 6.26): DTNNM and MRL ϕ lie close to both the K_{max} axes and L_1. DTNNM R_s = 1.284 MRL R_s = 1.168. **Location L47 (Fig 6.26): :** DTNNM and MRL ϕ lie close to L_1 and the K_{int} axes. DTNNM R_s = 1.444 and MRL R_s = 1.232. The DTNNM at L47 and L44 are relatively high. For both of these samples, this may be due to the orientation of the beds during deformation. K_{max} is trending NE-SE possibly indicating some palaeocurrent control. At L47 and L44, the fabric has been interpreted as an early LPS fabric both in the field and by the AMS stereonets (Chapter 4 and Chapter 5). The DTNNM R_s value may be measuring a combination of both the palaeocurrent lineation and subsequent early LPS which occurred in the same trend as the palaeocurrent lineation.

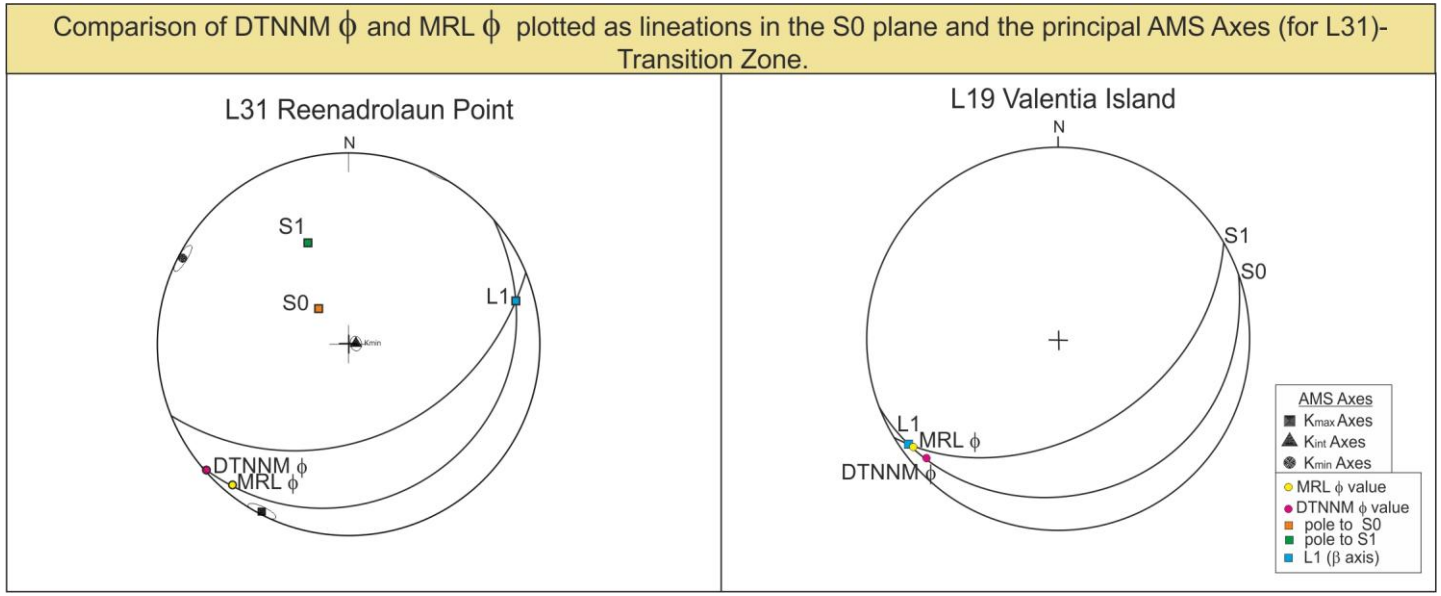

Figure 6.27 Stereonet plots for locations L31 & L19 (Transition Zone) showing the planes S_0 and S_1 and the AMS principal axes for L31. The ϕ values are plotted as lineations for DTNNM and MRL on the S_0 plane.

Location L31 (Fig 6.27): Both DTNNM and MRL ϕ lie close to the average K_{max} axis which lies closer to a NE-SW palaeocurrent direction but also moderately close to L_1. DTNNM and MRL ϕ and K_{max} in this case more likely represents a palaeocurrent direction.Strain values: DTNNM = 1.29 and MRL= 1.196. **Location L19 (Fig 6.27):** DTNNM and MRL ϕ both lie close to L_1.The strain values are relatively low with DTNNM R_s = 1.17 and MRL R_s = 1.144.

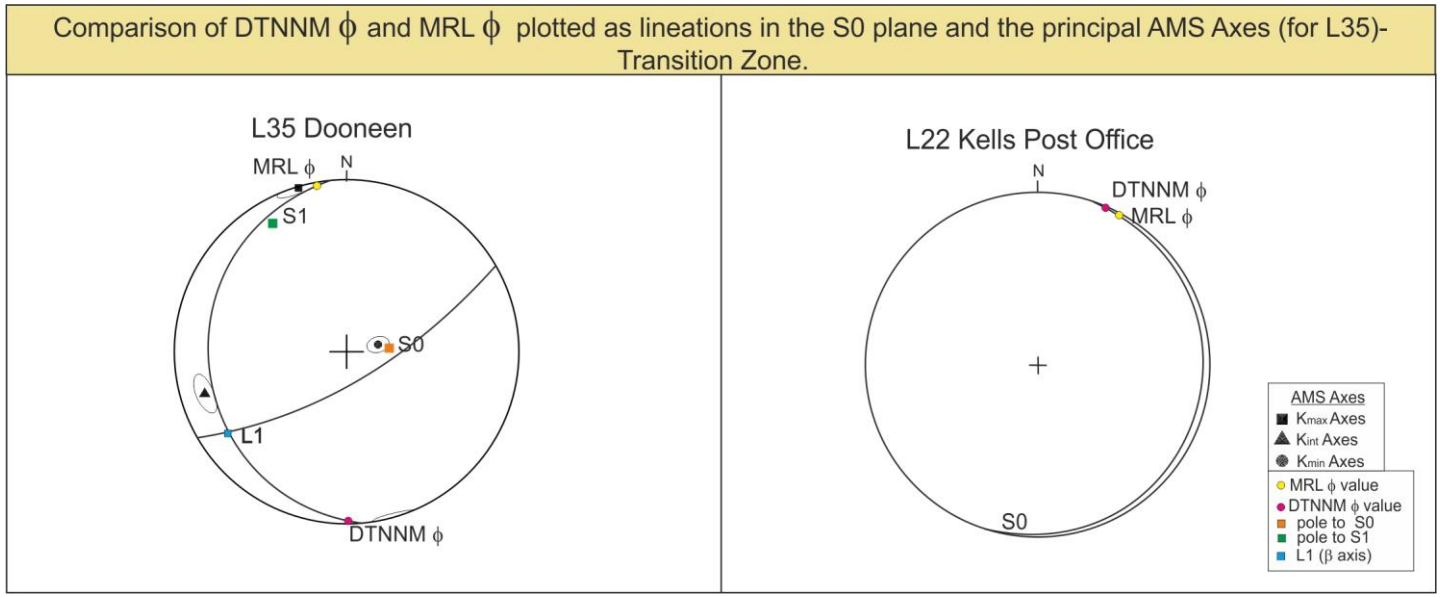

Figure 6.28 Stereonet plots for locations L35 & L22 (Transition Zone) showing the planes S_0 .The DTNNM and MRL ϕ values are plotted as lineations on the S_0 plane.

Location L35 (Fig 6.28): Both MRL ϕ and DTNNM ϕ lies closer to K_{max} and the pole to S1. This strain value for DTNNM is relatively high where R_s = 1.34795. MRL R_s is lower and mostly reflects the strain of the quartz clasts = 1.15595. Due to their orientation MRL, DTNNM and K_{max} may be more related to a northerly paleaocurrent direction as they do not lie close to L1. **Location L22 (Fig 6.28):** There is no S_1 recorded in the field in this location. DTNNM and MRL ϕ possible represent a NE-SW palaeocurrent lineation. MRL = 1.111 DTNNM = 1.171. DTNNM and MRL ϕ are unlikely to represent a tectonic lineation (L1) as the nearest cleavage reading is orientated approximately 082 75 S (Map Insert 1: Cleavage Results).

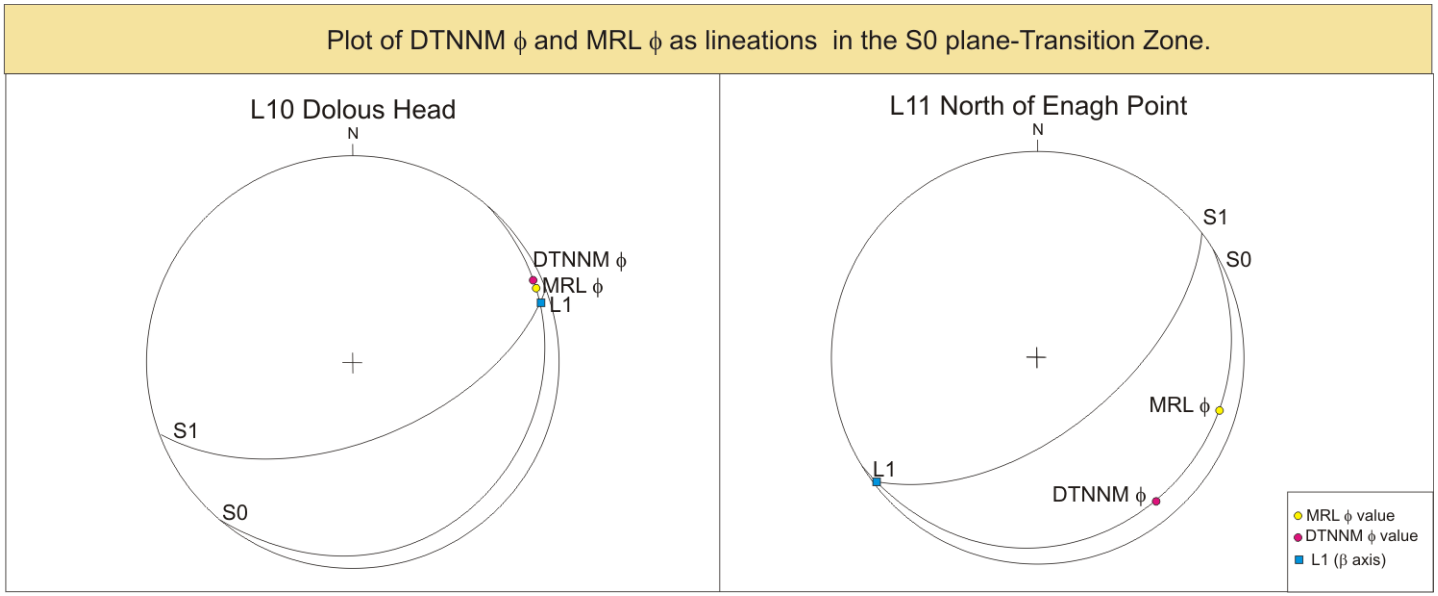

Figure 6.29 Stereonet plots for locations L10 & L11 (Transition zone) showing the planes S_0 and S_1. The ϕ values for DTNNM and MRL are plotted as lineations on the S_0 plane.

Location L10 (Fig 6.29): DTNNM and MRL ϕ lie very close to L_1. DTNNM R_s = 1.119 MRL R_s = 1.189. **Location L11 (Fig 6.29):** DTNNM and MRL ϕ do not lie close to L_1. This may be due to the lack of a dominant tectonic fabric. The strain value for MRL at L11 is 1.16224 and for DTNNM is 1.13601. This is a low strain sample with no distinct linear fabric.

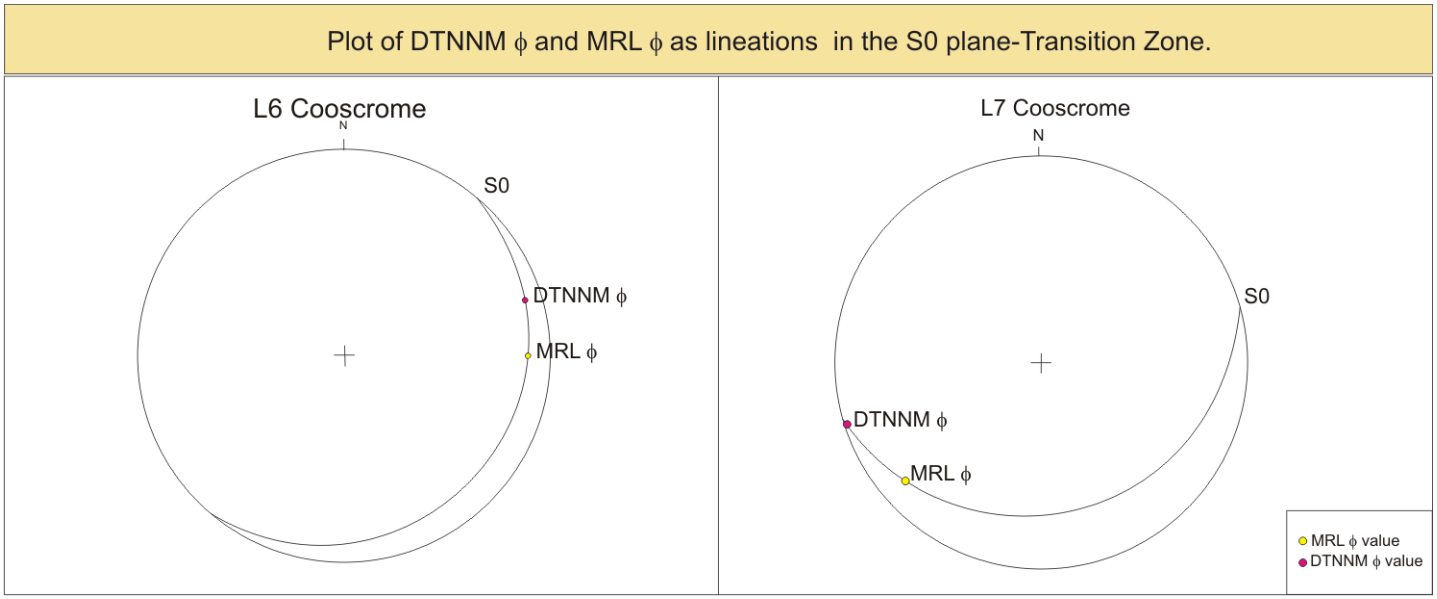

Figure 6.30 Stereonet plots for locations L6 & L7 (Transition zone) showing the planes S_0 and S_1 (where applicable). The ϕ values for DTNNM and MRL are plotted as lineations on the S_0 plane.

Location L6 (Fig 6.30): No cleavage was found at this site however DTNNM ϕ could possible be tracking a regional tectonic fabric. DTNNM ϕ may lie close to an expected L_1 as the cleavage in this area strikes 058 °. DTNNM R_s = 1.117 MRL R_s = 1.190. **Location L7(Fig 6.30):** DTNNM ϕ possible lies close to a regional L_1 MRL lies closer to a NE-SW palaeocurrent orientation. DTNNM ϕ may lie close to an expected L_1 as the cleavage in this area strikes 058 °. DTNNM R_s = 1.106 MRL R_s = 1.142.

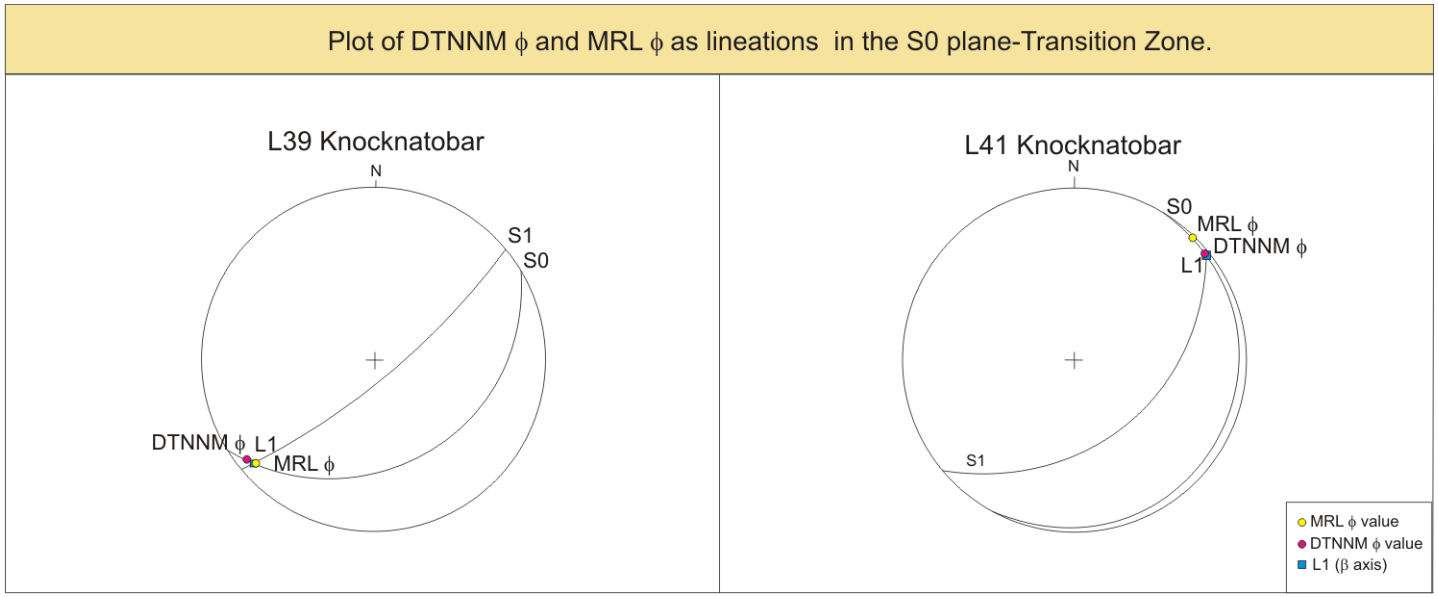

Figure 6.31 Stereonet plots for locations L39 & L41(Transition Zone) showing the planes S_0 and S_1 .The ϕ values for DTNNM and MRL are plotted as lineations on the S_0 plane.

Location L39 (Fig 6.31): DTNNM and MRL ϕ lie close to L_1. DTNNM R_s = 1.292 MRL R_s = 1.235.**Location L41 (Fig 6.31):** DTNNM and MRL ϕ lie close to L_1. DTNNM R_s = 1.129 MRL R_s = 1.084.

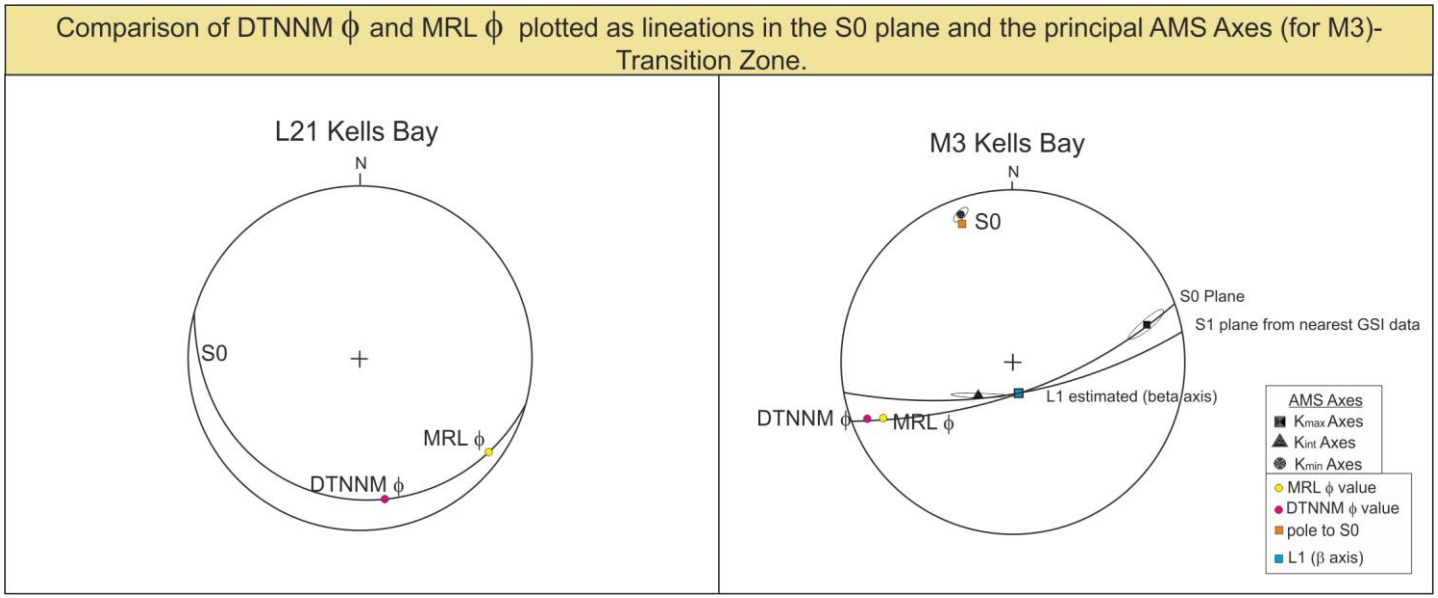

Figure 6.32 Stereonet plots for locations L21 and M3 (Transition Zone) showing the planes S_0 and S_1 and the principal AMS axes for M3. The ϕ values are plotted as lineations for DTNNM and MRL on the S_0 plane.

Location L21 (Fig 6.32): No cleavage has been found at this site. It is unlikely that DTNNM ϕ and MRL ϕ are tracking a regional tectonic fabric as they do not lie close to an expected L_1 for the area (Location L21 lies aprox 300 m from M3). Neither DTNNM or MRL appear to be representing any distinct fabric. This is reflected in the low strain values for L21 for MRL R_s = 1.035. DTNNM R_s = 1.204. **Location M3 (Fig 6.32):** Both DTNNM and MRL ϕ plot close to the K_{max} axes of the AMS ellipsoid. ϕ in this case may be representative of a palaeocurrent lineation trending NE –SW. L_1 is represented by the K_{int} axes and is not close to ϕ for DTNNM or MRL. DTNNM and MRL for M3 may therefore be mostly influenced by sedimentary features. The strain values for M3 are low with DTNNM R_s = 1.135 and MRL R_s = 1.083.

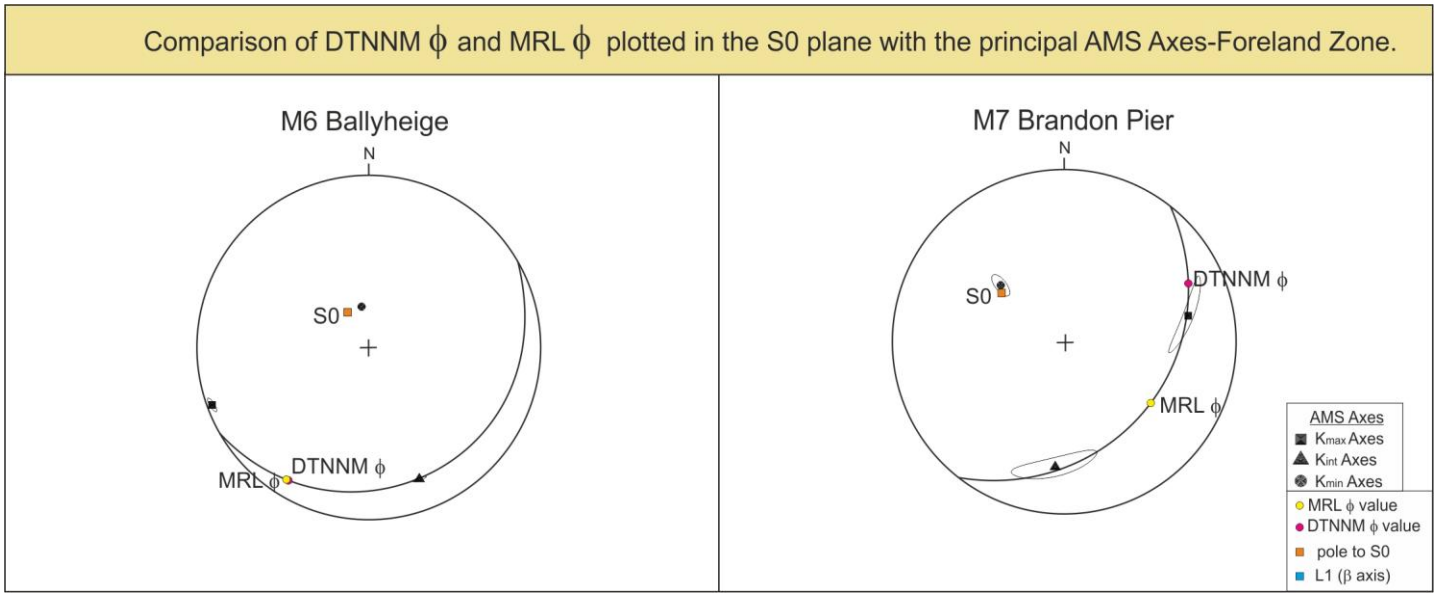

Figure 6.33 Stereonet plots for locations M6 and M7 showing the planes S_0 (No S1 found at locations). The ϕ values for DTNNM and MRL are plotted as lineations on the S_0 plane.

Location M6: (Fig 6.33): MRL and DTNNM ϕ plot close together but do not lie particularly close to any of the AMS axes. This is reflected in the low strain values: MRL = 1.093 and DTNNM = 1.069. There is no S1 in this area. MRL and DTNNM ϕ may be represenative of a NE-SW palaeocurrent lineation.**Location M7 (Fig 6.33):** The AMS fabric is strongly girdled in this location (Chapter 5). DTNNM ϕ lies close to K_{max} . There is not a strong relationship between MRL ϕ and any of the axes. DTNNM ϕ may be representative of a NE-SW palaeocurrent lineation. This is reflected in low strain values where MRL R_s = 1.027 and DTNNM R_s = 1.045.

6.9 Discussion of Results - ϕ and AMS

Relating the ϕ orientation with the principal AMS axes can help reveal what fabrics the ϕ value is representing and hence the strain analysis results. Table 6.3 summarizes the relationship of DTNNM and MRL ϕ values, the ϕ orientations, the principal AMS axes (for the AMS locations), the AMS ellipsoid interpretation and gives an interpretation of what ϕ represents in the field.

- **The Intrabasinal Zone**

In the Intrabasinal zone, as previously discussed there are generally higher R_s strain values for both DTNNM and MRL. In many of the AMS location, in the Intrabasinal Zone, the ϕ orientations for DTNNM and MRL ϕ mostly coincide with the K_{max} axes and/or L_1 with the associated AMS ellipsoids controlled by S1 (cleavage). In some of the AMS samples, DTNNM and MRL ϕ lies close to K_{int} and L_1 and the AMS ellipsoid is S1 controlled. In the locations that have not been analysed using AMS, DTNNM and MRL ϕ generally lie parallel to sub-parallel to the L_1 direction. The above indicates that for the Intrabasinal Zone the long axes of strain ellipsoid for MRL and DTNNM parallel the regional tectonic extension direction. In the Intrabasinal Zone, there are some notable cases where the DTNNM and MRL ϕ lie closer to the AMS K_{max} axes and the K_{max} axes do not lie particularly close to L_1. At location A1: Portmagee Quarry, the DTNNM and MRL ϕ both plot closer to the K_{max} axes than they do with L_1. At A1: Portmagee, the K_{max} axes have been rotated 10° from the L_1 orientation as a result of further deformation (See chapter 5-AMS results). Also, at location M5 the DTNNM and MRL ϕ both plot closer to the K_{max} axes than they do with L_1. This again may indicate that the strain fabric recorded by DTNNM and MRL is closely related to the K_{max} axes of the AMS ellipsoid, which may indicate a rotation of the AMS axes due to further deformation as in sample A1.

- **The Transition Zone**

As previously discussed the strain values in the Transition Zone are generally lower but with some occasional anomalously high values.

In many cases in the Transition Zone, DTNNM and MRL ϕ lie close to either:

- L_1 and the K_{max} axes or

- L_1 and the K_{int} axes or
- L1 (on samples with no AMS analysis).

This indicates that for most cases DTNNM and MRL are tracking the regional tectonic fabric even in cases of low strain. In the Transition Zone there are more occurrences of DTNNM and MRL ϕ coinciding with L_1 and K_{int} than there is in the Intrabasinal Zone indicating that K_{int} plays a greater role in representing the extensional direction due to lower strain. Also DTNNM and MRL ϕ track L_1 where L_1 is part of an early LPS fabric as interpreted by the AMS ellipsoids.

In some cases, DTNNM and/or MRL ϕ coincides with the K_{max} axes and the K_{max} axes does not lie close to L_1, but instead lies closer to a NE-SW trend. At these locations ϕ and K_{max} are interpreted to represent a NE-SW palaeocurrent direction as is documented in the literature on the Munster Basin (Graham, 1983; Russell, 1984; Williams et al., 1989)

In some locations no tectonic cleavage is present, however an estimation of where the regional tectonic cleavage would be expected to lie (if plotted), results in the DTNNM and MRL ϕ values being plotted in close proximity to the expected lineations e.g. Locations: (L6 & L7).

In the Transition zone in some locations the MRL and DTNNM ϕ value does not coincide with L_1 or a principal AMS axes and this is associated with low strain values - these locations are interpreted as low strain with no distinct tectonic fabric:

L11: DTNNM and MRLϕ not distinctly represented.
L21: DTNNM and MRLϕ not distinctly represented.
M7: MRLϕ not distinctly represented.

Table 6.3: shows the strain analysis locations in order from south to north and summarizes the interpretation for DTNNM ϕ and MRL ϕ.

Location (from south to north). * = AMS location	**DTNNM ϕ lies closest to:**	**DTNNM R_s value**	**DTNNM ϕ interpreted to represent:**	**MRL ϕ lies closest to:**	**MRL Rs value**	**MRL ϕ interpreted to represent:**	**AMS ellipsoid interpreted to represent**	**Zone**
M4-Broad Strand*	$K_{max} + L_1$	1.57413	L_1	$K_{max} + L_1$	1.27605	L_1	S_1	Intrabasinal Zone
A7-Lambs Head	L_1	1.20096	L_1	L_1	1.30891	L_1	N/A	Intrabasinal Zone
A8-Rossmore*	K_{max}	1.14232	L_1	K_{min} (Inverse magnetic fabric)	1.15988	Pole to S1	S_1	Intrabasinal Zone
A14-Kilgarvin*	$K_{int} + L_1$	1.50258	L_1	$K_{int} + L_1$	1.42645	L_1	S_1	Intrabasinal Zone
A6-Caherdaniel*	$K_{max} + L_1$	1.20397	L_1	$K_{max} + L_1$	1.38196	L_1	Intermediate between S1 and S0	Intrabasinal Zone
A9-Molls Gap*	Not represented	1.22443	Not defined	K_{max}	1.12971	Unknown	S_1	Intrabasinal Zone
AM1-South of Lough Caragh*	$K_{max} + L_1$	1.32629	L_1	$K_{max} + L_1$	1.26302	L_1	S_1	Intrabasinal Zone
A4-South East of Keel Bay*	$K_{max} + L_1$	1.21603	L_1	$K_{max} + L_1$	1.16514	L_1	S0	Intrabasinal Zone
A3M-Keel Bay*	$K_{max} + L_1$	1.53916	L_1	$K_{max} + L_1$	1.35498	L_1	S_1	Intrabasinal Zone
A2-Killabounia*	$K_{max} + L_1$	1.41579	L_1	$K_{max} + L_1$	1.39484	L_1	S_1	Intrabasinal Zone
A1-Portmagee Quarry*	$K_{max} + L1$	1.1794	L1	K_{max}	1.2349	L1	S1	Intrabasinal Zone

Table 6.3 Continued								
M5-Lough Acoose*	K_{max}	1.19302	Further tectonic strain	K_{max}	1.20962	Further tectonic strain	S_1	Intrabasinal Zone
L23-Rheencaheragh	L_1	1.24869	L_1	L_1	1.30956	L_1	N/A	Intrabasinal Zone
L26-Reenard Point	L_1	1.30125	L_1	L_1	1.24331	L_1	N/A	Intrabasinal Zone
M8-Glenflesk Quarry*	$K_{int} + L_1$	1.15664	L_1	$K_{int} + L_1$	1.24014	L_1	S1	Intrabasinal Zone
A10-Gap of Dunloe North*	K_{max}	1.09039	K_{max}	K_{max}	1.06922	K_{max}	Intermediate between S0/S1	Transition Zone
L44-Culoo Rocks*	$K_{max} + L_1$	1.28436	L_1	$K_{max} + L_1$	1.16775	L_1	Early LPS	Transition Zone
L19- Valentia Island	L_1	1.17069	L_1	L_1	1.14383	L_1	N/A	Transition Zone
AM11-Lough Caragh North*	$K_{int} + L_1$	1.20934	L_1	$K_{int} + L_1$	1.08096	L_1	Early LPS	Transition Zone
L31-Reenadrolaun Point*	K_{max}	1.13986	NE-SW palaeocurrent lineation.	K_{max}	1.26214	NE-SW palaeocurrent lineation.	S0	Transition Zone
L35-Dooneen*	K_{max}	1.08311	NE-SW Palaeocurrent	K_{max}	1.01122	NE-SW Palaeocurrent	S0	Transition Zone
L11-North Enagh Point	Not Represented	1.13601	No distinct lineation.	Not Represented	1.16224	No distinct lineation.	N/A	Transition Zone
L6-Cooscrome	L_1	1.11671	L_1	NE-SW	1.18987	NE-SW Palaeocurrent	N/A	Transition Zone
L7-Cooscrome	L_1	1.10647	L_1	L_1	1.14187	L_1	N/A	Transition Zone
L10-Dolous Head	L_1	1.11863	L_1	L_1	1.18854	L_1	N/A	Transition Zone
L41-Knocknatobar	L1	1.1293	L1	L_1	1.08372	L1	N/A	Transition Zone

Table 6.3 Continued								
L22-Kells Bay Post Office	NE-SW Palaeocurrent	1.1708	NE-SW palaeocurrent lineation.	NE-SW Palaeocurrent	1.11133	NE-SW palaeocurrent lineation.	N/A	Transition Zone
L39-Knocknatobar	L_1	1.29153	L_1	L_1	1.23496	L_1	N/A	Transition Zone
L47-Coosfada*	K_{int} + L_1	1.44428	L_1	K_{max}	1.23221	NE-SW Palaeocurrent lineation.	Early LPS	Transition Zone
M3-Kells Bay*	K_{max}	1.13481	NE-SW palaeocurrent lineation	K_{max}	1.08335	NE-SW palaeocurrent lineation	S0	Transition Zone
L21-Kells Bay	Not represented	1.2043	No distinct lineation	Not represented	1.03498	No distinct lineation	N/A	Transition Zone
M7- Brandon Pier*	K_{max}	1.04481	Weak NE-SW palaeocurrent lineation.	none	1.02682	No distinct lineation	S0	Foreland Zone
M6-Ballyheige*	NE-SW direction	1.09317	Weak NE-SW palaeocurrent lineation.	NE-SW direction	1.0693	Weak NE-SW palaeocurrent lineation.	S0	Foreland Zone

Table 6.4. Summarizes the average strain values, the interpretation for MRL and DTNNM ϕ, the asssociated AMS ellipsoid types, and the cleavage behaviour for each zone.

Zone	Locations (See Table 6.2)	Average R_s Value MRL	Average R_s Value DTNNM	MRL ϕ represents:	DTNNM ϕ represents:	AMS ellipsoids controlled by (where applicable)	Cleavage behaviour
Intrabasinal (South of the CF)	M4-M8	1.273	1.295	Mostly L_1	Mostly L_1	S_1	• Axial planar steeply dipping cleavage.
Transition Zone (North of the CF)	A10 – L21	1.143	1.177	L_1, NE-SW palaeocurrent lineations, & no distinct fabric.	L_1, NE-SW palaeocurrent lineations & No distinct fabric	S_0 and early LPS fabrics	• Early LPS fabric. • passively rotated S1 or • Zero cleavage.
Foreland Zone	M6 & M7	1.048	1.069	Weak palaeocurrent lineation and no distinct fabric	Weak palaeocurrent lineation & no distinct fabric	S_0 controlled	• spaced disjunctive S1 or • Zero cleavage.

6.10 Microstructures and Strain Analysis

6.10.1 Introduction

Interpreting strain analysis benefits from the consideration of microstructural deformation processes which affect the overall fabric of the rock. A full detailed microstructural study of these rocks in thin section may allow classification of the samples into low, medium and high strain zones, this is however beyond the scope of this study. Instead, a brief outline of microstructural deformation mechanism is discussed and some thin section descriptions of the samples are presented. The ϕ angles, which represent the orientation of the long axes of the strain ellipse for both DTNNM and MRL are also plotted on the thin section pictures in order to allow a comparison of the strain analysis results with the features seen in thin section.

6.10.2 Deformation Processes in Low Grade Metamorphic Conditions

The samples from the study area are quartz arenites and have under gone diagentic compaction and low-grade, sub-greenschist facies metamorphism. Temperatures attained during metamorphism in the Munster Basin have been previously estimated at 280-315°C (Meere, 1995 b) and 340-350°C (Blackmore, 1995).

In diagenetic and low grade metamorphic conditions deformation processes include brittle deformation and pressure solution (Passchier and Trouw, 2005). Pressure solution which involves the dissolution from one part of the grain and subsequent re-precipitation of dissolved material in low mean stress sites, may result in a change in grain shape which is unrelated to the internal deformation of the grain (Passchier and Trouw, 2005) and can also contribute to the formation of a secondary foliation by aiding in the elongation of minerals (e.g. Williams, 1972; Passchier and Trouw, 2005). Solution transfer as a result of stress may contribute to the formation of a foliation by dissolving micas or material between the micas, which lie in the shortening direction and therefore resulting in rotation of the micas or by transferring and depositing more material onto the micas perpendicular to the shortening direction (i.e. in the extension direction; Passchier and Trouw, 2005). As well as by the mechanism of pressure solution micas commonly deform by undulose extinction, folding and kinking (e.g. Lister and Snoke, 1984; Bell et al., 1986 b; cited by Passchier and Trouw, 2005) and fracturing (Kronenberg et al., 1990; Shea and Kronenberg 1992; Mares and Kronenberg

1993 cited by Passchier and Trouw, 2005). At temperatures up to 300°C deformation mechanisms of quartz mostly include pressure solution (Kerrich et al., 1977), solution transfer of material and brittle fracturing (Groshhong, 1988a; Knipe 1989; Dunlap et al., 1997; van Daalen et al., 1999; Stipp et al., 2002).

Recrystallisation processes affect grain boundaries and include grain boundary mobility (GBM), bulging recrystallisation (BLG) and subgrain rotation recrystallisation (SGR), (Passchier and Trouw, 2005). Bulging Recrystallisation (BLG) occurs at low temperatures (280 °C – 400 °C) and involves the bulging of one crystal into another by grain boundary migration (Fig 6.34; e.g. Stipp et al., 2002). This type of grain boundary migration often occurs at triple junctions and the edges of old grains (Passchier and Trouw, 2005).

Crystal plastic deformation may occur at certain strain rates, temperature and with the presence of fluids and occurs at higher temperatures than brittle deformation and pressure solution (Passchier and Trouw, 2005). Undulose extinction in quartz indicates that crystalplastic deformation has occurred (Passchier and Trouw, 2005). At 300-400°C there may be sweeping undulose extinction (Passchier and Trouw, 2005). Crystal plastic deformation can result in grains with an elongate shape in the XY plane (Passchier and Trouw, 2005) which is known as shape preferred orientation. A grain shaped preferred orientation (GSPO) or shaped preferred orientation is one that is composed of minerals that are elongated as a result of deformation (Figure 6.35, Passchier and Trouw, 2005). The term GSPO is applicable to describing quartz but not micas as these minerals are already elongated prior to deformation (Passchier and Trouw, 2005). GSPO can develop in primary grains but is more common in secondary recrystallised grains (Means, 1981; Lister and Snoke, 1984). GSPO can occur as a result of crystal plastic processes and solution transfer (Passchier and Trouw, 2005). The strength of the GSPO is related to the degree of finite strain (Passchier and Trouw, 2005), however the relationship between GSPO and finite strain is not straight forward, for example grains may deform passively , there may be overprinting SPO's or static recrystallisation may have occured (Passchier and Trouw, 2005). The relationship of the GSPO to finite strain axes also depends on whether the strain was coaxial or non coaxial (Passchier and Trouw, 2005). If the strain was coaxial, then the GSPO will be parallel to

the finite strain axes, if the strain was non coaxial then the GSPO will not necessarily be parallel with the finite strain axes (Passchier and Trouw, 2005).

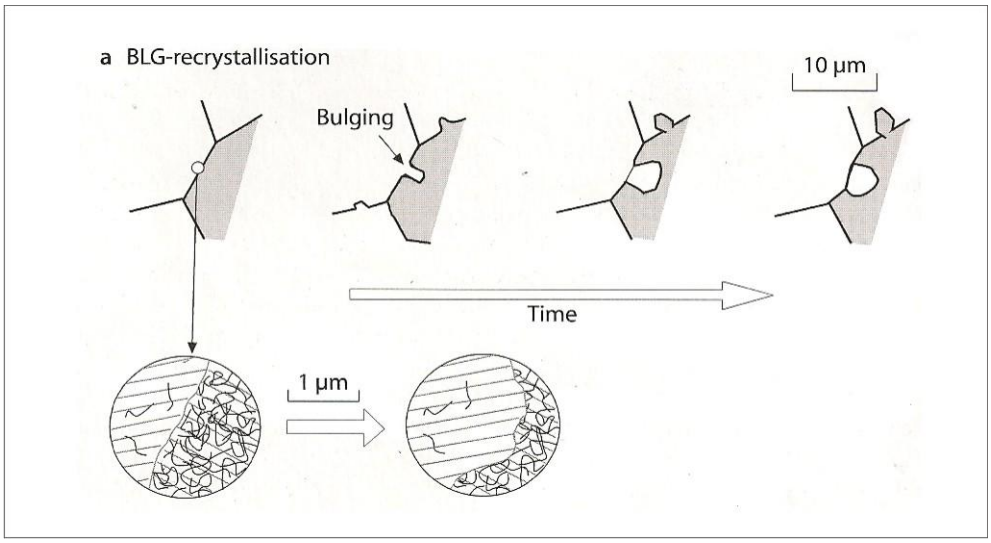

Figure 6.34 Shows the mechanism of BLG recrystallization from Passchier and Trouw (2005).

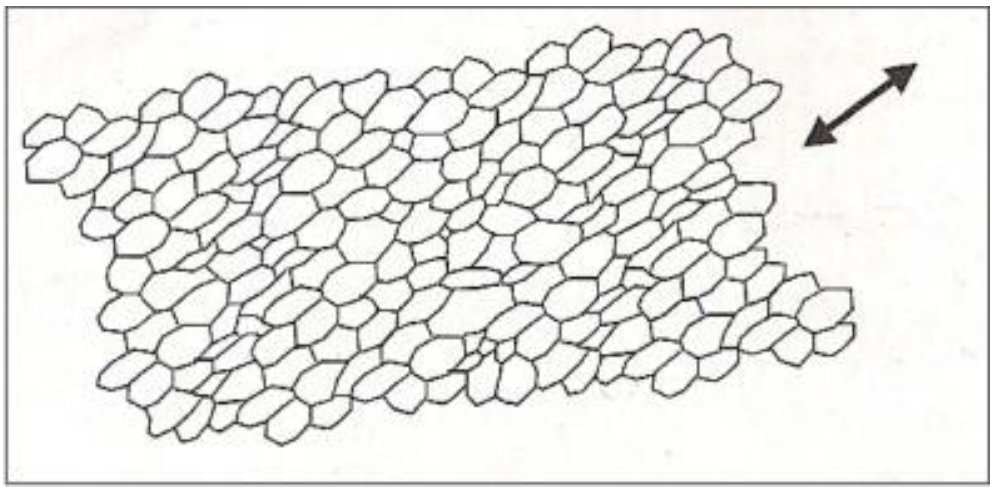

Figure 6.35 Shows a grain shape preferred orientation (Paschier and Trouw, 2005).

6.10.3 Results - Comparison of Microstructures and Strain Analysis

Samples in the Intrabasinal Zone generally appear to have features such as interlocking grain boundaries, a GSPO defined by elongated quartz clasts and in some cases minor amounts of an anastomosing mica fabric (Fig 6.36, 6.37 & 6.38). In one of the samples it is possible to observe minor amounts of grain boundary migration (GBM), where one quartz grain bulges into another - SE of Keel Bay (Fig 6.38). Microboudinaged quartz is observed in Sample A14 – Kilgarvin (Fig 6.37). The visible tectonic fabric observed in thin section often lies close to parallelism with the orientation of ϕ which marks the long axes of the strain ellipse for DTNNM and MRL (Fig 6.36, 6.37, 6.38). This shows

that both DTNNM and MRL are sensitive to the tectonic fabric seen in thin section. There is generally a stronger tectonic fabric visible in thin section in the Intrabasinal Zone than in the Transition Zone and Foreland Zone. Microstructural features observed in the Intrabasinal Zone, appear to reflect a higher deformational regime consistent with the strain analysis results.

North of the Coomnacronia Fault in the Transition Zone and Foreland Zone, the majority of samples show no distinct tectonic fabric, although sample L10: Dolous Head shows a weak GSPO of the quartz grains (Fig 6.41) and DTNNM ϕ and MRL ϕ lie subparallel to this weak fabric. In the Transition Zone and Foreland Zone, quartz grains are often well rounded to sub rounded (Fig 6.39, 6.40 & 6.41), although sample M6: Ballyheige (Fig 6.41) in the Foreland Zone consists of more angular quartz grains, but these do not form part of a GSPO. In most of the samples from the Transition Zone and the Foreland Zone the orientation of the DTNNM ϕ and MRL ϕ do not appear to be aligned with any visible microstructural fabric. Microstructural features observed in the Transition Zone and Foreland Zone, appear to reflect a lower deformational regime consistent with the strain analysis results.

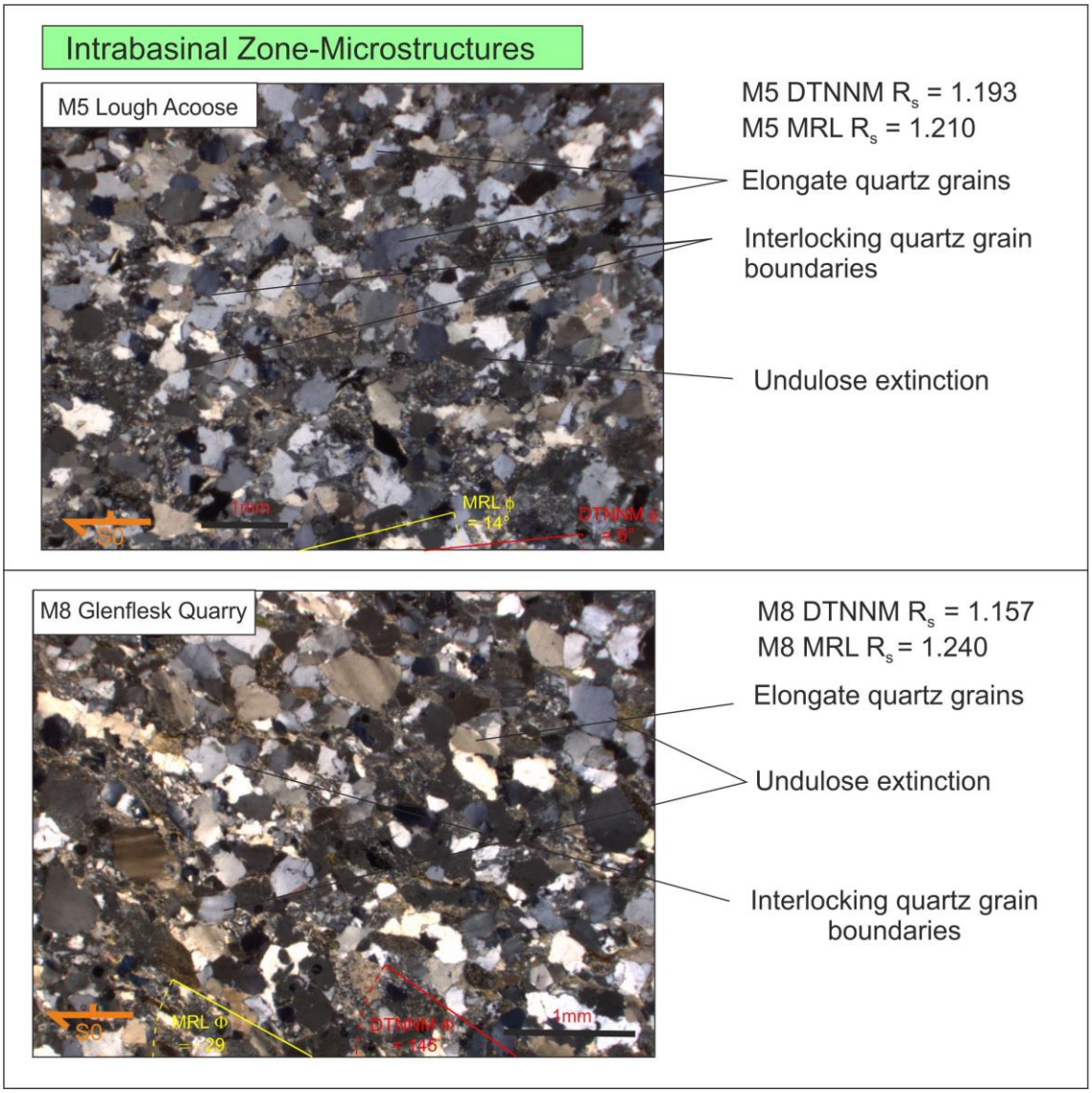

Figure 6.36 Sample M5: Lough Acoose from the Intrabasinal Zone shows elongate quartz grains, interlocking quartz grain boundaries and undulose extinction. Both MRL ϕ and DTNNM ϕ lie parallel to subparallel to the long axes of the quartz grains. Sample M8 similarly shows elongate quartz grains, undulose extinction and interlocking quartz grain boundaries. Both MRL ϕ and DTNNM ϕ lie parallel to subparallel to the long axes of the quartz grains.

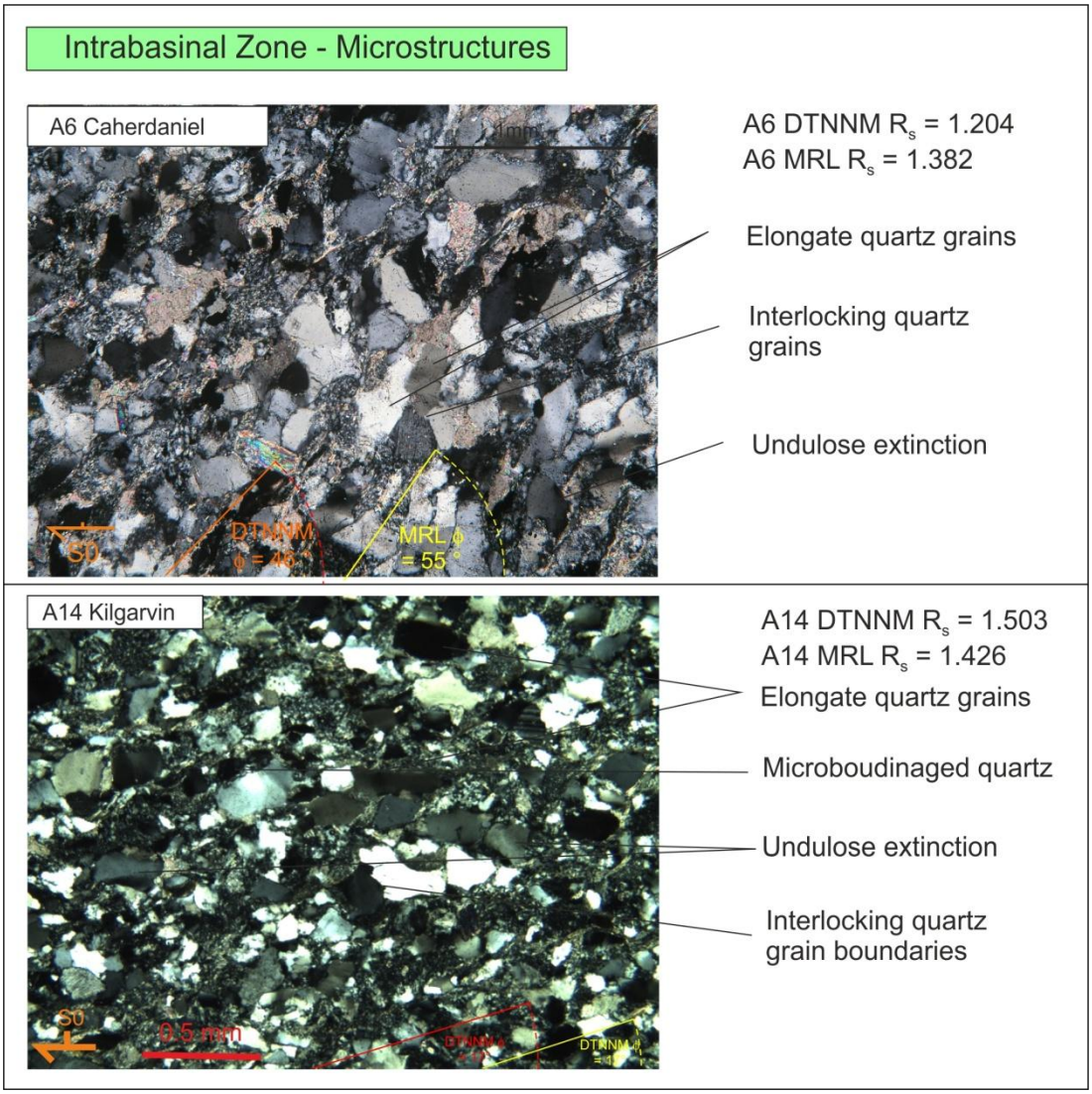

Figure 6.37 Sample A6 shows a clear tectonic fabric defined by a grain shape preferred orientation (GSPO) consisting of elongate quartz grains. The quartz grains are interlocking and display undulose extinction. Both MRL ϕ and DTNNM ϕ lie parallel to subparallel to the long axes of the quartz grains. Sample A14 shows similar characteristics to A6, with elongated quartz grains defining a strong GSPO. DTNNM ϕ and MRL ϕ lie close to parallelism with some of the long axes of the quartz elongated quartz grains. The R_s values for DTNNM and MRL for both sample A6 and A14 are high reflecting the strong tectonic fabric seen in thin section.

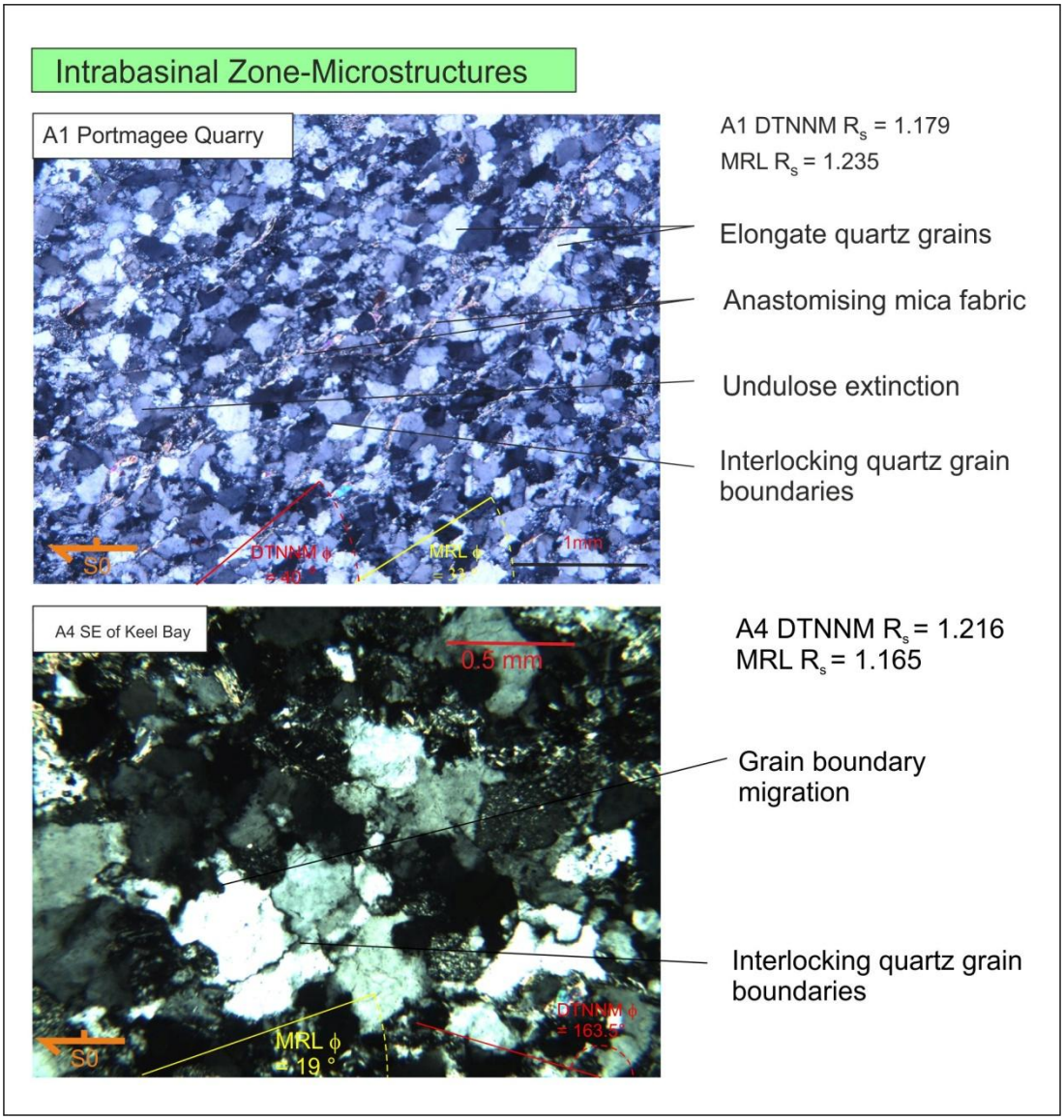

Figure 6.38 Sample A1Portmagee Quarry consists of a strong GSPO consisting of elongate quartz grains. There is also some minor amounts of anastomising micas which lie parallel to the GSPO. Both DTNNM ϕ and MRL ϕ lie close to parallelism with the direction of the GSPO. Quartz grain boundaries are interlocking and there is some undulose extinction. Sample A4 shows some grain boundary migrations and interlocking grain boundaries.

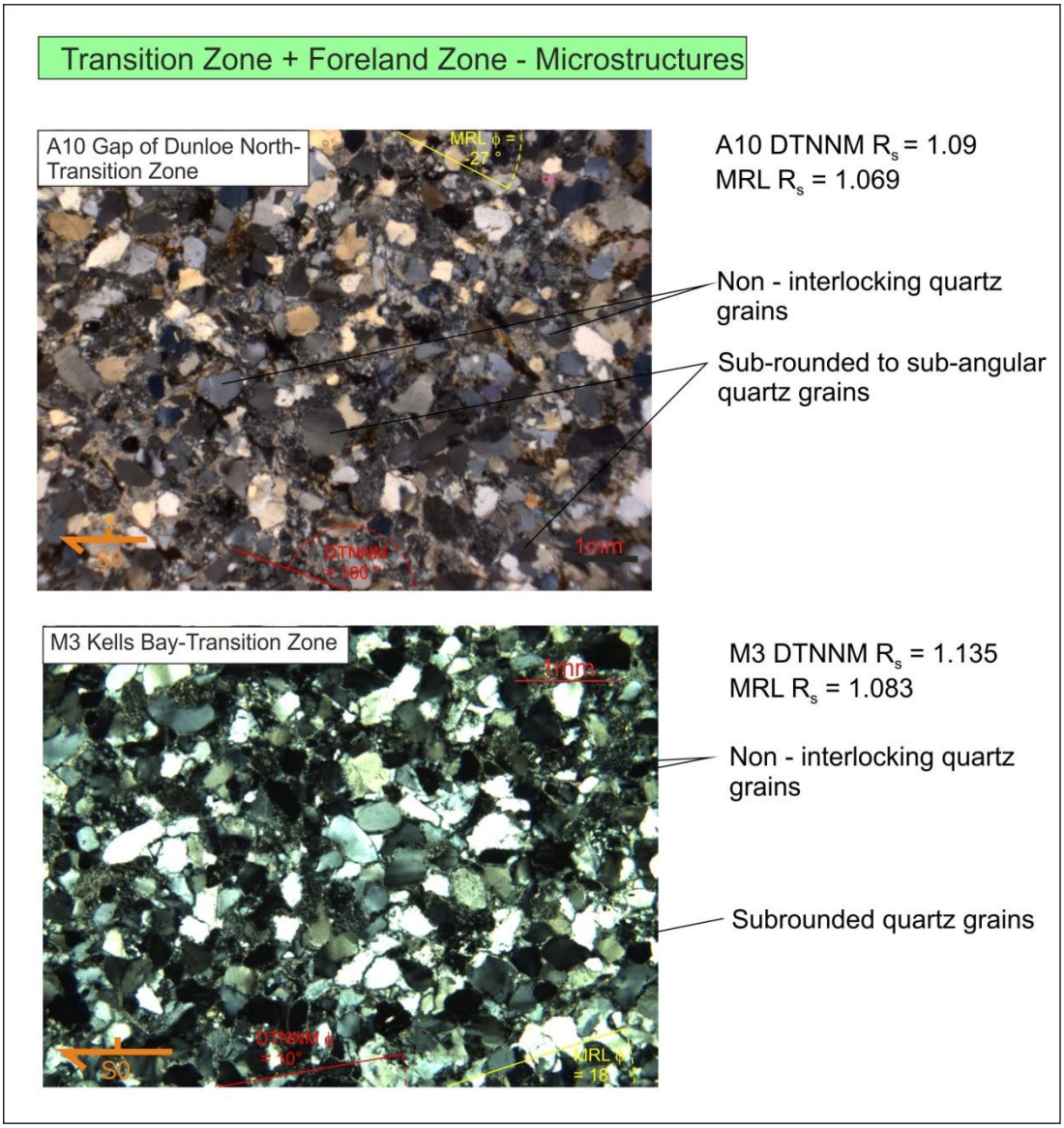

Figure 6.39 Sample A10 Gap of Dunloe North consists of subrounded to well rounded quartz grains which are mostly non- interlocking. There does not appear to be a dominant GSPO although the DTNNM ϕ and the MRL ϕ appear to track a weak tectonic fabric. Both DTNNM and MRL R_s values are low for sample A10. Sample M3 consists of sub rounded to well rounded quartz grains which are not closely interlocking. There is no dominant tectonic fabric. DTNNM and MRL R_s values are low for this sample.

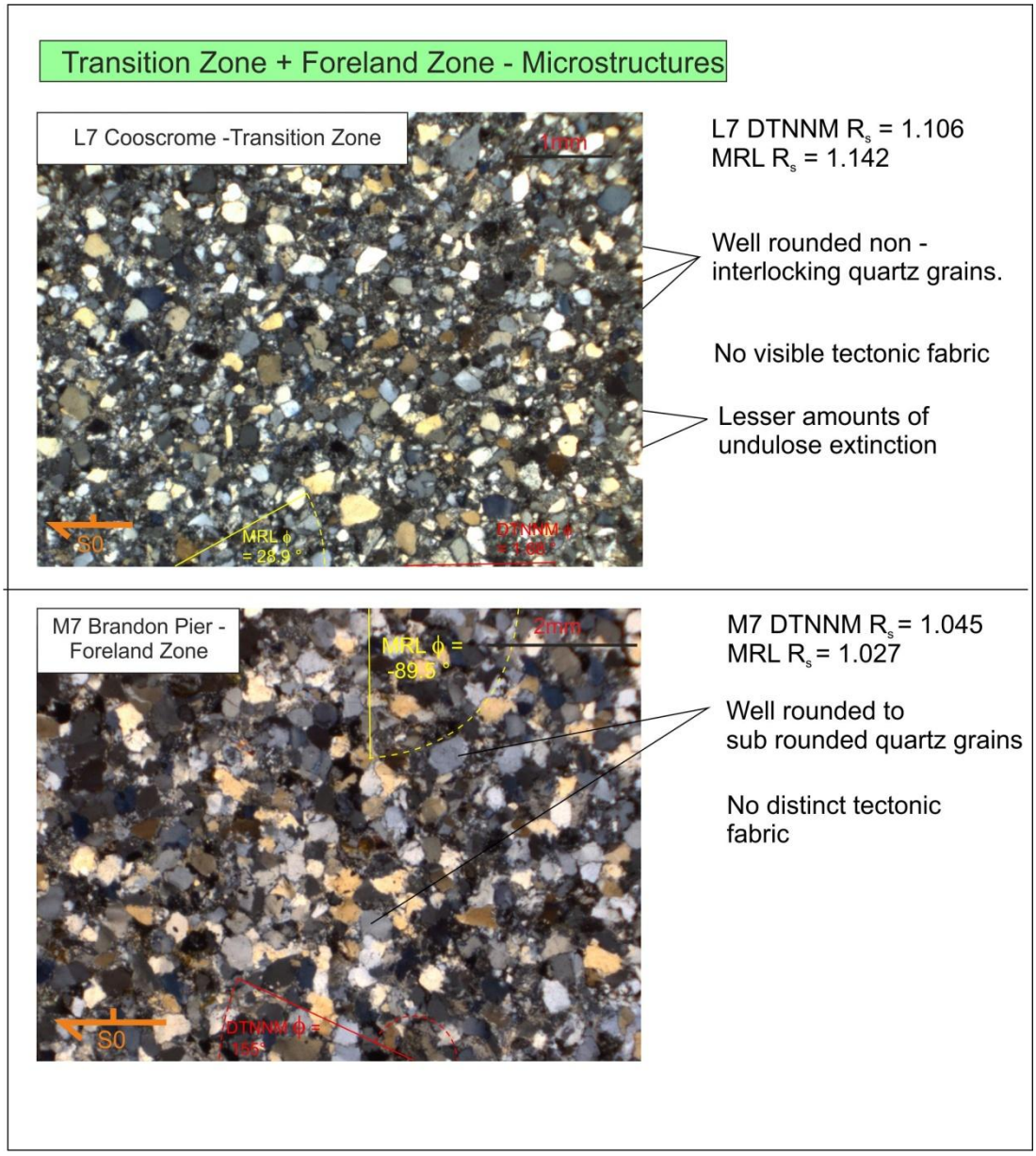

Figure 6.40 Sample L7 consists of non interlocking well rounded quartz grains with minor amounts of undulose extinction. DTNNM R_s and MRL R_s values are moderate to low. There is no distinct tectonic fabric. Sample M7 consists of well rounded to subrounded quartz grains. There is no distinct tectonic fabric. DTNNM R_s and MRL R_s values are low.

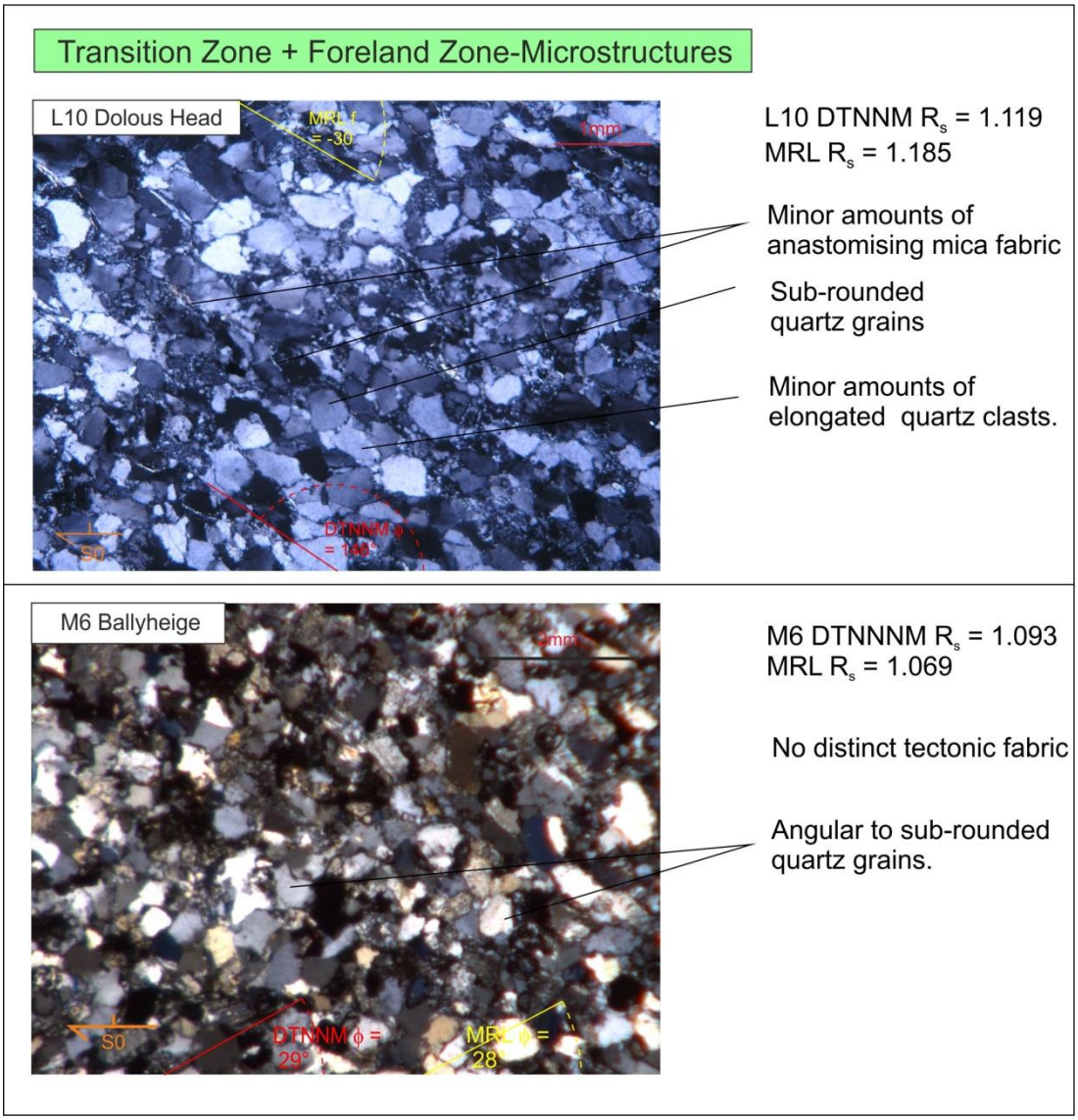

Figure 6.41 Sample L10: there is a moderate tectonic fabric defined by elongate quartz grains with minor amounts of anastomising mica fabric. Quartz grains are subrounded to sub angular. Both DTNNM ϕ and MRL ϕ lies close to parallelism with the direction of the tectonic fabric. DTNNM and MRL R_s values are moderate. Sample M6 consists of angular to subrounded quartz grains and there is no distinct tectonic fabric. DTNNM and MRL R_s values are low.

6.11 Strain Analysis Conclusions

R_s values for both the DTNNM and the MRL method generally decrease from south to north across the study area (Fig 6.11 & 6.13). For both of the methods there is a general drop in the average R_s value to the north of the Coomnacronia Fault indicating that this fault marks a strain boundary. Three strain zones have been identified based on the DTNNM and MRL results. The Intrabasinal Zone has moderate to higher strain values and the values are generally more consistent. The long axis of the strain ellipsoid for both DTNNM and MRL ϕ mostly represent L_1 in the Intrabasinal Zone. There is a visible tectonic fabric in the form of a GSPO of quartz seen in thin section in the Intrabasinal Zone, which often lies parallel to the long axes of the strain ellipse for both DTNNM and MRL. Strain values in the Transition Zone are predominantly lower but with some occasional higher values for DTNNM. These occasional higher values are a result of DTNNM being sensitive to a combination of both an original NE-SW palaeocurrent lineation and subsequent early LPS. DTNNM may be more sensitive to the overall fabric in the early stages of deformation than MRL. DTNNM which measures the object to object distances of the quartz clasts may be affected more so by the matrix due to the relative hardness of quartz grains. In the Transition Zone DTNNM and MRL ϕ mostly track the L_1 direction but also in some cases track a NE-SW palaeocurrent direction and in cases for very low strain do not track an obvious fabric. The DTNNM and MRL strain results in the Foreland Zone are low. In both the Transition Zone and the Foreland Zone most thin sections display no distinct tectonic fabric in the form of a GSPO. In general DTNNM values are higher than MRL values. MRL is more sensitive to the deformation of quartz grains. Also DTTNM may be more affected by variations in lithology as variations in lithology would affect the percentage of matrix. MRL would also have sensitivity to variations in lithology as the lower the content of matrix the more grain to grain contacts and hence the higher the deformation of quartz grains.

Chapter 7:
Discussion

Chapter 7: Discussion

7.1 Introduction

In south west Ireland, Middle-Upper Devonian Old Red Sandstone (ORS) is found in the Dingle Basin, Munster Basin and Kerry Head and lies upon Caledonian/Acadian Basement. The ORS and overlying Carboniferous underwent Variscan deformation at the end of the Carboniferous. Variscan deformation decreases from south to north across south west Ireland (e.g. Gill, 1962; Sanderson, 1984; Cooper et al., 1984, 1986; Bresser and Walter, 1999) and has a close relationship to the pre-existing Caledonian structures (e.g. Price and Todd, 1988; Meere, 1995; Landes, 2003). In the Munster Basin, deformation involved early layer parallel shortening (LPS), folding and thrusting (e.g. Cooper et al., 1986).

7.2 The Northern Margin of the Munster Basin

There are a number of hypothesis concerning the location of the northern margin of the Munster Basin, with much of the research having been carried out in the mid 80's. A number of authors (e.g. Meere, 1997; Vermeulen, 1998; Landes 2000) have since revisited the issue of the precise location of this northern margin. Fig 7.1 summarizes the various suggestions for the northern margin in the western part of the Munster Basin.

- **The Dingle Dungarvan Line (DDL)**

The Dingle-Dungarvan Line (DDL; Fig 7.1) is considered by (e.g. Price and Todd, 1988) to be the northern margin of the Munster Basin. The DDL lies in Dingle Bay and can be traced inland expressing itself as the Killarney-Mallow Fault Zone (KMFZ) in the east (Fig 7.1). The Killarney-Mallow Fault Zone is considered by some authors to be the northern margin of the Munster Basin (Price and Todd, 1988; Meere, 1997; Landes, 2000; 2003). The KMFZ has also been suggested as the location for the main cleavage front (Meere, 1997).

- **The Dingle Bay Lineament**

Price and Todd (1988) and Todd (1988), have also suggested the northern margin to be located at the Dingle Bay Lineament, a line which lies in Dingle Bay and is considered to be a reactivated Caledonian structure (Fig 7.1). This has been discussed in Chapter 2.

- **The Dingle Bay-Galtee Mountains Line (DBGML) or Dingle Bay Galtee Fault Zone (DBGFZ)**

The northern depositional margin of the Munster Basin has also been suggested to lie at the Dingle Bay Galtee Mountains Line (Todd, 1989; Williams et al., 1989) which is also termed the Dingle Bay Galtee Fault Zone (Williams, 1989). In the west the DBGML lies in the area between the Iveragh Peninsula and the Dingle Peninsula. Heading towards the east the DBGML sweeps to the north east, north of the Galtee Mountains (Chapter 2). However, a number of authors have interpreted the DBGML to be a northwards dipping structure based on Varnet Line B (e.g. Vermeulen, 1998; Landes, 2003; Fig 7.1 and discussed in Chapter 2.) Williams (1989) suggest that the DBGFZ was the northern margin of the Munster Basin. Palaeoflow directions are not influenced by the DBGFZ to the north of the fault or within the basin (Capewell, 1951; 1965; Bridge et al., 1980; Bridge and Diemer, 1983). Williams (1989) suggests from this that the DBGFZ had little topographic relief.

- **The Valentia Comeragh Mountains Fault Line (VCMF)**

The VCMF which includes the KMFZ , the Muckcross-Millstreet Fault, the Black Lake Fault and the Coomnacronia Fault in the west has been previously put forward by Meere (*pers comm*.), McCarthy (2014) and Ennis et al., (2015; Fig 7.2 and 7.3) as a fault system bounding the northern margin of the Munster Basin. Ennis et al. (2015) refers to the VCMF as the Coomnacronia-Killarney Mallow Fault Zone CKMFZ (Fig 7.3). In the west Meere (*pers comm*.) suggests this to lie along the Coomnacronia Fault. McCarthy (2014) suggests that a basement high lies to the north of the VCMF (Fig 7.2). This study has investigated the Coomnacronia Fault as a potential basin margin structure.

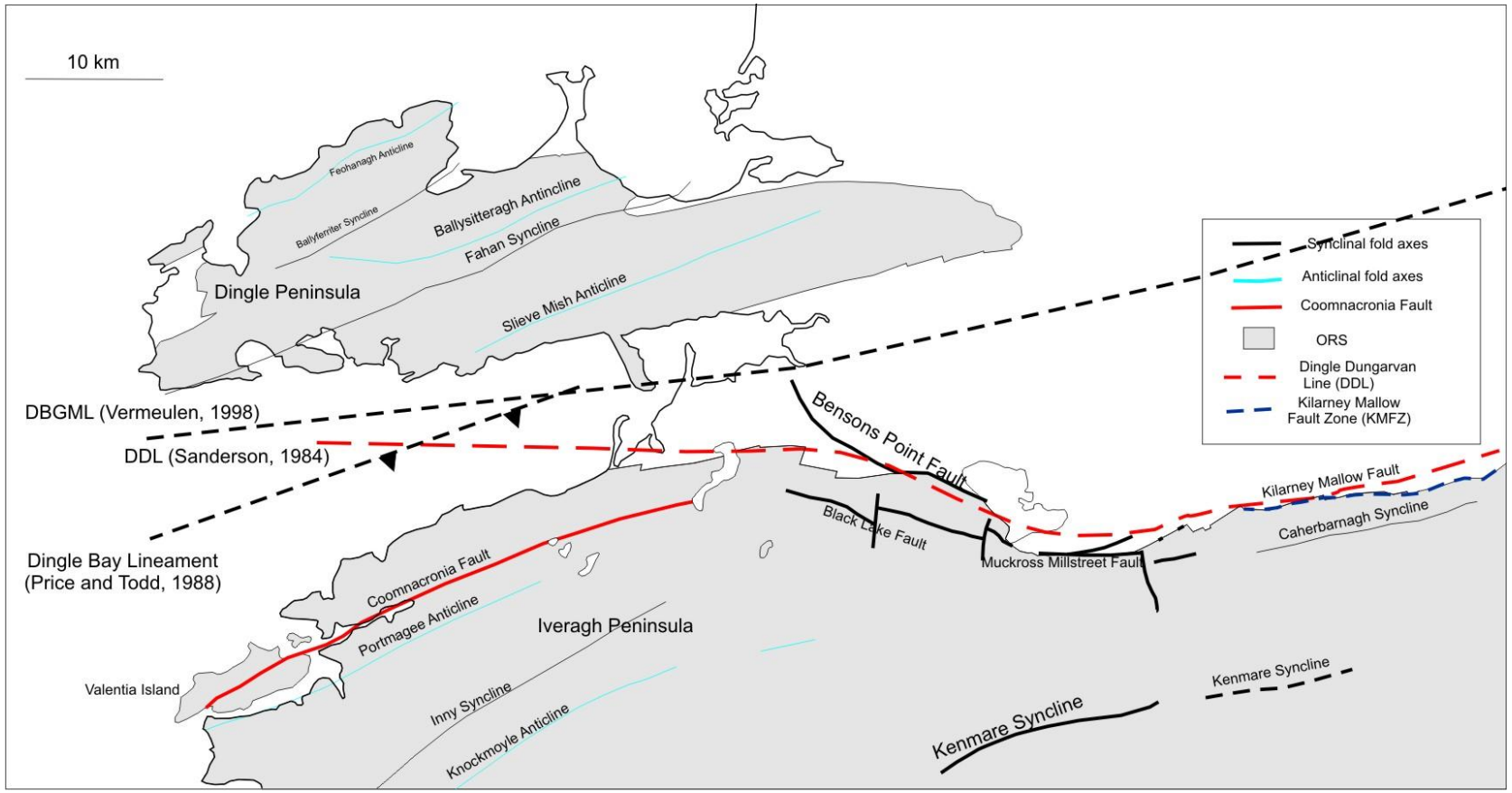

Figure 7.1 shows the Coomnacronia Fault, the Dingle-Dungarvan Line (DDL), the Black Lake Fault, the Killarney Mallow Fault (KMF), the Dingle Bay Galtee Mountains (DBGML) Line and the Dingle Bay Lineament and some of the other main structures on the Iveragh and Dingle Peninsula. Compliled and modified from Pracht (1996), Sanderson (1984), Price and Todd (1988) and Vermeulen (1998).

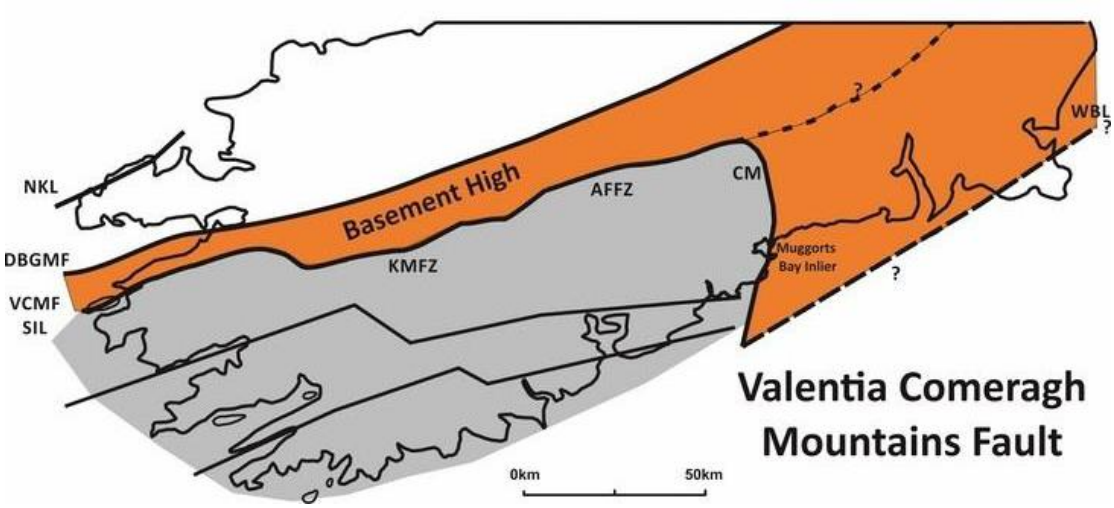

Figure 7.2 shows the basement high to the north of the Valentia Comeragh Mountains Fault Line (VCMF). KMFZ – Kilarney Mallow Fault Zone, AFFZ –Ardfinnan Fault Zone, NKL – North Kerry Lineament, DBGMF- Dingle Bay Galtee Mountains Fault, SIL – South Ireland Lineament, CM- Comeragh Mountains, WBL – Wexford Bay Lineament. From McCarthy (Phd, 2014).

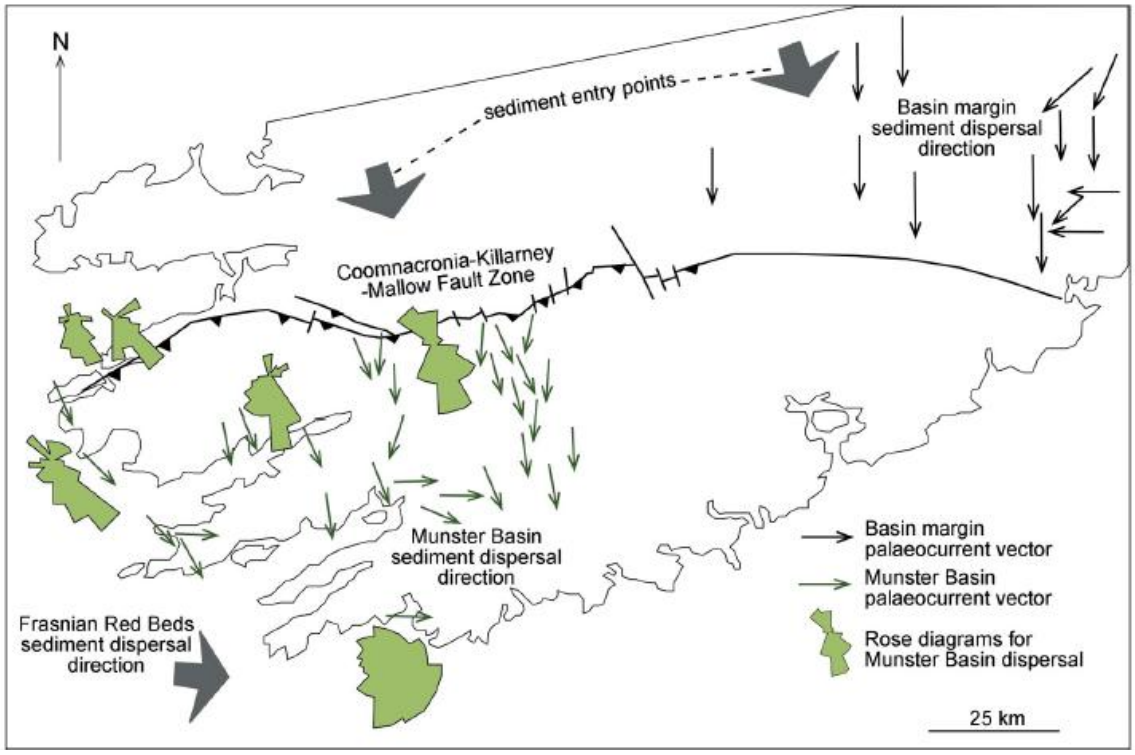

Figure 7.3 shows the Coomnacronia - Kilarney - Mallow - Fault Zone, CKMFZ as the northern margin of the Munster Basin. From Ennis et al. (2015).

7.3 The Coomnacronia Fault – A Proposed Basin Margin Fault

Given the ambiguity surrounding the northern margin of the Munster Basin as previously discussed, there is an obvious gap in the research concerning the margin in the western part of the Munster Basin. Notably the Coomnacronia Fault has not previously been investigated as a basin margin fault despite many features which indicate that it could be a marginal fault. The Coomnacronia Fault is a major map scale fault that lies laterally to the west of Muckcross - Milstreet Fault, the Black Lake Fault and the Killarney Mallow Fault Zone (Fig 7.1). Capewell (1975) describes the Coomnacronia Fault as a thrust fault and also suggested that a zone of tilted folds which lies to the north of the Coomnacronia Fault on the Iveragh Peninsula is actually part of the foreland to the north. Williams (2002) consider the Coomnacronia Fault to be intrabasinal but also suggest that there is major southwest thickening of sediments. Morris (1980) indicates the influence of Caledonian Basement in the vicinity of the fault (Cahersiveen) based on the presence of NE-SW gravity anomalies. Subsequent to Meere's (1997) strain work on the KMF, it seems plausible that the CF lying laterally to the west of the KMFZ is a more likely location for a potential basin margin fault.

7.4 Results.

South of the Coomnacronia Fault-The Intrabasinal Zone

The Intrabasinal Zone is proposed in this study to lie to the south of the Coomnacronia Fault and is characterised by large scale (10-15km wavelength) anticlines and synclines with a steeply dipping axial planar cleavage. To the immediate south of the Coomnacronia Fault Variscan cleavage strikes concordantly along the fault (Map Insert 2: Cleavage Results) and generally dips at 60° to the south which is the estimated dip of the Coomnacronia Fault (Capewell, 1975). Cleavage lying concordant to the fault indicates that the geometry of this fault is impacting the cleavage orientations within the basin fill. The strike of the cleavage maintains a concordant relationship with the fault. In the Intrabasinal Zone, the AMS fabrics are controlled predominantly by the cleavage i.e. the K_{min} axes of the AMS fabric ellipsoid lies parallel to the pole to cleavage plane and the AMS ellipsoid is either strongly prolate or oblate lying in the cleavage plane.

Thermomagnetic studies (Chapter 5) on 4 samples indicate that paramagnetic minerals (micas) are predominantly responsible for the magnetic susceptibility of these samples. The low mean values for magnetic susceptibility for all of the samples (Chapter 5), also suggests paramagnetic (mica) control. Micas lying parallel to or anastomising elongate quartz grains as part of a GSPO (Chapter 6) are sometimes observed in the Intrabasinal Zone. In the Intrabasinal Zone, the average strain estimates for the Delaunay Triangulation Nearest Neighbour Method: DTNNM $R_s = 1.296$ and for the Mean Radial Length method: MRL $R_s = 1.269$ which are higher than the averages for the Transition Zone. The strain values are all relative values allowing comparison of the zones, but are an underestimate of the total strain (Meere, P.A. *pers comms,* 2016). The ϕ value for DTNNM and MRL in most cases is orientated parallel or subparallel to the intersection lineation and/or the K_{max} axes of the AMS ellipsoids indicating that both DTNNM and MRL are indicative of tectonic fabric in the Intrabasinal Zone. Another indication of a higher strain regime can be observed in the microstructures of the Intrabasinal Zone. Quartz grains are interlocking, display undulose extinction and a tectonic fabric defined by elongated quartz grains and anastomising micas. It is clear from the above that the material to the south of the CF has undergone significant Variscan deformation. Should the CF merely be an Intrabasinal normal fault and/or a late stage thrust fault, then it would be expected that these characteristic, high-strain features found to the south of the Coomnacronia Fault would continue in the ORS to the north of the fault as far as the previously suggested basin margins (the DDL or DBGFZ). This is not the case. The northern coast of the Iveragh Peninsula has been called the Transition Zone and displays a distinct structural style and strain regime to that south of the Coomncronia Fault.

North of the Coomnacronia Fault (Iveragh Peninsula) –The Transition Zone

North of the Coomnacronia Fault, this study proposes a newly characterised zone: The Transition Zone to be located. Here the tectonic style changes abruptly with the presence of passively rotated cleavage and fabrics indicative of an early LPS deformation event. Folding in this area consists of overturned folds verging to the north. This type of passively rotated cleavage has not been observed in any other part of the inverted Munster Basin. AMS ellipsoids are controlled by bedding and/or an early LPS fabric and are consistent with a lower level deformation regime. AMS ellipsoids which show characteristic control by LPS (i.e. K_{max} perpendicular to bedding and girdled fabrics- Chapter 5) are only found in the zone to the north of the CF. The average strain

values for the Transition Zone are lower with the Delaunay Triangulation Nearest Method: DTNNM R_s = 1.203 and the Mean Radial Length Method: MRL R_s= 1.142. There are some locations with notably low strain values i.e. (e.g. M3 Kells Bay, where DTNNM R_s = 1.135, MRL R_s = 1.083 & A10- Gap of Dunloe North, where DTNNM R_s = 1.09 and MRL R_s = 1.069). The ϕ values for both the MRL and the DTNNM are often orientated parallel to sub-parallel with the bedding/cleavage intersection lineation or the K_{max} or K_{int} axes of the AMS ellipsoids. In some cases the ϕ values plots closer to a NE-SW trend than to the intersection lineation which may be reflective of sedimentary fabrics associated with NE-SW directed fluvial palaeocurrents as documented by Graham (1983), Russell (1984), Williams et al. (1989) Chapter 2 and Chapter 6. However there is also the possibility that in the Transition Zone, this NE-SW lineation that is picked up by both the K_{max} axes of the AMS ellipsoid and the ϕ for MRL and DTNNM could be due to the influence of Caledonian basement on the strain fabrics. Thermomagnetic studies have been carried out on three samples (Chapter 5) from the Transition Zone, indicating that paramagnetic minerals are responsible the magnetic susceptibility of these samples. The mean susceptibility is low (Chapter 5) indicating paramagnetic control of the AMS ellipsoids. Clearly the Transition Zone has not suffered the same degree and style of deformation as the Intrabasinal Zone.

The Foreland Zone

The Foreland Zone comprises the UORS of the Dingle Peninsula and Kerry Head to the north and has already been defined in the literature as lying to the north of the basin margin fault (Chapter 2). However, in order to allow for an end to end comparison, this study was extended into the Foreland Zone. In the Foreland zone, cleavage is generally absent (e.g. M7 Brandon Pier, M6 Ballyheige) or spaced and disjunctive (e.g. UORS at Bulls Head; Meere and Mulchrone, 2006). The AMS ellipsoids are oblate and lie in the bedding plane but the K_{max} axes still tracks a regional lineation indicating the beginnings of an early bedding/cleavage intersection lineation. Thermomagnetic studies have been carried out on sample M6-Ballyheige and the results show that paramagnetic minerals are responsible for the AMS ellipsoid. Similarly these samples in the Foreland zone have low mean susceptibilities indicating paramagnetic control on AMS ellipsoids. The strain analysis results are low with the average DTNNM R_s = 1.069 and MRL R_s = 1.048. There is no obvious tectonic fabric in the thin sections from the Foreland Zone.

7.5 Discussion of Results

7.5.1 Comparison with Global Inversion Studies

There are a number of mechanisms (as discussed in Chapter 1) by which inversion along the Coomnacronia Fault may have occurred. This study has investigated the effect of the Coomnacronia Fault on deformation styles from the south to the north of the fault. Based on the results from Chapters 4, 5, and 6, the Coomnacronia Fault has been proposed as the main northern basin margin fault and the most likely mechanisms that have effected deformation during inversion of this fault are basement buttressing and the development of a footwall shortcut. Rigid basement blocks play an important role in the deformation of the synrift fill and this may be expressed as strong chevron folding in the hanging wall (Chapter 1). Most notably this has been observed at Lake Coomnacronia (Chapter 4: Section 4.5.3) where there is strong chevron folding in the hangingwall in close proximity to the Coomnacronia Fault. Comparable studies to this include, Corfield et al. (1996) who discuss the occurrence of chevron folds found in synrift sediments in close proximity to the basin bounding block in the Dublin Basin, which lies in the foreland of the Irish Variscides (Fig 7.4). In a more generic sense, Corfield et al. (1996) also suggests that the varying styles of end carboniferous inversion across the British Isles are a mostly controlled by the influence of the basement and not the direction of shortening. The influence of the basement block on the cover sequence is also investigated by Bailey (2002), who shows that basement buttressing plays an important role in the geometry of the folds in the cover sequence. Bailey (2002) have looked at basement buttressing in the Tye River Fault zone, in the Blue Ridge Provence in the Appalachians and show that basement buttressing played a role both in the early stages of deformation and the later stages. Bailey (2002) also suggest that there is a recognisable systematic change in fold profiles directly related to highs in the basement. The systematic change in fold profiles in the area across the Coomnacronia Fault, although not the main focus of this study, has been discussed previously by Capewell (1975) who indicates a ‘zone of tilted folds’ (Section 2.14.2) and also in this study overturned folds have been observed to the north of the Coomnacronia Fault (Section 4.5.5). This change in fold profiles would be compatible with the existence of a basement high along the north coast of the Iveragh Peninsula.

Figure 7.4 a) Left shows chevron folding in the hanging wall as shown in **b) below** (from Corfield et al. (1996). Chevron folding occurs in the synrift fill as result basement buttressing by the northern basin margin fault. The area has in located in the Foreland and has undergone Variscan deformation at the end of the Carboniferous. from Corfield et al. (1996).

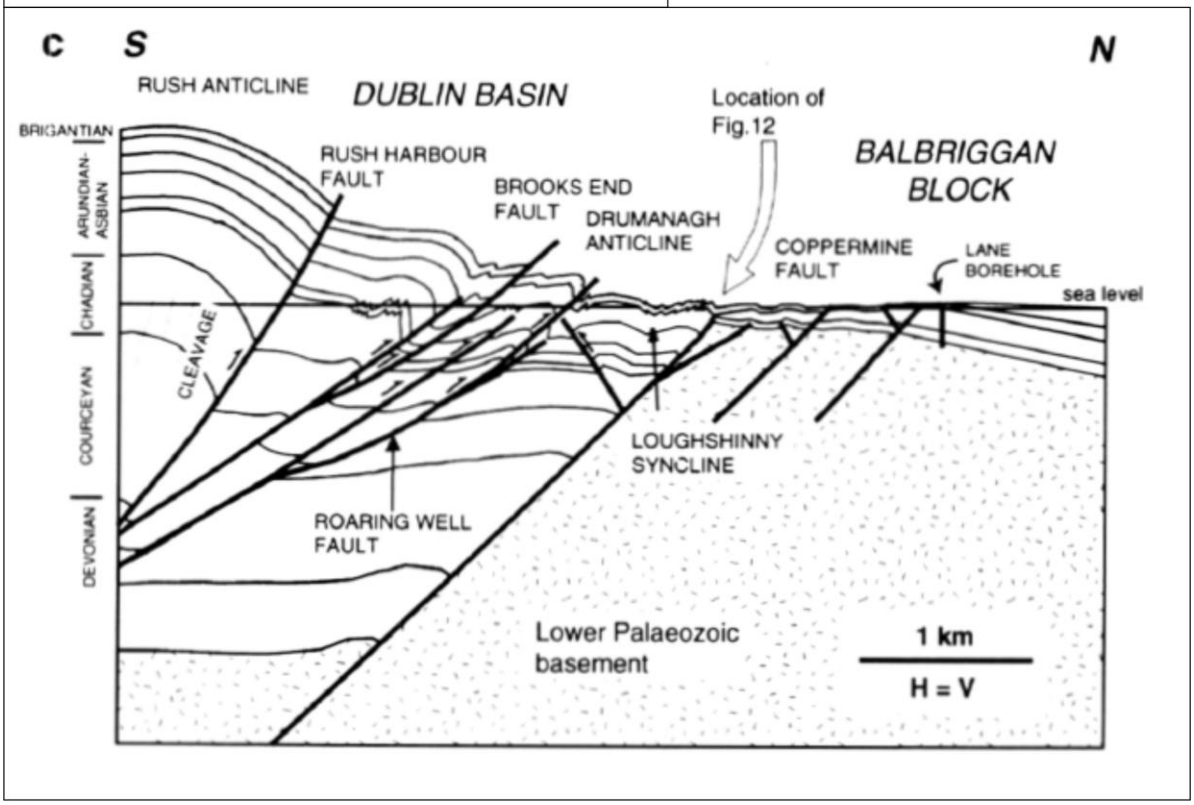

Inversion using a footwall shortcut has also been documented in a number of studies (Chapter 1; e.g. Giambiagi et al., 2009). A good analogy could be drawn between how the Coomnacronia Fault may have functioned as a basin margin fault and the Benton Fault in SW Dyfed, Wales (*pers comm*. Cooper, 2016; Powell, 1989; Fig 7.5). Powell (1989) examines the Benton Fault and other faults which are were originally extensional faults that controlled Devonian to Lower Carboniferous sedimentation, that have been reactivated as reverse faults during Variscan compression. The Benton Fault is one of the major faults that controlled sedimentation (pre-Variscan). Powell (1989) has put forward a model for the Benton Fault where a footwall shortcut develops during Variscan inversion, segmenting a unit consisting of some of the basement (Precambrian) from the horst block along with the overlying ORS units (Fig 7.5). This unit was

transported 3 km over the foreland during inversion. This type of structural mechanism would explain well the findings for the footwall of the Coomnacronia Fault in this study.

In order to allow the passive rotation of the autochtonous unit to the north of the Coomnacronia Fault, a footwall shortcut has been proposed. As well as the proposed existence of a footwall shortcut to the north, the steepness of the Coomnacronia Fault and the strong chevron folding found to the south of fault indicates that basement buttressing also played a role in deformation observed in the hangingwall. Therefore it is suggested that both of these mechanisms have played a part in the deformation of both the hanging wall units and the footwall units.

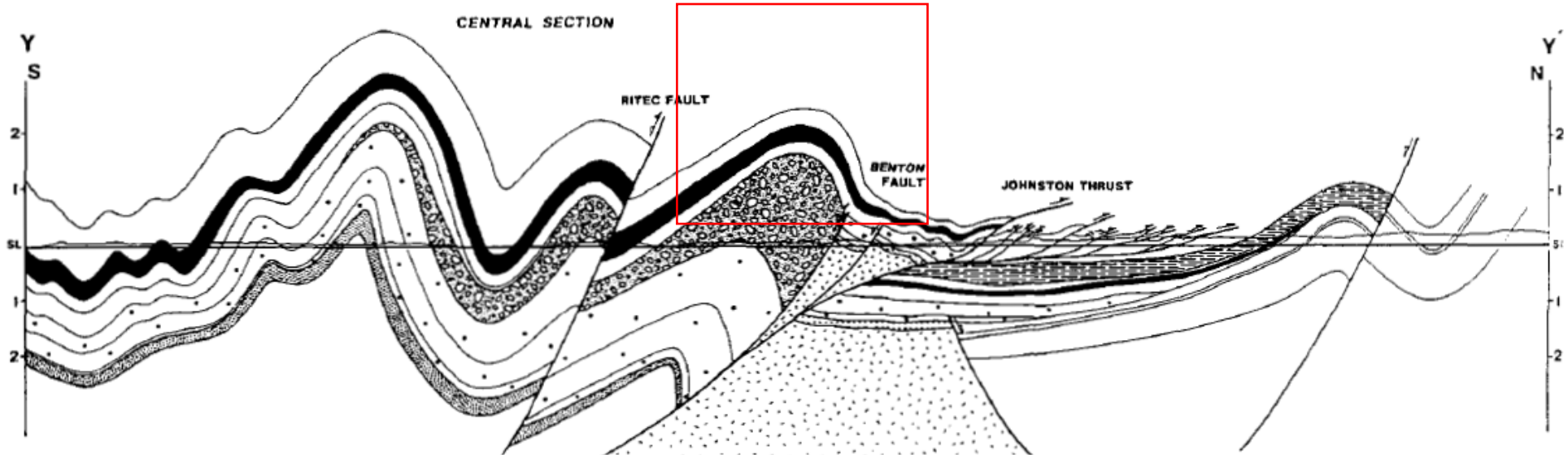

Figure 7.5 The Benton Fault (Area inside red box) may be a possible analogy for the behaviour of the Coomnacronia Fault as a basin margin fault. From Powel (1989).

7.5.2 Tectonic History

The following tectonic history (as illustrated in Fig 7.6) of the western sector of the Munster Basin is put forward in order to explain the findings in this study.

1) During Munster Basin sedimentation, the CF was initially an extensional fault delineating the northern margin of the basin.

2) During the early stages of inversion of the basin, Mid- Upper ORS material which lay to the south of the CF and thinner peripheral Mid – Upper ORS to the north (footwall) of the CF underwent, layer parallel shortening (LPS) followed by gentle folding.

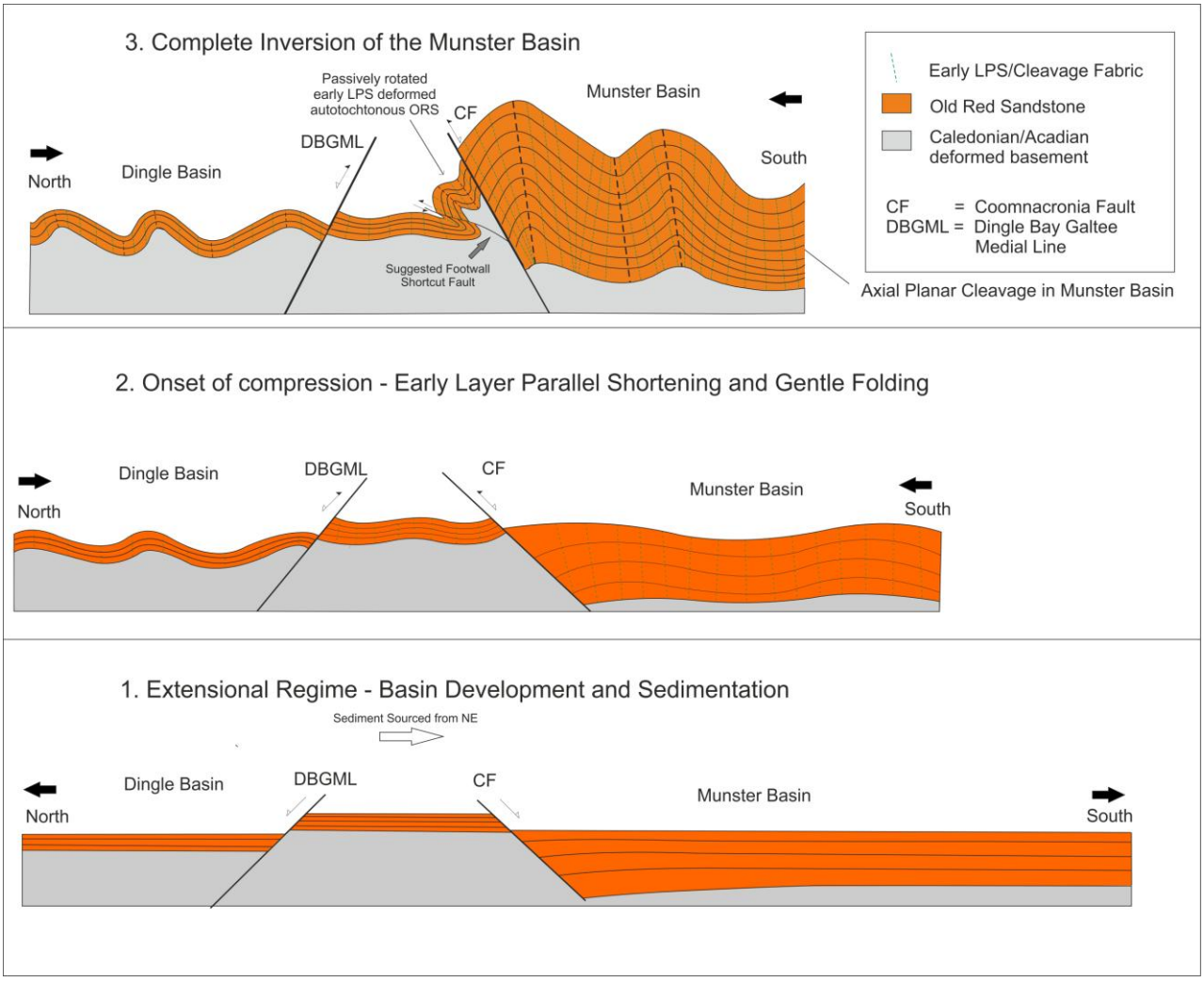

Figure 7.6 shows the progression from the extensional regime of the Munster Basin to complete inversion.

3) As inversion continued, the remaining material in the Munster Basin underwent continual deformation resulting in tightening of folding and a pervasive steeply dipping axial planar cleavage. To the north of the CF, a footwall shortcut may have developed in

response to inversion of the CF. This shortcut may have involved some of the Caledonian/Acadian basement horst block in a similar scenario to that of Powell's (1989) model as previously discussed (Fig 7.5). The movement along the footwall shortcut allowed for a rotation of the footwall unit with associated folding resulting in passively rotated early LPS fabric.

A summary of the tectonic zones is presented in Fig 7.7 and Map Insert 4. The ORS material to the south of the CF underwent the full extent of intrabasinal Variscan deformation resulting in the higher more consistent strain values and AMS ellipsoids controlled by cleavage (Fig 7.7). The results of the strain analysis are comparable with some of the findings in the microstructures. The thinner ORS material to the north preserved the early LPS fabric and underwent lower deformation, as indicated by lower strain R_s values, AMS ellipsoids characteristically controlled by bedding or LPS fabrics and lower deformation microstructure features.

7.6 Discussion of Methods

AMS has proven to be a very useful tool in foreland fold and thrust belts in previous studies (Chapter 3) and in this one. AMS is highly sensitive to the evolution of fabrics from primary sedimentary foliations to late tectonic overprint fabrics. AMS has also proven to be an effective complimentary study along with strain analysis and field work, in deciphering the location of the basin margin fault (the CF). AMS is an efficient and quick tool which is especially effective in the initial stages of a study, as a means to detecting variations in low strain. There is a very strong correlation of the orientation of the strain analysis long axis, ϕ, and the principal AMS axes indicating the accuracy of both of these methods. Although the MRL principally records strain of the quartz clasts and AMS is predominantly controlled by the paramagnetic minerals, the coincidence of the AMS axes and the long axis of the strain ellipsoid suggests that there is an intrinsic relationship between the quartz fabric and mica fabric which evolves as strain progresses. As strain increases the quartz grains formed a GSPO and the long axes of the micas may lie parallel or subparallel to the long axes of the quartz grains.

In general DTNNM measures higher strain than MRL, indicating that DTNNM is more sensitive to strain taken up by the matrix. Further work could involve quantifying the differences between DTNNM and MRL by detailed petrological analysis of the matrix proportions verses clast proportions. This also may also give an insight into the amount of strain taken up by early LPS.

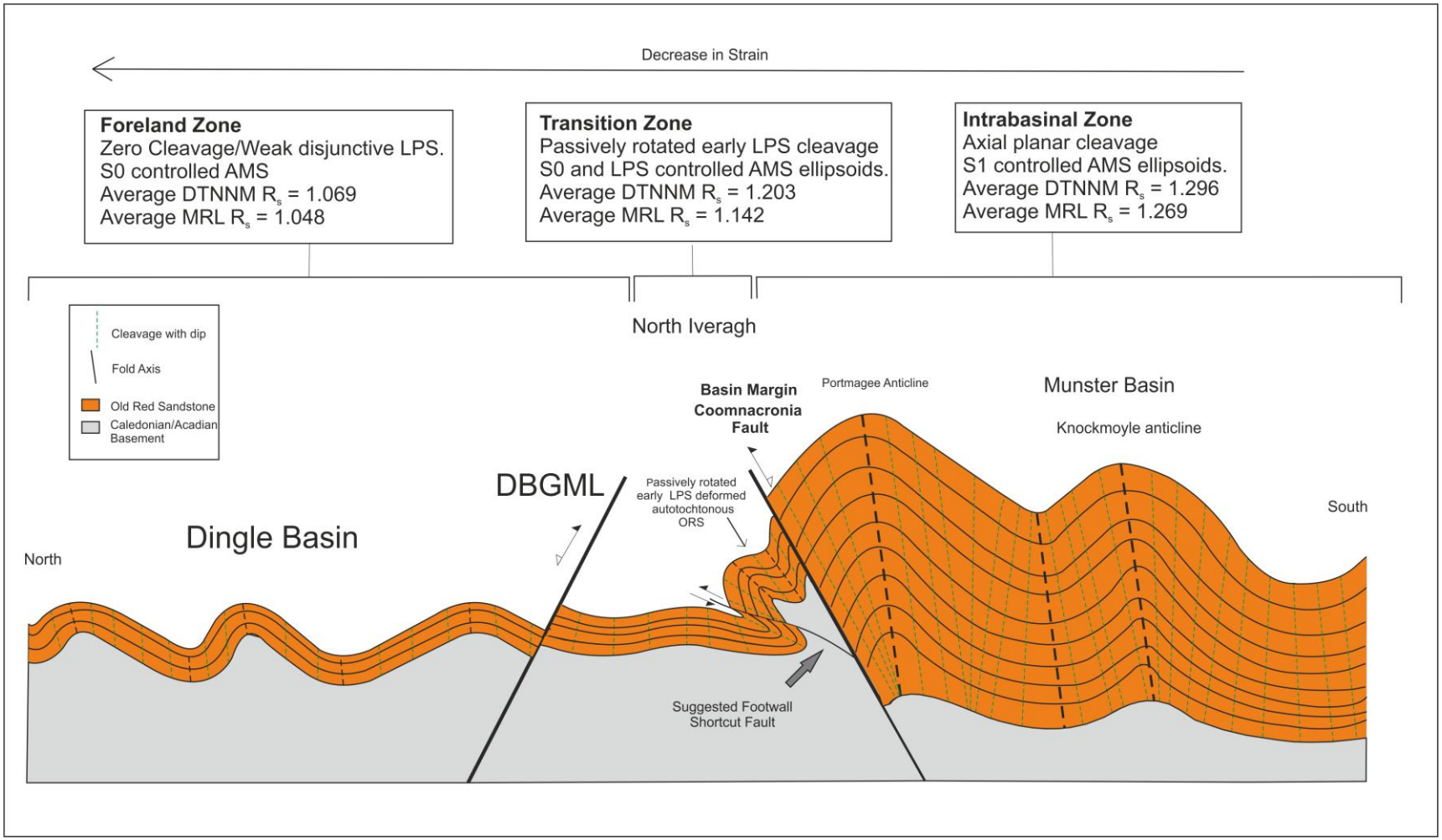

Figure 7.7 Schematic showing the development of cleavage zones and associated zones in ORS (pre-erosinal) across the main structural elements from south to north.

7.7 Further Work

There are a number of further studies which could develop upon the findings of this study. Temperature studies e.g. illite crystallinity (e.g. Kisch, 1983) may be a useful way of measuring any variations in temperature attained during low grade metamorphism. This method was used by Primmer (1985) in the anchizone to epizone of the Variscan in north Cornwall (Warr et al., 1991), and major temperature zones were found to be bound by a large scale fault, the Rusey Fault. Andrews et al. (1996) have also investigated the Rusey Fault using vitrinite reflectance data. These methods, alongside other geothermometry methods could be used in order to investigate if the Coomnacronia Fault marks any change in the temperatures attained during metamorphism. Previous illite crystallinity studies have been carried out in the south of the Munster Basin by Meere (1995), but not in the vicinity of the CF.

Fluid inclusion studies could also be used in order to investigate the CF as a basin margin fault. Previous fluid inclusion studies have also been carried out by Meere (1995) in the south of the Munster Basin, but none have been carried out in the region of the Coomnacronia Fault. Fluid inclusion studies may provide valuable insight into the role that the CF played as a basin margin fault.

Further detailed investigation into the nature of the LPS fabric would be desirable. Microstructural techniques could be used to compare the LPS fabric in the Transition Zone with the cleavage zones in the Intrabasinal Zone. This could involve looking at the preferred crystal orientation and microstructural deformation mechanisms using techniques such as EBSD or Neutron Texture goniometry. XRD could be used in order to understand better the distribution of micas and hence integrate this with the analysis of the LPS Fabric. A study could be carried out into the role of detrital and authigenic micas in LPS and cleavage development.

The depth of the basement in the area of the transition zone would be a key indicator that the CF is a basin margin structure and that the area lying to the north of the CF on the Iveragh Peninsula is a basement high. Geophysical surveys such as seismic refraction and gravity anomalies could be carried out on the northern Iveragh Peninsula with this purpose in mind.

A detailed tectono-stratigraphic study involving detailed mapping of lithological units across the CF, could be undertaken in order to investigate if the outcrop pattern fits best

with the CF being an intrabasinal fault or a basin margin fault. More detailed field work could be carried out on the Coomnacronia Fault and its fault movement history starting at its initiation as a basin margin fault during sedimentation to its reactivation as a reverse fault during Variscan deformation. Lake Coomnacronia would provide an excellent location for the detailed analysis of the CF's tectonic history, as in this location the CF can be observed in outcrop as a number of imbricate thrust faults.

Chapter 8:
Conclusions

Chapter 8: Conclusions

8.1 Tectonic Zones in the Western Irish Variscides

- This study proposes a new tectonic zonation scheme in the region of the northern margin of the Munster Basin, which builds upon and modifies the zones of Gill (1962) and subsequently Cooper (1986) in the south western Irish Variscides.
- The Coomnacronia Fault marks the boundary between a higher strain zone to the south - the Intrabasinal Zone and a lower strain zone to the north - the Transition Zone.

8.2 The Intrabasinal Zone

- The Intrabasinal Zone lies to the south of the Coomnacronia Fault and consists of mid-upper ORS that underwent the full extent of Variscan deformation, evident from the existence of a full penetrative steeply dipping axial planar cleavage, higher more consistent strain values, AMS ellipsoids controlled by cleavage and microstructures reflecting this higher strain zone.
- The Intrabasinal Zone has higher average strain values with the Delaunay Triangulation Nearest Neighbour Method (DTNNM) R_s = 1.296 and the Mean Radial Length Method (MRL) R_s = 1.269**.**
- AMS ellipsoids are predominantly controlled by cleavage indicating a complete tectonic overprint of primary sedimentary fabrics. The orientations of the principal AMS axes correlate closely with the long axes of the strain ellipse.
- Microstructures are indicative of a higher strain regime with the presence of a grain shaped preferred orientation (GSPO) defined by elongated quartz clasts, the long axes of which parallels the orientation of the principal strain axes.

8.3 The Transition Zone

- The Transition Zone is located to the north of the Coomnacronia Fault on the Iveragh Peninsula and shows evidence of having undergone a lower strain regime.
- Strain results are generally lower in the Transition Zone with the average DTNNM R_s = 1.203 and average MRL R_s= 1.142.
- The ORS of the Transition Zone is autochtonous and underwent early layer parallel shortening (LPS). The LPS fabric has been passively rotated with bedding, within a unit possibly underlain by a footwall shortcut.

- AMS ellipsoids are controlled by primary sedimentary fabrics and early layer parallel shortening (LPS) fabrics. The AMS fabrics have not undergone a complete tectonic overprint as in the Intrabasinal Zone.
- Microstructures are reflective of a lower strain regime compared to that of the Intrabasinal Zone.

8.4 The Foreland Zone

- The ORS on the Dingle Peninsula is part of the Foreland Zone. In this zone the cleavage is rare and disjunctive and steeply dipping. In this zone, AMS ellipsoids are controlled by primary sedimentary fabrics. There are lower average strain values in the Foreland Zone with the average DTNNM R_s = 1.069 the average MRL R_s = 1.048.

8.5 The Coomnacronia Fault

- The Coomnacronia Fault has a direct impact on the orientation of both the strike and the dip of cleavage in the Munster Basin, indicating its effect on deformation patterns. The Coomnacronia Fault is the location of a Variscan cleavage front, marks a significant tectonic boundary and possibly defines the location of the Variscan Front in the western part of the Irish Variscides.
- The Coomnacronia Fault was an initial extensional fault that bound the northern margin of the Munster Basin during sedimentation. The Coomnacronia Fault subsequently acted as a reverse fault during the onset of Variscan compression at the end of the Carboniferous. During inversion, a footwall shortcut is proposed to have developed to the north of the CF, which resulted in the rotation of the unit with associated passive rotation of the early tectonic fabric, lying immediately to the north of the Coomnacronia Fault.
- Inversion mechanisms along the Coomnacronia Fault involving a footwall shortcut explain better the nature of deformation patterns found in the vicinity of the northern margin of the Munster Basin, with a passively rotated tectonic fabric and lower strain in the footwall of the Coomnacronia Fault.

8.6 The Northern Margin of the Munster Basin and the Variscan Front

- The Coomnacronia Fault is considered to be the location of the northern margin of the Munster Basin in the west, and is the lateral continuation of the northern margin further to the east denoted by the Kilarney Mallow Fault Zone (KMFZ). This proposed basin margin fault lies further to the south than the previously suggested locations for the margin which were the Dingle Dungarvan Line (DDL) and the Dingle May Galtee Mountains Line (DBGML)/Dingle Bay Galtee Fault Zone (DBGFZ).
- The Variscan Front is considered to be the line along which tectonic deformation significantly decreases and this coincides with the northern margin of the Munster Basin.

References.

Abouzakhm, A.G. & Tarling, D.H. 1975. Magnetic anisotropy and susceptibility of late Precambrian tillites from northwestern Scotland. *Journal of the Geological Society*, **131**, 647-652.

Ailleres, L. & Champenois, M. 1994. Refinements to the Fry method (1979) using image processing. *Journal of Structural Geology*, **16**, 1327-1330.

Ailleres, L., Champenois, M., Macaudiere, J. & Bertrand, J.M. 1995. Use of image analysis in the measurement of finite strain by the normalized Fry method: geological implications for the 'Zone Houillere' (Brianconnais zone, French Alps). *Mineralogical Magazine*, **59**, 179-188.

Alexander, A.C. & Shail, R.K. 1995. Late Variscan structures on the coast between Perranporth and St. Ives, Cornwall. *Proceedings of the Ussher Society*, **8**, 398-398.

Allmendinger, R.W., Nelson, K.D., Potter, C.J., Barazangi, M., Brown, L.D. & Oliver, J.T. 1987. Deep seismic reflection characteristics of the continental crust. *Geology*, **15**, 304-310.

Anderson, M.W. & Morris, A. 2004. The puzzle of axis-normal magnetic lineations in folded low-grade sediments (Bude Formation, SW England). In: Martín-Hernández, F., Lüneburg, C.M., Aubourg, C., Jackson, M. (Eds.), Magnetic Fabric; Methods and Applications: *Geological Society Special Publication*, **238**, 175-190.

Aranguren, A., Cuevas, J. & Tubı´a, J.M. 1996. Composite magnetic fabrics from S-C mylonites. *Journal of Structural Geology*, **18**, 863-869.

Aubourg, C., Rochette, P. & Vialon, P. 1991. Subtle stretching lineation revealed by magnetic fabric of Callovian-Oxfordian black shales (French Alps). *Tectonophysics*, **185**, 211-223.

Aubourg, C., De Lamotte, D.F., Poisson, A. & Mercier, E. 1997. Magnetic fabrics and oblique ramp-related folding: a case study from the western Taurus (Turkey). *Journal of Structural Geology*, **19**, 1111-1120.

Aubourg, C., Hebert, R., Jolivet, L. & Cartayrade, G. 2000. The magnetic fabric of metasediments in a detachment shear zone: the example of Tinos Island (Greece). *Tectonophysics*, **321**, 219-236.

Aubourg, C. & Robion, P. 2002. Composite ferromagnetic fabrics (magnetite, greigite) measured by AMS and partial AARM in weakly strained sandstones from western Makran, Iran. *Geophysical Journal International*, **151**, 729-737.

Aubourg, C., Smith, B., Bakhtari, H., Guya, N., Eshragi, A., Lallemant, S. & Delaunay, S. 2004. Post-Miocene shortening pictured by magnetic fabric across the Zagros-Makran syntaxis (Iran). *Geological Society of America Special Papers*, **383**, 17-40.

Autran et al. 1980. Rhenohercyian Europe central germany. Forum of European Geological Surveys (FOREGS) - *From the Geological and Tectonic Framework of Europe*, 2005.

Averbuch, O, Frizon de Lamotte, D. & Kissel, C. 1992. Magnetic fabric as a structural indicator of the deformation path within a fold-thrust structure: a test case from the Corbieres (NE Pyrenees, France). *Journal of Structural Geology*, **14**, 461-474.

References

Avison, M. 1984. Contemporaneous faulting and the eruption and preservation of the Lough Guitane volcanic complex, Co. Kerry. *Journal of the Geological Society, London*, **141**, 501-10.

Badham, J.P.N. 1982. Strike-slip orogens - an explanation for the Hercynides. *Journal of the Geological Society*, **139**, 493-504.

Badham, J.P.N. & Halls, C. 1975. Microplate tectonics, oblique collisions, and evolution of the Hercynian orogenic systems. *Geology*, **3**, 373-376.

Bailey, C.M., Giorgis, S. & Coiner, L. 2002. Tectonic inversion and basement buttressing: an example from the central Apalachian Blue Ridge province. *Journal of Structural Geology*, **24**, 925-936.

Bakhtari, H.R., de Lamotte, D. F., Aubourg, C. & Hassanzadeh, J. 1998. Magnetic fabrics of tertiary sandstones from the Arc of Fars (Eastern Zagros, Iran). *Tectonophysics*, **284**, 299-316.

Bamford, M.L.F. & Ford, M. 1990. Flexural shear in a periclinal fold from the Irish Variscides. *Journal of Structural Geology*, **12**, 59-67.

Banerjee, S.K. & Stacey, F.D. 1967. The high field torque meter method of measuring magnetic anisotropy of rocks. *Developments in Solid Earth Geophysics*, **3**, 470.

Bascou, J., Raposo, M.I.B., Vauchez, A. & Egydio-Silva, M. 2002. Titanohematite lattice-preferred orientation and magnetic anisotropy in high-temperature mylonites. *Earth and Planetary Science Letters*, **198**, 77-92.

Behr, H. J., Walliser, O.H. & Weber, K. 1980. The development of the Rheno-hercynian and Saxo-thuringian zones of the mid-European Variscides. *Geology of Europe*, 77-89.

Bell, T. H. 1986. Foliation development and refraction in metamorphic rocks: reactivation of earlier foliations and decrenulation due to shifting patterns of deformation partitioning. *Journal of Metamorphic Geology*, **4**, 421-444.

Bina, M. & Daly, L. 1994. Mineralogical change and self-reversed magnetizations in pyrrhotite resulting from partial oxidation; geophysical implications. *Physics of the Earth and Planetary Interiors*, **85**, 83-99.

Blackmore, R. 1995. Low-grade metamorphism in the upper Palaeozoic Munster Basin, southern Ireland. *Irish Journal of Earth Sciences*, **14,** 115-133.

Borradaile, G. 1976. A strain study of a granite–granite gneiss transition and accompanying schistosity formation in the Betic orogenic zone, SE, Spain. *Journal of the Geological Society*, **132**, 417-428.

Borradaile, G.J. 1987a. Anisotropy of magnetic susceptibility: rock composition versus strain. *Tectonophysics*, **138**, 327-329.

Borradaile, G.J. 1987b. Analysis of strained sedimentary fabrics: review and tests. *Canadian Journal of Earth Sciences*, **24**, 442-455.

Borradaile, G.J. 1988. Magnetic susceptibility, petrofabrics and strain. *Tectonophysics*, **156**, 1-20.

References

Borradaile, G.J. 1991. Correlation of strain with anisotropy of magnetic susceptibility (AMS). *Pure and Applied Geophysics*, **135**, 15-29.

Borradaile, G.J. 2001. Magnetic fabrics and petrofabrics: their orientation distributions and anisotropies. *Journal of Structural Geology,* **23**, 1581-1596.

Borradaile, G.J. & Alford, C. 1987. Relationship between magnetic susceptibility and strain in laboratory experiments. *Tectonophysics*, **133**, 121-135.

Borradaile, G.J. & Alford, C. 1988. Experimental shear zones and magnetic fabrics. *Journal of Structural Geology*, **10**, 895-904.

Borradaile, G.J. & Geneviciene, I. 2008. Late proterozoic reconstructions of North-West Scotland and Central Canada: Magnetic fabrics, paleomagnetism and tectonics. *Journal of Structural Geology,* **30**, 1466-1488.

Borradaile, G.J. & Henry, B. 1997. Tectonic applications of magnetic susceptibility and its anisotropy. *Earth-Science Reviews*, **42**, 49-93.

Borradaile, G.J. & Jackson, M. 2004. Anisotropy of magnetic susceptibility (AMS), magnetic petrofabrics of deformed rocks. In: Martín-Hernandez, F., Lünenburg, C.M., Aubourg, C., Jackson, M. (Eds.), Magnetic Fabrics. *Geological Society of London Special Publication* No, **238**, pp. 299-360.

Borradaile, G.J. & Jackson, M. 2010. Structural geology, petrofabrics and magnetic fabrics (AMS, AARM, AIRM). *Journal of Structural Geology*, **32**, 1519-1551.

Borradaile, G.J. & Lucas, K. 2003. Tectonics of the Akamas and Mamonia ophiolites, Western Cyprus: magnetic petrofabrics and paleomagnetism. *Journal of Structural Geology,* **25**, 2053-2076.

Borradaile, G., Mothersill, J., Tarling, D. & Alford, C. 1986. Sources of magnetic susceptibility in a slate. *Earth and Planetary Science Letters*, **76**, 336-340.

Borradaile, G.J. & Stupavsky, M. 1995. Anisotropy of magnetic susceptibility: measurement schemes. *Geophysical Research Lett*ers, **15**, 1957-1960.

Borradaile, G.J., Tella, S. & McArthur, J. 1989. Magnetic fabric as a kinematic indicator of faults, a test case. *Annales de Tectonicae,* **3**, 3-11.

Borradaile, G.J., Werner, T. & Lagroix, F. 1999. Magnetic fabrics and anisotropy-controlled thrusting in the Kapuskasing Stuctural Zone, Canada. *Tectonophysics,* **302**, 241-256.

Borradaile, G.J. & Puumala, M. A. 1989. Synthetic magnetic fabrics in a plasticene medium. *Tectonophysics*, **164**, 73-78.

Boyd, J.D. & Sloan, R.J. 2000. Initiation and early development of the Dingle Basin, SW Ireland, in the context of the closure of the Iapetus Ocean. *Geological Society, London, Special Publications*, **180**, 123-145.

Bresser, G. & Walter, R. 1999. A new structural model for the SW Irish Variscides, The Variscan front of the NW Euroean Rhenohercynian. *Tectonophysics*, **309**, 197-209.

References

Bresser, G. & Hilgers, C. 1996. Struktur und Metamorphoseentwicklung im SW-irischen Außenvariszikum am Beispiel eines geologischen Profils von Killarney nach Bantry. Unpublised Diploma Thesis, RWTH Aachen, 331 pp.

Bridge, J.S. & Diemer, J.A. 1983. Quantitative interpretation of an evolving ancient river system. *Sedimentology*, **30**, 599-623.

Brokmeier, H.G. 1994 Texture analysis by neutron diffraction. In Materials Science Forum, **157**, 59-70.

Brown, A.C. 1979. The Navan (Tara) deposit. In: Brown, A.C. (ed.) Prospecting in areas of glaciated terrane, 25-33. *Irish Association for Economic Geology*.

Burmeister, K.C., Harrison, M.J., Marshak, S., Ferre, E.C., Bannister, R.A. & Kodama, K.P. 2009. Comparision of Fry strain ellipse and AMS ellipsoid trends to tectonic fabric trends in very low-strain sandstone of the Appalachian fold-thrust belt. *Journal of Structural Geology*, **31**, 1028 – 1038.

Butler, R.F. 1992. Paleomagnetism: Magnetic Domains to Geologic Terranes, Blackwell, 319 p.

Butler, R.W.H. 1989. The influence of pre-existing basin structure on thrust system evolution in the Western Alps. In Cooper, M.A. & Williams, G.D. (eds) Inversion Tectonics, *Geological Society of London Special Publication*, **44**, 105-122.

Callot, J. P., Robion, P., Sassi, W., Guiton, M. L. E., Faure, J. L., Daniel, J.M. & Schmitz, J. 2010. Magnetic characterisation of folded aeolian sandstones: Interpretation of magnetic fabrics in diamagnetic rocks. *Tectonophysics*, **495**, 230-245.

Capewell, J.G. 1951.The Old Red Sandstone of the Inch and Annascaul District, Co. Kerry. In *Proceedings of the Royal Irish Academy*. Section B: Biological, Geological, and Chemical Science, **54**, 141-168. Royal Irish Academy.

Capewell, J.G. 1957. The stratigraphy and structure of the country around Sneem, Co. Kerry. Proc. R.I.A., **58**, 167-183.

Capewell, J.G. 1965. The old red sandstone of Slieve Mish, Co. Kerry. *Proceedings of the Royal Irish Academy*, **64**, 165-174.

Capewell, G. 1975. The Old Red Sandstone Group of Iveragh, Co. Kerry. *Proceedings of the Royal Irish Academy*, **15**, 155-171.

Carmichael, R.S. 1982. CRC handbook of physical properties of Rocks. CRC Press. Inc..

Chadima, M., Hansen, A., Hirt, A. M., Hrouda, F. & Siemes, H. 2004. Phyllosilicate preferred orientation as a control of magnetic fabric: evidence from neutron texture goniometry and low and high-field magnetic anisotropy (SE Rhenohercynian Zone of Bohemian Massif). *Geological Society, London, Special Publications*, **238**, 361-380.

Chadima, M., Hrouda, F. & Melichar, R. 2006. Magnetic fabric study of the SE Rhenohercynian Zone (Bohemian Massif): Implications for dynamics of the Paleozoic accretionary wedge. *Tectonophysics*, **418**, 93-109.

References

Chew, D.M. & Stillman, C. J. 2009. Late Caledonian orogeny and magmatism. *The geology of Ireland*, **2,** 143-174.

Choudhury, K.R. & Mulchrone, K. 2006. A comparative error analysis of manual versus automated methods of data acquisition for algebraic strain estimation. *Tectonophysics,* **421,** 209-230.

Cifelli, F., Mattei, M., Chadima, M., Lenser, S. & Hirt, A.M. 2009. The magnetic fabric in "undeformed clays": AMS and neutron texture analyses from the Rif Chain (Morocco). *Tectonophysics*, **466**, 79-88.

Clayton, G. 1989. Vitrinite reflectance data from the Kinsale Harbour-Old Head of Kinsale area, southern Ireland, and its bearing on the interpretation of the Munster Basin. *Journal of the Geological Society, London*, **146**, 611-616.

Clayton. G. & Graham, J.R. 1974. Miospore assemblages from the Devonian Sherkin Formation of south-west County Cork. Republic of Ireland. *Pollen et Spores,* **16**, 565-588.

Clayton, G., Graham, J.R., Higgs, K., Holland, C.H. & Naylor, D. 1980. Devonian rocks in Ireland: A review. *Journal of Earth Sciences, Royal Dublin Society,* **2**, 161-183.

Clayton, G. & Higgs, K. 1979. The Tournaisian marine transgression in Ireland. *Journal of Earth Sciences, Royal Dublin Society*, **2**, 1-10.

Coe, K. & Selwood, E.B. 1963. The stratigraphy and structure of part of the Beara Peninsula, Co. Cork. In Proceedings of the Royal Irish Academy. Section B: Biological, *Geological, and Chemical Science*, (pp. 33-59). Hodges, Figgis, & Co.

Cogné, J.P. & Perroud, H. 1988. Anisotropy of magnetic susceptibility as a strain gauge in the Flamanville granite, NW France. *Physics of the Earth and Planetary Interiors*, **51**, 264-270.

Coller, D.W. 1984. Variscan structures in the Upper Palaeozoic rocks of west central Ireland. In: Hutton, D.H., Sanderson, D.J. (Eds.), Variscan Tectonics of the North Atlantic Region. *Geological Society of London, Special Publication***, 14**, 185-194.

Colthrust, J.R.J. 1978. Old Red Sandstone Rocks Surrounding the Slievenamon Inlier, Counties Tipperary and Kilkenny. *Journal of Earth Sciences*, **1,** 77-103.

Cooper, M.A., Collins, D., Ford, M., Murphy, F.X. & Trayner, P.M. 1984. Structural style, shortening estimates and the thrust front of the Irish Variscides. In: Hutton, D.H. & Sanderson, D.J. (Eds.), Variscan Tectonics of the North Atlantic Region. *Geological Society of London, Special Publication,* **14**, 185-194.

Cooper, M.A., Collins, D.A., Ford, M., Murphy, F.X., Trayner, P.M. & O' Sullivan, M. 1986. Structural evolution of the Irish Variscides. *Journal of the Geological Society*, London, **143**, 53-61.

Cooper, M. & Trayner, M. 1986. Thrust-surface geometry: implications for thrust-belt evolution and section-balancing techniques. *Journal of Structural Geology*, **8**, 305-312.

Cooper, M.A. & Williams, G.D. (eds) 1989. Inversion Tectonics. *Geological Society of London Special Publications*, **44**, 378 p.

References

Cooper, M.A., Williams, G.D., de Graciansky, Murphy, R.W., Needham, T., de Paor, D., Stoneley, R., Todd, S.P., Turner, J.P. & Ziegler, P.A. 1989. Inversion Tectonics – a discussion. *Geological Society Special Publications*, **44,** 335-347.

Corfield, S. M., Gawthorpe, R. L., Gage, M., Fraser, A. J. & Besly, B. M. (1996). Inversion tectonics of the Variscan foreland of the British Isles. *Journal of the Geological Society*, **153**, 17-32.

Cotter, E. & Graham, J.R. 1991. Coastal plain sedimentation in the late Devonian of southern Ireland; hummocky cross-stratification in fluvial deposits? *Sedimentary Geology*, **72**, 201-224.

Daly, L. 1972. Utilisation des mesures d'anisotropie de susceptibilité magnétique dans les reconstitutions paléogéographiques. *Memoirs, Bureau de Recherches Géologiques et Minières*, **77**, 839-843.

De Graciansky, P. C., Dardeau, G., Lemoine, M. & Tricart, P. (1989). The inverted margin of the French Alps and foreland basin inversion. *Geological Society, London, Special Publications*, ***44***, 87-104.

Debacker, T.N., Hirt, A.M., Sintubin, M. & Robion, P. 2009. Differences between magnetic and mineral fabrics in low grade, cleaved siliciclastic pelites: A case study from the Anglo-Brabant Deformation Belt (Belgium). *Tectonophysics*, **366**, 32-46.

Debacker, T.N., Robion, P. & Sintubin, M. 2004. The anisotropy of magnetic susceptibility (AMS) in low-grade, cleaved pelitic rocks: influence of cleavage/bedding angle and type and relative orientation of magnetic carriers. In: Martín-Hernández, F., Lüneburg, C.M., Aubourg, C., Jackson, M. (Eds.), Magnetic Fabric, Methods and Applications*: Geological Society Special Publication*, **238**, 77-108.

Debacker, T.N., Sintubin, M. & Verniers, J. 2004. Transitional geometries between gently plunging and steeply plunging folds: an example from the Lower Palaeozoic Brabant Massif, Anglo-Brabant deformation belt, Belgium. *Journal of the Geological Society*, **161**, 641-652.

Debacker, T.N., van Noorden, M. & Sintubin, M. 2006. Distinguishing syn-cleavage folds from pre-cleavage folds to which cleavage is virtually axial planar: examples from the Cambrian core of the Lower Palaeozoic Anglo-Brabant Deformation Belt (Belgium). *Journal of Structural Geology*, **28**, 1123-1138.

De Lamotte, D.F., Souque, C., Grelaud, S. & Robion, P. 2002. Early record of tectonic magnetic fabric during inversion of a sedimentary basin Short review and examples from the Corbières transfer zone (France). *Bulletin de la Société Géologique de France*, **173**, 461-469.

De Paor, D.C. 1983. Orthographic analysis of geological structures – 1 Deformation Theory. *Journal Structural Geology*, **5**, 255-277.

Dewey, J.F. 1966. Kink bands in Lower Carbonieferous slates of Rush, Co. Dublin. *Geological Magazine* **103**, 138-412.

Dewey, J.F. 1982. Plate tectonics and the evolution of the British Isles. *Journal of the Geological Society of London*, **139**, 371- 412.

Diemer J.A., Bridge, J.S. & Sanderson, D. J. 1987. Revised geology of Kerry Head, County Kerry, *Irish Journal of Earth Sciences*, **8**, 113-138.

References

Doran, R.J.P., Holland, C.H. & Jackson, A.A. 1973.The sub-Old Red Sandstone surface in southern Ireland. In Proceedings of the Royal Irish Academy. Section B: Biological, Geological, and Chemical Science (pp. 109-128). Royal Irish Academy.

Duermeijer, C.E., van Vugt, N., Langereis, C.G., Meulenkamp, J.E. & Zachariasse, W.J. 1998. A major late Tortonian rotation phase in the Crotone basin using AMS as tectonic tilt correction and timing of the opening of the Tyrrhenian basin. *Tectonophysics,* **287**, 233-249.

Dunlap, W.J., Hirth, G. & Teyssier, C. 1997. Thermomechanical evolution of a ductile duplex. *Tectonics*, **16**, 983-1000.

Dunlop, D. & O¨zdemir, O. 1997. Rock Magnetism: Fundamentals and Frontiers, *Cambridge University Press*, New York.

Dunlop, D.J. & O¨zdemir, O. 2001. Rock Magnetism: Fundamentals and Frontiers. Cambridge, *Cambridge University Press*.

Dunlop, D.J., Stacey, F.D. & Gillingham, D.E. 1974. The origin of thermoremanent magnetization: contribution of pseudo-single-domain magnetic moments. *Earth and Planetary Science Letters*, **21**, 288-294.

Dunnet, D. 1969. A technique of finite strain analysis using elliptical particles. *Tectonophysics*, **7**, 117-136.

Dunnet, D. & Siddans, A. 1971. Non-random sedimentary fabrics and their modification bystrain. *Tectonophysics,* **12**, 307-325.

Dunning, F.W. 1966. Tectonic Map of Great Britain and Northern Ireland. *Institute of Geological Sciences, England.*

Dunning, F.W. 1980. United Kingdom, geotectonic position. In: Bordas and 26th Int. Geolog. Congress (eds). Geology of the European Countries. 331-337. Graham & Trotman, London.

Efron, B 1979.Bootstrap methods: another look at the jackknife. *The Annals of Statistics* **7**, 1-26.

Elliott, D. 1970. Determination of finite strain and initial shape from deformed elliptical objects. *Geological Society of America Bulletin*, **81**, 2221-2236.

Engelder, T. & Marshak S. 1985. Disjunctive cleavage formed at shallow depths in sedimentary rocks. *Journal of Structural Geology*, **7**, 327-344.

Ennis, M., Meere, P.A., Timmerman, M.J. & Sudo, M. 2015. Post-Acadian sediment recycling in the Devonian Old Red Sandstone of Southern Ireland. *Gondwana Research*, **28**, 1415-1433.

Erslev, E. 1988. Normalized center-to-center strain analysis of packed aggregates. *Journal of Structural Geology*, **10**, 201-209.

Erslev, E. & Ge, H. 1990. Least-squares center-to-center and mean object ellipse fabric analysis. *Journal of Structural Geology*, **12**, 1047-1059.

References

Evans, M.A., Lewchuk, M.T. & Elmore, R.D. 2003. Strain partitioning of deformation mechanisms in limestones: examining the relationship of strain and anisotropy of magnetic susceptibility (AMS). *Journal of Structural Geology,* **25**, 1525-1549.

Feinberg, J.M., Wenk, H. R., Scott, G.R. & Renne, P.R. 2006. Preferred orientation and anisotropy of seismic and magnetic properties in gabbronorites from the Bushveld layered intrusion. *Tectonophysics,* **420**, 345-356.

Ferré, E.C. & Améglio, L. 2000. Preserved magnetic fabrics vs. annealed microstructures in the syntectonic recrystallised George granite, South Africa. *Journal of Structural Geology*, **22**, 1199-1219.

Fitter, F.P. 1989. Coaxial strain modification of anisotropy of magnetic susceptibility: a theoretical study in two dimensions. MS University of Texas at Arlington. Arlington.

Flinn, D. 1962. On folding during three-dimensional progressive deformation. Quarterly *Journal of the Geological Society of London,* **118**, 385 -433.

Flinn, D. 1965. On the symmetry principle and the deformation ellipsoid. *Geological Magazine,* **102**, 36-45.

Ford, M. 1987. Practical application of the sequential balancing technique: an example from the Irish Variscides. *Journal of the Geological Society, London,* **144**, 885-891.

Ford, M. 1990. The stratigraphy and structure of the Galley Head Culmination Zone: and area of enhanced shortening related to basin geometry within the Irish Variscides. *Geological Journal*, **25**, 145-159.

Ford, M., Brown, C. & Readman, P. 1991. Analysis and tectonic interpretation of gravity data over the Variscides of southwest Ireland. *Journal of the Geological Society, London*, **148**, 137-148.

Ford, M. & Edwards, H.E. 1990. Discussion of a Model for the development of the Irish Variscides. *Journal of the Geological Society,* **147**, 566-571.

Ford, M. & Ferguson, C.C. 1985. Cleavage strain in the Variscan Fold Belt, County Cork, Ireland, estimated from stretched arsenopyrite rosettes. *Journal of Structural Geology,* **7**, 217-223.

Ford, M., Klemperer, S.L. & Ryan, P.D. 1992. Deep structure of southern Ireland: a new geological synthesis using BIRPS deep reflection profiling. *Journal of the Geological Society, London,* **149**, 915-922.

Franke, W. 1989. Tectono-stratigraphic units in the Variscan belt of central Europe. *Geological Society of America, Special Paper,* **230**, 67-89.

Franke, W., Haak, V., Oncken, O. & Tanner,D. 2000. Orogenic processes: quantification and modelling in the Variscan belt. *Geological Society, London, Special Publications*, **179**, 1-3.

Friedman, M. & Higgs, N. G. 1981. Calcite fabrics in experimental shear zones. In Mechanical behavior of crustal rocks, *American Geophysical Union Monograph***, 24**, 11-27.

Friend, P.F., Williams, B.P.J., Ford, M. & Williams, E.A. 2000. Kinematics and dynamics of Old Red Sandstone basins. *Geological Society of London, Special Publications*, **180**, 29-60.

References

Frizon de Lamotte, D., Mercier, E., Dupre la Tour, A., Robion, P. & Averbuch, O. 1997. Cinématique du plissement et déformation interne des roches. L'exemple du pli de Lagrasse (Aude, France). *Comptes rendus de l'Académie des sciences. Série 2. Sciences de la terre et des planètes*, **324**, 591-598.

Fry, N.1979. Density distribution techniques and strained length methods for determination of finite strains. *Journal of Structural Geology*, **1**, 221-229.

Fry, N. 1979. Random point distributions and strain measurement in rocks. *Tectonophysics*, **60**, 89-105.

Fueten, F., Robin, P.Y.F. & Schweinberger, M. 2002. Finite element modelling of the evolution of pressure solution cleavage. *Journal of Structural Geology*, **24**, 1055-1064.

Gaillot, P., de Saint-Blanquat, M. & Bouchez, J. L. 2006. Effects of magnetic interactions in anisotropy of magnetic susceptibility: Models, experiments and implications for igneous rock fabrics quantification. *Tectonophysics*, **418**, 3-19.

Gardiner, P.R.R. & MacCarthy, I.A.J. 1980. The late Palaeozoic evolution of southern Ireland in the context of tectonic basins and their transatlantic significance. In: Geology of the North Atlantic borderlands (Eds. Kerr, J.W., and Fergusson, A.J.), *Canadian Society of Petroleum Geologists*, Memoir **7**, 683-725.

Gay, N. C. 1968. Pure shear and simple shear deformation of inhomogeneous viscous fluids. 1. Theory. *Tectonophysics*, **5**, 211-234.

Gayer, R., Garven, G. & Rickard, D. 1998. Fluid migration and coal-rank development in foreland basins. *Geology*, **26**, 679-682.

Giambiagi, L., Ghiglione, M., Cristallini, E. & Bottesi, G. 2009. Kinematic models of basement cover interaction: Insights from the Malargüe fold and thrust belt, Mendoza, Argentina. *Journal of Structural Geology*, **31**, 1443-1457.

Gibbs, A.D. 1984. Structural evolution of extensional basin margins. Journal of the *Geological Society of London*, **141**, 609-620.

Gil, A., Lago, M., Gale, C., Pocovi, E. & Arranz, E. 2002. Magnetic fabric in folded sills and lava flows. A case study in the Permian basalts of the Anayet Massif (Pyrenean Axial Zone, Spain). *Tectonophysics*, **350**, 1-15.

Gill, W.D. 1962. The Variscan fold belt in Ireland. In: Coe,K. (Ed.), Some Aspects of the Variscan Fold Belt. *University Press, Manchester*, pp. 41-64.

Girdler, R. W. 1961. The measurement and computation of anisotropy of magnetic susceptibility of rocks. *Geophysical Journal International*, **5**, 34-44.

Glennie, K.W. & Boegner, P.L.E. 1981. Sole Pit Inversion Tectonics. *In:* Illing, L.V. & Hobson, G.D. (eds) *Petroleum Geology of the Continental Shelf of Northwest Europe*. Institute of Petroleum, London, 110-120.

Goodwin L.B. & Tikoff B. 2002. Competency contrasts, kinematics, and the development of foliations and lineations in the crust. *Journal Structural Geology*, **24**, 1065-1085.

References

Goldstein, A.G. 1980. Magnetic susceptibility anisotropy of mylonites from the Lake Char mylonite zone, southeastern New England. *Tectonophysics,* **66**, 197-211.

Goldstein, A.G. & Brown, L.L. 1988. Magnetic susceptibility anisotropy of mylonites from the Brevard Zone, North Carolina, USA. *Physics of the Earth and Planetary Interiors,* **51**, 290-300.

Gosselet, J. 1888. L'Ardenne. Mémoires pour servir à l'explication de la carte géologique détaillée de la France.

Graham, J.R. 1975. Analysis of an upper Palaeozoic transgressive sequence in southwest County Cork, Eire. *Sedimentary Geology,* **13**, 267-290.

Graham, J.R. 1983. Analysis of the upper Devonian Munster Basin, an example of a fluvial distributary system. *Special Publications,International Association of Sedimentologists,* **6**, 473-483.

Graham, J.R. 2009. Devonian. In: The Geology of Ireland (eds C.H. Holland & I.S. Sanders), pp. 175-214. Dunedin Academic Press, Edinburgh. An authorative review of the Irish Old Red Sandstone basins.

Graham, J.R., James, A. & Russell, K.J. 1992. Basin History deduced from subtle changes in fluvial style: a study of distal alluvium from the Devonian of southwest Ireland. Transactions of the Royal Society of Edinburgh: *Earth Sciences*, **83**, 655-667.

Graham, J.R. & Reilly, T. A. 1972. The Sherkin Formation (Devonian) of south-west County Cork. Bulletin. *Geological Survey of Ireland*, **1**, 281-300.

Graham, J.R., Russell, K.J. & Stillman, C.J. 1995. Late Devonian magmatism in west Kerry and its relationship to the development of the Munster basin. *Irish Journal of Earth Sciences*, **14**, 7-23.

Graham, J.W. 1954. Magnetic susceptibility anisotropy, an unexploited petrofabric element. *Geological Society of America Bulletin*, **65**, 1257-1258.

Gray D.R. 1981. Compound tectonic fabrics in singly folded rocks from SW Virginia, USA. *Tectonophysics*, **78**, 229-248.

Gregoire, V., Darrozes, J., Gaillot, P. & Nedelec, A. 1998. Magnetic grain shape fabric and distribution anisotropy vs rock magnetic fabric: a three-dimensional case study. *Journal of Structural Geology*, **20**, 937-944.

Groshong, R.H. (1988). Low-temperature deformation mechanisms and their interpretation. *Geological Society of America Bulletin*, **100**, 1329-1360.

Gutiérrez-Alonso, G., Fernández-Suárez, J. & Weil, A.B. 2004. Orocline triggered lithospheric delamination. *Geological Society of America Special Papers,* **383**, 121-130.

Halliday, A.N. & Mitchell, J.G. 1983. K-Ar ages of clay concentrates from Irish ore bodies and their bearing on timing of mineralisation. Transactions of the Royal Society of Edinburgh: *Earth Sciences,* **74**, 1-14.

Hamilton, N. & Rees, A.I. 1970. Magnetic fabric of sediments from the Shelf at La Jolla (California). *Marine Geology,* **9**, M6-M11.

References

Hamblin, W.K. 1965. Origin of 'reverse drag' on the downthrow side of normal faults. *Geological Society of America Bulletin,* **76**, 1145-1164.

Hanna, S.S. & Graham, R.H. 1988. A structural context of strain measurements on reduction spots in the Alps Maritimes and the Hercynian fold belt of Southern Britain. *Annales Tectonicae,* **2**, 71-83

Hansen, A., Chadima, M., Cifelli, F., Brokmeier, H.G. & Siemes, H. 2004. Neutron pole figures compared with magnetic preferred orientations of different rock types. *Physica B* **350**, 120-122.

Harland, W.B. & Bayly, M.B. 1958. Tectonic Regimes. *Geological Magazine*, **95**, 89-104.

Hayward, A.B. & Graham, R.H. (1989). Some geometrical characteristics of inversion. *Geological Society, London, Special Publications*, **44,** 17-39.

Hellinger S.J. & Sclater, J.G. 1983. Some comments on two layer extension models for the evolution of sedimentary basins. *Journal of Geophysical Research*, **88**, 8251-69.

Henry, B. & Daly, L. 1983. From qualitative to quantitative magnetic anisotropy analysis; the prospect of finite strain calibration. *Tectonophysics*, **98**, 327-336.

Henry, B. & Hrouda, F. 1989. Analyse de la deformation finie des roches par détermination de leur anisotropie de susceptibilite magnétique. C. R. Acad. Sci. Paris, 308(B): 731-737.

Henry, B., Jordanova, D., Jordanova, N., Souque, C. & Robion, P. 2003. Anisotropy of magnetic susceptibility of heated rocks. *Tectonophysics*, **366**, 241-258.

Hext, G.R. 1963. The estimation of second-order tensors, with related tests and designs. *Biometrika*, **50**, 353-373.

Higgs, K. & Russell, K.J. 1981. Upper Devonian microfloras from southeast Iveragh, County Kerry, Ireland. *Geological Survey of Ireland Bulletin*, **3**, 17-50.

Hirt, A.M., Julivert, M. & Soldevila, J. 2000. Magnetic fabric and deformation in the Navia-Alto Sil slate belt, northwestern Spain. *Tectonophysics,* **320**, 1-16.

Hnat, J.S., van der Pluijm, B.A., Van der Voo, R. & Thomas, W.A. 2008. Differential displacement and rotation in thrust fronts: A magnetic, calcite twinning and palinspastic study of the Jones Valley thrust, Alabama, US Appalachians. *Journal of Structural Geology*, **30**, 725-738.

Ho, N.C., Peacor, D.R. & van der Pluijm, B.A. 1996. Contrasting roles of detrital and authigenic phyllosilicates during slaty cleavage development. *Journal of Structural Geology*, **18**, 615-623.

Ho, N.C., van der Pluijm, B.A. & Peacor, D.R. 2001. Static recrystallization and preferred orientation of phyllosillicates: Michigamme Formation, Northern Michigan, USA. *Journal of Structural Geology*, **23**, 887-893.

Holland, C.H. 1987. Stratigraphical and structural relationships of the Dingle Group (Silurian), County Kerry, Ireland. *Geological Magazine*, **124**, 33-42

References

Hopkinson, J. 1889. Magnetic and other Physical properties of iron at high temperatures. *Philosophical Transactions of the Royal Society of London*, Series A 180, p. 443.

Horne, R.R. 1971. Aeolian cross-stratification in the Devonian of the Dingle Peninsula, County Kerry, Ireland. *Geological Magazine*, **103**, 151-158.

Horne, R.R. 1974. The lithostratigraphy of the late Silurian to early Carboniferous of the Dingle Peninsula of County Kerry. *Geological Survey of Ireland Bulletin*, **1**, 395-428.

Housen, B.A., van der Pluijm, B.A. & Essene, E.J. 1995. Plastic behaviour of magnetite and high strains obtained from magnetic fabrics in the Parry Sound shear zone, Ontario Grenville Province. *Journal of Structural Geology*, **17**, 265-278.

Housen, B. A., Richter, C. & van der Pluijm, B. A. 1993. Composite magnetic anisotropy fabrics: experiments, numerical models and implications for the quantification of rock fabrics. *Tectonophysics*, **220**, 1-12.

Howard, D. W. 1975. Deep-Seated Igneous Intrusions in Co. Kerry. Proceedings of the Royal Irish Academy. Section B: *Biological, Geological, and Chemical Science*, **75**, 173-183.

Hrouda, F. 1982. Magnetic anisotropy of rocks and its application in geology and geophysics. *Geophysical Surveys*, **5**, 37-82.

Hrouda, F. 1987. Mathematical model relationship between the paramagnetic anisotropy and strain in slates. *Tectonophysics*, **142**, 323-327.

Hrouda, F. 1994. A Technique for the measurement of thermal changes of magnetic susceptibility of weakly magnetic rocks by the CS-2 Apparatus and KLY-2 Kappabridge, *Geophysical Journal International*, **118**, 604-612.

Hrouda, F. 2003. Indices for numerical characterization of the alteration processes of magnetic minerals taking place during investigation of temperature variation of magnetic susceptibility, *Studia Geophysica et Geodaetica*, **47**, 847-861.

Hrouda, F. 2009. Determination of field-independent and field-dependant components of anisotropy of susceptibility through standard AMS measurements in variable low fields 1: Theory. *Tectonophysics*, **466**, 114-122.

Hrouda, F. Chlupáčová, M. & Mrázová, Š. 2006. Low-field variation of magnetic susceptibility as a tool for magnetic mineralogy of rocks. *Physics of the Earth and Planetary Interiors*, **154**, 323-336.

Hrouda, F. & Hruskova, L. 1990. On the detection of weak strain parallel to the bedding by magnetic anisotropy: a mathematical model study. *Studia Geophysica et Geodaetica*, **34**, 327-341.

Hrouda, F. & Janák, F. 1976. The changes in shape of the magnetic susceptibility ellipsoid during progressive metamorphism and deformation.*Tectonophysics*, **34**, 135-148.

Hrouda, F. & Jelinek, V. 1990. Resolution of ferrimagnetic and paramagnetic anisotropies in rocks, using combined low-field and high-field measurements. *Geophysical Journal International*, **103**, 75-84.

References

Hrouda, F. & Jezek, J. 1999. Theoretical models for the relationship between magnetic anisotropy and strain: effect of triaxial magnetic grains. *Tectonophysics*, **301**, 183-190.

Hrouda, F. & Jezek, J. 2002. A technique for numerical modelling of magnetic anisotropy to strain relationship. *Physics and Chemistry of the Earth*, **27**, 1247-1252.

Hrouda, F. & Kahan, S. 1991. The magnetic fabric relationship between sedimentary and basement nappes in the High Tatra Mts. (N Slovakia). *Journal of Structural Geology*, **13**, 431-442.

Hrouda, F., Krejci, O., Potfaj, M. & Stranik, Z. 2009. Magnetic fabric and weak deformation in sandstones of accretionary prisms of the Flysch and Klippen Belts of the Western Carpathians: Mostly offscraping indicated. *Tectonophysics*, **479,** 254 – 270.

Hrouda, F. & Lanza, R. 1989. Magnetic fabric in the Biella and Traversella stocks (Periadriatic Line): implications for the mode of emplacement. *Physics of the earth and planetary interiors*, **56**, 337-348.

Hrouda, F., Schulmann, K., Suppes, M., Ullemayer, K., de Wall, H. & Weber, K. 1997. Quantitative relationship between low-field AMS and phyllosilicate Fabric: A review. *Physics and Chemistry of the Earth*, **22**, 153-156.

Hudson, R.S., Clarke, M.J. & Bertrand, T.P. 1966. The Lower Carboniferous (Dinantian) Stratigraphy of the Castleisland area, Co. Kerry, Ireland. *Scientific Proceedings of the Royal Dublin Society*, **2**, 297-317.

Hussain, S.M. 1957. The geology of the Kenmare syncline, Co. Kerry, Ireland. *Unpublished PhD thesis*, Univ. Coll. London. UK.

Hutton, D. H. & Sanderson, D. J. (Eds.). 1984. Variscan tectonics of the North Atlantic region.

Imaz, A.G., Pocoví, A., Lago, M. & Parés, J.M. (2000). Effect of lithostatic pressure and tectonic deformation on the magnetic fabric (anisotropy of magnetic susceptibility) in low-grade metamorphic rocks. *Journal of Geophysical Research*, Solid Earth, **105**, 21305-21317.

Ising, G. 1942. On the magnetic properties of varved clay. Arkiv för Matematik. Astronomi och Fysik **29**, 1-37.

Ishii, K. 1988. Grain growth and reorientation of phyllo-silicate minerals during the development of slaty cleavage in the South Kitakami Mountains, NE Japan. *Journal of Structural Geology*, **10**, 145-154.

Jackson, M. 1991. Anisotropy of magnetic remanence: a brief review of mineralogical sources, physical origins, and geological application, and comparison with susceptibility anisotropy. *Pure and Applied Geophysics*, **136**, 1-28.

Jackson, M., Sprowl, D. & Ellwood, B. 1989. Anisotropies of partial anhysteretic remanence and susceptibility in compacted black shales: Grainsize-and composition-dependent magnetic fabric. *Geophysical Research Letters*, **16**, 1063-1066.

Jacob, G., Kisch, H.J. & van der Pluijm, B.A. 2000. The relationship of phyllosilicate orientation, X-ray diffraction intensity ratios, and c/b fissility ratios in metasedimentary rocks

of the Helvetic zone of the Swiss Alps and the Caledonides of Jamtland, central western Sweden. *Journal of Structural Geology*, **22**, 245-258.

James, A. & Graham, J.R. 1995. Stratigraphy and structure of Devonian fluvial sediments, western Beara Peninsula, south-west Ireland. *Geological Journal*, **30**, 165-182.

Janak, F. 1965. Determination of anisotropy of magnetic susceptibility of rocks. *Studia Geophysica et Geodaetica*, **9**, 290-301.

Jelinek, V. 1977. The statistical theory of measuring anisotropy of magnetic susceptibility of rocks and its application. *Geofyzika, Brno*, **87**, 4.

Jelinek, V. 1981. Characterization of the magnetic fabric of rocks. *Tectonophysics*, **79**, 63-7.

Jessell, M.W. 1987. Grain-boundary migration microstructures in a naturally deformed quartzite. *Journal of Structural Geology*, **9**, 1007-1014

Jezek, J. & Hrouda, F. 2002. A technique for numerical modelling of magnetic anisotropy to strain relationship. *Physics and Chemistry of the Earth*, **27**, 1247-1252

Jezek, J. & Hrouda, F. 2002. Software for modelling the magnetic anisotropy of strained rocks. *Computers and Geosciences*, **28**, 1061-1068.

Jezek, J. & Hrouda, F. 2007. A program for inverse strain estimation from magnetic susceptibility. *Computers and Geoscience*, **33**, 749-759.

Jones, P.C. & Naylor, D. 2003. Namurian rocks of Whiddy Island, west Cork: A sedimentological outline and palaeogeographical implications. *Irish Journal of Earth Sciences*, **21**, 115-132.

Jordan P.G. 1987. The deformational behaviour of bimineralic limestone-halite aggregates. *Tectonophysics*, **135**, 185-197.

Jukes, J.B. 1861. Explanations to accompany Sheets 147 and 157 of the Maps of the Geological Survey of Ireland. *Memoirs of the Geological Survey of Ireland.*

Jukes, J. B. 1864. Explanation to accompany Sheet 192 and part of Sheet 199. *Memoirs of the Geological Survey of Ireland.*

Kanagawa, K. 1991. Change in dominant mechanisms for phyllosilicate preferred orientation during cleavage development in the Kitakami slates of NE Japan. *Journal of Structural Geology*, **13**, 927-943.

Keegan, J.B. & Penney, S.R. 1978. Lower Carboniferous miospore assemblages from the Portlaw area, county Waterford, Ireland. *Pollen et spores*. Kiujpers, 1975

Keeley, M.L. 1996. The Irish Variscides:problems, perspectives and some solutions. *Terra Nova*, **8**, 259-269.

Kelso, P.R., Tikoff, B., Jackson, M. & Sun, W. 2002. A new method for the separation of paramagnetic and ferromagnetic susceptibility anisotropy using low field and high field methods. *Geophysical Journal International*, **151**, 345-359.

References

Kerrich, R., Beckinsale, R.D. & Durham, J.J. 1977. The transition between deformation regimes dominated by intercrystalline diffusion and intracrystalline creep evaluated by oxygen isotope thermometry. *Tectonophysics*, **38,** 241-257.

Kisch, H. 1998. Criteria for incipient slaty and crenulation cleavage development in Tertiary flysch of the Helvetic zone of the Swiss Alps. *Journal of Structural Geology,* **20**, 601-615.

Kissel, C., Barrier, E., Laj, C. & Lei, T.Q. 1986. Magnetic fabric in "undeformed" marine clays from compressional zones. *Tectonics*, **5**, 769-781.

Klapper, G., Feist, R. & House, M.R. 1987. Decision on the boundary stratotype for the middle upper Devonian series boundary. *Episodes*, **10**, 97-101.

Klemperer, S.L. & Hobbs, R. 1991. The BIRPS atlas-deep seismic profiles around the British Isle. *University Press, Cambridge*.

Kligfield, R., Owens, W. H. & Lowrie, W. 1981. Magnetic susceptibility, anisotropy, strain, and progressive deformation in Permian sediments from the Maritime Alps (France). *Earth and Planetary Science Letters*, **55**, 181-189.

Kneen, S. 1976. The relationship between the magnetic and strain fabrics of some haematite-bearing Welsh, slates. *Earth and Planetary Earth Sciences,* **31**, 413-416.

Knipe, R.J. 1979. Chemical changes during slaty cleavage development. *Bulletin De Mineralogie*, **102**, 206-209.

Knipe, R.J. 1981. The interaction of deformation and metamorphism in slates. *Tectonophysics* **78**, 249-272.

Knipe, R.J. 1985. Footwall geometry and the rheology of thrust sheets. Journal of Structural Geology, **7**, 1-10.

Knipe, R.J. 1989. Deformation mechanisms-recognition from natural tectonites. *Journal of Structural Geology*, **11**, 127-146.

Kossmat, F. 1927. Gliederung des varistischen Gebirgsbaus. *Abhandlungen Sächsisches Geologisches Landesamt*, **1**, 1–39.

Kröner, A., Hegner, E., Lehmann, B., Heinhorst, J., Wingate, M.T.D., Liu, D.Y. & Ermelov, P. 2008. Palaeozoic arc magmatism in the Central Asian Orogenic Belt of Kazakhstan: SHRIMP zircon ages and whole-rock Nd isotopic systematics. *Journal of Asian Earth Sciences, **32,*** 118-130.

Kronenberg, A.K. Kirby, S.H. & Pinkston, J. 1990. Basal slip and mechanical anisotropy of biotite. *Journal of Geophysical Research*: Solid Earth, **95**, 19257-19278.

Lagroix, F. & Borradaile, G.J. 2000. Tectonics of the circum-Troodos sedimentary cover of Cyprus from rock magnetic and structural observations. *Journal of Structural Geology*, **22**, 453-469.

Lagroix, F. & Banerjee, S.K. 2002. Paleowind directions from the magnetic fabric of loess profiles in central Alaska. *Earth and Planetary Science Letters*, **195**, 99-112.

References

Lagroix, F. & Banerjee, S.K. 2004. The regional and temporal significance of primary aeolian magnetic fabrics preserved in Alaskan loess. *Earth and Planetary Science Letters*, **225**, 379-395.

Lamarche, G. & Rochette, P. 1987. Microstructural analysis and origin of lineations in the magnetic fabric of some Alpine slates. *Tectonophysics*, **139**, 285-293.

Lamplugh, G. W. (1920). Gault and Lower Greensand Near Leighton Buzzard. *Geological Magazine*, ***57***, 234-237.

Landes, M. 2001. A wide-angle seismic study of SW Ireland, Ph.D. thesis, *The National University of Ireland, Ireland*, 192pp.

Landes, M., O' Reilly, B.M., Readman, P.W., Shannon, P.M. & Prodehl, C. 2003. VARNET-96: three-dimensional upper crustal velocity structure of SW Ireland. *Geophysical Journal International*, **153**, 424-442.

Landes, M., Prodehl, C., Hauser, F., Jacob, A.W.B. & Vermeulen, N.J. 2000. VARNET-96: Influence of Variscan and Caledonian orogenies oncrustal structure in SW Ireland. *Geophysical Journal International*, **140**, 660-676.

Landes, M., Ritter, J. R. R., Readman, P.W. & O'Reilly, B. M. 2005. A review of the Irish crustal structure and signatures from the Caledonian and Variscan Orogenies. *Terra Nova*, **17**, 111-120.

Lattard, D., Engelmann, R., Kontny, A. & Sauerzapf, U. 2006. Curie temperatures of synthetic titanomagnetites in the Fe-Ti-O system: Effects of composition, crystal chemistry, and thermomagnetic methods. Journal of Geophysical Research: *Solid Earth*, 111(B12).

Lee, J.H., Peacor, D.R., Lewis, D. D. & Wintsch, R.P. 1984. Chlorite-illite/muscovite interlayered and interstratified crystals: a TEM/STEM study. *Contributions to Mineralogy and Petrology*, **88**, 372-385.

Lee, J. H., Peacor, D. R., Lewis, D. D. & Wintsch, R. P. 1986. Evidence for syntectonic crystallization for the mudstone to slate transition at Lehigh Gap, Pennsylvania, USA. *Journal of Structural Geology*, **8**, 767-780.

Lee, T.Q., Kissel, C., Laj, C., Horng, C. S. & Lue, Y. T. (1990). Magnetic fabric analysis of the Plio-Pleistocene sedimentary formations of the Coastal Range of Taiwan. *Earth and Planetary Science Letters*, **98**, 23-32.

Leeder , M.R. & Alexander, J. 1987. The origin and tectonic significance of asymmetrical meander belts. *Sedimentology*, **34**, 217-226.

Leeder, M.R. & Gawthorpe, R.L. 1987. Sedimentary models for extensional tilt-block/half graben basins. 139-152 in Coward, M.P., Dewey, J.F. & Hancock, P.L. (editors) Continental Extensional Tectonics. *Geological Society of London Special Publication*, 28.

Le Gall, B. 1991 Crustal evolutionary model for the Variscides of Ireland and Wales from SWAT seismic data. *Journal of the Geological Society*, **148**, 759-774.

Le Theoff, B. 1979. Non-coaxial deformation of elliptical particles. *Tectonophysics*, **53**, T7-T13.

References

Leveridge B.E. & Hartly, A.J. 2006. The Variscan Orogeny: the development and deformation of Devonian/Carboniferous basins in SE England and South Wales. In: The Geology of England and Wales (eds P.J. Brenchley, & P.F. Rawson),pp. 226-255. *The Geological Society London.*

Leveridge, B. E. & Shail, R. K. 2011. The Gramscatho basin, south Cornwall, UK: Devonian active margin successions. *Proceedings of the Geologists' Association*, **122**, 568-615.

Lisle, R. 1977a. Estimation of the tectonic strain ratio from the mean shape of deformed elliptical objects. *Geologie en Mijnbouw*, **56**, 140-144.

Lisle, R. 1977b. Clastic grain shape and orientation in relation to cleavage from the Aberystwyth Grits, Wales. *Tectonophysics,* **39**, 381–395.

Lisle, R. 1985. Geological Strain Analysis: A Manual for the Rf/ϕ Method. *Pergamon Press.*

Lister, G.S. & Snoke, A. W. 1984. SC mylonites. *Journal of Structural Geology*, **6**, 617-638.

Louis, L., Robion, P. & David, C. 2004. A single method for the inversion of anisotropic data sets with application to structural studies. *Journal of Structural Geology,* **26**, 2065-2072.

Lowrie, W. & Hirt, A.M. 1987. Anisotropy of magnetic susceptibility in the Scaglia Rossa pelagic limestone. *Earth and Planetary Science Letters*, **82**, 349-356.

Luneburg, C.M. & Lebit, D.W.H. 1998. The development of a single cleavage in an area of repeated folding. *Journal of Structural Geology,* **20**, 1531-1548.

Luneburg, C.M., Lampert, S.A., Lebit, H.D., Hirt, A.M., Casey, M. & Lowrie, W. 1999. Magnetic anisotropy, rock fabrics and finite strain in deformed sediments of SW Sardinia (Italy). *Tectonophysics,* **307**, 51-74.

MacCarthy, I.A.J. 1987. Transgressive facies in the South Munster Basin, Ireland. *Sedimentology*, **34**, 389-422.

MacCarthy, I.A.J. 1990. Alluvial sedimentation patterns in the Munster Basin, Ireland. *Sedimentology*, **37**, 685-712.

MacCarthy, I. A. & Gardiner, P. R. 1987. Dinantian cyclicity: a case history from the Munster Basin of southern Ireland. *Geological Journal*. Special issue, 199-237.

MacCarthy, I.A.J., Gardiner, P.R.R & Horne, R.R. 1978. The Lithostratigraphy of the Devonian-Early Carboniferous succession in parts of Counties Cork and Waterford, *Ireland. Geological Surey of Ireland, Bulletin,* **2**, 265-305.

Magee, C. 2011. Emplacement of sub-volcanic cone sheet intrusions (Doctoral dissertation, University of Birmingham).

Makris, J., Egloff, R., Jacob, A.W.B., Mohr, P., Murphy, T. & Ryan, P. 1988. Continental crust under the southern Porcupine Seabight west of Ireland. *Earth and Planetary Science Letters*, **89**, 387–397.

Mallik, J., Mathew, G. & Greiling, R.O. 2009. Magnetic fabric variations along the fault related anticlines of Eastern Kachchh, Western India. *Tectonophysics,* **473**, 428 – 445.

References

Mares, V.M. & Kronenberg, A.K. 1993. Experimental deformation of muscovite. *Journal of Structural Geology*, **15**, 1061-1075.

Marshak, S. & Engelder, T. 1985. Development of cleavage in limestones of a fold-thrust belt in eastern New York. *Journal of Structural Geology*, **7**, 345-359.

Martín-Hernández F. & Ferre, E.C. 2007. Separation of paramagnetic and ferromagnetic anisotropies: a review. *Journal of Geophysical Research*, 112. doi:10.1029/2006JB004340.

Martín-Hernández, F. & Hirt, A.M. 2001. Separation of ferrimagnetic and paramagnetic anisotropies using a high-field torsion magnetometer. *Tectonphysics*, **337**, 209-221.

Martín-Hernández F. & Hirt, A.M. 2003. The anisotropy of magnetic susceptibility in biotite, muscovite and chlorite single crystals. *Tectonophysics*, **367**, 13-28.

Martín-Hernández, F., Luneburg, C.M., Aubourg, C. & Jackson, M. 2004. Magnetic Fabric: methods and applications. *Geological Society, Special Publications*, **238**, 1-7.

Masson, F., Jacob, W.B., Prodehl, C., Readman, P.W., Shanon, P.M., Schulze, A. & Enderle, U. 1998. A wide-angle seismic traverse through the Variscan of southwest Ireland. *Geophysical Journal International*, **134**, 689-705.

Mathews, S.C. 1978. Caledonian connexions of Variscan tectonism Z. Dt. Geol. Ges. **129**, 423-428.

Matthews, P., Bond,R., Berg,J. & VanDen 1974. An algebraic method of strain analysis using elliptical markers. *Tectonophysics*, **24**, 31-67.

Matthews, S.C., Naylor, D. & Sevastopulo, G.D. 1983. Palaeozoic sedimentary sequence as a reflection of deep structure in southwest Ireland. *Sedimentary Geology*, **34**, 83-95.

Matte, P. 1986. Tectonics and plate tectonics model for the Variscan belt of Europe. *Tectonophysics*, **126**, 329-374.

Matte, P. 2001. The Variscan collage and orogeny (480–290 Ma) and the tectonic definition of the Armorica microplate: a review. *Terra Nova*, **13**, 122-128.

Mattei, M., Speranza, F., Argentieri, A., Rossetti, F., Sagnotti, L.Z. & Funiciello, R. 1999. Extensional tectonics in the Amantea basin (Calabria, Italy): a comparison between structural and magnetic anisotropy data. *Tectonophysics*, **307**, 33-49.

Max, M.D. & Lefort, J.P. 1984. Does the Variscan front in Ireland follow a dextral shear zone? In: Hutton, D.H., Sanderson, D.J. (Eds.), Variscan Tectonics of the North Atlantic Region. *Geological Society of London, Special Publication*, **14**, 177-183.

Max, M.D. & Long, C.B. 1985. Pre-Caledonian basement in Ireland and its cover relationships. *Geological Journal*, Vol. **20**, 341-366.

Max, M.D. & Riddihough, R.P. 1975. Continuation of the Highland Boundary fault in Ireland. *Geology*, **3**, 206-210.

McCann, T. 2008. The Geology of Central Europe. Precambrian and Palaeozoic. *The Geological Society.*

References

McClay, K.R., Insley, M.W. & Anderton, R. (1989). Inversion of the Kechika Trough, northeastern British Columbia, Canada. *Geological Society, London, Special Publications*, ***44***, 235-257.

McClay, K.R. & Buchanan, P.G. 1992. Thrust faults in inverted extensional basins. In McClay 1992. Thrust Tectonics. Springer Netherlands. 93-104.

McKenzie, D. 1978. Some remarks on the development of sedimentary basins. *Earth and Planetery Science Letters*. **40**, 25-32

McKenzie, D. & Jackson, J. 1983. The relationship between strain rates, crustal thickening, palaeomagnetism, finite strain and fault movements within a deforming zone. *Earth and Planetary Science Letters*, **65**, 182-202.

McKerrow, W.S. 1988. Wenlock to Givetian deformation in the British Isles and the Canadian Appalachians. *Geological Society, London, Special Publications*, **38**, 437-448.

McCarthy, D.J. 2014. Application of semi-automated strain analysis techniques and anisotropy of magnetic susceptibility in fold and thrust belts. PhD Thesis, University College Cork.

McCarthy, D.J., Meere, P.A. & Petronis, M.S. 2015. A comparison of the effectiveness of clast based finite strain analysis techniques to AMS in sandstones from the Sevier Thrust Belt, Wyoming. *Tectonophysics*, **639**, 68-81.

McClay, K.R. & Price, N.J. (Eds.). 1981. Thrust and nappe tectonics (No. 9). Wiley-Blackwell.

Means WD. 1979. Stress and Strain. Springer-Verlag, Berlin Heidel Berg New York.

Means, W.D. 1981. The concept of steady-state foliation. *Tectonophysics*, **78**, 179-199.

Means, W.D., Williams, P. F. & Hobbs, B. E. 1984. Incremental deformation and fabric development in a KCl/mica mixture. *Journal of Structural Geology*, **6**, 391-398.

Meere, P.A. 1992. Structural and metamorphic studies of the Irish Variscides from the Killarney-Baltimore tansect, southwest Ireland. PhD thesis, National University of Ireland.

Meere, P.A. 1995 a. High and low density fluids in a quartz vein from the Irish Variscides. *Journal of Structural Geology*, **17**, 435-446.

Meere, P.A. 1995 b. The structural evolution of the western Irish Variscides: An example of obstacle tectonics? *Tectonophysics*, **246**, 97-112.

Meere, P.A. 1995 c. Sub-greenschist facies metamorphism from the Variscides of SW Ireland: an early syn-extensional peak thermal event. *Journal of the Geological Society*, London, **152**, 511-521.

Meere, P.A., MacCarthy, I.A.J., Reavy, J., Allen, A. & Higgs, K. 2013. Geology of Ireland, A Field Guide. *The Collins Press.*

Meere, P.A. & Mulchrone, K.F. 2006. Timing of deformation within Old Red Sandstone lithologies from the Dingle Peninsula, SW Ireland. *Journal of the Geological Society*, London, **163**, 461-469.

References

Meere, P.A., Mulchrone, K. F. & Timmerman, M. 2013. Shear folding in low-grade metasedimentary rocks: Reverse shear along cleavage at a high angle to the maximum compressive stress. *Geology,* **41**, 879-882

Meere, P.A., Mulchrone, K. F., Sears, J. W. & Bradway, M. D. 2008. The effect of non-passive clast behaviour in the estimation of finite strain in sedimentary rocks. *Journal of Structural Geology,* **30**, 1264-1271.

Moore, 1975. Fault Tectonics at Tynagh mine, Ireland. Trans. Instn. Min. Metal.84b 141-145

Mulchrone, K.F. 2003. Application of Delaunay triangulation to the nearest neighbour method of strain analysis. *Journal of Structural Geology,* **25**, 689-702.

Mulchrone, K.F., McCarthy, D. J. & Meere, P.A. 2013. Mathematica code for image analysis, semi-automatic parameter extraction and strain analysis. *Computers & Geosciences,* **61**, 64-70.

Mulchrone, K.F. & Meere, P.A 2001. A Windows program for the analysis of tectonic strain using deformed elliptical markers. *Computers & Geosciences,* **27**, 1251-1255.

Mulchrone, K.F. & Meere, P.A. 2007. Strain refraction, viscosity ratio and multi-layer deformation: A mechanical approach. *Journal of Structural Geology,* **29**, 453-466.

Mulchrone, K.F., Meere, P.A. & Choudhury, K.R., 2005. SAPE: a program for semi-automatic parameter extraction for strain analysis. *Journal of Structural Geology,* **27**, 2084-2098.

Murphy, F.C. 1985. Non-axial planar cleavage and Caledonian sinistral transpression in eastern Ireland. *Geological Journal,* **20**, 257-279.

Murphy, F.X. 1990. The role of pressure solution and intermicrolithon-slip in the development of disjunctive cleavage domains: a study from Helvick Head in the Irish Variscides. *Journal of Structural Geology,* **12**, 69-81.

Murphy, F.X. 1990. The Irish Variscides: a fold belt developed within a major surge zone. *Journal of the Geological Society,* London, **147**, 451-460.

Murphy, F.X. 1988. The Origin of Variscan kink bands: a study from the Dungarvan Syncline, southern Ireland. *Geological Magazine,* **125**, 641-650.

Murphy, J.B., Pisarevsky, S.A., Nance, R.D. & Keppie, J.D. 2004a. Neoproterozoic Early Paleozoic evolution of peri-Gondwanan terranes: implications for Laurentia–Gondwana connections. *International Journal of Earth Sciences,* **93**, 659-682.

Murphy, T. 1960. Gravity anomaly map of Ireland, Sheet 5, South-West. Commun. Dublin Institute of Advanced Studies, Geophys. Bull., No. 18.

Murphy, T. 1962. Some Unusual Low Bouguer Anomalies of Small Extent in Central Ireland and Their Connection with Geological STRUCTURE*.Geophysical Prospecting, **10**, 258-270.

Murphy, T. 1974. Gravity anomaly map of Ireland. Commun. Dublin Institute of Advanced Studies, Geophys. Bull., No. 32.

References

Muxworthy, A.R. & Williams, W. 2004. Distribution anisotropy: the influence of magnetic interactions on the anisotropy of magnetic remanence. In: Martín-Hernández, F., Lüneburg, C.M., Aubourg, C., Jackson, M. (Eds.), Magnetic Fabrics. *Geological Society of London Special Publication*, **238**, 37-48.

Nagata, T. 1961 Rock Magnetism, 2nd edition, Maruzen, Tokyo, 350 p

Nakamura, N. & Borradaile, G. 2001. Do reduction spots predate finite strain? A magnetic diagnosis of Cambrian slates in North Wales. *Tectonophysics*, **340**, 133-139.

Nakamura, N. & Borradaile, G.J. 2001. Strain, anisotropy of anhysteretic remanence, and anisotropy of magnetic susceptibility in a slaty tuff. *Physics of the Earth and Planetary Interiors*, **125**, 85-93.

Nance, R.D., Gutierrez-Alonso, G., Keppie, J.D., Linnemann, U., Murphy, J.B., Quesada, C., Strachan, R.A. & Woodcock, N.H. 2010. Evolution of the Rheic Ocean. *Gondwana Research*, **17**, 194-222.

Nance, R.D., Murphy, J.B., Strachan, R.A., Keppie, J.D., Gutiérrez-Alonso, G., Fernández-Suárez, J., Quesada, C., Linnemann, U., D'Lemos, R. & Pisarevsky, S.A. 2008. Neoproterozoic–early Paleozoic tectonostratigraphy and palaeogeography of the peri-Gondwanan terranes: Amazonian v. West African connection. In: Ennih, N., Liégeois, J-P. (Eds.), The boundaries of the West African Craton: *Geological Society of London Special Publication*, **297**, 345-383.

Naylor, D. 1966. The upper Devonian and Carboniferous geology of the Old Head of Kinsale. Co. Cork. *Scientific Proceedings, Royal Dublin Society*, Series A, 2,229-247.

Naylor, D. 1975. Upper Devonian-Lower Carboniferous stratigraphy along the south coast of Dunmanus Bay, Co. Cork. *Proceedings of the Royal Irish Academy*, **75**, 317-337.

Naylor, D. 1978. A structural section across the Variscan fold belt, southwest Ireland. Journal of *Earth Science, Royal Dublin Society*, **1**, 63-70.

Naylor, D. & Jones P.C. 1967. Sedimentation and tectonic setting of the Old Red Sandstone of south west Ireland. In: OSWALDD, H. (ed.) International Symposium of the Devonian System, 2, Alberta Society of Petroleum Geologists, Calgary, 1089-1099.

Naylor, D., Jones, P.C. & Clarke, M.J. 1969. The stratigraphy of the Cork beds (Upper Devonian and Carboniferous) in southwest Ireland. *Scientific proceedings, Royal Dublin Society, Series A*, Vol. **3**, 171-191.

Naylor, D., Reilly, T.A., Sevastopulo, G.D. & Sleeman, A.G. 1983. Stratigraphy and structure in the Irish Variscides. In: Hancock, P.L. (Ed.) The Variscan Fold Belt in the British Isles. Adam Hilger, Bristol.

Naylor, D. & Sevastopoulo, G.D. 1979. The Hercynian 'Front' in Ireland. Krystalinikum, **14**, 77-90.

Naylor, D., Sevastopulo, G.D., Sleeman, A.G, Reilly, T.A. 1981. The Variscan fold belt in Ireland. *The Variscan Orogen in Europe*, **60**, 49-66.

Nex, P.A.M., Kinnaird, J. A. & Ixer, R. 2003. Localized ductile thrusting north of the Variscan Front, Ross Island, southwest Ireland. *Geological Journal*, **38**, 15-29.

References

Nye, J.F., 1957 Physical Properties of Crystals, Clarendon Press, Oxford, 322 p.

O' Connor, P.J. & Brück, P.M. 1978. Age and Origin of the Leinster Granite. *Journal of Earth Sciences,* **1**, pp. 105-113.

O' Reilly, B.M., Readman, P.W & Murphy, T. 1996. The gravity signature of Caledonian and Variscan tectonics in Ireland. *Physics and Chemistry of the Earth,* **21**, 299-304.

Oliva-Urcia, B., Larrasoaña, J. C., Pueyo, E. L., Gil, A., Mata, P., Parés, J. M. & Pueyo, O. 2009. Disentangling magnetic subfabrics and their link to deformation processes in cleaved sedimentary rocks from the Internal Sierras (west central Pyrenees, Spain). *Journal of Structural Geology*, **31**,163-176.

Oliva-Urcia, B., Rahl, J. M., Schleicher, A. M. & Parés, J. M. 2010. Correlation between the anisotropy of the magnetic susceptibility, strain and X-ray Texture Goniometry in phyllites from Crete, Greece. *Tectonophysics*, **486**, 120-131.

O' Rourke, J. 1993.Computational Geometry in C, *Cambridge University Press, Cambridge.*

Orlicky, O. 1990. Detection of magnetic carriers in rocks: results of susceptibility changes in powdered rock samples induced by temperature. *Physics of the Earth and Planetary Interiors*, **63**, 66-70.

O'Reilly, W. 1984. Rock and Mineral Magnetism. Blackie, Glasgow, UK, 220 pp.

Ori, G.G. and Penney, S.R. 1982. The stratigraphy and sedimentology of the Old Red Sandstone sequence at Dunmore East, Co. Waterford. *Journal of Earth Sciences,* **5**, 43-59.

Owens, W.H. 1972. Strain modification of angular density distributions. *Tectonophysics*, **16**, 249-261.

Owens, W.H. 1974. Mathematical model studies on factors affecting the magnetic anisotropy of deformed rocks. *Tectonophysics*, **24**, 115-131.

Owens, W.H. 2000. Statistical applications to second-rank tensors in magnetic fabric analysis. *Geophysical Journal International*, **142**, 527-538.

Owens, W.H. & Bamford, D. 1976. Magnetic, seismic, and other anisotropic properties of rock fabrics. *Philosophical Transactions of the Royal Society of London A: Mathematical, Physical and Engineering Sciences*, ***283***, 55-68.

Owens, W.H. & Rutter, E.H. 1978. The development of magnetic susceptibility anisotropy through crystallographic preferred orientation in a calcite rock. *Physics of the Earth and Planetary Interiors,* **16**, 215-222.

Parés, J.M. 2004. How deformed are weakly deformed mudrocks? Insights from magnetic magnetic anisotropy. In: Martin-Hernandez, F., Lüneburg, C., Aubourg, C., Jackson, M. (Eds.), Magnetic Fabrics: Methods and Applications. *Geological Society, Special Publications, London,* **238**, 191-203.

Parés, J.M. & Dinarés-Turell, J. 1993. Magnetic Fabric in Two Sedimentary Rock-Types from the Southern Pyrenees. *Journal of Geomagnetism and Geoelectricity,* **45**, 193-205.

References

Pares, J.M. & Van der Pluijm, B.A. 2002. Evaluating magnetic lineations (AMS) in deformed rocks. *Tectonophysics*, **350**, 283-298.

Pares, J.M. & Van der Pluijm, B.A. 2003. Magnetic fabrics and strain in pencil structures of the Knobs Formation, Valley and Ridge Province, US Appalachians. *Journal of Structural, Geology,* **25**, 1349-1358.

Pares, J.M. & Van der Pluijm, B.A. 2004. Correlating magnetic fabrics with finite strain: Comparing results from mudrocks in the Variscan and Appalachian Orogens. *Geologica Acta,* **2**, 213-220.

Pares, J.M. & Van der Pluijm, B.A. 2014. Low-temperature AMS and the quantification of subfabrics in deformed rocks. *Tectonophysics,* **629**, 55-62.

Pares, J.M., Van der Pluijm, B.A. & Dinares-Turell, J. 1999. Evolution of magnetic fabrics during incipient deformation of mudrocks (Pyrenees, northern Spain). *Tectonophysics, **307***, 1-14.

Pare´s, J.M., Van der Pluijm, B.A. & Holladay, L. 2000. Low-temperature of the anisotropy of magnetic susceptibility. AGU Fall Meeting, San Francsico, California.

Parkin, J. 1976. Silurian rocks of the Bull's Head, Annascaul and Derrymore Glen inliers, Dingle Peninsula, County Kerry. *Proceedings of the Royal Irish Academy*, **76B**, 577-606.

Passchier, C.W. & Trouw, R. A.J. 2005. Microtectonics, 366 pp. *Springer*, Berlin.

Penney, S.R., 1980. A new look at the Old Red Sandstone succession of the Comeragh Mountains, County Waterford. *Journal of Earth Sciences*, **3**, 155-178.

Perarnau, A. & Tarling, D. H. 1985. Thermal enhancement of magnetic fabric in Cretaceous sandstones. *Journal of the Geological Society,* **142**, 1029-1034.

Perparata, F.P., Shamos, M.I. 1985. Computational Geometry: An Introduction. Springer, NewYork, 412pp.

Petrovský, E. & Kapička, A. 2006. On determination of the Curie point from thermomagnetic curves. *Journal of Geophysical Research*: Solid Earth, 111(B12).

Phillips, W.E.A., Stillman, C.J. & Murphy, T. 1976. A Caledonian plate tectonic model. *Journal of the Geological Society of London*, **132**, 579-609.

Piazolo, S. & Passchier, C. W. 2002. Controls on lineation development in low to medium grade shear zones: a study from the Cap de Creus peninsula, NE Spain. *Journal of Structural Geology*, **24**, 25-44.

Pickering, K.T. 2008. The destruction of Iapetus and Tornquist's Oceans. *Geology Today,* **5**, 160-166.

Piper, J.D.A., Elliot, M.T. & Kneller, B.C. 1996. Anisotropy of magnetic susceptibility in a Palaeozoic Flysch basin: the Windermere Supergroup, northern England. *Sedimentary Geology*, **106**, 235-258.

References

Polat, G., Lebedev, S., Readman, P. W., O'Reilly, B. M. & Hauser, F. 2012. Anisotropic Rayleigh-wave tomography of Ireland's crust: Implications for crustal accretion and evolution within the Caledonian Orogen. *Geophysical Research Letters*, 39(4).

Potter, D.K. & Stephenson, A. 1988. Single-domain particles in rocks and magnetic fabric analysis. *Geophysical Research Letters*, **15**, 1097-1100.

Powell, C.M. 1989. Structural controls on Palaeozoic basin evolution and inversion in southwest Wales. *Journal of the Geological Society*, **146**, 439-446.

Pracht, M. 1996. The geology of Dingle Bay. Bedrock Geology 1: 100,000 Map Series, Sheet 20, *Geological Survey of Ireland*, Dublin.

Pracht, M. & Sleeman, A.G. 2002. Geology of West Cork: a geological description of West Cork and adjacent parts of Kerry to accompany the bedrock geology 1: 100,000 scale map series, sheet 24, West Cork. Department of Public Enterprise.

Price, C.A. 1989. Some thoughts on the subsidence and evolution of the Munster Basin, Southern Ireland. In: Arthurson, R.S., Gutteridge, P., Nolan, S.C. (Eds.), Role of Tectonics in Devonian and Carboniferous Sedimentation in the BritishIsles. *Special Publication of the Yorkshire Geological Society***, 6**, 111-122.

Price, C.A. & Todd, S.P. 1988. A model for the development of the Irish Variscides. *Journal of the Geological Society London*, **145**, 935-939.

Primmer, T.J. (1985). A transition from diagenesis to greenschist facies within a major Variscan fold/thrust complex in south-west England. *Mineralogical Magazine*, **49**, 365-374.

Quesada, C., Bellido, F., Dallmeyer, R.D., Gil-Ibarguchi, I., Oliveira, J.T., Pérez Estaún, A., Ribeiro, A., Robardet, M. & Silva, J.B. 1991. Terranes within the Iberian Massif: correlations with West African sequences. In: Dallmeyer, R.D., Lécorché, J. (Eds.),The West African Orogens and Circum-Atlantic Correlatives. Springer, Berlin Heidelberg New York, pp. 267-293.

Quinn, D., Meere, P.A. & Wartho, J.A. 2005. A chronology of foreland deformation: ultra-violet laser 40 Ar/39 Ar dating of syn/late-orogenic intrusions from the Variscides of southwest Ireland. *Journal of Structural Geology*, **27**, 1413-1425.

Rahl, J.M., Anderson, K.M., Brandon, M.T. & Fassoulas, C. 2005. Raman spectroscopic carbonaceous material thermometry of low-grade metamorphic rocks: calibration and application to tectonic exhumation in Crete, Greece. *Earth & Planetary Science Letters*, **240**, 339-354.

Ramsay, J.G. 1967. Folding and fracturing of rocks. New York, MacGraw-Hill, 568p.

Ramsay, J.G. & Huber, M. I. 1983. Strain Analysis, The Techniques of Modern Structural Geology, vol. 1. Strain Analysis. *Academic Press, London*.

Rathore, J.S. 1979. Magnetic susceptibility anisotropy in the Cambrian slate belt of North Wales and correlation with strain. *Tectonophysics*, **53**, 83-97.

Rathore, J.S. 1980. Magnetic susceptibility anisotropy from the Borrowdale Volcanic Group in the English Lake District and their correlation with strain. *Tectonophysics*, **57**, 207-220.

References

Rathore, J.S. & Heinz, H. 1980. The application of magnetic susceptibility anisotropy analyses to the study of tectonic events on the Periadriatic Line.Mitt. Österr. Geol. Ges., **71**, 275-290.

Rathore, J.S. & Henry, B. 1982. Comparison of strain and magnetic fabrics in Dalradian rocks from the southwest Highlands of Scotland. *Journal of Structural Geology*, **4**, 373-384.

Read, H.H.& Watson, J. 1975. The Hercynides and Uralides with their Forelands. In Introduction to Geology (pp. 58-98). Macmillan Education UK.

Readman, P.W., O'Reilly, B.M. & Murphy, T. 1997. Gravity gradients and upper-crustal tectonic fabrics, Ireland. *Journal of the Geological Society*, London, **154**, 817-828.

Ree J., H. 1991. An experimental steady-state foliation. *Journal of Structural Geology*, **13**, 1001-1011.

Reilly, T.A. & Graham, J.R. 1972. The historical and geological setting of the Glandore mines, southwest County Cork. *Bulletin of the Geological Survey of Ireland*, **2**, 1-13.

Reilly, T.A. & Graham, R.J. 1976. The stratigraphy of the Roaringwater Bay area of south-west County Cork. *Bulletin of the Geological Survey of Ireland*, **2**, 1-13.

Rey, P., Burg, J.P. & Casey, M. 1997. The Scandinavian Caledonides and their relationship to the Variscan belt. In: Orogeny Through Time (J.P. Burg and M. Ford, eds). *Geological Society, London, Special Publications,* **121**, 179-200.

Richmond, L.K. & Williams, B.P.J. 2000. A new terrane in the Old Red Sandstone of the Dingle Peninsula, SW Ireland. In: Friend, P.F. & Williams, B.P.J. (eds) New Perspectives on the Old Red Sandstone. *Geological Society, London, Special Publications*, **180**, 147-183.

Richter, C. & Van der Pluijm, B.A. 1994. Separation of paramagnetic and ferrimagnetic susceptiblities using low temperature magnetic susceptiblities and comparison with high field methods. *Physics of the Earth and Planetary Interiors*, **82**, 113-123.

Richter, C., Van der Pluijm, B.A. & Housen, B.A. 1993. The quantification of crystallographic preferred orientation using magnetic anisotropy. *Journal of Structural Geology*, **15**, 113-116.

Ring, U. & Brandon, M.T. 1999. Rheology and stability of accretionary wedges; an example from the Franciscan Complex, USA. In: Dietrich, P.G., Franke, W., Merkel, B.J., Herzig, P. (Eds.), 89th Annual Meeting of the Geologische Vereinigung; Old crust, New Problems; Geodynamics and utilization; Abstracts and Programme; Includes the Final International Colloquium of the DFG Priority Programme "Orogenic Processes; Quantification and Modeling in the Variscan Belt". Terra Nostra (Bonn). 99-1, 168.

Ramsay, J.G. 1982. Rock ductility and its influence on the development of tectonic structures in mountain belts. *Mountain Building Processes*, 111-127.

Robin, P.F. & Torrance, J.G. 1987. Statistical analysis of the effect of sample size on paleostrain calculation. I. Single face measurements. *Tectonophysics*, **138**, 311-317.

Rochette, P. 1987. Magnetic susceptibility of the rock matrix related to magnetic fabric studies. *Journal of Structural Geology*, **9**, 1015-1020.

References

Rochette, P. & Lamarche, G. 1986. Evolution des propriétés magnétiques lors des transformations minérales dans les roches: exemple du Jurassique Dauphinois (Alpes françaises). *Bulletin de Minéralogie*, **109**, 687-696.

Rochette, P. & Vialon, P. 1984. Development of planar and linear fabrics in Dauphinois shales and slates (French Alps) studied by magnetic anisotropy and its mineralogical control. *Journal Structural Geology*, **6**, 33-38.

Rochette, P., Jackson, M. & Aubourg, C. 1992. Rock magnetism and the interpretation of anisotropy of magnetic susceptibility. *Review of Geophysics*, **30**, 209-226.

Robin, P.Y.F. 1977. Determination of geologic strain using randomly oriented strain markers of any shape. *Tectonophysics*, **42**, T7-T16.

Robinson, K.W., Shannon, P.M. & Young, D.G.G. (1981). The Fastnet Basin: an integrated analysis. Petroleum Geology of the Continental Shelf of North-West Europe, Heyden, London, 432-444.

Robion, P., Averbuch, O. & Sintubin, M. 1999. Fabric development and metamorphic evolution of lower Palaeozoic slaty rocks from the Rocroi massif (French-Belgian Ardennes): new constraints from magnetic fabrics, phyllosilicate preferred preferred orientation and illite crystallinity data. *Tectonophysics*, **309**, 257-273.

Robion, P., Frizon de Lamotte, D., Kissel, C. & Aubourg, C. 1995. Tectonic verses mineralogical contribution to the magnetic fabrics of epimetamorphic slaty rocks: an example from the Ardennes Massif (France-Belgium). *Journal of Structural Geology*, **17**, 1111-1124.

Robion, P., Grelaud, S. & Frizon de Lamotte, D. 2007. Pre-folding magetic fabrics in fold-and-thrust belts: Why the apparent internal deformation of the sedimentary rocks from the Minervois basin (NE-Pyrenees, France) is so high compared to the Potwar basin (SW-Himalaya, Pakistan)? *Sedimentary Geology*, **196**, 181-200.

Rochette, P. & Fillion, G. 1988. Identification of multicomponent anisotropies in rocks using various field and temperature values in a cryogenic magnetometer. *Physics of the Earth and Planetary Interiors*, **51**, 379-386.

Rothery, E. 1989. Transpression in the Variscan foreland: a study in east-central Ireland. *Irish Journal of Earth Sciences*, 1-12.

Roure, F., Swennen, R., Schneider, F., Faure, J.L., Ferket, H., Guilhaumou, N. & Vandeginste, V. 2005. Incidence and importance of tectonics and natural fluid migration on reservoir evolution in foreland fold-and-thrust belts. *Oil & Gas Science and Technology*, **60**, 67-106.

Ruf, A.S., Naruk, S.J., Butler, R.F. & Calderone, G.J. 1988. Strain and magnetic fabric in the Santa Catalina and Pinaleno mountains metamorphic core complex mylonite zones, Arizona. *Tectonics*, **7**, 235–248

Russell, K.J. 1978. Vertebrate fossils from the Iveragh Peninsula and the age of the Old Red Sandstone. *Journal of Earth Sciences Royal Dublin Society*, **1**, 151-162.

Ryan, P.D. & Dewey, J.F. 1991. A geological and tectonic cross-section of the Caledonides of western Ireland. *Journal of the Geological Society*, **148**, 173-180.

Sagnotti, L. & Speranza, F. 1993. Magnetic fabric analysis of the Plio-Pleistocene clayey units of the Sant'Arcangelo basin, southern Italy. *Physics of the Earth and Planetary Interiors*, **77**, 165-176.
Sagnotti, L., Speranza, F., Winkler, A., Mattei, M. & Funiciello, R., 1998. Magnetic fabric of clay sediments from the external northern Apennines (Italy). *Physics of the Earth and Planetary Interiors*, **105**, 73-93.

Saint-Bezar, B., Herbert, R.L., Aubourg, C., Robion, P., Swennen, R. & Frizon de Lamotte, D. 2002. Magnetic fabric and petrographic investigation of hematite-bearing sandstones within ramp-related folds: examples from the South Atlas Front (Morrocco). *Journal of Structural Geology*, **24**, 1507-1520.

Sanderson, D.J. 1984. Structural variation across the northern margin of the Variscides in NW Europe. In: Hutton, D.H., Sanderson, D.J. (Eds.), Variscan Tectonics of the North Atlantic Region. *Geological Society of London, Special Publication***, 14**, 149-165.

Schmidt, V., Hirt, A.M., Leiss, B., Burlini, L. & Walter, J.M. 2009. Quantitative correlation of texture and magnetic anisotropy of compacted calcite-muscovite aggregates. *Journal of Structural Geology*, **31,** 1062-1073.

Schmidt, V., Hirt, A.M., Rosselli, P. & Martín-Hernández, F. 2007 b. Separation of diamagnetic and paramagnetic anisotropy by high-field, low-temperature torque measurements. *Geophysical Journal International*, **168**, 40-47.

Schwehr, K. & Tauxe, L. 2003. Characterization of soft-sediment deformation: Detection of cryptoslumps using magnetic methods. *Geological Society of America*, **31**, 203-206.

Seago, R.D. & Chapman, T. J. 1988. The confrontation of structural styles and the evolution of a foreland basin in central SW England. *Journal of the Geological Society*, **145**, 789-800

Shackleton, R.M. 1984. Thin skinned tectonics, basement control and the Variscan Front. In: Hutton, D.H.W. & Sanderson, D.J. (eds) Variscan Tectonics in the North Atlantic Region. *Special Publication of the Geological Society*, London, **14**, 125-30.

Shail, R.K. 1991. Field excursion to the Gramscatho group of south Cornwall. Proceedings of the Ussher society. **7**, 427 – 428.

Sherlock, S.C., Kelley, S. P., Zalasiewicz, J. A., Schofield, D. I., Evans, J. A., Merriman, R. J. & Kemp, S. J. 2003. Precise dating of low-temperature deformation: Strain-fringe analysis by 40Ar-39Ar laser microprobe. *Geology*, **31**, 219-222.

Shea, W.T. & Kronenberg, A.K. 1992. Rheology and deformation mechanisms of an isotropic mica schist. *Journal of Geophysical Research*, Solid Earth, **97**, 15201-15237.

Shimamoto, T. & Ikeda, Y. 1976. A simple algebraic method for strain estimation from deformed ellipsoidal objects. 1. Basic theory. *Tectonophysics*, **36**, 315-337.

Siegesmund, S. 1995. Control of magnetic rock fabrics by mica preferred orientation: a quantitative approach. *Journal of Structural Geology*, **17**, 1601-1613.

Siegesmund, S. 1996. The significance of rock fabrics for the geological interpretation of geophysical anisotropies. *Petrophysical and Seismic Features of the exposed lower continental crust in Calabria (Italy).* **85**, 8-109.

Siddans, A.W.B. 1972. Slaty cleavage - a review of research since 1815. *Earth-Science Reviews*, **8**, 205-232.

Silva, P. F., Marques, F. O., Miranda, J. M., Henry, B. & Mateus, A. 2001. Anisotropy of magnetic susceptibility constraints on Variscan obduction processes in the Bragança Massif (NE Portugal). *Tectonophysics*, **341**, 95-119.

Sintubin, M. 1994b. Phyllosillicate preferred orientation in relation to strain path determination in the lower Palaeozoic Stavelot-Venn Massif (Ardennes, Belgium). *Tectonophysics*, **237**, 215-231.

Sintubin, M. 1998. Mica (110) pole figures in support of Marchian behaviour of phyllosilicates during the development of phyllosilicate preferred orientation. *Material Science Forum*, **273-275**, 601-606.

Sintubin, M. 1999. Arcuate fold and cleavage patterns in the southeastern part of the Anglo-Brabant Fold Belt (Belgium): tectonic implications. *Tectonophysics*, **309**, 81-97.

Sintubin, M. Wenk, H. R. & Phillips, D. S. 1995. Texture development in platy materials: Comparison of Bi2223 aggregates with phyllosilicate fabrics. *Materials Science and Engineering*, **202**, 157-171.

Sloan, R.J. & Bennett, M.C. 1990. Geochemical character of Silurian volcanism in SW Ireland. *Journal of the Geological Society*, **147**, 1051-1060.

Somma, R. 2006. The south-western side of the Calabrian Arc (Peloritani Mountains): Geological, structural and AMS evidence for passive clockwise rotations. *Journal of Geodynamics*, **41**, 422-439.

Soper, N.J., Webb, B.C. & Woodcock, N.H. 1987. Late Caledonian (Acadian) transpression in north-west England: timing, geometry and geotectonic significance. *Proceedings of the Yorkshire Geological Society*, **47.**

Soper, N.J. & Woodcock, N.H. 1990. Silurian collision and sediment dispersal patterns in southern Britain. *Geological Magazine*, **127**, 527-542.

Soper, N.J. & Woodcock, N.H. 2003. The lost Lower Old Red Sandstone of England and Wales: a record of post-Iapetan flexure or Early Devonian transtension? *Geological Magazine*, **140**, 627-647.

Soto, R., Larrasoana, J.C., Arlegui, L. E., Beamud, E., Oliva-Urcia, Belen & Simon, J. L. 2009. Reliability of magnetic fabric of weakly deformed mudrocks as a palaeostress indicator in compressive settings. *Journal of Structural Geology*, **31**, 512-522.

Soto, R., Mattei, M. & Casas, A.M. 2003.Relationship between AMS and folding in an area of superimposed folding (Cotiella-Boixols nappe, Southern Pyrenees). *Geodynamica Acta*, **16**, 171-185.

Sloan, R.J. & Willams, B.P.J. 1991. Volcano-tectonic control of offshore to tidal-flat regressive cycles from the Dunquin Group (Silurian) of southwestIreland. In: MACDONALD, D.I.M. (ed.) Sea level changes at active place margins: process and product. *International Association of Sedimentologists, Special Publications*, **12**, 105-119.

References

Stampfli, G.M., Hochard, C., Vérard, C. & Wilhem, C. 2013. The formation of Pangea. *Tectonophysics*, **593**, 1-19.

Stephenson, A. 1994. Distribution anisotropy, two simple models for magnetic lineation and foliation. *Physics of the Earth and Planetary Interiors*, **82**, 49-53.

Stetsky R.M. 1978. Mechanisms of high temperature temperature frictional sliding in Westerly Granite. *Canadian Journal Earth Science*, **15**, 361-375.

Stetsky R.M., Brace W.F., Riley D.K. & Robin P.Y.F. 1974. Friction in faulted rock at high temperature and pressure. *Tectonophysics* **78**, 585-600.

Stephenson, A., Sadikun, S. & Potter, D.K. 1986. A theoretical and experimental comparison of the anisotropies of magnetic susceptibility and remanence in rocks and minerals. *Geophysiccal Journal of the Royal Astronomical Society*, **84**, 185-200.

Stevenson, C.T.E. 2005. Granite Emplacement and Magma Flow in Contrasting Tectonic Environments Using Anisotropy of Magnetic Susceptibility (Doctoral dissertation, University of Birmingham).

Stille, H. 1951. die MitteleuropäischeVariszische Grundgebirge im Bilde des Gesamteuropäischen. In: Beihefte zum Geologischen Jahrbuch Heft 2. Geologische Landesanstalt der Bundespepublik Deutschland, Hannover, 138 p.

Stille, H. 1924. Grundfragen der vergleichenden Tektonik: pp443; *Borntraeger, Berlin.*

Stipp, M., StuÈnitz, H., Heilbronner, R. & Schmid, S. M. 2002. The eastern Tonale fault zone: a 'natural laboratory'for crystal plastic deformation of quartz over a temperature range from 250 to 700 C. *Journal of Structural Geology*, **24**, 1861-1884.

StÖssel, I. 1993. Geologie der Umgbung von Cahersiveen, Co. Kerry. Unpublished Diploma Arbeit, ETH-Zurich, Switzerland.

Suess, E. 1886. Über unterbrochene Gebirgsfaltung. Sitzungsberichte der kaiserlichen Akademie der Wissenschaften in Wien, mathematischnaturwissenschaftliche Klasse, Abteilung 1, **94**, 111-117.

Swager, N. 1985. Solution transfer, mechanical rotation, and kink-band boundary migration during crenulation-cleavage development. *Journal of Structural Geology*, **7**, 421-429.

Tarling, D.H. & Hrouda, F. 1993. The Magnetic Anisotropy of Rocks. Chapman & Hall, London.

Thompson R. & Oldfield, F., Environmental Magnetism, 227 pp., Allen & Unwin, Boston, 1986.

Tikoff, B. & Greene, D. 1997. Stretching lineations in transpressional shear zones: an example from Sierra Nevada Batholith, California. *Journal of Structural Geology*, **19**, 29-39.

Todd, S.P. 1989. Role of the Dingle Bay Lineament in the evolution of the Old Red Sandstone of southwest Ireland. In: Arthurton, R.S., Gutteridge, P. & Nolan, S.C. (eds) Role of Tectonics in Devonian and Carboniferous Sedimentation in the British Isles. *Yorkshire Geological Society, Special Publications*, **6**, 35-54.

References

Todd, S.P. 1991. The Silurian Rocks of Inishnabro, Blasket Islands, County Kerry and theis regional significance. *Irish Journal of Earth Science*, **11**, 91-98.

Todd, S.P. 2015. Structure of the Dingle Peninsula, SW Ireland: evidence for the nature and timing of Caledonian, Acadian and Variscan tectonics. *Geological Magazine*, **152**, 242-268.

Todd, S.P., Boyd, J.D. & Dodd, C.D. 1988a. Old Red Sandstone sedimentation and basin development in the Dingle Peninsula, southwest Ireland. In McMillan, N.J., Embry, A.F., & Glass, D.J. (eds) The Devonian of the World. *Canadian Society of Petroleum Geologists Memoir*, **14**, 251-268.

Todd, S.P., Williams, B.P.J. & Hancock, P.L. 1988b. Lithostratigraphy and structure of the Old Red Sandstone of the northern Dingle Peninsula, Co. Kerry, southwest Ireland. *Geological Journal*, **23**, 107-120.

Trayner, P.M. & Cooper, M.A. 1984. Cleavage geometry and the development of the Church Bay Anticline, Co. Cork, Ireland. *Journal of Structural Geology*, **6**, 83-87.

Tucker, R.D. & McKerrow, W.S. 1995. Early Paleozoic chronology: a review in light of new U-Pb zircon ages from Newfoundland and Britain. *Canadian Journal of Earth Sciences*, **32**, 368-379.

Tullis, T.E. & Wood, D.S. 1975. Correlation of finite strain from both reduction bodies and preferred orientation of mica in slate from Wales. *Geological Society of America Bulletin*, **86**, 632-638.

Ullemeyer, K., Braun, G., Dahms, M., Kruhl, J.H., OlesenØ, N. & Siegesmund, S. 2000. Texture analysis of a muscovite-bearing quartzite: a comparison of some currently used techniques. *Journal of Structural Geology*, **22**, 1541-1557.

Uyeda, S., Fuller, M.D., Belshé, J.C., Girdler, R.W. 1963. Anisotropy of magnetic susceptibility of rocks and minerals. *Journal of Geophysical Research*, **68**, 279-291.

Van Daalen, M., Heilbronner, R. & Kunze, K. 1999. Orientation analysis of localized shear deformation in quartz fibres at the brittle-ductile transition. *Tectonophysics*, **303**, 83-107.

Van Veen, P.M. & Van der Zwan, C.J. 1980. Palynological evidence concerning the Middle/Late Devonian age of the Green Sandstone Formation McGillycuddy's Reeks, southwest Ireland. *Geologie en Mijnbouw*. Netherlands Journal of Geosciences, **59**, 405-408.

Vasiliev. I., Matenco, L. & Krijgsman, W. 2009. The syn- and post-collisional evolution of the Romanian Carpathian foredeep: New constraints from anisotropy of magnetic susceptibility and paleostress analyses. *Tectonophysics*, **473**, 457-465.

Veloso, E.E., Anma, R., Ota, T., Komiya, T., Kagashima, S. & Yamazaki, T. 2007. Paleocurrent patterns of the sedimentary sequence of the Taitao ophiolite constrained by anisotropy of magnetic susceptibility and palaeomagnetic analyses. *Sedimentary Geology*, **201**, 446-460.

Vermeulen, N.J., Shannon, P.M., Landes, M., Masson, F. & Group, V. 1998. Seismic evidence for subhorizontal crustal detachments beneath the Irish Variscides. *Irish Journal of Earth Sciences*, 1-18.

References

Walsh, P.T. 1968. The Old Red Sandstone west of Killarney, Co. Kerry, Ireland. *Proceedings of the Royal Irish Acadamy*, **66**, 9-26.

Warr, L.N. 1993. Basin development and foreland basin development in the Rhenohercynian of south west England. In: Gayer, R.A., Greiling, R. & Vogel, A., (eds). The Rhenohercynian and Sub-Variscan fold belts. Earth Evolution Series, Viewig & Sohn, Braunschweig/Wiesbaden 197-224.

Warr, L.N. 2009. The Variscan Orogeny: the welding of Pangaea. *Geological history of Britain and Ireland*, 271.

Warr, L.N. 2012. The Variscan Cycle: Consolidation of Pangea. In Strachan, R. A. & Woodcock, N.H. (Eds.). 2012. Geological history of Britain and Ireland. Wiley-Blackwell Science.

Wartho, J. A., Quinn, D. & Meere, P. A. 2006. The timing of Variscan deformation: UV laser 40 Ar/39 Ar dating of syn/ late-orogenic intrusions from SW Ireland. *Geochimica et Cosmochimica Acta*, **70**, A690.

Weber, K., 1981. The structural development of the Rheinische Schiefergebirge. *Geol. Mijnbouw*, **60**, 149-159.

Weil, A.B. Van der Voo, R. & Van der Pluijm, B.A. 2001. Oroclinal bending and evidence against the Pangea megashear: The Cantabria-Asturias arc (northern Spain). *Geology*, **29**, 991-994.

Weil, A.B. & Yonkee, W. A. 2012. Layer-parallel shortening across the Sevier fold-thrust belt and Laramide foreland of Wyoming: spatial and temporal evolution of a complex geodynamic system. *Earth and Planetary Science Letters*, **357**, 405-420.

White S.H. & Johnston D.C. 1981. A microstructural and microchemical study of cleavage lamellae in a slate. *Journal of Structural Geology*, **3**, 279-290.

White S.H. & Knipe R.J. 1978. Microstructure and cleavage development in selected slates. *Contributions to Mineralogy and Petrology*, **66**, 165-174.

Williams, E.A. 2000. Flexural cantilever models of extensional subsidence in the Munster Basin (SW Ireland) and Old Red Sandstone fluvial dispersal systems. From: Friend, P.F. & Williams, B.P.J. (eds). New perspectives on the Old Red Sandstone. *Geological Society, London, Special Publications*, **180**, 239-269.

Williams, E.A., Bamford, M.L.F., Cooper, M.A., Edwards, H.E., Ford, M., Grant, G.G., MacCarthy, I.A.J., McAfee, A.M. & O'Sullivan, M.J. 1989. Tectonic Controls and sedimentary response in the Devonian-Carboniferous Munster and South Munster basins, south-west Ireland. In: Arthurton, R. S., Gutteridge, P. & Nolan, S.C. (eds) Role of Tectonics in Devonian and Carboniferous Sedimentation in the British Isles. *Special Publication of the Yorkshire Geological Society*.

Williams, E.A., Ford, M. & Edwards, H.E. 1990. Discussion of a model for the development of the Irish Variscides. *Journal of the Geological Society*, **147**, 566-571.

Williams, E.A., Ford, M., Edwards, H. & O'Sullivan, M.J. 1993. An outline of evolution of the Late Devonian Munster basin, southwest Ireland. In R.A. Gayer, R.O. Greiling and A.K. Vogel (eds), Rhenohercynian and subvariscan fold belts, 131-8.

References

Williams, E.A., Sergeev, S.A., Stossel, I. & Ford, M. 1997. An Eifelian U-Pb zircon date for the Enagh Tuff Bed from the Old Red Sandstone of the Munster Basin in NW Iveragh, SW Ireland. *Journal of the Geological Society, London*, **154**, 189-193.

Williams, E.A., Sergeev, S.A., Stossel, I., Ford, M. & Higgs, K.T. 2000. U-Pb zircon geochronology of silicic tuffs and chronostratigraphy of the earliest Old Red Sandstone in the Munster Basin, SW Ireland. In Friend, P.F. & Williams, B.P.J. (Eds.). New Perspectives on the Old Red Sandstone. *Geological Society London, Special Publications*, **180**, 269-302.

Williams, E.A., Sergeev, S. A., Stössel, I. & Ford, M.1997. An Eifelian U-Pb zircon date for the Enagh Tuff Bed from the Old Red Sandstone of the Munster Basin in NW Iveragh, SW Ireland. *Journal of the Geological Society*, **154**, 189-193.

Williams, G.D., Powell, C.M. & Cooper, M.A. 1989. Geometry and kinematics of inversion tectonics. *Geological Society, London, Special Publications*, **44**, 3-15.

Wilson C.J.L. 1980. Shear zones in a pegmatite: a study of albite-mica-quartz deformation. *Journal Stuctural Geology*, **2**, 203-209.

Wingfield, R.T.R. 1966. The Geology of Kenmare and Killarney. Unpublished Ph.D. thesis, Univ. of Dublin.

Winkler, A., Alfonsi, L., Florindo, F., Sagnotti, L. & Speranza, F. 1997. The magnetic anisotropy of rocks: principles, techniques and geodynamic applications in the Italian peninsula. *Annali di Geofisica*, Vol. XL, N.3 p 729-740.

Woodcock, N.H. & Strachan, R.A. 2000. The Caledonian Orogeny: a multiple plate collision. In: Geological History of Britain and Ireland (N.H.Woodcock and R.A. Strachan, eds) Blackwell Science, London.

Woodcock, N.H., Soper, N.J. & Strachan, R.A. 2007. A Rheic cause for the Acadian deformation in Europe. *Journal of the Geological Society*, **164**, 1023-1036.

Wood, D.S., Oertel, G., Singh, J. & Benett, H.F. 1976. Strain and anisotropy in rocks. *Philosophical Transactions of the Royal Society of London, Series A*, **283**, 27-42.

Wu, S. & Groshong, R.H. 1991. Low-temperature deformation of sandstone, southern Appalachian fold-thrust belt. *Geological Society of America Bulletin*, **103**, 861-875.

Witt, K. 1996. Geologische Kartierung der su¨dwest-irischen Aussenzone des Variszikums in der Bantrymulde. Unpubl. Diplomkartierung, RWTH Aachen, 80 pp.

Yu, H. & Zheng, Y. 1984. A statistical analysis applied to the $R_{f/phi}$ method. *Tectonophysics* **110**, 151-155.

Ziegler, P. 1989. Evolution of Laurussia. Kluwer, Dordrecht.

Ziegler, P.A. 1978a. In tectonics and geophysics of continental rifts (ed. I. B. Ramberg & E.-R. Neumann) (N.A.T.O. Advanced Study Institute, Series C), pp. 249-277. Dordrecht:D. Reidel.

Ziegler, P.A. 1978b *Geologie en Mijnbouw*. **57**, 589-626.

References

Zhao, X., Riisager, P., Antretter, M., Carlut, J., Lippert, P., Liu, Q. & Kanamatsu, T. 2006. Unraveling the magnetic carriers of igneous cores from the Atlantic, Pacific, and the southern Indian oceans with rock magnetic characterization. *Physics of the Earth and Planetary Interiors*, **156**, 294-328.

Online references:

http://www2.ulg.ac.be/geolsed/MS/Chadima-training.pdf
Georient software: http://www2.ulg.ac.be/geolsed/MS/Chadima-training.pdf

Appendix A: Field Data and AMS Site Data.

TABLE A.1 SITES WITH SINGLE POINT CLEAVAGE AND BEDDING READINGS

No.	Location	Grid Ref	Latitude/Longitude	Fm.	Lithology	S0 bedding LHR	S1 cleavage LHR
L1	Coonama Harbour	44815 58432	51°59'20.94"N 10°12'46.07"W	BSF	sandstone	215 42 N	050 55 S
L4	Near Cooncrome	44495 58145	51°57'44.94"N 10°15'23.54"W	BSF	sandstone	340 10 E	058 40 S
L5	Near Cooncrome	44525 58142	51°57'45.66"N 10°15'31.49"W	BSF	sandstone	078 70 S	090 20 S
L6	Cooncrome Harbour East	44448 58162	51°57'54.51"N 10°15'51.48"W	BSF	sandstone	040 15 S	N/A
L7	Cooncrome Harbour West	44432 58171	51°57'55.16"N 10°15'57.44"W	BSF	sandstone	075 28 S	N/A
L8	Road to Coonama	44831 58262	51°58'28.87"N 10°12'20.83"W	BSF	sandstone	055 70 N	060 42 S
L13	White Bay Beach	44355 57944	51°56'40.79"N 10°16'34.00"W	BSF	sandstone	230 60 N	070 60 S
L14	Cahersiveen railway/river north	44735 58025	51°57'12.31"N 10°13'18.01"W	VSF	siltstone	190 25 N	060 75 S
L15	Kerry way Coars.	45445 57872	51°56'35.25"N 10° 7'2.17"W	SFSF	siltstone	not visible	060 80 S
L16	Coars Roadcut.	45458 57920	51°56'43.53"N 10° 6'55.15"W	SFSF	siltstone	not visible	080 80 S
L17	Coars.	45384 57925	51°56'44.75"N 10° 7'32.20"W	SFSF	siltstone	not visible	070 80 S
L18	Bray Head.	43309 57309	51°53'3.18"N 10°25'31.63"W	VSF	siltstone	300 20 N	080 65 S
L20	Coonama Harbour Point East.	44834 58501	51°59'44.56"N 10°12'40.69"W	BSF	sandstone	065 20 S	070 70 S
L21	Kells Bay West	45549 58805	52° 1'31.19"N 10° 6'20.24"W	BSF	sandstone	105 20 S	N/A
L22	Kells Bay Post Office	45602 59676	52° 0'48.44"N 10° 5'52.41"W	BSF	sandstone	020 05 S	N/A
L23	Reencaheragh Bay Portmagee.	43585 57278	51°53'3.71"N 10°22'50.40"W	VSF	sandstone	060 55 S	062 48 S
L25	Marina Cahersiveen.	44661 57961	51°56'50.14"N 10°14'11.07"W	VSF	siltstone	240 70 N	065 60 S
L26	Reenard Point	44345 57765	51°55'47.65"N 10°16'41.66"W	VSF	sandstone	038 25 S	065 70 S
L27	Manix point	44562 57918	51°56'30.40"N 10°14'43.42"W	VSF	siltstone	not visible	055 68 S
L28	Valentia Pier Opposite Portmagee.	43700 57341	51°53'18.11"N 10°22'7.15"W	VSF	siltstone	250 60 N	065 40 S
L30	Valentia Fort Point	44033 57824	51°55'59.82"N 10°19'20.16"W	VSF	sandstone	230 10 N	080 48 S
L33	Cahersiveen railway/river south	44745 58005	51°57'7.26"N 10°13'10.16"W	VSF	siltstone	not visible	060 45 S
L34	Near Cahergal stone fort	44435 58051	51°57'17.47"N 10°15'53.33"W	VSF	siltstone	not visible	070 45 S
L37	Coosmaraka, Valencia N coast	43431 57555	51°53'44.77"N 10°25'24.21"W	VSF	sandstone	265 08 N	060 42 S
L38.2	Beenaryraka Head, Valentia	43442 57605	51°54'44.23"N 10°24'20.79"W	VSF	sandstone	235 30 N	050 45 S
L46	Portmagee East of Bridge	43794 57298	51°53'4.93"N 10°21'10.83"W	VSF	siltstone	210 45 N	060 65 S
L12	Ballycarbary Castle	44460 57980	51°56'50.43"N 10°15'41.98"W	BSF	siltstone	070 85 S	070 60 S
L39	Knocknatobar	44951 58468	51°59'42.84"N 10°11'55.43"W	BSF	sandstone	058 39 S	N/A
L41	Knocknatobar mountain	44950 58368	51°58'46.18"N 10°11'46.00"W	BSF	sandstone	030 05 S	050 50 S
A21	Round corner from Cooncrome	44446 58171	51°57'55.63"N 10°15'49.99"W	SFSF	sandstone	250 80 N	060 25 S

	location.	Grid Reference	Lat/Long	Fm.	Lithology	S0 LHR	S1 LHR
L60	Torc Waterfall	49661 58478	52° 0'17.89"N 9°30'22.35"W	SFSF	siltstone	none	082 42 S
L61	South of White Bay	44352 57875	51°56'22.16"N 10°16'35.39"W	BSSF	sandstone	254 78 N	078 60 S
L62	Near Ballykneally				sandstone	070 64 S	068 78 N
A1	Portmagee Quarry	44439 57185	51°52'37.24"N 10°15'41.64"W	SFSF	sandstone	060 45 S	062 72 S
A2	Killabounia	44155 56981	51°51'28.22"N 10°18'0.03"W	SFSF	sandstone	050 40 S	056 80 E
A3M	Keel Bay	43905 56853	51°50'46.32"N 10°20'8.42"W	SFSF	sandstone	046 60 S	052 78 N
A4	Se of Keel Bay	44006 56658	51°49'50.36"N 10°19'18.94"W	SFSF	Sandstone	050 70 S	060 75 N
A6	Caherdaniel	45215 55997	51°46'24.44"N 10° 8'42.11"W	SFSF	Sandstone	120 32 S	065 88 S
A8	Turn of Rossmore	47562 56618	51°50'0.80"N 9°48'20.29"W	BSF	sandstone	250 18 N	070 85 N
A9	Molls Gap	48637 57730	51°56'14.30"N 9°39'10.31"W	SFSF	sandstone	070 52 S	058 80 S
A14	Kilgarvain	50763 58097	51°58'23.32"N 9°20'35.94"W	SFSF	sandstone	072 30 S	065 85 N
A10	Gap Dunloe North	48768 58788	52° 2'0.42"N 9°38'13.94"W	BSF	sandstone	100 30 S	076 72 S
A12	Gap Dunoe South	48765 58806	52° 0'36.39"N 9°38'17.86"W	SFSF	sandstone	040 30 S	076 72 S
L44	Culoo Rocks	43545 57635	51°54'52.98"N 10°23'30.05"W	VSF	sandstone	056 28 N	050 20 S
L47	Coosfada	44457 58350	51°58'47.24"N 10°15'55.10"W	BSF	sandstone	240 58 N	060 30 S
L31	Reenadrolaun Point	43836 57850	51°55'55.39"N 10°21'1.36"W	VSF	sandstone	050 20 S	068 48 S
M5	Lough Acoose	47609 58494	52° 0'9.94"N 9°48'16.20"W	LASF	sandstone	100 40 S	075 55 S
AM1	South of Lough Caragh	47470 57837	51°56'33.16"N 9°49'20.16"W	BSF	sandstone	078 42 S	070 85 S
AM11	North of Lough Caragh	47242 59195	52° 3'54.73"N 9°51'39.72"W	BSF	sandstone	262 52 N	068 40 S
L35	Dooneen	45022 58340	51°58'45.13"N 10°10'50.56"W	BSF	sandstone	175 10 S	062 55 S (in area)
M8	Glenflesk Quarry	50666 58614	52° 1'8.68"N 9°21'38.04"W	SFSF	sandstone	232 80 N	060 60 S
M2	Rheencaheragh Bay	43565 57288	51°53'1.97"N 10°23'13.65"W	VSF	sandstone	090 42 N	058 53 S
M3	Kells Bay	45567 58803	52° 1'29.97"N 10° 6'8.01"W	BSF	sandstone	070 75 S	N/A
M6	Ballyheige	47489 62801	52°23'20.06"N 9°50'12.36"W	KS	sandstone	060 20 S	N/A
M7	Brandon Pier	45255 61516	52°16'8.58"N 10° 9'33.18"W	CA	sandstone	038 38 S	N/A
A13	Dunmore East	66894 60087	52° 9'19.76"N 6°59'33.21"W	TF	sandstone	140 08 S	N/A
M4	Broad Strand	55147 54114	51°37'15.27"N 8°41'55.31"W	WS	sandstone	075 80 S	078 80 N
A15	Bulls Head Dingle	44950 59752	52° 6'28.11"N 10°11'41.18"W	LS	sandstone	062 35 S	N/A

BSF = Ballinskelligs Sandstone Fm, VSF = Valentia Slate Fm, LASF = Lough Acoose Sandstone Fm, SFSF = St. Finan's Sanstone Fm, LS = Lough Slat Conglomerate ,CA = Capagh Sandstone Formation , WS = White strand Formation, KS = Kilmore Sandstone Formation, TF = Templetown Formation.

L23 Reencaheragh bay S1	L25 Cahersiveen Marina	L28 Valentia Pier	Gap of Dunloe N	Gap of Dunloe S	L60 Torc Waterfall
060 50 S	060 58 S	058 40 S	078 70 S	076 58 S	080 42 S
065 52 S	058 62 S	060 42 S	080 68 S	074 52 S	080 45 S
062 55 S	060 64 S	058 38 S	078 70 S	070 55 S	080 48 S
060 55 S	060 58 S	062 40 S	075 72 S	070 60 S	082 50 S
055 52 S	062 58 S	060 44 S	080 69 S	062 54 S	082 44 S
055 48 S	062 57 S	060 40 S	085 65 S	065 55 S	078 40 S
052 40 S	060 55 S	070 40 S	075 58 S	070 56 S	082 48 S
050 50 S	060 58 S	060 38 S	080 52 S	070 58 S	085 52 S
055 50 S	058 58 S	062 46 S	075 55 S	065 50 S	078 45 S
050 55 S	062 60 S	060 40 S	072 58 S	072 52 S	075 46 S
052 48 S	060 55 S	062 46 S	070 55 S	060 58 S	085 42 S
058 56 S	058 54 S	060 40 S	082 58 S	060 54 S	076 48 S
050 40 S	062 60 S	062 46 S	075 60 S	064 52 S	082 35 S
055 45 S	061 53 S	064 40 S	070 60 S	065 58 S	078 50 S
068 45 S	058 56 S	060 46 S	072 55 S	062 58 S	
060 58 S	062 55 S	060 38 S	085 50 S	062 62 S	
070 52 S	064 53 S	063 44 S	082 52 S		
065 62 S	062 58 S	065 42 S	080 68 S		
060 60 S	060 57 S	058 38 S	078 62 S		
060 50 S	055 50 S	058 46 S	080 60 S		
052 56 S	065 53 S	056 40 S	078 65 S		
058 58 S		062 48 S	072 62 S		
062 48 S					
058 55 S					
056 52 S					
062 58 S					
058 58 S					
060 54 S					
060 50 S					
060 60 S					
058 58 S					

L38.2 Beenakryraka Head S1 Cleavage			
054 38 S	050 40 S	052 40 S	060 52 S
048 36 S	054 40 S	055 45 S	
052 38 S	052 42 S	056 42 S	
050 38 S	050 38 S	050 38 S	

Appendices

L53 Derrynane Beach GR: 4524 5584 **Lat/Long** 51°45'36.05"N 10° 8'20.02"W Fold Hinge Line = 40-245			
		Pairs from same limb.	
Fold 2	Pairs	**S0**	**S1**
on southern limb:		110 48 S	068 76 N
		170 38 W	070 86 N
		118 42 S	072 82 N
		120 45 S	080 72 N
northern limb:		050 48 N	070 80 S
		040 48 N	080 80 S
		030 42 N	090 84 S
Fold 3		Fold Hinge Line = 30-230	
	Pairs	S0	S1
		010 48 N	065 80 S
		120 48 S	065 82 N
Fold 1		Fold Hinge line = 38-235	
	Pairs	S0	S1
		080 45 S	050 86 N
		088 52 S	050 85 N
		088 52 N	050 85 S
at fold axial plane		145 38 S	050 90 S

Canglass Point				
		S0	S1	L1
FoldLimb1	**Pair 1**	060 80 N	040 20 S	00-060
	Pair 2	060 60 N	040 30 S	
	Pair3	062 40 N	040 40 S	05-045
	Pair 4	horizontal	048 62 S	00- 046
		S0	S1	L1
Fold Limb 2	**Pair 1**	055 10 S	056 68S	02-060
		S0	S1	
Fold Limb 3	**Pair 1**	062 68 S	055 20 S	
	Pair 2	040 15 S	056 68 S	

L55 Near to Rossbeigh-Iveragh Peninsula GR: 4626 5901 **Lat/Long** 52° 2'45.05"N 10° 0'12.20"W				
Fold 1:	Verging to the North		Fold Axial Plane = 062 54 S	
		Pairs	**S0**	**S1**
	on southern Limb :	a	060 20 S	078 80 S
		b	060 05 S	078 65 S
	at fold hinge	d	080 40 N	060 48 S
	on northern Limb:	e	070 70 N	070 25 S
		f	080 88 N	080 18 S
Fold 2 :	**Verging to the North**		Fold Axial Plane = 062 60 S	
		Pairs	**S0**	**S1**
	on southern limb:	a	060 18 S	070 72 S
		b	060 25 S	060 65 S
	on northern limb:	c	062 70 N	072 38 S
		d	060 88 S	068 20 S
Fold 3	Verging to the North		Fold Axial Plane = 070 55 S	

Appendices

Ballinskelligs Pier GR: 4434 5643 **Lat/Long** 51°48'32.95"N 10°16'17.14"W		
S0	**S1**	**L1**
080 46 N	050 80 S	
070 42 N	052 78 S	
078 32 N	052 80 S	
056 58 N	040 50 S	20-218

L1 Coonama Harbour	
S0	S1
234 60 N	060 38 S
232 54 N	050 60 S
132 08 S	060 64 S
235 20 S	060 30 S
	050 70 S

Ballagisheen Pass **GR:** 4669 5791 **Lat/Long :** 51°56'54.69"N 9°56'6.77"W	
Pairs:	
S0	**S1**
058 56 N	060 68 S
060 58 N	064 82 S
058 52 N	060 60 S
	060 62 S
	062 58 S
	058 60 S

Appendices

Samples Analysed						
No.	**Location**	**Fm.**	**No. of Cores analysed (AMS)**	**Strain analysis**	**Thermomagnetic studies**	**Thin Section Analysis**
A1	Portmagee Quarry	SFSF				✓
A2	Killabounia.	SFSF	10	✓	✓	
A3M	Keel Bay.	SFSF	9	✓		
A4	SE of Keel Bay.	SFSF	9	✓		✓
A6	Road to Caherdaniel.	SFSF	11	✓		✓
A8	Turn off Rossmore.	BSF	19	✓	✓	
A9	Molls Gap.	SFSF	16	✓		
A10	Gap of Dunloe South.	BSF	13	✓		✓
A12	Gap of Dunloe North.	SFSF	9	✓		
A13	Dunmore East.	TF	9	✓		
A14	Kilgarvin.	SFSF	10	✓	✓	✓
A15	Bulls Head Dingle Peninsula.	LS	8	✓		
M2	Rheencaheragh.	VSF	21	✓		
M3	Kells Bay.	BSF	16	✓		✓
M4	Broad Strand.	WS	25	✓		
M5	Lough Acoose.	LASF	13	✓		✓
M6	Ballyheige.	KS	26	✓	✓	✓
M7	Brandon Pier.	CA	7	✓		✓
M8	Glenflesk Quarry.	SFS	28	✓		✓
L7	Cooscrome	BSF	N/A	✓		✓
L10	Dolous Head	BSF	N/A	✓		✓
L39	Knocknatobar	BSF	N/A	✓		✓
L21	Kells Bay West	BSF	N/A	✓		✓

Samples Analysed continued.						
Location No.	**Location**	**Fm.**	**No of Cores analysed**	**Strain analysis**	**Thermomagnetic studies**	**Thin Section Analysis**
L31	Reenadrolaun Point, Valentia Island.	VSF	15	✓	✓	
AM1	Lough Caragh North.	BSF	10	✓	✓	
AM11	South of Lough Caragh.	BSF	8	✓	✓	
L35	Dooneen.	BSF	7	✓		
L44	Culoo Rocks, Valentia Island.	VSF	13	✓		
L47	Coosfada.	BSF	8	✓	✓	✓
L22	Kells Bay Post Office	BSF		✓		

TABLE A.2 FIELD DATA COLLECTED FROM AMS SITES

A1 Portmagee Quarry				
S0	**S0 (continued)**	**S1**	**L1**	**L1 (continued)**
070 45 S	072 48 S	068 74 S	09- 235	09-238
070 50 S	068 52 S	068 65 S	12- 255	09- 244
065 45 S	060 44 S	067 65 S	14- 242	10 -242
062 48 S	058 58 S	062 72 S	16- 242	08- 242
080 48 S	060 54 S	064 72 S	12- 236	08- 240
065 50 S	065 48 S	068 64 S	12- 235	06- 238
070 50 S	058 58 S	059 70 S	10- 234	08- 242
072 52 S	070 45 S	058 78 S	12- 230	08- 236
072 48 S	075 45 S	060 72 S	12- 240	10- 244
065 48 S	076 50 S	064 69 S	09- 240	10- 236
068 50 S		060 60 S	14- 242	10- 244
065 50 S		060 68 S	12- 240	10- 236
060 49 S		070 65 S	10- 240	12- 236
065 60 S		060 72 S	10- 240	09- 244
065 56 S		060 75 S	12- 235	08- 240
068 48 S		058 80 S	14- 230	10- 242
070 52 S		060 72 S	10- 235	
066 48 S		070 70 S		

A2 Killabounia		
S0	**S1**	
050 40 S	056 80 S	
040 42 S	060 85 S	
038 50 S	058 78 S	
048 55 S	054 90 S	
048 55 S	052 78 S	
050 52 S	050 78 S	
	052 86 S	
	048 80 S	
	050 82 S	
	048 82 S	
	052 80 S	
	046 80 S	
	052 90 S	
	054 78 S	
	052 84 S	
	048 90 S	
	050 85 S	

A3M Keel Bay		
S0	**S1**	**L1**
045 55 S	050 72 N	12 052
048 58 S	052 88 N	14 053
042 46 S	052 65 N	10 050
045 45 S	054 80 N	09 050
038 48 S	058 66 S	09 042
040 55 S	056 64 S	15 050
052 48 S	058 70 S	
052 46 S	050 65 S	
050 52 S	050 88 S	
052 52 S	052 86 S	
056 40 S	050 84 N	
042 38 S	048 82 N	
038 42 S	048 85 N	
045 40 S	052 78 N	
	054 84 N	
	048 80 S	
	048 80 S	
	052 82 S	
	050 82 S	
	052 78 S	
	050 74 S	
	052 86 S	
	055 85 N	
	052 80 N	

A6 Caherdaniel			
S0	**S1**	**S1 (Continued)**	**L1**
125 36 S	065 90 S	065 88 N	42 238
120 32 S	060 85 S	066 88 N	36 236
112 38 S	064 85 N	065 90 S	35 230
125 38 S	065 88 S	060 85 S	38 232
120 38 S	060 86 S	064 85 N	35 230
125 35 S	060 90 S	065 88 S	38 232
125 30 S	070 86 S	060 88 S	35 235
	064 88 S		38 238
	065 88 S		38 228
	058 86 N		32 235
	056 84 N		35 230
	065 90 S		30 238
	065 85 N		32 236
	064 86 N		30 238
	060 88 N		32 232
	058 82 N		32 234
	062 85 N		38 228
	064 90 S		32 235
	058 88 N		32 238
	058 88 N		30 240
	060 90 S		32 240
	065 88 N		
	065 88 N		
	064 88 S		

A10 Gap of Dunloe North	
S0	S1
110 38 S	076 72 S
128 36 S	078 68 S
098 38 S	080 48 S
108 28 S	078 64 S
105 28 S	070 55 S
100 42 S	080 58 S
120 35 S	078 42 S
105 38 S	080 56 S
105 30 S	065 58 S
105 38 S	070 60 S
098 48 S	080 66 S
115 48 S	
114 40 S	
090 44 S	
080 44 S	
080 44 S	
100 38 S	
100 44 S	
108 38 S	
110 30 S	

A12 Gap of Dunloe South	
S0	S1
055 32 S	080 64 S
055 28 S	076 50 S
080 30 S	068 52 S
082 18 S	066 66 S
065 38 S	056 52 S
080 30 S	076 56 S
058 32 S	065 52 S
080 58 S	
060 36 S	
082 30 S	
066 32 S	
062 40 S	
050 32 S	
048 30 S	
050 28 S	
064 44 S	

L44 Culoo Rocks		
S0	S1	L1
228 10 N	050 38 S	04 054
235 08 N	060 20 S	04 055
232 08 N	056 20 S	04 235
228 10 N	054 35 S	04 052
228 15 N	048 42 S	02 232
062 08 N	042 35 S	06 238
060 12 N	045 50 S	08 046
040 06 N	052 56 S	02 048
	050 50 S	
	054 62 S	
	060 28 S	
	058 36 S	
	060 18 S	
	058 28 S	
	052 26 S	
	054 20 S	
	058 38 S	
	050 44 S	

Appendices

AM1			
S0	**S1**	**S1 (Continued)**	**L1**
080 32 S	074 68 S	072 65 S	15 248
080 30 S	076 78 S	076 70 S	12 240
076 35 S	075 78 S	078 68 S	10 246
075 32 S	080 70 S	065 72 S	08 242
080 38 S	068 65 S	068 76 S	10 250
082 36 S	075 68 S	075 72 S	16 250
	070 72 S		10 252
	066 75 S		12 246
	072 74 S		08 245
	078 72 S		10 245
	075 78 S		08 248
	076 62 S		10 246
	074 78 S		
	074 74 S		
	072 66 S		
	072 58 S		
	068 76 S		
	080 60 S		
	072 76 S		
	080 70 S		
	074 72 S		
	070 70 S		
	065 58 S		
	080 65 S		

AM11		
S0	**S1**	**L1**
262 40 N	075 80 N	08 078
268 40 N	068 40 S	12 076
256 52 N	050 40 S	08 074
260 52 N	045 38 S	08 075
256 46 N		12 080
260 48 N		12 075
260 50 N		05 074
266 46 N		08 078
252 62 N		10 080
262 58 N		12 060
262 58 N		
260 58 N		

L35 Dooneen	
S0	**S1**
175 20 S	060 76 S
178 15 S	062 60 S
190 20 S	060 58 S
	056 80 S
	058 70 S
	070 68 S
	060 45 S
	058 38 S
	062 55 S
	062 48 S
	056 40 S
	060 42 S
	060 38 S
	062 40 S
	058 52 S

Appendices

L47 Coosfada	
S0	**S1**
228 68 N	065 32 S
232 75 N	050 30 S
240 82 N	055 28 S
240 65 N	060 42 S
228 78 N	
228 70 N	
220 66 N	
240 68 N	
230 72 N	

M5 Lough Acoose		
S0	**S0 (continued)**	**S1**
070 38 S	100 36 S	080 52 S
075 42 S	090 38 S	078 56 S
100 40 S	086 38 S	076 54 S
082 25 S	088 48 S	075 55 S
080 48 S	086 40 S	074 54 S
080 32 S	088 32 S	076 48 S
082 46 S	086 46 S	074 62 S
080 40 S		078 50 S
080 40 S		
082 36 S		
085 40 S		

L31 Reenadrolaun Point	
050 25 N	038 40 S
050 08 S	054 52 S
045 30 S	060 48 S
	052 40 S
	058 40 S
	065 36 S
	062 44 S
	068 48 S
	068 38 S

Appendix B: AMS Methodology

i) AMS Block Sampling and Drilling.

Bedding was recorded in the field using left hand rule and marked on the block sample. The block sample was removed using a hammer and chisel. Any cleavage on or close to the sample was recorded.The orientated sandstone blocks were drilled in the laboratory at the University of Birmingham. The block samples were placed on the drilling table and clamped down in order to stabilize them during drilling. With each sample the drill dip and drill pitch was measured and recorded prior to drilling, using the left hand rule (AMS sample preparation Appendix). The surface was marked with white marker using the left hand rule (See Fig 5.1). The location of each core within the block sample was also recorded in the case of any variations or anomalies within the block sample itself. The cores were drilled using 25 mm in diameter diamond tipped non magnetic drill bit cooled with water. Once the cores were drilled, they were then allowed to dry and were trimmed and cut into cylinders of 22mm length and 25 mm diameter. Any cores above this size or with irregular edges were either re-trimmed and/or sanded down, and the size rechecked with a callipers. The number of cores from each sample ranges from 7 to 28. The cores were then labelled and re-marked using the left hand rule (Fig 5.1). Any cores that broken during drilling were super glued back together using non magnetic glue.

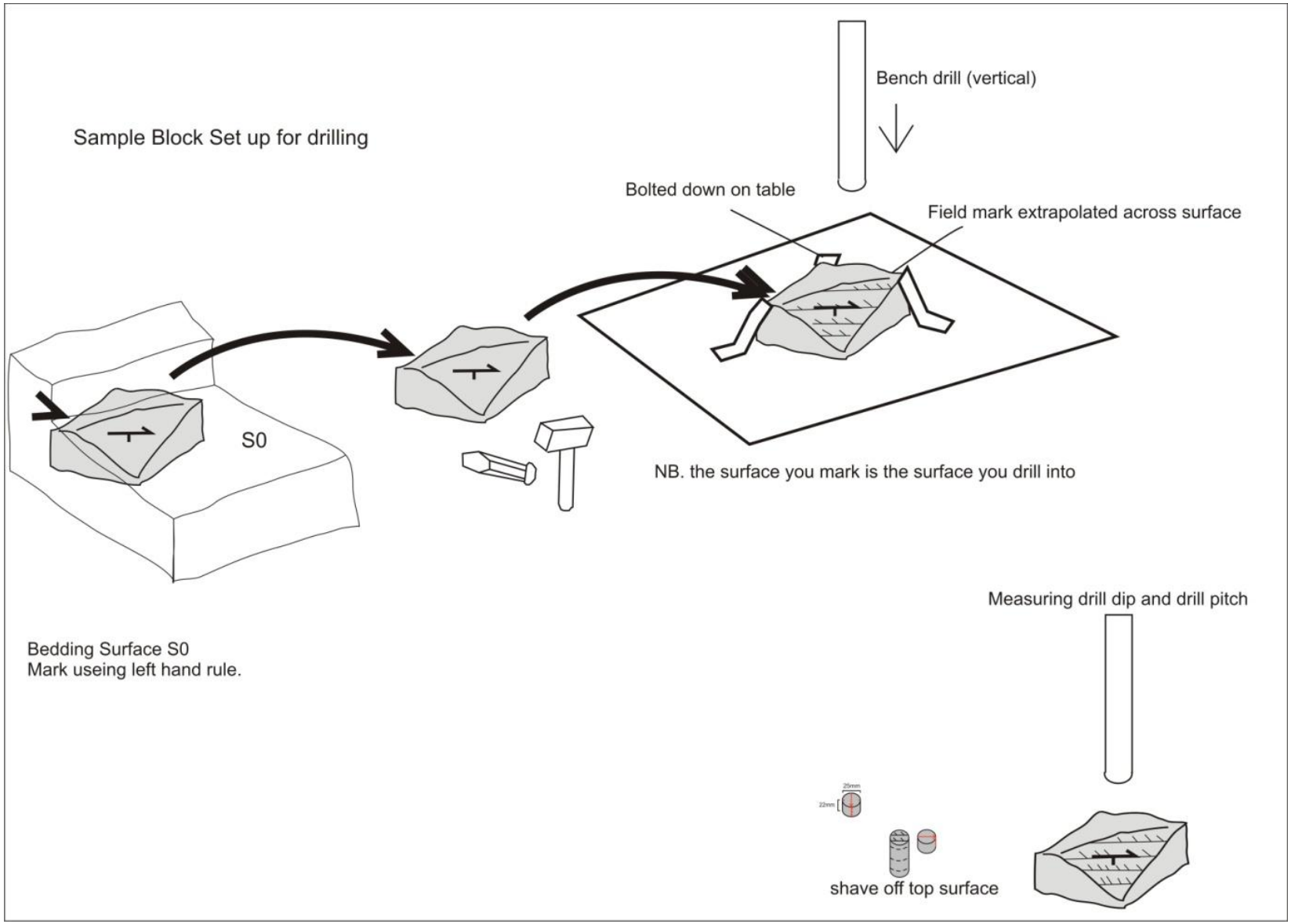

Fig A.1 Shows the method of block sampling and drilling (modified after Stevenson, 2005).

ii) Measuring the Drill Dip and Pitch.

The drill dip and the drill Pitch are required for each sample .

- Measure the angle between the strike of the sample on the drilling platform and the original field strike reading using left hand rule. Count the angular distance clockwise from the drill pitch plane. (This is measure in the plane parallel to the surface of the block).
- Measure the dip of the drilling plane. (Drill Dip)

Analysis using the Kappabridge:

First block of the day:

1. C:\KLY3\data\chloe
2. file name-(block name)
3. specimen name (eg a.1, a.2 …)

For a new block type # and press enter (after analysing when saving).
Select option 3 for non orientated.
F1 = axis 1
F2 = axis 2
F3 = axis 3
F4 = bulk anisotropy.
F5 = save

Enter specimen name.

Press enter…gives data.

Press escape to begin new sample.

Saved onto floppy disk.

Transfer to PC and use the following programmes by transferring them into a new folder named after the specimen.

Programmes used:

These following programmes process the raw AMS data and correct for field orientations and carry out the statistical analysis necessary to obtain 95% confidence (Owens, 1994; Jelineck, 1978).The processed data from these programmes was then converted to plots using Ghostgum software: GSview 3.2.

Appendices

List of Programmes for Processing AMS data.

MANIFIG	MEASAVER
ANISPLOT	JELANEW5
LFPLOT.FOR	JELANEW6
LFPLOT	BODGE 1
MEASUER	

To plot the AMS stereonet.

Open with gsview32

File-convert-pdfwrite-300 resolution

Save to AMS results M*

Call M*.plt

Open with adobe acrobat

Can now be opened in corel draw (as curves).

Example of output for sample M4: Broad Strand.

m4.ave = file name

Nrpt = 25 = number of cores

Mean: 0.96480 1.04083 -0.00546 0.01051 0.01981

Susc	Dec	Dip	
1.046	76.7	-3.2	Susc = K_{max}
0.998	357.1	72.8	Susc = K_{int}
0.956	345.7	-16.9	Susc = K_{min}

Covariance matrix for mean in reference frame, on 24 d.f.
0.52342E-05-0.58069E-05-0.19604E-07-0.18406E-05-0.13939E-05
-0.58069E-05 0.66294E-05-0.18846E-07 0.21185E-05 0.14931E-05
-0.19604E-07-0.18846E-07 0.46670E-06 0.32822E-07-0.19708E-06
-0.18406E-05 0.21185E-05 0.32822E-07 0.76497E-06 0.41208E-06
-0.13939E-05 0.14931E-05-0.19708E-06 0.41208E-06 0.60875E-06

95% LIMITS ON PRIN SUSCYS (MAX,INT,MIN) : 0.529E-02 0.691E-03 0.528E-02

Principal susceptibility differences; 95% limits:
K(1) - K(2) = 0.481E-01 +/- 0.539E-02
K(2) - K(3) = 0.413E-01 +/- 0.537E-02
K(1) - K(3) = 0.894E-01 +/- 0.106E-01

MU = 49.4 +/- 3.6 μ value
M = 1.17 RANGE 1.33 1.03

L	F	H
4.81 +/- 0.54	4.13 +/- 0.54	8.94 +/- 1.06

DIRECTIONAL ERRORS, ERANG, FOR AXIS IP. ERANG(1) MAKES ANGLE AWPJK WITH AXIS JP.
IP = 1 JP = 2 AWPJK = 144.4 ERANG 2.18 1.01
IP = 2 JP = 3 AWPJK = 69.6 ERANG 1.93 1.37
IP = 3 JP = 1 AWPJK = 139.6 ERANG 1.68 1.26

Appendices

Appendix C) AMS Pl6 Files (Un-normalised means)

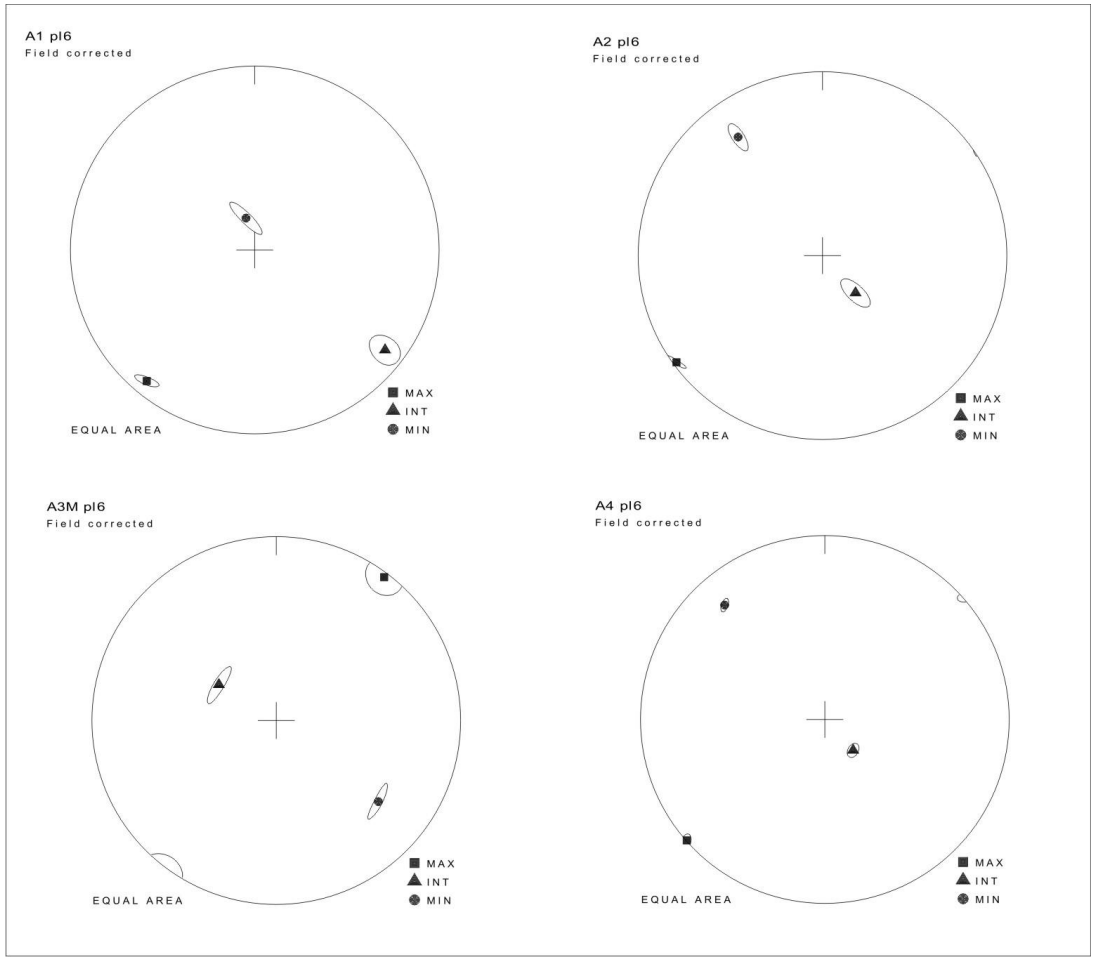

Appendices

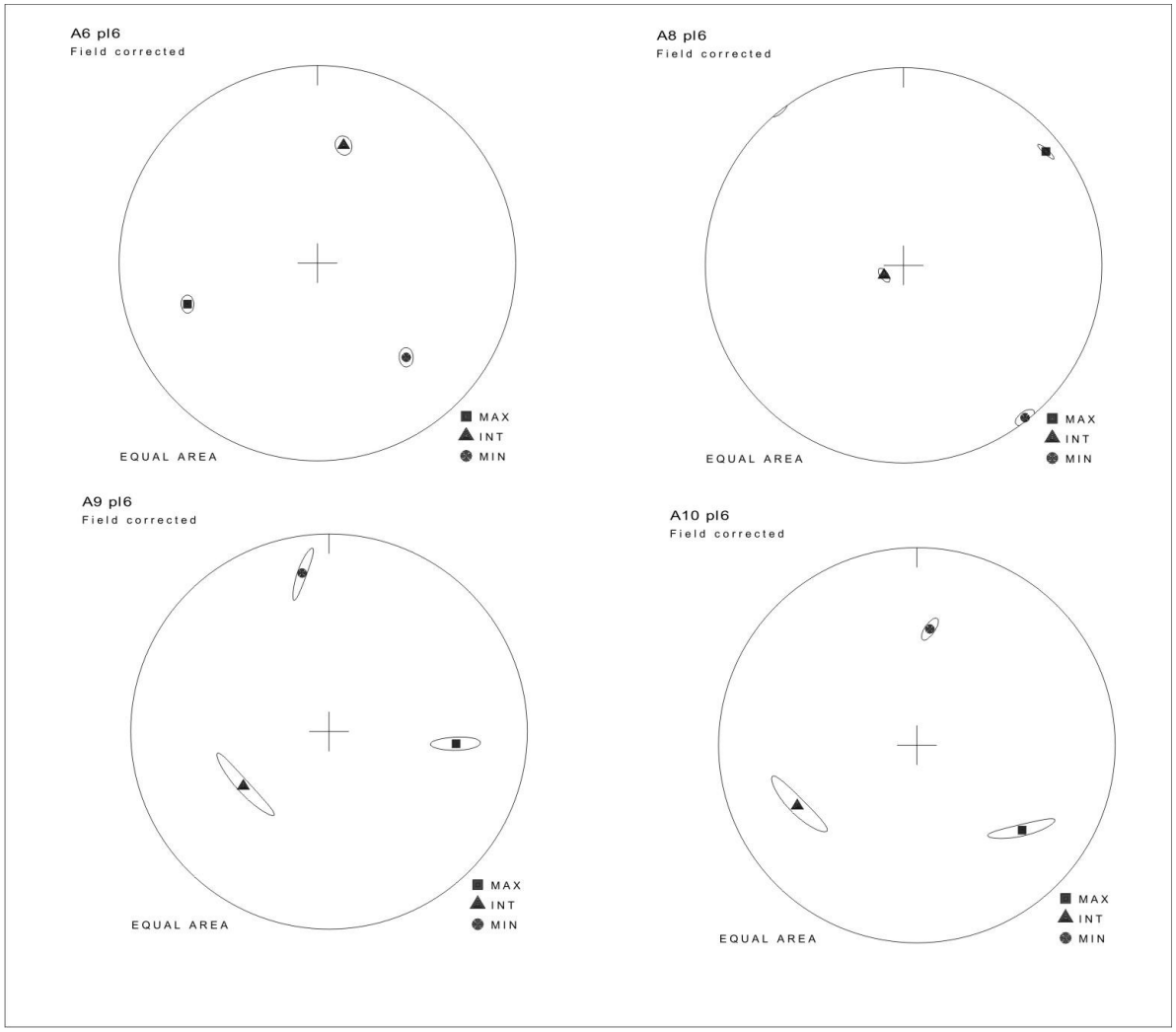
A6 pl6
Field corrected
EQUAL AREA
MAX
INT
MIN
A8 pl6
Field corrected
EQUAL AREA
MAX
INT
MIN
A9 pl6
Field corrected
EQUAL AREA
MAX
INT
MIN
A10 pl6
Field corrected
EQUAL AREA
MAX
INT
MIN

Appendices

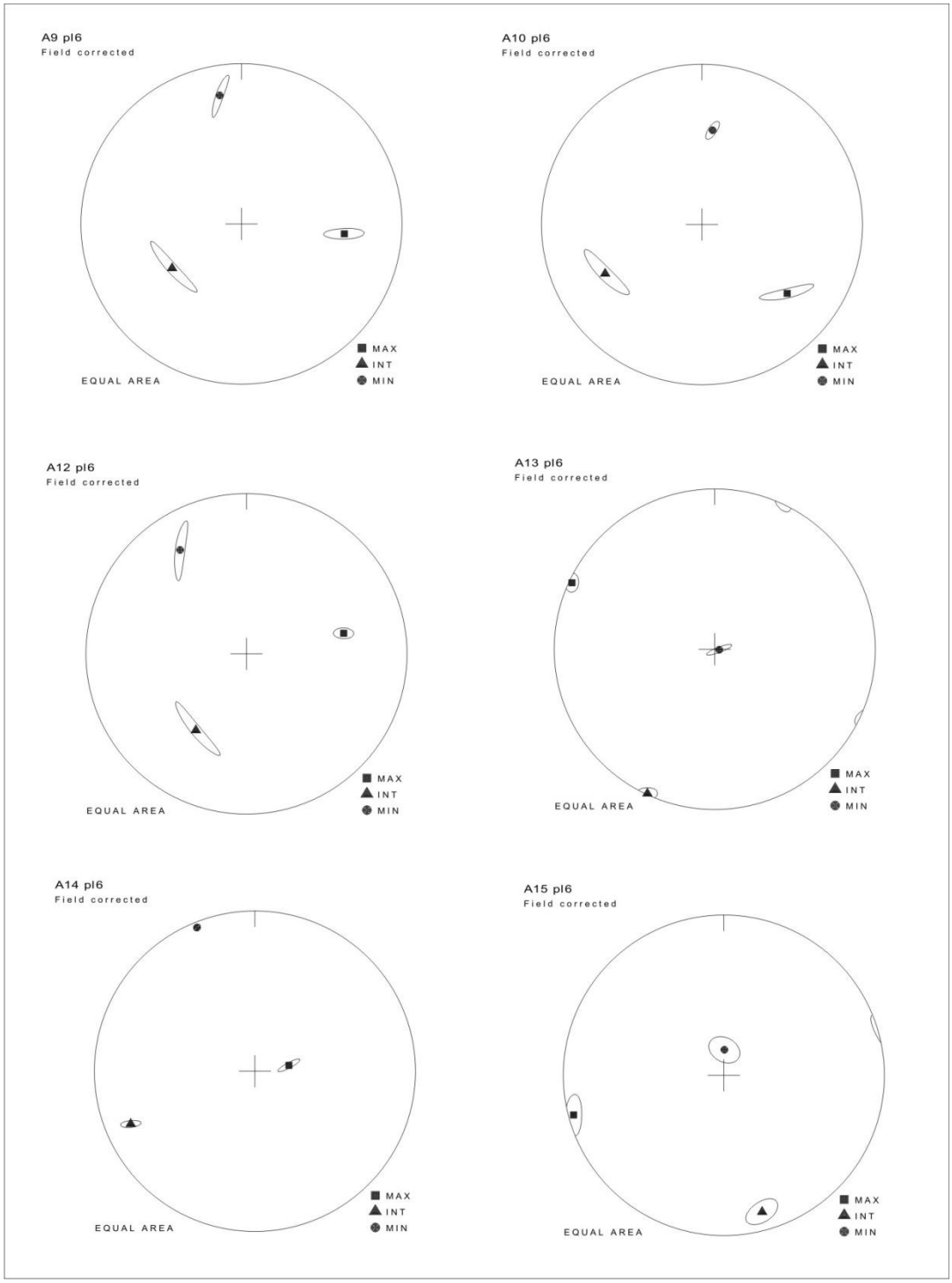
A9 pl6
Field corrected
EQUAL AREA
MAX
INT
MIN
A10 pl6
Field corrected
EQUAL AREA
MAX
INT
MIN
A12 pl6
Field corrected
EQUAL AREA
MAX
INT
MIN
A13 pl6
Field corrected
EQUAL AREA
MAX
INT
MIN
A14 pl6
Field corrected
EQUAL AREA
MAX
INT
MIN
A15 pl6
Field corrected
EQUAL AREA
MAX
INT
MIN

Appendices

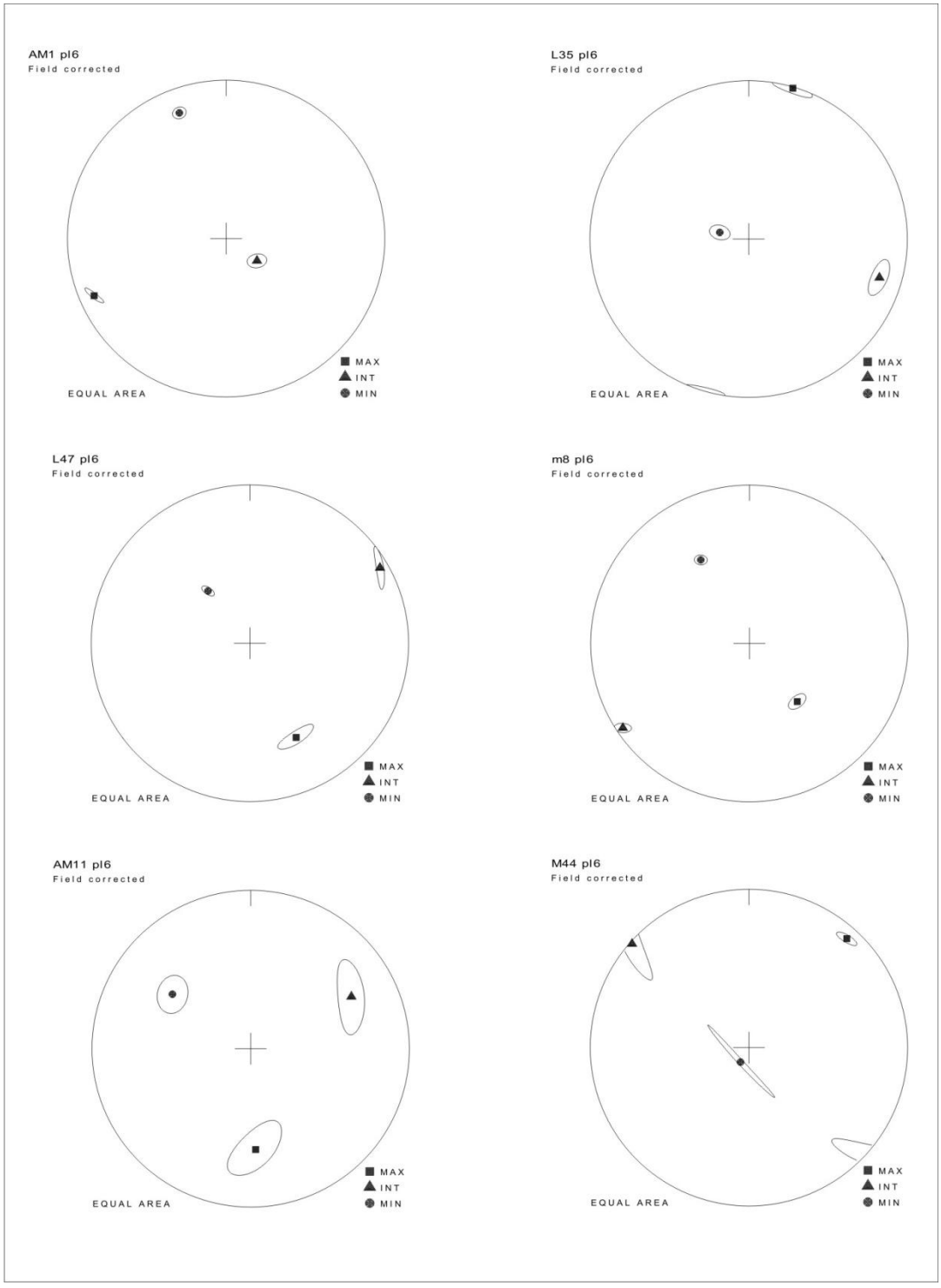
AM1 pl6
Field corrected
EQUAL AREA
MAX
INT
MIN
L35 pl6
Field corrected
EQUAL AREA
MAX
INT
MIN
L47 pl6
Field corrected
EQUAL AREA
MAX
INT
MIN
m8 pl6
Field corrected
EQUAL AREA
MAX
INT
MIN
AM11 pl6
Field corrected
EQUAL AREA
MAX
INT
MIN
M44 pl6
Field corrected
EQUAL AREA
MAX
INT
MIN

Appendices

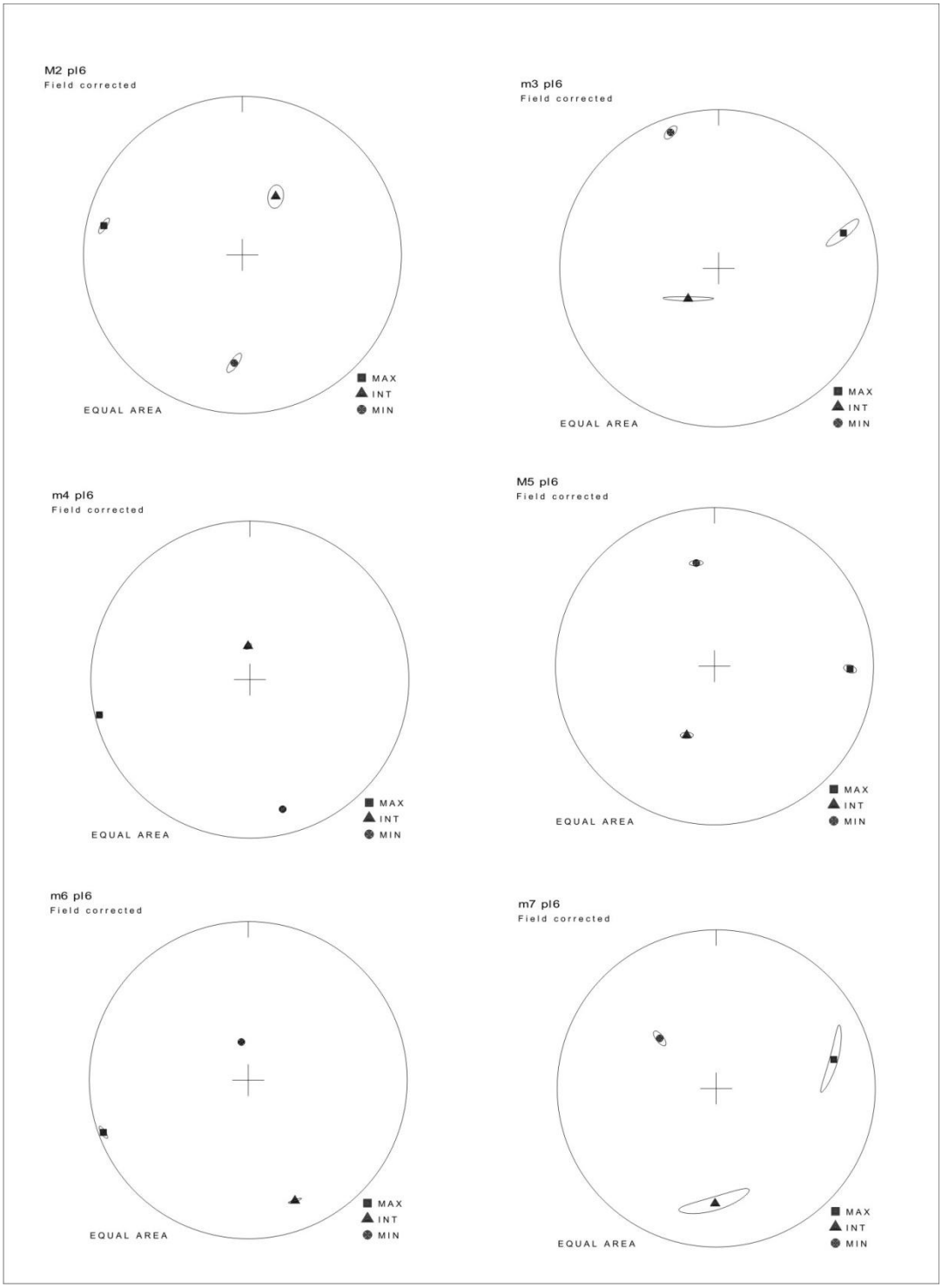
M2 pl6
Field corrected
EQUAL AREA
MAX
INT
MIN
m3 pl6
Field corrected
EQUAL AREA
MAX
INT
MIN
m4 pl6
Field corrected
EQUAL AREA
MAX
INT
MIN
M5 pl6
Field corrected
EQUAL AREA
MAX
INT
MIN
m6 pl6
Field corrected
EQUAL AREA
MAX
INT
MIN
m7 pl6
Field corrected
EQUAL AREA
MAX
INT
MIN

Appendix D : Strain Analysis

Code for Mathematica (Mulchrone et al., 2013):

```
<< "C:\\Users\\Chloe\\Documents\\Thesis Chapters 2013\\chapter 6 strain
   analysis\\Strain Analysis 2014\\A1 test\\Strain Analysis Notebook.m"
SetDirectory["C:\\Users\\Chloe\\Documents\\Thesis Chapters
   2013\\chapter 6 strain analysis\\Strain Analysis 2014\\A1 test"]
Import["L47 Coosfada F1(1) 200dpi trace.bmp"]
```

```
C:\Users\Chloe\Documents\Thesis Chapters
  2013\chapter 6 strain analysis\Strain Analysis 2014\A1 test
```

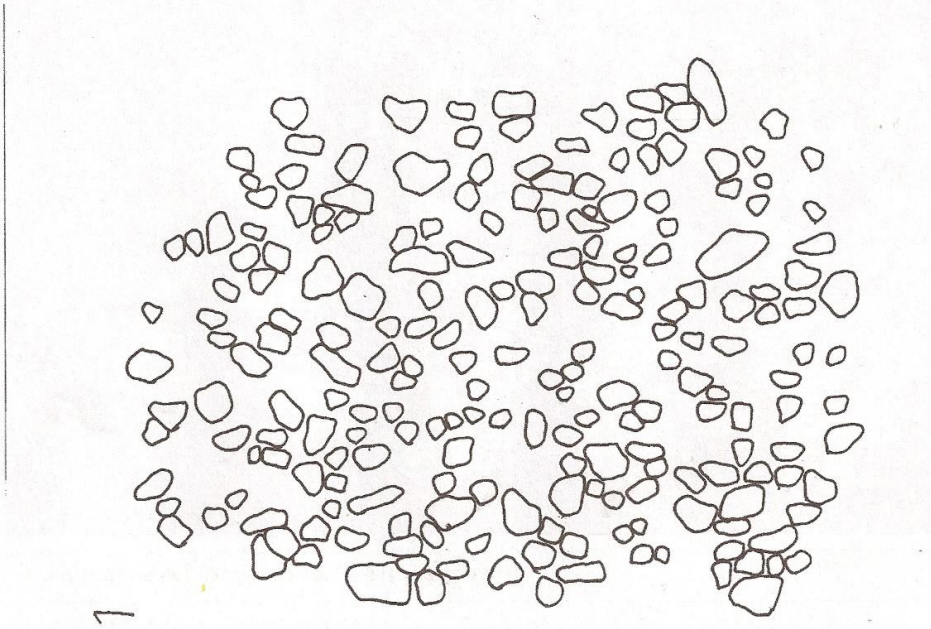

Appendices


```
res1 = AnalyzeImage["L47 Coosfada F1(1) 200dpi trace.bmp"]
```

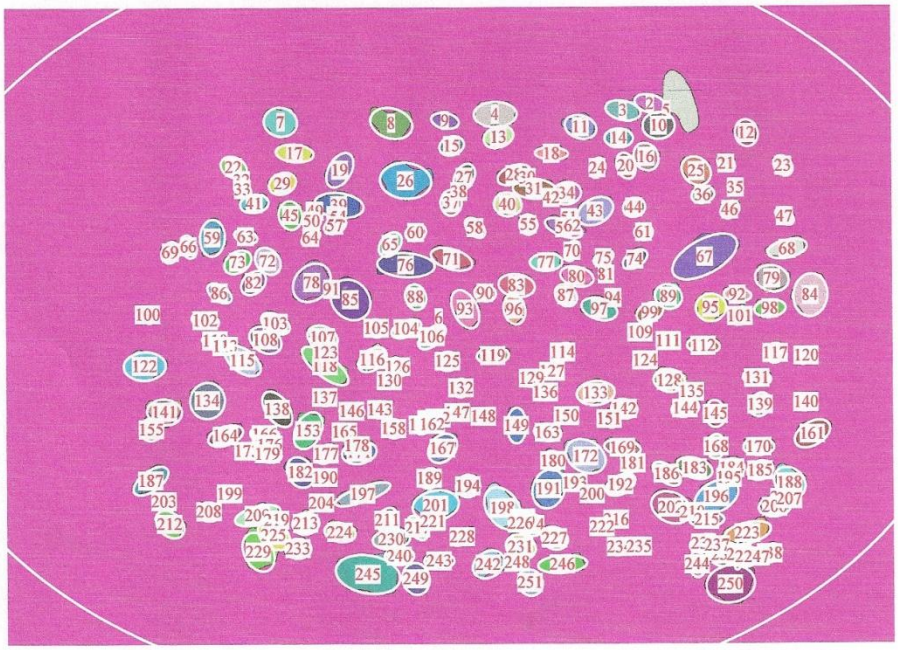

A very large output was generated. Here is a sample of it:

```
{{2 → {30.7419, {1702.39, 1425.14}, 84.0293, 47.1464, 2.87064, 2},
  3 → {34.0202, {1630.81, 1407.75}, 93.8944, 50.9791, 2.92417, 3}, <<246>>,
  250 → {55.0887, {1906.45, 156.443}, 128.791, 97.7237, -2.97756, 250}, 251 →
    {33.4969, {1377.92, 162.668}, 71.415, 63.8305, -1.02437, 251}}, {<<1>>}}
```

Show Less | Show More | Show Full Output | Set Size Limit...

Appendices


```
res2 = RefineImageData[res1, {239, 226, 219, 176, 162, 6, 91, 42, 62,
    54, 113, 38, 49, 210, 237, 178, 160, 159, 195, 247, 175, 174, 53, 48,
    32, 5, 30, 247, 220, 221, 218, 52, 157, 207, 205, 51, 248, 123, 156}];
```

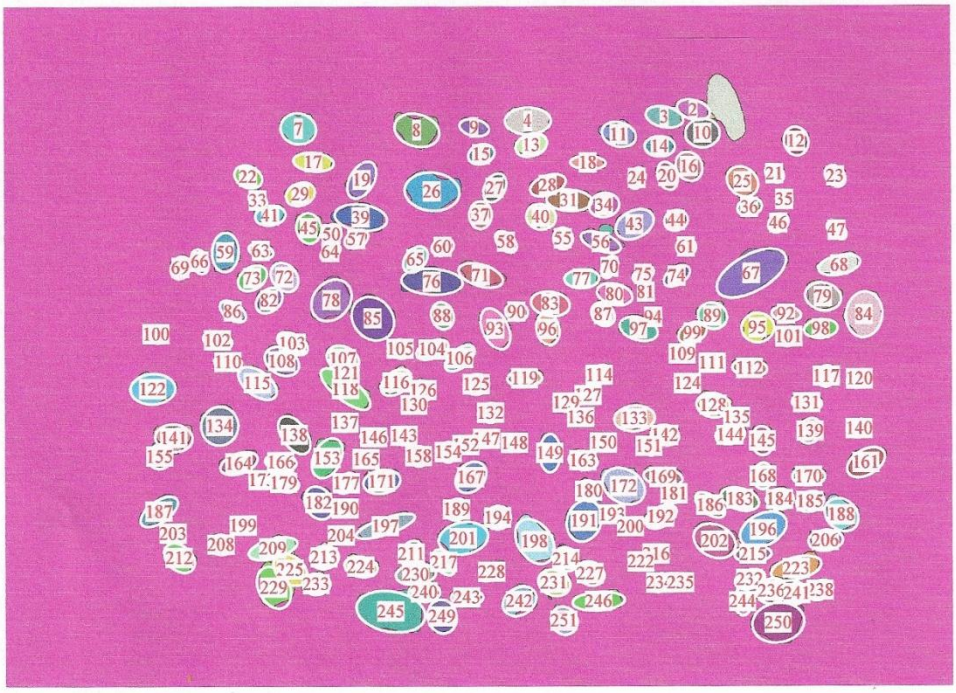

```
mres = ExtractData[res2];
nnres = AnalyseDataPolar[mres[[1]], 1000]
nnres[[1]] / nnres[[2]]
```

```
{1.10475, 0.764913, 174.044}
```

```
1.44428
```

```
CreateNNPlotPolar[mres[[1]], nnres]
```

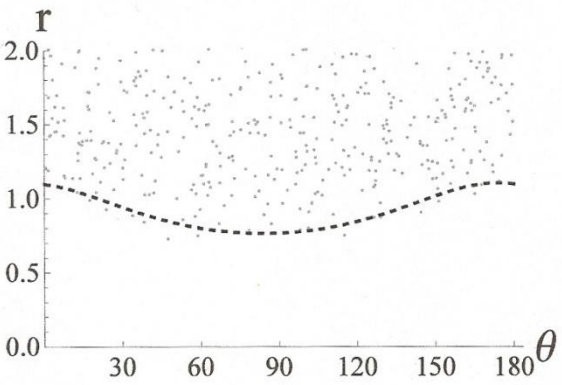

Appendices


```
CreateNNPlotCartesian[mres[[1]], nnres]
```

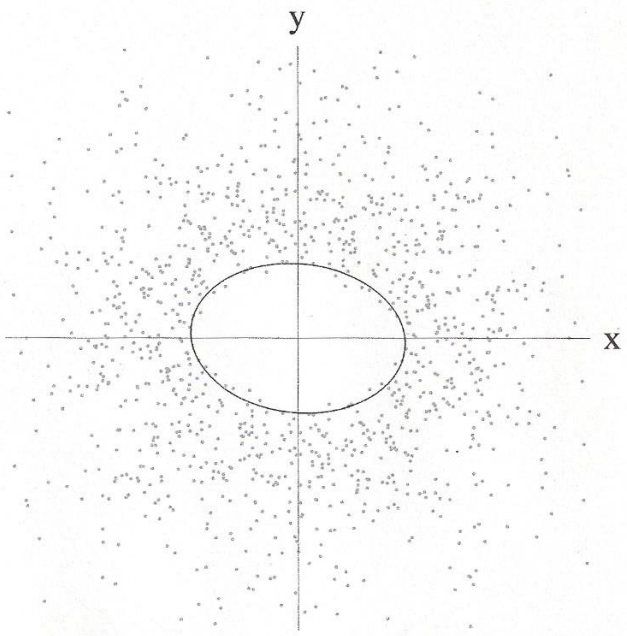


```
bres = Quiet[BootStrapPolar[mres[[1]], 1000, 1000]];
CreateBootStrapPlot[bres]
```

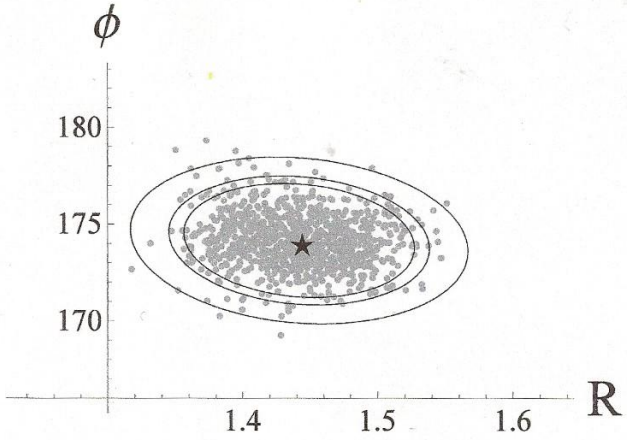


```
MRL[mres[[2]]]
{1.23221, 0.888995}
```

Appendices


```
bsMRL = BootStrapMRL[mres[[2]], 1000];
CreateBootStrapPlot[bsMRL]
```

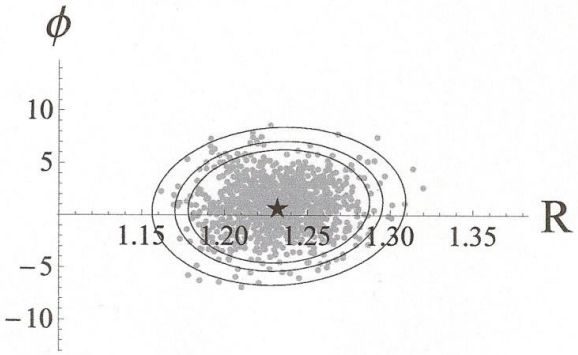

.....

.....

Appendices

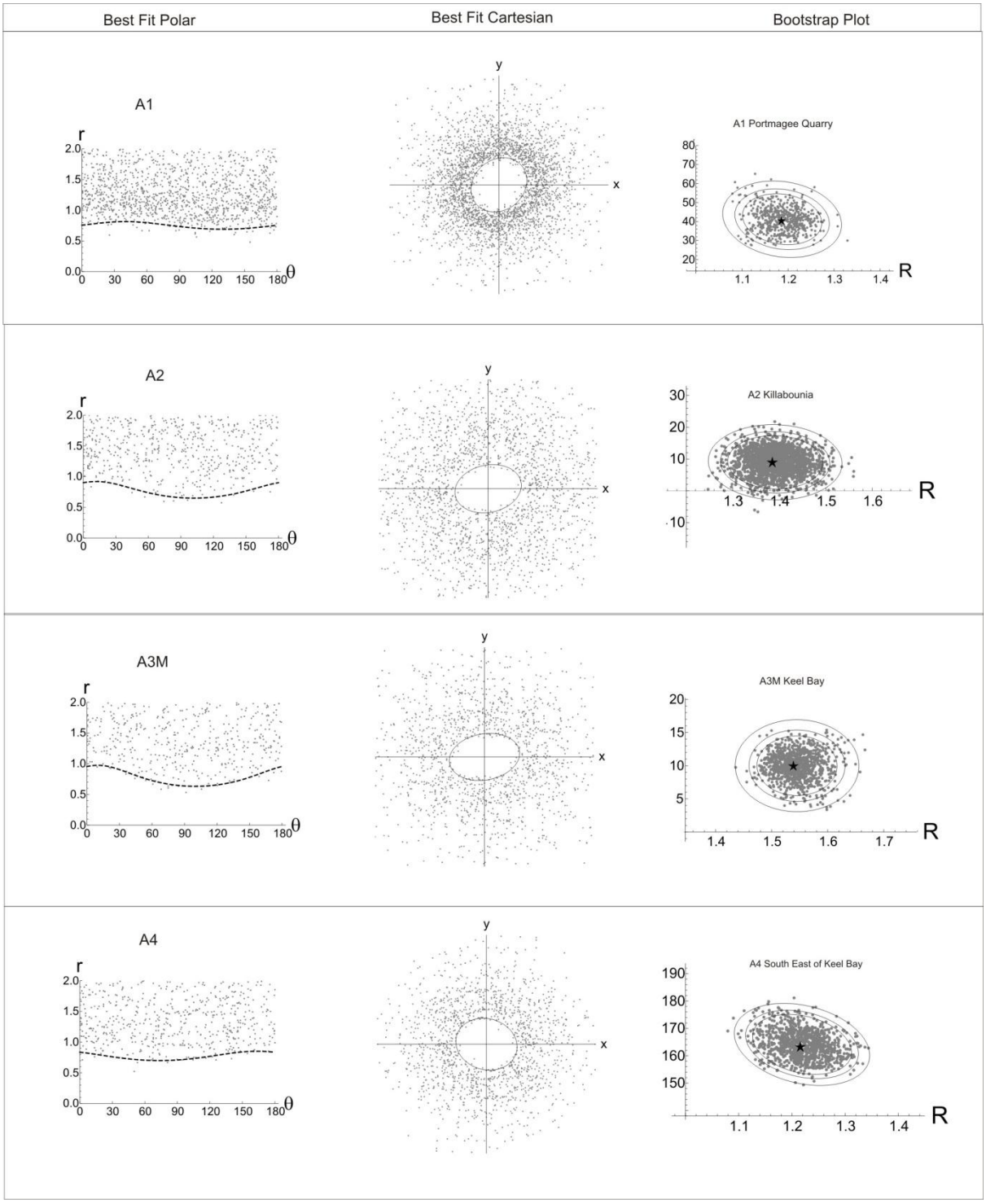

DTNNM best fit polar and cartesian plots and confidence limits at 90, 95 and 99% for locations –A1, A2, A3M, A4.

Appendices

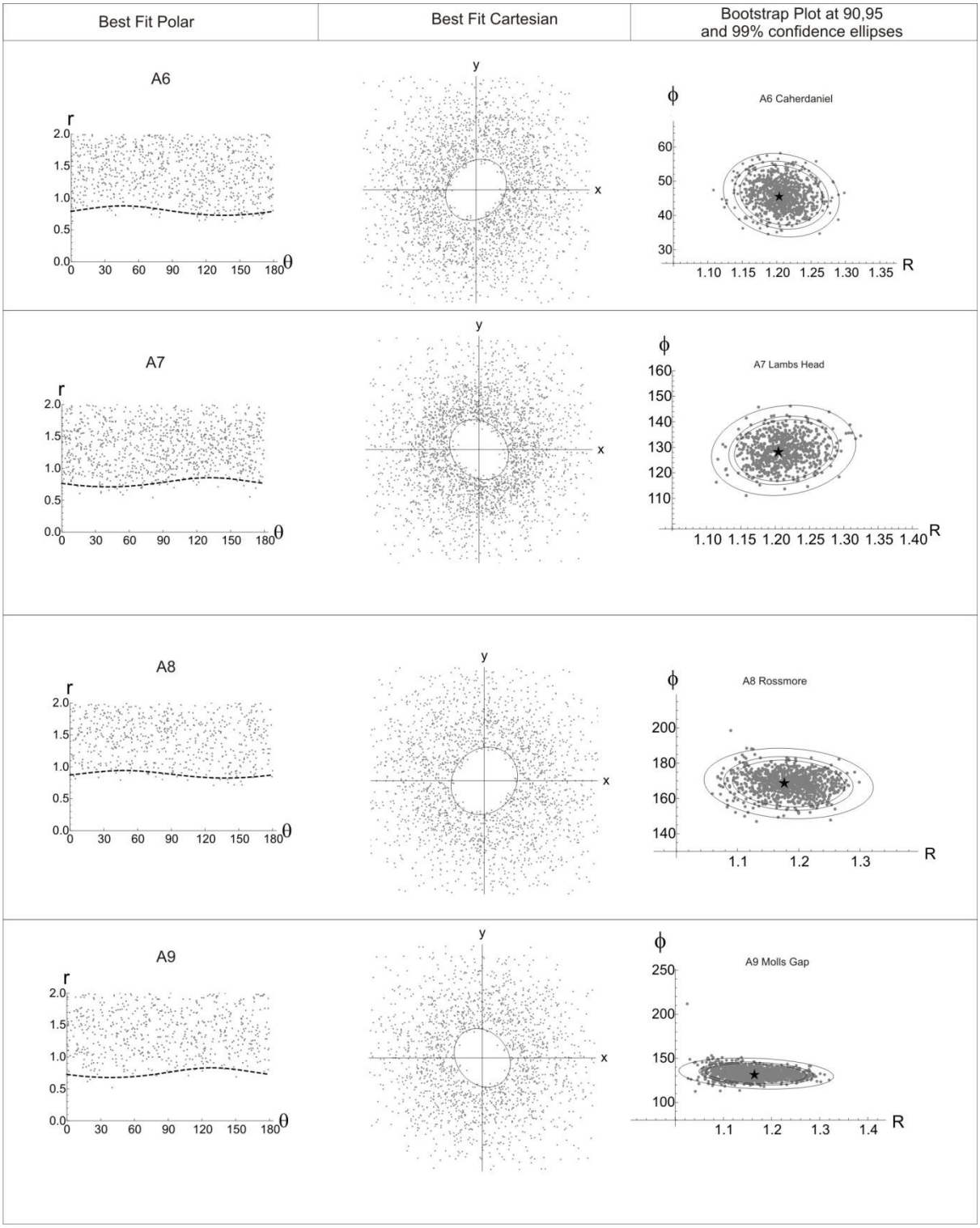

DTNNM best fit polar and cartesian plots and confidence limits at 90, 95 and 99% for locations –A6, A7, A8, A9

Appendices

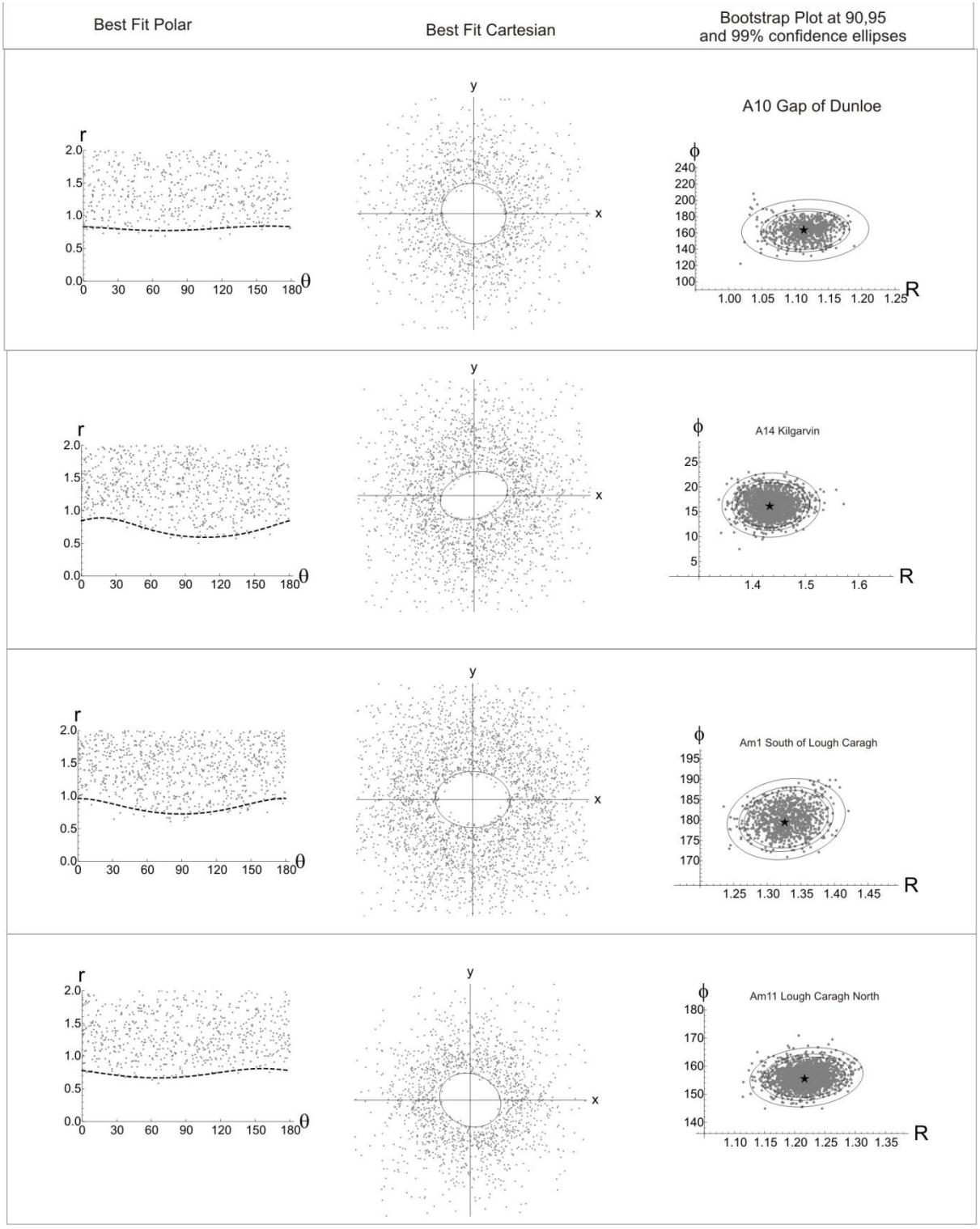

DTNNM best fit polar and cartesian plots and confidence limits at 90, 95 and 99% for locations A10,A14, AM1 and AM11.

Appendices

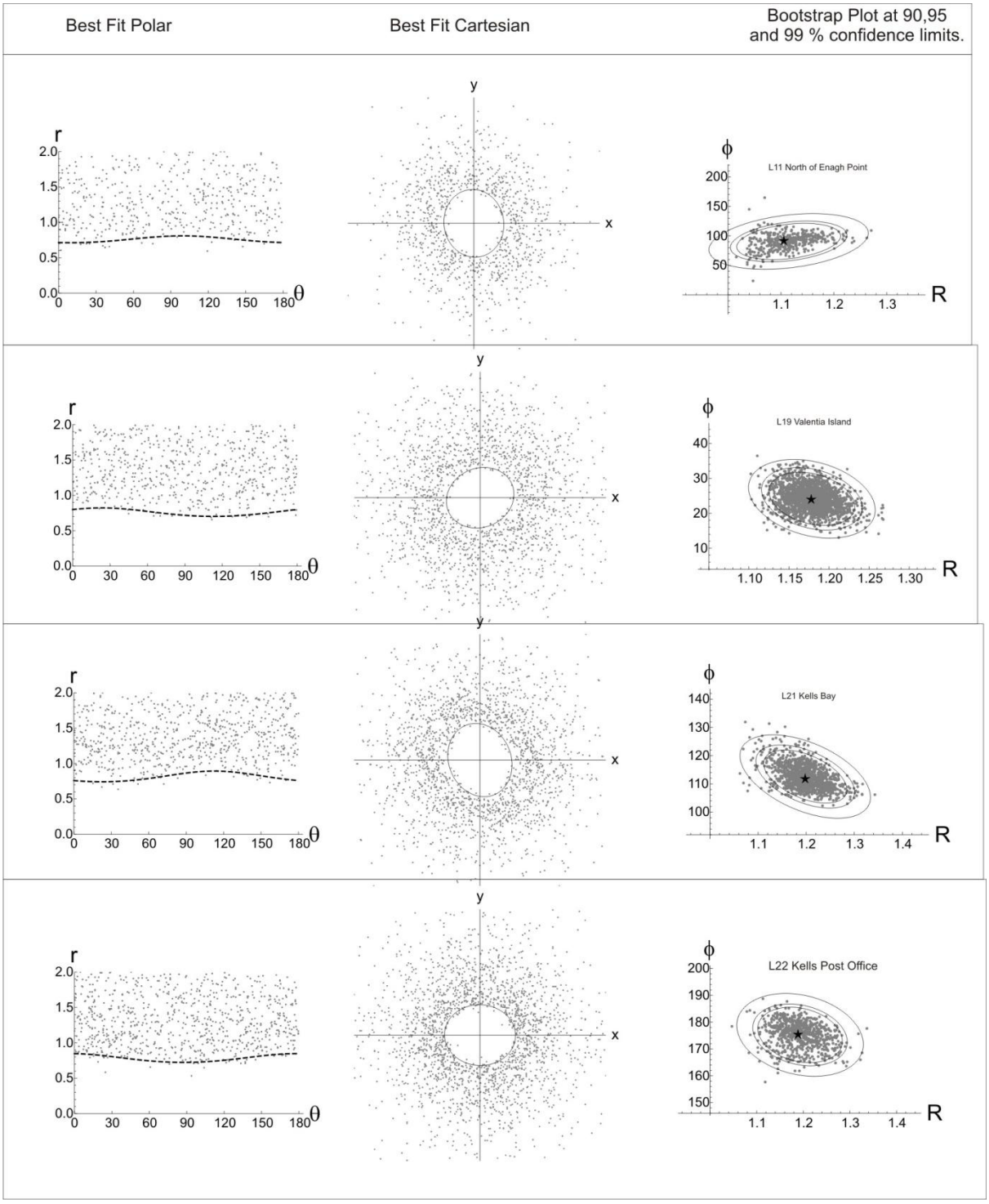

DTNNM best fit polar and cartesian plots and confidence limits at 90, 95 and 99% for locations L11, L19, L21, L22

Appendices

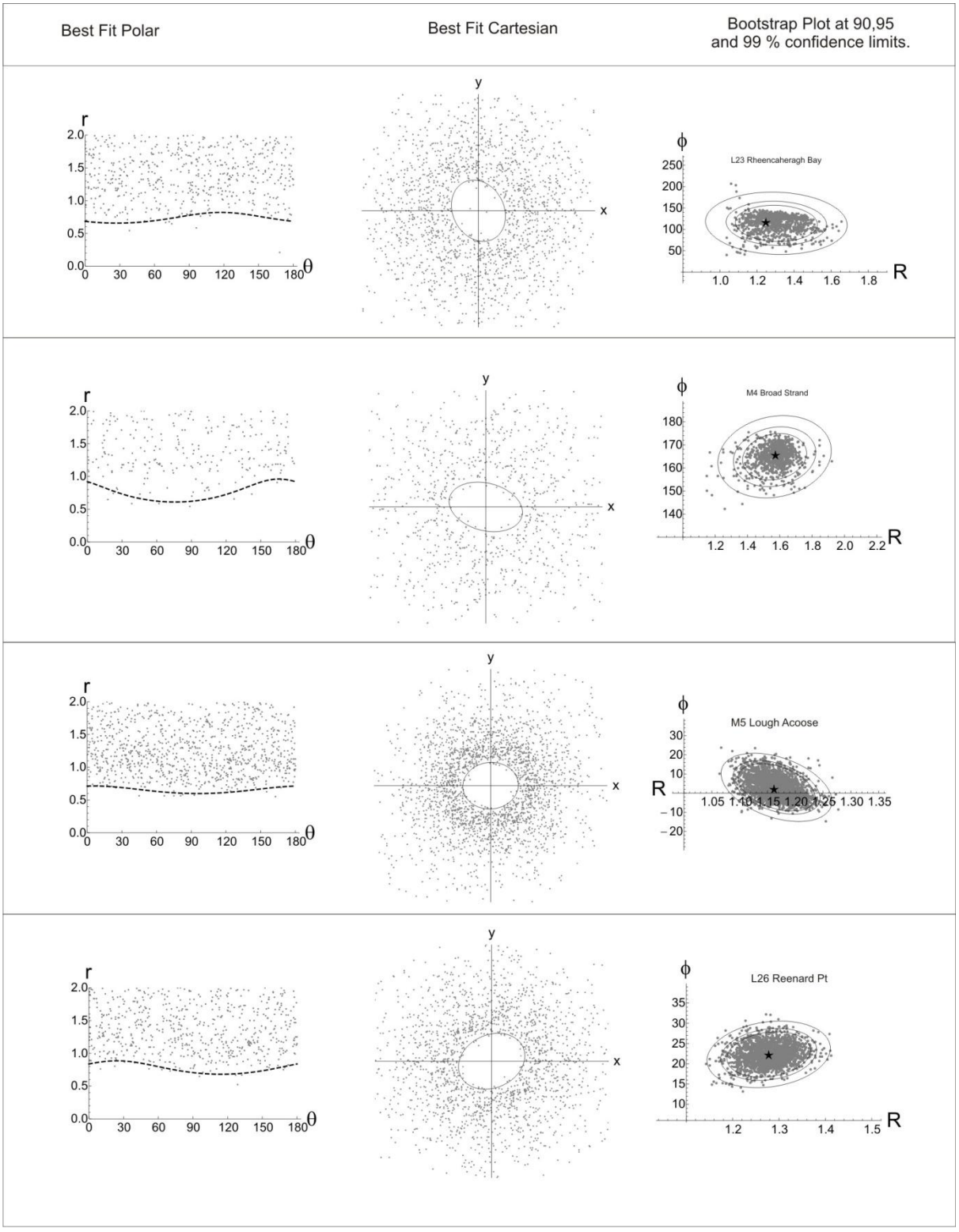

DTNNM best fit polar and cartesian plots and confidence limits at 90, 95 and 99% for locations L23,M4, M5, L26.

Appendices

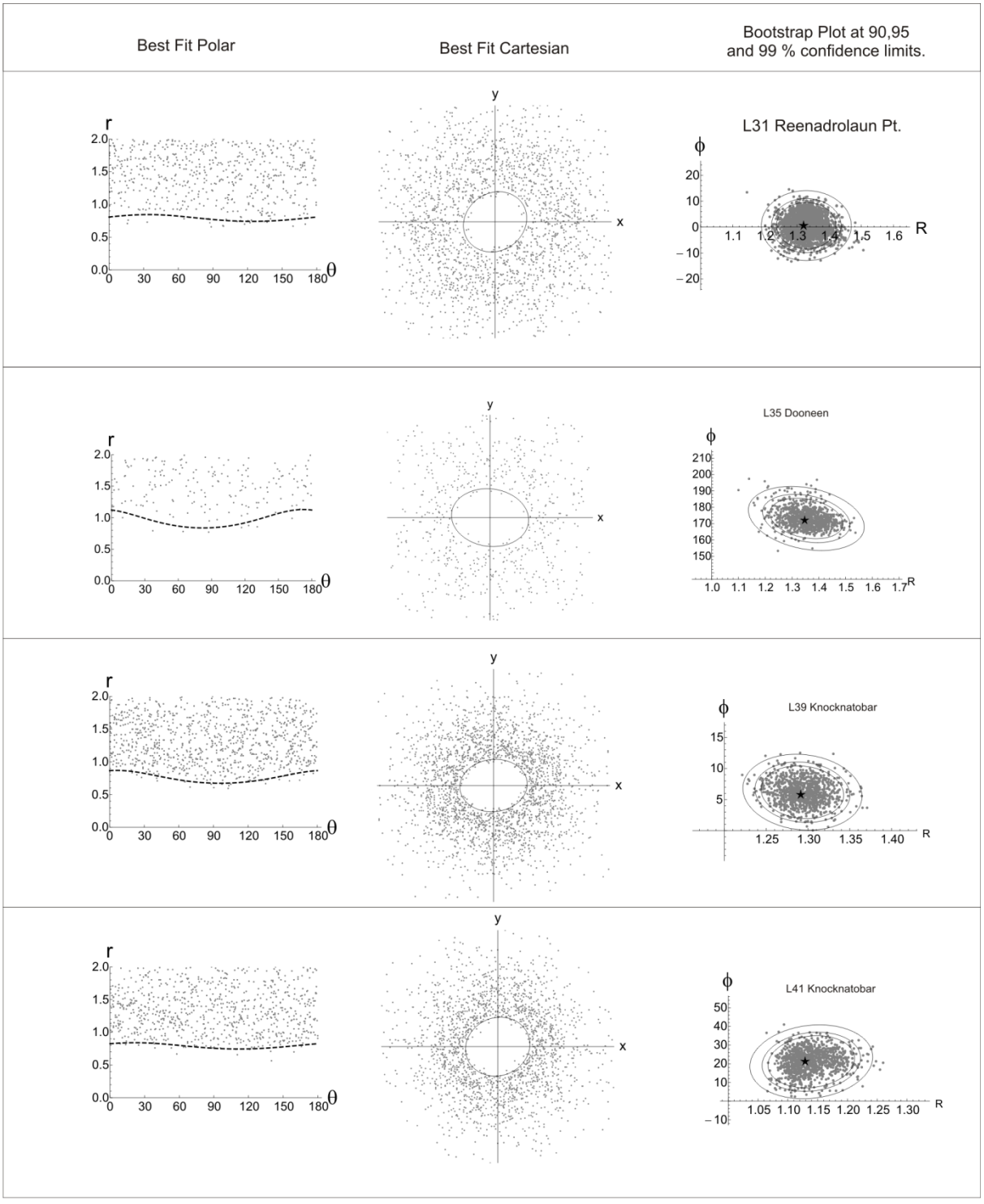

DTNNM best fit polar and cartesian plots and confidence limits at 90, 95 and 99% for locations L31, L35, L39, L41.

Appendices

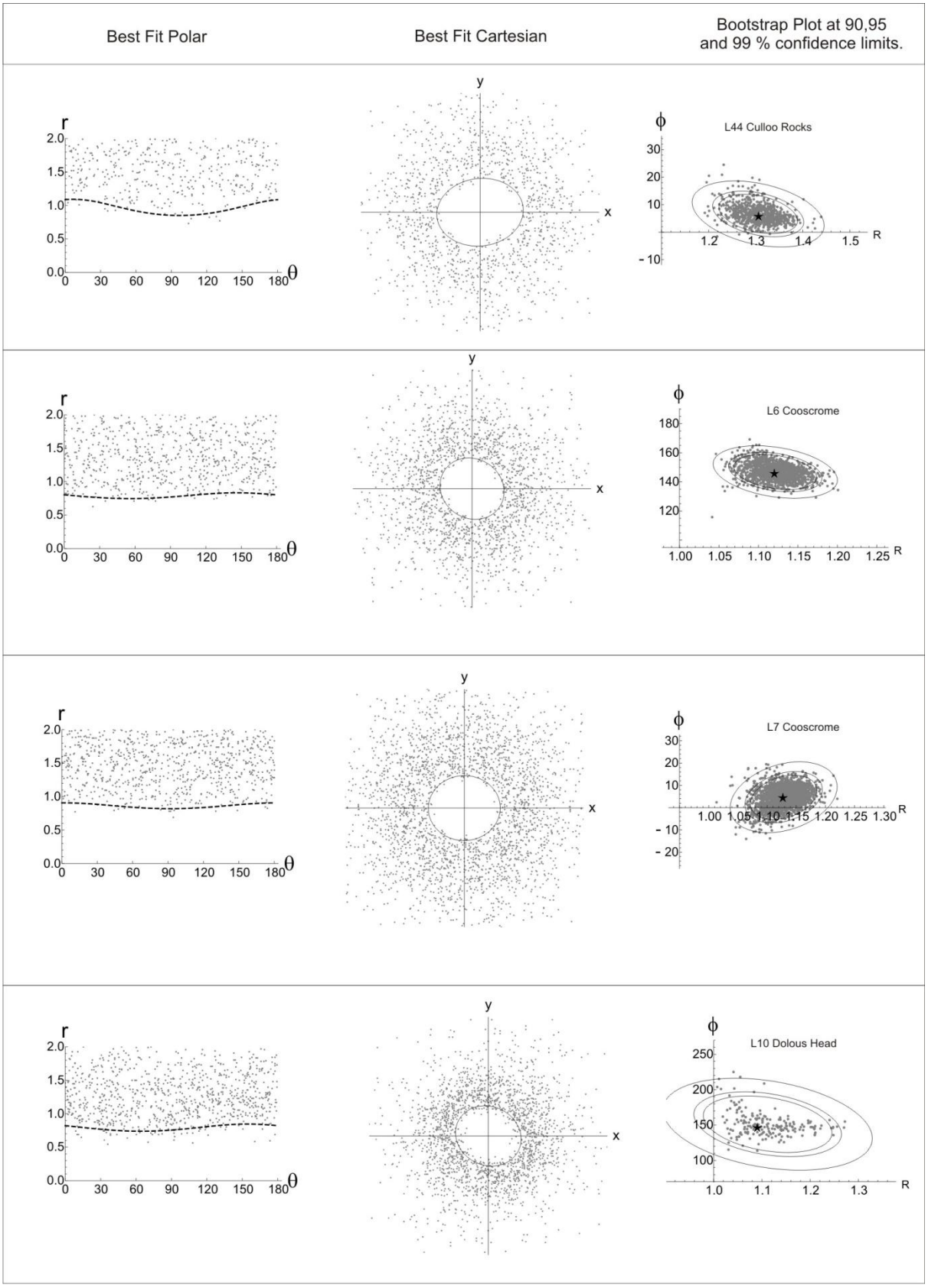

DTNNM best fit polar and cartesian plots and confidence limits at 90, 95 and 99% for locations L44, L6, L7 & L10.

Appendices

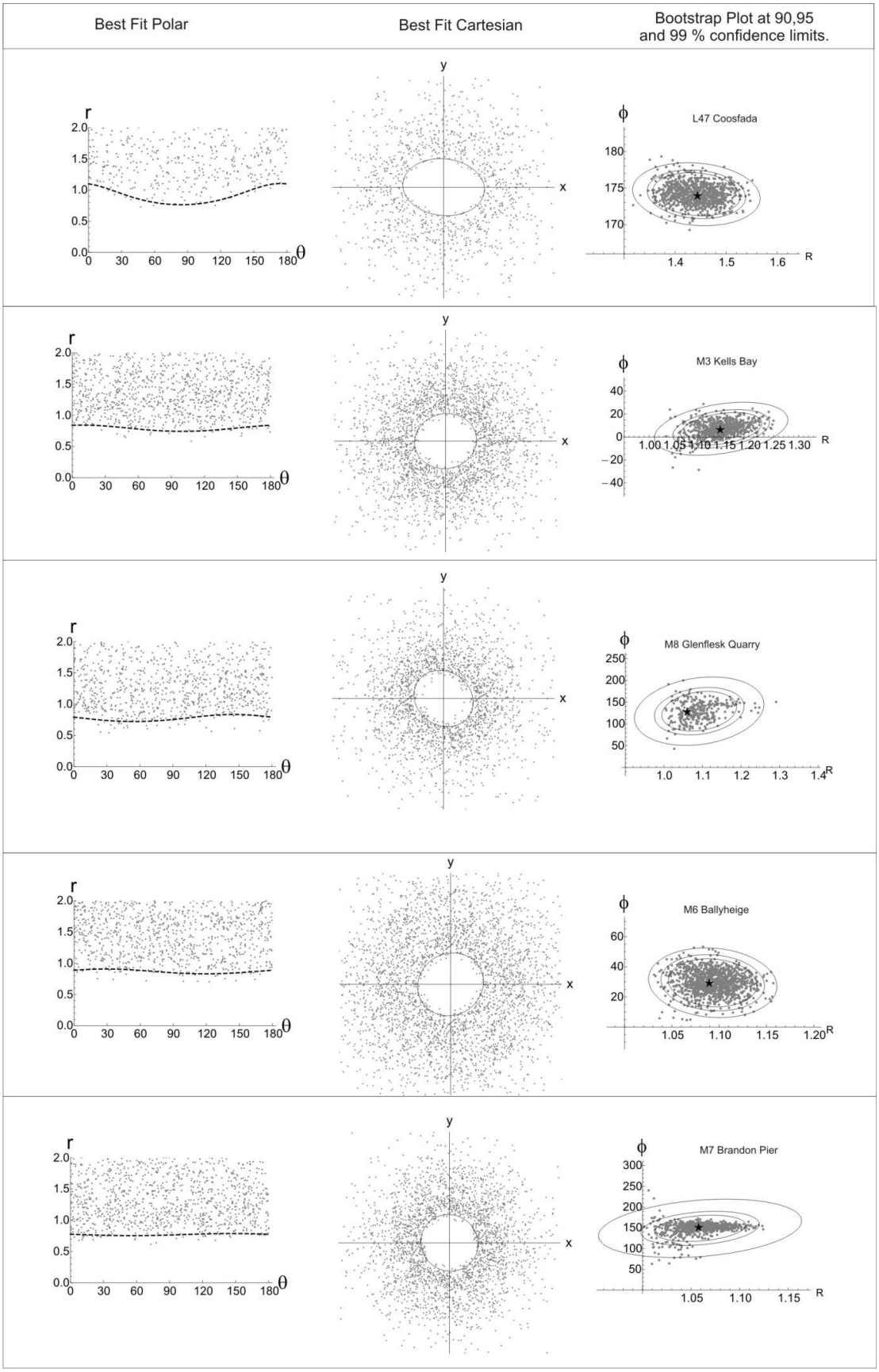

DTNNM best fit polar and cartesian plots and confidence limits at 90, 95 and 99% for locations L47, M3, M6, M6, M7

Appendices

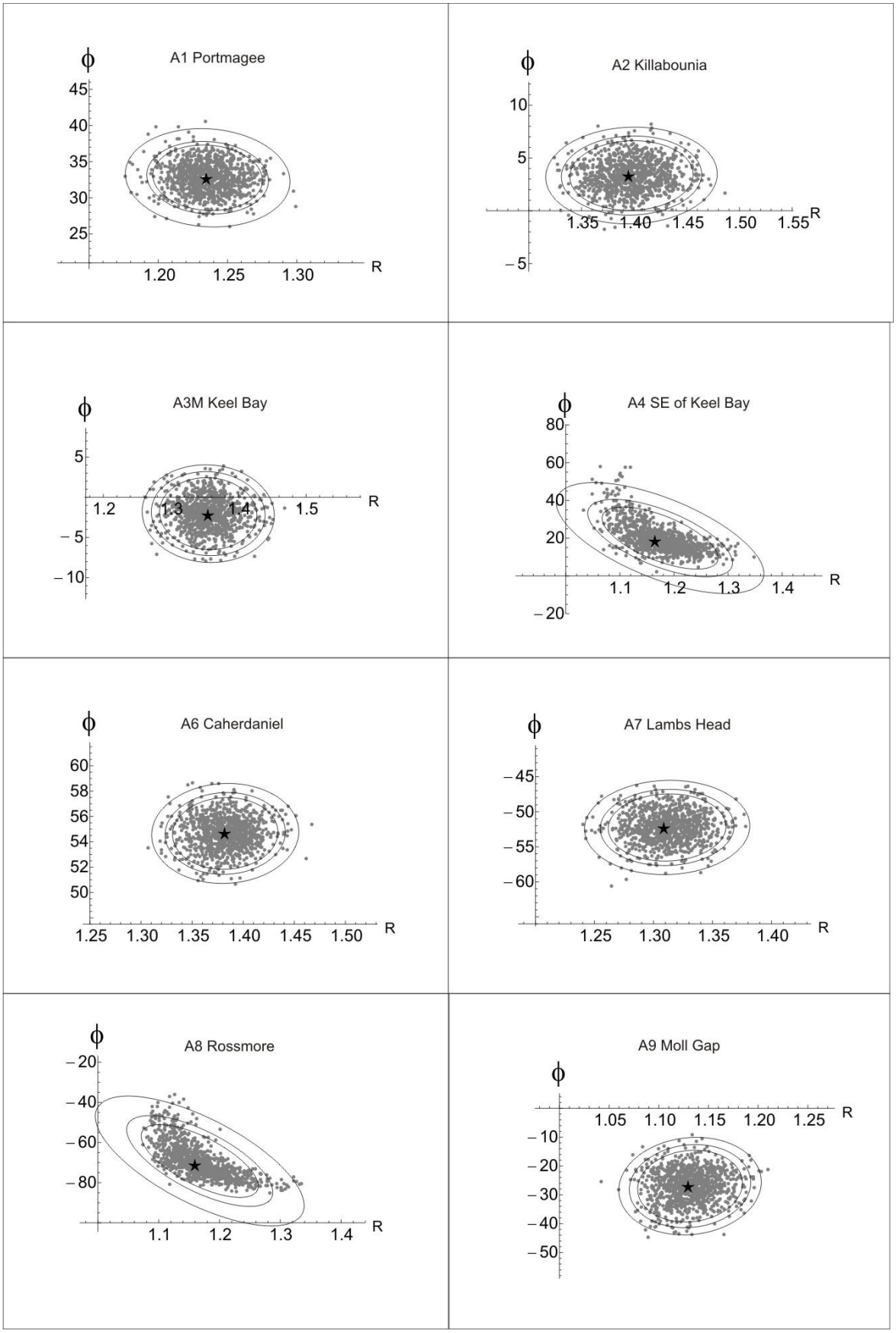

MRL plots showing confidence limits at 90, 95 and 99% for locations A1, A2, A3M, A4, A6, A7, A8, A9.

Appendices

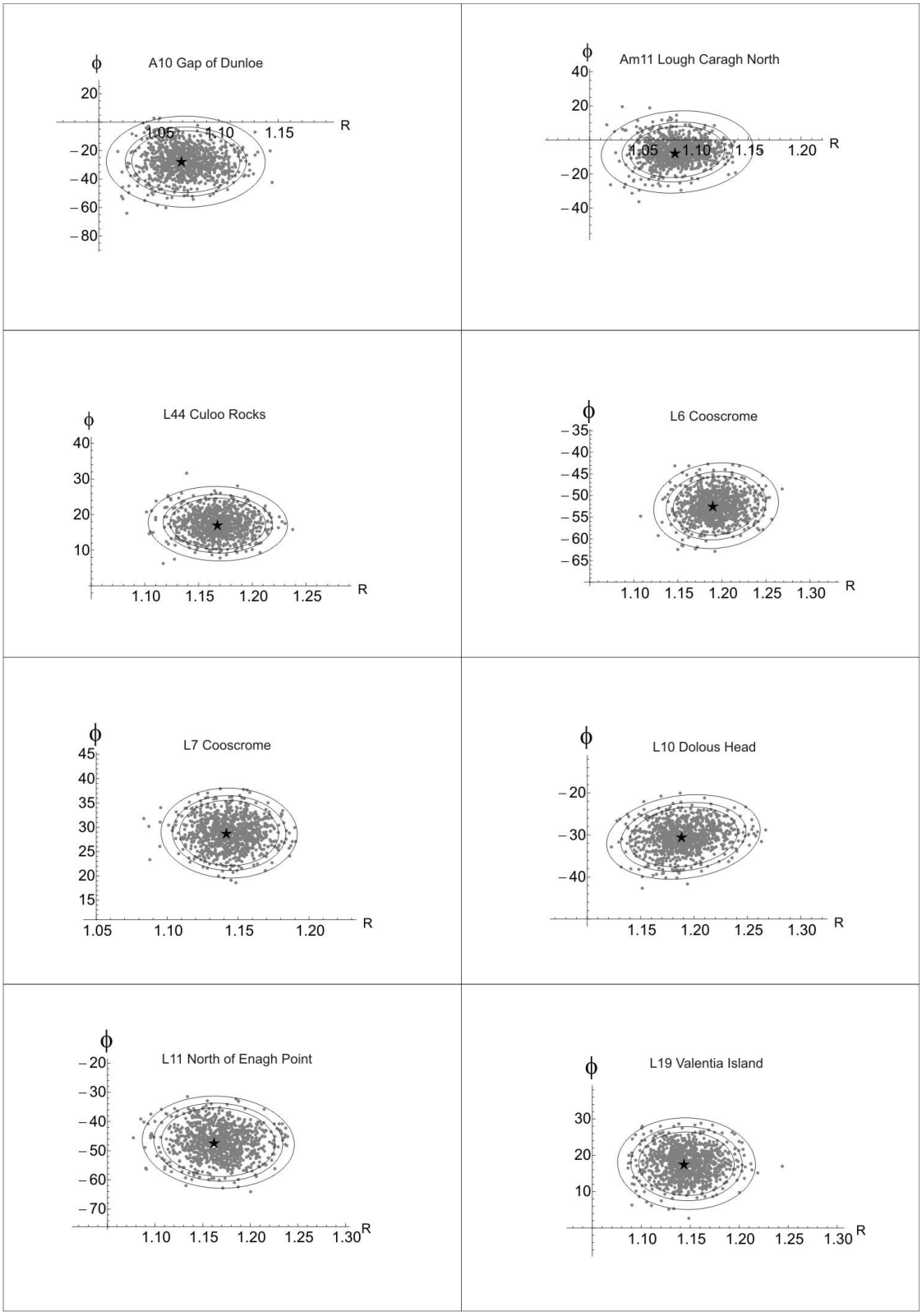

MRL plots showing confidence limits at 90, 95 and 99% for locations in the Transition Zone- A10, AM11, L44, L6,L7, L10, L11, L19**.**

Appendices

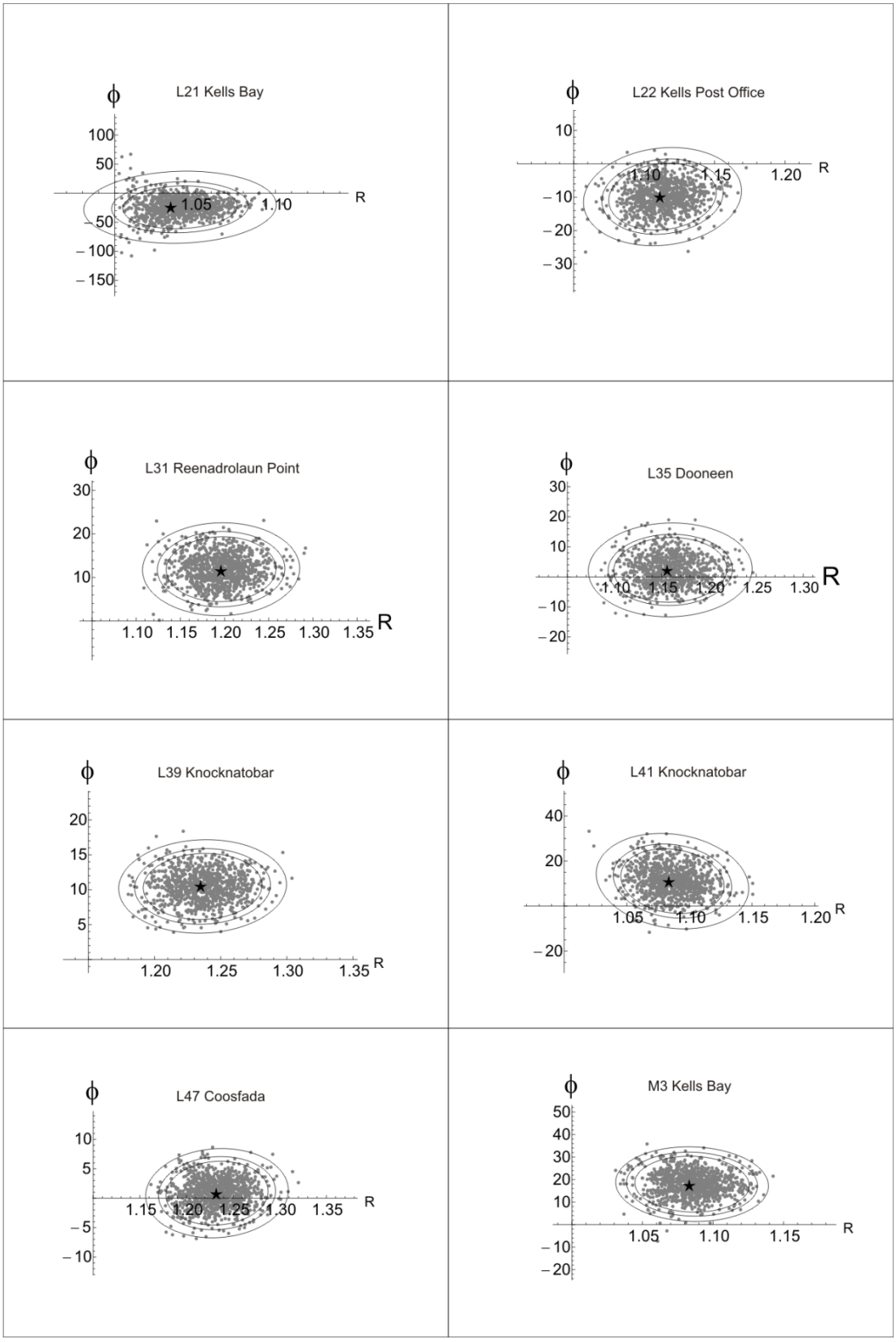

MRL plots showing confidence limits at 90, 95 and 99% for locations in the Transition Zone- L21, L22, L31, L35, L39, L41, L47, M3.

Appendices

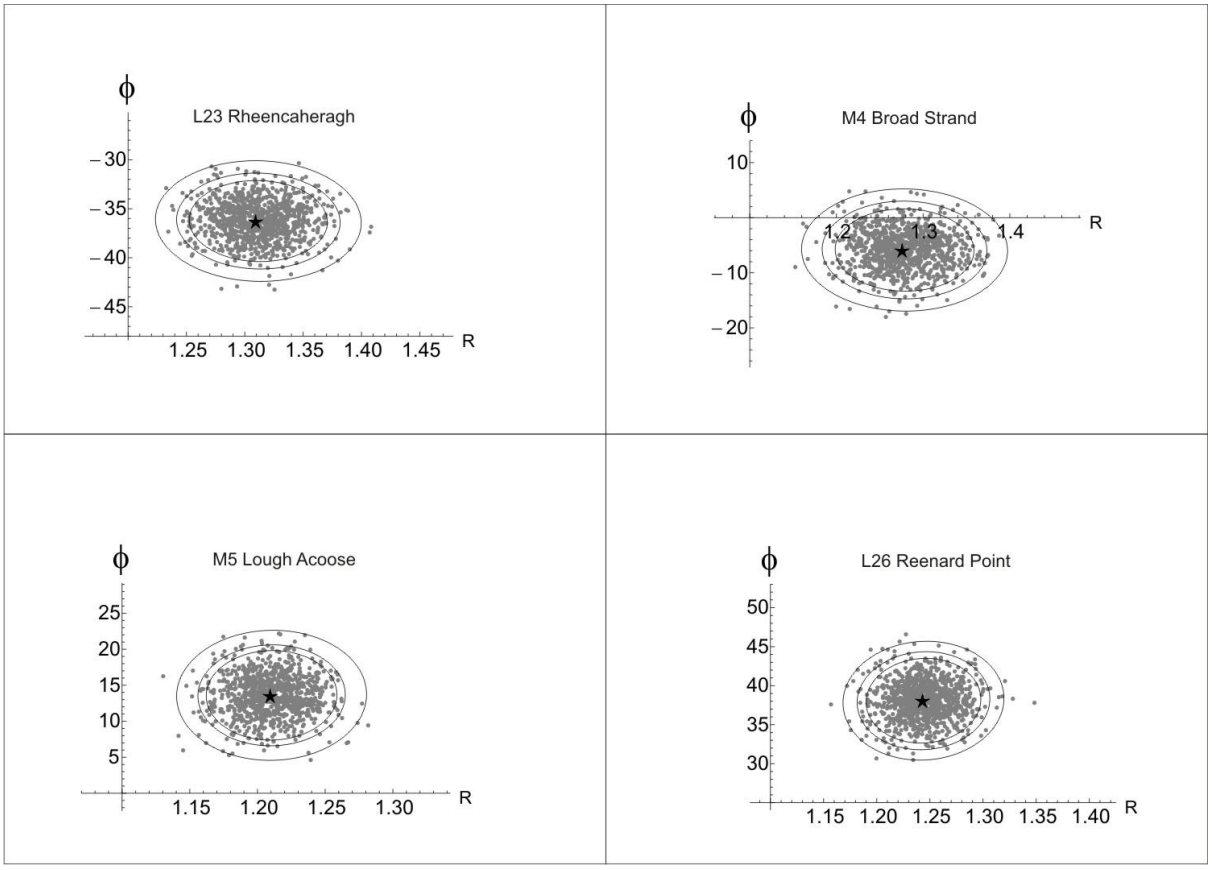

MRL plots showing confidence limits at 90, 95 and 99% for locations in the Intabasinal Zone –L23, M4, M5, L26.

Apendix E: Thermomagnetics

The Variaiton of Magnetic Susceptibility with Temperature.

i) Sample Preparation.

For each sample, approximately one half of a standard AMS core was crushed into a powder using the rock crusher. The powder was sieved using a 250 micron sieve in order to ensure all particle sizes are 250 microns or less. The sample were powdered to a very fine scale and allowed to dry in order to allow the sample to be placed into a thin test tube and prevent clumping and scraping on the thermometer.

ii) Apparatus.

The KLY-3S Kappabridge pick up unit is connected to the CS-3 Temperature Control unit and the spinning specimen magnetic susceptibility Anisotropy Meter. The CS-3 Temperature Control Unit is used for magnetic susceptibility temperature variations measurements. Distilled water is pumped into and out of the KLY-3 Kappabridge pick up unit in order to cool it. The Dell latitude XP run on Ms-Dos is plugged into the KLY 3 anisotropy meter. The KLY-3S Kappabridge measures the susceptibility from approximately 28 ° C to approximately 660° C and cooling back to room temperature. There are approximatley 540 to 670 readings taken for each sample. See Cur files on disc.

The samples are crushed but not too fine to avoid the creation of single domain particles.

iii) Measuring-Method.

1). Switch off everything first.

2). Ensure that the test tube and the thermometer is clean and not damp -use some Gauze.

3). Fill up the test tube approximately 2-3 cm high with powdered sample.

4). Allow the powder to flow sideways by gently shaking the test tube subhorizontally. This ensures space for the thermometer to be placed in the test tube and reach the end of the test tube. Tip the test tube back to the vertical position.

5). Place the thermometer into the test tube and place the cover over them both to secure them together.

6). Place the test tube with powder and thermometer securely into the temperature variation holder

(At the top of the test tube there is a small inlet which can be used to pump argon gas into in order to prevent oxidation of the sediment. In this case however argon was unavailable for use. Observing the oxidation of the specimen can tell more about the relative content of magnetite due to the oxidation of magnetite to maghaemite.)

7). Switch on the KLY-3 anisotropy meter-This will switch on the CS-3 temperature control unit and the Kly-3 Pick up unit also.

8). Switch on the Dell.

9) Running the Programme SUSTE.

Type:

cd kly3\suste

suste

(Programme starts up Agico Suste 2000)

10). Cur files produced are saved on the disc. A correction for the magnetic susceptibility of the holder is made (magnetic susceptibility of the holder = **-140×10^{-6}**).

Results for the Anisotropy of Magnetic Susceptibility across the northern margin of the Munster Basin, South West Ireland.

Carboniferous
- Limestone
- Ballyheige (ORS)
- Ballinskelligs
- Lough Acoose
- St Finans
- Valentia Slate Conglomerates

Upper Devonian / Middle Devonian — Iveragh Group — Sandstone

Devonian
- Upper — Slieve Mish group
- Middle — Caherbla group
- Lower — Dingle group

Sandstone & Conglomerates

Silurian
- Siltstone & Lst

Ordovician
- Siltstone & Mudstone

Igneous
- Dolerite

CF Coomnacronia Fault
Anticline
Syncline
Proposed Basin Margin

Geological Map based on
Geology of Dingle Bay Sheet 21, 20 & 24
Scale 1:100,000
Pracht(1995,1997,2001)

Foreland Zone:

Low deformation.

Bedding controlled AMS Fabrics/Primary sedimentary Fabrics.

Characterised by K_{min} axes // to the pole to S0
No visible tectonic fabric recorded by AMS ellipsoids.

M7,M6 & A15

Oblate AMS ellipsoids.

- S0: Pole to bedding (Hand sample reading)
- S1: Pole to Cleavage (Hand Sample or local reading)
- K1: maximum susceptibility axes
- K2: intermediate susceptibility axes
- K3: minimum susceptibility axes

K1>K2>K3

Oblate magnetic fabric where: $0 < \mu < 45$

Prolate magnetic fabric where: $45 < \mu < 90$

N

10 km

M7 Brandon Pier — M7 μ = 19.6

M6 Ballyheige — M6 μ = 13.5

A15 Dingle Peninsula — A15 μ = 37.2

N

IRELAND

Area of AMS analysis

Kerry Head
Dingle Peninsula
Iveragh Peninsula

A13
M10
M4

Other AMS ellipsoids.

A13 Dunmore East ** — A13 μ = 9.8

M4 Broad Strand * — M4 μ = 49.4

M10 Kenmare — M10 μ = 68.9

A13 & M4: Outside of mapped area. See Ireland Map.
A13 shows behaviour of AMS in Undeformed Old Red Sandstone.
M4 from south coast (Zone 1, Intrabasinal zone shows cleavage controlled AMS fabric).
M10:An example of a limestone sample shows more scattered AMS axes. Kmax is // to the pole to S1.

Transition Zone:
Moderate/Low Deformation.

Two Main Types:

i) Primary bedding controlled fabrics:

K_{min} is // to the pole to S0:
L31,M3, M2, L35

ii) Bedding and early layer parallel shortening fabrics.

Evidence of early LPS
1. K_{max} is // to the pole to bedding and // to the LPS plane:

Seen in : L47, Am11

2. First signs of LPS: grouping of K_{max} and a girdle of K_{int} and K_{min} : M44

Oblate and Prolate AMS ellipsoids.

Am11 Lough Caragh North — Am11 μ = 15.6

L35 Dooneen — L35 μ = 30.7

M3 Kells Bay — M3 μ = 16.9

A10 Gap of Dunloe North — A10 μ = 14.4

M44 Culoo Rocks — M44 μ = 80.4

L31 Valentia Island — L31 μ = 52

L47 Coosfada — L47 μ = 9.4

M2 Rheencaheragh — M2 μ = 69.2

A2 Killabounia — A2 μ = 62.7

M5 Lough Acoose — M5 μ = 42.9

A12 Gap of Dunloe — A12 μ = 59

M8 Glenflesk Quarry — M8 μ = 21.6

Intrabasinal Zone:
High deformation/moderate deformation.

a) Complete Tectonic Overprint: The AMS ellipsoids have been completely rotated into the cleavage plane.
Characterised by cleavage controlled AMS ellipsoids.
K_{min} // to the pole to S1 and L1 // to K_{max} or K_{int} AMS axes:

A2, A3M, Am1, M5, A14, M8, A8, A4-(S1 lies very close to S0)

Further deformation or transpression related: A1, A9

b) Incomplete Tectonic Overprint: Occurs as the AMS ellipsoids have been incompletely rotated from the bedding plane into the cleavage plane.
L1 // to K_{max} or K_{int}.

K_{int} and K_{min} occupy an intermediate position between bedding fabric and cleavage fabric: A6, A12

Oblate and Prolate AMS Ellipsoids

S - Line section for μ values against distance

A3M Keel Bay — A3M μ = 36

A4 East of Keel — A4 μ = 33.1

A1 Portmagee Quarry — A1 μ = 66

A6 Caherdaniel — A6 μ = 64.5

A8 Rossmore — A8 μ = 58.2

Am1 South of Lough Caragh — Am1 μ = 54.9

A9 Molls Gap — A9 μ = 22.8

A14 Kilgarvan — A14 μ = 9.1

Cleavage Map of the Iveragh Peninsula, South West Ireland.

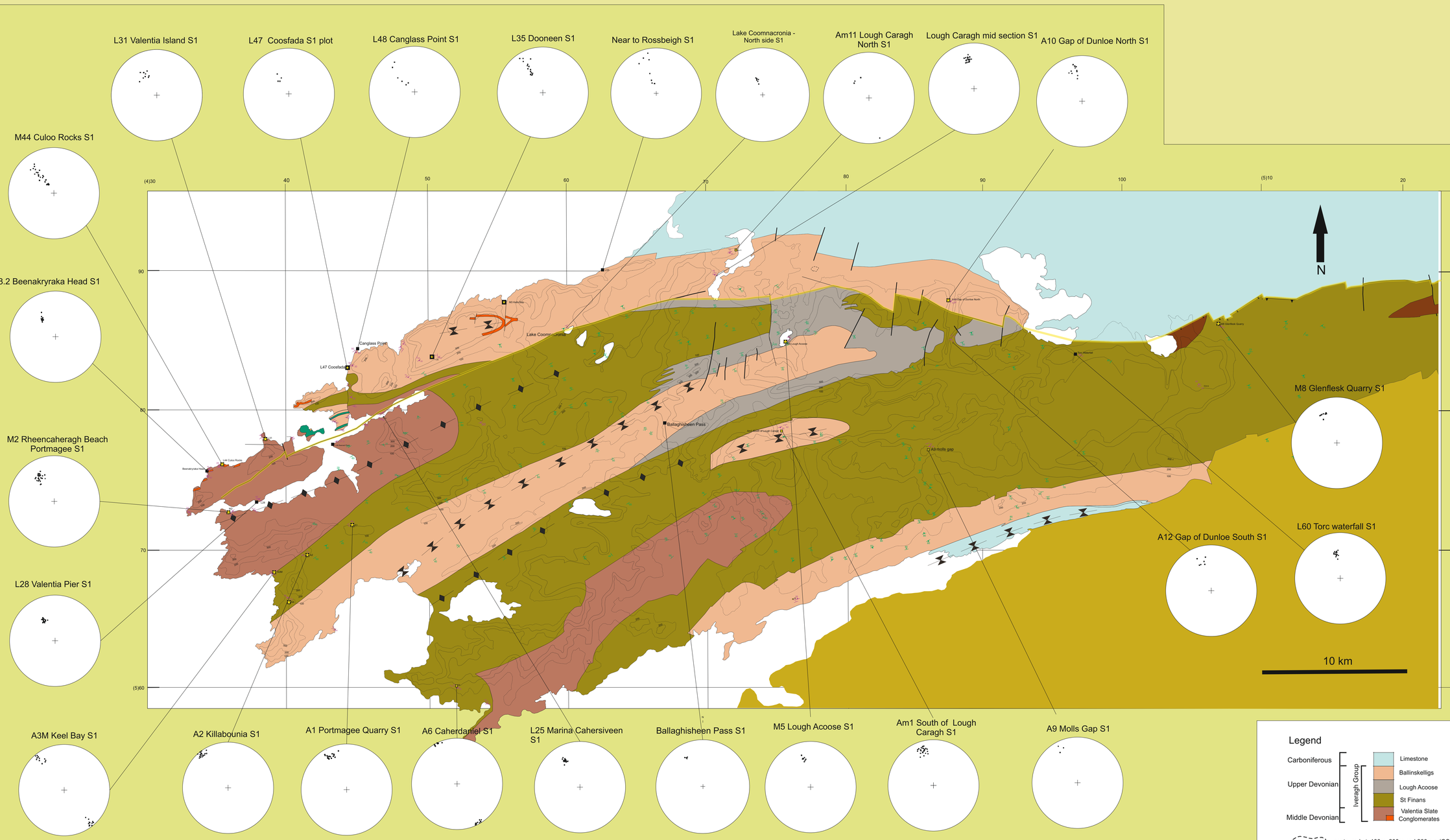

Strain Analysis Results showing DTNNM R_s and MRL R_s values across the northern margin of the Munster Basin, South West Ireland.

M6 Ballyheige
DTNNM = 1.093
MRL = 1.069

M7 Brandon Pier
DTNNM = 1.045
MRL = 1.027

M4 Broad Strand
DTNNM Rs = 1.574
MRL Rs = 1.276

A13 Dunmore East
DTNNM Rs = 1.292
MRL Rs = 1.093

N

IRELAND

Kerry Head
Dingle Peninsula
Iveragh Peninsula

A13

M4

Carboniferous
Upper Devonian
Middle Devonian
Iveragh Group
Limestone
Ballyheige
Ballinskelligs
Lough Acoose
St Finans
Valentia Slate Conglomerates
Sandstone
Devonian
Upper
Middle
Lower
Slieve Mish group
Caherbla group
Dingle group
Sandstone & Conglomerates
Silurian
Ordovician
Siltstone & Lst
Siltstone & Mudstone
Igneous
Dolerite
Proposed Basin Margin
Coomnacronia Fault
Anticline
Syncline
Contoured to 300 + (OSI Ireland)

L6 Cooscrome
DTNNM = 1.117
MRL = 1.190

L47 Coosfada
DTNNM = 1.444
MRL = 1.232

L39 Knocknatobar
DTNNM = 1.292
MRL = 1.235

L21 Kells Bay
DTNNM = 1.204
MRL = 1.035

M3 Kells Bay
DTNNM =1.135
MRL = 1.083

Am11 Lough Caragh North
DTNNM = 1.209
MRL = 1.081

A10 Gap of Dunloe North
DTNNM = 1.09
MRL = 1.069

L22 Kells Bay Post Office
DTNNM = 1.171
MRL = 1.111

L35 Dooneen
DTNNM = 1.348
MRL = 1.155

L41 Knocknatobar
DTNNM = 1.129
MRL = 1.084

L11North of Enagh Point
DTNNM = 1.136
MRL = 1.162

L10 Dolous Head
DTNNM = 1.119
MRL = 1.189

L7 Cooscrome
DTNNM = 1.106
MRL = 1.142

L19 Valentia
DTNNM = 1.171
MRL = 1.144

L31 Reenadrolaun Point
DTNNM = 1.290
MRL = 1.196

L44 Culoo Rocks
DTNNM = 1.284
MRL = 1.168

L23 Rheencaheragh Bay
DTNNM = 1.249
MRL = 1.310

L26 Reenard Pt
DTNNM = 1.301
MRL = 1.243

A3M Keel Bay
DTNNM = 1.539
MRL = 1.355

A2 Killabounia
DTNNM = 1.348
MRL = 1.264

A4 South East of Keel Bay
DTNNM = 1.216
MRL = 1.165

A1 Portmagee Quarry
DTNNM = 1.179
MRL = 1.235

A6 Caherdaniel
DTNNM = 1.204
MRL = 1.382

A7 Lambs Head
DTNNM = 1.201
MRL = 1.309

Line : Strain values verses distance

A8 Rossmore
DTNNM = 1.142
MRL = 1.160

Am1 South of Lough Caragh
DTNNM = 1.326
MRL= 1.263

A9 Molls Gap
DTNNM = 1.309
MRL = 1.199

M5 Lough Acoose
DTNNM = 1.193
MRL = 1.210

A14 Kilgarvan
DTNNM= 1.503
MRL = 1.426

M8 Glenflesk Quarry
DTNNM = 1.157
MRL = 1.240

10 km

Summary of Variscan Tectonic Zones in Old Red Sandstone Across the Northern Margin of the Munster Basin.